

# Fluid mechanics, turbulent flow and turbulence modeling

Lars Davidson

Division of Fluid Dynamics  
Department of Applied Mechanics  
Chalmers University of Technology  
SE-412 96 Göteborg, Sweden

<http://www.tfd.chalmers.se/~lada>, [lada@chalmers.se](mailto:lada@chalmers.se)

March 19, 2013

## Abstract

This course material is used in two courses in the International Master's programme **Applied Mechanics** at Chalmers. The two courses are *TME225 Mechanics of fluids*, and *MTF270 Turbulence Modeling*. MSc students who follow these courses are supposed to have taken one basic course in fluid mechanics.

This document can be downloaded at  
[http://www.tfd.chalmers.se/~lada/MoF/lecture\\_notes.html](http://www.tfd.chalmers.se/~lada/MoF/lecture_notes.html)

and

[http://www.tfd.chalmers.se/~lada/comp\\_turb\\_model/lecture\\_notes.html](http://www.tfd.chalmers.se/~lada/comp_turb_model/lecture_notes.html)

The Fluid courses in the MSc programme are presented at  
<http://www.tfd.chalmers.se/~lada/msc/msc-programme.html>

The MSc programme is presented at  
<http://www.chalmers.se/en/education/programmes/masters-info/Pages/Applied-Mechanics.aspx>

# Contents

<b>1 Motion, flow</b>	<b>9</b>
1.1 Eulerian, Lagrangian, material derivative . . . . .	9
1.2 Viscous stress, pressure . . . . .	10
1.3 Strain rate tensor, vorticity . . . . .	11
1.4 Product of a symmetric and antisymmetric tensor . . . . .	13
1.5 Deformation, rotation . . . . .	14
1.6 Irrotational and rotational flow . . . . .	16
1.6.1 Ideal vortex line . . . . .	17
1.6.2 Shear flow . . . . .	18
1.7 Eigenvalues and eigenvectors: physical interpretation . . . . .	19
<b>2 Governing flow equations</b>	<b>21</b>
2.1 The Navier-Stokes equation . . . . .	21
2.1.1 The continuity equation . . . . .	21
2.1.2 The momentum equation . . . . .	21
2.2 The energy equation . . . . .	22
2.3 Transformation of energy . . . . .	23
2.4 Left side of the transport equations . . . . .	24
2.5 Material particle vs. control volume (Reynolds Transport Theorem) .	25
<b>3 Exact solutions to the Navier-Stokes equation: two examples</b>	<b>27</b>
3.1 The Rayleigh problem . . . . .	27
3.2 Flow between two plates . . . . .	30
3.2.1 Curved plates . . . . .	30
3.2.2 Flat plates . . . . .	31
3.2.3 Force balance . . . . .	33
3.2.4 Balance equation for the kinetic energy . . . . .	34
<b>4 Vorticity equation and potential flow</b>	<b>36</b>
4.1 Vorticity and rotation . . . . .	36
4.2 The vorticity transport equation in three dimensions . . . . .	37
4.3 The vorticity transport equation in two dimensions . . . . .	40
4.3.1 Boundary layer thickness from the Rayleigh problem . . . . .	41
<b>5 Turbulence</b>	<b>43</b>
5.1 Introduction . . . . .	43
5.2 Turbulent scales . . . . .	44
5.3 Energy spectrum . . . . .	45
5.4 The cascade process created by vorticity . . . . .	49
<b>6 Turbulent mean flow</b>	<b>53</b>
6.1 Time averaged Navier-Stokes . . . . .	53
6.1.1 Boundary-layer approximation . . . . .	54
6.2 Wall region in fully developed channel flow . . . . .	54
6.3 Reynolds stresses in fully developed channel flow . . . . .	58
6.4 Boundary layer . . . . .	60
<b>7 Probability density functions</b>	<b>62</b>

<b>8 Transport equations for kinetic energy</b>	<b>65</b>
8.1 The Exact $k$ Equation . . . . .	65
8.1.1 Spectral transfer dissipation $\varepsilon_\kappa$ vs. “true” viscous dissipation, $\varepsilon$	68
8.2 The Exact $k$ Equation: 2D Boundary Layers . . . . .	68
8.3 Spatial vs. spectral energy transfer . . . . .	70
8.4 The overall effect of the transport terms . . . . .	71
8.5 The transport equation for $\bar{v}_i \bar{v}_i / 2$ . . . . .	71
<b>9 Transport equations for Reynolds stresses</b>	<b>74</b>
9.1 Reynolds shear stress vs. the velocity gradient . . . . .	78
<b>10 Correlations</b>	<b>80</b>
10.1 Two-point correlations . . . . .	80
10.2 Auto correlation . . . . .	82
<b>11 Reynolds stress models and two-equation models</b>	<b>84</b>
11.1 Mean flow equations . . . . .	84
11.1.1 Flow equations . . . . .	84
11.1.2 Temperature equation . . . . .	85
11.2 The exact $\overline{v'_i v'_j}$ equation . . . . .	85
11.3 The exact $\overline{v'_i \theta'}$ equation . . . . .	86
11.4 The $k$ equation . . . . .	88
11.5 The $\varepsilon$ equation . . . . .	89
11.6 The Boussinesq assumption . . . . .	89
11.7 Modelling assumptions . . . . .	90
11.7.1 Production terms . . . . .	91
11.7.2 Diffusion terms . . . . .	91
11.7.3 Dissipation term, $\varepsilon_{ij}$ . . . . .	93
11.7.4 Slow pressure-strain term . . . . .	93
11.7.5 Rapid pressure-strain term . . . . .	96
11.7.6 Wall model of the pressure-strain term . . . . .	102
11.8 The $k - \varepsilon$ model . . . . .	104
11.9 The modelled $\overline{v'_i v'_j}$ equation with IP model . . . . .	105
11.10 Algebraic Reynolds Stress Model (ASM) . . . . .	105
11.11 Explicit ASM (EASM or EARSM) . . . . .	106
11.12 Boundary layer flow . . . . .	107
<b>12 Reynolds stress models vs. eddy-viscosity models</b>	<b>109</b>
12.1 Stable and unstable stratification . . . . .	109
12.2 Curvature effects . . . . .	110
12.3 Stagnation flow . . . . .	113
12.4 RSM/ASM versus $k - \varepsilon$ models . . . . .	114
<b>13 Realizability</b>	<b>115</b>
13.1 Two-component limit . . . . .	116
<b>14 Non-linear Eddy-viscosity Models</b>	<b>118</b>
<b>15 The V2F Model</b>	<b>121</b>
15.1 Modified V2F model . . . . .	124

15.2 Realizable V2F model . . . . .	125
15.3 To ensure that $v^2 \leq 2k/3$ [1] . . . . .	125
<b>16 The SST Model</b>	<b>126</b>
<b>17 Overview of RANS models</b>	<b>130</b>
<b>18 Large Eddy Simulations</b>	<b>131</b>
18.1 Time averaging and filtering . . . . .	131
18.2 Differences between time-averaging (RANS) and space filtering (LES) . . . . .	132
18.3 Resolved & SGS scales . . . . .	133
18.4 The box-filter and the cut-off filter . . . . .	134
18.5 Highest resolved wavenumbers . . . . .	135
18.6 Subgrid model . . . . .	135
18.7 Smagorinsky model vs. mixing-length model . . . . .	136
18.8 Energy path . . . . .	136
18.9 SGS kinetic energy . . . . .	137
18.10 LES vs. RANS . . . . .	137
18.11 The dynamic model . . . . .	138
18.12 The test filter . . . . .	139
18.13 Stresses on grid, test and intermediate level . . . . .	140
18.14 Numerical dissipation . . . . .	141
18.15 Scale-similarity Models . . . . .	142
18.16 The Bardina Model . . . . .	143
18.17 Redefined terms in the Bardina Model . . . . .	143
18.18 A dissipative scale-similarity model. . . . .	144
18.19 Forcing . . . . .	145
18.20 Numerical method . . . . .	146
18.20.1 RANS vs. LES . . . . .	147
18.21 One-equation $k_{sgs}$ model . . . . .	148
18.22 Smagorinsky model derived from the $k_{sgs}$ equation . . . . .	148
18.23 A dynamic one-equation model . . . . .	149
18.24 A Mixed Model Based on a One-Eq. Model . . . . .	150
18.25 Applied LES . . . . .	150
18.26 Resolution requirements . . . . .	150
<b>19 Unsteady RANS</b>	<b>152</b>
19.1 Turbulence Modelling . . . . .	155
19.2 Discretization . . . . .	155
<b>20 DES</b>	<b>157</b>
20.1 DES based on two-equation models . . . . .	158
20.2 DES based on the $k - \omega$ SST model . . . . .	159
<b>21 Hybrid LES-RANS</b>	<b>160</b>
21.1 Momentum equations in hybrid LES-RANS . . . . .	164
21.2 The equation for turbulent kinetic energy in hybrid LES-RANS . . . . .	164
21.3 Results . . . . .	164
<b>22 The SAS model</b>	<b>167</b>
22.1 Resolved motions in unsteady . . . . .	167

22.2	The von Kármán length scale . . . . .	167
22.3	The second derivative of the velocity . . . . .	169
22.4	Evaluation of the von Kármán length scale in channel flow . . . . .	169
<b>23</b>	<b>The PANS Model</b>	<b>172</b>
<b>24</b>	<b>Hybrid LES/RANS for Dummies</b>	<b>176</b>
24.1	Introduction . . . . .	176
24.1.1	Reynolds-Averaging Navier-Stokes equations: RANS . . . . .	176
24.1.2	Large Eddy Simulations: LES . . . . .	176
24.1.3	Zonal LES/RANS . . . . .	177
24.2	The PANS $k - \varepsilon$ turbulence model . . . . .	177
24.3	Zonal LES/RANS: wall modeling . . . . .	178
24.3.1	The interface conditions . . . . .	178
24.3.2	Results . . . . .	179
24.4	Zonal LES/RANS: embedded LES . . . . .	179
24.4.1	The interface conditions . . . . .	179
24.4.2	Results . . . . .	181
<b>25</b>	<b>Inlet boundary conditions</b>	<b>182</b>
25.1	Synthesized turbulence . . . . .	182
25.2	Random angles . . . . .	182
25.3	Highest wave number . . . . .	183
25.4	Smallest wave number . . . . .	183
25.5	Divide the wave number range . . . . .	183
25.6	von Kármán spectrum . . . . .	184
25.7	Computing the fluctuations . . . . .	184
25.8	Introducing time correlation . . . . .	184
<b>26</b>	<b>Overview of LES, hybrid LES-RANS and URANS models</b>	<b>187</b>
<b>27</b>	<b>Best practice guidelines (BPG)</b>	<b>190</b>
27.1	EU projects . . . . .	190
27.2	Ercoftac workshops . . . . .	190
27.3	Ercoftac Classical Database . . . . .	191
27.4	ERCOFTAC QNET Knowledge Base Wiki . . . . .	191
<b>A</b>	<b>TME225: <math>\epsilon - \delta</math> identity</b>	<b>192</b>
<b>B</b>	<b>TME225 Assignment 1: laminar flow</b>	<b>193</b>
B.1	Fully developed region . . . . .	194
B.2	Wall shear stress . . . . .	194
B.3	Inlet region . . . . .	194
B.4	Wall-normal velocity in the developing region . . . . .	195
B.5	Vorticity . . . . .	195
B.6	Deformation . . . . .	195
B.7	Dissipation . . . . .	195
B.8	Eigenvalues . . . . .	195
B.9	Eigenvectors . . . . .	196
<b>C</b>	<b>TME225: Fourier series</b>	<b>197</b>

C.1	Orthogonal functions . . . . .	197
C.2	Trigonometric functions . . . . .	198
C.3	Fourier series of a function . . . . .	200
C.4	Derivation of Parseval's formula . . . . .	200
C.5	Complex Fourier series . . . . .	202
<b>D</b>	<b>TME225: Why has the energy spectrum, <math>E</math>, such strange dimensions?</b>	<b>203</b>
D.1	An example . . . . .	203
D.2	An example: Matlab code . . . . .	205
<b>E</b>	<b>TME225 Assignment 2: turbulent flow</b>	<b>209</b>
E.1	Time history . . . . .	209
E.2	Time averaging . . . . .	209
E.3	Mean flow . . . . .	210
E.4	The time-averaged momentum equation . . . . .	210
E.5	Wall shear stress . . . . .	211
E.6	Resolved stresses . . . . .	211
E.7	Fluctuating wall shear stress . . . . .	211
E.8	Production terms . . . . .	211
E.9	Pressure-strain terms . . . . .	211
E.10	Dissipation . . . . .	212
E.11	Do something fun! . . . . .	212
<b>F</b>	<b>TME225 Learning outcomes 2012</b>	<b>213</b>
<b>G</b>	<b>MTF270: Some properties of the pressure-strain term</b>	<b>224</b>
<b>H</b>	<b>MTF270: Galilean invariance</b>	<b>225</b>
<b>I</b>	<b>MTF270: Computation of wavenumber vector and angles</b>	<b>227</b>
I.1	The wavenumber vector, $\kappa_j^n$ . . . . .	227
I.2	Unit vector $\sigma_i^n$ . . . . .	228
<b>J</b>	<b>MTF270: 1D and 3D energy spectra</b>	<b>229</b>
J.1	Energy spectra from two-point correlations . . . . .	230
<b>K</b>	<b>MTF270, Assignment 1: Reynolds averaged Navier-Stokes</b>	<b>232</b>
K.1	Two-dimensional flow . . . . .	232
K.2	Analysis . . . . .	232
	K.2.1 The momentum equations . . . . .	233
	K.2.2 The turbulent kinetic energy equation . . . . .	234
	K.2.3 The Reynolds stress equations . . . . .	234
K.3	Compute derivatives on a curvi-linear mesh . . . . .	236
	K.3.1 Geometrical quantities . . . . .	237
<b>L</b>	<b>MTF270, Assignment 2: LES</b>	<b>238</b>
L.1	Task 2.1 . . . . .	238
L.2	Task 2.2 . . . . .	240
L.3	Task 2.3 . . . . .	240
L.4	Task 2.4 . . . . .	241
L.5	Task 2.5 . . . . .	242

L.6	Task 2.6 . . . . .	242
L.7	Task 2.7 . . . . .	243
L.8	Task 2.8 . . . . .	244
L.9	Task 2.9 . . . . .	244
L.10	Task 2.10 . . . . .	244
L.11	Task 2.11 . . . . .	245
<b>M</b>	<b>MTF270: Compute energy spectra from LES/DNS data using Matlab</b>	<b>246</b>
M.1	Introduction . . . . .	246
M.2	An example of using FFT . . . . .	246
M.3	Energy spectrum from the two-point correlation . . . . .	248
M.4	Energy spectra from the autocorrelation . . . . .	250
<b>N</b>	<b>MTF270, Assignment 4: Hybrid LES-RANS</b>	<b>251</b>
N.1	Time history . . . . .	251
N.2	Mean velocity profile . . . . .	252
N.3	Resolved stresses . . . . .	252
N.4	Turbulent kinetic energy . . . . .	253
N.5	The modelled turbulent shear stress . . . . .	253
N.6	Turbulent length scales . . . . .	253
N.7	SAS turbulent length scales . . . . .	253
<b>O</b>	<b>MTF270, Assignment 5: Embedded LES with PANS</b>	<b>255</b>
O.1	Time history . . . . .	255
O.2	Resolved stresses . . . . .	256
O.3	Turbulent viscosity . . . . .	256
O.4	Modelled stresses . . . . .	257
O.5	Turbulent SGS dissipation . . . . .	257
<b>P</b>	<b>MTF270: Transformation of a tensor</b>	<b>259</b>
P.1	Rotation to principal directions . . . . .	260
P.2	Transformation of a velocity gradient . . . . .	261
<b>Q</b>	<b>MTF270: Green's formulas</b>	<b>262</b>
Q.1	Green's first formula . . . . .	262
Q.2	Green's second formula . . . . .	262
Q.3	Green's third formula . . . . .	262
Q.4	Analytical solution to Poisson's equation . . . . .	265
<b>R</b>	<b>MTF270: Learning outcomes for 2012</b>	<b>266</b>
<b>S</b>	<b>References</b>	<b>273</b>

# TME225 Mechanics of fluids

**L. Davidson**

Division of Fluid Dynamics, Department of Applied Mechanics  
Chalmers University of Technology, Göteborg, Sweden  
<http://www.tfd.chalmers.se/~lada>, lada@chalmers.se

This report can be downloaded at  
<http://www.tfd.chalmers.se/~lada/MoF/>

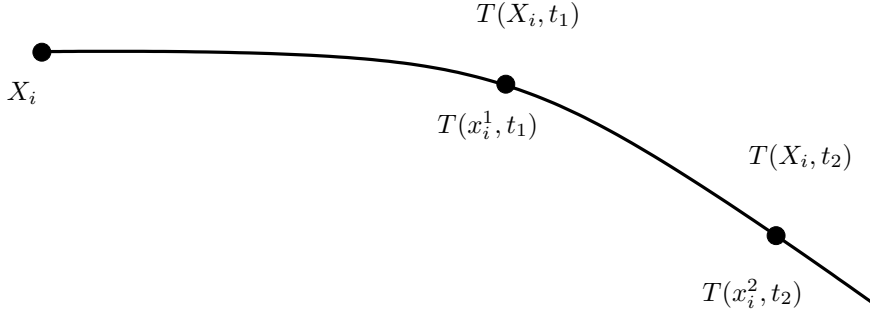


Figure 1.1: The temperature of a fluid particle described in Lagrangian,  $T(X_i, t)$ , or Eulerian,  $T(x_i, t)$ , approach.

# 1 Motion, flow

## 1.1 Eulerian, Lagrangian, material derivative

See also [2], Chapt. 3.2.

Assume a fluid particle is moving along the line in Fig. 1.1. We can choose to study its motion in two ways: Lagrangian or Eulerian.

In the Lagrangian approach we keep track of its original position ( $X_i$ ) and follow its path which is described by  $x_i(X_i, t)$ . For example, at time  $t_1$  the temperature of the particle is  $T(X_i, t_1)$ , and at time  $t_2$  its temperature is  $T(X_i, t_2)$ , see Fig. 1.1. This approach is not used for fluids because it is very tricky to define and follow a fluid particle. It is however used when simulating movement of particles in fluids (for example soot particles in gasoline-air mixtures in combustion applications). The speed of the particle is then expressed as a function of time and its position at time zero, i.e.  $v_i = v_i(X_i, t)$ .

In the Eulerian approach we pick a position, e.g.  $x_i^1$ , and watch the particle pass by. This approach is used for fluids. The temperature of the fluid,  $T$ , for example, is expressed as a function of the position, i.e.  $T = T(x_i)$ , see Fig. 1.1. It may be that the temperature at position  $x_i$ , for example, varies in time,  $t$ , and then  $T = T(x_i, t)$ .

Now we want to express how the temperature of a fluid particle varies. In the Lagrangian approach we first pick the particle (this gives its starting position,  $X_i$ ). Once we have chosen a particle its starting position is fixed, and temperature varies only with time, i.e.  $T(t)$  and the temperature gradient can be written  $dT/dt$ .

In the Eulerian approach it is a little bit more difficult. We are looking for the temperature gradient,  $dT/dt$ , but since we are looking at fixed points in space we need to express the temperature as a function of both time and space. From classical mechanics, we know that the velocity of a fluid particle is the time derivative of its space location, i.e.  $v_i = dx_i/dt$ . The chain-rule now gives

$$\frac{dT}{dt} = \frac{\partial T}{\partial t} + \frac{dx_j}{dt} \frac{\partial T}{\partial x_j} = \frac{\partial T}{\partial t} + v_j \frac{\partial T}{\partial x_j} \quad (1.1)$$

Note that we have to use partial derivative on  $T$  since it is a function of more than one (independent) variable. The first term on the right side is the **local rate of change**; by this we mean that it describes the variation of  $T$  in time at position  $x_i$ . The second term on the right side is called the **convective rate of change**, which means that it describes

**local rate  
of change**  
**Conv. rate  
of change**

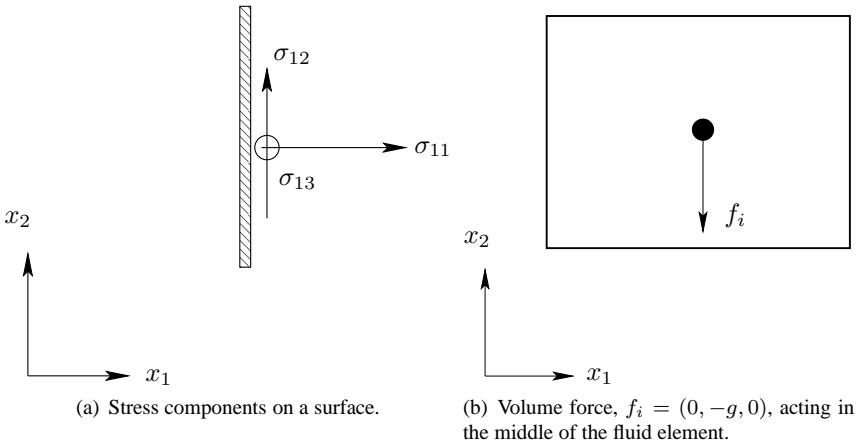


Figure 1.2: Stress tensor and volume (gravitation) force.

the variation of  $T$  in space when it passes the point  $x_i$ . The left side in Eq. 1.1 is called the **material derivative** and is in this text denoted by  $dT/dt$ .

Equation 1.1 can be illustrated as follows. Put your finger out in the blowing wind. The temperature gradient you're finger experiences is  $\partial T/\partial t$ . Imagine that you're a fluid particle and that you ride on a bike. The temperature gradient you experience is the material derivative,  $dT/dt$ .

**Exercise 1** Write out Eq. 1.1, term-by-term.

## 1.2 Viscous stress, pressure

See also [2], Chaps. 6.3 and 8.1.

We have in Part I [3] derived the balance equation for linear momentum which reads

$$\boxed{\rho \dot{v}_i - \sigma_{ji,j} - \rho f_i = 0} \quad (1.2)$$

Switch notation for the material derivative and derivatives so that

$$\rho \frac{dv_i}{dt} = \frac{\partial \sigma_{ji}}{\partial x_j} + \rho f_i \quad (1.3)$$

where the first and the second term on the right side represents, respectively, the net force due to surface and volume forces ( $\sigma_{ij}$  denotes the stress tensor). Stress is force per unit area. The first term includes the viscous stress tensor,  $\tau_{ij}$ . As you have learnt earlier, the first index relates to the surface at which the stress acts and the second index is related to the stress component. For example, on a surface whose normal is  $n_i = (1, 0, 0)$  act the three stress components  $\sigma_{11}$ ,  $\sigma_{12}$  and  $\sigma_{13}$ , see Fig. 1.2a; the volume force acts in the middle of the fluid element, see Fig. 1.2b.

In the present notation we denote the velocity vector by  $\mathbf{v} = v_i = (v_1, v_2, v_3)$  and the coordinate by  $\mathbf{x} = x_i = (x_1, x_2, x_3)$ . In the literature, you may find other notations of the velocity vector such as  $u_i = (u_1, u_2, u_3)$ . If no tensor notation is used the velocity vector is usually denoted as  $(u, v, w)$  and the coordinates as  $(x, y, z)$ .

**Material derivative**

The diagonal components of  $\sigma_{ij}$  represent normal stresses and the off-diagonal components of  $\sigma_{ij}$  represent the shear stresses. In Part I [3] you learnt that the pressure is defined as minus the sum of the normal stress, i.e.

$$p = -\sigma_{kk}/3 \quad (1.4)$$

The pressure,  $p$ , acts as a normal stress. In general, pressure is a thermodynamic property,  $p_t$ , which can be obtained – for example – from the ideal gas law. In that case the thermodynamics pressure,  $p_t$ , and the mechanical pressure,  $p$ , may not be the same but Eq. 1.4 is nevertheless used. The *viscous* stress tensor,  $\tau_{ij}$ , is obtained by subtracting the trace,  $\sigma_{kk}/3 = -p$ , from  $\sigma_{ij}$ ; the stress tensor can then be written as

$$\sigma_{ij} = -p\delta_{ij} + \tau_{ij} \quad (1.5)$$

$\tau_{ij}$  is the deviator of  $\sigma_{ij}$ . The expression for the viscous stress tensor is found in Eq. 2.4 at p. 21. The minus-sign in front of  $p$  appears because the pressure acts *into* the surface. When there's no movement, the viscous stresses are zero and then of course the normal stresses are the same as the pressure. In general, however, the normal stresses are the sum of the pressure and the viscous stresses, i.e.

$$\sigma_{11} = -p + \tau_{11}, \quad \sigma_{22} = -p + \tau_{22}, \quad \sigma_{33} = -p + \tau_{33}, \quad (1.6)$$

**Exercise 2** Consider Fig. 1.2. Show how  $\sigma_{21}, \sigma_{22}, \sigma_{23}$  act on a surface with normal vector  $n_i = (0, 1, 0)$ . Show also how  $\sigma_{31}, \sigma_{32}, \sigma_{33}$  act on a surface with normal vector  $n_i = (0, 0, 1)$ .

**Exercise 3** Write out Eq. 1.5 on matrix form.

### 1.3 Strain rate tensor, vorticity

See also [2], Chapt. 3.5.3, 3.6.

We need an expression for the viscous stresses,  $\tau_{ij}$ . They will be expressed in the velocity gradients,  $\frac{\partial v_i}{\partial x_j}$ . Hence we will now discuss the velocity gradients.

The velocity gradient tensor can be split into two parts as

$$\begin{aligned} \frac{\partial v_i}{\partial x_j} &= \frac{1}{2} \left( \underbrace{\frac{\partial v_i}{\partial x_j} + \frac{\partial v_i}{\partial x_j}}_{2\partial v_i / \partial x_j} + \underbrace{\frac{\partial v_j}{\partial x_i} - \frac{\partial v_j}{\partial x_i}}_{=0} \right) \\ &= \frac{1}{2} \left( \frac{\partial v_i}{\partial x_j} + \frac{\partial v_j}{\partial x_i} \right) + \frac{1}{2} \left( \frac{\partial v_i}{\partial x_j} - \frac{\partial v_j}{\partial x_i} \right) = S_{ij} + \Omega_{ij} \end{aligned} \quad (1.7)$$

where

$S_{ij}$  is a *symmetric* tensor called the **strain-rate tensor**

$\Omega_{ij}$  is a *anti-symmetric* tensor called the **vorticity tensor**

The vorticity tensor is related to the familiar **vorticity vector** which is the curl of the velocity vector, i.e.  $\boldsymbol{\omega} = \nabla \times \mathbf{v}$ , or in tensor notation

$$\omega_i = \epsilon_{ijk} \frac{\partial v_k}{\partial x_j} \quad (1.8)$$

**Strain-rate tensor  
vorticity tensor**

If we set, for example,  $i = 3$  we get

$$\omega_3 = \partial v_2 / \partial x_1 - \partial v_1 / \partial x_2. \quad (1.9)$$

The vorticity represents rotation of a fluid particle. Inserting Eq. 1.7 into Eq. 1.8 gives

$$\omega_i = \epsilon_{ijk} (S_{kj} + \Omega_{kj}) = \epsilon_{ijk} \Omega_{kj} \quad (1.10)$$

since  $\epsilon_{ijk} S_{kj} = 0$  because the product of a symmetric tensor ( $S_{kj}$ ) and an anti-symmetric tensor ( $\epsilon_{ijk}$ ) is zero. Let us show this for  $i = 1$  by writing out the full equation. Recall that  $S_{ij} = S_{ji}$  (i.e.  $S_{12} = S_{21}$ ,  $S_{13} = S_{31}$ ,  $S_{23} = S_{32}$ ) and  $\epsilon_{ijk} = -\epsilon_{ikj} = \epsilon_{jki}$  etc (i.e.  $\epsilon_{123} = -\epsilon_{132} = \epsilon_{231} \dots, \epsilon_{113} = \epsilon_{221} = \dots \epsilon_{331} = 0$ )

$$\begin{aligned} \epsilon_{1jk} S_{kj} &= \epsilon_{111} S_{11} + \epsilon_{112} S_{21} + \epsilon_{113} S_{31} \\ &\quad + \epsilon_{121} S_{12} + \epsilon_{122} S_{22} + \epsilon_{123} S_{32} \\ &\quad + \epsilon_{131} S_{13} + \epsilon_{132} S_{23} + \epsilon_{133} S_{33} \\ &= 0 \cdot S_{11} + 0 \cdot S_{21} + 0 \cdot S_{31} \\ &\quad + 0 \cdot S_{12} + 0 \cdot S_{22} + 1 \cdot S_{32} \\ &\quad + 0 \cdot S_{13} - 1 \cdot S_{23} + 0 \cdot S_{33} \\ &= S_{32} - S_{23} = 0 \end{aligned} \quad (1.11)$$

Now let us invert Eq. 1.10. We start by multiplying it with  $\epsilon_{i\ell m}$  so that

$$\epsilon_{i\ell m} \omega_i = \epsilon_{i\ell m} \epsilon_{ijk} \Omega_{kj} \quad (1.12)$$

The  $\epsilon$ - $\delta$ -identity gives (see Table A.1 at p. A.1)

$$\epsilon_{i\ell m} \epsilon_{ijk} \Omega_{kj} = (\delta_{\ell j} \delta_{mk} - \delta_{\ell k} \delta_{mj}) \Omega_{kj} = \Omega_{m\ell} - \Omega_{\ell m} = 2\Omega_{m\ell} \quad (1.13)$$

This can easily be proved by writing all the components, see Table A.1 at p. A.1. Hence we get with Eq. 1.8

$$\Omega_{m\ell} = \frac{1}{2} \epsilon_{i\ell m} \omega_i = \frac{1}{2} \epsilon_{\ell mi} \omega_i = -\frac{1}{2} \epsilon_{m\ell i} \omega_i \quad (1.14)$$

or, switching indices

$$\Omega_{ij} = -\frac{1}{2} \epsilon_{ijk} \omega_k \quad (1.15)$$

A much easier way to go from Eq. 1.10 to Eq. 1.15 is to write out the components of Eq. 1.10. Here we do it for  $i = 1$

$$\omega_1 = \epsilon_{123} \Omega_{32} + \epsilon_{132} \Omega_{23} = \Omega_{32} - \Omega_{23} = -2\Omega_{23} \quad (1.16)$$

and we get

$$\Omega_{23} = -\frac{1}{2} \omega_1 \quad (1.17)$$

which indeed is identical to Eq. 1.15.

**Exercise 4** Write out the second and third component of the vorticity vector given in Eq. 1.8 (i.e.  $\omega_2$  and  $\omega_3$ ).

**Exercise 5** Complete the proof of Eq. 1.11 for  $i = 2$  and  $i = 3$ .

**Exercise 6** Write out Eq. 1.16 also for  $i = 2$  and  $i = 3$  and find an expression for  $\Omega_{12}$  and  $\Omega_{13}$  (cf. Eq. 1.17). Show that you get the same result as in Eq. 1.15.

**Exercise 7** In Eq. 1.17 we proved the relation between  $\Omega_{ij}$  and  $\omega_i$  for the off-diagonal components. What about the diagonal components of  $\Omega_{ij}$ ? What do you get from Eq. 1.7?

**Exercise 8** From your course in linear algebra, you should remember how to compute a vector product using Sarrus' rule. Use it to compute the vector product

$$\boldsymbol{\omega} = \nabla \times \mathbf{v} = \begin{bmatrix} \hat{\mathbf{e}}_1 & \hat{\mathbf{e}}_2 & \hat{\mathbf{e}}_3 \\ \frac{\partial}{\partial x_1} & \frac{\partial}{\partial x_2} & \frac{\partial}{\partial x_3} \\ v_1 & v_2 & v_3 \end{bmatrix}$$

Verify that this agrees with the expression in tensor notation in Eq. 1.8.

## 1.4 Product of a symmetric and antisymmetric tensor

In this section we show the proof that the product of a symmetric and antisymmetric tensor is zero. First, we have the definitions:

- A tensor  $a_{ij}$  is symmetric if  $a_{ij} = a_{ji}$ ;
- A tensor  $b_{ij}$  is antisymmetric if  $b_{ij} = -b_{ji}$ .

It follows that for an antisymmetric tensor that all diagonal components must be zero; for example,  $b_{11} = -b_{11}$  can only be satisfied if  $b_{11} = 0$ .

The (inner) product of a symmetric and antisymmetric tensor is always zero. This can be shown as follows

$$a_{ij}b_{ij} = a_{ji}b_{ij} = -a_{ij}b_{ji},$$

where we first used the fact that  $a_{ij} = a_{ji}$  (symmetric), and then that  $b_{ij} = -b_{ji}$  (antisymmetric). Since the indices  $i$  and  $j$  are both dummy indices we can interchange them, so that

$$a_{ij}b_{ij} = -a_{ji}b_{ij} = -a_{ij}b_{ij},$$

and thus the product must be zero.

This can of course also be shown by writing out  $a_{ij}b_{ij}$  on component form, i.e.

$$\begin{aligned} a_{ij}b_{ij} &= \underline{\underline{a_{11}b_{11}}} + \underline{\underline{a_{12}b_{12}}} + \underline{\underline{a_{13}b_{13}}} \\ &\quad + \underline{\underline{a_{21}b_{21}}} + \underline{\underline{a_{22}b_{22}}} + \underline{\underline{a_{23}b_{23}}} \\ &\quad + \underline{\underline{a_{31}b_{31}}} + \underline{\underline{a_{32}b_{32}}} + \underline{\underline{a_{33}b_{33}}} = 0 \end{aligned}$$

The underlined terms are zero; terms I cancel each other as do terms II and III.

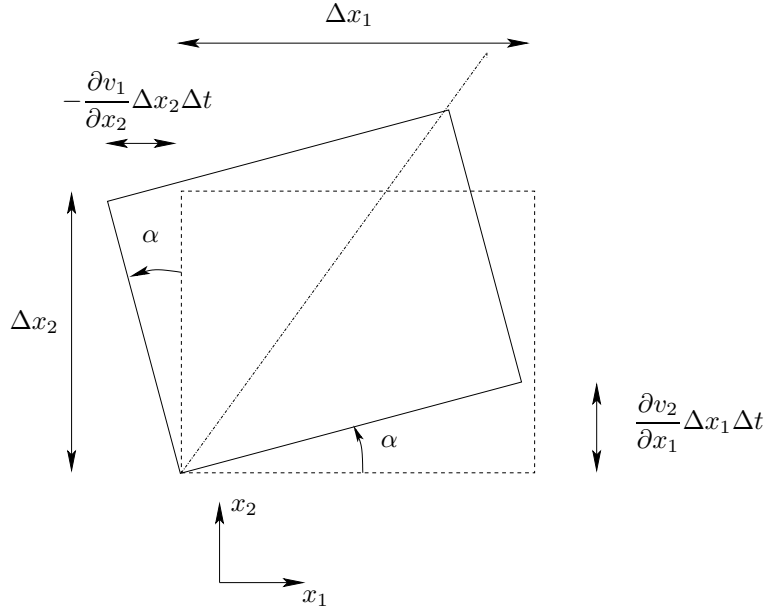


Figure 1.3: Rotation of a fluid particle during time  $\Delta t$ . Here  $\partial v_1 / \partial x_2 = -\partial v_2 / \partial x_1$  so that  $-\Omega_{12} = \omega_3 / 2 = \partial v_2 / \partial x_1 > 0$ .

## 1.5 Deformation, rotation

See also [2], Chapt. 3.3.

The velocity gradient can, as shown above, be divided into two parts:  $S_{ij}$  and  $\Omega_{ij}$ . We have shown that the latter is connected to *rotation* of a fluid particle. During rotation the fluid particle is not deformed. This movement can be illustrated by Fig. 1.3. The vertical movement ( $v_2$ ) of the lower-right corner ( $x_1 + \Delta x_1$ ) of the particle in Fig. 1.3 is estimated as follows. The velocity at the lower-left corner is  $v_2(x_1)$ . Now we need the velocity at the lower-right corner which is located at  $x_1 + \Delta x_1$ . It is computed using the first term in the Taylor series as<sup>1</sup>

$$v_2(x_1 + \Delta x_1) = v_2(x_1) + \Delta x_1 \frac{\partial v_2}{\partial x_1}$$

It is assumed that the fluid particle in Fig. 1.3 is rotated the angle  $\alpha$  during the time  $\Delta t$ . The vorticity during this rotation is  $\omega_3 = \partial v_2 / \partial x_1 - \partial v_1 / \partial x_2 = -2\Omega_{12}$ . The vorticity  $\omega_3$  should be interpreted as twice the average rotation of the horizontal edge ( $\partial v_2 / \partial x_1$ ) and vertical edge ( $-\partial v_1 / \partial x_2$ ).

Next let us have a look at the deformation caused by  $S_{ij}$ . It can be divided into two parts, namely shear and elongation (also called extension or dilatation). The deformation due to shear is caused by the off-diagonal terms of  $S_{ij}$ . In Fig. 1.4, a pure shear deformation by  $S_{12} = (\partial v_1 / \partial x_2 + \partial v_2 / \partial x_1) / 2$  is shown. The deformation due to elongation is caused by the diagonal terms of  $S_{ij}$ . Elongation caused by  $S_{11} = \partial v_1 / \partial x_1$  is illustrated in Fig. 1.5.

**rotation**

<sup>1</sup>this corresponds to the equation for a straight line  $y = kx + \ell$  where  $k$  is the slope which is equal to the derivative of  $y$ , i.e.  $dy/dx$

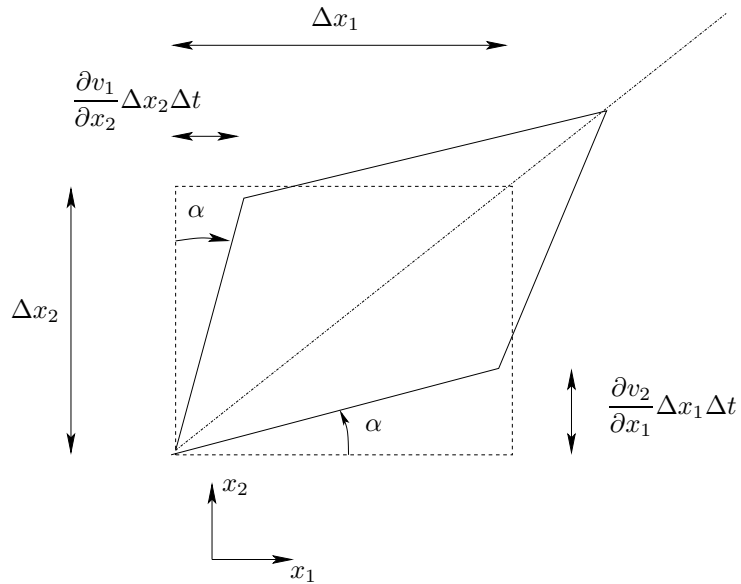


Figure 1.4: Deformation of a fluid particle by shear during time  $\Delta t$ . Here  $\partial v_1 / \partial x_2 = \partial v_2 / \partial x_1$  so that  $S_{12} = \partial v_1 / \partial x_2 > 0$ .

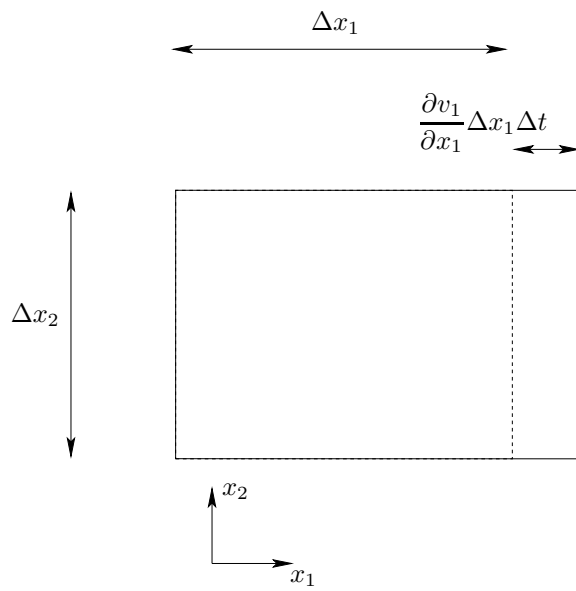


Figure 1.5: Deformation of a fluid particle by elongation during time  $\Delta t$ .

In general, a fluid particle experiences a combination of rotation, deformation and elongation as indeed is given by Eq. 1.7.

**Exercise 9** Consider Fig. 1.3. Show and formulate the rotation by  $\omega_1$ .

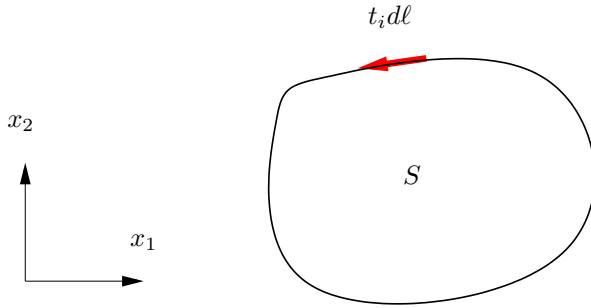


Figure 1.6: The surface,  $S$ , is enclosing by the line  $\ell$ . The vector,  $t_i$ , denotes the unit tangential vector of the enclosing line,  $\ell$ .

**Exercise 10** Consider Fig. 1.4. Show and formulate the deformation by  $S_{23}$ .

**Exercise 11** Consider Fig. 1.5. Show and formulate the elongation by  $S_{22}$ .

## 1.6 Irrational and rotational flow

In the previous subsection we introduced different types of movement of a fluid particle. One type of movement was rotation, see Fig. 1.3. Flows are often classified based on rotation: they are *rotational* ( $\omega_i \neq 0$ ) or *irrotational* ( $\omega_i = 0$ ); the latter type is also called inviscid flow or potential flow. We'll talk more about that later on. In this subsection we will give examples of one irrotational and one rotational flow. In potential flow, there exists a potential,  $\Phi$ , from which the velocity components can be obtained as

$$v_k = \frac{\partial \Phi}{\partial x_k} \quad (1.18)$$

Before we talk about the ideal vortex line in the next section, we need to introduce the concept **circulation**. Consider a closed line on a surface in the  $x_1 - x_2$  plane, see Fig. 1.6. When the velocity is integrated along this line and projected onto the line we obtain the circulation

$$\Gamma = \oint v_m t_m d\ell \quad (1.19)$$

Using Stokes's theorem we can relate the circulation to the vorticity as

$$\Gamma = \int_{\ell} v_m t_m d\ell = \int_S \varepsilon_{ijk} \frac{\partial v_k}{\partial x_j} n_i dS = \int_S \omega_3 dS \quad (1.20)$$

where  $n_i = (0, 0, 1)$  is the unit normal vector of the surface  $S$ . Equation 1.20 reads in vector notation

$$\Gamma = \int_{\ell} \mathbf{v} \cdot \mathbf{t} d\ell = \int_S (\nabla \times \mathbf{v}) \cdot \mathbf{n} dS = \int_S \omega_3 dS \quad (1.21)$$

The circulation is useful in aeronautics and windpower engineering where the lift of an airfoil or a rotorblade is expressed in the circulation for a 2D section. The lift force is computed as

$$L = \rho V \Gamma \quad (1.22)$$

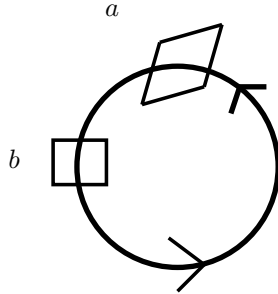


Figure 1.7: Ideal vortex. The fluid particle (i.e. its diagonal, see Fig. 1.3) does not rotate.

where  $V$  is the velocity around the airfoil (for a rotorblade it is the relative velocity, since the rotorblade is rotating). In a recent MSc thesis project, an inviscid simulation method (based on the circulation and vorticity sources) was used to compute the aerodynamic loads for windturbines [4].

**Exercise 12** *In potential flow  $\omega_i = \varepsilon_{ijk} \partial v_k / \partial x_j = 0$ . Multiply Eq. 1.18 by  $\varepsilon_{ijk}$  and derivate with respect to  $x_k$  (i.e. take the curl of) and show that the right side becomes zero as it should, i.e.  $\varepsilon_{ijk} \partial^2 \Phi / (\partial x_k \partial x_j) = 0$ .*

### 1.6.1 Ideal vortex line

The ideal vortex line is an irrotational (potential) flow where the fluid moves along circular paths, see Fig. 1.7. The velocity field in polar coordinates reads

$$v_\theta = \frac{\Gamma}{2\pi r}, \quad v_r = 0 \quad (1.23)$$

where  $\Gamma$  is the circulation. Its potential reads

$$\Phi = \frac{\Gamma\theta}{2\pi} \quad (1.24)$$

The velocity,  $v_\theta$ , is then obtained as

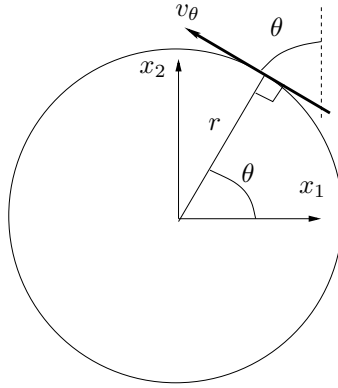
$$v_\theta = \frac{1}{r} \frac{\partial \Phi}{\partial \theta} = \frac{\Gamma}{2\pi r}$$

To transform Eq. 1.23 into Cartesian velocity components, consider Fig. 1.8. The Cartesian velocity vectors are expressed as

$$\begin{aligned} v_1 &= -v_\theta \sin(\theta) = -v_\theta \frac{x_2}{r} = -v_\theta \frac{x_2}{(x_1^2 + x_2^2)^{1/2}} \\ v_2 &= v_\theta \cos(\theta) = v_\theta \frac{x_1}{r} = v_\theta \frac{x_1}{(x_1^2 + x_2^2)^{1/2}} \end{aligned} \quad (1.25)$$

Inserting Eq. 1.25 into Eq. 1.23 we get

$$v_1 = -\frac{\Gamma x_2}{2\pi(x_1^2 + x_2^2)}, \quad v_2 = \frac{\Gamma x_1}{2\pi(x_1^2 + x_2^2)}. \quad (1.26)$$

Figure 1.8: Transformation of  $v_\theta$  into Cartesian components.

To verify that this flow is a potential flow, we need to show that the vorticity,  $\omega_i = \varepsilon_{ijk} \partial v_k / \partial x_j$  is zero. Since it is a two-dimensional flow ( $v_3 = \partial / \partial x_3 = 0$ ),  $\omega_1 = \omega_2 = 0$ , we only need to compute  $\omega_3 = \partial v_2 / \partial x_1 - \partial v_1 / \partial x_2$ . The velocity derivatives are obtained as

$$\frac{\partial v_1}{\partial x_2} = -\frac{\Gamma}{2\pi} \frac{x_1^2 - x_2^2}{(x_1^2 + x_2^2)^2}, \quad \frac{\partial v_2}{\partial x_1} = \frac{\Gamma}{2\pi} \frac{x_2^2 - x_1^2}{(x_1^2 + x_2^2)^2} \quad (1.27)$$

and we get

$$\omega_3 = \frac{\Gamma}{2\pi} \frac{1}{(x_1^2 + x_2^2)^2} (x_2^2 - x_1^2 + x_1^2 - x_2^2) = 0 \quad (1.28)$$

which shows that the flow is indeed a potential flow, i.e. *irrotational* ( $\omega_i \equiv 0$ ). Note that the deformation is not zero, i.e.

$$S_{12} = \frac{1}{2} \left( \frac{\partial v_1}{\partial x_2} + \frac{\partial v_2}{\partial x_1} \right) = \frac{\Gamma}{2\pi} \frac{x_2^2}{(x_1^2 + x_2^2)^2} \quad (1.29)$$

Hence a fluid particle in an ideal vortex does deform but it does not rotate (i.e. its diagonal does not rotate, see Fig. 1.7).

It may be little confusing that the flow path forms a *vortex* but the flow itself has no *vorticity*. Thus one must be very careful when using the words “vortex” and “vorticity”. By vortex we usually mean a recirculation region of the mean flow. That the flow has no vorticity (i.e. no rotation) means that a fluid particle moves as illustrated in Fig. 1.7. As a fluid particle moves from position *a* to *b* – on its counter-clockwise-rotating path – the particle itself is not rotating. This is true for the whole flow field, except at the center where the fluid particle does rotate. This is a singular point as is seen from Eq. 1.23 for which  $\omega_3 \rightarrow \infty$ .

**vortex vs.  
vorticity**

Note that generally a vortex has vorticity, see Section 4.2. The ideal vortex is a very special flow case.

### 1.6.2 Shear flow

Another example – which is rotational – is a shear flow in which

$$v_1 = cx_2^2, \quad v_2 = 0 \quad (1.30)$$

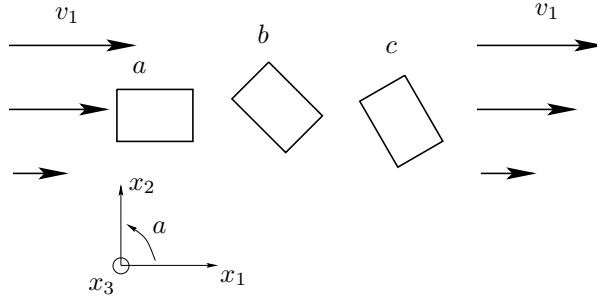


Figure 1.9: A shear flow. The fluid particle rotates.  $v_1 = cx_2^2$ .

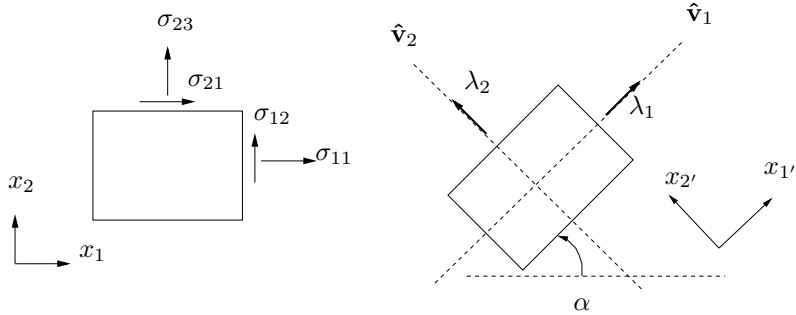


Figure 1.10: A two-dimensional fluid element. Left: in original state; right: rotated to principal coordinate directions.  $\lambda_1$  and  $\lambda_2$  denote eigenvalues;  $\hat{\mathbf{v}}_1$  and  $\hat{\mathbf{v}}_2$  denote unit eigenvectors.

with  $c, x_2 > 0$ , see Fig. 1.9. The vorticity vector for this flow reads

$$\omega_1 = \omega_2 = 0, \quad \omega_3 = \frac{\partial v_2}{\partial x_1} - \frac{\partial v_1}{\partial x_2} = -2cx_2 \quad (1.31)$$

When the fluid particle is moving from position  $a$ , via  $b$  to position  $c$  it is indeed rotating. It is rotating in clockwise direction. Note that the positive rotating direction is defined as the counter-clockwise direction, indicated by  $\alpha$  in Fig. 1.9. This is why the vorticity,  $\omega_3$ , is negative ( $= -2cx_2$ ).

## 1.7 Eigenvalues and eigenvectors: physical interpretation

See also [2], Chapt. 2.5.5.

Consider a two-dimensional fluid (or solid) element, see Fig. 1.10. In the left figure it is oriented along the  $x_1 - x_2$  coordinate system. On the surfaces act normal stresses ( $\sigma_{11}, \sigma_{22}$ ) and shear stresses ( $\sigma_{12}, \sigma_{21}$ ). The stresses form a tensor,  $\sigma_{ij}$ . Any tensor has eigenvectors and eigenvalues (also called principal vectors and principal values). Since  $\sigma_{ij}$  is symmetric, the eigenvalues are real (i.e. not imaginary). The eigenvalues are obtained from the characteristic equation, see [2], Chapt. 2.5.5 or Eq. 13.5 at p. 115. When the eigenvalues have been obtained, the eigenvectors can be computed. Given the eigenvectors, the fluid element is rotated  $\alpha$  degrees so that its edges are aligned with the eigenvectors,  $\hat{\mathbf{v}}_1 = \hat{x}_{1'}$  and  $\hat{\mathbf{v}}_2 = \hat{x}_{2'}$ , see right part of Fig. 1.10. Note that the

sign of the eigenvectors is not defined, which means that the eigenvectors can equally well be chosen as  $-\hat{\mathbf{v}}_1$  and/or  $-\hat{\mathbf{v}}_2$ . In the principal coordinates  $x_{1'} - x_{2'}$  (right part of Fig. 1.10), there are no shear stresses on the surfaces of the fluid element. There are only normal stresses. This is the very definition of eigenvectors. Furthermore, the eigenvalues are the normal stresses in the principal coordinates, i.e.  $\lambda_1 = \sigma_{1'1'}$  and  $\lambda_2 = \sigma_{2'2'}$ .

## 2 Governing flow equations

See also [2], Chaps. 5 and 8.1.

### 2.1 The Navier-Stokes equation

#### 2.1.1 The continuity equation

The first equation is the continuity equation (the balance equation for mass) which reads [3]

$$\boxed{\dot{\rho} + \rho v_{i,i} = 0} \quad (2.1)$$

Change of notation gives

$$\frac{d\rho}{dt} + \rho \frac{\partial v_i}{\partial x_i} = 0 \quad (2.2)$$

For incompressible flow ( $\rho = \text{const}$ ) we get

$$\frac{\partial v_i}{\partial x_i} = 0 \quad (2.3)$$

#### 2.1.2 The momentum equation

The next equation is the momentum equation. We have formulated the constitutive law for Newtonian viscous fluids [3]

$$\sigma_{ij} = -p\delta_{ij} + 2\mu S_{ij} - \frac{2}{3}\mu S_{kk}\delta_{ij} \quad (2.4)$$

Inserting Eq. 2.4 into the balance equations, Eq. 1.3, we get

$$\rho \frac{dv_i}{dt} = -\frac{\partial p}{\partial x_i} + \frac{\partial \tau_{ji}}{\partial x_j} + \rho f_i = -\frac{\partial p}{\partial x_i} + \frac{\partial}{\partial x_j} \left( 2\mu S_{ij} - \frac{2}{3}\mu \frac{\partial v_k}{\partial x_k} \delta_{ij} \right) + \rho f_i \quad (2.5)$$

where  $\mu$  denotes the dynamic viscosity. This is the *Navier-Stokes* equations (sometimes the continuity equation is also included in the name “Navier-Stokes”). It is also called the *transport equation for momentum*. If the viscosity,  $\mu$ , is constant it can be moved outside the derivative. Furthermore, if the flow is incompressible the second term in the parenthesis on the right side is zero because of the continuity equation. If these two requirements are satisfied we can also re-write the first term in the parenthesis as

$$\frac{\partial}{\partial x_j} (2\mu S_{ij}) = \mu \frac{\partial}{\partial x_j} \left( \frac{\partial v_i}{\partial x_j} + \frac{\partial v_j}{\partial x_i} \right) = \mu \frac{\partial^2 v_i}{\partial x_j \partial x_j} \quad (2.6)$$

because of the continuity equation. Equation 2.5 can now – for constant  $\mu$  and incompressible flow – be written

$$\rho \frac{dv_i}{dt} = -\frac{\partial p}{\partial x_i} + \mu \frac{\partial^2 v_i}{\partial x_j \partial x_j} + \rho f_i \quad (2.7)$$

In inviscid (potential) flow, there are no viscous (friction) forces. In this case, the Navier-Stokes equation reduces to the *Euler equations*

$$\rho \frac{dv_i}{dt} = -\frac{\partial p}{\partial x_i} + \rho f_i \quad (2.8)$$

**Euler  
equations**

**Exercise 13** Equation 1.3 states that mass times acceleration is equal to the sum of forces (per unit volume). Write out the momentum equation (without using the summation rule) for the  $x_1$  direction and show the surface forces and the volume force on a small, square fluid element (see lecture notes of Toll & Ekh [3]). Now repeat it for the  $x_2$  direction.

**Exercise 14** Formulate the Navier-Stokes equation for incompressible flow but non-constant viscosity.

## 2.2 The energy equation

See also [2], Chaps. 6.4 and 8.1.

We have in Part I [3] derived the energy equation which reads

$$\boxed{\rho \dot{u} - v_{i,j} \sigma_{ji} + q_{i,i} = \rho z} \quad (2.9)$$

where  $u$  denotes internal energy.  $q_i$  denotes the conductive heat flux and  $z$  the net radiative heat source. The latter can also be seen as a vector,  $z_{i,rad}$ ; for simplicity, we neglect the radiation from here on. Change of notation gives

$$\rho \frac{du}{dt} = \sigma_{ji} \frac{\partial v_i}{\partial x_j} - \frac{\partial q_i}{\partial x_i} \quad (2.10)$$

In Part I [3] we formulated the constitutive law for the heat flux vector (Fourier's law)

$$q_i = -k \frac{\partial T}{\partial x_i} \quad (2.11)$$

Inserting the constitutive laws, Eqs. 2.4 and 2.11, into Eq. 2.10 gives

$$\rho \frac{du}{dt} = -p \frac{\partial v_i}{\partial x_i} + \underbrace{2\mu S_{ij} S_{ij} - \frac{2}{3} \mu S_{kk} S_{ii}}_{\Phi} + \frac{\partial}{\partial x_i} \left( k \frac{\partial T}{\partial x_i} \right) \quad (2.12)$$

where we have used  $S_{ij} \partial v_i / \partial x_j = S_{ij} (S_{ij} + \Omega_{ij}) = S_{ij} S_{ij}$  because the product of a symmetric tensor,  $S_{ij}$ , and an anti-symmetric tensor,  $\Omega_{ij}$ , is zero. Two of the viscous terms (denoted by  $\Phi$ ) represent irreversible viscous heating (i.e. transformation of kinetic energy into thermal energy); these terms are important at high-speed flow<sup>2</sup> (for example re-entry from outer space) and for highly viscous flows (lubricants). The first term on the right side represents reversible heating and cooling due to compression and expansion of the fluid. Equation 2.12 is the *transport equation for (internal) energy*,  $u$ .

Now we assume that the flow is incompressible (i.e. the velocity should be smaller than approximately 1/3 of the speed of sound) for which

$$du = c_p dT \quad (2.13)$$

where  $c_p$  is the heat capacity (see Part I) [3] so that Eq. 2.12 gives ( $c_p$  is assumed to be constant)

$$\rho c_p \frac{dT}{dt} = \Phi + \frac{\partial}{\partial x_i} \left( k \frac{\partial T}{\partial x_i} \right) \quad (2.14)$$

---

<sup>2</sup>High-speed flows relevant for aeronautics will be treated in detail in the course “Compressible flow” in the MSc programme.

The dissipation term is simplified to  $\Phi = 2\mu S_{ij} S_{ij}$  because  $S_{ii} = \partial v_i / \partial x_i = 0$ . If we furthermore assume that the heat conductivity coefficient is constant and that the fluid is a gas or a common liquid (i.e. not an lubricant oil), we get

$$\frac{dT}{dt} = \alpha \frac{\partial^2 T}{\partial x_i \partial x_i} \quad (2.15)$$

where  $\alpha = k / (\rho c_p)$  is the *thermal diffusivity*.

$$Pr = \frac{\nu}{\alpha} \quad (2.16)$$

**thermal  
diffusivity**

is defined where  $\nu = \mu / \rho$  is the kinematic viscosity. The physical meaning of the Prandtl number is the ratio of how well the fluid diffuses momentum to the how well it diffuses internal energy (i.e. temperature).

The dissipation term,  $\Phi$ , is neglected in Eq. 2.15 because one of two assumptions are valid:

1. The fluid is a gas with low velocity (lower than 1/3 of the speed of sound); this assumption was made when we assumed that the fluid is incompressible
2. The fluid is a common liquid (i.e. not an lubricant oil). In lubricant oils the viscous heating (i.e. the dissipation,  $\Phi$ ) is large. One example is the oil flow in a gearbox in a car where the temperature usually is more than 100°C higher when the car is running compared to when it is idle.

**Exercise 15** Write out and simplify the dissipation term,  $\Phi$ , in Eq. 2.12. The first term is positive and the second term is negative; are you sure that  $\Phi > 0$ ?

### 2.3 Transformation of energy

Now we will derive the equation for the kinetic energy,  $k = v_i v_i / 2$ . Multiply Eq. 1.3 with  $v_i$

$$\rho v_i \frac{dv_i}{dt} - v_i \frac{\partial \sigma_{ji}}{\partial x_j} - v_i \rho f_i = 0 \quad (2.17)$$

Using the product rule backwards (Trick 2, see Eq. 8.4), the first term on the left side can be re-written

$$\rho v_i \frac{dv_i}{dt} = \frac{1}{2} \rho \frac{d(v_i v_i)}{dt} = \rho \frac{dk}{dt} \quad (2.18)$$

$(v_i v_i / 2 = k)$  so that

$$\rho \frac{dk}{dt} = v_i \frac{\partial \sigma_{ji}}{\partial x_j} + \rho v_i f_i \quad (2.19)$$

Re-write the stress-velocity term so that

$$\rho \frac{dk}{dt} = \frac{\partial v_i \sigma_{ji}}{\partial x_j} - \sigma_{ji} \frac{\partial v_i}{\partial x_j} + \rho v_i f_i \quad (2.20)$$

This is the *transport equation for kinetic energy*,  $k$ . Adding Eq. 2.20 to Eq. 2.10 gives

$$\rho \frac{d(u + k)}{dt} = \frac{\partial \sigma_{ji} v_i}{\partial x_j} - \frac{\partial q_i}{\partial x_i} + \rho v_i f_i \quad (2.21)$$

This is an equation for the sum of internal and kinetic energy,  $u + k$ . This is the *transport equation for total energy*,  $u + k$ .

Let us take a closer look at Eqs. 2.10, 2.20 and 2.21. First we separate the term  $\sigma_{ji}\partial v_i/\partial x_j$  in Eqs. 2.10 and 2.20 into work related to the pressure and viscous stresses respectively (see Eq. 1.5), i.e.

$$\sigma_{ji}\frac{\partial v_i}{\partial x_j} = \underbrace{-p\frac{\partial v_i}{\partial x_i}}_{\mathbf{a}} + \underbrace{\tau_{ji}\frac{\partial v_i}{\partial x_j}}_{\mathbf{b}=\Phi} \quad (2.22)$$

The following things should be noted.

- The physical meaning of the **a**-term in Eq. 2.22 – which includes the pressure,  $p$  – is heating/cooling by compression/expansion. This is a reversible process, i.e. no loss of energy but only transformation of energy.
- The physical meaning of the **b**-term in Eq. 2.22 – which includes the viscous stress tensor,  $\tau_{ij}$  – is a dissipation, which means that kinetic energy is transformed to thermal energy. It is denoted  $\Phi$ , see Eq. 2.12, and is called viscous dissipation. It is always positive and represents irreversible heating.
- The dissipation,  $\Phi$ , appears as a sink term in the equation for the kinetic energy,  $k$  (Eq. 2.20) and it appears as a source term in the equation for the internal energy,  $u$  (Eq. 2.10). The transformation of kinetic energy into internal energy takes place through this source term.
- $\Phi$  does not appear in the equation for the total energy  $u+k$  (Eq. 2.21); this makes sense since  $\Phi$  represents a energy transfer between  $u$  and  $k$  and does not affect their sum,  $u+k$ .

Dissipation is very important in turbulence where transfer of energy takes place at several levels. First energy is transferred from the mean flow to the turbulent fluctuations. The physical process is called production of turbulent kinetic energy. Then we have transformation of kinetic energy from turbulence kinetic energy to thermal energy; this is turbulence dissipation (or heating). At the same time we have the usual viscous dissipation from the mean flow to thermal energy, but this is much smaller than that from the turbulence kinetic energy. For more detail, see section 2.4 in [5]<sup>3</sup>.

## 2.4 Left side of the transport equations

So far, the left side in transport equations have been formulated using the material derivative,  $d/dt$ . Let  $\Psi$  denote a transported quantity (i.e.  $\Psi = v_i, u, T \dots$ ); the left side of the equation for momentum, thermal energy, total energy, temperature etc reads

$$\rho \frac{d\Psi}{dt} = \rho \frac{\partial \Psi}{\partial t} + \rho v_j \frac{\partial \Psi}{\partial x_j} \quad (2.23)$$

This is often called the *non-conservative* form. Using the continuity equation, Eq. 2.2, it can be re-written as

$$\begin{aligned} \rho \frac{d\Psi}{dt} &= \rho \frac{\partial \Psi}{\partial t} + \rho v_j \frac{\partial \Psi}{\partial x_j} + \Psi \underbrace{\left( \frac{d\rho}{dt} + \rho \frac{\partial v_j}{\partial x_j} \right)}_{=0} = \\ &\quad \rho \frac{\partial \Psi}{\partial t} + \rho v_j \frac{\partial \Psi}{\partial x_j} + \Psi \left( \frac{\partial \rho}{\partial t} + v_j \frac{\partial \rho}{\partial x_j} + \rho \frac{\partial v_j}{\partial x_j} \right) \end{aligned} \quad (2.24)$$

---

<sup>3</sup>can be downloaded from <http://www.tfd.chalmers.se/~lada>

**non-  
conserv-  
ative**

The two underlined terms will form a time derivative term, and the other three terms can be collected into a convective term, i.e.

$$\rho \frac{d\Psi}{dt} = \underline{\rho \frac{\partial \Psi}{\partial t}} + \underline{\rho v_j \frac{\partial \Psi}{\partial x_j}} \quad (2.25)$$

Thus, left sided of the temperature equation and the Navier-Stokes, for example, can be written in three different ways (by use of the chain-rule and the continuity equation)

$$\begin{aligned} \rho \frac{dv_i}{dt} &= \rho \frac{\partial v_i}{\partial t} + \rho v_j \frac{\partial v_i}{\partial x_j} = \underline{\frac{\partial \rho v_i}{\partial t}} + \underline{\frac{\partial \rho v_j v_i}{\partial x_j}} \\ \rho \frac{dT}{dt} &= \rho \frac{\partial T}{\partial t} + \rho v_j \frac{\partial T}{\partial x_j} = \underline{\frac{\partial \rho v_i}{\partial t}} + \underline{\frac{\partial \rho v_j T}{\partial x_j}} \end{aligned} \quad (2.26)$$

The continuity equation can also be written in three ways (by use of the chain-rule)

$$\frac{d\rho}{dt} + \rho \frac{\partial v_i}{\partial x_i} = \underline{\frac{\partial \rho}{\partial t}} + v_i \frac{\partial \rho}{\partial x_i} + \rho \frac{\partial v_i}{\partial x_i} = \underline{\frac{\partial \rho}{\partial t}} + \underline{\frac{\partial \rho v_i}{\partial x_i}} \quad (2.27)$$

The forms on the right sides of Eqs. 2.26 and 2.27 are called the *conservative* form. When solving transport equations (such as the Navier-Stokes) numerically using finite volume methods, the left sides in the transport equation are always written as the expressions on the right side of Eqs. 2.26 and 2.27; in this way Gauss law can be used to transform the equations from a volume integral to a surface integral and thus ensuring that the transported quantities are *conserved*. The results may be inaccurate due to too coarse a numerical grid, but no mass, momentum, energy etc is lost (provided a transport equation for the quantity is solved): “what comes in goes out”.

**conservative**

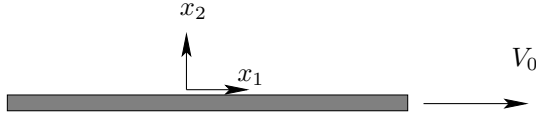
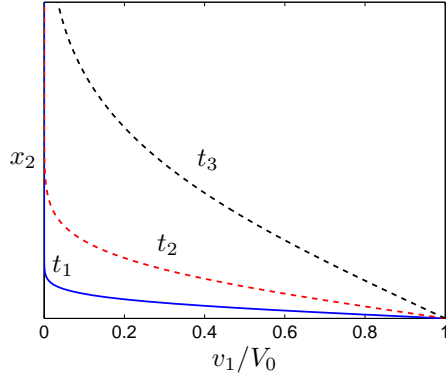
## 2.5 Material particle vs. control volume (Reynolds Transport Theorem)

See also lecture notes of Toll & Ekh [3] and [2], Chapt. 5.2.

In Part I [3] we initially derived all balance equations (mass, momentum and energy) for a collection of *material particles*. The conservation of mass,  $d/dt \int \rho dV = 0$ , Newton's second law,  $d/dt \int \rho v_i = F_i$  etc were derived for a collection of particles in the volume  $V_{part}$ , where  $V_{part}$  is a volume that includes the same fluid particles all the time. This means that the volume,  $V_{part}$ , must be moving and it may expand or contract (if the density is non-constant), otherwise particles would move across its boundaries. The equations we have looked at so far (the continuity equation 2.3, the Navier-Stokes equation 2.7, the energy equations 2.12 and 2.20) are all given for a fixed control volume. How come? The answer is the Reynolds transport theorem, which converts the equations from being valid for a moving volume with a collection,  $V_{part}$ , to being valid for a fixed volume,  $V$ . The Reynolds transport theorem reads

$$\begin{aligned} \frac{d}{dt} \int_{V_{part}} \Phi dV &= \int_V \left( \frac{\partial \Phi}{\partial t} + \Phi \frac{\partial v_i}{\partial x_i} \right) dV \\ &= \int_V \left( \frac{\partial \Phi}{\partial t} + v_i \frac{\partial \Phi}{\partial x_i} + \Phi \frac{\partial v_i}{\partial x_i} \right) dV = \int_V \left( \frac{\partial \Phi}{\partial t} + \frac{\partial v_i \Phi}{\partial x_i} \right) dV \\ &= \int_V \frac{\partial \Phi}{\partial t} dV + \int_S v_i n_i \Phi dS \end{aligned} \quad (2.28)$$

where  $V$  denotes a fixed non-deformable volume in space. The divergence theorem was used to obtain the last line and  $S$  denotes the bounding surface of volume  $V$ . The last term on the last line represents the net flow of  $\Phi$  across the fixed non-deformable volume,  $V$ .  $\Phi$  in the equation above can be  $\rho$  (mass),  $\rho v_i$  (momentum) or  $\rho u$  (energy). This equation applies to *any* volume at *every* instant and the restriction to a collection of a material particles is no longer necessary. Hence, in fluid mechanics the transport equations (Eqs. 2.2, 2.5, 2.10, ...) are valid both for a material collection of particles as well as for a *volume*; the latter is usually fixed (this is not necessary).

Figure 3.1: The plate moves to the right with speed  $V_0$  for  $t > 0$ .Figure 3.2: The  $v_1$  velocity at three different times.  $t_3 > t_2 > t_1$ .

### 3 Exact solutions to the Navier-Stokes equation: two examples

#### 3.1 The Rayleigh problem

Imagine the sudden motion of an infinitely long flat plate. For time greater than zero the plate is moving with the speed  $V_0$ , see Fig. 3.1.

Because the plate is infinitely long, there is no  $x_1$  dependency. Hence the flow depends only on  $x_2$  and  $t$ , i.e.  $v_1 = v_1(x_2, t)$  and  $p = p(x_2, t)$ . Furthermore,  $\partial v_1 / \partial x_1 = \partial v_3 / \partial x_3 = 0$  so that the continuity equation gives  $\partial v_2 / \partial x_2 = 0$ . At the lower boundary ( $x_2 = 0$ ) and at the upper boundary ( $x_2 \rightarrow \infty$ ) the velocity component  $v_2 = 0$ , which means that  $v_2 = 0$  in the entire domain. So, Eq. 2.7 gives (no body forces, i.e.  $f_1 = 0$ ) for the  $v_1$  velocity component

$$\rho \frac{\partial v_1}{\partial t} = \mu \frac{\partial^2 v_1}{\partial x_2^2} \quad (3.1)$$

We will find that the diffusion process depends on the kinematic viscosity,  $\nu = \mu/\rho$ , rather than the dynamic one,  $\mu$ . The boundary conditions for Eq. 3.1 are

$$v_1(x_2, t = 0) = 0, \quad v_1(x_2 = 0, t) = V_0, \quad v_1(x_2 \rightarrow \infty, t) = 0 \quad (3.2)$$

The solution to Eq. 3.1 is shown in Fig. 3.2. For increasing time ( $t_3 > t_2 > t_1$ ), the moving plate affects the fluid further and further away from the plate.

It turns out that the solution to Eq. 3.1 is a *similarity solution*; this means that the number of independent variables is reduced by one, in this case from two ( $x_2$  and  $t$ ) to one ( $\eta$ ). The similarity variable,  $\eta$ , is related to  $x_2$  and  $t$  as

$$\eta = \frac{x_2}{2\sqrt{\nu t}} \quad (3.3)$$

If the solution of Eq. 3.1 depends only on  $\eta$ , it means that the solution for a given fluid will be the same (“similar”) for many (infinite) values of  $x_2$  and  $t$  as long as the ratio  $x_2/\sqrt{\nu t}$  is constant. Now we need to transform the derivatives in Eq. 3.1 from  $\partial/\partial t$  and  $\partial/\partial x_2$  to  $d/d\eta$  so that it becomes a function of  $\eta$  only. We get

$$\begin{aligned}\frac{\partial v_1}{\partial t} &= \frac{dv_1}{d\eta} \frac{\partial \eta}{\partial t} = -\frac{x_2 t^{-3/2}}{4\sqrt{\nu}} \frac{dv_1}{d\eta} = -\frac{1}{2} \frac{\eta}{t} \frac{dv_1}{d\eta} \\ \frac{\partial v_1}{\partial x_2} &= \frac{dv_1}{d\eta} \frac{\partial \eta}{\partial x_2} = \frac{1}{2\sqrt{\nu t}} \frac{dv_1}{d\eta} \\ \frac{\partial^2 v_1}{\partial x_2^2} &= \frac{\partial}{\partial x_2} \left( \frac{\partial v_1}{\partial x_2} \right) = \frac{\partial}{\partial x_2} \left( \frac{1}{2\sqrt{\nu t}} \frac{dv_1}{d\eta} \right) = \frac{1}{2\sqrt{\nu t}} \frac{\partial}{\partial x_2} \left( \frac{dv_1}{d\eta} \right) = \frac{1}{4\nu t} \frac{d^2 v_1}{d\eta^2}\end{aligned}\quad (3.4)$$

We introduce a non-dimensional velocity

$$f = \frac{v_1}{V_0} \quad (3.5)$$

Inserting Eqs. 3.4 and 3.5 in Eq. 3.1 gives

$$\frac{d^2 f}{d\eta^2} + 2\eta \frac{df}{d\eta} = 0 \quad (3.6)$$

We have now successfully transformed Eq. 3.1 and reduced the number of independent variables from two to one. Now let us find out if the boundary conditions, Eq. 3.2, also can be transformed in a physically meaningful way; we get

$$\begin{aligned}v_1(x_2, t = 0) &= 0 \Rightarrow f(\eta \rightarrow \infty) = 0 \\ v_1(x_2 = 0, t) &= V_0 \Rightarrow f(\eta = 0) = 1 \\ v_1(x_2 \rightarrow \infty, t) &= 0 \Rightarrow f(\eta \rightarrow \infty) = 0\end{aligned}\quad (3.7)$$

Since we managed to transform both the equation (Eq. 3.1) and the boundary conditions (Eq. 3.7) we conclude that the transformation is suitable.

Now let us solve Eq. 3.6. Integration once gives

$$\frac{df}{d\eta} = C_1 \exp(-\eta^2) \quad (3.8)$$

Integration a second time gives

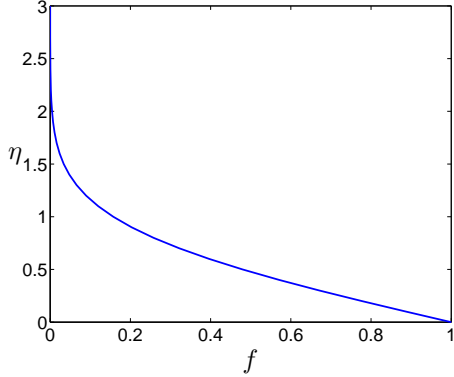
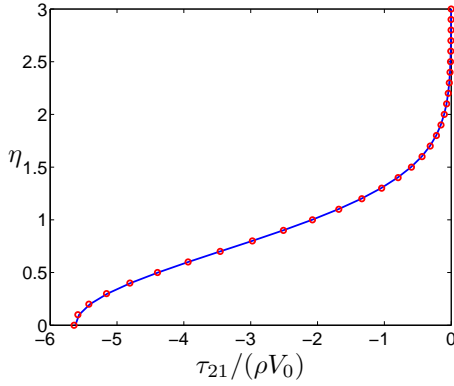
$$f = C_1 \int_0^\eta \exp(-\eta'^2) d\eta' + C_2 \quad (3.9)$$

The integral above is the error function

$$\text{erf}(\eta) \equiv \frac{2}{\sqrt{\pi}} \int_0^\eta \exp(-\eta'^2) d\eta' \quad (3.10)$$

At the limits, the error function takes the values 0 and 1, i.e.  $\text{erf}(0) = 0$  and  $\text{erf}(\eta \rightarrow \infty) = 1$ . Taking into account the boundary conditions, Eq. 3.7, the final solution to Eq. 3.9 is (with  $C_2 = 1$  and  $C_1 = -2/\sqrt{\pi}$ )

$$f(\eta) = 1 - \text{erf}(\eta) \quad (3.11)$$

Figure 3.3: The velocity,  $f = v_1/V_0$ , given by Eq. 3.11.Figure 3.4: The shear stress for water ( $\nu = 10^{-6}$ ) obtained from Eq. 3.12 at time  $t = 100\,000$ .

The solution is presented in Fig. 3.3. Compare this figure with Fig. 3.2 at p. 27; all graphs in that figure collapse into one graph in Fig. 3.3. To compute the velocity,  $v_1$ , we pick a time  $t$  and insert  $x_2$  and  $t$  in Eq. 3.3. Then  $f$  is obtained from Eq. 3.11 and the velocity,  $v_1$ , is computed from Eq. 3.5. This is how the graphs in Fig. 3.2 were obtained.

From the velocity profile we can get the shear stress as

$$\tau_{21} = \mu \frac{\partial v_1}{\partial x_2} = \frac{\mu V_0}{2\sqrt{\nu t}} \frac{df}{d\eta} = -\frac{\mu V_0}{\sqrt{\pi \nu t}} \exp(-\eta^2) \quad (3.12)$$

where we used  $\nu = \mu/\rho$ . Figure 3.4 presents the shear stress,  $\tau_{21}$ . The solid line is obtained from Eq. 3.12 and circles are obtained by evaluating the derivative,  $df/d\eta$ , numerically using central differences  $(f_{j+1} - f_{j-1})/(\eta_{j+1} - \eta_{j-1})$ .

As can be seen from Fig. 3.4, the magnitude of the shear stress increases for decreasing  $\eta$  and it is largest at the wall,  $\tau_w = -\rho V_0/\sqrt{\pi t}$

The vorticity,  $\omega_3$ , across the boundary layer is computed from its definition (Eq. 1.31)

$$\omega_3 = -\frac{\partial v_1}{\partial x_2} = -\frac{V_0}{2\sqrt{\nu t}} \frac{df}{d\eta} = \frac{V_0}{\sqrt{\pi \nu t}} \exp(-\eta^2) \quad (3.13)$$

From Fig. 3.2 at p. 27 it is seen that for large times, the moving plate is felt further and further out in the flow, i.e. the thickness of the boundary layer,  $\delta$ , increases. Often

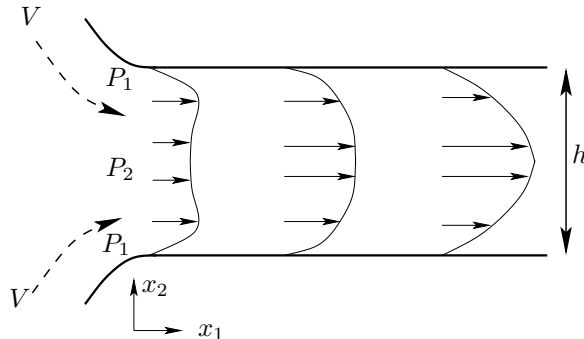


Figure 3.5: Flow in a horizontal channel. The inlet part of the channel is shown.

the boundary layer thickness is defined by the position where the local velocity,  $v_1(x_2)$ , reaches 99% of the freestream velocity. In our case, this corresponds to the point where  $v_1 = 0.01V_0$ . From Fig. 3.3 and Eq. 3.11 we find that this occurs at

$$\eta = 1.8 = \frac{\delta}{2\sqrt{\nu t}} \Rightarrow \delta = 3.6\sqrt{\nu t} \quad (3.14)$$

It can be seen that the boundary layer thickness increases with  $t^{1/2}$ . Equation 3.14 can also be used to estimate the *diffusion length*. After, say, 10 minutes the diffusion length for air and water, respectively, are

$$\begin{aligned} \delta_{air} &= 10.8\text{cm} \\ \delta_{water} &= 2.8\text{cm} \end{aligned} \quad (3.15)$$

As mentioned in the beginning of this section, note that the diffusion length is determined by the kinematic viscosity,  $\nu = \mu/\rho$  rather than by dynamic one,  $\mu$ .

The diffusion length can also be used to estimate the thickness of a developing boundary layer, see Section 4.3.1.

**diffusion length**

**Exercise 16** Consider the graphs in Fig. 3.3. Create this graph with Matlab.

**Exercise 17** Consider the graphs in Fig. 3.2. Note that no scale is used on the  $x_2$  axis and that no numbers are given for  $t_1$ ,  $t_2$  and  $t_3$ . Create this graph with Matlab for both air and engine oil. Choose suitable values on  $t_1$ ,  $t_2$  and  $t_3$ .

**Exercise 18** Repeat the exercise above for the shear stress,  $\tau_{21}$ , see Fig. 3.4.

## 3.2 Flow between two plates

Consider steady, incompressible flow in a two-dimensional channel, see Fig. 3.5, with constant physical properties (i.e.  $\mu = \text{const}$ ).

### 3.2.1 Curved plates

Provided that the walls at the inlet are well curved, the velocity near the walls is larger than in the center, see Fig. 3.5. The reason is that the flow (with velocity  $V$ ) following the curved wall must change its direction. The physical agent which accomplish this is the pressure gradient which forces the flow to follow the wall as closely as possible

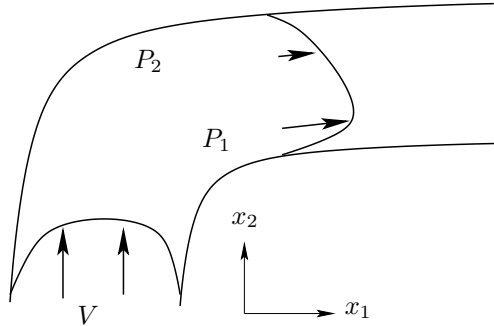


Figure 3.6: Flow in a channel bend.

(if the wall is not sufficiently curved a separation will take place). Hence the pressure in the center of the channel,  $P_2$ , is higher than the pressure near the wall,  $P_1$ . It is thus easier (i.e. less opposing pressure) for the fluid to enter the channel near the walls than in the center. This explains the high velocity near the walls.

The same phenomenon occurs in a channel bend, see Fig. 3.6. The flow  $V$  approaches the bend and the flow feels that it is approaching a bend through an increased pressure. The pressure near the outer wall,  $P_2$ , must be higher than that near the inner wall,  $P_1$ , in order to force the flow to turn. Hence, it is easier for the flow to sneak along the inner wall where the opposing pressure is smaller than near the outer wall: the result is a higher velocity near the inner wall than near the outer wall. In a three-dimensional duct or in a pipe, the pressure difference  $P_2 - P_1$  creates secondary flow downstream the bend (i.e. a swirling motion in the  $x_2 - x_3$  plane).

### 3.2.2 Flat plates

The flow in the inlet section (Fig. 3.5) is two dimensional. Near the inlet the velocity is largest near the wall and further downstream the velocity is retarded near the walls due to the large viscous shear stresses there. The flow is accelerated in the center because the mass flow at each  $x_1$  must be constant because of continuity. The acceleration and retardation of the flow in the inlet region is “paid for” by a pressure loss which is rather high in the inlet region; if a separation occurs because of sharp corners at the inlet, the pressure loss will be even higher. For large  $x_1$  the flow will be fully developed; the region until this occurs is called the *entrance region*, and the entrance length can, for moderately disturbed inflow, be estimated as [6]

$$\frac{x_{1,e}}{D_h} = 0.016 Re_{D_h} \equiv 0.016 \frac{VD_h}{\nu} \quad (3.16)$$

where  $V$  denotes the bulk (i.e. the mean) velocity, and  $D_h = 4A/S_p$  where  $D_h$ ,  $A$  and  $S_p$  denote the hydraulic diameter, the cross-sectional area and the perimeter, respectively. For flow between two plates we get  $D_h = 2h$ .

Let us find the governing equations for the fully developed flow region; in this region the flow does not change with respect to the streamwise coordinate,  $x_1$  (i.e.  $\partial v_1 / \partial x_1 = \partial v_2 / \partial x_1 = 0$ ). Since the flow is two-dimensional, it does not depend on the third coordinate direction,  $x_3$  (i.e.  $\partial / \partial x_3$ ), and the velocity in this direction is zero, i.e.  $v_3 = 0$ . Taking these restrictions into account the continuity equation can be

simplified as (see Eq. 2.3)

$$\frac{\partial v_2}{\partial x_2} = 0 \quad (3.17)$$

Integration gives  $v_2 = C_1$  and since  $v_2 = 0$  at the walls, it means that

$$v_2 = 0 \quad (3.18)$$

across the entire channel (recall that we are dealing with the part of the channel where the flow is fully developed; in the inlet section  $v_2 \neq 0$ , see Fig. 3.5).

Now let us turn our attention to the momentum equation for  $v_2$ . This is the vertical direction ( $x_2$  is positive upwards, see Fig. 3.5). The gravity acts in the negative  $x_2$  direction, i.e.  $f_i = (0, -\rho g, 0)$ . The momentum equation can be written (see Eq. 2.7 at p. 21)

$$\rho \frac{dv_2}{dt} \equiv \rho v_1 \frac{\partial v_2}{\partial x_1} + \rho v_2 \frac{\partial v_2}{\partial x_2} = -\frac{\partial p}{\partial x_2} + \mu \frac{\partial^2 v_2}{\partial x_2^2} - \rho g \quad (3.19)$$

Since  $v_2 = 0$  we get

$$\frac{\partial p}{\partial x_2} = -\rho g \quad (3.20)$$

Integration gives

$$p = -\rho g x_2 + C_1(x_1) \quad (3.21)$$

where the integration “constant”  $C_1$  may be a function of  $x_1$  but not of  $x_2$ . If we denote the pressure at the lower wall (i.e. at  $x_2 = 0$ ) as  $P$  we get

$$p = -\rho g x_2 + P(x_1) \quad (3.22)$$

Hence the pressure,  $p$ , decreases with vertical height. This agrees with our experience that the pressure decreases at high altitudes in the atmosphere and increases the deeper we dive into the sea. Usually the *hydrostatic pressure*,  $P$ , is used in incompressible flow. This pressure is zero when the flow is *static*, i.e. when the velocity field is zero. However, when you want the *physical* pressure, the  $\rho g x_2$  as well as the surrounding atmospheric pressure must be added.

**hydrostatic pressure**

We can now formulate the momentum equation in the streamwise direction

$$\rho \frac{dv_1}{dt} \equiv \rho v_1 \frac{\partial v_1}{\partial x_1} + \rho v_2 \frac{\partial v_1}{\partial x_2} = -\frac{dp}{dx_1} + \mu \frac{\partial^2 v_1}{\partial x_1^2} \quad (3.23)$$

where  $p$  was replaced by  $P$  using Eq. 3.22. Since  $v_2 = \partial v_1 / \partial x_1 = 0$  the left side is zero so

$$\mu \frac{\partial^2 v_1}{\partial x_1^2} = \frac{dp}{dx_1} \quad (3.24)$$

Since the left side is a function of  $x_2$  and the right side is a function of  $x_1$ , we conclude that they both are equal to a constant. The velocity,  $v_1$ , is zero at the walls, i.e.

$$v_1(0) = v_1(h) = 0 \quad (3.25)$$

where  $h$  denotes the height of the channel, see Eq. 3.5. Integrating Eq. 3.24 twice and using Eq. 3.25 gives

$$v_1 = -\frac{h}{2\mu} \frac{dp}{dx_1} x_2 \left(1 - \frac{x_2}{h}\right) \quad (3.26)$$

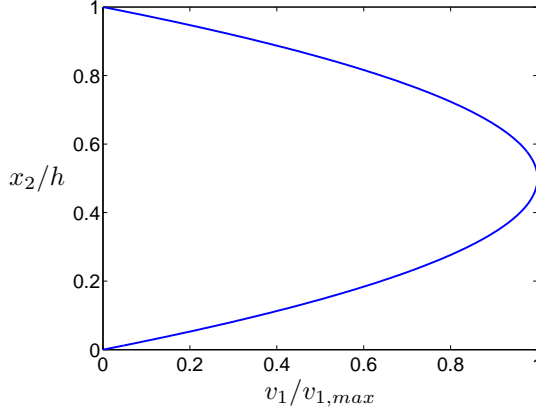


Figure 3.7: The velocity profile in fully developed channel flow, Eq. 3.28.

The minus sign on the right side appears because the pressure gradient is decreasing for increasing  $x_1$ ; the pressure is *driving* the flow. The negative pressure gradient is constant (see Eq. 3.24) and can be written as  $-dP/dx_1 = \Delta P/L$ .

The velocity takes its maximum in the center, i.e. for  $x_2 = h/2$ , and reads

$$v_{1,max} = \frac{h}{2\mu} \frac{\Delta P}{L} \frac{h}{2} \left(1 - \frac{1}{2}\right) = \frac{h^2}{8\mu} \frac{\Delta P}{L} \quad (3.27)$$

We often write Eq. 3.26 on the form

$$\frac{v_1}{v_{1,max}} = \frac{4x_2}{h} \left(1 - \frac{x_2}{h}\right) \quad (3.28)$$

The mean velocity (often called the bulk velocity) is obtained by integrating Eq. 3.28 across the channel, i.e.

$$v_{1,mean} = \frac{v_{1,max}}{h} \int_0^h 4x_2 \left(1 - \frac{x_2}{h}\right) dx_2 = \frac{2}{3} v_{1,max} \quad (3.29)$$

The velocity profile is shown in Fig. 3.7

Since we know the velocity profile, we can compute the wall shear stress. Equation 3.26 gives

$$\tau_w = \mu \frac{\partial v_1}{\partial x_2} = -\frac{h}{2} \frac{dP}{dx_1} = \frac{h}{2} \frac{\Delta P}{L} \quad (3.30)$$

Actually, this result could have been obtained by simply taking a force balance of a slice of the flow far downstream.

### 3.2.3 Force balance

To formulate a force balance in the  $x_1$  direction, we start with Eq. 1.3 which reads for  $i = 1$

$$\rho \frac{dv_1}{dt} = \frac{\partial \sigma_{j1}}{\partial x_j} \quad (3.31)$$

The left hand side is zero since the flow is fully developed. Forces act on a volume and its bounding surface. Hence we integrate Eq. 3.31 over the volume of a slice (length

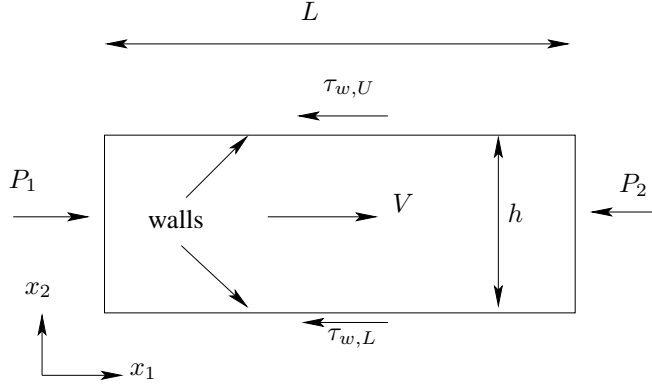


Figure 3.8: Force balance of the flow between two plates.

$L$ ), see Fig. 3.8

$$0 = \int_V \frac{\partial \sigma_{j1}}{\partial x_j} dV \quad (3.32)$$

Recall that this is the form on which we originally derived the momentum balance (Newton's second law) in Part I. [3] Now use Gauss divergence theorem

$$0 = \int_V \frac{\partial \sigma_{j1}}{\partial x_j} dV = \int_S \sigma_{j1} n_j dS \quad (3.33)$$

The bounding surface consists in our case of four surfaces (lower, upper, left and right) so that

$$0 = \int_{S_{left}} \sigma_{j1} n_j dS + \int_{S_{right}} \sigma_{j1} n_j dS + \int_{S_{lower}} \sigma_{j1} n_j dS + \int_{S_{upper}} \sigma_{j1} n_j dS \quad (3.34)$$

The normal vector on the lower, upper, left and right are  $n_{i,lower} = (0, -1, 0)$ ,  $n_{i,upper} = (0, 1, 0)$ ,  $n_{i,left} = (-1, 0, 0)$ ,  $n_{i,right} = (1, 0, 0)$ . Inserting the normal vectors and using Eq. 1.5 give

$$0 = - \int_{S_{left}} (-p + \tau_{11}) dS + \int_{S_{right}} (-p + \tau_{11}) dS - \int_{S_{lower}} \tau_{21} dS + \int_{S_{upper}} \tau_{21} dS \quad (3.35)$$

$\tau_{11} = 0$  because  $\partial v_1 / \partial x_1 = 0$  (fully developed flow). The shear stress at the upper and lower surfaces have opposite sign because  $\tau_w = \mu(\partial v_1 / \partial x_2)_{lower} = -\mu(\partial v_1 / \partial x_2)_{upper}$ . Using this and Eq. 3.22 give (the gravitation term on the left and right surface cancels and  $P$  and  $\tau_w$  are constants and can thus be taken out in front of the integration)

$$0 = P_1 Wh - P_2 Wh - 2\tau_w LW \quad (3.36)$$

where  $W$  is the width (in  $x_3$  direction) of the two plates (for convenience we set  $W = 1$ ). With  $\Delta P = P_1 - P_2$  we get Eq. 3.30.

### 3.2.4 Balance equation for the kinetic energy

In this subsection we will use the equation for kinetic energy, Eq. 2.20. Let us integrate this equation in the same way as we did for the force balance. The left side of Eq. 2.20

is zero because we assume that the flow is fully developed; using Eq. 1.5 gives

$$\begin{aligned} 0 &= \frac{\partial v_i \sigma_{ji}}{\partial x_j} - \sigma_{ji} \frac{\partial v_i}{\partial x_j} + \underbrace{\rho v_i f_i}_{=0} \\ &= -\frac{\partial v_j p}{\partial x_j} + \frac{\partial v_i \tau_{ji}}{\partial x_j} + p \delta_{ij} \frac{\partial v_i}{\partial x_j} - \underbrace{\tau_{ji} \frac{\partial v_i}{\partial x_j}}_{\Phi} \end{aligned} \quad (3.37)$$

On the first line  $v_i f_i = v_1 f_1 + v_2 f_2 = 0$  because  $v_2 = f_1 = 0$ . The third term on the second line  $p \delta_{ij} \partial v_i / \partial x_j = p \partial v_i / \partial x_i = 0$  because of continuity. The last term corresponds to the viscous dissipation term,  $\Phi$  (i.e. loss due to friction), see Eq. 2.22 (term **b**). Now we integrate the equation over a volume

$$0 = \int_V \left( -\frac{\partial p v_j}{\partial x_j} + \frac{\partial \tau_{ji} v_i}{\partial x_j} - \Phi \right) dV \quad (3.38)$$

Gauss divergence theorem on the two first terms gives

$$0 = \int_S (-p v_j + \tau_{ji} v_i) n_j dS - \int_V \Phi dV \quad (3.39)$$

where  $S$  is the surface bounding the volume. The unit normal vector is denoted by  $n_j$  which points *out* from the volume. For example, on the right surface in Fig. 3.8 it is  $n_j = (1, 0, 0)$  and on the lower surface it is  $n_j = (0, -1, 0)$ . Now we apply Eq. 3.39 to the fluid enclosed by the flat plates in Fig. 3.8. The second term is zero on all four surfaces and the first term is zero on the lower and upper surfaces (see Exercises below). We replace the pressure  $p$  with  $P$  using Eq. 3.22 so that

$$\begin{aligned} \int_{S_{left} \& S_{right}} (-P v_1 + \rho g x_2 v_1) n_1 dS &= -(P_2 - P_1) \int_{S_{left} \& S_{right}} v_1 n_1 dS \\ &= \Delta P v_{1,mean} W h \end{aligned}$$

because  $\rho g x_2 n_1 v_1$  on the left and right surfaces cancels;  $P$  can be taken out of the integral as it does not depend on  $x_2$ . Finally we get

$$\Delta P = \frac{1}{W h v_{1,mean}} \int_V \Phi dV \quad (3.40)$$

**Exercise 19** For the fully developed flow, compute the vorticity,  $\omega_i$ , using the exact solution (Eq. 3.28).

**Exercise 20** Show that the first and second terms in Eq. 3.39 are zero on the upper and the lower surfaces in Fig. 3.8.

**Exercise 21** Show that the second term in Eq. 3.39 is zero also on the left and right surfaces in Fig. 3.8 (assume fully developed flow).

**Exercise 22** Using the exact solution, compute the dissipation,  $\Phi$ , for the fully developed flow.

**Exercise 23** From the dissipation, compute the pressure drop. Is it the same as that obtained from the force balance (if not, find the error; it should be!).

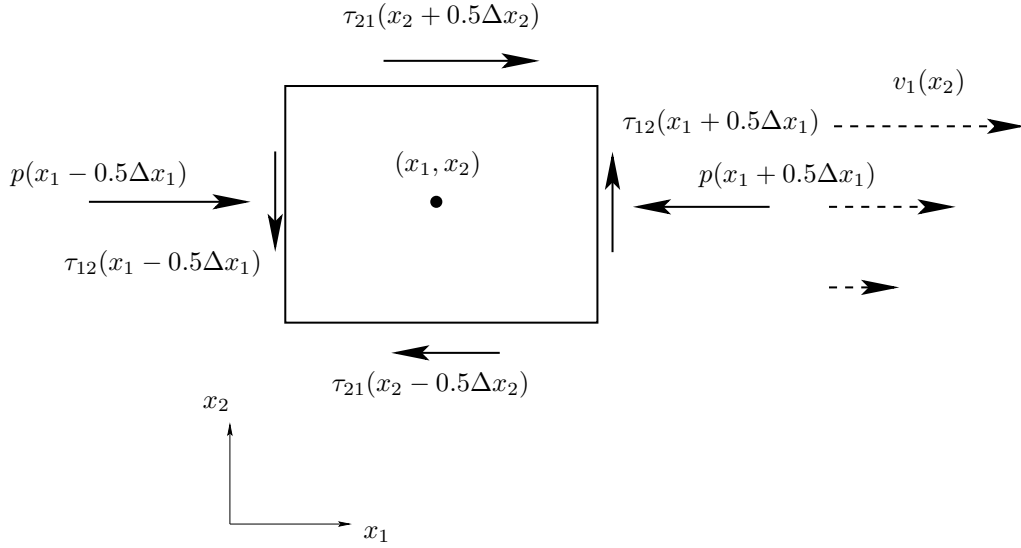


Figure 4.1: Surface forces in the  $x_1$  direction acting on a fluid particle (assuming  $\tau_{11} = \tau_{22} = 0$ ).  $v_1 = cx_2^2$  and  $v_2 = 0$ .  $\partial\tau_{12}/\partial x_1 = 0$ ,  $\partial\tau_{21}/\partial x_2 > 0$ .  $v_1$  velocity field indicated by dashed vectors.

## 4 Vorticity equation and potential flow

### 4.1 Vorticity and rotation

Vorticity,  $\omega_i$ , was introduced in Eq. 1.8 at p. 11. As shown in Fig. 1.3 at p. 14, vorticity is connected to rotation of a fluid particle. Figure 4.1 shows the surface forces in the  $x_1$  momentum equation acting on a fluid particle in a shear flow. Looking at Fig. 4.1 it is obvious that only the shear stresses are able to rotate the fluid particle; the pressure acts through the center of the fluid particle and is thus not able to affect rotation of the fluid particle.

Let us have a look at the momentum equations in order to show that the viscous terms indeed can be formulated with the vorticity vector,  $\omega_i$ . In incompressible flow the viscous terms read (see Eqs. 2.4, 2.5 and 2.6)

$$\frac{\partial \tau_{ji}}{\partial x_j} = \mu \frac{\partial^2 v_i}{\partial x_j \partial x_j} \quad (4.1)$$

The right side can be re-written using the tensor identity

$$\frac{\partial^2 v_i}{\partial x_j \partial x_j} = \frac{\partial^2 v_j}{\partial x_j \partial x_i} - \left( \frac{\partial^2 v_j}{\partial x_j \partial x_i} - \frac{\partial^2 v_i}{\partial x_j \partial x_j} \right) = \frac{\partial^2 v_j}{\partial x_j \partial x_i} - \varepsilon_{inm} \varepsilon_{mjk} \frac{\partial^2 v_k}{\partial x_j \partial x_n} \quad (4.2)$$

Let's verify that

$$\left( \frac{\partial^2 v_j}{\partial x_j \partial x_i} - \frac{\partial^2 v_i}{\partial x_j \partial x_j} \right) = \varepsilon_{inm} \varepsilon_{mjk} \frac{\partial^2 v_k}{\partial x_j \partial x_n} \quad (4.3)$$

Use the  $\varepsilon - \delta$ -identity (see Table A.1 at p. 38)

$$\varepsilon_{inm} \varepsilon_{mjk} \frac{\partial^2 v_k}{\partial x_j \partial x_n} = (\delta_{ij} \delta_{nk} - \delta_{ik} \delta_{nj}) \frac{\partial^2 v_k}{\partial x_j \partial x_n} = \frac{\partial^2 v_k}{\partial x_i \partial x_k} - \frac{\partial^2 v_i}{\partial x_j \partial x_j} \quad (4.4)$$

The first term on the right side is zero because of continuity and hence we find that Eq. 4.2 can indeed be written as

$$\frac{\partial^2 v_i}{\partial x_j \partial x_j} = \frac{\partial^2 v_j}{\partial x_j \partial x_i} - \varepsilon_{inm} \varepsilon_{mjk} \frac{\partial^2 v_k}{\partial x_j \partial x_n} \quad (4.5)$$

At the right side we recognize the vorticity,  $\omega_m = \varepsilon_{mjk} \partial v_k / \partial x_j$ , so that

$$\frac{\partial^2 v_i}{\partial x_j \partial x_j} = \frac{\partial^2 v_j}{\partial x_j \partial x_i} - \varepsilon_{inm} \frac{\partial \omega_m}{\partial x_n} \quad (4.6)$$

where the first on the right side is zero because of continuity, so that

$$\frac{\partial^2 v_i}{\partial x_j \partial x_j} = -\varepsilon_{inm} \frac{\partial \omega_m}{\partial x_n} \quad (4.7)$$

In vector notation the identity Eq. 4.6 reads

$$\nabla^2 \mathbf{v} = \nabla(\nabla \cdot \mathbf{v}) - \nabla \times \nabla \times \mathbf{v} = -\nabla \times \boldsymbol{\omega} \quad (4.8)$$

Using Eq. 4.7, Eq. 4.1 reads

$$\frac{\partial \tau_{ji}}{\partial x_j} = -\mu \varepsilon_{inm} \frac{\partial \omega_m}{\partial x_n} \quad (4.9)$$

Thus, there is a one-to-one relation between the viscous term and vorticity: no viscous terms means no vorticity and vice versa. An imbalance in shear stresses (left side of Eq. 4.9) causes a change in vorticity, i.e. generates vorticity (right side of Eq. 4.9). Hence, inviscid flow (i.e. friction-less flow) has no rotation. (The exception is when vorticity is transported *into* an inviscid region, but also in that case no vorticity is generated or destroyed: it stays constant, unaffected.) Inviscid flow is often called *irrotational* flow (i.e. no rotation) or *potential* flow. The vorticity is always created at boundaries, see Section 4.3.1.

**potential**

The main points that we have learnt in this section are:

1. The viscous terms are responsible for creating vorticity; this means that the vorticity can't be created or destroyed in inviscid (friction-less) flow
2. The viscous terms in the momentum equations can be expressed in  $\omega_i$ ; considering Item 1 this was to be expected.

**Exercise 24** Prove the first equality of Eq. 4.7 using the  $\varepsilon$ - $\delta$ -identity.

**Exercise 25** Write out Eq. 4.9 for  $i = 1$  and verify that it is satisfied.

## 4.2 The vorticity transport equation in three dimensions

Up to now we have talked quite a lot about vorticity. We have learnt that physically it means rotation of a fluid particle and that it is only the viscous terms that can cause rotation of a fluid particle. The terms inviscid, irrotational and potential flow all denote *frictionless flow* which is equivalent to zero vorticity. There is a small difference between the three terms because there may be vorticity in inviscid flow that is convected into the flow at the inlet(s); but also in this case the vorticity is not affected once it has

**friction-less**

entered the inviscid flow region. However, mostly no distinction is made between the three terms.

In this section we will derive the transport equation for vorticity in incompressible flow. As usual we start with the Navier-Stokes equation, Eq. 2.7 at p.21. First, we re-write the convective term of the incompressible momentum equation (Eq. 2.7) as

$$v_j \frac{\partial v_i}{\partial x_j} = v_j (S_{ij} + \Omega_{ij}) = v_j \left( S_{ij} - \frac{1}{2} \varepsilon_{ijk} \omega_k \right) \quad (4.10)$$

where Eq. 1.15 on p. 12 was used. Inserting  $S_{ij} = (\partial v_i / \partial x_j + \partial v_j / \partial x_i) / 2$  and multiplying by two gives

$$2v_j \frac{\partial v_i}{\partial x_j} = v_j \left( \frac{\partial v_i}{\partial x_j} + \frac{\partial v_j}{\partial x_i} \right) - \varepsilon_{ijk} v_j \omega_k \quad (4.11)$$

The second term on the right side can be written as

$$v_j \frac{\partial v_j}{\partial x_i} = \frac{1}{2} \frac{\partial(v_j v_j)}{\partial x_i} = \frac{\partial k}{\partial x_i} \quad (4.12)$$

where  $k = v_j v_j / 2$ . Equation 4.11 can now be written as

$$v_j \frac{\partial v_i}{\partial x_j} = \underbrace{\frac{\partial k}{\partial x_i}}_{\text{no rotation}} - \underbrace{\varepsilon_{ijk} v_j \omega_k}_{\text{rotation}} \quad (4.13)$$

The last term on the right side is the vector product of  $\mathbf{v}$  and  $\boldsymbol{\omega}$ , i.e.  $\mathbf{v} \times \boldsymbol{\omega}$ .

The trick we have achieved is to split the convective term into one term without rotation (first term on the right side of Eq. 4.13) and one term including rotation (second term on the right side). Inserting Eq. 4.13 into the incompressible momentum equation (Eq. 2.7) yields

$$\frac{\partial v_i}{\partial t} + \underbrace{\frac{\partial k}{\partial x_i}}_{\text{no rotation}} - \underbrace{\varepsilon_{ijk} v_j \omega_k}_{\text{rotation}} = -\frac{1}{\rho} \frac{\partial p}{\partial x_i} + \nu \frac{\partial^2 v_i}{\partial x_j \partial x_j} + f_i \quad (4.14)$$

The volume source is in most engineering flows represented by the gravity which, i.e.  $f_i = g_i$ . Since the vorticity vector is defined by the cross product  $\varepsilon_{pqi} \partial v_i / \partial x_q$  ( $\nabla \times \mathbf{v}$  in vector notation, see Exercise 8), we start by applying the operator  $\varepsilon_{pqi} \partial / \partial x_q$  to the Navier-Stokes equation (Eq. 4.14) so that

$$\begin{aligned} & \varepsilon_{pqi} \frac{\partial^2 v_i}{\partial t \partial x_q} + \varepsilon_{pqi} \frac{\partial^2 k}{\partial x_i \partial x_q} - \varepsilon_{pqi} \varepsilon_{ijk} \frac{\partial v_j \omega_k}{\partial x_q} \\ &= -\varepsilon_{pqi} \frac{1}{\rho} \frac{\partial^2 p}{\partial x_i \partial x_q} + \nu \varepsilon_{pqi} \frac{\partial^3 v_i}{\partial x_j \partial x_j \partial x_q} + \varepsilon_{pqi} \frac{\partial g_i}{\partial x_q} \end{aligned} \quad (4.15)$$

where the body force  $f_i$  was replaced by  $g_i$ . We know that  $\varepsilon_{ijk}$  is anti-symmetric in all indices, and hence the second term on line 1 and the first term on line 2 are zero (product of a symmetric and an anti-symmetric tensor). The last term on line 2 is zero because the gravitation vector,  $g_i$ , is constant. The last term on line 1 is re-written using the  $\varepsilon$ - $\delta$  identity (see Table A.1 at p. A.1)

$$\begin{aligned} \varepsilon_{pqi} \varepsilon_{ijk} \frac{\partial v_j \omega_k}{\partial x_q} &= (\delta_{pj} \delta_{qk} - \delta_{pk} \delta_{qj}) \frac{\partial v_j \omega_k}{\partial x_q} = \frac{\partial v_p \omega_k}{\partial x_k} - \frac{\partial v_q \omega_p}{\partial x_q} \\ &= v_p \frac{\partial \omega_k}{\partial x_k} + \omega_k \frac{\partial v_p}{\partial x_k} - v_q \frac{\partial \omega_p}{\partial x_q} - \omega_p \frac{\partial v_q}{\partial x_q} \end{aligned} \quad (4.16)$$

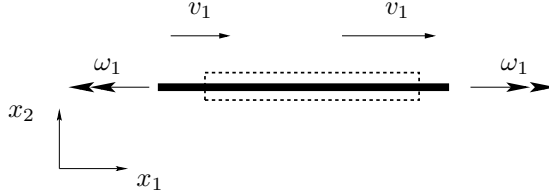


Figure 4.2: Vortex stretching. Dashed lines denote fluid element before stretching.  
 $\frac{\partial v_1}{\partial x_1} > 0$ .

Using the definition of  $\omega_i$  we find that its divergence

$$\frac{\partial \omega_i}{\partial x_i} = \frac{\partial}{\partial x_i} \left( \varepsilon_{ijk} \frac{\partial v_k}{\partial x_j} \right) = \varepsilon_{ijk} \frac{\partial^2 v_k}{\partial x_j \partial x_i} = 0 \quad (4.17)$$

is zero (product of a symmetric and an anti-symmetric tensor). Using the continuity equation ( $\partial v_q / \partial x_q = 0$ ) and Eq. 4.17, Eq. 4.16 can be written

$$\varepsilon_{pqi} \varepsilon_{ijk} \frac{\partial v_j \omega_k}{\partial x_q} = \omega_k \frac{\partial v_p}{\partial x_k} - v_k \frac{\partial \omega_p}{\partial x_k} \quad (4.18)$$

The second term on line 2 in Eq. 4.15 can be written as

$$\nu \varepsilon_{pqi} \frac{\partial^3 v_i}{\partial x_j \partial x_j \partial x_q} = \nu \frac{\partial^2}{\partial x_j \partial x_j} \left( \varepsilon_{pqi} \frac{\partial v_i}{\partial x_q} \right) = \nu \frac{\partial^2 \omega_p}{\partial x_j \partial x_j} \quad (4.19)$$

Inserting Eqs. 4.18 and 4.19 into Eq. 4.15 gives finally

$$\frac{d\omega_p}{dt} \equiv \frac{\partial \omega_p}{\partial t} + v_k \frac{\partial \omega_p}{\partial x_k} = \omega_k \frac{\partial v_p}{\partial x_k} + \nu \frac{\partial^2 \omega_p}{\partial x_j \partial x_j} \quad (4.20)$$

We recognize the usual unsteady term, the convective term and the diffusive term. Furthermore, we have got rid of the pressure gradient term. That makes sense, because as mentioned in connection to Fig. 4.1, the pressure cannot affect the rotation (i.e. the vorticity) of a fluid particle since the pressure acts through its center. Equation 4.20 has a new term on the right-hand side which represents amplification and rotation/tilting of the vorticity lines. If we write it term-by-term it reads

$$\omega_k \frac{\partial v_p}{\partial x_k} = \begin{cases} \omega_1 \frac{\partial v_1}{\partial x_1} + \omega_2 \frac{\partial v_1}{\partial x_2} + \omega_3 \frac{\partial v_1}{\partial x_3}, & p = 1 \\ \omega_1 \frac{\partial v_2}{\partial x_1} + \omega_2 \frac{\partial v_2}{\partial x_2} + \omega_3 \frac{\partial v_2}{\partial x_3}, & p = 2 \\ \omega_1 \frac{\partial v_3}{\partial x_1} + \omega_2 \frac{\partial v_3}{\partial x_2} + \omega_3 \frac{\partial v_3}{\partial x_3}, & p = 3 \end{cases} \quad (4.21)$$

The diagonal terms in this matrix represent *vortex stretching*. Imagine a slender, cylindrical fluid particle with vorticity  $\omega_i$  and introduce a cylindrical coordinate system with the  $x_1$ -axis as the cylinder axis and  $r_2$  as the radial coordinate (see Fig. 4.2) so that  $\omega_i = (\omega_1, 0, 0)$ . We assume that a positive  $\partial v_1 / \partial x_1$  is acting on the fluid cylinder; it will act as a source in Eq. 4.20 increasing  $\omega_1$  and it will stretch the cylinder. The volume of the fluid element must stay constant during the stretching (the incompressible

**Vortex stretching**

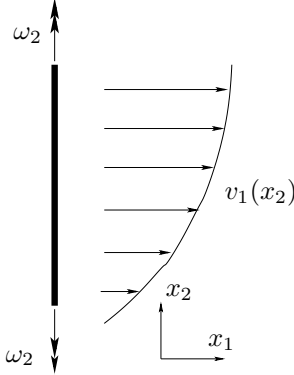


Figure 4.3: Vortex tilting.

continuity equation), which means that the radius of the cylinder will decrease. Hence vortex stretching will either make a fluid element longer and thinner (as in the example above) or shorter and thicker (when  $\partial v_1 / \partial x_1 < 0$ ).

The off-diagonal terms in Eq. 4.21 represent *vortex tilting*. Again, take a slender fluid particle, but this time with its axis aligned with the  $x_2$  axis, see Fig. 4.3. The velocity gradient  $\partial v_1 / \partial x_2$  will tilt the fluid particle so that it rotates in clock-wise direction. The second term  $\omega_2 \partial v_1 / \partial x_2$  in line one in Eq. 4.21 gives a contribution to  $\omega_1$ . This means that vorticity in the  $x_2$  direction, through the source term  $\omega_2 \partial v_1 / \partial x_2$ , creates vorticity in the  $x_1$  direction..

**Vortex  
tilting**

Vortex stretching and tilting are physical phenomena which act in three dimensions: fluid which initially is two dimensional becomes quickly three dimensional through these phenomena. Vorticity is useful when explaining why turbulence must be three-dimensional, see Section 5.4.

### 4.3 The vorticity transport equation in two dimensions

It is obvious that the vortex stretching/tilting has no influence in two dimensions; in this case the vortex stretching/tilting term vanishes because the vorticity vector is orthogonal to the velocity vector (for a 2D flow the velocity vector reads  $v_i = (v_1, v_2, 0)$  and the vorticity vector reads  $\omega_i = (0, 0, \omega_3)$  so that the vector  $\omega_k \partial v_p / \partial x_k = 0$ ). Thus in two dimensions the vorticity equation reads

$$\frac{d\omega_3}{dt} = \nu \frac{\partial^2 \omega_3}{\partial x_\alpha \partial x_\alpha} \quad (4.22)$$

(Greek indices are used to indicate that they take values 1 or 2). This equation is exactly the same as the transport equation for temperature in incompressible flow, see Eq. 2.15. This means that vorticity diffuses in the same way as temperature does. In fully developed channel flow, for example, the vorticity and the temperature equations reduce to

$$0 = \nu \frac{\partial^2 \omega_3}{\partial x_2^2} \quad (4.23a)$$

$$0 = k \frac{\partial^2 T}{\partial x_2^2} \quad (4.23b)$$

For the temperature equation the heat flux is given by  $q_2 = -\partial T / \partial x_2$ ; with a hot lower wall and a cold upper wall (constant wall temperatures) the heat flux is constant and goes from the lower wall to the upper wall. We have the same situation for the vorticity. Its gradient, i.e. the vorticity flux,  $\gamma_2 = -\partial \omega_3 / \partial x_2$ , is constant across the channel. You have plotted this quantity in TME225 Assignment 1.

If wall-normal temperature derivative  $\partial T / \partial x_2 = 0$  at both walls (*adiabatic* walls), the heat flux is zero at the walls and the temperature will be equal to an arbitrary constant in the entire domain. It is only when the wall-normal temperature derivative at the walls are non-zero that a temperature field is created in the domain. The same is true for  $\omega_3$ : if  $\partial \omega_3 / \partial x_2 = 0$  at the walls, the flow will not include any vorticity. Hence, vorticity is – in the same way as temperature – generated at the walls.

#### 4.3.1 Boundary layer thickness from the Rayleigh problem

In Section 3.1 we studied the Rayleigh problem (unsteady diffusion). As shown above, the two-dimensional unsteady temperature equation is identical to the two-dimensional unsteady equation for vorticity. The diffusion time,  $t$ , or the diffusion length,  $\delta$ , in Eq. 3.14 can now be used to estimate the thickness of a developing boundary layer (recall that the limit between the boundary layer and the outer free-stream region can be defined by vorticity: inside the vorticity is non-zero and outside it is zero).

In a boundary layer the streamwise pressure gradient is zero. This means that

$$\mu \frac{\partial^2 v_1}{\partial x_2^2} \Big|_{wall} = 0$$

because, at the wall, the only non-zero terms in the Navier-Stokes equation are the streamwise pressure gradient and the wall-normal diffusion term (see, for example, Eqs. 2.7 and 3.23). Hence, the flux of vorticity

$$\gamma_2 = -\frac{\partial \omega_3}{\partial x_2} \Big|_{wall} = \frac{\partial^2 v_1}{\partial x_2^2} \Big|_{wall} = 0$$

(recall that  $(\partial v_2 / \partial x_1)_{wall} = 0$ ) along the wall which means that no vorticity is created along the boundary. The vorticity in a developing boundary layer is created at the leading edge of the plate (note that in channel flow, vorticity is indeed created along the walls because in this case the streamwise pressure gradient is not zero). The vorticity generated at the leading edge is transported along the wall by convection and at the same time it is transported by diffusion away from the wall.

Below we will estimate the boundary layer thickness using the expression derived for the Rayleigh problem. In a boundary layer there is vorticity and outside the boundary layer it is zero (in this flow, the vorticity is created at time  $t = 0^+$  when the plate instantaneously accelerates from rest to velocity  $V_0$ ). Hence, if we can estimate how far from the wall the vorticity diffuses, this gives us an estimation of the boundary layer thickness.

Consider the boundary layer in Fig. 4.4. At the end of the plate the boundary thickness is  $\delta(L)$ . The time it takes for a fluid particle to travel from the leading edge of the plate to  $x = L$  is  $L/V_0$ . During this time vorticity will be transported by diffusion in the  $x_2$  direction the length  $\delta$  according Eq. 3.14. If we assume that the fluid is air with the speed  $V_0 = 3m/s$  and that the length of the plate  $L = 2m$  we get from Eq. 3.14 that  $\delta(L) = 1.2cm$ .

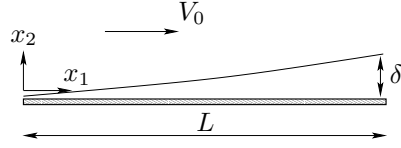


Figure 4.4: Boundary layer. The boundary layer thickness,  $\delta$ , increases for increasing streamwise distance from leading edge ( $x_1 = 0$ ).

**Exercise 26** Note that the estimate above is not quite accurate because in the Rayleigh problem we assumed that the convective terms are zero, but in a developing boundary layer, as in Fig. 4.4, they are not ( $v_2 \neq 0$  and  $\partial v_1 / \partial x_1 \neq 0$ ). The proper way to solve the problem is to use Blasius solution (you have probably learnt about this in your first fluid mechanics course; if not, you should go and find out). Blasius solution gives

$$\frac{\delta}{L} = \frac{5}{Re_L^{1/2}}, \quad Re_L = \frac{V_0 L}{\nu} \quad (4.24)$$

Compute what  $\delta(L)$  you get from Eq. 4.24.

**Exercise 27** Assume that we have a developing flow in a pipe (radius  $R$ ) or between two flat plates (separation distance  $h$ ). We want to find out how long distance it takes for the the boundary layers to merge. Equation 3.14 can be used with  $\delta = R$  or  $h$ . Make a comparison with this and Eq. 3.16.

## 5 Turbulence

### 5.1 Introduction

Almost all fluid flow which we encounter in daily life is turbulent. Typical examples are flow around (as well as *in*) cars, aeroplanes and buildings. The boundary layers and the wakes around and after bluff bodies such as cars, aeroplanes and buildings are turbulent. Also the flow and combustion in engines, both in piston engines and gas turbines and combustors, are highly turbulent. Air movements in rooms are turbulent, at least along the walls where wall-jets are formed. Hence, when we compute fluid flow it will most likely be turbulent.

In turbulent flow we usually divide the velocities in one time-averaged part  $\bar{v}_i$ , which is independent of time (when the mean flow is steady), and one fluctuating part  $v'_i$  so that  $v_i = \bar{v}_i + v'_i$ .

There is no definition on turbulent flow, but it has a number of characteristic features (see Pope [7] and Tennekes & Lumley [8]) such as:

**I. Irregularity.** Turbulent flow is irregular and chaotic (they may seem random, but they are governed by Navier-Stokes equation, Eq. 2.7). The flow consists of a spectrum of different scales (eddy sizes). We do not have any exact definition of an *turbulent eddy*, but we suppose that it exists in a certain region in space for a certain time and that it is subsequently destroyed (by the cascade process or by dissipation, see below). It has a characteristic velocity and length (called a velocity and length scale). The region covered by a large eddy may well enclose also smaller eddies. The largest eddies are of the order of the flow geometry (i.e. boundary layer thickness, jet width, etc). At the other end of the spectra we have the smallest eddies which are dissipated by viscous forces (stresses) into thermal energy resulting in a temperature increase. Even though turbulence is chaotic it is deterministic and is described by the Navier-Stokes equations.

turbulent  
eddy

**II. Diffusivity.** In turbulent flow the diffusivity increases. The turbulence increases the exchange of momentum in e.g. boundary layers, and reduces or delays thereby separation at bluff bodies such as cylinders, airfoils and cars. The increased diffusivity also increases the resistance (wall friction) and heat transfer in internal flows such as in channels and pipes.

**III. Large Reynolds Numbers.** Turbulent flow occurs at high Reynolds number. For example, the transition to turbulent flow in pipes occurs that  $Re_D \simeq 2300$ , and in boundary layers at  $Re_x \simeq 500\,000$ .

**IV. Three-Dimensional.** Turbulent flow is always three-dimensional and unsteady. However, when the equations are time averaged, we can treat the flow as two-dimensional (if the geometry is two-dimensional).

**V. Dissipation.** Turbulent flow is dissipative, which means that kinetic energy in the small (dissipative) eddies are transformed into thermal energy. The small eddies receive the kinetic energy from slightly larger eddies. The slightly larger eddies receive their energy from even larger eddies and so on. The largest eddies extract their energy from the mean flow. This process of transferring energy from the largest turbulent scales (eddies) to the smallest is called the *cascade process*.

cascade  
process

**VI. Continuum.** Even though we have small turbulent scales in the flow they are much larger than the molecular scale and we can treat the flow as a continuum.

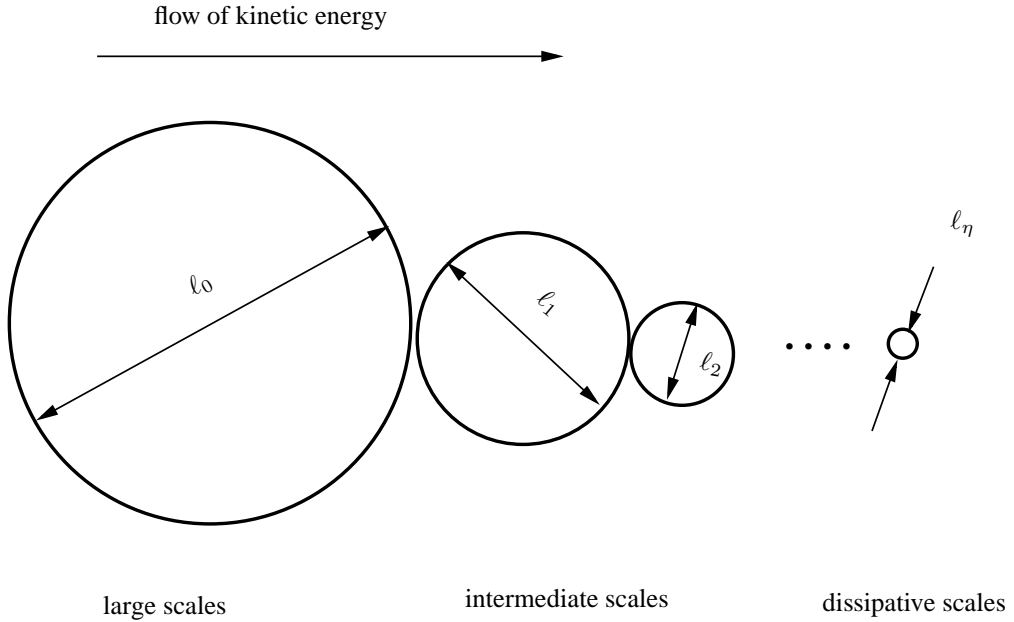


Figure 5.1: Cascade process with a spectrum of eddies. The energy-containing eddies are denoted by  $v_0$ ;  $\ell_1$  and  $\ell_2$  denotes the size of the eddies in the inertial subrange such that  $\ell_2 < \ell_1 < \ell_0$ ;  $\ell_\eta$  is the size of the dissipative eddies.

## 5.2 Turbulent scales

The largest scales are of the order of the flow geometry (the boundary layer thickness, for example), with length scale  $\ell_0$  and velocity scale  $v_0$ . These scales extract kinetic energy from the mean flow which has a time scale comparable to the large scales, i.e.

$$\frac{\partial \bar{v}_1}{\partial x_2} = \mathcal{O}(t_0^{-1}) = \mathcal{O}(v_0/\ell_0) \quad (5.1)$$

Part of the kinetic energy of the large scales is lost to slightly smaller scales with which the large scales interact. Through the *cascade process*, kinetic energy is in this way transferred from the largest scale to the smallest scales. At the smallest scales the frictional forces (viscous stresses) become large and the kinetic energy is transformed (dissipated) into thermal energy. The kinetic energy transferred from eddy-to-eddy (from an eddy to a slightly smaller eddy) is the same *per unit time* for each eddy size.

The dissipation is denoted by  $\varepsilon$  which is energy per unit time and unit mass ( $\varepsilon = [m^2/s^3]$ ). The dissipation is proportional to the kinematic viscosity,  $\nu$ , times the fluctuating velocity gradient up to the power of two (see Section 8.1). The friction forces exist of course at all scales, but they are largest at the smallest eddies. In reality a small fraction is dissipated at all scales. However it is assumed that most of the energy that goes into the large scales per unit time (say 90%) is finally dissipated at the smallest (dissipative) scales.

The smallest scales where dissipation occurs are called the Kolmogorov scales whose velocity scale is denoted by  $v_\eta$ , length scale by  $\ell_\eta$  and time scale by  $\tau_\eta$ . We assume that these scales are determined by viscosity,  $\nu$ , and dissipation,  $\varepsilon$ . The argument is as follows.

**viscosity:** Since the kinetic energy is destroyed by viscous forces it is natural to assume that viscosity plays a part in determining these scales; the larger viscosity, the larger scales.

**dissipation:** The amount of energy that is to be dissipated is  $\varepsilon$ . The more energy that is to be transformed from kinetic energy to thermal energy, the larger the velocity gradients must be.

Having assumed that the dissipative scales are determined by viscosity and dissipation, we can express  $v_\eta$ ,  $\ell_\eta$  and  $\tau_\eta$  in  $\nu$  and  $\varepsilon$  using dimensional analysis. We write

$$\begin{aligned} v_\eta &= \nu^a \varepsilon^b \\ [m/s] &= [m^2/s] [m^2/s^3] \end{aligned} \quad (5.2)$$

where below each variable its dimensions are given. The dimensions of the left and the right side must be the same. We get two equations, one for meters [m]

$$1 = 2a + 2b, \quad (5.3)$$

and one for seconds [s]

$$-1 = -a - 3b, \quad (5.4)$$

which give  $a = b = 1/4$ . In the same way we obtain the expressions for  $\ell_\eta$  and  $\tau_\eta$  so that

$$v_\eta = (\nu \varepsilon)^{1/4}, \quad \ell_\eta = \left( \frac{\nu^3}{\varepsilon} \right)^{1/4}, \quad \tau_\eta = \left( \frac{\nu}{\varepsilon} \right)^{1/2} \quad (5.5)$$

### 5.3 Energy spectrum

As mentioned above, the turbulence fluctuations are composed of a wide range of scales. We can think of them as eddies, see Fig. 5.1. It turns out that it is often convenient to use Fourier series to analyze turbulence. In general, any periodic function,  $g$ , with a period of  $2L$  (i.e.  $g(x) = g(x + 2L)$ ), can be expressed as a Fourier series, i.e.

$$g(x) = \frac{1}{2}a_0 + \sum_{n=1}^{\infty} (a_n \cos(\kappa_n x) + b_n \sin(\kappa_n x)) \quad (5.6)$$

where  $x$  is a spatial coordinate and

$$\kappa_n = \frac{n\pi}{L} \quad \text{or} \quad \kappa = \frac{2\pi}{L} \quad (5.7)$$

Variable  $\kappa_n$  is called the wavenumber. The Fourier coefficients are given by

$$\begin{aligned} a_n &= \frac{1}{L} \int_{-L}^L g(x) \cos(\kappa_n x) dx \\ b_n &= \frac{1}{L} \int_{-L}^L g(x) \sin(\kappa_n x) dx \end{aligned}$$

Parseval's formula states that

$$\int_{-L}^L g^2(x) dx = \frac{L}{2} a_0^2 + L \sum_{n=1}^{\infty} (a_n^2 + b_n^2) \quad (5.8)$$

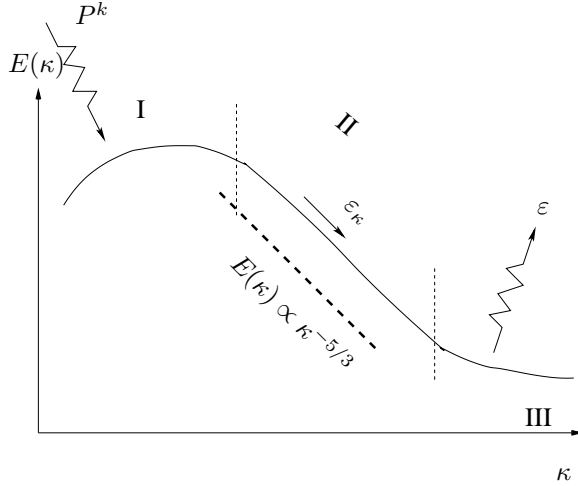


Figure 5.2: Spectrum for turbulent kinetic energy,  $k$ . I: Range for the large, energy containing eddies. II: the inertial subrange. III: Range for small, isotropic scales. For a discussion of  $\varepsilon_\kappa$  vs.  $\varepsilon$ , see Section 8.1.1. The wavenumber,  $\kappa$ , is proportional to the inverse of the length scale of a turbulent eddy,  $\ell_\kappa$ , i.e.  $\kappa \propto \ell_\kappa^{-1}$ . For a discussion of  $\varepsilon_\kappa$  vs.  $\varepsilon$ , see Section 8.1.1.

For readers not familiar to Fourier series, a brief introduction is given in Section C. An example of a fourier series and spectra are given in Section D. Let now  $g$  be a fluctuating velocity component, say  $v'_1$ . The left side of Eq. 5.8 expresses  $v'^2_1$  in physical space (vs.  $x$ ) and the right side  $v'^2_1$  in wavenumber space (vs.  $\kappa_n$ ). The reader who is not familiar to the term “wavenumber”, is probably more familiar to “frequency”. In that case, express  $g$  in Eq. 5.6 as a series in *time* rather than in *space*. In this case the left side of Eq. 5.8 expresses  $v'^2_1$  as a function of time and the right side expresses  $v'^2_1$  as a function of frequency.

The turbulent scales are distributed over a range of scales which extends from the largest scales which interact with the mean flow to the smallest scales where dissipation occurs, see Fig. 5.1. Now let us think about how the kinetic energy of the eddies varies with eddy size. Intuitively we assume that large eddies have large fluctuating velocities which implies large kinetic energy,  $v'_i v'_i / 2$ . It is now convenient to study the kinetic energy of each eddy size in wavenumber space. In wavenumber space the energy of eddies can be expressed as

$$E(\kappa) d\kappa \quad (5.9)$$

where Eq. 5.9 expresses the contribution from the scales with wavenumber between  $\kappa$  and  $\kappa + d\kappa$  to the turbulent kinetic energy  $k$ . The energy,  $E(\kappa)$ , corresponds to  $g^2(\kappa)$  in Eq. 5.8. The dimension of wavenumber is one over length; thus we can think of wavenumber as proportional to the inverse of an eddy’s diameter, i.e.  $\kappa \propto 1/d$ . The total turbulent kinetic energy is obtained by integrating over the whole wavenumber space i.e.

$$k = \int_0^\infty E(\kappa) d\kappa = L \sum g^2(\kappa_n) \quad (5.10)$$

Think of this equation as a way to compute the kinetic energy by first sorting all eddies by size (i.e. wavenumber), then computing the kinetic energy of each eddy size (i.e.

$E(\kappa)d\kappa$ , and finally summing the kinetic energy of all eddy sizes (i.e. carrying out the integration). Note that the physical meaning of  $E$  is kinetic energy *per unit wavenumber* of eddies of size  $\ell_\kappa \propto \kappa^{-1}$ . Hence the dimension of  $E$  is  $v^2/\ell$ , see Eq. 5.10; for a discussion on the dimension of  $E$ , see Appendix D.

The kinetic energy is the sum of the kinetic energy of the three fluctuating velocity components, i.e.

$$k = \frac{1}{2} \left( \overline{v_1'^2} + \overline{v_2'^2} + \overline{v_3'^2} \right) = \frac{1}{2} \overline{v_i' v_i'} \quad (5.11)$$

The spectrum of  $E$  is shown in Fig. 5.2. We find region I, II and III which correspond to:

- I. In this region we have the large eddies which carry most of the energy. These eddies interact with the mean flow and extract energy from the mean flow. This energy transfer takes place via the production term,  $P^k$ , in the transport equation for turbulent kinetic energy, see Eq. 8.14. The energy extracted per unit time by the largest eddies is transferred (per unit time) to slightly smaller scales. The eddies' velocity and length scales are  $v_0$  and  $\ell_0$ , respectively.
- III. Dissipation range. The eddies are small and isotropic and it is here that the dissipation occurs. The energy transfer from turbulent kinetic energy to thermal energy (increased temperature) is governed by  $\varepsilon$  in the transport equation for turbulent kinetic energy, see Eq. 8.14. The scales of the eddies are described by the Kolmogorov scales (see Eq. 5.5)

- II. Inertial subrange. The existence of this region requires that the Reynolds number is high (fully turbulent flow). The eddies in this region represent the mid-region. This region is a “transport region” (i.e. in wavenumber space) in the cascade process. The “transport” in wavenumber space is called *spectral transfer*. Energy per time unit,  $P^k = \varepsilon$ , is coming from the large eddies at the lower part of this range and is transferred per unit time to the dissipation range at the higher part. Note that the relation  $P^k = \{\text{dissipation at small scales}\}$ , see Fig. 5.2, is given by the assumption of the cascade process, i.e. that the energy transfer per unit time from eddy-size-to-eddy-size is the same for all eddy sizes.

The kinetic energy,  $k_\kappa = v_{\kappa,i}' v_{\kappa,i}' / 2$ , of an eddy of size (lengthscale),  $1/\kappa$ , represents the kinetic energy of all eddies of this size. The kinetic energy of all eddies (of all size) is computed by Eq. 5.11. The eddies in this region are independent of both the large, energy-containing eddies and the eddies in the dissipation range. One can argue that the eddies in this region should be characterized by the spectral transfer of energy per unit time ( $\varepsilon$ ) and the size of the eddies,  $1/\kappa$ . Dimensional analysis gives

$$\begin{aligned} \frac{E}{[m^3/s^2]} &= \frac{\kappa^a}{[1/m]} \frac{\varepsilon^b}{[m^2/s^3]} \end{aligned} \quad (5.12)$$

We get two equations, one for meters [m]

$$3 = -a + 2b,$$

and one for seconds [s]

$$-2 = -3b,$$

**spectral transfer**

so that  $b = 2/3$  and  $a = -5/3$ . Inserted in Eq. 5.12 we get

$$E(\kappa) = C_K \varepsilon^{\frac{2}{3}} \kappa^{-\frac{5}{3}} \quad (5.13)$$

where the Kolmogorov constant  $C_K \simeq 1.5$ . This is a very important law (Kolmogorov spectrum law or the  $-5/3$  law) which states that, if the flow is fully turbulent (high Reynolds number), the energy spectra should exhibit a  $-5/3$ -decay in the inertial region (region II, Fig. 5.2).

Above we state that the small eddies are *isotropic*. This means that – in average – the eddies have no preferred direction, i.e. the fluctuations in all directions are the same so that  $\overline{v_1'^2} = \overline{v_2'^2} = \overline{v_3'^2}$ . Note that is not true instantaneously, i.e. in general  $v'_1 \neq v'_2 \neq v'_3$ . Furthermore, isotropic turbulence implies that if a coordinate direction is switched, nothing should be changed. For example if the  $x_1$  coordinate direction is rotated  $180^\circ$  the  $\overline{v'_1 v'_2}$  should remain the same, i.e.  $\overline{v'_1 v'_2} = -\overline{v'_1 v'_2}$ . This is possible only if  $\overline{v'_1 v'_2} = 0$ . Hence, all shear stresses are zero in isotropic turbulence. Using our knowledge in tensor notation, we know that an isotropic tensor can be written as  $\text{const.} \delta_{ij}$ . Hence, the Reynolds stress tensor for small scales can be written as  $\overline{v'_i v'_j} = \text{const.} \delta_{ij}$  which, again, shows us that the shear stresses are zero in isotropic turbulence.

**isotropic turbulence**

As discussed on p. 44, the concept of the cascade process assumes that the energy extracted per unit time by the large turbulent eddies is transferred (per unit time) by non-linear interactions through the inertial range to the dissipative range where the kinetic energy is transformed (per unit time) to thermal energy (increased temperature). The spectral transfer rate of kinetic energy from eddies of size  $1/\kappa$  to slightly smaller eddies can be estimated as follows. An eddy loses (part of) its kinetic energy during one revolution. The kinetic energy of the eddy is proportional to  $v_\kappa^2$  and the time for one revolution is proportional to  $\ell_\kappa/v_\kappa$ . Hence, the energy spectral transfer rate,  $\varepsilon_\kappa$ , for an eddy of length scale  $1/\kappa$  can be estimated as (see Fig. 5.2)

$$\varepsilon_\kappa = \mathcal{O}\left(\frac{v_\kappa^2}{\ell_\kappa/v_\kappa}\right) = \mathcal{O}\left(\frac{v_\kappa^3}{\ell_\kappa}\right) \quad (5.14)$$

Kinetic energy is transferred per unit time to smaller and smaller eddies until the transfer takes place by dissipation (i.e. increased temperature) at the Kolmogorov scales. In the inertial subrange, the cascade process assumes that  $\varepsilon_\kappa = \varepsilon$ . Applying Eq. 5.14 for the large energy-containing eddies gives

$$\varepsilon_0 = \mathcal{O}\left(\frac{v_0^2}{\ell_0/v_0}\right) = \mathcal{O}\left(\frac{v_0^3}{\ell_0}\right) = \varepsilon_\kappa = \varepsilon \quad (5.15)$$

The dissipation at small scales (large wavenumbers) is determined by how much energy per unit time enters the cascade process at the large scales (small wavenumbers). We can now estimate the ratio between the large eddies (with  $v_0$  and  $\ell_0$ ) to the Kolmogorov eddies ( $v_\eta$  and  $\ell_\eta$ ). Equations 5.5 and 5.15 give

$$\begin{aligned} \frac{v_0}{v_\eta} &= (\nu \varepsilon)^{-1/4} v_0 = (\nu v_0^3 / \ell_0)^{-1/4} v_0 = (v_0 \ell_0 / \nu)^{1/4} = Re^{1/4} \\ \frac{\ell_0}{\ell_\eta} &= \left(\frac{\nu^3}{\varepsilon}\right)^{-1/4} \ell_0 = \left(\frac{\nu^3 \ell_0}{v_0^3}\right)^{-1/4} \ell_0 = \left(\frac{\nu^3}{v_0^3 \ell_0^3}\right)^{-1/4} = Re^{3/4} \\ \frac{\tau_0}{\tau_\eta} &= \left(\frac{\nu \ell_0}{v_0^3}\right)^{-1/2} \tau_0 = \left(\frac{v_0^3}{\nu \ell_0}\right)^{1/2} \frac{\ell_0}{v_0} = \left(\frac{v_0 \ell_0}{\nu}\right)^{1/2} = Re^{1/2} \end{aligned} \quad (5.16)$$

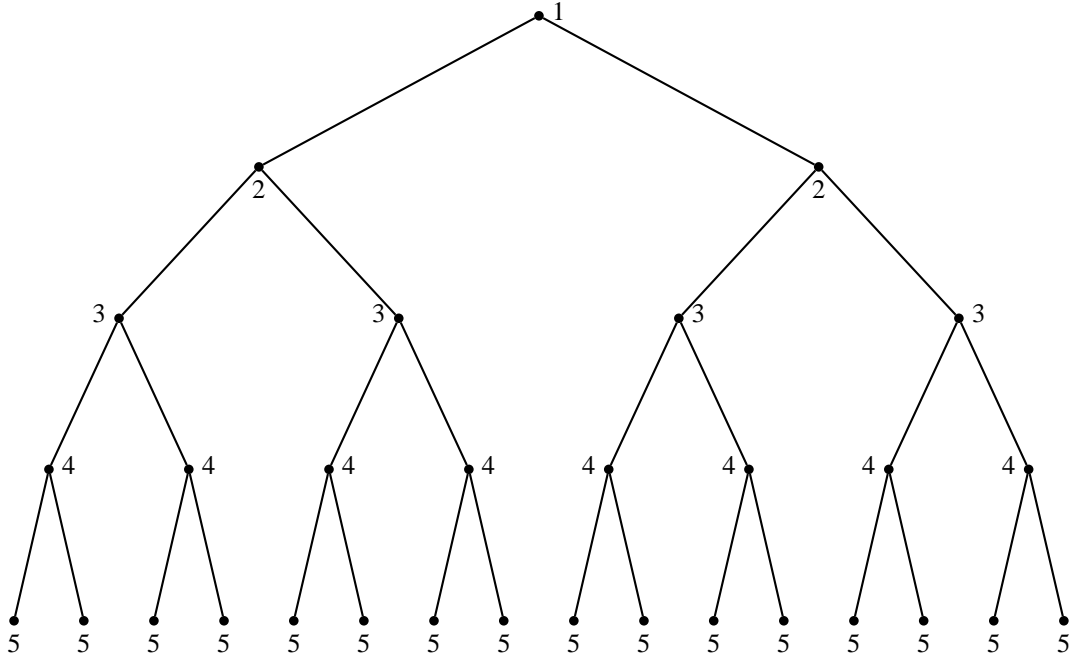


Figure 5.3: Family tree of turbulent eddies (see also Table 5.1). Five generations. The large original eddy, with axis aligned in the  $x_1$  direction, is 1<sup>st</sup> generation. Adapted from [9]

where  $Re = v_0 \ell_0 / \nu$ . We find that the ratio of the velocity, length and time scales of the energy-containing eddies to the Kolmogorov eddies increases with increasing Reynolds number. This means that the eddy range (wavenumber range) of the intermediate region, (region II, the inertial region), increases with increasing Reynolds number. Hence, the larger the Reynolds number, the larger the wavenumber range of the intermediate range where the eddies are independent of both the large scales and the viscosity.

#### 5.4 The cascade process created by vorticity

The interaction between vorticity and velocity gradients is an essential ingredient to create and maintain turbulence. Disturbances are amplified by interaction between the vorticity vector and the velocity gradients; the disturbances are turned into chaotic, three-dimensional fluctuations, i.e. into turbulence. Two idealized phenomena in this interaction process can be identified: vortex stretching and vortex tilting.

The equation for the instantaneous vorticity ( $\omega_i = \bar{\omega}_i + \omega'_i$ ) reads (see Eq. 4.20)

$$\frac{\partial \omega_i}{\partial t} + v_j \frac{\partial \omega_i}{\partial x_j} = \omega_j \frac{\partial v_i}{\partial x_j} + \nu \frac{\partial^2 \omega_i}{\partial x_j \partial x_j} \quad (5.17)$$

$$\omega_i = \epsilon_{ijk} \frac{\partial v_k}{\partial x_j}$$

As we learnt in Section 4.2 this equation is not an ordinary convection-diffusion equation: it has an additional term on the right side which represents amplification and

generation	$x_1$	$x_2$	$x_3$
$1^{st}$	1	0	0
$2^{nd}$	0	1	1
$3^{rd}$	2	1	1
$4^{th}$	2	3	3
$5^{th}$	6	5	5
$6^{th}$	10	11	11
$7^{th}$	22	21	21

Table 5.1: Number of eddies at each generation with their axis aligned in the  $x_1$ ,  $x_2$  or  $x_3$  direction, see Fig. 5.3.

rotation/tilting of the vorticity lines (the first term on the right side). The  $i = j$  components of this term represent (see Eq. 4.21) *vortex stretching*. A positive  $\partial v_1 / \partial x_1$  will stretch the cylinder, see Fig. 4.2 and from the requirement that the volume must not change (incompressible continuity equation) we find that the radius of the cylinder will decrease. We have neglected the viscosity since viscous diffusion at high Reynolds number is much smaller than the turbulent one and since viscous dissipation occurs at small scales (see p. 44). Thus we can assume that there are no viscous stresses acting on the cylindrical fluid element surface which means that the angular momentum

$$r^2 \omega_1 = \text{const.} \quad (5.18)$$

remains constant as the radius of the fluid element decreases. Note that also the circulation,  $\Gamma$  – which is the integral of the tangential velocity round the perimeter, see Eq. 1.19 – is constant. Equation 5.18 shows that the vorticity increases if the radius decreases (and vice versa). As was mentioned above, the continuity equation shows that stretching results in a decrease of the radius of a slender fluid element and an increase of the vorticity component (i.e. the tangential velocity component) aligned with the element. For example, an extension of a fluid element in one direction ( $x_1$  direction) decreases the length scales in the  $x_2$  direction and increases  $\omega'_1$ , see Fig. 5.4. The increased  $\omega'_1$  means that the velocity scale in the  $x_2$  direction is increased, see Fig. 5.5. The increased  $v'_2$  velocity component will stretch smaller fluid elements aligned in the  $x_2$  direction, see Fig. 5.5. This will increase their vorticity  $\omega'_2$  and decrease its radius,  $r_2$ . In the same way will the increased  $\omega'_1$  also stretch a fluid element aligned in the  $x_3$  direction and increase  $\omega'_3$  and decrease  $r_3$ . At each stage, the length scale of the eddies – whose velocity scale are increased – decreases. Figure 5.3 illustrates how a large eddy whose axis is oriented in the  $x_1$  axis in a few generations creates – through vortex stretching – smaller and smaller eddies with larger and larger velocity gradients. Here a generation is related to a wavenumber in the energy spectrum (Fig. 5.2); young generations correspond to high wavenumbers. The smaller the eddies, the less the original orientation of the large eddy is recalled. In other words, the small eddies “don’t remember” the characteristics of their original ancestor. The small eddies have no preferred direction. They are *isotropic*. The creation of multiple eddies by vortex stretching from one original eddy is illustrated in Fig. 5.3 and Table 5.1. The large original eddy ( $1^{st}$  generation) is aligned in the  $x_1$  direction. It creates eddies in the  $x_2$  and  $x_3$  direction ( $2^{nd}$  generation), which in turn each create new eddies in the  $x_1$  and  $x_3$  ( $3^{rd}$  generation) and so on. For each generation the eddies become more and more isotropic as they get smaller.

### Vortex stretching

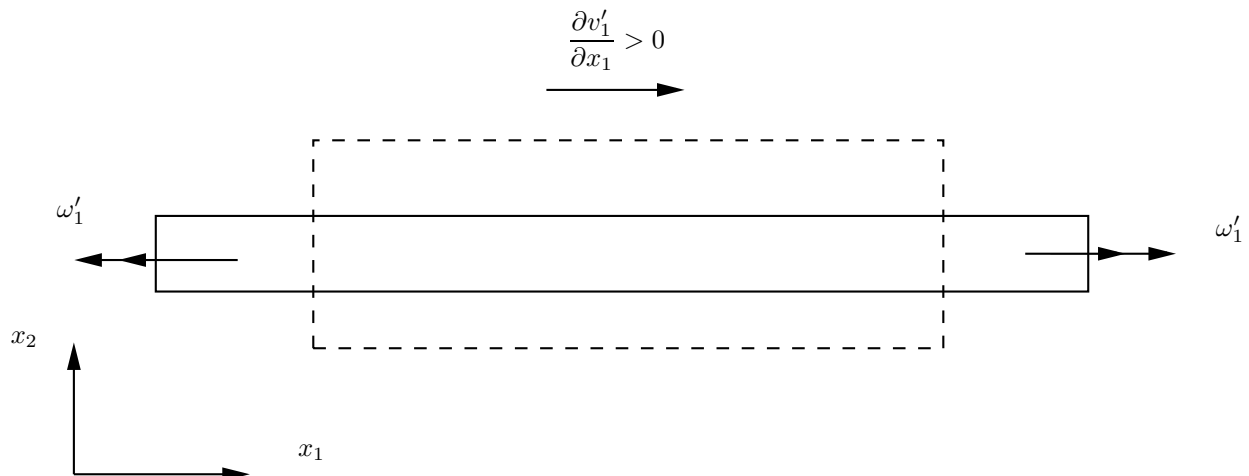


Figure 5.4: A fluid element is stretched by  $\frac{\partial v'_1}{\partial x_1} > 0$ . Its radius decreases (from dashed line to solid line).

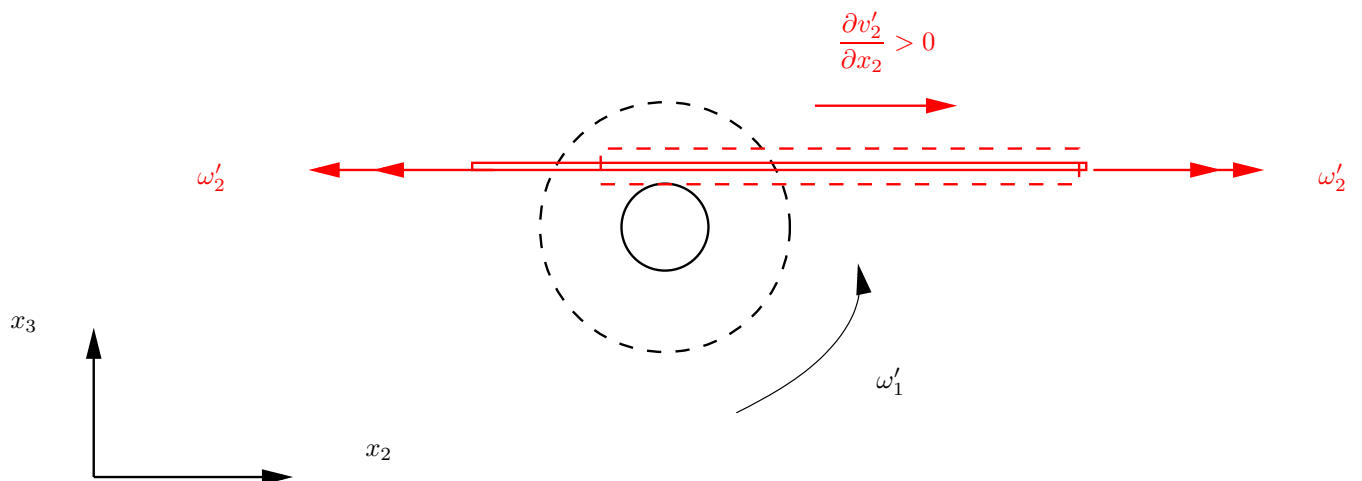


Figure 5.5: The rotation rate of the fluid element (black circles) in Fig. 5.4 increases and its radius decreases. This creates a positive  $\frac{\partial v'_2}{\partial x_2} > 0$  which stretches the small red fluid element aligned in the  $x_2$  direction and increases  $\omega'_2$ . The radius of the red fluid element decreases.

The  $i \neq j$  components in the first term on the right side in Eq. 4.21 represent *vortex tilting*. Again, take a slender fluid element, now with its axis aligned with the  $x_2$  axis, Fig. 4.2. The velocity gradient  $\partial v_1 / \partial x_2$  will tilt the fluid element so that it rotates in the clock-wise direction. As a result, the second term  $\omega_2 \partial v_1 / \partial x_2$  in line one in Eq. 4.21 gives a contribution to  $\omega_1$ . This shows how vorticity in one direction is transferred to the other two directions through vortex tilting.

Vortex stretching and vortex tilting qualitatively explain how interaction between vorticity and velocity gradient create vorticity in all three coordinate directions from a disturbance which initially was well defined in one coordinate direction. Once this process has started it continues, because vorticity generated by vortex stretching and vortex tilting interacts with the velocity field and creates further vorticity and so on. The vorticity and velocity field becomes chaotic and three-dimensional: turbulence has been created. The turbulence is also maintained by these processes.

From the discussion above we can now understand why turbulence always must be three-dimensional (Item IV on p. 43). If the instantaneous flow is two-dimensional ( $x_1 - x_2$  plane) we find that the vortex-stretching/tilting term on the right side of Eq. 5.17 vanishes because the vorticity vector and the velocity vector are orthogonal. The only non-zero component of vorticity vector is  $\omega_3$  because

$$\begin{aligned}\omega_1 &= \frac{\partial v_3}{\partial x_2} - \frac{\partial v_2}{\partial x_3} \equiv 0 \\ \omega_2 &= \frac{\partial v_1}{\partial x_3} - \frac{\partial v_3}{\partial x_1} \equiv 0.\end{aligned}$$

Since  $v_3 = 0$ , we get  $\omega_j \partial v_i / \partial x_j = 0$ .

**Vortex  
tilting**

## 6 Turbulent mean flow

### 6.1 Time averaged Navier-Stokes

When the flow is turbulent it is preferable to decompose the instantaneous variables (for example the velocity components and the pressure) into a mean value and a fluctuating value, i.e.

$$\begin{aligned} v_i &= \bar{v}_i + v'_i \\ p &= \bar{p} + p' \end{aligned} \quad (6.1)$$

where the bar,  $\bar{\cdot}$ , denotes the time averaged value. One reason why we decompose the variables is that when we measure flow quantities we are usually interested in their mean values rather than their time histories. Another reason is that when we want to solve the Navier-Stokes equation numerically it would require a very fine grid to resolve all turbulent scales and it would also require a fine resolution in time (turbulent flow is always unsteady).

The continuity equation and the Navier-Stokes equation for incompressible flow with constant viscosity read

$$\frac{\partial v_i}{\partial x_i} = 0 \quad (6.2)$$

$$\rho \frac{\partial v_i}{\partial t} + \rho \frac{\partial v_i v_j}{\partial x_j} = - \frac{\partial p}{\partial x_i} + \mu \frac{\partial^2 v_i}{\partial x_j \partial x_j} \quad (6.3)$$

The gravitation term,  $-\rho g_i$ , has been omitted which means that the  $p$  is the *hydrostatic* pressure (i.e. when  $v_i \equiv 0$ , then  $p \equiv 0$ , see p. 32). Inserting Eq. 6.1 into the continuity equation (6.2) and the Navier-Stokes equation (6.3) we obtain the *time averaged* continuity equation and Navier-Stokes equation

$$\frac{\partial \bar{v}_i}{\partial x_i} = 0 \quad (6.4)$$

$$\rho \frac{\partial \bar{v}_i \bar{v}_j}{\partial x_j} = - \frac{\partial \bar{p}}{\partial x_i} + \frac{\partial}{\partial x_j} \left( \mu \frac{\partial \bar{v}_i}{\partial x_j} - \rho \bar{v}'_i \bar{v}'_j \right) \quad (6.5)$$

It is assumed that the mean flow is steady. This equation is the time-averaged Navier-Stokes equation and it is often called the *Reynolds equation*. A new term  $\rho \bar{v}'_i \bar{v}'_j$  appears on the right side of Eq. 6.5 which is called the *Reynolds stress tensor*. The tensor is symmetric (for example  $\bar{v}'_1 \bar{v}'_2 = \bar{v}'_2 \bar{v}'_1$ ). It represents correlations between fluctuating velocities. It is an additional stress term due to turbulence (fluctuating velocities) and it is unknown. We need a model for  $\bar{v}'_i \bar{v}'_j$  to close the equation system in Eq. 6.5. This is called the *closure problem*: the number of unknowns (ten: three velocity components, pressure, six stresses) is larger than the number of equations (four: the continuity equation and three components of the Navier-Stokes equations).

The continuity equation applies both for the instantaneous velocity,  $v_i$  (Eq. 6.2), and for the time-averaged velocity,  $\bar{v}_i$  (Eq. 6.4); hence it applies also for the fluctuating velocity,  $v'_i$ , i.e.

$$\frac{\partial v'_i}{\partial x_i} = 0 \quad (6.6)$$

**Reynolds equations**

**closure problem**

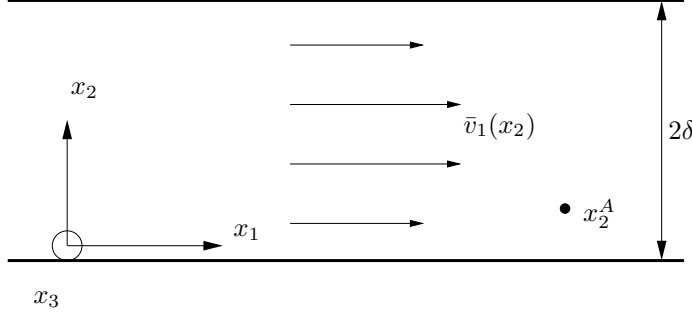


Figure 6.1: Flow between two infinite parallel plates. The width (i.e. length in the  $x_3$  direction) of the plates,  $Z_{max}$ , is much larger than the separation between the plates, i.e.  $Z_{max} \gg \delta$ .

### 6.1.1 Boundary-layer approximation

For steady ( $\partial/\partial t = 0$ ), two-dimensional ( $\bar{v}_3 = \partial/\partial x_3 = 0$ ) boundary-layer type of flow (i.e. boundary layers along a flat plate, channel flow, pipe flow, jet and wake flow, etc.) where

$$\bar{v}_2 \ll \bar{v}_1, \quad \frac{\partial \bar{v}_1}{\partial x_1} \ll \frac{\partial \bar{v}_1}{\partial x_2}, \quad (6.7)$$

First we re-write the left side of Eq. 6.5 using the continuity equation

$$\rho \frac{\partial \bar{v}_i \bar{v}_j}{\partial x_j} = \rho \bar{v}_j \frac{\partial \bar{v}_i}{\partial x_j} + \underbrace{\rho \bar{v}_i \frac{\partial \bar{v}_j}{\partial x_j}}_{=0} = \rho \bar{v}_j \frac{\partial \bar{v}_i}{\partial x_j} \quad (6.8)$$

Using Eq. 6.8. Eq. 6.5 can be written

$$\rho \bar{v}_1 \frac{\partial \bar{v}_1}{\partial x_1} + \rho \bar{v}_2 \frac{\partial \bar{v}_1}{\partial x_2} = - \frac{\partial \bar{p}}{\partial x_1} + \frac{\partial}{\partial x_2} \left[ \mu \frac{\partial \bar{v}_1}{\partial x_2} - \rho \overline{v'_1 v'_2} \right] \quad (6.9)$$

$x_1$  and  $x_2$  denote the streamwise and wall-normal coordinate, respectively, see Fig. 6.1. Note that the two terms on the left side are of the same order, because they both include the product of one large ( $\bar{v}_1$  or  $\partial/\partial x_2$ ) and one small ( $\bar{v}_2$  or  $\partial/\partial x_1$ ) part.

In addition to the viscous shear stress,  $\mu \partial \bar{v}_1 / \partial x_2$ , an additional *turbulent* one – a Reynolds shear stress – appears on the right side of Eq. 6.9. The total shear stress is thus

$$\tau_{12,tot} = \mu \frac{\partial \bar{v}_1}{\partial x_2} - \rho \overline{v'_1 v'_2} \quad (6.10)$$

## 6.2 Wall region in fully developed channel flow

The region near the wall is very important. Here the velocity gradient is largest as the velocity drops down to zero at the wall over a very short distance. One important quantity is the wall shear stress which is defined as

$$\tau_w = \mu \frac{\partial \bar{v}_1}{\partial x_2} \Big|_w \quad (6.11)$$

From the wall shear stress, we can define a *wall friction velocity*,  $u_\tau$ , as

$$\tau_w = \rho u_\tau^2 \Rightarrow u_\tau = \left( \frac{\tau_w}{\rho} \right)^{1/2} \quad (6.12)$$

In order to take a closer look at the near-wall region, let us, again, consider fully developed channel flow between two infinite plates, see Fig. 6.1. In fully developed channel flow, the streamwise derivative of the streamwise velocity component is zero (this is the definition of fully developed flow), i.e.  $\partial \bar{v}_1 / \partial x_1 = 0$ . The continuity equation gives now  $\bar{v}_2 = 0$ , see Eq. 3.18 at p. 32. The first term on the left side of Eq. 6.9 is zero because we have fully developed flow ( $\partial \bar{v}_1 / \partial x_1 = 0$ ) and the last term is zero because  $\bar{v}_2 \equiv 0$ . The streamwise momentum equation, Eq. 6.9, can now be written

$$0 = -\frac{\partial \bar{p}}{\partial x_1} + \frac{\partial}{\partial x_2} \left( \mu \frac{\partial \bar{v}_1}{\partial x_2} - \rho \bar{v}'_1 \bar{v}'_2 \right) \quad (6.13)$$

We know that the first term is a function only of  $x_1$  and the two terms in parenthesis are functions of  $x_2$  only; hence they must be constant (see Eq. 3.24 and the text related to this equation), i.e.

$$\begin{aligned} -\frac{\partial \bar{p}}{\partial x_1} &= \text{-constant} \\ \frac{\partial}{\partial x_2} \left( \mu \frac{\partial \bar{v}_1}{\partial x_2} - \rho \bar{v}'_1 \bar{v}'_2 \right) &= \frac{\partial \tau_{12,tot}}{\partial x_2} = \text{constant} \end{aligned} \quad (6.14)$$

where the total stress,  $\tau_{12,tot}$ , is given by Eq. 6.10. Integrating Eq. 6.13 from  $x_2 = 0$  to  $x_2$

$$\tau_{12,tot}(x_2) - \tau_w = \frac{\partial \bar{p}}{\partial x_1} x_2 \Rightarrow \tau_{12,tot} = \tau_w + \frac{\partial \bar{p}}{\partial x_1} x_2 = \tau_w \left( 1 - \frac{x_2}{\delta} \right) \quad (6.15)$$

At the last step we used the fact that the pressure gradient balances the wall shear stress, i.e.  $-\partial \bar{p} / \partial x_1 = \tau_w / \delta$ , see Eq. 3.30 (note that  $h = 2\delta$ ) and Eq. 6.31.

The wall region can be divided into one outer and one inner region, see Fig. 6.2. The inner region includes the viscous region (dominated by the viscous diffusion) and the logarithmic region (dominated by turbulent diffusion); the logarithmic region is sometimes called the *inertial region*, because the turbulent stresses stem from the inertial (i.e. the non-linear convection) term. The buffer region acts as a transition region between these two regions where viscous diffusion of streamwise momentum is gradually replaced by turbulent diffusion. In the inner region, the total shear stress is approximately constant and equal to the wall shear stress  $\tau_w$ , see Fig. 6.3. Note that the total shear stress is constant only close to the wall (Fig. 6.3b); further away from the wall it decreases (in fully developed channel flow it decreases linearly with the distance from the wall, see Eq. 6.15 and Fig. 6.3a). The Reynolds shear stress vanishes at the wall because  $v'_1 = v'_2 = 0$ , and the viscous shear stress attains its wall-stress value  $\tau_w = \rho u_\tau^2$ . As we go away from the wall the viscous stress decreases and the turbulent one increases and at  $x_2^+ \simeq 11$  they are approximately equal. In the logarithmic layer the viscous stress is negligible compared to the Reynolds stress.

At the wall, the velocity gradient is directly related to the wall shear stress, i.e. (see Eq. 6.11 and 6.12)

$$\left. \frac{\partial \bar{v}_1}{\partial x_2} \right|_w = \frac{\tau_w}{\mu} = \frac{\rho}{\mu} u_\tau^2 = \frac{1}{\nu} u_\tau^2 \quad (6.16)$$

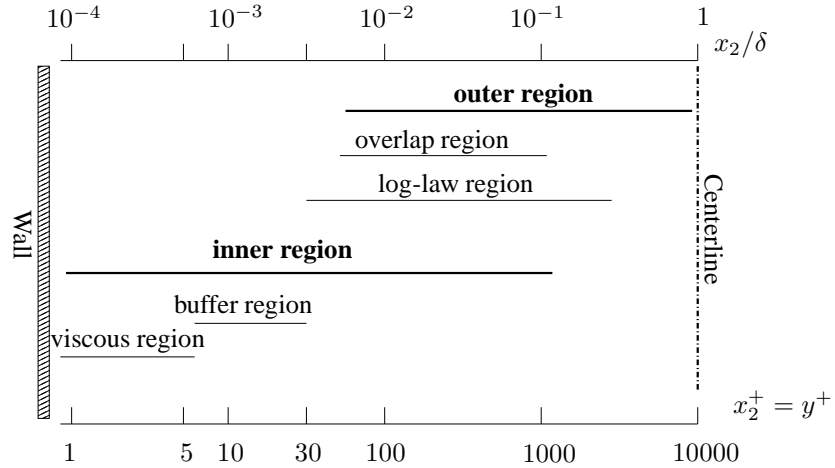


Figure 6.2: The wall region (adapted from Ch.7 in [7]) for  $Re_\tau = 10\,000$ .  $\delta$  denotes half width of the channel, see Fig. 6.1 and  $x_2^+ = x_2 u_\tau / \nu$  denotes the normalized wall distance.

Integration gives (recall that both  $\nu$  and  $u_\tau^2$  are constant)

$$\bar{v}_1 = \frac{1}{\nu} u_\tau^2 x_2 + C_1$$

Since the velocity,  $\bar{v}_1$ , is zero at the wall, the integration constant  $C_1 = 0$  so that

$$\frac{\bar{v}_1}{u_\tau} = \frac{u_\tau x_2}{\nu} \quad (6.17)$$

Equation 6.17 is expressed in *inner scaling* (or wall scaling) which means that  $\bar{v}_1$  and  $x_2$  are normalized with quantities related to the wall, i.e. the friction velocity stemming from the wall shear stress and the viscosity (here we regard viscosity as a quantity related to the wall, since the flow is dominated by viscosity). Often the plus-sign ('+') is used to denote inner scaling and equation Eq. 6.17 can then be written

$$\bar{v}_1^+ = x_2^+ \quad (6.18)$$

Further away from the wall at  $30 \lesssim x_2^+ \lesssim 3000$  (or  $0.003 \lesssim x_2/\delta \lesssim 0.3$ ), we encounter the *log-law region*, see Fig. 6.2. In this region the flow is assumed to be independent of viscosity. The Reynolds shear stress,  $\rho \bar{v}_1' \bar{v}_2'$ , is in the region  $x_2^+ \lesssim 200$  (i.e.  $x_2/\delta \lesssim 0.1$ ) fairly constant and approximately equal to  $\tau_w$ , see Fig. 6.3b. Hence the friction velocity,  $u_\tau$ , is a suitable velocity scale in the inner logarithmic region; it is used in the entire region.

What about the length scale? Near the wall, an eddy cannot be larger than the distance to the wall and it is the distance to the wall that sets an upper limit on the eddy-size. Hence it seems reasonable to take the wall distance as the characteristic length scale; a constant is added so that

$$\ell = \kappa x_2. \quad (6.19)$$

The velocity gradient can now be estimated as

$$\frac{\partial \bar{v}_1}{\partial x_2} = \frac{u_\tau}{\kappa x_2} \quad (6.20)$$

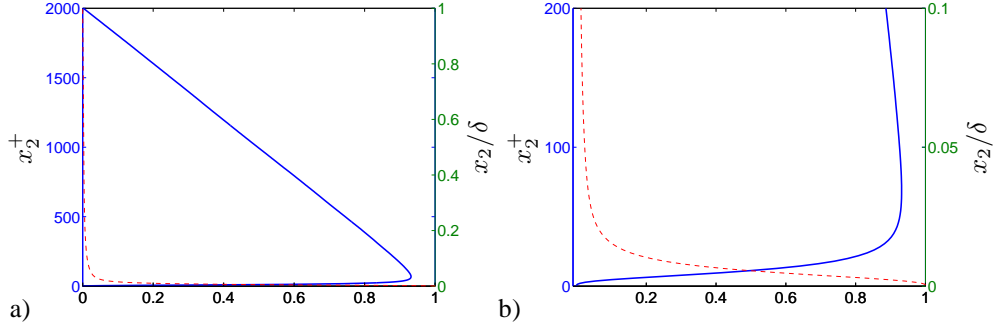


Figure 6.3: Reynolds shear stress.  $Re_\tau = 2000$ . a) lower half of the channel; b) zoom near the wall. DNS data [10, 11]. — :  $-\overline{v'_1 v'_2}/\tau_w$ ; - - - :  $\mu(\partial \bar{v}_1 / \partial x_2)/\tau_w$ .

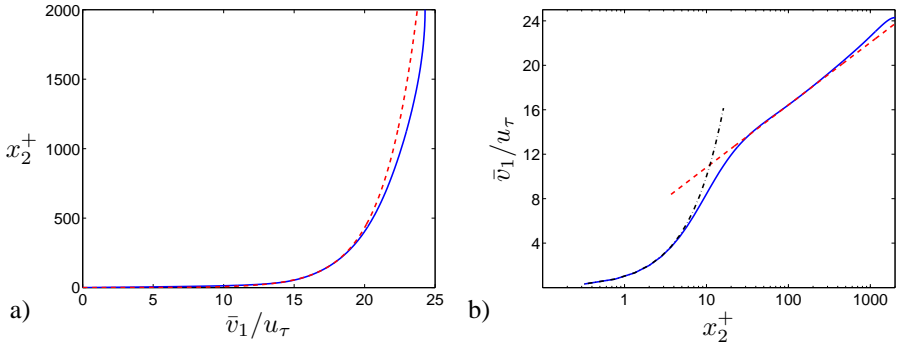


Figure 6.4: Velocity profiles in fully developed channel flow.  $Re_\tau = 2000$ . — : DNS data [10, 11]; - - - :  $\bar{v}_1/u_\tau = (\ln x_2^+)/0.41 + 5.2$ ; - - - - :  $\bar{v}_1/u_\tau = x_2^+$ .

based on the velocity scale,  $u_\tau$ , and the length scale  $\kappa x_2$ . Another way of deriving the expression in Eq. 6.20 is to use the Boussinesq assumption (see Eq. 11.30) in which a turbulent Reynolds stress is assumed to be equal to the product between the turbulent viscosity and the velocity gradient as

$$-\overline{v'_1 v'_2} = \nu_t \frac{\partial \bar{v}_1}{\partial x_2} \quad (6.21)$$

The turbulent viscosity,  $\nu_t$ , represents the turbulence and has the same dimension as  $\nu$ , i.e. [ $m^2/s$ ]. Hence  $\nu_t$  can be expressed as a product of a turbulent velocity scale and a turbulent length scale, and in the log-law region that gives

$$\nu_t = u_\tau \kappa x_2 \quad (6.22)$$

so that Eq. 6.21 gives (inserting  $-\overline{v'_1 v'_2} = u_\tau^2$ )

$$u_\tau^2 = \kappa u_\tau x_2 \frac{\partial \bar{v}_1}{\partial x_2} \Rightarrow \frac{\partial \bar{v}_1}{\partial x_2} = \frac{u_\tau}{\kappa x_2} \quad (6.23)$$

In non-dimensional form Eqs. 6.20 and 6.23 read

$$\frac{\partial \bar{v}_1^+}{\partial x_2^+} = \frac{1}{\kappa x_2^+} \quad (6.24)$$

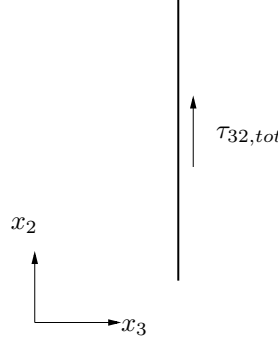


Figure 6.5: Symmetry plane of channel flow.

Integration gives now

$$\begin{aligned}\bar{v}_1^+ &= \frac{1}{\kappa} \ln(x_2^+) + B \quad \text{or} \\ \frac{\bar{v}_1}{u_\tau} &= \frac{1}{\kappa} \ln\left(\frac{x_2 u_\tau}{\nu}\right) + B\end{aligned}\tag{6.25}$$

where  $B$  is an integration constant. From Eq. 6.25 we can define the *viscous length scale*,  $\ell_\nu$ , as

$$x_2^+ = x_2/\ell_\nu \Rightarrow \ell_\nu = \frac{\nu}{u_\tau}\tag{6.26}$$

Equation 6.25 is the logarithmic law due to von Kármán [12]. The constant,  $\kappa$ , is called the von Kármán constant. The constants in the log-law are usually set to  $\kappa = 0.41$  and  $B = 5.2$ . log-law

As can be seen in Fig. 6.2 the log-law applies for  $x_2^+ \lesssim 3000$  ( $x_2/\delta \lesssim 0.3$ ). Figure 6.4 – where the Reynolds number is lower than in Fig. 6.2 – show that the log-law fit the DNS up to  $x_2^+ \lesssim 500$  ( $x_2/\delta \lesssim 0.25$ ).

In the outer region of the boundary layer, the relevant length scale is the boundary layer thickness. The resulting velocity law is the *defect law*

$$\frac{\bar{v}_{1,c} - \bar{v}_1}{u_\tau} = F_D\left(\frac{x_2}{\delta}\right)\tag{6.27}$$

where  $c$  denotes centerline.

### 6.3 Reynolds stresses in fully developed channel flow

The flow is two-dimensional ( $\bar{v}_3 = 0$  and  $\partial/\partial x_3 = 0$ ). Consider the  $x_2 - x_3$  plane, see Fig. 6.5. Since nothing changes in the  $x_3$  direction, the viscous shear stress

$$\tau_{32} = \mu \left( \frac{\partial \bar{v}_3}{\partial x_2} + \frac{\partial \bar{v}_2}{\partial x_3} \right) = 0\tag{6.28}$$

because  $\bar{v}_3 = \partial \bar{v}_2 / \partial x_3 = 0$ . The turbulent part shear stress,  $\overline{v'_2 v'_3}$ , can be expressed using the Boussinesq assumption (see Eq. 11.30)

$$-\rho \overline{v'_2 v'_3} = \mu_t \left( \frac{\partial \bar{v}_3}{\partial x_2} + \frac{\partial \bar{v}_2}{\partial x_3} \right) = 0\tag{6.29}$$

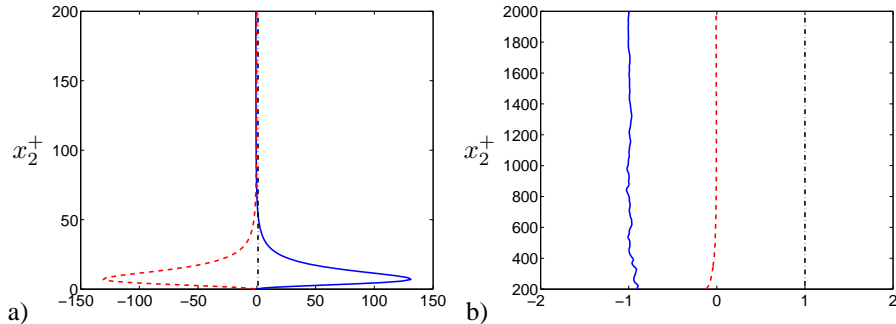


Figure 6.6: Fully developed channel flow.  $Re_\tau = 2000$ . Forces in the  $\bar{v}_1$  equation, see Eq. 6.13. a) near the lower wall of the channel; b) lower half of the channel excluding the near-wall region. DNS data [10, 11]. — :  $-\rho(\partial v'_1 v'_2 / \partial x_2) / \tau_w$ ; - - - :  $\mu(\partial^2 \bar{v}_1 / \partial x_2^2) / \tau_w$ ; - - :  $-(\partial \bar{p} / \partial x_1) / \tau_w$ .

and it is also zero since  $\bar{v}_3 = \partial \bar{v}_2 / \partial x_3 = 0$ . With the same argument,  $\overline{v'_1 v'_3} = 0$ . However note that  $\overline{v'_3}^2 = \overline{v_3^2} \neq 0$ . The reason is that although the *time-averaged* flow is two-dimensional (i.e.  $\bar{v}_3 = 0$ ), the instantaneous turbulent flow is always three-dimensional and unsteady. Hence  $v_3 \neq 0$  and  $v'_3 \neq 0$  so that  $v'_3^2 \neq 0$ . Consider, for example, the time series  $v_3 = v'_3 = (-0.25, 0.125, 0.125, -0.2, 0.2)$ . This gives

$$\bar{v}_3 = (-0.25 + 0.125 + 0.125 - 0.2 + 0.2)/5 = 0$$

but

$$\overline{v'_3}^2 = \overline{v_3^2} = [(-0.25)^2 + 0.125^2 + 0.125^2 + (-0.2)^2 + 0.2^2] / 5 = 0.03475 \neq 0.$$

Figure 6.3 presents the Reynolds and viscous shear stresses for fully developed flow. As can be seen, the viscous shear stress is negligible except very near the wall. It is equal to one near the wall and decreases rapidly for increasing wall distance. On the other hand, the Reynolds shear stress is zero at the wall (because the fluctuating velocities are zero at the wall) and increases for increasing wall distance. The intersection of the two shear stresses takes place at  $x_2^+ \simeq 11$ .

Looking at Eq. 6.13 we find that it is not really the shear stress that is interesting, but its gradient. The gradient of the shear stress,  $-\partial(\rho v'_1 v'_2) / \partial x_2$  and  $\mu \partial^2 \bar{v}_1 / \partial x_2^2$  represent, together with the pressure gradient,  $-\partial \bar{p} / \partial x_1$ , the *forces* acting on the fluid. Figure 6.6 presents the forces. Start by looking at Fig. 6.6b which shows the forces in the region away from the wall. The pressure gradient is constant and equal to one: this is the force *driving* the flow. This agrees – fortunately – with our intuition. We can imagine that the fluid (air, for example) is driven by a fan. Another way to describe the behaviour of the pressure is to say that there is a pressure drop. The pressure must decrease in the streamwise direction so that the pressure gradient term,  $-\partial \bar{p} / \partial x_1$ , in Eq. 6.13 takes a positive value which pushes the flow in the  $x_1$  direction. The force that balances the pressure gradient is the gradient of the Reynolds shear stress. This is the force *opposing* the movement of the fluid. This opposing force has its origin at the walls due to the viscous wall force (viscous shear stress multiplied by area).

Now let's have a look at the forces in the near-wall region, see Fig. 6.6a. Here the forces are two orders of magnitude larger than in Fig. 6.6b but they act over a very thin region ( $x_2^+ \leq 40$  or  $x_2/\delta < 0.02$ ). In this region the shear stress gradient term is

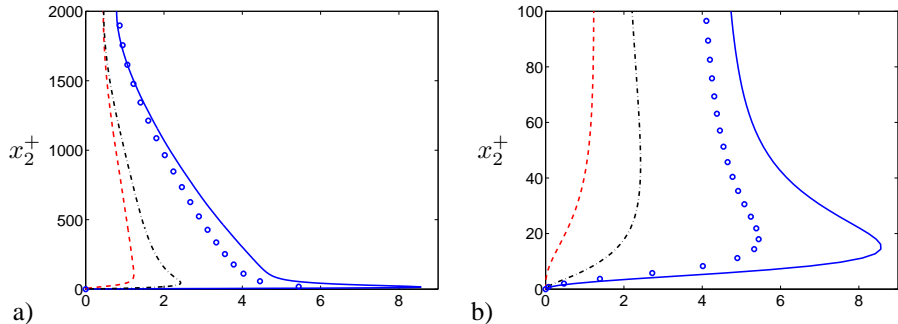


Figure 6.7: Normal Reynolds stresses and turbulent kinetic energy.  $Re_\tau = 2000$ . DNS data [10, 11]. —:  $\rho v_1'^2 / \tau_w$ ; - - :  $\rho v_2'^2 / \tau_w$ ; - · - :  $\rho v_3'^2 / \tau_w$ ; ○:  $k / u_\tau^2$ .

driving the flow and the opposing force is the viscous force. We can of course make a force balance for a section of the channel, as we did for laminar flow, see Eq. 3.36 at p. 34 and Fig. 3.8 at p. 34 which reads

$$0 = \bar{p}_1 Z_{max} 2\delta - \bar{p}_2 Z_{max} 2\delta - 2\tau_w L Z_{max} \quad (6.30)$$

where  $L$  is the length of the section. We get

$$\frac{\Delta \bar{p}}{L} = -\frac{\partial \bar{p}}{\partial x_1} = \frac{\tau_w}{\delta} \quad (6.31)$$

As can be seen the pressure drop is directly related to the wall shear stress. In turbulent flow the velocity profile in the center region is much flatter than in laminar flow (cf. Fig. 6.4 and Fig. 3.7 at p. 33). This makes the velocity gradient near the wall (and the wall shear stress,  $\tau_w$ ) much larger in turbulent flow than in laminar flow: Eq. 6.31 shows why the pressure drop is larger in the former case compared to the latter; or — in other words — why a larger fan is required to push the flow in turbulent flow than in laminar flow.

Figure 6.7 presents the normal Reynolds stresses,  $\rho v_1'^2$ ,  $\rho v_2'^2$  and  $\rho v_3'^2$ . As can be seen, the streamwise stress is largest and the wall-normal stress is smallest. The former is largest because the mean flow is in this direction; the latter is smallest because the turbulent fluctuations are damped by the wall. The turbulent kinetic energy,  $k = \overline{v_i' v_i'}/2$ , is also included. Note that this is smaller than  $v_1'^2$ .

## 6.4 Boundary layer

Up to now we have mainly discussed fully developed channel flow. What is the difference between that flow and a boundary layer flow? First, in a boundary layer flow the convective terms are not zero (or negligible), i.e. the left side of Eq. 6.9 is not zero. The flow in a boundary layer is continuously developing, i.e. its thickness,  $\delta$ , increases continuously for increasing  $x_1$ . The flow in a boundary layer is described by Eq. 6.9. Second, in a boundary layer flow the wall shear stress is not determined by the pressure drop; the convective terms must also be taken into account. Third, the outer part of the boundary layer is highly intermittent, consisting of turbulent/non-turbulent motion.

However, the inner region of a boundary layer ( $x_2/\delta < 0.1$ ) is principally the same as for the fully developed channel flow, see Fig. 6.8: the linear and the log-law regions

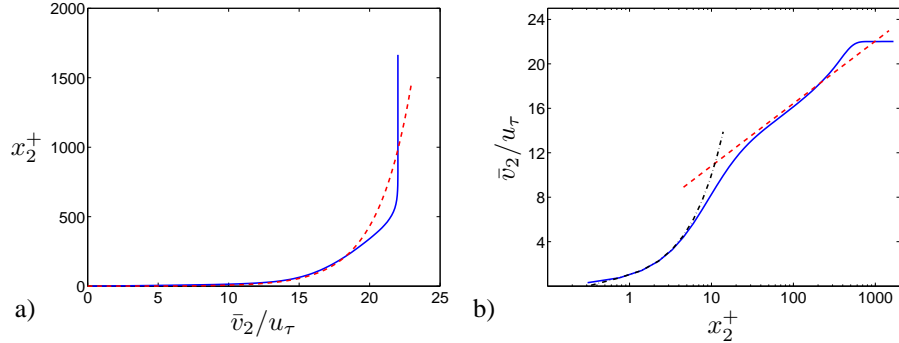
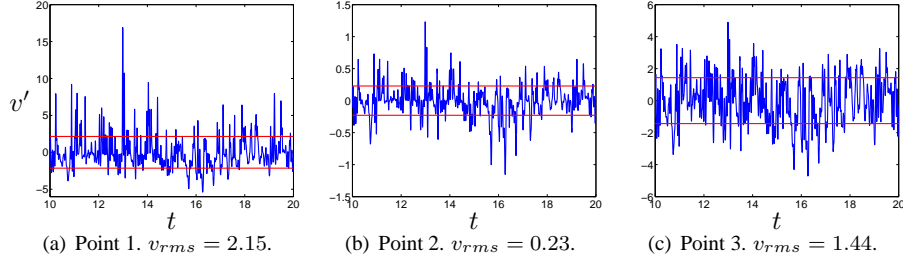


Figure 6.8: Velocity profiles in a boundary layer along a flat plate. — : DNS data [13];  
 - - :  $\bar{v}_2/u_\tau = (\ln x_2^+)/0.41 + 5.2$ ; - · - :  $\bar{v}_2/u_\tau = x_2^+$ .

are very similar for the two flows. However, in boundary layer flow the log-law is valid only up to approximately  $x_2/\delta \simeq 0.1$  (compared to approximately  $x_2/\delta \simeq 0.3$  in channel flow)

Figure 7.1: Time history of  $v'$ . Horizontal red lines show  $\pm v_{rms}$ .

## 7 Probability density functions

Some statistical information is obtained by forming the mean and second moments, for example  $\bar{v}$  and  $\overline{v'^2}$ , as was done in Section 6. The *root-mean-square* (RMS) can be defined from the second moment as

$$v_{rms} = \left( \overline{v'^2} \right)^{1/2} \quad (7.1)$$

The RMS is the same as the *standard deviation* which is equal to the square-root of the *variance*. In order to extract more information, probability density function is a useful statistical tool to analyze turbulence. From the velocity signals we can compute the probability densities (sometimes called *histograms*). With a probability density,  $f_v$ , of the  $v$  velocity, the mean velocity is computed as

$$\bar{v} = \int_{-\infty}^{\infty} v f_v(v) dv \quad (7.2)$$

Normalize the probability functions, so that

$$\int_{-\infty}^{\infty} f_v(v) dv = 1 \quad (7.3)$$

Here we integrate over  $v$ . The mean velocity can of course also be computed by integrating over time, as we do when we define a time average, (see Eq. 6.1 at p. 53), i.e.

$$\bar{v} = \frac{1}{2T} \int_{-T}^{T} v dt \quad (7.4)$$

where  $T$  is “sufficiently” large.

Consider the probability density functions of the fluctuations. The second moment corresponds to the variance of the fluctuations (or the square of the RMS, see Eq. 7.1), i.e.

$$\overline{v'^2} = \int_{-\infty}^{\infty} v'^2 f_{v'}(v') dv' \quad (7.5)$$

As in Eq. 7.4,  $\overline{v'^2}$  is usually computed by integrating in time, i.e.

$$\overline{v'^2} = \frac{1}{2T} \int_{-T}^{T} v'^2(t) dt$$

A probability density function is symmetric if positive values are as frequent and large as the negative values. Figure 7.1 presents the time history of the  $v'$  history at

**root-mean-square**  
**RMS**

**standard deviation**  
**variance**

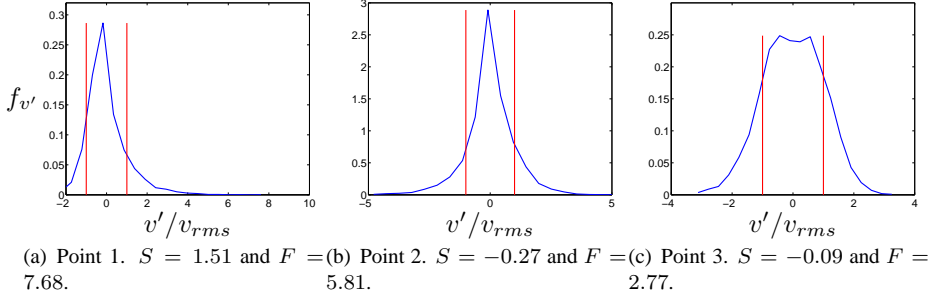


Figure 7.2: Probability density functions av time histories in Fig. 7.1. Vertical red lines show  $\pm v_{rms}$ . The skewness,  $S$ , and the flatness,  $F$ , are given for the three time histories.

three different points in a flow (note that  $\bar{v}' = 0$ ). The red horizontal lines indicate the RMS value of  $v'$ . The resulting probability densities functions are shown in Fig. 7.2. The red vertical lines show plus and minus RMS of  $v'$ . Let us analyze the data at the three points.

**Point 1.** The time history of the velocity fluctuation (Fig. 7.1a) shows that there exists large positive values but no large negative values. The positive values are often larger than  $+v_{rms}$  (the peak is actually close to  $8v_{rms}$ ) but the negative values are seldom smaller than  $-v_{rms}$ . This indicates that the distribution of  $v'$  is skewed towards the positive side. This is confirmed in the PDF distribution, see Fig. 7.2a.

**Point 2.** The fluctuations at this point are much smaller and the positive values are as large the negative values; this means that the PDF should be symmetric which is confirmed in Fig. 7.2b. The extreme values of  $v'$  are approximately  $\pm 1.5v_{rms}$ , see Figs. 7.1b and 7.2b.

**Point 3.** At this point the time history (Fig. 7.1c) shows that the fluctuations are clustered around zero and much values are within  $\pm v_{rms}$ . The time history shows that the positive and the negative values have the same magnitude. The PDF function in Fig. 7.2c confirms that there are many value around zero, that the extreme value are small and that positive and negative values are equally frequent (i.e. the PDF is symmetric).

In Fig. 7.2 we can judge whether the PDF is symmetric, but instead of “looking” at the probability density functions, we should use a definition of the degree of symmetry, which is the *skewness*. It is defined as

$$\overline{v'^3} = \int_{-\infty}^{\infty} v'^3 f_{v'}(v') dv'$$

and is commonly normalized by  $v_{rms}^3$ , so that the skewness,  $S_{v'}$ , of  $v'$  is defined as

$$S_{v'} = \frac{1}{v_{rms}^3} \int_{-\infty}^{\infty} v'^3 f_{v'}(v') dv' = \frac{1}{2v_{rms}^3 T} \int_{-T}^{T} v'^3(t) dt$$

Note that  $f$  must be normalized (see Eq. 7.3).

skewness

There is yet another statistical quantity which sometimes is used for describing turbulent fluctuations, namely the *flatness*. The variance (the square of RMS) tells us how large the fluctuations are in average, but it does not tell us if the time history includes few very large fluctuations or if all are rather close to  $v_{rms}$ . The flatness gives this information, and it is defined computed from  $v'^4$  and normalized by  $v_{rms}^4$ , i.e. flatness

$$F = \frac{1}{v_{rms}^4} \int_{-\infty}^{\infty} v'^4 f_{v'}(v) dv$$

The fluctuations at Point 1 (see Fig. 7.1a) includes some samples which are very large and hence its flatness is large (see caption in Fig. 7.2a), whereas the fluctuation for Point 3 all mostly clustered within  $\pm 2v_{rms}$  giving a small flatness, see Fig. 7.1c and the caption in Fig. 7.2c. For a Gaussian distribution

$$f(v') = \frac{1}{v_{rms}} \exp\left(-\frac{v' - v_{rms}}{2v_{rms}^2}\right)$$

for which  $F = 3$ .

## 8 Transport equations for kinetic energy

In this section and Section 9 we will derive various transport equations. There are two tricks which often will be used. Both tricks simply use the product rule for derivative backwards.

**Trick 1:** Using the product rule we get

$$\frac{\partial A_i B_j}{\partial x_k} = A_i \frac{\partial B_j}{\partial x_k} + B_j \frac{\partial A_i}{\partial x_k} \quad (8.1)$$

This expression can be re-written as

$$A_i \frac{\partial B_j}{\partial x_k} = \frac{\partial A_i B_j}{\partial x_k} - B_j \frac{\partial A_i}{\partial x_k} \quad (8.2)$$

and then we call it the “product rule backwards”.

**Trick 2:** Using the product rule we get

$$\frac{1}{2} \frac{\partial A_i A_i}{\partial x_j} = \frac{1}{2} \left( A_i \frac{\partial A_i}{\partial x_j} + A_i \frac{\partial A_i}{\partial x_j} \right) = A_i \frac{\partial A_i}{\partial x_j} \quad (8.3)$$

This trick is usually used backwards, i.e.

$$A_i \frac{\partial A_i}{\partial x_j} = \frac{1}{2} \frac{\partial A_i A_i}{\partial x_j} \quad (8.4)$$

### 8.1 The Exact $k$ Equation

The equation for turbulent kinetic energy,  $k = \frac{1}{2} \overline{v'_i v'_i}$ , is derived from the Navier-Stokes equation. Again, we assume incompressible flow (constant density) and constant viscosity (cf. Eq. 6.3). We subtract Eq. 6.5 from Eq. 6.3 and divide by density, multiply by  $v'_i$  and time average which gives

$$\begin{aligned} & \overline{v'_i \frac{\partial}{\partial x_j} [v_i v_j - \bar{v}_i \bar{v}_j]} = \\ & -\frac{1}{\rho} \overline{v'_i \frac{\partial}{\partial x_i} [p - \bar{p}]} + \nu \overline{v'_i \frac{\partial^2}{\partial x_j \partial x_i} [v_i - \bar{v}_i]} + \overline{\frac{\partial v'_i v'_j}{\partial x_j} v'_i} \end{aligned} \quad (8.5)$$

Using  $v_j = \bar{v}_j + v'_j$ , the left side can be rewritten as

$$\overline{v'_i \frac{\partial}{\partial x_j} [(\bar{v}_i + v'_i)(\bar{v}_j + v'_j) - \bar{v}_i \bar{v}_j]} = \overline{v'_i \frac{\partial}{\partial x_j} [\bar{v}_i v'_j + v'_i \bar{v}_j + v'_i v'_j]}. \quad (8.6)$$

Using the continuity equation  $\partial v'_j / \partial x_j = 0$  (see Eq. 6.6), the first term is rewritten as

$$\overline{v'_i \frac{\partial}{\partial x_j} (\bar{v}_i v'_j)} = \overline{v'_i v'_j} \frac{\partial \bar{v}_i}{\partial x_j}. \quad (8.7)$$

For the second term in Eq. 8.6 we start using  $\partial \bar{v}_j / \partial x_j = 0$

$$\overline{v'_i \frac{\partial}{\partial x_j} (v'_i \bar{v}_j)} = \bar{v}_j v'_i \overline{\frac{\partial v'_i}{\partial x_j}} \quad (8.8)$$

Next, we use **Trick 2**

$$\bar{v}_j \left( v'_i \frac{\partial v'_i}{\partial x_j} \right) = \bar{v}_j \frac{\partial}{\partial x_j} \overline{\left( \frac{1}{2} v'_i v'_i \right)} = \bar{v}_j \frac{\partial}{\partial x_j} (k) = \frac{\partial}{\partial x_j} (\bar{v}_j k) \quad (8.9)$$

The third term in Eq. 8.6 can be written as (replace  $\bar{v}_j$  by  $v'_j$  and use the same technique as in Eq. 8.9)

$$\frac{1}{2} \frac{\partial}{\partial x_j} \overline{(v'_j v'_i v'_i)}. \quad (8.10)$$

The first term on the right side of Eq. 8.5 is re-written using the continuity equation as

$$-\frac{1}{\rho} v'_i \frac{\partial p'}{\partial x_i} = -\frac{1}{\rho} \frac{\partial p' v'_i}{\partial x_i} \quad (8.11)$$

The second term on the right side of Eq. 8.5 can be written

$$\nu \overline{v'_i \frac{\partial^2 v'_i}{\partial x_j \partial x_j}} = \nu \overline{\frac{\partial}{\partial x_j} \left( \frac{\partial v'_i}{\partial x_j} v'_i \right)} - \nu \overline{\frac{\partial v'_i}{\partial x_j} \frac{\partial v'_i}{\partial x_j}} \quad (8.12)$$

applying **Trick 1** (if we apply the product rule on the first term on the right side of Eq. 8.12 we get the left side and the second term on the right side). For the first term in Eq. 8.12 we use the same trick as in Eq. 8.9 so that

$$\begin{aligned} \nu \overline{\frac{\partial}{\partial x_j} \left( \frac{\partial v'_i}{\partial x_j} v'_i \right)} &= \nu \overline{\frac{\partial}{\partial x_j} \left( \frac{1}{2} \left( \frac{\partial v'_i}{\partial x_j} v'_i + \frac{\partial v'_i}{\partial x_j} v'_i \right) \right)} = \\ \nu \overline{\frac{\partial}{\partial x_j} \left( \frac{1}{2} \left( \frac{\partial v'_i}{\partial x_j} v'_i \right) \right)} &= \nu \frac{1}{2} \frac{\partial^2 v'_i v'_i}{\partial x_j \partial x_j} = \nu \frac{\partial^2 k}{\partial x_j \partial x_j} \end{aligned} \quad (8.13)$$

The last term on the right side of Eq. 8.5 is zero because it is time averaging of a fluctuation, i.e.  $\bar{a}\bar{b}' = \bar{a}\bar{b}' = 0$ . Now we can assemble the transport equation for the turbulent kinetic energy. Equations 8.7, 8.9, 8.11, 8.12 and 8.13 give

$$\underbrace{\frac{\partial \bar{v}_j k}{\partial x_j}}_I = -\underbrace{\overline{v'_i v'_j} \frac{\partial \bar{v}_i}{\partial x_j}}_{II} - \underbrace{\frac{\partial}{\partial x_j} \left[ \frac{1}{\rho} \overline{v'_j p'} + \frac{1}{2} \overline{v'_j v'_i v'_i} - \nu \frac{\partial k}{\partial x_j} \right]}_{III} - \underbrace{\nu \overline{\frac{\partial v'_i}{\partial x_j} \frac{\partial v'_i}{\partial x_j}}}_{IV} \quad (8.14)$$

The terms in Eq. 8.14 have the following meaning.

#### I. Convection.

**II. Production,  $P^k$ .** The large turbulent scales extract energy from the mean flow. This term (including the minus sign) is almost always positive. It is largest for the energy-containing eddies, i.e. for small wavenumbers, see Fig. 5.2.

**III.** The two first terms represent **turbulent diffusion** by pressure-velocity fluctuations, and velocity fluctuations, respectively. The last term is viscous diffusion.

**IV. Dissipation,  $\varepsilon$ .** This term is responsible for transformation of kinetic energy at small scales to thermal energy. The term (excluding the minus sign) is always positive (it consists of velocity gradients squared). It is largest for large wavenumbers, see Fig. 5.2

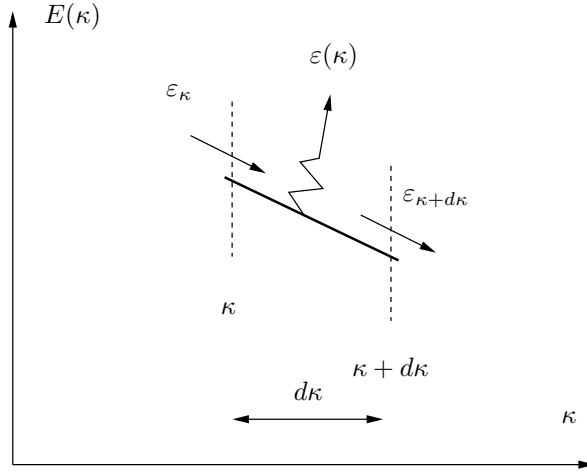


Figure 8.1: Zoom of the energy spectrum for a wavenumber located in Region II or III, see Fig. 5.2.

The transport equation for  $k$  can also be written in a simplified easy-to-read symbolic form as

$$C^k = P^k + D^k - \varepsilon \quad (8.15)$$

where  $C^k$ ,  $P^k$ ,  $D^k$  and  $\varepsilon$  correspond to terms I-IV in Eq. 8.14.

Above, it is stated that the production takes place at the large energy-containing eddies, i.e. we assume that the large eddies contribute much more to the production term more than the small eddies. There are two arguments for this:

1. The Reynolds stresses (which appear in  $P^k$ ) are larger for large eddies than for small eddies
2. In order to extract energy from the mean flow, the time scale of the eddy and the mean velocity gradient,  $\partial \bar{v}_i / \partial x_j$ , must be of the same magnitude. This requirement is best satisfied by the large scales. In the fully turbulent region of a boundary layer, for example, both time scales are proportional to  $\kappa x_2 / u_\tau$ . The magnitude of the velocity gradient is given by Eq. 6.20 and the time scale of a large eddy is given by  $\ell_0 / v_0 = \kappa x_2 / u_\tau$ . Actually, in the cascade process we argue that the smaller the eddies, the less they remember the characteristic of mean flow gradient (i.e. its magnitude, direction, time scale etc)

In the cascade process (see Section 5.3) we assume that the viscous dissipation,  $\varepsilon$ , takes places at the smallest scales. How do we know that the majority of the dissipation takes place at the smallest scales? First, let us investigate how the time scale varies with eddy size. Consider the inertial subrange. The energy that is transferred in spectral space per unit time,  $\varepsilon_\kappa$ , is equal to the viscous dissipation,  $\varepsilon$ . How large is  $\varepsilon$  at wavenumber  $\kappa$  (denoted by  $\varepsilon_\kappa$ )? Recall that the viscous dissipation,  $\varepsilon$ , is expressed as the viscosity times the square of the velocity gradient, see Eq. 8.14. The velocity gradient for an eddy characterized by velocity  $v_\kappa$  and lengthscale  $\ell_\kappa$  can be estimated as

$$\left( \frac{\partial v}{\partial x} \right)_\kappa \propto \frac{v_\kappa}{\ell_\kappa} \propto (v_\kappa^2)^{1/2} \kappa \quad (8.16)$$

since  $\ell_\kappa \propto \kappa^{-1}$ . Now we know that the energy spectrum  $E \propto v_\kappa^2/\kappa \propto \kappa^{-5/3}$  in the inertial region which gives

$$\left(\frac{\partial v}{\partial x}\right)_\kappa \propto \left(\kappa^{-2/3}\right)^{1/2} \kappa \propto \kappa^{-1/3} \kappa \propto \kappa^{2/3} \quad (8.17)$$

Thus the viscous dissipation at wavenumber  $\kappa$  can be estimated as

$$\varepsilon(\kappa) \propto \left(\frac{\partial v}{\partial x}\right)_\kappa^2 \propto \kappa^{4/3}, \quad (8.18)$$

i.e.  $\varepsilon(\kappa)$  does indeed increase for increasing wavenumber.

The energy transferred from eddy-to-eddy in spectral space can also be used for estimating the velocity gradient of an eddy. The cascade process assumes that this energy transfer is the same for each eddy, i.e.  $\varepsilon_\kappa = \varepsilon = v_\kappa^3/\ell_\kappa = \ell_\kappa^2/\tau_\kappa^3 = \ell_0^2/\tau_0^3$ , see Eq. 5.14. We find from  $\ell_\kappa^2/\tau_\kappa^3 = \ell_0^2/\tau_0^3$  that for decreasing eddy size (decreasing  $\ell_\kappa$ ), the time scale,  $\tau_\kappa$ , also decreases, i.e.

$$\tau_\kappa = \left(\frac{\ell_\kappa}{\ell_0}\right)^{2/3} \tau_0 \quad (8.19)$$

where  $\tau_0$  and  $\ell_0$  are constants (we have chosen the large scales,  $\tau_0$  and  $\ell_0$ ). Hence

$$\left(\frac{\partial v}{\partial x}\right)_\kappa = \tau_\kappa^{-1} \propto \ell_\kappa^{-2/3} \propto \kappa^{2/3}, \quad (8.20)$$

which is the same as Eq. 8.17.

### 8.1.1 Spectral transfer dissipation $\varepsilon_\kappa$ vs. “true” viscous dissipation, $\varepsilon$

As a final note to the discussion in the previous section, it may be useful to look at the difference between the spectral transfer dissipation  $\varepsilon_\kappa$ , and the “true” viscous dissipation,  $\varepsilon$ ; the former is the energy transferred from eddy to eddy per unit time, and the latter is the energy transformed per unit time to internal energy for the entire spectrum (occurring mainly at the small, dissipative scales), see Fig. 5.2. Now consider Fig. 8.1 which shows a zoom of the energy spectrum. We assume that no mean flow energy production occurs between  $\kappa$  and  $\kappa + d\kappa$ , i.e. the region may be in the  $-5/3$  region or in the dissipation region. Turbulent kinetic per unit time energy enters at wavenumber  $\kappa$  at a rate of  $\varepsilon_\kappa$  and leaves at wavenumber  $\kappa + d\kappa$  at a rate of  $\varepsilon_{\kappa+d\kappa}$ . If  $\kappa$  and  $\kappa + d\kappa$  are located in the inertial region (i.e. the  $-5/3$  region), then the usual assumption is that  $\varepsilon_\kappa \simeq \varepsilon_{\kappa+d\kappa}$  and that there is no viscous dissipation to internal energy, i.e.  $\varepsilon(\kappa) \simeq 0$ . If there is viscous dissipation at wavenumber  $\kappa$  (which indeed is the case if the zoomed region is located in the dissipative region), then  $\varepsilon(\kappa)$  is simply obtained through an energy balance, i.e.

$$\varepsilon(\kappa) = \varepsilon_{\kappa+d\kappa} - \varepsilon_\kappa \quad (8.21)$$

## 8.2 The Exact $k$ Equation: 2D Boundary Layers

In 2D boundary-layer flow, for which  $\partial/\partial x_2 \gg \partial/\partial x_1$  and  $\bar{v}_2 \ll \bar{v}_1$ , the exact  $k$  equation reads

$$\begin{aligned} \frac{\partial \bar{v}_1 k}{\partial x_1} + \frac{\partial \bar{v}_2 k}{\partial x_2} &= -\overline{v'_1 v'_2} \frac{\partial \bar{v}_1}{\partial x_2} \\ &- \frac{\partial}{\partial x_2} \left[ \frac{1}{\rho} \overline{p' v'_2} + \frac{1}{2} \overline{v'_2 v'_i v'_i} - \nu \frac{\partial k}{\partial x_2} \right] - \nu \frac{\partial v'_i}{\partial x_j} \frac{\partial v'_i}{\partial x_j} \end{aligned} \quad (8.22)$$

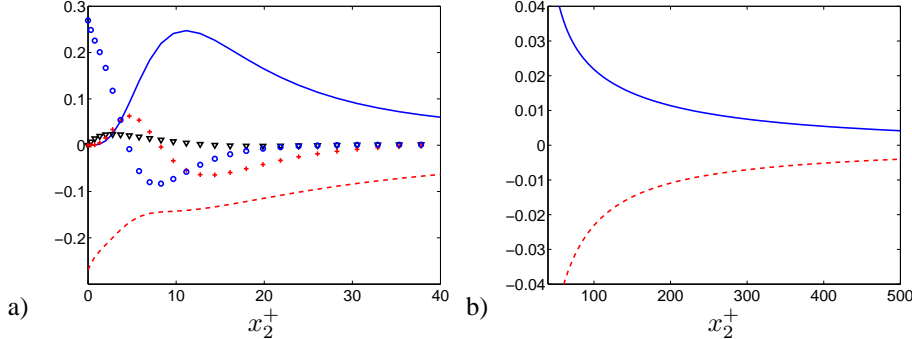


Figure 8.2: Channel flow at  $Re_\tau = 2000$ . Terms in the  $k$  equation scaled by  $u_\tau^4/\nu$ .  $Re_\tau = 2000$ . a) Zoom near the wall; b) Outer region. DNS data [10, 11].  $\text{---} : P^k$ ;  $\text{---} : -\varepsilon$ ;  $\nabla : -\partial \bar{v}' p' / \partial x_2$ ;  $+ : -\partial v'_1 v'_2 / 2 \partial x_2$ ;  $\circ : \nu \partial^2 k / \partial x_2^2$ .

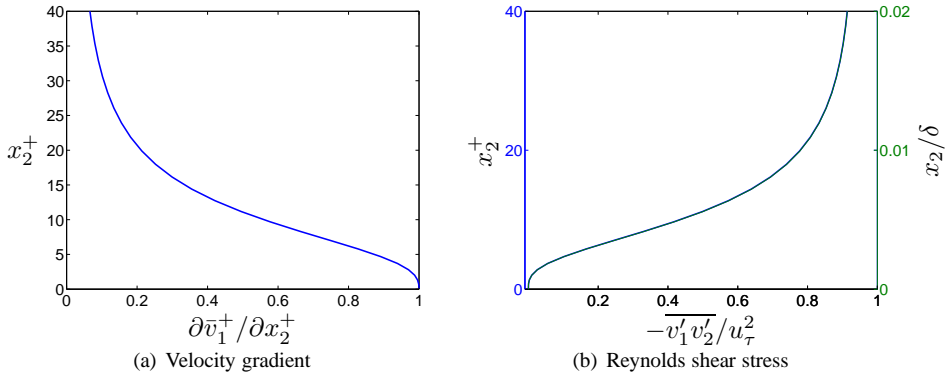


Figure 8.3: Channel flow at  $Re_\tau = 2000$ . DNS data [10, 11].

Note that the dissipation includes all derivatives. This is because the dissipation term is at its largest for small, isotropic scales for which all derivatives are of the same order and hence the usual boundary-layer approximation  $\partial/\partial x_1 \ll \partial/\partial x_2$  does not apply for these scales.

Figure 8.2 presents the terms in Eq. 8.22 for fully developed channel flow. The left side is – since the flow is fully developed – zero. In the outer region (Fig. 8.2b) all terms are negligible except the production term and the dissipation term which balance each other. This is called *local equilibrium*, see p. 70. Closer to the wall (Fig. 8.2a) the other terms do also play a role. Note that the production and the dissipation terms close to the wall are two orders of magnitude larger than in the logarithmic region (Fig. 8.2b). At the wall the turbulent fluctuations are zero which means that the production term is zero. Since the region near the wall is dominated by viscosity the turbulent diffusion terms due to pressure and velocity are also small. The dissipation term and the viscous diffusion term attain their largest value at the wall and they much be equal to each other since all other terms are zero or negligible.

The turbulence kinetic energy is produced by its main source term, the production term,  $P^k = -\bar{v}'_1 \bar{v}'_2 \partial \bar{v}_1 / \partial x_2$ . The velocity gradient is largest at the wall (see Fig. 8.3a) where the shear stress is zero (see Fig. 8.3b)); the former decreases and the magnitude of the latter increases with wall distance and their product takes its maximum at  $x_2^+ \simeq$

local equilibrium

11. Since  $P^k$  is largest here so is also  $k$ , see Fig. 6.7.  $k$  is transported in the  $x_2$  direction by viscous and turbulent diffusion and it is destroyed (i.e. dissipated) by  $\varepsilon$ .

### 8.3 Spatial vs. spectral energy transfer

In Section 5.3 we discussed *spectral* transfer of turbulent kinetic energy from large eddies to small eddies (which also applies to the transport of the Reynolds stresses). In Section 8.1 we derived the equation for *spatial* transport of turbulent kinetic energy. How are the spectral transfer and the spatial transport related? The reason that we in Section 5.3 only talked about spectral transfer was that we assumed homogeneous turbulence in which the spatial derivatives of the time-averaged turbulent quantities are zero, for example  $\partial \bar{v}_1^2 / \partial x_i = 0$ ,  $\partial k / \partial x_i = 0$  etc. (Note that the derivatives of the *instantaneous* turbulent fluctuations are non-zero even in homogeneous turbulence, i.e.  $\partial v'_1 / \partial x_i \neq 0$ ; the instantaneous flow field in turbulent flow is – as we mentioned at the very beginning at p. 43 – *always* three-dimensional and unsteady). In homogeneous turbulence the spatial transport terms (i.e. the convective term, term **I**, and the diffusion terms, term **III** in Eq. 8.14) are zero. Hence, in homogeneous turbulence there is no time-averaged spatial transport. However, there is *spectral transfer* of turbulent kinetic energy which takes place in wavenumber space, from large eddies to small eddies. The production term (term **II** in Eq. 8.14) corresponds to the process in which large energy-containing eddies extract energy from the mean flow. The dissipation term (term **IV** in Eq. 8.14) corresponds to transformation of the turbulent kinetic energy at the small eddies to thermal energy. However, real flows are hardly ever homogeneous. Some flows may have one or two homogeneous directions. Consider, for example, fully developed channel turbulent flow. If the channel walls are very long and wide compared to the distance between the walls,  $2\delta$ , then the turbulence (and the flow) is homogeneous in the streamwise direction and the spanwise direction, i.e.  $\partial \bar{v}_1 / \partial x_1 = 0$ ,  $\partial \bar{v}_i^2 / \partial x_1 = 0$ ,  $\partial \bar{v}_i^2 / \partial x_3 = 0$  etc.

**homogeneous turbulence**

In non-homogeneous turbulence, the cascade process is not valid. Consider a large, turbulent eddy at a position  $x_2^A$  (see Fig. 6.1) in fully developed channel flow. The instantaneous turbulent kinetic energy,  $k_\kappa = v'_{\kappa,i} v'_{\kappa,i} / 2$ , of this eddy may either be transferred in wavenumber space or transported in physical (spatial) space, or both. It may first be transported in physical space towards the center, and there lose its kinetic energy to smaller eddies. This should be kept in mind when thinking in terms of the cascade process. Large eddies which extract their energy from the mean flow may not give their energy to the slightly smaller eddies as assumed in Figs. 5.2 and 5.1, but  $k_\kappa$  may first be transported in physical space and then transferred in spectral space.

In the inertial range (Region II), however, the cascade process is still a good approximation even in non-homogeneous turbulence. The reason is that the transfer of turbulent kinetic energy,  $k_\kappa$ , from eddy-to-eddy, occurs at a much faster rate than the spatial transport by convection and diffusion. In other words, the time scale of the cascade process is much smaller than that of convection and diffusion which have no time to transport  $k_\kappa$  in space before it is passed on to a smaller eddy by the cascade process. We say that the turbulence at these scales is in *local equilibrium*. The turbulence in the buffer layer and the logarithmic layer of a boundary layer (see Fig. 6.2) is also in local equilibrium. In Townsend [14], this is (approximately) stated as:

**local equilibrium**

the local rates of turbulent kinetic energy (i.e. production and dissipation) are so large that aspects of the turbulent motion concerned with these processes are independent of conditions elsewhere in the flow.

This statement simply means that production is equal to dissipation, i.e.  $P^k = \varepsilon$ , see Fig. 8.2.

In summary, care should be taken in non-homogeneous turbulence, regarding the validity of the cascade process for the large scales (Region I).

## 8.4 The overall effect of the transport terms

The overall effect (i.e. the net effect) of the production term is to increase  $k$ , i.e. if we integrate the production term over the entire domain,  $V$ , we get

$$\int_V P_k dV > 0 \quad (8.23)$$

Similarly, the net effect of the dissipation term is a negative contribution, i.e.

$$\int_V -\varepsilon dV < 0 \quad (8.24)$$

What about the *transport* terms, i.e. convection and diffusion? Integration of the convection term over the entire volume,  $V$ , gives, using Gauss divergence law,

$$\int_V \frac{\partial \bar{v}_j k}{\partial x_j} dV = \int_S \bar{v}_j k n_j dS \quad (8.25)$$

where  $S$  is the bounding surface of  $V$ . This shows that the net effect of the convection term occurs only at the boundaries. Inside the domain, the convection merely transports  $k$  without adding or subtracting anything to the integral of  $k$ ,  $\int_V k dV$ ; the convection acts as a source term in part of the domain, but in the remaining part of the domain it acts as an equally large sink term. Similarly for the diffusion term, we get

$$\begin{aligned} & - \int_V \frac{\partial}{\partial x_j} \left( \frac{1}{2} \bar{v}'_j \bar{v}'_k \bar{v}'_k + \frac{1}{\rho} \bar{p}' \bar{v}'_j - \nu \frac{\partial k}{\partial x_j} \right) V \\ &= - \int_S \left( \frac{1}{2} \bar{v}'_j \bar{v}'_k \bar{v}'_k + \frac{1}{\rho} \bar{p}' \bar{v}'_j - \nu \frac{\partial k}{\partial x_j} \right) n_j dS \end{aligned} \quad (8.26)$$

The only net contribution occurs at the boundaries. Hence, Eqs. 8.25 and 8.26 show that the transport terms only – as the word implies – *transports*  $k$  without giving any net effect except at the boundaries. Mathematically these terms are called *divergence terms*, i.e. they can both be written as the divergence of a vector  $A_j$ ,

$$\frac{\partial A_j}{\partial x_j} \quad (8.27)$$

where  $A_j$  for the convection and the diffusion term reads

$$A_j = \begin{cases} \bar{v}_j k & \text{convection term} \\ - \left( \frac{1}{2} \bar{v}'_j \bar{v}'_k \bar{v}'_k + \frac{1}{\rho} \bar{p}' \bar{v}'_j - \nu \frac{\partial k}{\partial x_j} \right) & \text{diffusion term} \end{cases} \quad (8.28)$$

## 8.5 The transport equation for $\bar{v}_i \bar{v}_i / 2$

The equation for  $K = \bar{v}_i \bar{v}_i / 2$  is derived in the same way as that for  $\bar{v}'_i \bar{v}'_i / 2$ . Multiply the time-averaged Navier-Stokes equations, Eq. 6.5, by  $\bar{v}_i$  so that

$$\bar{v}_i \frac{\partial \bar{v}_i \bar{v}_j}{\partial x_j} = -\frac{1}{\rho} \bar{v}_i \frac{\partial \bar{p}}{\partial x_i} + \nu \bar{v}_i \frac{\partial^2 \bar{v}_i}{\partial x_j \partial x_j} - \bar{v}_i \frac{\partial \bar{v}'_i \bar{v}'_j}{\partial x_j}. \quad (8.29)$$

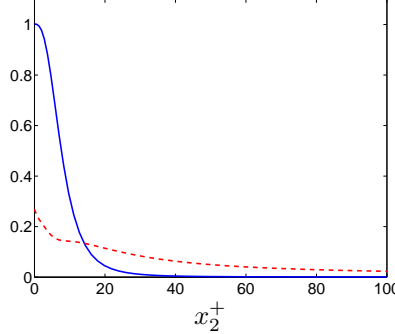


Figure 8.4: Channel flow at  $Re_\tau = 2000$ . Comparison of mean and fluctuating dissipation terms. Both terms are normalized by  $u_\tau^4/\nu$ . DNS data [10, 11]. — :  $\nu(\partial \bar{v}_1 / \partial x_2)^2$ ; - - - :  $\varepsilon$ .

Using the continuity equation and **Trick 2** the term on the left side can be rewritten as

$$\bar{v}_i \frac{\partial \bar{v}_i \bar{v}_j}{\partial x_j} = \bar{v}_j \bar{v}_i \frac{\partial \bar{v}_i}{\partial x_j} = \frac{1}{2} \bar{v}_j \frac{\partial \bar{v}_i \bar{v}_i}{\partial x_j} = \frac{\partial \bar{v}_j K}{\partial x_j} \quad (8.30)$$

Using the continuity equation, the first term on the right side of Eq. 8.29 can be written as

$$-\bar{v}_i \frac{\partial \bar{p}}{\partial x_i} = -\frac{\partial \bar{v}_i \bar{p}}{\partial x_i}. \quad (8.31)$$

The viscous term in Eq. 8.29 is rewritten in the same way as the viscous term in Section 8.1, see Eqs. 8.12 and 8.13, i.e.

$$\nu \bar{v}_i \frac{\partial^2 \bar{v}_i}{\partial x_j \partial x_j} = \nu \frac{\partial K}{\partial x_j \partial x_j} - \nu \frac{\partial \bar{v}_i}{\partial x_j} \frac{\partial \bar{v}_i}{\partial x_j}. \quad (8.32)$$

Equations 8.30, 8.31 and 8.32 inserted in Eq. 8.29 gives

$$\frac{\partial \bar{v}_j K}{\partial x_j} = \nu \frac{\partial^2 K}{\partial x_j \partial x_j} - \frac{1}{\rho} \frac{\partial \bar{v}_i \bar{p}}{\partial x_i} - \nu \frac{\partial \bar{v}_i}{\partial x_j} \frac{\partial \bar{v}_i}{\partial x_j} - \bar{v}_i \frac{\partial \bar{v}'_i \bar{v}'_j}{\partial x_j}. \quad (8.33)$$

The last term is rewritten using **Trick 1** as

$$-\bar{v}_i \frac{\partial \bar{v}'_i \bar{v}'_j}{\partial x_j} = -\frac{\partial \bar{v}_i \bar{v}'_i \bar{v}'_j}{\partial x_j} + \bar{v}'_i \bar{v}'_j \frac{\partial \bar{v}_i}{\partial x_j}. \quad (8.34)$$

Note that the first term on the right side differs to the corresponding term in Eq. 8.14 by a factor of two since “Trick 2” cannot be used because  $\bar{v}_i \neq v'_i$ . Inserted in Eq. 8.33 gives (cf. Eq. 8.14)

$$\frac{\partial \bar{v}_j K}{\partial x_j} = \underbrace{\bar{v}'_i \bar{v}'_j \frac{\partial \bar{v}_i}{\partial x_j}}_{-P^k, \text{ sink}} - \frac{\partial}{\partial x_j} \left( \frac{1}{\rho} \bar{v}_j \bar{p} + \bar{v}_i \bar{v}'_i \bar{v}'_j - \nu \frac{\partial K}{\partial x_j} \right) - \underbrace{\nu \frac{\partial \bar{v}_i}{\partial x_j} \frac{\partial \bar{v}_i}{\partial x_j}}_{\varepsilon_{mean}, \text{ sink}} \quad (8.35)$$

On the left side we have the usual convective term. On the right side we find:

- loss of energy to  $k$  due to the production term

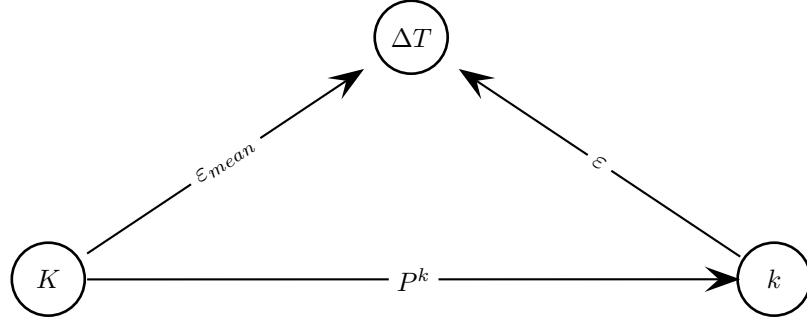


Figure 8.5: Transfer of energy between mean kinetic energy ( $K$ ), turbulent kinetic energy ( $k$ ) and internal energy (denoted as an increase in temperature,  $\Delta T$ ).  $K = \frac{1}{2} \bar{v}_i \bar{v}_i$  and  $k = \frac{1}{2} v'_i v'_i$ .

- diffusion by pressure-velocity interaction
- diffusion by velocity-stress interaction
- viscous diffusion
- viscous dissipation,  $\varepsilon_{mean}$

Note that the first term in Eq. 8.35 is the same as the first term in Eq. 8.14 but with opposite sign: here we clearly can see that the main source term in the  $k$  equation (the production term) appears as a sink term in the  $K$  equation.

In the  $K$  equation the dissipation term and the negative production term (representing loss of kinetic energy to the  $k$  field) read

$$-\nu \frac{\partial \bar{v}_i}{\partial x_j} \frac{\partial \bar{v}_i}{\partial x_j} + \overline{v'_i v'_j} \frac{\partial \bar{v}_i}{\partial x_j}, \quad (8.36)$$

and in the  $k$  equation the production and the dissipation terms read

$$-\overline{v'_i v'_j} \frac{\partial \bar{v}_i}{\partial x_j} - \nu \frac{\partial \bar{v}'_i}{\partial x_j} \frac{\partial \bar{v}'_i}{\partial x_j} \quad (8.37)$$

The gradient of the time-averaged velocity field,  $\bar{v}_i$ , is much smoother than that of the fluctuating velocity field,  $v'_i$ . In fully turbulent flow, the dissipation by the fluctuations,  $\varepsilon$ , is much larger than the dissipation by the mean flow (left side of Eq. 8.36). This is seen in Fig. 8.4. The energy flow from the mean flow to internal energy is illustrated in Fig. 8.5. The major part of the energy flow goes from  $K$  to  $k$  and then to dissipation.

In the viscous-dominated wall region, the mean dissipation,  $\nu(\partial \bar{v}_1 / \partial x_2)^2$ , is much larger than  $\varepsilon$ . At the wall, the mean dissipation takes the value  $\nu = 1/2000$  (normalized by  $u_\tau^4 / \nu$ ).

## 9 Transport equations for Reynolds stresses

In Section 8 we derived transport equations for kinetic turbulent energy,  $k$ , which is the trace of the Reynolds stress tensor  $\overline{v'_i v'_j}$  divided by two, i.e.  $k = \overline{v'_i v'_i}/2$ . This means that  $k$  is equal to twice the sum of the diagonal components of  $\overline{v'_i v'_j}$ , i.e.  $k = 0.5(\overline{v'_1^2} + \overline{v'_2^2} + \overline{v'_3^2})$ . Here we will now derive the transport equation for the Reynolds stress tensor. This is an unknown in the time-averaged Navier-Stokes equations, Eq. 6.5, which must be known before Eq. 6.5 can be solved. The most accurate way to find  $\overline{v'_i v'_j}$  is, of course, to solve a transport equation for it. This is computationally expensive since we then need to solve six additional transport equations (recall that  $\overline{v'_i v'_j}$  is symmetric, i.e.  $\overline{v'_1 v'_2} = \overline{v'_2 v'_1}$  etc.) Often, some simplifications are introduced, in which  $\overline{v'_i v'_j}$  is modelled by expressing it in a turbulent viscosity and a velocity gradient. Two-equations models are commonly used in these simplified models; no transport equation for  $\overline{v'_i v'_j}$  is solved. This is the subject of *Turbulence Modelling* which you will learn about in other courses in the MSc programme.

Now let's start to derive the transport equation for  $\overline{v'_i v'_j}$ . This approach is very similar to that we used when deriving the  $k$  equation in Section 8.1. Steady, incompressible flow with constant density and viscosity is assumed. Subtract Eq. 6.5 from Eq. 6.3 and divide by density, multiply by  $v'_j$  and time average and we obtain

$$\begin{aligned} & \overline{v'_j \frac{\partial}{\partial x_k} [v_i v_k - \bar{v}_i \bar{v}_k]} = \\ & -\frac{1}{\rho} \overline{v'_j \frac{\partial}{\partial x_i} p'} + \nu \overline{v'_j \frac{\partial^2 v'_i}{\partial x_k \partial x_k}} + \overline{\frac{\partial v'_i v'_k}{\partial x_k} v'_j} \end{aligned} \quad (9.1)$$

Equation 6.5 is written with the index  $i$  as free index, i.e.  $i = 1, 2$  or  $3$  so that the equation is an equation for  $v_1$ ,  $v_2$  or  $v_3$ . Now write Eq. 6.5 as an equation for  $v_j$  and multiply this equation by  $v'_i$ . We get

$$\begin{aligned} & \overline{v'_i \frac{\partial}{\partial x_k} [v_j v_k - \bar{v}_j \bar{v}_k]} = \\ & -\frac{1}{\rho} \overline{v'_i \frac{\partial}{\partial x_j} p'} + \nu \overline{v'_i \frac{\partial^2 v'_j}{\partial x_k \partial x_k}} + \overline{\frac{\partial v'_j v'_k}{\partial x_k} v'_i} \end{aligned} \quad (9.2)$$

It may be noted that Eq. 9.2 is conveniently obtained from Eq. 9.1 by simply switching indices  $i$  and  $j$ . Adding Eqs. 9.1 and 9.2 together gives

$$\begin{aligned} & \overline{v'_j \frac{\partial}{\partial x_k} [v_i v_k - \bar{v}_i \bar{v}_k]} + \overline{v'_i \frac{\partial}{\partial x_k} [v_j v_k - \bar{v}_j \bar{v}_k]} = \\ & -\frac{1}{\rho} \overline{v'_i \frac{\partial p'}{\partial x_j}} - \frac{1}{\rho} \overline{v'_j \frac{\partial p'}{\partial x_i}} \\ & + \nu \overline{v'_i \frac{\partial^2 v'_j}{\partial x_k \partial x_k}} + \nu \overline{v'_j \frac{\partial^2 v'_i}{\partial x_k \partial x_k}} \\ & + \overline{\frac{\partial v'_j v'_k}{\partial x_k} v'_i} + \overline{\frac{\partial v'_i v'_k}{\partial x_k} v'_j} \end{aligned} \quad (9.3)$$

Note that each line in the equation is *symmetric*: if you switch indices  $i$  and  $j$  in any of the terms nothing changes. This is important since the tensor  $\overline{v'_i v'_j}$  is symmetric.

Furthermore, you can check that the equation is correct according to the tensor notation rules. Indices  $i$  and  $j$  appear once in each term (not more and not less) and index  $k$  (the dummy index) appears exactly twice in each term (implying summation). Note that it is correct to use any other index than  $k$  in some terms (but you must not use  $i$  and  $j$ ). You could, for example, replace  $k$  with  $m$  in the first term and with  $q$  in the second term; it is permissible, but usually we use the same dummy index in every term.

Using  $v_i = \bar{v}_i + v'_i$ , the first line can be rewritten as

$$\overline{v'_j \frac{\partial}{\partial x_k} [\bar{v}_i v'_k + v'_i \bar{v}_k + v'_i v'_k]} + \overline{v'_i \frac{\partial}{\partial x_k} [\bar{v}_j v'_k + v'_j \bar{v}_k + v'_j v'_k]} \quad (9.4)$$

Using the continuity equation the first terms in the two groups are rewritten as

$$\overline{v'_j v'_k} \frac{\partial \bar{v}_i}{\partial x_k} + \overline{v'_i v'_k} \frac{\partial \bar{v}_j}{\partial x_k} \quad (9.5)$$

We merge the second terms in the two groups in Eq. 9.4.

$$\begin{aligned} \overline{v'_j \frac{\partial v'_i \bar{v}_k}{\partial x_k}} + \overline{v'_i \frac{\partial v'_j \bar{v}_k}{\partial x_k}} &= \bar{v}_k v'_j \overline{\frac{\partial v'_i}{\partial x_k}} + \bar{v}_k v'_i \overline{\frac{\partial v'_j}{\partial x_k}} \\ &= \bar{v}_k \frac{\partial v'_i v'_j}{\partial x_k} = \frac{\partial v'_i v'_j \bar{v}_k}{\partial x_k} \end{aligned} \quad (9.6)$$

The continuity equation was used twice (to get the right side on the first line and to get the final expression) and the product rule was used backwards to get the second line. Re-writing also the third terms in the two groups in Eq. 9.4 in the same way, the second and the third terms in Eq. 9.4 can be written

$$\frac{\partial \overline{v'_i v'_j} \bar{v}_k}{\partial x_k} + \frac{\partial \overline{v'_i v'_j v'_k}}{\partial x_k} \quad (9.7)$$

The second line in Eq. 9.3 is also re-written using **Trick 1**

$$-\frac{1}{\rho} \frac{\partial}{\partial x_j} \overline{v'_i p'} - \frac{1}{\rho} \frac{\partial}{\partial x_i} \overline{v'_j p'} + \frac{1}{\rho} \overline{p' \frac{\partial v'_i}{\partial x_j}} + \frac{1}{\rho} \overline{p' \frac{\partial v'_j}{\partial x_i}} \quad (9.8)$$

It will later turn out that it is convenient to express all derivatives as  $\partial/\partial x_k$ . Therefore we re-write the derivative in the two first terms as

$$\frac{\partial}{\partial x_j} = \delta_{jk} \frac{\partial}{\partial x_k} \text{ and } \frac{\partial}{\partial x_i} = \delta_{ik} \frac{\partial}{\partial x_k} \quad (9.9)$$

so that

$$-\delta_{jk} \frac{1}{\rho} \frac{\partial}{\partial x_k} \overline{v'_i p'} - \delta_{ik} \frac{1}{\rho} \frac{\partial}{\partial x_k} \overline{v'_j p'} + \frac{1}{\rho} \overline{p' \frac{\partial v'_i}{\partial x_j}} + \frac{1}{\rho} \overline{p' \frac{\partial v'_j}{\partial x_i}} \quad (9.10)$$

The third line in Eq. 9.3 is also re-written using **Trick 1**

$$\nu \frac{\partial}{\partial x_k} \left( \overline{v'_i \frac{\partial v'_j}{\partial x_k}} \right) + \nu \frac{\partial}{\partial x_k} \left( \overline{v'_j \frac{\partial v'_i}{\partial x_k}} \right) - 2\nu \overline{\frac{\partial v'_i}{\partial x_k} \frac{\partial v'_j}{\partial x_k}}$$

**Trick 1** is used – again – to merge the two first terms so that the third line in Eq. 9.3 reads

$$\begin{aligned} & \nu \frac{\partial}{\partial x_k} \left( \overline{v'_i \frac{\partial v'_j}{\partial x_k}} + v'_j \overline{\frac{\partial v'_i}{\partial x_k}} \right) - 2\nu \overline{\frac{\partial v'_i}{\partial x_k} \frac{\partial v'_j}{\partial x_k}} \\ &= \nu \frac{\partial}{\partial x_x} \left( \overline{\frac{\partial v'_i v'_j}{\partial x_k}} \right) - 2\nu \overline{\frac{\partial v'_i}{\partial x_k} \frac{\partial v'_j}{\partial x_k}} = \nu \overline{\frac{\partial^2 v'_i v'_j}{\partial x_k \partial x_k}} - 2\nu \overline{\frac{\partial v'_i}{\partial x_k} \frac{\partial v'_j}{\partial x_k}} \end{aligned} \quad (9.11)$$

The terms on the fourth line in Eq. 9.3 are zero because  $\bar{a}\bar{b}' = \bar{a}\bar{b}' = 0$ . We can now put everything together. Put the first term in Eq. 9.7 on the left side and the second term on the right side together with Eqs. 9.5, 9.10 and 9.11 so that

$$\begin{aligned} & \underbrace{\frac{\partial}{\partial x_k} (\bar{v}_k \overline{v'_i v'_j})}_{\text{I}} = \underbrace{-\overline{v'_j v'_k} \frac{\partial \bar{v}_i}{\partial x_k} - \overline{v'_i v'_k} \frac{\partial \bar{v}_j}{\partial x_k}}_{\text{II}} \\ & - \underbrace{\frac{\partial}{\partial x_k} \left( \overline{v'_i v'_j v'_k} + \frac{1}{\rho} \delta_{jk} \overline{v'_i p'} + \frac{1}{\rho} \delta_{ik} \overline{v'_j p'} - \nu \overline{\frac{\partial v'_i v'_j}{\partial x_k}} \right)}_{\text{III}} \\ & + \underbrace{\frac{1}{\rho} p' \left( \overline{\frac{\partial v'_i}{\partial x_j} + \frac{\partial v'_j}{\partial x_i}} \right)}_{\text{V}} - \underbrace{2\nu \overline{\frac{\partial v'_i}{\partial x_k} \frac{\partial v'_j}{\partial x_k}}}_{\text{IV}} \end{aligned} \quad (9.12)$$

Note that the manipulation in Eq. 9.9 allows the diffusion (term III) to be written on a more compact form. After a derivation, it is always useful to check that the equation is correct according to the tensor notation rules.

- Every term – or group of terms – should include the free indices  $i$  and  $j$  (only once);
- Every term – or group of terms – should be symmetric in  $i$  and  $j$ ;
- A dummy index (in this case index  $k$ ) must appear exactly twice (=summation) in every term

Equation 9.12 can also be written in a simplified easy-to-read symbolic form as

$$C_{ij} = P_{ij} + D_{ij} + \Pi_{ij} - \varepsilon_{ij} \quad (9.13)$$

where  $\Pi_{ij}$  denotes the pressure-strain term

$$\Pi_{ij} = \frac{p'}{\rho} \left( \overline{\frac{\partial v'_i}{\partial x_j} + \frac{\partial v'_j}{\partial x_i}} \right) \quad (9.14)$$

Equation 9.12 is the (exact) transport equation of the Reynolds stress,  $\overline{v'_i v'_j}$ . It is called the *Reynolds stress equations*. Since it is an equation for a second-order tensor, it consists of nine equations, but since it is symmetric we only need to consider six of them. Compare Eq. 9.12 with the equation for turbulent kinetic energy, Eq. 8.14. An alternative – and maybe easier – way to derive Eq. 8.14 is to first derive Eq. 9.12 and then take the trace (setting  $i = j$ ) and dividing by two. In both the  $k$  and the  $\overline{v'_i v'_j}$  equations there is a convection term (I), a production term (II), a diffusion term

**Reynolds  
stress  
equations**

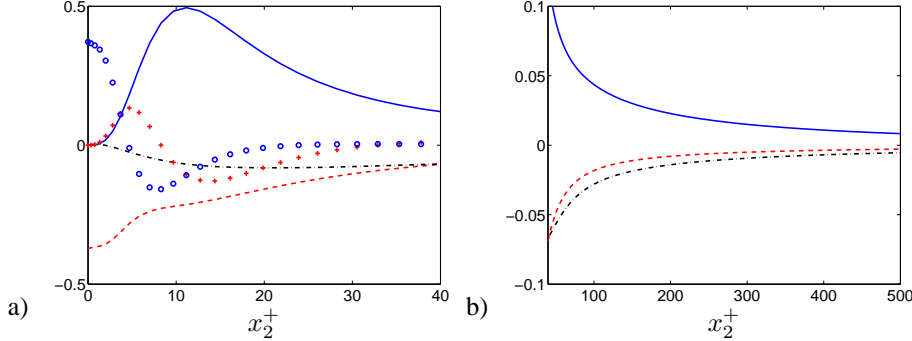


Figure 9.1: Channel flow at  $Re_\tau = 2000$ . Terms in the  $\overline{v_1'^2}$  equation scaled by  $u_\tau^4/\nu$ .  
a) Zoom near the wall; b) Outer region. DNS data [10, 11]. —:  $P_{11}$ ; - - -:  $\Pi_{11}$ ; +:  $-\partial(\overline{v_2'v_1'^2})/\partial x_2$ ; o:  $\nu\partial^2\overline{v_1'^2}/\partial x_2^2$ .

(III) and a dissipation term (IV). In the  $\overline{v_i'v_j'}$  equation there is a fifth term (V), see Eq. 9.14, which is called the pressure strain term. The physical meaning of this term is to redistribute energy between the normal stress components (if we transform Eq. 9.12 to the principal coordinates of  $\overline{v_i'v_j'}$  there are no shear stresses, only normal stresses). The average of the normal stresses is  $\overline{v_{av}^2} = \overline{v_i'v_i'}/3$ . For a normal stress that is larger than  $\overline{v_{av}^2}$ , the pressure-strain term is negative and vice-versa. It is often called the *Robin Hood* term because it – as Robin Hood – “takes from the rich and gives to the poor”. Note that the trace of the pressure-strain term is zero, i.e.

$$\Pi_{ii} = \frac{1}{\rho} p' \left( \overline{\frac{\partial v'_i}{\partial x_i}} + \overline{\frac{\partial v'_i}{\partial x_i}} \right) = 0 \quad (9.15)$$

because of the continuity equation and this is the reason why this term does not appear in the  $k$  equation.

For 2D boundary layer flow, Eq. 9.12 reads

$$\begin{aligned} \frac{\partial}{\partial x_1} (\bar{v}_1 \overline{v_i'v_j'}) + \frac{\partial}{\partial x_2} (\bar{v}_2 \overline{v_i'v_j'}) &= -\overline{v_j'v_2'} \frac{\partial \bar{v}_i}{\partial x_2} - \overline{v_i'v_2'} \frac{\partial \bar{v}_j}{\partial x_2} \\ &- \frac{\partial}{\partial x_2} \left( \overline{v_i'v_j'v_2'} + \frac{1}{\rho} \delta_{j2} \overline{v_i'p'} + \frac{1}{\rho} \delta_{i2} \overline{v_j'p'} - \nu \frac{\partial \overline{v_i'v_j'}}{\partial x_2} \right) \\ &+ \frac{1}{\rho} p' \left( \overline{\frac{\partial v'_i}{\partial x_j}} + \overline{\frac{\partial v'_j}{\partial x_i}} \right) - 2\nu \frac{\partial v'_i}{\partial x_k} \frac{\partial v'_j}{\partial x_k} \end{aligned} \quad (9.16)$$

Now let's look at this equation for fully developed channel flow for which

$$\begin{aligned} \bar{v}_2 &= \bar{v}_3 = 0 \\ \frac{\partial \overline{(\cdot)}}{\partial x_1} &= \frac{\partial \overline{(\cdot)}}{\partial x_3} = 0 \end{aligned} \quad (9.17)$$

The second line shows that it is the streamwise and spanwise derivative that operate on *time-averaged* quantities that are zero, not those that operate on instantaneous quantities such as in  $\varepsilon_{ij}$  and  $\Pi_{ij}$ .

The production term in Eq. 9.16 reads

$$P_{ij} = -\overline{v_j'v_2'} \frac{\partial \bar{v}_i}{\partial x_2} - \overline{v_i'v_2'} \frac{\partial \bar{v}_j}{\partial x_2} \quad (9.18)$$

**pressure strain**

**Robin Hood**

For the  $\overline{v_1'^2}$  ( $i = j = 1$ ),  $\overline{v_2'^2}$  ( $i = j = 2$ ),  $\overline{v_3'^2}$  ( $i = j = 3$ ) and  $\overline{v'_1 v'_2}$  ( $i = 1, j = 2$ ) equations we get

$$P_{11} = -2\overline{v'_1 v'_2} \frac{\partial \bar{v}_1}{\partial x_2} \quad (9.19a)$$

$$P_{22} = -2\overline{v'_2 v'_2} \frac{\partial \bar{v}_2}{\partial x_2} = 0 \quad (9.19b)$$

$$P_{33} = -2\overline{v'_3 v'_2} \frac{\partial \bar{v}_3}{\partial x_2} = 0 \quad (9.19c)$$

$$P_{12} = -\overline{v'_2 v'_2} \frac{\partial \bar{v}_1}{\partial x_2} - \overline{v'_1 v'_2} \frac{\partial \bar{v}_2}{\partial x_2} = -\overline{v'_2} \frac{\partial \bar{v}_1}{\partial x_2} \quad (9.19d)$$

using Eq. 9.17.

Figure 9.1 presents the terms in the  $\overline{v_1'^2}$  equation (Eq. 9.16 with  $i = j = 1$ ). As we saw for the  $k$  equation, the production term,  $P_{11}$ , reaches its maximum at  $x_2 \simeq 11$  where also  $\overline{v_1'^2}$  takes its maximum (Fig. 6.7). The pressure-strain term,  $\Pi_{11}$ , and the dissipation term act as sink terms. In the outer region (Fig. 9.1b) the production term balances the pressure-strain term and the dissipation term.

The terms in the wall-normal stress equation,  $\overline{v_2'^2}$ , are shown in Fig. 9.2. Here we find – as expected – that the pressure-strain term,  $\Pi_{22}$ , acts as the main source term. As mentioned previously,  $\Pi_{22}$  – the “Robin Hood” term – takes from the “rich”  $\overline{v_1'^2}$  equation and gives to the “poor”  $\overline{v_2'^2}$  equation energy because  $\overline{v_1'^2}$  is large and  $\overline{v_2'^2}$  is small.

Figure 9.3 presents the terms in the  $\overline{v'_1 v'_2}$  equation. The production term – which should be a source term – is here negative. Indeed it should be. Recall that  $\overline{v'_1 v'_2}$  is here negative and hence its source must be negative; or, rather, the other way around:  $\overline{v'_1 v'_2}$  is negative because its production term,  $P_{12} = -\overline{v'_2} \partial \bar{v}_1 / \partial x_2$ , is negative since  $\partial \bar{v}_1 / \partial x_2 > 0$ . Note that in the upper half of the channel  $\partial \bar{v}_1 / \partial x_2 < 0$  and hence  $P_{12}$  and  $\overline{v'_1 v'_2}$  are positive. Furthermore, note that the dissipation,  $\varepsilon_{12}$ , is zero. This is because dissipation takes place at the smallest scales and they are isotropic. That implies there is no correlation between two fluctuating velocity components, e.g.  $\overline{v'_1 v'_2} = 0$  (in general, for  $i \neq j$ , the stresses  $\overline{v'_i v'_j}$  in isotropic turbulence are zero). Hence, also their gradients are zero so that

$$\varepsilon_{12} = 2\nu \frac{\partial \bar{v}_1}{\partial x_k} \frac{\partial \bar{v}_2}{\partial x_k} = 0 \quad (9.20)$$

However, very close to the wall,  $x_2^+ \leq 10$ ,  $\varepsilon_{12} \neq 0$  because here the wall affects the dissipative scales making them non-isotropic;  $\varepsilon_{12}$  is positive since  $\overline{v'_1 v'_2} < 0$ , see Fig. 9.3.

If you want to learn more how to derive transport equations of turbulent quantities, see [15] which can be downloaded [here](#)

<http://www.tfd.chalmers.se/~lada/allpaper.html>

## 9.1 Reynolds shear stress vs. the velocity gradient

In boundary-layer type of flow, the Reynolds shear stress and the velocity gradient  $\partial \bar{v}_1 / \partial x_2$  have nearly always opposite signs. For channel flow, for example, Eq. 9.19 shows that  $P_{12}$  is negative (and hence also  $\overline{v'_1 v'_2}$ ) in the lower half because  $\partial \bar{v}_1 / \partial x_2 > 0$  and it is positive in the upper half because  $\partial \bar{v}_1 / \partial x_2 < 0$ . This can also be shown by physical argumentation. Consider the flow in a boundary layer, see Fig. 9.4. A fluid

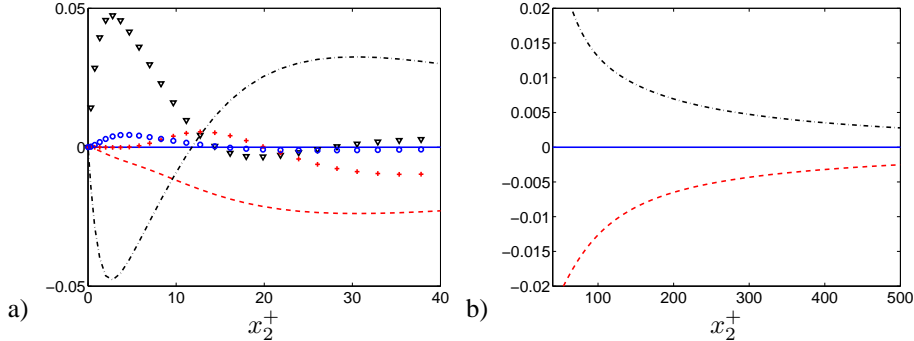


Figure 9.2: Channel flow at  $Re_\tau = 2000$ . Terms in the  $\overline{v_2'^2}$  equation scaled by  $u_\tau^4/\nu$ .  
a) Zoom near the wall; b) Outer region. DNS data [10, 11]. — :  $P_{22}$ ; - - - :  $-\varepsilon_{22}$ ;  
 $\nabla$  :  $-2\partial\overline{v'_2 p'}/\partial x_2$ ; - - :  $\Pi_{22}$ ; + :  $-\partial(\overline{v'_2 v'_2'^2})/\partial x_2$ ; ○ :  $\nu\partial^2\overline{v'_2'^2}/\partial x_2^2$ .

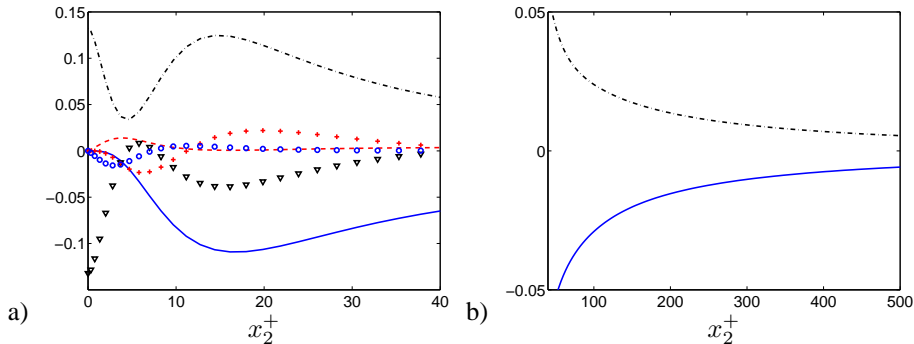


Figure 9.3: Channel flow at  $Re_\tau = 2000$ . Terms in the  $\overline{v'_1 v'_2}$  equation scaled by  $u_\tau^4/\nu$ .  
a) Zoom near the wall; b) Outer region. DNS data [10, 11]. — :  $P_{12}$ ; - - - :  $-\varepsilon_{12}$ ;  
 $\nabla$  :  $-\partial\overline{v'_2 p'}/\partial x_2$ ; - - :  $\Pi_{12}$ ; + :  $-\partial(\overline{v'_1 v'_2'^2})/\partial x_2$ ; ○ :  $\nu\partial^2\overline{v'_1 v'_2'}/\partial x_2^2$ .

particle is moving downwards (particle drawn with solid line) from  $x_{2,B}$  to  $x_{2,A}$  with (the turbulent fluctuating) velocity  $v'_2$ . At its new location the  $v_1$  velocity is in average smaller than at its old, i.e.  $\bar{v}_1(x_{2,A}) < \bar{v}_1(x_{2,B})$ . This means that when the particle at  $x_{2,B}$  (which has streamwise velocity  $v_1(x_{2,B})$ ) comes down to  $x_{2,A}$  (where the streamwise velocity is  $v_1(x_{2,A})$ ) it has an excess of streamwise velocity compared to its new environment at  $x_{2,A}$ . Thus the streamwise fluctuation is positive, i.e.  $v'_1 > 0$  and the correlation between  $v'_1$  and  $v'_2$  is in average negative ( $\overline{v'_1 v'_2} < 0$ ).

If we look at the other particle (dashed line in Fig. 9.4) we reach the same conclusion. The particle is moving upwards ( $v'_2 > 0$ ), and it is bringing a deficit in  $v_1$  so that  $v'_1 < 0$ . Thus, again,  $v'_1 v'_2 < 0$ . If we study this flow for a long time and average over time we get  $\overline{v'_1 v'_2} < 0$ . If we change the sign of the velocity gradient so that  $\partial\bar{v}_1/\partial x_2 < 0$  we will find that the sign of  $\overline{v'_1 v'_2}$  also changes.

In cases where the shear stress and the velocity gradient have the same sign (for example, in a wall jet) the reason is that the other terms (usually the transport terms) are more important than the production term.

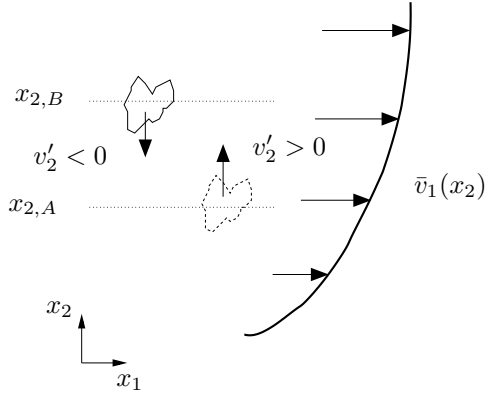
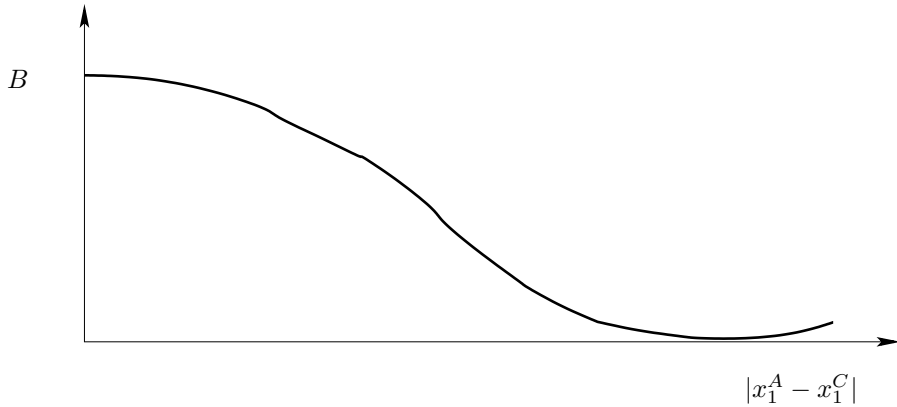
Figure 9.4: Sign of the Reynolds shear stress  $-\rho\overline{v'_1 v'_2}$  in a boundary layer.

Figure 10.1: Two-point correlation.

## 10 Correlations

### 10.1 Two-point correlations

Two-point correlations are useful when describing some characteristics of the turbulence. Pick two points along the  $x_1$  axis, say  $x_1^A$  and  $x_1^C$ , and sample the fluctuating velocity in, for example, the  $x_1$  direction. We can then form the correlation of  $v'_1$  at these two points as

$$B_{11}(x_1^A, x_1^C) = \overline{v'_1(x_1^A)v'_1(x_1^C)} \quad (10.1)$$

Often, it is expressed as

$$B_{11}(x_1^A, \hat{x}_1) = \overline{v'_1(x_1^A)v'_1(x_1^A + \hat{x}_1)} \quad (10.2)$$

where  $\hat{x}_1 = x_1^C - x_1^A$  is the separation distance between point  $A$  and  $C$ .

It is obvious that if we move point  $A$  and  $C$  closer to each other,  $B_{11}$  increases; when the two points are moved so close that they merge, then  $B_{11} = \overline{v'^2}(x_1^A)$ . If, on the other hand, we move point  $C$  further and further away from point  $A$ , then  $B_{11}$  will go to zero. Furthermore, we expect that the two-point correlation function will be related to the largest eddies. It is convenient to normalize  $B_{11}$  so that it varies between

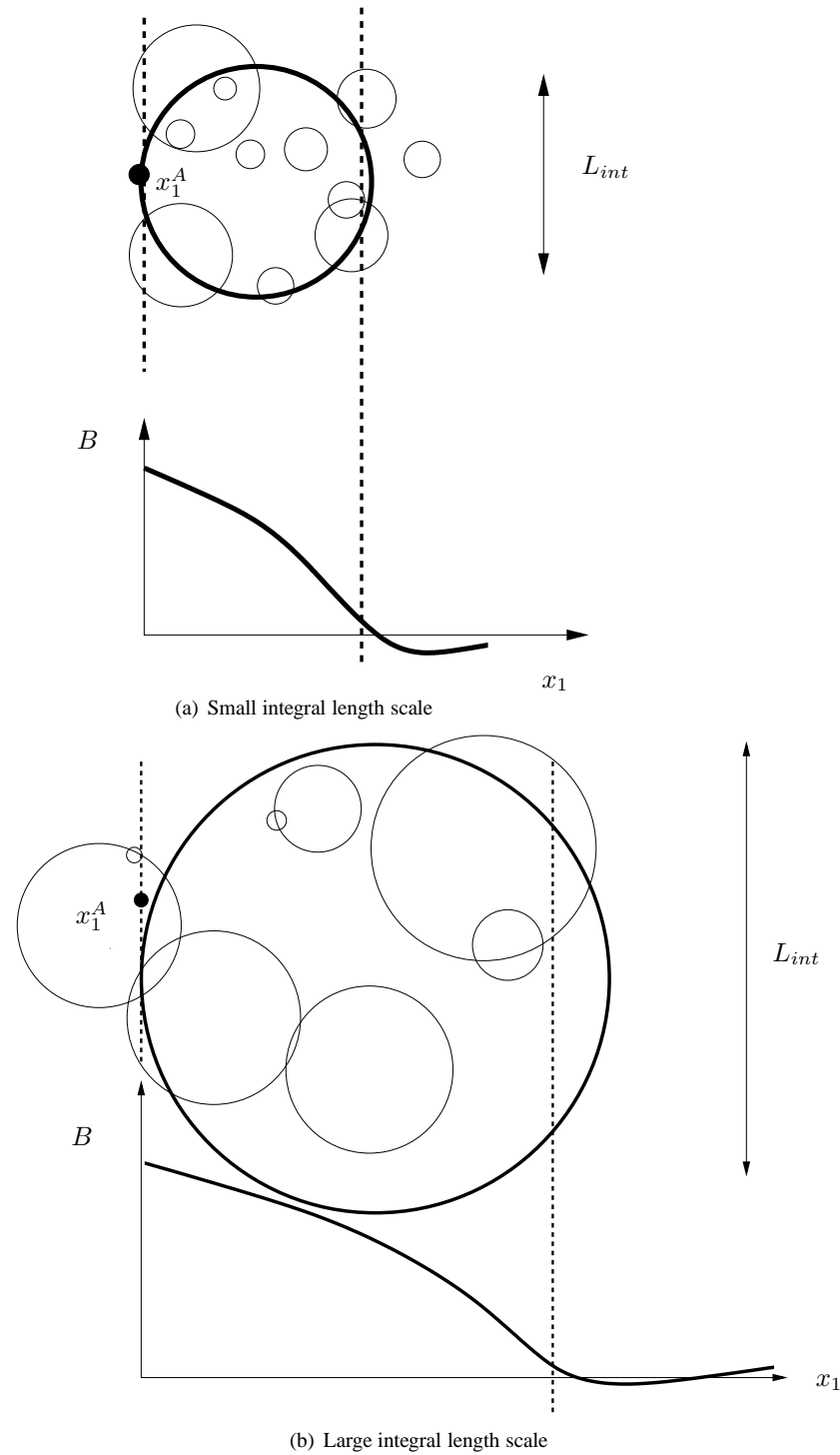


Figure 10.2: Schematic relation between the two-point correlation, the largest eddies (thick lines) and the integral length scale,  $L_{int}$ .

-1 and +1. The normalized two-point correlation reads

$$B_{11}^{norm}(x_1^A, \hat{x}_1) = \frac{1}{v_{1,rms}(x_1^A)v_{1,rms}(x_1^A + \hat{x}_1)} \overline{v'_1(x_1^A)v'_1(x_1^A + \hat{x}_1)} \quad (10.3)$$

where subscript *rms* denotes root-mean-square, which for  $v'_1$ , for example, is defined as

$$v_{1,rms} = \left( \overline{v'^2_1} \right)^{1/2} \quad (10.4)$$

RMS is the same as *standard deviation* (Matlab command `std`) which is the square-root of the *variance* (Matlab command `var`).

Consider a flow where the largest eddies have an eddy scale (length scale) of  $L_{int}$ , see Fig. 10.2. We expect that the two point correlation,  $B_{11}$ , approaches zero for separation distance,  $|x_1^A - x_1^C| > L_{int}$  because for separation distances larger than  $|x_1^A - x_1^B|$  there is no correlation between  $v'_1(x_1^A)$  and  $v'_1(x_1^C)$ . Hence, flows with large eddies will have a two-point correlation function which decreases slowly with separation distance. For flows with small eddies, the two-point correlation,  $B_{11}$ , decreases rapidly with  $\hat{x}_1$ .

If the flow is homogeneous (see p.70) in the  $x_1$  direction, the two-point correlation does not depend on the location of  $x_1^A$ , i.e. it is only dependent on the separation of the two points,  $\hat{x}_1$ .

From the two-point correlation,  $B_{11}$ , an integral length scale,  $L_{int}$ , can be computed which is defined as the integral of  $B_{11}$  over the separation distance, i.e.

**integral  
length scale**

$$L_{int}(x_1) = \int_0^\infty \frac{B_{11}(x_1, \hat{x}_1)}{v_{1,rms}^A v_{1,rms}^C} d\hat{x}_1 \quad (10.5)$$

If the flow is homogeneous in the  $x_1$  direction then  $L_{int}$  does not depend on  $x_1$ .

## 10.2 Auto correlation

Auto correlation is a “two-point correlation” in time, i.e. the correlation of a turbulent fluctuation with a separation in time. If we again choose the  $v'_1$  fluctuation, the auto correlation reads

$$B_{11}(t^A, \hat{t}) = \overline{v'_1(t^A)v'_1(t^A + \hat{t})} \quad (10.6)$$

where  $\hat{t} = t^C - t^A$ , is the time separation distance between time  $A$  and  $C$ . If the mean flow is steady, the “time direction” is homogeneous and  $B_{11}$  is independent on  $t^A$ ; in this case the auto-correlation depends only on time separation,  $\hat{t}$ , i.e.

$$B_{11}(\hat{t}) = \overline{v'_1(t)v'_1(t + \hat{t})} \quad (10.7)$$

where the right side is time-averaged over  $t$ .

The normalized auto-correlation reads

$$B_{11}^{norm}(\hat{t}) = \frac{1}{v_{1,rms}^2} \overline{v'_1(t)v'_1(t + \hat{t})} \quad (10.8)$$

In analogy to the integral length scale,  $L_{int}$ , the *integral time scale*,  $T_{int}$ , is defined as (assuming steady flow)

**integral  
time scale**

$$T_{int} = \int_0^\infty B_{11}^{norm}(\hat{t}) d\hat{t} \quad (10.9)$$

# MTF270 Turbulence Modelling

**L. Davidson**

Division of Fluid Dynamics, Department of Applied Mechanics  
Chalmers University of Technology, Göteborg, Sweden  
<http://www.tfd.chalmers.se/~lada>, lada@chalmers.se

This report can be downloaded at

[http://www.tfd.chalmers.se/~lada/comp\\_turb\\_model/lecture\\_notes.html](http://www.tfd.chalmers.se/~lada/comp_turb_model/lecture_notes.html)

## 11 Reynolds stress models and two-equation models

### 11.1 Mean flow equations

#### 11.1.1 Flow equations

For incompressible turbulent flow, all variables are divided into a mean part (time averaged) and fluctuating part. For the velocity vector this means that  $v_i$  is divided into a mean part  $\bar{v}_i$  and a fluctuating part  $v'_i$  so that  $v_i = \bar{v}_i + v'_i$ . Time average and we get (see Eq. 6.4 at. p. 53):

$$\frac{\partial \bar{v}_i}{\partial x_j} = 0 \quad (11.1)$$

$$\frac{\partial \rho_0 \bar{v}_i}{\partial t} + \frac{\partial}{\partial x_j} (\rho_0 \bar{v}_i \bar{v}_j) = -\frac{\partial \bar{p}}{\partial x_i} + \mu \frac{\partial^2 \bar{v}_i}{\partial x_j \partial x_j} - \frac{\partial \tau_{ij}}{\partial x_j} - \beta \rho_0 (\bar{\theta} - \theta_0) g_i \quad (11.2)$$

(note that  $\theta$  denotes temperature) where  $\rho_0$  is a constant reference density and  $f_i = -\beta(\bar{\theta} - \theta_0)g_i$  and the turbulent stress tensor (also called *Reynolds stress tensor*) is written as:

$$\tau_{ij} = \rho_0 \overline{v'_i v'_j}$$

**Reynolds  
stress  
tensor**

The pressure,  $\bar{p}$ , denotes the hydro-static pressure, see Eq. 3.22, which means that when the flow is still (i.e.  $\bar{v}_i \equiv 0$ ), then the pressure is zero (i.e.  $\bar{p} \equiv 0$ ).

The body force  $f_i$  – which was omitted for convenience in Eq. 6.4 – has here been re-introduced. The body force in Eq. 11.2 is due to buoyancy, i.e. density differences. The basic form of the buoyancy force is  $f_i = g_i$  where  $g_i$  denotes gravitational acceleration. Since the pressure,  $\bar{p}$ , is defined as the hydro-static pressure we must rewrite the buoyancy source as

$$\rho_0 f_i = (\rho - \rho_0) g_i \quad (11.3)$$

so that  $\bar{p} \equiv 0$  when  $\bar{v}_i \equiv 0$  (note that the true pressure decreases upwards as  $\rho g \Delta h$  where  $\Delta h$  denotes change in height). If we let density depend on pressure and temperature, differentiation gives

$$d\rho = \left( \frac{\partial \rho}{\partial \theta} \right)_p d\theta + \left( \frac{\partial \rho}{\partial p} \right)_\theta dp \quad (11.4)$$

Our flow is incompressible, which means that the density does not depend on pressure, i.e.  $\partial \rho / \partial p = 0$ ; it may, however, depend on temperature and mixture composition. Hence the last term in Eq. 11.4 is zero and we introduce the volumetric thermal expansion,  $\beta$ , so that

$$\begin{aligned} \beta &= -\frac{1}{\rho_0} \left( \frac{\partial \rho}{\partial \theta} \right)_p \Rightarrow \\ d\rho &= -\rho_0 \beta d\theta \Rightarrow \rho - \rho_0 = -\beta \rho_0 (\theta - \theta_0) \end{aligned} \quad (11.5)$$

where  $\beta$  is a physical property which is tabulated in physical handbooks. For a perfect gas it is simply  $\beta = \theta^{-1}$  (with  $\theta$  in degrees Kelvin). Now we can re-write the buoyancy source as

$$\rho_0 f_i = (\rho - \rho_0) g_i = -\rho_0 \beta (\bar{\theta} - \theta_0) g_i \quad (11.6)$$

which is the last term in Eq. 11.2. Consider the case where  $x_3$  is vertically upwards. Then  $g_i = (0, 0, -g)$  and a large temperature in Eq. 11.6 results in a force vertically upwards, which agrees well with our intuition.

### 11.1.2 Temperature equation

The instantaneous temperature,  $\theta$ , is also decomposed into a mean and a fluctuating component as  $\theta = \bar{\theta} + \theta'$ . The transport equation for  $\theta$  reads (see Eq. 2.15 where temperature was denoted by  $T$ )

$$\frac{\partial \theta}{\partial t} + \frac{\partial v_i \theta}{\partial x_i} = \alpha \frac{\partial^2 \theta}{\partial x_i \partial x_i} \quad (11.7)$$

where  $\alpha = k/(\rho c_p)$ , see Eq. 2.15 on p. 23. Introducing  $\theta = \bar{\theta} + \theta'$  we get

$$\frac{\partial \bar{\theta}}{\partial t} + \frac{\partial \bar{v}_i \bar{\theta}}{\partial x_i} = \alpha \frac{\partial^2 \bar{\theta}}{\partial x_i \partial x_i} - \frac{\partial \overline{v'_i \theta'}}{\partial x_i} \quad (11.8)$$

The last term on the right side is an additional term whose physical meaning is turbulent heat flux vector. This is similar to the Reynolds stress tensor on the right side of the time-averaged momentum equation, Eq. 11.2. The total heat flux vector – viscous plus turbulent – in Eq. 11.8 reads (cf. Eq. 2.11)

$$\frac{q_{i,tot}}{\rho c_p} = \frac{q_i}{\rho c_p} + \frac{q_{i,turb}}{\rho c_p} = -\alpha \frac{\partial \bar{\theta}}{\partial x_i} - \overline{v'_i \theta'} \quad (11.9)$$

## 11.2 The exact $\overline{v'_i v'_j}$ equation

Now we want to solve the time-averaged continuity equation (Eq. 11.1) and the three momentum equations (Eq. 11.2). Unfortunately there are ten unknowns; the four usual ones ( $\bar{v}_i$ ,  $\bar{p}$ ) plus six turbulent stresses,  $\overline{v'_i v'_j}$ . We must *close* this equation system; it is called the *closure problem*. We must find some new equations for the turbulent stresses. We need a turbulence model.

**closure problem**

The most comprehensive turbulence model is to derive exact transport equations for the turbulent stresses. An exact equation for the Reynolds stresses can be derived from the Navies-Stokes equation. It is emphasized that this equation is exact; or, rather, as exact as the Navier-Stokes equations. The derivation follows the steps below.

- Set up the momentum equation for the instantaneous velocity  $v_i = \bar{v}_i + v'_i \rightarrow$  Eq. (A)
- Time average  $\rightarrow$  equation for  $\bar{v}_i$ , Eq. (B)
- Subtract Eq. (B) from Eq. (A)  $\rightarrow$  equation for  $v'_i$ , Eq. (C)
- Do the same procedure for  $v_j \rightarrow$  equation for  $v'_j$ , Eq. (D)
- Multiply Eq. (C) with  $v'_j$  and Eq. (D) with  $v'_i$ , time average and add them together  $\rightarrow$  equation for  $\overline{v'_i v'_j}$

In Section 9 at p. 74 these steps are given in some detail. More details can also be found in [15] (set the SGS tensor to zero, i.e.  $\tau_{ij}^a = 0$ ).

The final  $\overline{v'_i v'_j}$ -equation (Reynolds Stress equation) reads (see Eq. 9.12)

$$\begin{aligned} \frac{\partial \overline{v'_i v'_j}}{\partial t} + \bar{v}_k \frac{\partial \overline{v'_i v'_j}}{\partial x_k} &= -\overline{v'_i v'_k} \frac{\partial \bar{v}_j}{\partial x_k} - \overline{v'_j v'_k} \frac{\partial \bar{v}_i}{\partial x_k} + \underbrace{\frac{p'}{\rho} \left( \frac{\partial v'_i}{\partial x_j} + \frac{\partial v'_j}{\partial x_i} \right)}_{\Pi_{ij}} \\ &\quad - \underbrace{\frac{\partial}{\partial x_k} \left[ \overline{v'_i v'_j v'_k} + \frac{p' v'_j}{\rho} \delta_{ik} + \frac{p' v'_i}{\rho} \delta_{jk} \right]}_{D_{ij,t}} + \nu \underbrace{\frac{\partial^2 \overline{v'_i v'_j}}{\partial x_k \partial x_k}}_{D_{ij,\nu}} \\ &\quad - \underbrace{g_i \beta \overline{v'_j \theta'}}_{G_{ij}} - g_j \beta \overline{v'_i \theta'} - 2\nu \underbrace{\frac{\partial v'_i}{\partial x_k} \frac{\partial v'_j}{\partial x_k}}_{\varepsilon_{ij}} \end{aligned} \quad (11.10)$$

where  $D_{ij,t}$  and  $D_{ij,\nu}$  denote turbulent and viscous diffusion, respectively. The total diffusion reads  $D_{ij} = D_{ij,t} + D_{ij,\nu}$ . This is analogous to the momentum equation where we have gradients of viscous and turbulent stresses which correspond to viscous and turbulent diffusion. Equation 11.10 can symbolically be written

$$C_{ij} = P_{ij} + \Pi_{ij} + D_{ij} + G_{ij} - \varepsilon_{ij}$$

where

$C_{ij}$  Convection

$P_{ij}$  Production

$\Pi_{ij}$  Pressure-strain

$D_{ij}$  Diffusion

$G_{ij}$  Buoyancy production

$\varepsilon_{ij}$  Dissipation

### 11.3 The exact $\overline{v'_i \theta'}$ equation

If temperature variations occurs we must solve for the mean temperature field, see Eq. 11.8. To obtain the equation for the fluctuating temperature, subtract Eq. 11.8 from Eq. 11.7

$$\frac{\partial \theta'}{\partial t} + \frac{\partial}{\partial x_k} (v'_k \bar{\theta} + \bar{v}_k \theta' + v'_k \theta') = \alpha \frac{\partial^2 \theta'}{\partial x_k \partial x_k} + \frac{\partial \overline{v'_k \theta'}}{\partial x_k} \quad (11.11)$$

To get the equation for the fluctuating velocity,  $v'_i$ , subtract the equation for the mean velocity  $\bar{v}_i$  (Eq. 11.2) from the equation for the instantaneous velocity,  $v_i$  (Eq. 6.3) so that

$$\frac{\partial v'_i}{\partial t} + \frac{\partial}{\partial x_k} (v'_k \bar{v}_i + \bar{v}_k v'_i + v'_k v'_i) = -\frac{1}{\rho} \frac{\partial p'}{\partial x_i} + \nu \frac{\partial^2 v'_i}{\partial x_k \partial x_k} + \frac{\partial \overline{v'_i v'_k}}{\partial x_k} - g_i \beta \theta' \quad (11.12)$$

Multiply Eq. 11.11 with  $v'_i$  and multiply Eq. 11.12 with  $\theta'$ , add them together and time average

$$\begin{aligned} & \overline{\frac{\partial v'_i \theta'}{\partial t}} + \overline{v'_i \frac{\partial}{\partial x_k} (v'_k \bar{\theta} + \bar{v}_k \theta' + v'_k \theta')} + \theta' \overline{\frac{\partial}{\partial x_k} (\bar{v}_i v'_k + \bar{v}_k v'_i + v'_i v'_k)} \\ &= - \overline{\frac{\theta' \partial p'}{\rho \partial x_i}} + \alpha \overline{v'_i \frac{\partial^2 \theta'}{\partial x_k \partial x_k}} + \nu \theta' \overline{\frac{\partial^2 v'_i}{\partial x_k \partial x_k}} - g_i \beta \overline{\theta' \theta'} \end{aligned} \quad (11.13)$$

The Reynolds stress term in Eq. 11.12 multiplied by  $\theta'$  and time averaged is zero, i.e.

$$\overline{\frac{\partial v'_i v'_j}{\partial x_k} \theta'} = \overline{\frac{\partial v'_i v'_j}{\partial x_k} \bar{\theta'}} = 0$$

The first term in the two parentheses on line 1 in Eq. 11.13 are combined into two production terms (using the continuity equation,  $\partial v'_k / \partial x_k = 0$ )

$$\overline{v'_i v'_k} \frac{\partial \bar{\theta}}{\partial x_k} + \overline{v'_k \theta'} \frac{\partial \bar{v}}{\partial x_k} \quad (11.14)$$

The second term in the two parenthesis on the first line of Eq. 11.13 are re-written using the continuity equation

$$\overline{v'_i \frac{\partial \bar{v}_k \theta'}{\partial x_k}} + \theta' \overline{\frac{\partial \bar{v}_k v'_i}{\partial x_k}} = \bar{v}_k \left( \overline{v'_i \frac{\partial \theta'}{\partial x_k}} + \overline{\theta' \frac{\partial v'_i}{\partial x_k}} \right) \quad (11.15)$$

Now the two terms can be merged (product rule backwards)

$$\bar{v}_k \frac{\partial \overline{v'_i \theta'}}{\partial x_k} = \frac{\partial \bar{v}_k \overline{v'_i \theta'}}{\partial x_k} \quad (11.16)$$

where we used the continuity equation to obtain the right side. The last two terms in Eq. 11.13 are re-cast into turbulent diffusion terms using the same procedure as in Eqs. 11.15 and 11.16

$$\frac{\partial \overline{v'_i v'_k \theta'}}{\partial x_k} \quad (11.17)$$

The viscous diffusion terms on the right side are re-written using the product rule backwards (Trick 1, see p. 65)

$$\begin{aligned} \overline{\alpha v'_i \frac{\partial^2 \theta'}{\partial x_k \partial x_k}} &= \overline{\alpha v'_i \frac{\partial}{\partial x_k} \left( \frac{\partial \theta'}{\partial x_k} \right)} = \alpha \frac{\partial}{\partial x_k} \left( \overline{v'_i \frac{\partial \theta'}{\partial x_k}} \right) - \alpha \overline{\frac{\partial \theta'}{\partial x_k} \frac{\partial v'_i}{\partial x_k}} \\ \overline{\nu \theta' \frac{\partial^2 v'_i}{\partial x_k \partial x_k}} &= \nu \theta' \overline{\frac{\partial}{\partial x_k} \left( \frac{\partial v'_i}{\partial x_k} \right)} = \nu \frac{\partial}{\partial x_k} \left( \overline{\theta' \frac{\partial v'_i}{\partial x_k}} \right) - \nu \overline{\frac{\partial \theta'}{\partial x_k} \frac{\partial v'_i}{\partial x_k}} \end{aligned} \quad (11.18)$$

Inserting Eqs. 11.14, 11.16, 11.17 and 11.18 into Eq. 11.13 gives the transport equation for the heat flux vector  $v'_i \theta'$

$$\begin{aligned} & \overline{\frac{\partial v'_i \theta'}{\partial t}} + \frac{\partial}{\partial x_k} \bar{v}_k \overline{v'_i \theta'} = \underbrace{- \overline{v'_i v'_k} \frac{\partial \bar{\theta}}{\partial x_k}}_{P_{i\theta}} - \underbrace{\overline{v'_k \theta'} \frac{\partial \bar{v}_i}{\partial x_k}}_{\Pi_{i\theta}} - \underbrace{\overline{\frac{\theta' \partial p'}{\rho \partial x_i}}}_{D_{i\theta,t}} - \underbrace{\frac{\partial}{\partial x_k} \overline{v'_k v'_i \theta'}}_{D_{i\theta,\nu}} \\ &+ \underbrace{\alpha \frac{\partial}{\partial x_k} \left( \overline{v'_i \frac{\partial \theta'}{\partial x_k}} \right)}_{D_{i\theta,\nu}} + \nu \underbrace{\frac{\partial}{\partial x_k} \left( \overline{\theta' \frac{\partial v'_i}{\partial x_k}} \right)}_{\varepsilon_{i\theta}} - \underbrace{(\nu + \alpha) \frac{\partial}{\partial x_k} \overline{\frac{\partial v'_i}{\partial x_k} \frac{\partial \theta'}{\partial x_k}}}_{G_{i\theta}} - \underbrace{g_i \beta \overline{\theta'^2}}_{G_{i\theta}} \end{aligned} \quad (11.19)$$

where  $P_{i\theta}$ ,  $\Pi_{i\theta}$  and  $D_{i\theta,t}$  denote the production, scramble and turbulent diffusion term, respectively. The production term include one term with the mean velocity gradient and one term with the mean temperature gradient. On the last line,  $D_{i\theta,\nu}$ ,  $\varepsilon_{i\theta}$  and  $G_{i\theta}$  denote viscous diffusion, dissipation and buoyancy term, respectively. The unknown terms –  $\Pi_{i\theta}$ ,  $D_{i\theta}$ ,  $\varepsilon_{i\theta}$ ,  $G_{i\theta}$  – have to be modelled as usual; this is out of the scope of the present course but the interested reader is referred to [16].

It can be noted that there is no usual viscous diffusion term in Eq. 11.19. The reason is that the viscous diffusion coefficients are different in the  $v_i$  equation and the  $\theta$  equation ( $\nu$  in the former case and  $\alpha$  in the latter). However, if  $\nu \simeq \alpha$  (which corresponds to a Prandtl number of unity, i.e.  $Pr = \nu/\alpha \simeq 1$ , see Eq. 2.16), the diffusion term in Eq. 11.19 assumes the familiar form

$$\begin{aligned} & \alpha \overline{\frac{\partial}{\partial x_k} \left( v'_i \frac{\partial \theta'}{\partial x_k} \right)} + \nu \overline{\frac{\partial}{\partial x_k} \left( \theta' \frac{\partial v'_i}{\partial x_k} \right)} \\ &= \alpha \frac{\partial^2 \overline{v'_i \theta'}}{\partial x_k \partial x_k} - \alpha \frac{\partial}{\partial x_k} \left( \overline{\theta' \frac{\partial v'_i}{\partial x_k}} \right) + \nu \frac{\partial^2 \overline{v'_i \theta'}}{\partial x_k \partial x_k} - \nu \frac{\partial}{\partial x_k} \left( \overline{v'_i \frac{\partial \theta'}{\partial x_k}} \right) \\ &\simeq 2\nu \frac{\partial^2 \overline{v'_i \theta'}}{\partial x_k \partial x_k} - \nu \frac{\partial}{\partial x_k} \left( \overline{\theta' \frac{\partial v'_i}{\partial x_k}} \right) - \nu \frac{\partial}{\partial x_k} \left( \overline{v'_i \frac{\partial \theta'}{\partial x_k}} \right) \\ &= 2\nu \frac{\partial^2 \overline{v'_i \theta'}}{\partial x_k \partial x_k} = \left( \nu + \frac{\nu}{Pr} \right) \frac{\partial^2 \overline{v'_i \theta'}}{\partial x_k \partial x_k} \end{aligned} \quad (11.20)$$

Often the viscous diffusion is simplified in this way.

## 11.4 The $k$ equation

The turbulent kinetic energy is the sum of all normal Reynolds stresses, i.e.

$$k = \frac{1}{2} \left( \overline{v_1'^2} + \overline{v_2'^2} + \overline{v_3'^2} \right) \equiv \frac{1}{2} \overline{v'_i v'_i}$$

By taking the trace (setting indices  $i = j$ ) of the equation for  $\overline{v'_i v'_j}$  and dividing by two we get the equation for the turbulent kinetic energy:

$$\begin{aligned} \frac{\partial k}{\partial t} + \bar{v}_j \frac{\partial k}{\partial x_j} &= - \underbrace{\overline{v'_i v'_j} \frac{\partial \bar{v}_i}{\partial x_j}}_{P^k} - \underbrace{\nu \frac{\partial v'_i}{\partial x_j} \frac{\partial v'_i}{\partial x_j}}_{\varepsilon} \\ &\quad - \underbrace{\frac{\partial}{\partial x_j} \left\{ \overline{v'_j \left( \frac{p'}{\rho} + \frac{1}{2} v'_i v'_i \right)} \right\}}_{D_t^k} + \underbrace{\nu \frac{\partial^2 k}{\partial x_j \partial x_j}}_{D_\nu^k} \underbrace{- g_i \beta \overline{v'_i \theta'}}_{G^k} \end{aligned} \quad (11.21)$$

where – as in the  $\overline{v'_i v'_j}$  equation –  $D_t^k$  and  $D_\nu^k$  denotes turbulent and viscous diffusion, respectively. The total diffusion reads  $D^k = D_t^k + D_\nu^k$ . Equation 11.21 can symbolically be written:

$$C^k = P^k + D^k + G^k - \varepsilon \quad (11.22)$$

## 11.5 The $\varepsilon$ equation

Two quantities are usually used in eddy-viscosity model to express the turbulent viscosity. In the  $k - \varepsilon$  model,  $k$  and  $\varepsilon$  are used. The turbulent viscosity is then computed as

$$\nu_t = C_\mu \frac{k^2}{\varepsilon}$$

where  $C_\mu = 0.09$ . An exact equation for the transport equation for the dissipation

$$\varepsilon = \nu \frac{\partial v'_i}{\partial x_j} \frac{\partial v'_i}{\partial x_j}$$

can be derived (see, e.g., [17]), but it is very complicated and in the end many terms are found negligible. It is much easier to look at the  $k$  equation, Eq. 11.22, and to setup a similar equation for  $\varepsilon$ . The transport equation should include a convective term,  $C^\varepsilon$ , a diffusion term,  $D^\varepsilon$ , a production term,  $P^\varepsilon$ , a production term due to buoyancy,  $G^\varepsilon$ , and a destruction term,  $\Psi^\varepsilon$ , i.e.

$$C^\varepsilon = P^\varepsilon + D^\varepsilon + G^\varepsilon - \Psi^\varepsilon \quad (11.23)$$

The production and destruction terms,  $P^k$  and  $\varepsilon$ , in the  $k$  equation are used to formulate the corresponding terms in the  $\varepsilon$  equation. The terms in the  $k$  equation have the dimension  $\partial k / \partial t = [m^2/s^3]$  whereas the terms in the  $\varepsilon$  equation have the dimension  $\partial \varepsilon / \partial t = [m^2/s^4]$ . Hence, we must multiply  $P^k$  and  $\varepsilon$  by a quantity which has the dimension  $[1/s]$ . One quantity with this dimension is the mean velocity gradient which might be relevant for the production term, but not for the destruction. A better choice should be  $\varepsilon/k = [1/s]$ . Hence, we get

$$P^\varepsilon + G^\varepsilon - \Psi^\varepsilon = \frac{\varepsilon}{k} (c_{\varepsilon 1} P^k + c_{\varepsilon 1} G^k - c_{\varepsilon 2} \varepsilon) \quad (11.24)$$

where we have added new unknown coefficients in front of each term. The turbulent diffusion term is expressed in the same way as that in the  $k$  equation (see Eq. 11.36) but with its own turbulent Prandtl number,  $\sigma_\varepsilon$  (see Eq. 11.33), i.e.

$$D^\varepsilon = \frac{\partial}{\partial x_j} \left[ \left( \nu + \frac{\nu_t}{\sigma_\varepsilon} \right) \frac{\partial \varepsilon}{\partial x_j} \right] \quad (11.25)$$

The final form of the  $\varepsilon$  transport equation reads

$$\frac{\partial \varepsilon}{\partial t} + \bar{v}_j \frac{\partial \varepsilon}{\partial x_j} = \frac{\varepsilon}{k} (c_{\varepsilon 1} P^k + c_{\varepsilon 1} G^k - c_{\varepsilon 2} \varepsilon) + \frac{\partial}{\partial x_j} \left[ \left( \nu + \frac{\nu_t}{\sigma_\varepsilon} \right) \frac{\partial \varepsilon}{\partial x_j} \right] \quad (11.26)$$

Note that this is a *modelled* equation since we have modelled the production, destruction and turbulent diffusion terms.

## 11.6 The Boussinesq assumption

In the Boussinesq assumption an eddy (i.e. a *turbulent*) viscosity is introduced to model the unknown Reynolds stresses in Eq. 11.2. Consider the diffusion terms in the incompressible momentum equation in the case of non-constant viscosity (see Eq. 2.5)

$$\frac{\partial}{\partial x_j} \left\{ \nu \left( \frac{\partial \bar{v}_i}{\partial x_j} + \frac{\partial \bar{v}_j}{\partial x_i} \right) - \overline{v'_i v'_j} \right\} \quad (11.27)$$

Now we want to replace the Reynolds stress tensor,  $\overline{v'_i v'_j}$ , by a turbulent viscosity,  $\nu_t$ , so that the the diffusion terms can be written

$$\frac{\partial}{\partial x_j} \left\{ (\nu + \nu_t) \left( \frac{\partial \bar{v}_i}{\partial x_j} + \frac{\partial \bar{v}_j}{\partial x_i} \right) \right\} \quad (11.28)$$

Identification of Eqs. 11.27 and 11.28 gives

$$\overline{v'_i v'_j} = -\nu_t \left( \frac{\partial \bar{v}_i}{\partial x_j} + \frac{\partial \bar{v}_j}{\partial x_i} \right) \quad (11.29)$$

This equation is not valid upon contraction (the left side will be zero, but not the right side). Hence we add the trace of the left side to the right side so that

$$\overline{v'_i v'_j} = -\nu_t \left( \frac{\partial \bar{v}_i}{\partial x_j} + \frac{\partial \bar{v}_j}{\partial x_i} \right) + \frac{2}{3} \delta_{ij} k = -2\nu_t \bar{s}_{ij} + \frac{2}{3} \delta_{ij} k \quad (11.30)$$

Now the equation valid also when it is contracted (i.e taking the trace); after contraction both left and right side are equal (as they must be) and equal to  $\overline{v'_i v'_i} = 2k$ . When Eq. 11.30 is included in Eq. 11.2 we replace six turbulent stresses with one new unknown (the turbulent viscosity,  $\nu_t$ ). This is of course a drastic simplification.

If the mean temperature equation is solved for we need an equation for the heat flux vector,  $\overline{v'_i \theta'}$ . One option is to solve its transport equation, Eq. 11.19. If an eddy-viscosity model (i.e. Eq. 11.30) is used for the Reynolds stresses, an eddy-viscosity model is commonly used also for the heat flux vector. The Boussinesq assumption reads

$$\overline{v'_i \theta'} = -\alpha_t \frac{\partial \bar{\theta}}{\partial x_i} \quad (11.31)$$

where  $\alpha_t$  denotes the turbulent thermal diffusivity. It is usually obtained from the turbulent viscosity as

$$\alpha_t = \frac{\nu_t}{\sigma_\theta} \quad (11.32)$$

where  $\sigma_\theta$  is the turbulent Prandtl number; it is an empirical constant which is usually set to  $0.7 \leq \sigma_\theta \leq 0.9$ . The physical meaning of the turbulent Prandtl number,  $\sigma_\theta$ , is analogous to the physical meaning of the usual Prandtl number, see Eq. 2.16; it defines how efficient the turbulence transports (by diffusion) momentum compared to how efficient it transports thermal energy, i.e.

$$\sigma_\theta = \frac{\nu_t}{\alpha_t} \quad (11.33)$$

It is important to recognize that the viscosity ( $\nu$ ), the Prandtl number ( $Pr$ ), the thermal diffusivity ( $\alpha$ ) are *physical* parameters which depend on the fluid (e.g. water or air) and its conditions (e.g. temperature). However, the turbulent viscosity ( $\nu_t$ ), the turbulent thermal diffusivity ( $\alpha_t$ ) and the turbulent Prandtl number ( $\sigma_\theta$ ) depend on the flow (e.g. mean flow gradients and turbulence).

## 11.7 Modelling assumptions

Now we will compare the modelling assumptions for the unknown terms in the  $\overline{v'_i v'_j}$ ,  $\overline{v'_i \theta'}$ ,  $k$  and  $\varepsilon$  equations and formulate modelling assumptions for the remaining terms in the Reynolds stress equation. This will give us the Reynolds Stress Model [RSM] (also

called the Reynolds Stress underline Transport Model [RSTM]) where a (modelled) transport equation is solved for each stress. Later on, we will introduce a simplified algebraic model, which is called the Algebraic Stress Model [ASM] (this model is also called Algebraic Reynolds Stress Model, ARSM)

Summary of physical meaning:

$P_{ij}$ ,  $P_{i\theta}$  and  $P^k$  are production terms of  $\overline{v'_i v'_j}$ ,  $\overline{v'_i \theta'}$  and  $k$

$G_{ij}$ ,  $G_{i\theta}$  and  $G^k$  are production terms of  $\overline{v'_i v'_j}$ ,  $\overline{v'_i \theta'}$  and  $k$  due to buoyancy

$D_{ij,t}$ ,  $D_{i\theta,t}$ ,  $D_t^k$  are the turbulent diffusion terms of  $\overline{v'_i v'_j}$ ,  $\overline{v'_i \theta'}$  and  $k$

$\Pi_{i\theta}$  is the pressure-scramble terms of  $\overline{v'_i \theta'}$

$\Pi_{ij}$  is the pressure-strain correlation term, which promotes isotropy of the turbulence

$\varepsilon_{ij}$ ,  $\varepsilon_{i\theta}$  and  $\varepsilon$  are dissipation of  $\overline{v'_i v'_j}$ ,  $\overline{v'_i \theta'}$  and  $k$ , respectively. The dissipation takes place at the small-scale turbulence.

### 11.7.1 Production terms

In RSM and ASM the production terms are computed exactly

$$\begin{aligned} P_{ij} &= -\overline{v'_i v'_k} \frac{\partial \bar{v}_j}{\partial x_k} - \overline{v'_j v'_k} \frac{\partial \bar{v}_i}{\partial x_k}, \quad P^k = \frac{1}{2} P_{ii} = -\overline{v'_i v'_j} \frac{\partial \bar{v}_i}{\partial x_j} \\ P_{i\theta} &= -\overline{v'_i v'_k} \frac{\partial \bar{\theta}}{\partial x_k} - \overline{v'_k \theta'} \frac{\partial \bar{v}_i}{\partial x_k} \end{aligned} \quad (11.34)$$

The  $k$  is usually not solved for in RSM but a length-scale equation (i.e.  $\varepsilon$  or  $\omega$ ) is always part of an RSM and that equation includes  $P^k$ .

In the  $k - \varepsilon$  model, the Reynolds stresses in the production term are computed using the Boussinesq assumption, which gives

$$\begin{aligned} -\overline{v'_i v'_j} &= \nu_t \left( \frac{\partial \bar{v}_i}{\partial x_j} + \frac{\partial \bar{v}_j}{\partial x_i} \right) - \frac{2}{3} \delta_{ij} k \\ P^k &= \nu_t \left( \frac{\partial \bar{v}_i}{\partial x_j} + \frac{\partial \bar{v}_j}{\partial x_i} \right) \frac{\partial \bar{v}_i}{\partial x_j} = \nu_t 2 \bar{s}_{ij} (\bar{s}_{ij} + \Omega_{ij}) = 2 \nu_t \bar{s}_{ij} \bar{s}_{ij} \\ \bar{s}_{ij} &= \frac{1}{2} \left( \frac{\partial \bar{v}_i}{\partial x_j} + \frac{\partial \bar{v}_j}{\partial x_i} \right), \quad \Omega_{ij} = \frac{1}{2} \left( \frac{\partial \bar{v}_i}{\partial x_j} - \frac{\partial \bar{v}_j}{\partial x_i} \right) \end{aligned} \quad (11.35)$$

where on the second line we used the fact that  $\bar{s}_{ij} \Omega_{ij} = 0$  because the product between a symmetric tensor ( $\bar{s}_{ij}$ ) and an asymmetric tensor ( $\Omega_{ij}$ ) is zero.

### 11.7.2 Diffusion terms

The diffusion terms in the  $k$  and  $\varepsilon$ -equations in the  $k - \varepsilon$  model are modelled using the standard gradient hypothesis which reads

$$\begin{aligned} D^k &= \frac{\partial}{\partial x_j} \left[ \left( \nu + \frac{\nu_t}{\sigma_k} \right) \frac{\partial k}{\partial x_j} \right] \\ D^\varepsilon &= \frac{\partial}{\partial x_j} \left[ \left( \nu + \frac{\nu_t}{\sigma_\varepsilon} \right) \frac{\partial \varepsilon}{\partial x_j} \right] \end{aligned} \quad (11.36)$$

The gradient hypothesis simply assumes that turbulent diffusion acts as to even out all inhomogeneities. In other words, it assumes that the turbulent diffusion term,  $D_t^k$ , transports  $k$  from regions where  $k$  is large to regions where  $k$  is small. The turbulent diffusion flux of  $k$  is expressed as

$$d_{j,t}^k = \frac{1}{2} \overline{v'_j v'_i v'_i} = -\frac{\nu_t}{\sigma_k} \frac{\partial k}{\partial x_j} \quad (11.37)$$

Only the triple correlations are included since the pressure diffusion usually is negligible (see Fig. 8.2 at p. 69). Taking the divergence of Eq. 11.37 (including the minus sign in Eq. 11.21) gives the turbulent diffusion term in Eq. 11.36.

Solving the equations for the Reynolds stresses,  $\overline{v'_i v'_j}$ , opens possibilities for a more advanced model of the turbulent diffusion terms. Equation 11.37 assumes that if the gradient is zero in  $x_i$  direction, then there is no diffusion flux in that direction. A more general gradient hypothesis can be formulated without this limitation, e.g.

$$d_{j,t,G}^k \propto \overline{v'_j v'_k} \frac{\partial k}{\partial x_k} \quad (11.38)$$

which is called the general gradient diffusion hypothesis (GGDH). It was derived in [18] from the transport equation of the triple correlation  $\overline{v'_j v'_i v'_i}$ . In GGDH the turbulent flux  $d_{1,t,G}^k$ , for example, is computed as

$$d_{1,t,G}^k \propto \overline{v'_1 v'_1} \frac{\partial k}{\partial x_1} + \overline{v'_1 v'_2} \frac{\partial k}{\partial x_2} + \overline{v'_1 v'_3} \frac{\partial k}{\partial x_3} \quad (11.39)$$

Hence, even if  $\partial k / \partial x_1 = 0$  the diffusion flux  $d_{1,t,G}^k$  may be non-zero. A quantity of dimension [s] must be added to get the correct dimension, and as in Eq. 11.24 we take  $k/\varepsilon$  so that

$$d_{j,t,G}^k = c_k \frac{k}{\varepsilon} \overline{v'_j v'_k} \frac{\partial k}{\partial x_k} \quad (11.40)$$

The diffusion term,  $D_t^k$ , in the  $k$  equation is obtained by taking the divergence of this equation

$$D_t^k = \frac{\partial d_{j,t,G}^k}{\partial x_j} = \frac{\partial}{\partial x_j} \left( c_k \frac{k}{\varepsilon} \overline{v'_j v'_k} \frac{\partial k}{\partial x_k} \right) \quad (11.41)$$

This diffusion model may be used when the  $k$  equation is solved in an RSM or an ASM. The corresponding diffusion terms for the  $\varepsilon$  and  $\overline{v'_i v'_j}$  equations read

$$\begin{aligned} D_t^\varepsilon &= \frac{\partial}{\partial x_j} \left( c_\varepsilon \overline{v'_j v'_k} \frac{k}{\varepsilon} \frac{\partial \varepsilon}{\partial x_k} \right) \\ D_{ij,t} &= \frac{\partial}{\partial x_k} \left( c_k \overline{v'_k v'_m} \frac{k}{\varepsilon} \frac{\partial \overline{v'_i v'_j}}{\partial x_m} \right) \end{aligned} \quad (11.42)$$

Equation 11.42 often causes numerical problems. A more stable alternative is to model the diffusion terms as in 11.36 which for  $\overline{v'_i v'_j}$  reads

$$D_{ij,t} = \frac{\partial}{\partial x_m} \left( \frac{\nu_t}{\sigma_k} \frac{\partial \overline{v'_i v'_j}}{\partial x_m} \right) \quad (11.43)$$

### 11.7.3 Dissipation term, $\varepsilon_{ij}$

The dissipation term  $\varepsilon_{ij}$  (see Eq. 11.10) is active for the small-scale turbulence. Because of the cascade process and vortex stretching (see Figs. 5.2 and 5.3) the small-scale turbulence is isotropic. This means that the velocity fluctuations of the small-scale turbulence have no preferred direction, see p. 48. This gives:

1.  $\overline{v_1'^2} = \overline{v_2'^2} = \overline{v_3'^2}$ .
2. All shear stresses are zero, i.e.

$$\overline{v_i' v_j'} = 0 \quad \text{if } i \neq j$$

because the fluctuations in two different coordinate directions are not correlated.

What applies for the small-scale fluctuations (Items 1 and 2, above) must also apply to the gradients of the fluctuations, i.e.

$$\begin{aligned} \frac{\partial v'_1}{\partial x_k} \frac{\partial v'_1}{\partial x_k} &= \frac{\partial v'_2}{\partial x_k} \frac{\partial v'_2}{\partial x_k} = \frac{\partial v'_3}{\partial x_k} \frac{\partial v'_3}{\partial x_k} \\ \frac{\partial v'_i}{\partial x_k} \frac{\partial v'_j}{\partial x_k} &= 0 \quad \text{if } i \neq j \end{aligned} \quad (11.44)$$

The relations in Eq. 11.44 are conveniently expressed in tensor notation as

$$\varepsilon_{ij} = \frac{2}{3} \varepsilon \delta_{ij} \quad (11.45)$$

where the factor 2/3 is included so that  $\varepsilon = \frac{1}{2} \varepsilon_{ii}$  is satisfied, see Eqs. 11.10 and 11.21.

### 11.7.4 Slow pressure-strain term

The pressure-strain term,  $\Pi_{ij}$ , makes a large contribution to the  $\overline{v_i' v_j'}$  equation. In Section 9 it was shown that for channel flow it is negative for the streamwise equation,  $v_1'^2$ , and positive for the wall-normal,  $v_2'^2$ , and spanwise,  $v_3'^2$ , equations. Furthermore, it acts as a sink term for the shear stress equation. In summary, it was shown that the term acts as to make the turbulence more *isotropic*, i.e. decreasing the large normal stresses and the magnitude of the shear stress and increasing the small normal stresses. The pressure-strain term is often called the *Robin Hood* terms, because it “takes from the rich and gives to the poor”.

The role of the pressure strain can be described in physical terms as follows. Assume that two fluid particles with fluctuating velocities  $v'_1$  bounce into each other at  $O$  so that  $\partial v'_1 / \partial x_1 < 0$ , see Fig. 11.1. As a result the fluctuating pressure  $p'$  increases at  $O$  so that

$$p' \frac{\partial v'_1}{\partial x_1} < 0$$

The fluid in the  $x_1$  direction is performing work, moving fluid particles against the pressure gradient. The kinetic energy lost in the  $x_1$  direction is transferred to the  $x_2$  and  $x_3$  directions and we assume that the collision makes fluid particles move in the other two directions, i.e.

$$\frac{\partial v'_2}{\partial x_2} > 0, \quad \frac{\partial v'_3}{\partial x_3} > 0 \quad (11.46)$$

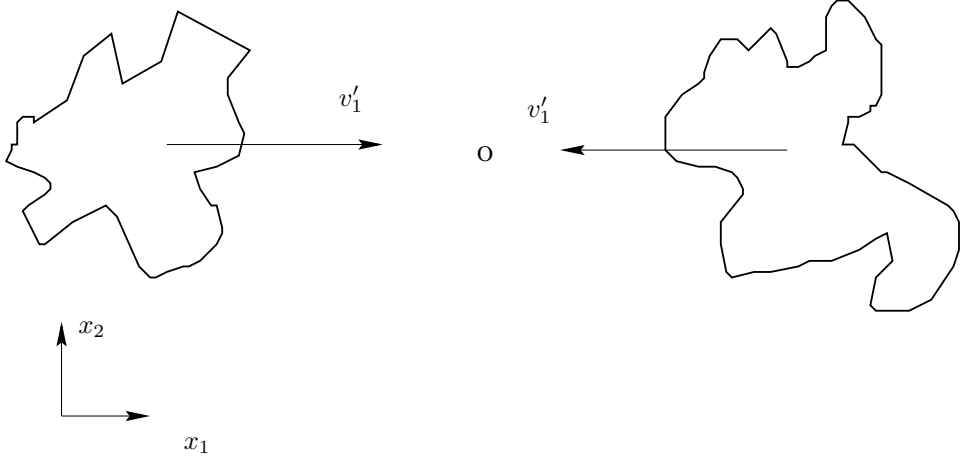


Figure 11.1: Physical illustration of the pressure-strain term.

Indeed, if  $\partial v'_1 / \partial x_1 < 0$ , the continuity equation gives  $\partial v'_2 / \partial x_2 + \partial v'_3 / \partial x_3 > 0$ . However, in Eq. 11.46 we assume that not only their sum is positive but also that they both are positive. If this is to happen the kinetic energy in the  $x_1$  direction must be larger than that in the  $x_2$  and  $x_3$  direction, i.e.  $\overline{v'^2_1} > \overline{v'^2_2}$  and  $\overline{v'^2_1} > \overline{v'^2_3}$ . If this were not true, the fluctuation  $v'_1$  would not be able to create an acceleration of both  $v'_2$  and  $v'_3$ .

The amount of kinetic energy transferred from the  $x_1$  direction to the  $x_2$  and  $x_3$  directions, should be proportional to the difference of their energy, i.e.

$$\begin{aligned} \frac{1}{\rho} \overline{p' \frac{\partial v'_1}{\partial x_1}} &\propto -\frac{1}{2} \left[ \left( \overline{v'^2_1} - \overline{v'^2_2} \right) + \left( \overline{v'^2_1} - \overline{v'^2_3} \right) \right] = - \left[ \overline{v'^2_1} - \frac{1}{2} \left( \overline{v'^2_2} + \overline{v'^2_3} \right) \right] \\ &= - \left[ \frac{3}{2} \overline{v'^2_1} - \frac{1}{2} \left( \overline{v'^2_1} + \overline{v'^2_2} + \overline{v'^2_3} \right) \right] = - \left( \frac{3}{2} \overline{v'^2_1} - k \right) \end{aligned} \quad (11.47)$$

The expression in Eq. 11.47 applies only to the normal stresses, i.e. the principal axis of  $\overline{v'_i v'_j}$ . By transforming to a coordinate system which is rotated  $\pi/4$  it is shown that the sign of  $\overline{p'(\partial v'_i / \partial x_j + \partial v'_j / \partial x_i)}$  and  $\overline{v'_i v'_j}$  are opposite. Assume that we express Eq. 11.47 in principal coordinates,  $(x_{1*}, x_{2*})$ , and then transform the equation to  $(x_1, x_2)$  by rotating it angle  $\alpha = \pi/4$ , see Appendix P. Replacing  $u_{12}$  in Eq. P.6b by  $\overline{v'_1 v'_2}$  we get

$$\overline{v'_1 v'_2} = 0.5 \left( \overline{v'^2_{1*}} - \overline{v'^2_{2*}} \right) \quad (11.48)$$

since  $\overline{v'_{1*} v'_{2*}} = \overline{v'_{2*} v'_{1*}}$ . Now we have transformed the right side of Eq. 11.47. Next step is to transform the left side, i.e. the velocity gradients. We use Eqs. P.6b and P.6c: replacing  $u_{12}$  and  $u_{21}$  by  $\partial v'_1 / \partial x_2$  and  $\partial v'_2 / \partial x_1$ , respectively, and adding them gives

$$\frac{\partial v'_2}{\partial x_1} + \frac{\partial v'_1}{\partial x_2} = \frac{\partial v'_{1*}}{\partial x_{1*}} - \frac{\partial v'_{2*}}{\partial x_{2*}} \quad (11.49)$$

the pressure-strain term in Eqs. 11.10 and 11.47 can be written

$$\overline{p' \left( \frac{\partial v'_2}{\partial x_1} + \frac{\partial v'_1}{\partial x_2} \right)} = \overline{p' \left( \frac{\partial v'_{1*}}{\partial x_{1*}} - \frac{\partial v'_{2*}}{\partial x_{2*}} \right)} \quad (11.50)$$

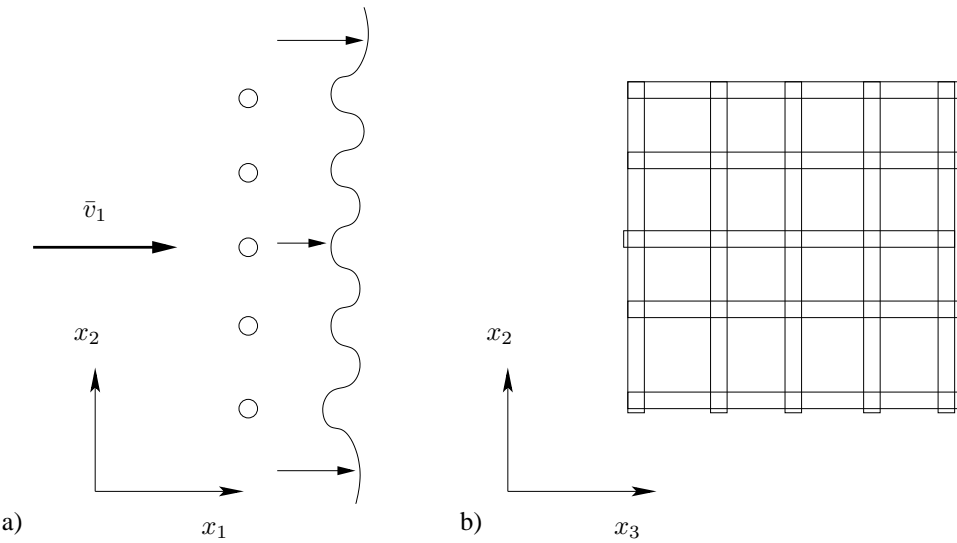


Figure 11.2: Decaying grid turbulence. The circles (a) and the thin rectangles (b) illustrates part of the grid which consists of a mesh of circular cylinders.

Now we apply Eq. 11.47 using the right side of Eq. 11.50

$$\overline{p' \left( \frac{\partial v'_{1*}}{\partial x_{1*}} - \frac{\partial v'_{2*}}{\partial x_{2*}} \right)} \propto - \left( \overline{v'^2_{1*}} - \overline{v'^2_{2*}} \right) \quad (11.51)$$

Inserting Eqs. 11.48 and 11.50 into Eq. 11.51 gives finally

$$\overline{p' \left( \frac{\partial v'_2}{\partial x_1} + \frac{\partial v'_1}{\partial x_2} \right)} = -\rho \overline{v'_1 v'_2} \quad (11.52)$$

This shows that the pressure-strain term acts as a sink term in the shear stress equation. Thus, Eqs. 11.47 and 11.52 lead us to write

$$\Phi_{ij,1} \equiv \overline{p' \left( \frac{\partial v'_i}{\partial x_j} + \frac{\partial v'_j}{\partial x_i} \right)} = -c_1 \rho \frac{\varepsilon}{k} \left( \overline{v'_i v'_j} - \frac{2}{3} \delta_{ij} k \right) \quad (11.53)$$

where  $\Phi$  denotes the *modelled* pressure-strain term and subscript 1 means the slow part; the concept “slow” and “rapid” is discussed at p. 96. We have introduced the turbulent time scale  $k/\varepsilon$ . This pressure-strain model for the slow part was proposed by Rotta in 1951 [19].

Let us investigate how Eq. 11.53 behaves for decaying grid turbulence, see Fig. 11.2. Flow from left with velocity  $\bar{v}_1$  passes through a grid. The grid creates velocity gradients behind the grid which generate turbulence. Further downstream the velocity gradients are smoothed out and the mean flow becomes constant. From this point and further downstream the flow represents homogeneous turbulence which is slowly approaching isotropic turbulence; furthermore the turbulence is slowly dying (i.e. decaying) due to dissipation. The exact  $\overline{v'_i v'_j}$  equation for this flow reads (no production or diffusion because of homogeneity)

$$\bar{v}_1 \frac{\partial \overline{v'_i v'_j}}{\partial x_1} = \frac{\overline{p'}}{\rho} \left( \frac{\partial v'_i}{\partial x_j} + \frac{\partial v'_j}{\partial x_i} \right) - \varepsilon_{ij} \quad (11.54)$$

Rotta's pressure-strain model is supposed to reduce anisotropy. Thus it should be interesting to re-write Eq. 11.54 expressed in the normalized anisotropy Reynolds stress tensor which is defined as

$$b_{ij} = \frac{\overline{v'_i v'_j}}{2k} - \frac{1}{3}\delta_{ij} \quad (11.55)$$

Note that when the turbulence is isotropic, then  $b_{ij} = 0$ . We introduce  $b_{ij}$  (Eq. 11.55), Rotta's model (Eq. 11.53) and the model for the dissipation tensor (11.45) into Eq. 11.54 so that

$$2\bar{v}_1 \left( \frac{\partial(kb_{ij})}{\partial x_1} + \delta_{ij} \frac{1}{3} \frac{\partial k}{\partial x_1} \right) = -2c_1 \varepsilon b_{ij} - \frac{2}{3} \delta_{ij} \varepsilon \quad (11.56)$$

Analogously to Eq. 11.54, the  $k$  equation in decaying grid turbulence reads

$$\bar{v}_1 \frac{\partial k}{\partial x_1} = -\varepsilon \quad (11.57)$$

Inserting Eq. 11.57 in Eq. 11.56 and dividing by  $2k$  we obtain

$$\bar{v}_1 \frac{\partial b_{ij}}{\partial x_1} = -c_1 \frac{\varepsilon}{k} b_{ij} - \frac{1}{3} \delta_{ij} \frac{\varepsilon}{k} + \frac{\varepsilon}{k} b_{ij} + \frac{1}{3} \delta_{ij} \frac{\varepsilon}{k} = \frac{\varepsilon}{k} b_{ij}(1 - c_1) \quad (11.58)$$

Provided that  $c_1 > 1$  Rotta's model does indeed reduce non-isotropy as it should.

The model of the slow pressure-strain term in Eq. 11.53 can be extended by including terms which are non-linear in  $\overline{v'_i v'_j}$ . To make it general it is enough to include terms which are quadratic in  $\overline{v'_i v'_j}$ , since according to the Cayley-Hamilton theorem, a second-order tensor satisfies its own characteristic equation (see Section 1.20 in [20]); this means that terms cubic in  $\overline{v'_i v'_j}$  can be expressed in terms linear and quadratic in  $\overline{v'_i v'_j}$ . The most general form of  $\Phi_{ij,1}$  can be formulated as [21]

$$\begin{aligned} \Phi_{ij,1} &= -c_1 \rho \left[ \varepsilon a_{ij} + c'_1 \left( a_{ik} a_{kj} - \frac{1}{3} \delta_{ij} a_{kl} a_{lk} \right) \right] \\ a_{ij} &= \frac{\overline{v'_i v'_j}}{k} - \frac{2}{3} \delta_{ij} \end{aligned} \quad (11.59)$$

$a_{ij}$  is the anisotropy tensor whose trace is zero. In isotropic flow all its components are zero. Note that the right side is trace-less (i.e. the trace is zero). This should be so since the exact form of  $\Phi_{ij}$  is trace-less, i.e.  $\Phi_{ii} = \overline{2p' \partial v'_i / \partial x_i} = 0$ .

### 11.7.5 Rapid pressure-strain term

Above a model for the slow part of the pressure-strain term was developed using physical arguments. Here we will carry out a mathematical derivation of a model for the rapid part of the pressure-strain term.

The notation "rapid" comes from a classical problem in turbulence called the rapid distortion problem, where a very strong velocity gradient  $\partial \bar{v}_i / \partial x_j$  is imposed so that initially the second term (the slow term) can be neglected, see Eq. 11.61. It is assumed that the effect of the mean gradients is much larger than the effect of the turbulence, i.e.

$$\left| \frac{\partial \bar{v}_i}{\partial x_j} \right| \Big/ (\varepsilon/k) \rightarrow \infty \quad (11.60)$$

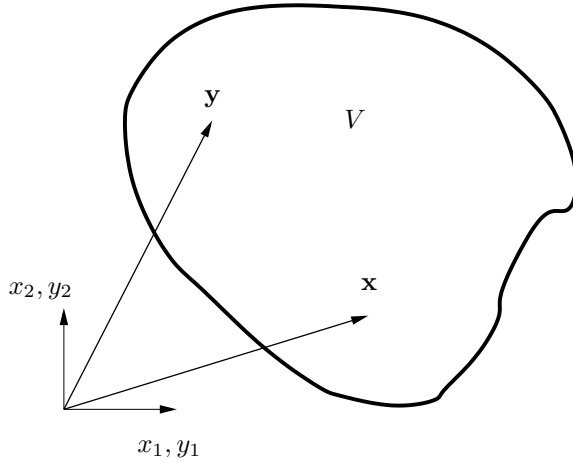


Figure 11.3: The exact solution to Eq. 11.62. The integral is carried out for all points,  $\mathbf{y}$ , in volume  $V$ .

Thus in this case it is the first term in Eq. 11.61 which gives the most “rapid” response in  $p'$ . The second “slow” term becomes important first at a later stage when turbulence has been generated.

Now we want to derive an exact equation for the pressure-strain term,  $\Pi_{ij}$ . Since it includes the fluctuating pressure,  $p'$ , we start by deriving an exact equation for  $p'$  starting from Navier-Stokes equations.

1. Take the divergence of incompressible Navier-Stokes equation assuming constant viscosity (see Eq. 6.3) i.e.  $\frac{\partial}{\partial x_i} \left( v_j \frac{\partial v_i}{\partial x_j} \right) = \dots \Rightarrow$  Equation **A**.
2. Take the divergence of incompressible time-averaged Navier-Stokes equation assuming constant viscosity (see Eq. 6.5) i.e.  $\frac{\partial}{\partial x_i} \left( \bar{v}_j \frac{\partial \bar{v}_i}{\partial x_j} \right) = \dots \Rightarrow$  Equation **B**.

Subtracting of Equation **B** from Equation **A** gives a Poisson equation for the fluctuating pressure  $p'$

$$\frac{1}{\rho} \frac{\partial^2 p'}{\partial x_j \partial x_j} = -2 \underbrace{\frac{\partial \bar{v}_i}{\partial x_j} \frac{\partial v'_j}{\partial x_i}}_{\text{rapid term}} - \underbrace{\frac{\partial^2}{\partial x_i \partial x_j} \left( v'_i v'_j - \bar{v}'_i \bar{v}'_j \right)}_{\text{slow term}} \quad (11.61)$$

For a Poisson equation

$$\frac{\partial^2 \varphi}{\partial x_j \partial x_j} = f \quad (11.62)$$

there exists an exact analytical solution given by Green's formula, see Appendix Q (it is derived from Gauss divergence law)

$$\varphi(\mathbf{x}) = -\frac{1}{4\pi} \int_V \frac{f(\mathbf{y}) dy_1 dy_2 dy_3}{|\mathbf{y} - \mathbf{x}|} \quad (11.63)$$

where the integrals at the boundaries vanish because it is assumed that  $f \rightarrow 0$  at the boundaries, see Fig. 11.3. Applying Eq. 11.63 on Eq. 11.61 gives

$$p'(\mathbf{x}) = \frac{\rho}{4\pi} \int_V \left[ \underbrace{2 \frac{\partial \bar{v}_i(\mathbf{y})}{\partial y_j} \frac{\partial v'_j(\mathbf{y})}{\partial y_i}}_{\text{rapid term}} + \underbrace{\frac{\partial^2}{\partial y_i \partial y_j} (v'_i(\mathbf{y}) v'_j(\mathbf{y}) - \overline{v'_i(\mathbf{y}) v'_j(\mathbf{y})})}_{\text{slow term}} \right] \frac{d\mathbf{y}^3}{|\mathbf{y} - \mathbf{x}|} \quad (11.64)$$

where  $d\mathbf{y}^3 = dy_1 dy_2 dy_3$ . Now make two assumptions in Eq. 11.64:

- i) the turbulence is homogeneous (i.e. the spatial derivative of all time-averaged fluctuating quantities is zero). This requirement is not as drastic as it may sound (very few turbulent flows are homogeneous). This term is indeed very small compared to the second derivative of the instantaneous fluctuations,  $v'_i(\mathbf{y}) v'_j(\mathbf{y})$ .
- ii) the variation of  $\partial \bar{v}_i / \partial x_j$  in space is small. The same argument can be used as above: the mean gradient  $\partial \bar{v}_i / \partial x_j$  varies indeed much more slowly than the instantaneous velocity gradient,  $\partial v'_j(\mathbf{y}) / \partial y_i$ .

Assumption i) means that the last term in the integral in Eq. 11.64 is zero, i.e.

$$\frac{\partial^2 \overline{v'_i v'_j}}{\partial y_i \partial y_j} = 0$$

Assumption ii) means that the mean velocity gradient can be taken outside the integral. Now multiply Eq. 11.64 with  $\partial v'_i / \partial x_j + \partial v'_j / \partial x_i$ . Since this term is not a function of  $\mathbf{y}$  it can be moved in under the integral. We obtain after time averaging

$$\begin{aligned} & \frac{1}{\rho} \overline{p'(\mathbf{x}) \left( \frac{\partial v'_i(\mathbf{x})}{\partial x_j} + \frac{\partial v'_j(\mathbf{x})}{\partial x_i} \right)} \\ &= \frac{\partial \bar{v}_k(\mathbf{x})}{\partial x_\ell} \underbrace{\frac{1}{2\pi} \int_V \left( \frac{\partial v'_i(\mathbf{x})}{\partial x_j} + \frac{\partial v'_j(\mathbf{x})}{\partial x_i} \right) \frac{\partial v'_\ell(\mathbf{y})}{\partial y_k} \frac{d\mathbf{y}^3}{|\mathbf{y} - \mathbf{x}|}}_{M_{ijk\ell}} \\ &+ \underbrace{\frac{1}{4\pi} \int_V \left( \frac{\partial v'_i(\mathbf{x})}{\partial x_j} + \frac{\partial v'_j(\mathbf{x})}{\partial x_i} \right) \frac{\partial^2}{\partial y_k \partial y_\ell} (v'_k(\mathbf{y}) v'_\ell(\mathbf{y})) \frac{d\mathbf{y}^3}{|\mathbf{y} - \mathbf{x}|}}_{A_{ij}} \end{aligned} \quad (11.65)$$

Note that the mean velocity gradient,  $\partial \bar{v} / \partial x_\ell$ , is taken at point  $\mathbf{x}$  because it has been moved out of the integral. In order to understand this better, consider the integral

$$f(x) = \int_0^L \frac{g(\xi) d\xi}{|x - \xi|} \quad (11.66)$$

Note that  $x$  and  $\xi$  are coordinates along the same axis (think of them as two different points along the  $x$  axis). If the two points,  $x$  and  $\xi$ , are far from each other, then the denominator is large and the contribution to the integral is small. Hence, we only need to consider  $\xi$  points which are close to  $x$ . If we assume that  $g(\xi)$  varies slowly with  $\xi$ ,

$g(\xi)$  can be moved out of the integral and since  $x$  is close to  $\xi$ , Eq. 11.66 can be written as

$$f(x) = g(x) \int_0^L \frac{d\xi}{|x - \xi|} \quad (11.67)$$

Going from Eq. 11.66 to Eq. 11.67 corresponds to moving the mean velocity gradient out of the integral. Equation 11.65 can be written on shorter form as

$$\overline{\frac{p'}{\rho} \left( \frac{\partial v'_i}{\partial x_j} + \frac{\partial v'_j}{\partial x_i} \right)} = A_{ij} + M_{ijkl} \frac{\partial \bar{v}_k}{\partial x_\ell} = \Phi_{ij,1} + \Phi_{ij,2} \quad (11.68)$$

where the first term represents the slow term,  $\Phi_{ij,1}$  (see Eq. 11.53), and second term the rapid term,  $\Phi_{ij,2}$  (index 2 denotes the rapid part).

Now we will take a closer look at rapid part (i.e. the second term) of  $M_{ijkl}$ . The second term of  $M_{ijkl}$  in the integral in Eq. 11.65 can be rewritten as

$$\begin{aligned} \overline{\frac{\partial v'_j(\mathbf{x})}{\partial x_i} \frac{\partial v'_\ell(\mathbf{y})}{\partial y_k}} &= \frac{\partial}{\partial y_k} \left( \overline{v'_\ell(\mathbf{y}) \frac{\partial v'_j(\mathbf{x})}{\partial x_i}} \right) - \overline{v'_\ell(\mathbf{y})} \overline{\frac{\partial^2 v'_j(\mathbf{x})}{\partial y_k \partial x_i}} \\ &= \frac{\partial^2}{\partial y_k \partial x_i} \left( \overline{v'_\ell(\mathbf{y}) v'_j(\mathbf{x})} \right) - \frac{\partial}{\partial y_k} \left( \overline{v'_j(\mathbf{x})} \frac{\partial v'_\ell(\mathbf{y})}{\partial x_i} \right) \\ &= \frac{\partial^2}{\partial y_k \partial x_i} \left( \overline{v'_\ell(\mathbf{y}) v'_j(\mathbf{x})} \right) \end{aligned} \quad (11.69)$$

$\partial^2 v'_j(\mathbf{x}) / \partial y_k \partial x_i$  on line 1 is zero because  $v'_j(\mathbf{x})$  is not a function of  $\mathbf{y}$ . For the same reason the last term on line 2 is zero.

Note that the terms above as well as in Eq. 11.65 are two-point correlations, the two points being  $\mathbf{x}$  and  $\mathbf{y}$ . Introduce the distance vector between the two points

$$r_i = y_i - x_i \quad (11.70)$$

Differentiating Eq. 11.70 gives

$$\frac{\partial}{\partial r_i} = \frac{\partial}{\partial y_i} - \frac{\partial}{\partial x_i} \quad (11.71)$$

Equation 11.70 is a coordinate transformation where we replace  $x_i$  and  $y_i$  with

- I.  $x_i$  and  $r_i$ , or
- II.  $y_i$  and  $r_i$ .

Assumption i) at p. 98 gives that  $\partial/\partial x_i = 0$  (Item I) or  $\partial/\partial y_i = 0$  (Item II). In other words, the two-point correlations are independent of where in space the two points are located; they are only dependent on the distance between the two points (i.e.  $r_i$ ). Hence we can replace the spatial derivative by the distance derivative, i.e.

$$\begin{aligned} \frac{\partial}{\partial x_i} &= - \frac{\partial}{\partial r_i} \\ \frac{\partial}{\partial y_i} &= \frac{\partial}{\partial r_i} \end{aligned} \quad (11.72)$$

We can now write  $M_{ijkl}$  in Eq. 11.65, using Eqs. 11.69 and 11.72, as

$$\begin{aligned} M_{ijkl} &= -\frac{1}{2\pi} \int_V \left[ \frac{\partial^2}{\partial r_k \partial r_i} \left( \overline{v'_\ell v'_j} \right) + \frac{\partial^2}{\partial r_k \partial r_j} \left( \overline{v'_\ell v'_i} \right) \right] \frac{d\mathbf{r}^3}{|\mathbf{r}|} \\ &= a_{ijkl} + a_{jikl} \end{aligned} \quad (11.73)$$

It can be shown that  $a_{ijkl}$  is symmetric with respect to index  $j$  and  $\ell$  (recall that  $v'_\ell$  and  $v'_j$  are not at the same point but separated by  $r_i$ ), i.e.

$$a_{ijkl} = a_{ilkj} \quad (11.74)$$

see Appendix G on p. 224. Furthermore, Eq. 11.73 is independent of in which order the two derivatives are taken, so that  $a_{ijkl}$  is symmetric with respect to  $i$  and  $k$ , i.e.

$$a_{ijkl} = a_{kjl} \quad (11.75)$$

Now let us formulate a general expression of  $a_{ijkl}$  which is linear in  $\overline{v'_i v'_j}$  and symmetric in  $(j, \ell)$  and  $(i, k)$ . We get

$$\begin{aligned} a_{ijkl} &= c_1 \delta_{ik} \overline{v'_j v'_\ell} \\ &\quad + c_2 \delta_{j\ell} \overline{v'_i v'_k} \\ &\quad + c_3 (\delta_{ij} \overline{v'_k v'_\ell} + \delta_{kj} \overline{v'_i v'_\ell} + \delta_{i\ell} \overline{v'_k v'_j} + \delta_{k\ell} \overline{v'_i v'_j}) \\ &\quad + c_4 \delta_{j\ell} \delta_{ik} k \\ &\quad + c_5 (\delta_{ij} \delta_{kl} + \delta_{jk} \delta_{il}) k \end{aligned} \quad (11.76)$$

Each line is symmetric in  $(j, \ell)$  and  $(i, k)$ . For example, on line 3, term 1 & term 3 and term 2 & term 4 are symmetric with respect to  $j$  and  $\ell$  and term 1 & term 2 and term 3 & term 4 are symmetric with respect to  $i$  and  $k$ .

Consider Eq. 11.65. Here it is seen that if  $i = j$  then  $M_{ijkl} = 0$  due to the continuity equation; looking at Eq. 11.73 we get

$$a_{iilk} = 0 \quad (11.77)$$

Applying this condition to Eq. 11.76 gives

$$\begin{aligned} 0 &= c_1 \delta_{ik} \overline{v'_i v'_\ell} + c_2 \delta_{i\ell} \overline{v'_i v'_k} + c_3 (3 \overline{v'_k v'_\ell} + \delta_{ki} \overline{v'_i v'_\ell} + \delta_{i\ell} \overline{v'_k v'_i} + \delta_{k\ell} \overline{v'_i v'_i}) \\ &\quad + c_4 \delta_{i\ell} \delta_{ik} k + c_5 (3 \delta_{kl} + \delta_{ik} \delta_{il}) k \\ &= c_1 \overline{v'_k v'_\ell} + c_2 \overline{v'_\ell v'_k} + c_3 (3 \overline{v'_k v'_\ell} + \overline{v'_k v'_\ell} + \overline{v'_k v'_\ell} + 2 \delta_{k\ell} k) \\ &\quad + c_4 \delta_{k\ell} k + c_5 (3 \delta_{kl} + \delta_{k\ell}) k \\ &= \overline{v'_k v'_\ell} (c_1 + c_2 + 5c_3) + k \delta_{k\ell} (c_4 + 2c_3 + 4c_5) \end{aligned} \quad (11.78)$$

Green's third formula reads (see Appendix G on p. 224)

$$a_{ijie} = 2 \overline{v'_j v'_\ell} \quad (11.79)$$

Using Eq. 11.79 in Eq. 11.76 gives

$$\begin{aligned} 2 \overline{v'_j v'_\ell} &= 3c_1 \overline{v'_j v'_\ell} + c_2 \delta_{j\ell} \overline{v'_i v'_i} + c_3 (\delta_{ij} \overline{v'_i v'_\ell} + \delta_{ij} \overline{v'_i v'_\ell} + \delta_{i\ell} \overline{v'_i v'_j} + \delta_{i\ell} \overline{v'_i v'_j}) \\ &\quad + (3c_4 \delta_{j\ell} + c_5 (\delta_{ij} \delta_{il} + \delta_{ji} \delta_{il})) k \\ &= 3c_1 \overline{v'_j v'_\ell} + 2c_2 \delta_{j\ell} k + 4c_3 \overline{v'_j v'_\ell} + (3c_4 + 2c_5) \delta_{j\ell} k \\ &= \overline{v'_j v'_\ell} (3c_1 + 4c_3) + \delta_{j\ell} k (2c_2 + 3c_4 + 2c_5) \end{aligned} \quad (11.80)$$

Equations 11.78 and 11.80 give four equations

$$\begin{aligned} c_1 + c_2 + 5c_3 &= 0, & c_4 + 2c_3 + 4c_5 &= 0 \\ 3c_1 + 4c_3 - 2 &= 0, & 2c_2 + 3c_4 + 2c_5 &= 0 \end{aligned} \quad (11.81)$$

for the five unknown constants. Let us express all constants in  $c_2$  which gives

$$c_1 = \frac{4c_2 + 10}{11}, \quad c_3 = -\frac{3c_2 + 2}{11}, \quad c_4 = -\frac{50c_2 + 4}{55}, \quad c_5 = \frac{20c_2 + 6}{55} \quad (11.82)$$

Inserting Eq. 11.82 into Eq. 11.76 and 11.68 gives

$$\begin{aligned} \phi_{ij,2} &= M_{ijkl} \frac{\partial \bar{v}_k}{\partial x_\ell} = (a_{ijkl} + a_{jikl}) \frac{\partial \bar{v}_k}{\partial x_\ell} \\ &= c_1 \left( \overline{v'_j v'_\ell} \frac{\partial \bar{v}_i}{\partial x_\ell} + \overline{v'_i v'_\ell} \frac{\partial \bar{v}_j}{\partial x_\ell} \right) + c_2 \left( \overline{v'_i v'_k} \frac{\partial \bar{v}_k}{\partial x_j} + \overline{v'_j v'_k} \frac{\partial \bar{v}_k}{\partial x_i} \right) \\ &\quad + c_3 \left( 2\delta_{ij} \overline{v'_k v'_\ell} \frac{\partial \bar{v}_k}{\partial x_\ell} + \overline{v'_i v'_\ell} \frac{\partial \bar{v}_j}{\partial x_\ell} + \overline{v'_j v'_\ell} \frac{\partial \bar{v}_i}{\partial x_\ell} + \overline{v'_k v'_j} \frac{\partial \bar{v}_k}{\partial x_i} + \overline{v'_k v'_i} \frac{\partial \bar{v}_k}{\partial x_j} \right) \\ &\quad + c_4 k \left( \frac{\partial \bar{v}_i}{\partial x_j} + \frac{\partial \bar{v}_j}{\partial x_i} \right) + c_5 k \left( \frac{\partial \bar{v}_j}{\partial x_i} + \frac{\partial \bar{v}_i}{\partial x_j} \right) \end{aligned} \quad (11.83)$$

We find that the  $c_1$  term and the second and third part of the  $c_3$  term can be merged. Furthermore, the  $c_2$  term and the third and fourth part of the  $c_3$  term can be merged as well as the  $c_4$  and  $c_5$  terms; using Eq. 11.81 we get

$$\begin{aligned} \phi_{ij,2} &= -\frac{c_2 + 8}{11} P_{ij} - \frac{8c_2 - 2}{11} \mathcal{D}_{ij} + \frac{6c_2 + 4}{11} P^k + \frac{4 - 60c_2}{55} k \bar{s}_{ij} \\ \mathcal{D}_{ij} &= -\overline{v'_i v'_k} \frac{\partial \bar{v}_k}{\partial x_j} - \overline{v'_j v'_k} \frac{\partial \bar{v}_k}{\partial x_i} \end{aligned} \quad (11.84)$$

Finally we re-write this equation so that it is expressed in trace-less tensors

$$\begin{aligned} \Phi_{ij,2} &= -\rho \frac{c_2 + 8}{11} \left( P_{ij} - \frac{2}{3} \delta_{ij} P^k \right) \\ &\quad - \rho \frac{8c_2 - 2}{11} \left( \mathcal{D}_{ij} - \frac{2}{3} \delta_{ij} P^k \right) - \frac{60c_2 - 4}{55} \rho k \bar{s}_{ij} \end{aligned} \quad (11.85)$$

where  $c_2 = 0.4$ . Note that  $\Phi_{ii} = 0$  as we required in Eq. 11.77. This pressure-strain model is called the LRR model and it was proposed in [22].

All three terms in Eq. 11.85 satisfy continuity and symmetry conditions. It might be possible to use a simpler pressure-strain model using one or any two terms. Since the first term is the most important one, a simpler model has been proposed [22, 23]

$$\Phi_{ij,2} = -c_2 \rho \left( P_{ij} - \frac{2}{3} \delta_{ij} P^k \right) \quad (11.86)$$

It can be noted that there is a close similarity between the Rotta model and Eq. 11.86: both models represent “return-to-isotropy”, the first expressed in  $\overline{v'_i v'_j}$  and the second in  $P_{ij}$ . The model in Eq. 11.86 is commonly called the IP model (IP=Isotropization by Production). Since two terms are omitted we should expect that the best value of  $\gamma$  should be different than  $(c_2 + 8)/11$ ; a value of  $\gamma = 0.6$  was ( $c_2 = -1.4$ ) found to give good agreement with experimental data. Since Eq. 11.86 is a truncated form of

	LRR model	LRR-IP model
$c_1$ (Eq. 11.53)	1.5	1.5
$c_2$ (Eq. 11.85)	0.4	—
$c_2$ (Eq. 11.86)	—	0.6

Table 11.1: Constants in the LRR and LRR-IP pressure-strain models.

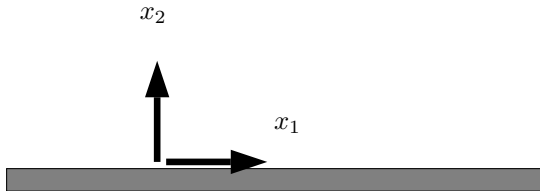


Figure 11.4: Modelling of wall correction in pressure-strain terms.

Eq. 11.85 it does not satisfy all requirements that Eq. 11.85 do. Equation 11.86 does satisfy symmetry condition and continuity but it does not satisfy the integral condition in Eq. 11.79. Although Eq. 11.86 is a simpler, truncated version of Eq. 11.85, it is often found to give more accurate results [24]. Since the IP model is both simpler and seems to be more accurate than Eq. 11.85, it is one of the most popular models of the rapid pressure-strain term. The coefficients for the slow and rapid terms in the LRR and LRR-IP models are summarized in Table 11.1

### 11.7.6 Wall model of the pressure-strain term

When we derived the rapid pressure-strain model using Green's function in Eq. 11.64 we neglected the influence of any boundaries. In wall-bounded domains it turns out that the effect of the walls must be taken into account. Both the rapid term in the LRR model and the IP model must be modified to include wall modelling.

The effect of the wall is to dampen turbulence. There are two main effects whose underlying physics are entirely different.

1. **Viscosity.** Close to the wall the viscous processes (viscous diffusion and dissipation) dominate over the turbulent ones (production and turbulent diffusion).
2. **Pressure.** When a fluid particle approaches a wall, the presence of the wall is felt by the fluid particle over a long distance. This is true for a fluid particle carried by the wind approaching a building as well as for a fluid particle carried by a fluctuating velocity approaching the wall in a turbulent boundary layer. In both cases it is the pressure that informs the fluid particle of the presence of the wall.

Since the pressure-strain term includes the fluctuating pressure, it is obviously the second of these two processes that we want to include in the wall model. Up to now we have introduced two terms for modelling the pressure-strain term, the slow and the

fast term. It is suitable to include a slow and a fast **wall model term**, i.e.

$$\Phi_{ij} = \Phi_{ij,1} + \Phi_{ij,2} + \Phi_{ij,1w} + \Phi_{ij,2w} \quad (11.87)$$

where subscript  $w$  denotes wall modelling.

Consider a wall, see Fig. 11.4. The pressure fluctuations dampens the wall-normal fluctuations. Furthermore, the damping effect of the wall should decrease for increasing wall distance. We need to scale the wall-normal distance with a relevant quantity and the turbulent length scale,  $k^{3/2}/\varepsilon$ , seems to be a good candidate. For the wall-normal fluctuations, the IP wall model reads [25]

$$\begin{aligned} \Phi_{22,1w} &= -2c_{1w} \frac{\varepsilon}{k} \overline{v_2'^2} f \\ f &= \frac{k^{\frac{3}{2}}}{2.55 |(x_i - x_{i,w})| \varepsilon} \end{aligned} \quad (11.88)$$

where  $|x_i - x_{i,w}|$  denotes the distance vector to the wall. As explained above, this damping is inviscid (due to pressure) and affects the turbulent fluctuations well into the log-region. It has nothing to do with viscous damping. Away from the wall, in the fully turbulent region, the damping function goes to zero since the distance to the wall ( $|x_i - x_{i,w}|$ ) increases faster than the turbulence length scale,  $k^{3/2}/\varepsilon$ . In the viscous region the wall model term,  $\Phi_{22,1w}$ , is not relevant and should be zero since it should account only for inviscid damping. Moreover, function  $f$  should not exceed one.

The IP wall model for the wall-parallel fluctuations reads

$$\Phi_{11,1w} = \Phi_{33,1w} = c_{1w} \frac{\varepsilon}{k} \overline{v_2'^2} f \quad (11.89)$$

The requirement that the sum of the pressure strain term should be zero. i.e.  $\Phi_{ii,1w} = 0$ , is now satisfied since  $\Phi_{11,1w} + \Phi_{22,1w} + \Phi_{33,1w} = 0$ .

The wall model for the shear stress is set as

$$\Phi_{12,1w} = -\frac{3}{2} c_{1w} \frac{\varepsilon}{k} \overline{v_1' v_2'} f \quad (11.90)$$

The factor 3/2 is needed to ensure that  $\Phi_{ii,1w} = 0$  is satisfied when the coordinate system is rotated. You can prove this by rotating the matrix  $[\Phi_{11,1w}, \Phi_{12,1w}; \Phi_{21,1w}, \Phi_{22,1w}]$  and taking the trace of  $\Phi$  in the principal coordinates system (i.e. taking the sum of the eigenvalues).

The general formula for a wall that is not aligned with a Cartesian coordinate axis reads [25]

$$\Phi_{ij,1w} = c_{1w} \frac{\varepsilon}{k} \left( \overline{v'_k v'_m} n_{k,w} n_{m,w} \delta_{ij} - \frac{3}{2} \overline{v'_k v'_i} n_{k,w} n_{j,w} - \frac{3}{2} \overline{v'_k v'_j} n_{i,w} n_{k,w} \right) f \quad (11.91)$$

An analogous wall model is used for the rapid part which reads

$$\Phi_{ij,2w} = c_{2w} \left( \Phi_{km,2} n_{k,w} n_{m,w} \delta_{ij} - \frac{3}{2} \Phi_{ki,2} n_{k,w} n_{j,w} - \frac{3}{2} \Phi_{kj,2} n_{i,w} n_{k,w} \right) f \quad (11.92)$$

### 11.8 The $k - \varepsilon$ model

The exact  $k$  equation is given by Eq. 11.21. By inserting the model assumptions for the turbulent diffusion (Eq. 11.36), the production (Eq. 11.35) and the buoyancy term (Eqs. 11.31 and 11.32) we get the *modelled* equation for  $k$

$$\frac{\partial k}{\partial t} + \bar{v}_j \frac{\partial k}{\partial x_j} = \nu_t \left( \frac{\partial \bar{v}_i}{\partial x_j} + \frac{\partial \bar{v}_j}{\partial x_i} \right) \frac{\partial \bar{v}_i}{\partial x_j} + g_i \beta \frac{\nu_t}{\sigma_\theta} \frac{\partial \bar{\theta}}{\partial x_i} - \varepsilon + \frac{\partial}{\partial x_j} \left[ \left( \nu + \frac{\nu_t}{\sigma_k} \right) \frac{\partial k}{\partial x_j} \right] \quad (11.93)$$

In the same way, the modelled  $\varepsilon$  equation is obtained from Eq. 11.26

$$\begin{aligned} \frac{\partial \varepsilon}{\partial t} + \bar{v}_j \frac{\partial \varepsilon}{\partial x_j} &= \frac{\varepsilon}{k} c_{\varepsilon 1} \nu_t \left( \frac{\partial \bar{v}_i}{\partial x_j} + \frac{\partial \bar{v}_j}{\partial x_i} \right) \frac{\partial \bar{v}_i}{\partial x_j} \\ &\quad + c_{\varepsilon 1} g_i \frac{\varepsilon}{k} \frac{\nu_t}{\sigma_\theta} \frac{\partial \bar{\theta}}{\partial x_i} - c_{\varepsilon 2} \frac{\varepsilon^2}{k} + \frac{\partial}{\partial x_j} \left[ \left( \nu + \frac{\nu_t}{\sigma_\varepsilon} \right) \frac{\partial \varepsilon}{\partial x_j} \right] \end{aligned} \quad (11.94)$$

The turbulent viscosity is computed as

$$\nu_t = c_\mu \frac{k^2}{\varepsilon} \quad (11.95)$$

The standard values for the coefficients read

$$(c_\mu, c_{\varepsilon 1}, c_{\varepsilon 2}, \sigma_k, \sigma_\varepsilon) = (0.09, 1.44, 1.92, 1, 1.3) \quad (11.96)$$

## 11.9 The modelled $\overline{v'_i v'_j}$ equation with IP model

With the models for diffusion, pressure-strain and dissipation we get

$$\begin{aligned}
& \bar{v}_k \frac{\partial \overline{v'_i v'_j}}{\partial x_k} = \text{(convection)} \\
& -\overline{v'_i v'_k} \frac{\partial \bar{v}_j}{\partial x_k} - \overline{v'_j v'_k} \frac{\partial \bar{v}_i}{\partial x_k} \quad \text{(production)} \\
& -c_1 \frac{\varepsilon}{k} \left( \overline{v'_i v'_j} - \frac{2}{3} \delta_{ij} k \right) \quad \text{(slow part)} \\
& -c_2 \left( P_{ij} - \frac{2}{3} \delta_{ij} P^k \right) \quad \text{(rapid part)} \\
& + c_{1w} \rho \frac{\varepsilon}{k} \left[ \overline{v'_k v'_m} n_k n_m \delta_{ij} - \frac{3}{2} \overline{v'_i v'_k} n_k n_j \right. \\
& \quad \left. - \frac{3}{2} \overline{v'_j v'_k} n_k n_i \right] f \quad \text{(wall, slow part)} \\
& + c_{2w} \left[ \Phi_{km,2} n_k n_m \delta_{ij} - \frac{3}{2} \Phi_{ik,2} n_k n_j \right. \\
& \quad \left. - \frac{3}{2} \Phi_{jk,2} n_k n_i \right] f \quad \text{(wall, rapid part)} \\
& \quad + \nu \frac{\partial^2 \overline{v'_i v'_j}}{\partial x_k \partial x_k} \quad \text{(viscous diffusion)} \\
& + \frac{\partial}{\partial x_k} \left[ c_k \overline{v'_k v'_m} \frac{k}{\varepsilon} \frac{\partial \overline{v'_i v'_j}}{\partial x_m} \right] \quad \text{(turbulent diffusion)} \\
& - g_i \beta \overline{v'_j \theta'} - g_j \beta \overline{v'_i \theta'} \quad \text{(buoyancy production)} \\
& - \frac{2}{3} \varepsilon \delta_{ij} \quad \text{(dissipation)}
\end{aligned} \tag{11.97}$$

## 11.10 Algebraic Reynolds Stress Model (ASM)

The Algebraic Reynolds Stress Model is a simplified Reynolds Stress Model. The RSM and  $k - \varepsilon$  models are written in symbolic form (see p. 86 & 88) as:

$$\begin{aligned}
\text{RSM : } & C_{ij} - D_{ij} = P_{ij} + \Phi_{ij} - \varepsilon_{ij} \\
k - \varepsilon : & C^k - D^k = P^k - \varepsilon
\end{aligned} \tag{11.98}$$

In ASM we assume that the transport (convective and diffusive) of  $\overline{v'_i v'_j}$  is related to that of  $k$ , i.e.

$$C_{ij} - D_{ij} = \frac{\overline{v'_i v'_j}}{k} (C^k - D^k)$$

Inserting Eq. 11.98 into the equation above gives

$$P_{ij} + \Phi_{ij} - \varepsilon_{ij} = \frac{\overline{v'_i v'_j}}{k} (P^k - \varepsilon) \tag{11.99}$$

Thus the transport equation (PDE) for  $\overline{v'_i v'_j}$  has been transformed into an *algebraic* equation based on the assumption in Eq. 11.98.

Now we want to re-write this equation as an equation for  $\overline{v'_i v'_j}$ . Insert the IP models for  $\Phi_{ij,1}$  (Eq. 11.53) and  $\Phi_{ij,2}$  (Eq. 11.86) and the isotropic model for  $\varepsilon_{ij}$  (Eq. 11.45) in Eq. 11.99 and multiply by  $k/\varepsilon$  so that

$$\begin{aligned} \frac{k}{\varepsilon} P_{ij} - c_1 \left( \overline{v'_i v'_j} - \frac{2}{3} \delta_{ij} k \right) - c_2 \frac{k}{\varepsilon} \left( P_{ij} - \frac{2}{3} \delta_{ij} P^k \right) - \frac{2}{3} \delta_{ij} k \\ + \frac{k}{\varepsilon} (\Phi_{ij,1w} + \Phi_{ij,2w}) = \frac{\overline{v'_i v'_j}}{\varepsilon} (P^k - \varepsilon) \end{aligned}$$

Collect all  $\overline{v'_i v'_j}$  terms so that

$$\begin{aligned} \overline{v'_i v'_j} \left( \frac{P^k}{\varepsilon} - 1 + c_1 \right) = \\ \frac{k}{\varepsilon} \left[ P_{ij} - c_2 \left( P_{ij} - \frac{2}{3} \delta_{ij} P^k \right) + \Phi_{ij,1w} + \Phi_{ij,2w} \right] + \frac{2}{3} \delta_{ij} k (-1 + c_1) \\ = \frac{k}{\varepsilon} \left[ P_{ij} \boxed{-\delta_{ij} \frac{2}{3} P^k} - c_2 \left( P_{ij} - \frac{2}{3} \delta_{ij} P^k \right) + \Phi_{ij,1w} + \Phi_{ij,2w} \right] + \boxed{\frac{2}{3} \delta_{ij} k (P^k / \varepsilon)} - 1 + c_1 \end{aligned}$$

where  $(2/3)\delta_{ij}P^k/\varepsilon$  was added and subtracted at the last line (shown in boxes). Dividing both sides by  $P^k/\varepsilon - 1 + c_1$  gives finally

$$\overline{v'_i v'_j} = \frac{2}{3} \delta_{ij} k + \frac{k}{\varepsilon} \frac{(1 - c_2) \left( P_{ij} - \frac{2}{3} \delta_{ij} P^k \right) + \Phi_{ij,1w} + \Phi_{ij,2w}}{c_1 + P^k / \varepsilon - 1} \quad (11.100)$$

In boundary layer flow Eq. 11.100 reads

$$-\overline{v'_1 v'_2} = \frac{2}{3} \underbrace{(1 - c_2) \frac{c_1 - 1 + c_2 P^k / \varepsilon}{(c_1 - 1 + P^k / \varepsilon)}}_{c_\mu} \frac{k^2}{\varepsilon} \frac{\partial \bar{v}}{\partial y}$$

As can be seen, this model can be seen as an extension of an eddy-viscosity model where the  $c_\mu$  constant is made a function of the ratio  $P^k/\varepsilon$ .

## 11.11 Explicit ASM (EASM or EARSM)

Equation 11.100 is an *implicit* equation for  $\overline{v'_i v'_j}$ , i.e. the Reynolds stresses appear both on the left and the right side of the equation. It would of course be advantageous to be able to get an *explicit* expression for the Reynolds stresses. Pope [26] managed to derive an explicit expression for ASM in two dimensions. He assumed that the Reynolds stress tensor can be expressed in the strain-rate tensor,  $\bar{s}_{ij}$ , and the vorticity tensor,  $\Omega_{ij}$ . Furthermore, he showed that the coefficients,  $G^{(n)}$ , in that expression can be a function of not more than the following five invariants

$$\begin{aligned} (k^2 / \varepsilon^2) \bar{s}_{ij} \bar{s}_{ji}, \quad (k^2 / \varepsilon^2) \bar{\Omega}_{ij} \bar{\Omega}_{ji}, \quad (k^3 / \varepsilon^3) \bar{s}_{ij} \bar{s}_{jk} \bar{s}_{ki} \\ (k^3 / \varepsilon^3) \bar{\Omega}_{ij} \bar{\Omega}_{jk} \bar{s}_{ki}, \quad (k^4 / \varepsilon^4) \bar{\Omega}_{ij} \bar{\Omega}_{jk} \bar{s}_{km} \bar{s}_{mi} \end{aligned} \quad (11.101)$$

In two dimension the expression reads

$$\overline{v'_i v'_j} = \frac{2}{3} k \delta_{ij} + G^{(1)} \frac{k^2}{\varepsilon} \bar{s}_{ij} + G^{(2)} \frac{k^3}{\varepsilon^2} (\bar{s}_{ik} \bar{\Omega}_{kj} - \bar{\Omega}_{ik} \bar{s}_{kj}) \quad (11.102)$$

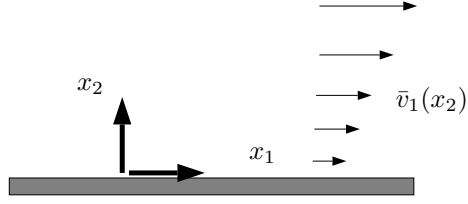


Figure 11.5: Boundary layer flow.

In general three-dimensional flow, the Reynolds stress tensor depends on 10 tensors,  $T_{ij}^n$  [26], i.e.

$$\begin{aligned}
 \overline{v'_i v'_j} - k\delta_{ij} &= \sum_{n=1}^{10} G^{(n)} T_{ij}^n \\
 T_{ij}^1 &= \bar{s}_{ij}, \quad T_{ij}^2 = \bar{s}_{ik}\bar{\Omega}_{kj} - \bar{s}_{jk}\bar{\Omega}_{ki}, \quad T_{ij}^3 = \bar{s}_{ik}\bar{s}_{kj} - \frac{1}{3}\delta_{ij}\bar{s}_{ik}\bar{s}_{ki} \\
 T_{ij}^4 &= \bar{\Omega}_{ik}\bar{\Omega}_{kj} - \frac{1}{3}\delta_{ij}\bar{\Omega}_{ik}\bar{\Omega}_{ki}, \quad T_{ij}^5 = \bar{\Omega}_{ik}\bar{s}_{km}\bar{s}_{mj} - \bar{s}_{im}\bar{s}_{mk}\bar{\Omega}_{kj} \\
 T_{ij}^6 &= \bar{\Omega}_{im}\bar{\Omega}_{mk}\bar{s}_{kj} + \bar{s}_{ik}\bar{\Omega}_{km}\bar{\Omega}_{mj} - \frac{2}{3}\delta_{ij}\bar{\Omega}_{pm}\bar{\Omega}_{mk}\bar{s}_{kp} \\
 T_{ij}^7 &= \bar{\Omega}_{im}\bar{s}_{mk}\bar{\Omega}_{kn}\bar{\Omega}_{nj} - \bar{\Omega}_{im}\bar{\Omega}_{mk}\bar{s}_{kn}\bar{\Omega}_{nj}, \quad T_{ij}^8 = \bar{s}_{im}\bar{\Omega}_{mk}\bar{s}_{kn}\bar{s}_{nj} - \bar{s}_{im}\bar{s}_{mk}\bar{\Omega}_{kn}\bar{s}_{nj} \\
 T_{ij}^9 &= \bar{\Omega}_{im}\bar{\Omega}_{mk}\bar{s}_{kn}\bar{s}_{nj} - \bar{s}_{im}\bar{s}_{mk}\bar{\Omega}_{kn}\bar{\Omega}_{nj} - \frac{2}{3}\delta_{ij}\bar{\Omega}_{pm}\bar{\Omega}_{mk}\bar{s}_{kn}\bar{s}_{np} \\
 T_{ij}^{10} &= \bar{\Omega}_{im}\bar{s}_{mk}\bar{s}_{kn}\bar{\Omega}_{np}\bar{\Omega}_{pj} - \bar{\Omega}_{im}\bar{\Omega}_{mk}\bar{s}_{kn}\bar{s}_{np}\bar{\Omega}_{pj}
 \end{aligned} \tag{11.103}$$

where  $T_{ij}^n$  may depend on the five invariants in Eq. 11.101. Equation 11.103 is a general form of a non-linear eddy-viscosity model. Any ASM may be written on the form of Eq. 11.103.

It may be noted that Eq. 11.103 includes only linear and quadratic terms of  $\bar{s}_{ij}$  and  $\bar{\Omega}_{ij}$ . That is because of Cayley-Hamilton theorem which states that a second-order tensor satisfies its own characteristic equation (see Section 1.20 in [20]); hence cubic terms or higher can recursively be expressed in linear ( $\bar{s}_{ij}$ ) and quadratic tensors ( $\bar{s}_{ik}\bar{s}_{kj}$ ). Furthermore, note that all terms in Eq. 11.103 are symmetric and traceless as required by the left side,  $\overline{v'_i v'_j} - 2\delta_{ij}k/3$ .

## 11.12 Boundary layer flow

Let us study boundary layer flow (Fig. 11.5) where  $\bar{v}_2 = 0$ ,  $\bar{v}_1 = \bar{v}_1(x_2)$ . In general the production  $P_{ij}$  has the form:

$$P_{ij} = -\overline{v'_i v'_k} \frac{\partial \bar{v}_j}{\partial x_k} - \overline{v'_j v'_k} \frac{\partial \bar{v}_i}{\partial x_k}$$

In this special case we get:

$$P_{11} = -2\overline{v'_1 v'_2} \frac{\partial \bar{v}_1}{\partial x_2}$$

$$P_{12} = -\overline{v'_2^2} \frac{\partial \bar{v}_1}{\partial x_2}$$

$$P_{22} = 0$$

Is  $\overline{v'_2^2}$  zero because its production term  $P_{22}$  is zero? No! The sympathetic term  $\Phi_{ij}$  which takes from the rich (i.e.  $\overline{v'_1^2}$ ) and gives to the poor (i.e.  $\overline{v'_2^2}$ ) saves the unfair situation! The IP model for  $\Phi_{ij,1}$  and  $\Phi_{ij,2}$  gives

$$\begin{aligned}\Phi_{22,1} &= c_1 \frac{\varepsilon}{k} \left( \frac{2}{3} k - \overline{v'_2^2} \right) > 0 \\ \Phi_{22,2} &= c_2 \frac{1}{3} P_{11} = -c_2 \frac{2}{3} \overline{v'_1 v'_2} \frac{\partial \bar{v}_1}{\partial x_2} > 0\end{aligned}$$

Note also that the dissipation term for the  $\overline{v'_1 v'_2}$  is zero, but it takes the value  $\frac{2}{3}\varepsilon$  for the  $\overline{v'_1^2}$  and  $\overline{v'_2^2}$  equations (see p. 93). Since the modelled  $\overline{v'_1 v'_2}$  does not have any dissipation term, the question arises: what is the main sink term in the  $\overline{v'_1 v'_2}$  equation? The answer is, again, the pressure strain term  $\Phi_{ij,1}$  and  $\Phi_{ij,2}$ .

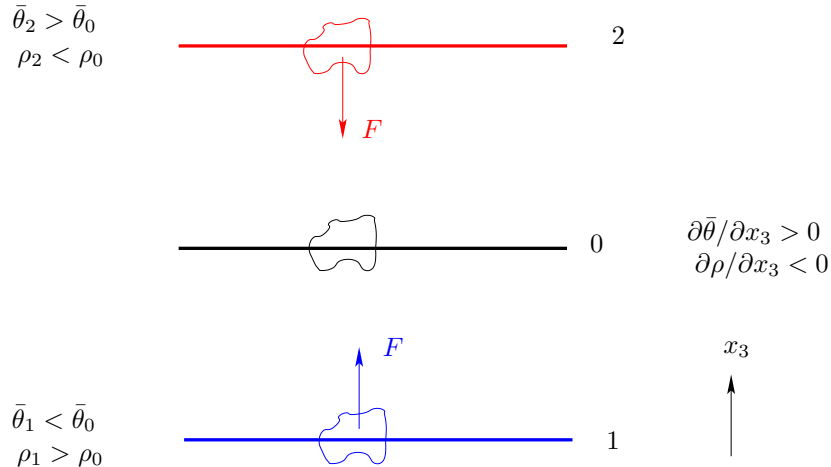


Figure 12.1: Stable stratification due to positive temperature gradient  $\partial\bar{\theta}/\partial x_3 > 0$ .

## 12 Reynolds stress models vs. eddy-viscosity models

In this section we present three fundamental physical processes which Reynolds stress models are able to handle whereas eddy-viscosity models fail. The reason for the superiority of the former model is in all cases that the production term is treated exactly, whereas it in eddy-viscosity models is modelled.

### 12.1 Stable and unstable stratification

In flows where buoyancy is dominating, the temperature has a large effect on the turbulence through the buoyancy term  $G_{ij}$ , see Eq. 11.10. If the temperature increases upwards (i.e.  $\partial\bar{\theta}/\partial x_3 > 0$ ), then the flow is **stably stratified**. This is illustrated in Fig. 12.1. Consider  $\partial\bar{\theta}/\partial x_3 > 0$ . This means that the density decreases with increasing vertical height, i.e.  $\partial\rho/\partial x_3 < 0$ . If a fluid particle is displaced from its equilibrium level 0 up to level 2, see Fig. 12.1, it is heavier than the surrounding at this new level ( $\rho_0 > \rho_2$ ). Hence, the buoyancy forces the particle back to its original position 0. In this way the vertical turbulent fluctuations are damped. Similarly if a particle originating at level 0, is moved down to level 1. Here it is lighter than its new environment, and hence buoyancy makes it to move make to its original level 0.

For the case of **unstable stratification**, the situation is reversed. Cold fluid is located on top of hot fluid, i.e.  $\partial\bar{\theta}/\partial x_3 < 0$  and  $\partial\rho/\partial x_3 > 0$ . In Fig. 12.1 we would then have  $\rho_2 > \rho_0$ . If a fluid particle at level 0 is displaced upwards to level 2, it is at this location lighter than its new environment; hence it continues to move upwards. If it is moved down to level 1 it is heavier than its new environments and it will then continue downwards. Hence, turbulent fluctuations are enhanced. This flow situation is called **unstable stratification**.

The production term due to buoyancy reads (see Eq. 11.10)

$$G_{33} = 2g\beta v'_3 \bar{\theta}' \quad (12.1)$$

since  $g_i = (0, 0, -g)$ . From the equation for the turbulent heat flux,  $\bar{v}'_3 \bar{\theta}'$  (i.e. Eq. 11.19

with  $i = 3$ ), we find the production term for  $\overline{v'_3 \theta'}$

$$P_{3\theta} = -\overline{v'_3 v'_k} \frac{\partial \bar{\theta}}{\partial x_k} - \overline{v'_k \theta'} \frac{\partial \bar{v}_3}{\partial x_k} \quad (12.2)$$

In the case illustrated in Fig. 12.1, the production term due to temperature gradient reads  $P_{3\theta} = -\overline{v'^2_3} \partial \bar{\theta} / \partial x_3 < 0$  (recall that we assume that buoyancy dominates so that the first term in Eq. 12.2 is much larger than the second one). Since the main source term in the  $\overline{v'_3 \theta'}$  equation,  $P_{3\theta}$ , is negative, it makes  $\overline{v'_3 \theta'} < 0$  so that  $G_{33} < 0$  (see Eq. 12.1). Thus, for the case illustrated in Fig. 12.1, we find that the production term,  $G_{33}$ , due to buoyancy yields a damping of the vertical fluctuations as it should.

Note that the horizontal turbulent fluctuations are not affected by the buoyancy term,  $G_{ij}$ , since  $G_{11} = G_{22} = 0$  because the gravity is in the  $x_3$  direction (i.e.  $g_1 = g_2 = 0$ ).

If the situation in Fig. 12.1 is reversed so that  $\partial \bar{\theta} / \partial x_3 < 0$  the vertical fluctuations are instead augmented. This is called **unstably stratified** conditions.

When eddy-viscosity models are used, transport equations are usually not solved for  $\overline{v'_i \theta'}$ . Instead the heat flux tensor is modelled with an eddy-viscosity assumption using the Boussinesq assumption, see Eq. 11.31. The buoyancy term,  $G^k$ , in the  $k$  equation reads, see Eq. 11.10 (take the trace of  $G_{ij}$  and divide by two)

$$G^k = 0.5 G_{ii} = -g_i \beta \overline{v'_i \theta'} \quad (12.3)$$

For  $g_i = (0, 0, -g)$ , it reads  $G^k = g \beta \overline{v'_3 \theta'}$  which with Eq. 11.31 gives

$$G^k = -g \beta \frac{\nu_t}{\sigma_\theta} \frac{\partial \bar{\theta}}{\partial x_3} \quad (12.4)$$

Hence it is seen that in stably stratified conditions,  $G^k < 0$  as required. The difference between an eddy-viscosity model and a Reynolds stress model, is that the former reduces  $k$  whereas the latter reduces only the vertical fluctuations.

## 12.2 Curvature effects

When the streamlines in boundary layer flow have a convex curvature, the turbulence is stabilized. This dampens the turbulence [27, 28], especially the shear stress and the Reynolds stress normal to the wall. Concave curvature destabilizes the turbulence. The ratio of boundary layer thickness  $\delta$  to curvature radius  $R$  is a common parameter for quantifying the curvature effects on the turbulence. The work reviewed by Bradshaw [27] demonstrates that even such small amounts of convex curvature as  $\delta/R = 0.01$  can have a significant effect on the turbulence. In [29] they carried out an experimental investigation on a configuration simulating the flow near a trailing edge of an airfoil, where they measured  $\delta/R \simeq 0.03$ . They reported a 50 percent decrease of  $\rho \overline{v'^2_2}$  (Reynolds stress in the normal direction to the wall) owing to curvature. The reduction of  $\rho \overline{v'^2_1}$  and  $-\rho \overline{v'_1 v'_2}$  was also substantial. In addition they reported significant damping of the turbulence in the shear layer in the outer part of the separation region.

An illustrative model case is curved boundary layer flow, see Fig. 12.2. A polar coordinate system  $r - \theta$  with  $\hat{\theta}$  locally aligned with the streamline is introduced. As  $v_\theta = v_\theta(r)$  (with  $\partial v_\theta / \partial r > 0$  and  $v_r = 0$ ), the radial inviscid momentum equation degenerates to

$$\frac{\rho v_\theta^2}{r} - \frac{\partial p}{\partial r} = 0 \quad (12.5)$$

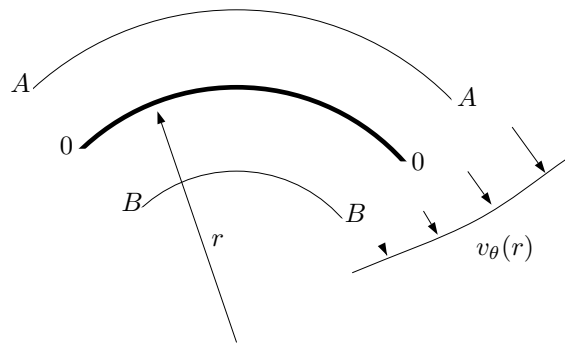


Figure 12.2: Flow in a polar coordinate system illustrating streamline curvature. The streamline is aligned with the  $\theta$  axis.

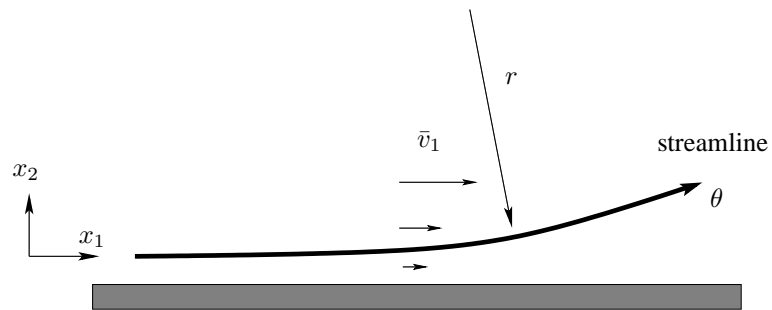


Figure 12.3: Streamline curvature occurring when the flow approaches, for example, a separation region or an obstacle.

	$\partial \mathbf{V}_\theta / \partial \mathbf{r} > \mathbf{0}$	$\partial \mathbf{V}_\theta / \partial \mathbf{r} < \mathbf{0}$
convex curvature	stabilizing	destabilizing
concave curvature	destabilizing	stabilizing

Table 12.1: Effect of streamline curvature on turbulence.

Here the variables are instantaneous or laminar. The centrifugal force exerts a force in the normal direction (outward) on a fluid following the streamline, which is balanced by the pressure gradient. Since we have assumed that  $\partial v_\theta / \partial r > 0$ , Eq. 12.5 shows that the pressure gradient increases with  $r$ . If the fluid is displaced by some disturbance (e.g. turbulent fluctuation) outwards to level A, it encounters a pressure gradient larger than that to which it was accustomed at  $r = r_0$ , as  $(v_\theta)_A > (v_\theta)_0$ , which from Eq. 12.5 gives  $(\partial p / \partial r)_A > (\partial p / \partial r)_0$ . Hence the fluid is forced back to  $r = r_0$ . Similarly, if the fluid is displaced inwards to level B, the pressure gradient is smaller here than at  $r = r_0$  and cannot keep the fluid at level B. Instead the centrifugal force drives it back to its original level.

It is clear from the model problem above that convex curvature, when  $\partial v_\theta / \partial r > 0$ , has a stabilizing effect on (turbulent) fluctuations, at least in the radial direction. It is discussed below how the Reynolds stress model responds to streamline curvature.

Assume that there is a flat-plate boundary layer flow, see Fig. 12.3. The ratio of the normal stresses  $\rho \bar{v}_1'^2$  to  $\rho \bar{v}_2'^2$  is typically 5. At one  $x_1$  station, the flow is deflected upwards. How will this affect turbulence? Let us study the effect of concave streamline curvature. The production terms  $P_{ij}$  owing to rotational strains ( $\partial \bar{v}_1 / \partial x_2$ ,  $\partial \bar{v}_2 / \partial x_1$ ) can be written as (see Eq. 11.10):

$$\text{RSM, } \overline{v_1'^2} - \text{eq. : } P_{11} = -2 \overline{v'_1 v'_2} \frac{\partial \bar{v}_1}{\partial x_2} \quad (12.6a)$$

$$\text{RSM, } \overline{v'_1 v'_2} - \text{eq. : } P_{12} = \boxed{-\overline{v_1'^2} \frac{\partial \bar{v}_2}{\partial x_1}} - \overline{v_2'^2} \frac{\partial \bar{v}_1}{\partial x_2} \quad (12.6b)$$

$$\text{RSM, } \overline{v_2'^2} - \text{eq. : } P_{22} = \boxed{-2 \overline{v'_1 v'_2} \frac{\partial \bar{v}_2}{\partial x_1}} \quad (12.6c)$$

$$k - \varepsilon \quad P^k = \nu_t \left( \frac{\partial \bar{v}_1}{\partial x_2} + \boxed{\frac{\partial \bar{v}_2}{\partial x_1}} \right)^2 \quad (12.6d)$$

The terms in boxes appear because of the streamline curvature.

As long as the streamlines are parallel to the wall, all production is a result of  $\partial \bar{v}_1 / \partial x_2$ . However as soon as the streamlines are deflected, there are more terms resulting from  $\partial \bar{v}_2 / \partial x_1$ . Even if  $\partial \bar{v}_2 / \partial x_1$  is much smaller than  $\partial \bar{v}_1 / \partial x_2$  it will still contribute non-negligibly to  $P_{12}$  as  $\rho \bar{v}_1'^2$  is much larger than  $\rho \bar{v}_2'^2$ . Thus the magnitude of  $P_{12}$  will increase ( $P_{12}$  is negative) as  $\partial \bar{v}_2 / \partial x_1 > 0$ . An increase in the magnitude of  $P_{12}$  will increase  $-\overline{v'_1 v'_2}$ , which in turn will increase  $P_{11}$  and  $P_{22}$ . This means that  $\rho \bar{v}_1'^2$  and  $\rho \bar{v}_2'^2$  will be larger and the magnitude of  $P_{12}$  will be further increased, and so on. It is seen that there is a positive feedback, which continuously increases the Reynolds stresses. The turbulence is *destabilized* owing to concave curvature of the streamlines. Note that eddy-viscosity models such as  $k - \varepsilon$  and  $k - \omega$  models cannot account for

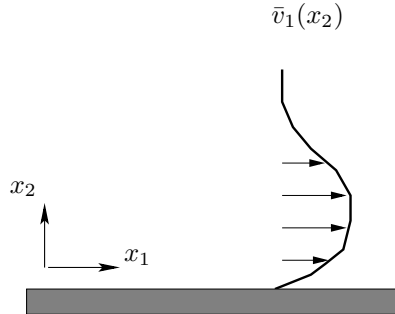


Figure 12.4: The velocity profile for a wall jet.

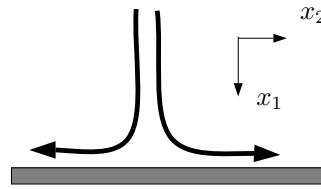


Figure 12.5: The flow pattern for stagnation flow.

streamline curvature since the two rotational strains,  $\partial\bar{v}_1/\partial x_2$  and  $\partial\bar{v}_2/\partial x_1$ , in the production term are multiplied by the same coefficient (the turbulent viscosity).

If the flow (concave curvature) is a wall jet flow where  $\partial\bar{v}_1/\partial x_2 < 0$  in the outer part (see Fig. 12.4) the situation will be reversed: the turbulence will be *stabilized*. If the streamline (and the wall) is deflected downwards, the situation will be as follows: the turbulence is stabilizing when  $\partial\bar{v}_1/\partial x_2 > 0$ , and destabilizing for  $\partial\bar{v}_1/\partial x_2 < 0$ .

The stabilizing or destabilizing effect of streamline curvature is thus dependent on the type of curvature (convex or concave), and whether there is an increase or decrease in momentum in the tangential direction with radial distance from its origin (i.e. the sign of  $\partial V_\theta/\partial r$ ). For convenience, these cases are summarised in Table 12.1. It should be noted that concave or convex depends on from which the streamline is viewed. The streamline in Fig. 12.3, for example, is concave when viewed from the wall but convex when viewed from the orig of the circle with radius  $r$ .

It should be mentioned that one part of the effect of curved streamlines in Eq. 12.6 is due to the transformation of the advective term of the  $\overline{v'_i v'_j}$ -equation (cf. polar coordinates where additional terms appear both in the momentum equations and the transport equation for  $\overline{v'_i v'_j}$ ). In [30] they proposed a correction term to take this effect into account.

## 12.3 Stagnation flow

The  $k - \varepsilon$  model does not model the normal stresses properly, whereas ASM/RSM do. The production term in the  $k$  equations for RSM/ASM and  $k - \varepsilon$  model in stagnation

flow (see Fig. 12.5) due to  $\partial\bar{v}_1/\partial x_1$  and  $\partial\bar{v}_2/\partial x_2$  is:

$$RSM : 0.5 (P_{11} + P_{22}) = -\overline{v'_1^2} \frac{\partial\bar{v}_1}{\partial x_1} - \overline{v'_2^2} \frac{\partial\bar{v}_2}{\partial x_2} = -\frac{\partial\bar{v}_1}{\partial x_1} (\overline{v'_1^2} - \overline{v'_2^2}) \quad (12.7)$$

$$k - \varepsilon : P^k = 2\nu_t \left\{ \left( \frac{\partial\bar{v}_1}{\partial x_1} \right)^2 + \left( \frac{\partial\bar{v}_2}{\partial x_2} \right)^2 \right\} \quad (12.8)$$

where continuity  $\partial\bar{v}_1/\partial x_1 = -\partial\bar{v}_2/\partial x_2$  has been employed. In RSM, the two terms are added with sign. In the  $k - \varepsilon$  model, however, the production will be large because the difference in sign of the two terms is not taken into account.

## 12.4 RSM/ASM versus $k - \varepsilon$ models

- Advantages with  $k - \varepsilon$  models (or eddy viscosity models):
  - i) simple due to the use of an isotropic eddy (turbulent) viscosity
  - ii) stable via stability-promoting second-order gradients in the mean-flow equations
  - iii) work reasonably well for a large number of engineering flows
- Disadvantages:
  - i) isotropic, and thus not good in predicting normal stresses ( $\overline{v'_1^2}, \overline{v'_2^2}, \overline{v'_3^2}$ )
  - ii) as a consequence of i) it is unable to account for curvature effects
  - iii) as a consequence of i) it is unable to account for irrotational strains (stagnation flow)
  - iv) in boundary layers approaching separation, the production due to normal stresses is of the same magnitude as that due to shear stresses [31].
- Advantages with ASM/RSM:
  - i) the production terms do not need to be modelled
  - ii) thanks to i) it can selectively augment or damp the stresses due to curvature effects (RSM is better than ASM because the convective terms are accounted for), boundary layers approaching separation, buoyancy etc.
- Disadvantages with ASM/RSM:
  - i) RSM is complex and difficult to implement, especially implicit ASM
  - ii) numerically unstable because small stabilizing second-order derivatives in the momentum equations (only laminar diffusion)
  - iii) CPU time consuming

## 13 Realizability

There are a number of realizability constraints. The usual two ones are that all normal stresses should stay positive and that the correlation coefficient for the shear stress should not exceed one, i.e.

$$\begin{aligned} \overline{v_i'^2} &\geq 0 \text{ for all } i \\ \frac{\overline{v_i' v_j'}}{\left(\overline{v_i'^2} \overline{v_j'^2}\right)^{1/2}} &\leq 1 \text{ no summation over } i \text{ and } j, i \neq j \end{aligned} \quad (13.1)$$

These criteria are seldom used in RSMs. However, satisfying the first criteria is actually of importance for eddy-viscosity models in stagnation flow [32]. Assume that the flow is in the  $x_1$  direction and that it approaches the wall (see Fig. 12.5). The Boussinesq assumption for the normal stress  $\overline{v_1'^2}$  reads (cf. Eq. 12.7)

$$\overline{v_1'^2} = \frac{2}{3}k - 2\nu_t \frac{\partial \bar{v}_1}{\partial x_1} = \frac{2}{3}k - 2\nu_t \bar{s}_{11} \quad (13.2)$$

It is seen that if  $\bar{s}_{11}$  gets too large then  $\overline{v_1'^2} < 0$  which is unphysical, i.e. non-realizable.

Let's now briefly repeat the concept "invariants". This means something that is independent of the coordinate system. Here we mean independent of rotation of the coordinate system. If a tensor is symmetric, then we know that it has real eigenvalues which means that we can rotate the coordinate system so that the off-diagonal components vanish (see, e.g., [20]). For the strain tensor this means that the off-diagonal components of  $\bar{s}_{ij}$  vanish and this is the coordinate system where the diagonal components become largest (e.g.  $\bar{s}_{11}$  in Eq. 13.2). Thus this is the coordinate system in which the danger of negative  $\overline{v_1'^2}$  from Eq. 13.2 is largest. The equation for finding the eigenvalues of a tensor  $C_{ij}$  is (see e.g. [20] or [33])

$$|C_{ij} - \delta_{ij}\lambda| = 0 \quad (13.3)$$

which gives, in 2D,

$$\begin{vmatrix} C_{11} - \lambda & C_{12} \\ C_{21} & C_{22} - \lambda \end{vmatrix} = 0 \quad (13.4)$$

The resulting equation is

$$\begin{aligned} \lambda^2 - I_1^{2D}\lambda + I_2^{2D} &= 0 \\ I_1^{2D} &= C_{ii} \\ I_2^{2D} &= \frac{1}{2}(C_{ii}C_{jj} - C_{ij}C_{ij}) = \det(C_{ij}) \end{aligned} \quad (13.5)$$

Since the above equation is the same irrespectively of how the coordinate system is rotated, it follows that its coefficients  $I_1^{2D}$  and  $I_2^{2D}$  are invariants.

In 3D Eq. 13.3 gives

$$\begin{vmatrix} C_{11} - \lambda & C_{12} & C_{13} \\ C_{21} & C_{22} - \lambda & C_{23} \\ C_{31} & C_{32} & C_{33} - \lambda \end{vmatrix} = 0 \quad (13.6)$$

which gives

$$\begin{aligned}\lambda^3 - I_1^{3D} \lambda^2 + I_2^{3D} \lambda - I_3^{3D} &= 0 \\ I_1^{3D} &= C_{ii} \\ I_2^{3D} &= \frac{1}{2}(C_{ii}C_{jj} - C_{ij}C_{ij}) \\ I_3^{3D} &= \frac{1}{6}(2C_{ij}C_{jk}C_{ki} - 3C_{ij}C_{ji}C_{kk} + C_{ii}C_{jj}C_{kk}) = \det(C_{ij})\end{aligned}\tag{13.7}$$

The invariants are  $I_1^{3D}$ ,  $I_2^{3D}$  and  $I_3^{3D}$ .

Let's go back to Eq. 13.2 and assume incompressible 2D flow. The first invariant reads (cf. Eq. 13.5)

$$I_1^{2D} = \bar{s}_{ii} = \bar{s}_{11} + \bar{s}_{22} = \lambda_1 + \lambda_2 = 0\tag{13.8}$$

It is zero due to the continuity equation. The second invariant of  $\bar{s}_{ij}$  reads

$$I_2^{2D} = -\bar{s}_{ij}\bar{s}_{ij}/2,\tag{13.9}$$

(see Eq. 13.5) which is the same in all coordinate systems (hence the name "invariant"). The solution to Eq. 13.5, using Eq. 13.8, is

$$\lambda_{1,2} = \pm (-I_2^{2D})^{1/2} = \pm \left(\frac{\bar{s}_{ij}\bar{s}_{ij}}{2}\right)^{1/2}\tag{13.10}$$

The eigenvalues of  $\bar{s}_{ij}$  correspond to the strains in the principal axis. As discussed above, we apply Eq. 13.2 in the principal coordinate directions of  $\bar{s}_{ij}$ . Hence,  $\bar{s}_{11}$  in Eq. 13.2 is replaced by the largest eigenvalue so that

$$\overline{v_1'^2} = \frac{2}{3}k - 2\nu_t\lambda_1\tag{13.11}$$

The requirement  $\overline{v_1'^2} \geq 0$  gives now together with Eq. 13.11

$$\nu_t \leq \frac{k}{3|\lambda_1|} = \frac{k}{3} \left(\frac{2}{\bar{s}_{ij}\bar{s}_{ij}}\right)^{1/2}\tag{13.12}$$

In 3D, Eq. 13.7 instead of Eq. 13.5 is used, and Eq. 13.10 is replaced by [32]

$$|\lambda_k| = k \left(\frac{2\bar{s}_{ij}\bar{s}_{ij}}{3}\right)^{1/2}\tag{13.13}$$

This is a simple modification of an eddy-viscosity model, and it ensure that the normal stresses stay positive.

### 13.1 Two-component limit

Another realizability constraint is to require that when  $\overline{v_i'^2}$  approaches zero near walls, it should do so smoothly. One way to ensure this is to require that the derivative of  $\overline{v_i'^2}$  should go to zero as  $\overline{v_i'^2}$  goes to zero, i.e.

$$\overline{v_i'^2} \rightarrow 0 \Rightarrow \frac{d\overline{v_i'^2}}{dt} \rightarrow 0\tag{13.14}$$

where  $d/dt$  denotes the material derivative (think of Eq. 13.14 in Lagrangian coordinates, i.e. we follow a fluid particle as it approaches the wall). Equation 13.14 requires that when  $\overline{v_i'^2}$  approaches zero, the left side (and thus also the right side) of the transport equation of  $\overline{v_i'^2}$  should also do so too. Since we are here concerned about the pressure-strain term, we'll take a look at how it behaves near walls when  $\overline{v_i'^2} \rightarrow 0$ . This is of some relevance in near-wall turbulence where the wall-normal stress goes to zero faster than the wall-parallel ones: this state of turbulence is called the two-component limit [34]. Neither the form of  $\Phi_{ij,2}$  in Eq. 11.86 nor Eq. 11.85 satisfy the requirement that  $\Phi_{22,2} = 0$  when  $\overline{v_2'^2} = 0$  [21]. In Eq. 11.86, for example,

$$\Phi_{22,2} \rightarrow \gamma \frac{2}{3} \delta_{ij} P^k \neq 0 \quad (13.15)$$

Very complex forms of  $\Phi_{ij,2}$  have been proposed [35] [CL96] which include terms cubic in  $\overline{v_i' v_j'}$ . The CL96 model does satisfy the two-component limit. Another advantage of the CL96 model is that it does not need any wall distances, which is valuable in complex geometries.

The models of the slow pressure-strain in Eq. 11.53 (linear model) and Eq. 11.59 (non-linear model) do also not satisfy the two-component limit. The Rotta model, for example, gives

$$\Phi_{22,1} \rightarrow c_1 \rho \frac{2\varepsilon}{3} \neq 0 \quad (13.16)$$

The only way to ensure this is to make  $c_1 \rightarrow 0$  when the wall is approached. A convenient parameter proposed in [34] is  $A$  which is an expression of  $A_2$  and  $A_3$  (the second and third invariant of  $a_{ij}$ , respectively), i.e.

$$A_2 = a_{ij} a_{ji}, \quad A_3 = a_{ij} a_{jk} a_{ki}, \quad A = 1 - \frac{9}{8}(A_2 - A_3) \quad (13.17)$$

The parameter  $A = 0$  in the two-component limit and  $A = 1$  in isotropic turbulence. Thus  $A$  is a suitable parameter to use when damping the constant  $c_1$  as the wall is approached.

## 14 Non-linear Eddy-viscosity Models

In traditional eddy-viscosity models the turbulent stress  $\overline{v'_i v'_j}$  is formulated from the Boussinesq assumption, i.e.

$$\begin{aligned} a_{ij} &= -2\nu_t \frac{\bar{s}_{ij}}{k} \\ \bar{s}_{ij} &= \frac{1}{2} \left( \frac{\partial \bar{v}_i}{\partial x_j} + \frac{\partial \bar{v}_j}{\partial x_i} \right) \end{aligned} \quad (14.1)$$

where the anisotropy tensor is defined as

$$a_{ij} \equiv \frac{\overline{v'_i v'_j}}{k} - \frac{2}{3} \delta_{ij} \quad (14.2)$$

The relation between the stress  $\overline{v'_i v'_j}$  and the velocity gradient in Eq. 14.1 is, as can be seen, linear. One way to make eddy-viscosity models more general is to include non-linear terms of the strain-rate (i.e. the velocity gradient) [26]. A subset of the most general form reads [36]

$$\begin{aligned} a_{ij} &= \boxed{-2c_\mu \tau \bar{s}_{ij}} \\ &+ c_1 \tau^2 \left( \bar{s}_{ik} \bar{s}_{kj} - \frac{1}{3} \bar{s}_{\ell k} \bar{s}_{\ell k} \delta_{ij} \right) + c_2 \tau^2 \left( \bar{\Omega}_{ik} \bar{s}_{kj} - \bar{s}_{ik} \bar{\Omega}_{kj} \right) \\ &+ c_3 \tau^2 \left( \bar{\Omega}_{ik} \bar{\Omega}_{jk} - \frac{1}{3} \bar{\Omega}_{\ell k} \bar{\Omega}_{\ell k} \delta_{ij} \right) + c_4 \tau^3 \left( \bar{s}_{ik} \bar{s}_{\ell k} \bar{\Omega}_{\ell j} - \bar{\Omega}_{i\ell} \bar{s}_{\ell k} \bar{s}_{kj} \right) \\ &+ c_5 \tau^3 \left( \bar{\Omega}_{i\ell} \bar{\Omega}_{\ell m} \bar{s}_{mj} + \bar{s}_{i\ell} \bar{\Omega}_{\ell m} \bar{\Omega}_{mj} - \frac{2}{3} \bar{\Omega}_{mn} \bar{\Omega}_{n\ell} \bar{s}_{\ell m} \delta_{ij} \right) \\ &+ c_6 \tau^3 \bar{s}_{k\ell} \bar{s}_{k\ell} \bar{s}_{ij} + c_7 \tau^3 \bar{\Omega}_{k\ell} \bar{\Omega}_{k\ell} \bar{s}_{ij} \\ \bar{\Omega}_{ij} &= \frac{1}{2} \left( \frac{\partial \bar{v}_i}{\partial x_j} - \frac{\partial \bar{v}_j}{\partial x_i} \right) \end{aligned} \quad (14.3)$$

where  $\tau$  is a turbulent time scale; for a non-linear  $k - \varepsilon$  model  $\tau = k/\varepsilon$ , and for a non-linear  $k - \omega$  model  $\tau = 1/\omega$ . The tensor groups correspond to a subset of Eq. 11.103:

Line 1:  $T_{ij}^1$ ,

Line 2:  $T_{ij}^3$  and  $T_{ij}^2$

Line 3:  $T_{ij}^4$  and  $T_{ij}^5$

Line 4:  $T_{ij}^6$

Line 5:  $T_{ij}^1$  multiplied by the invariants  $\bar{s}_{k\ell} \bar{s}_{k\ell}$  and  $\bar{\Omega}_{k\ell} \bar{\Omega}_{k\ell}$

The expression in Eq. 14.3 is cubic in  $\partial \bar{v}_i / \partial x_j$ . However, note that it is only quadratic in  $\bar{s}_{ij}$  and  $\bar{\Omega}_{ij}$ . This is due to Cayley-Hamilton theorem which states that a tensor is only linearly independent up to quadratic terms, see p. 96; this means that, for example,  $\bar{s}_{ij}^3 = \bar{s}_{ik} \bar{s}_{k\ell} \bar{s}_{\ell j}$  can be expressed as a linear combination of  $\bar{s}_{ij}^2 = \bar{s}_{ik} \bar{s}_{kj}$  and  $\bar{s}_{ij}$ .

$a_{ij}$  is symmetric and its trace is zero; it is easily verified that the right side of Eq. 14.3 also has these properties. Examples of non-linear models (sometimes also

called *explicit* algebraic Reynolds stress models, EARSM) in the literature are the models presented in [37, 38, 36, 39]. EARSMs are very popular — especially the model in [39] — in the aeronautical community where explicit time-marching solvers are used. They are computationally cheap, more accurate than linear eddy-viscosity models and they don't give rise to any numerical instabilities as in implicit solvers (like SIMPLE). In implicit solvers a large turbulent viscosity in the diffusion term of the momentum equations is needed to stabilize the solution procedure.

Let's take a closer look on Eq. 14.3 in fully developed channel flow ( $\bar{v}_2 = \bar{v}_3 = \partial/\partial x_1 = \partial/\partial x_3 \equiv 0$ ); we obtain

$$\begin{aligned} a_{11} &= \frac{1}{12}\tau^2 \left( \frac{\partial \bar{v}_1}{\partial x_2} \right)^2 (c_1 + 6c_2 + c_3) \\ a_{22} &= \frac{1}{12}\tau^2 \left( \frac{\partial \bar{v}_1}{\partial x_2} \right)^2 (c_1 - 6c_2 + c_3) \\ a_{33} &= -\frac{1}{6}\tau^2 \left( \frac{\partial \bar{v}_1}{\partial x_2} \right)^2 (c_1 + c_3) \\ a_{12} &= -c_\mu \tau \frac{\partial \bar{v}_1}{\partial x_2} + \frac{1}{4}\tau^3 \left( \frac{\partial \bar{v}_1}{\partial x_2} \right)^3 (-c_5 + c_6 + c_7) \end{aligned} \quad (14.4)$$

Using values on the constants as in [36], i.e  $c_1 = -0.05$ ,  $c_2 = 0.11$ ,  $c_3 = 0.21$ ,  $c_4 = -0.8$ ,  $c_5 = 0$ ,  $c_6 = -0.5$  and  $c_7 = 0.5$  we get

$$\begin{aligned} a_{11} &= \frac{0.82}{12}\tau^2 \left( \frac{\partial \bar{v}_1}{\partial x_2} \right)^2 \Rightarrow \bar{v}_1'^2 = \frac{2}{3}k + \frac{0.82}{12}k\tau^2 \left( \frac{\partial \bar{v}_1}{\partial x_2} \right)^2 \\ a_{22} &= \frac{-0.5}{12}\tau^2 \left( \frac{\partial \bar{v}_1}{\partial x_2} \right)^2 \Rightarrow \bar{v}_2'^2 = \frac{2}{3}k - \frac{0.5}{12}k\tau^2 \left( \frac{\partial \bar{v}_1}{\partial x_2} \right)^2 \\ a_{33} &= \frac{-0.16}{12}\tau^2 \left( \frac{\partial \bar{v}_1}{\partial x_2} \right)^2 \Rightarrow \bar{v}_3'^2 = \frac{2}{3}k - \frac{0.16}{12}k\tau^2 \left( \frac{\partial \bar{v}_1}{\partial x_2} \right)^2 \\ a_{12} &= -c_\mu \frac{k}{\varepsilon} \frac{\partial \bar{v}_1}{\partial x_2} \end{aligned} \quad (14.5)$$

We find that indeed the non-linear model gives anisotropic normal Reynolds stresses.

In Eqs. 14.4 and 14.5 we have assumed that the only strain is  $\partial \bar{v}_1 / \partial x_2$ . When we discussed streamline curvature effects at p. 113 we found that it is important to investigate the effect of secondary strains such as  $\partial \bar{v}_2 / \partial x_1$ . Let's write down Eq. 14.3 for the strain  $\partial \bar{v}_2 / \partial x_1$

$$\begin{aligned} a_{11} &= \frac{1}{12}\tau^2 \left( \frac{\partial \bar{v}_2}{\partial x_1} \right)^2 (c_1 - 6c_2 + c_3) \\ a_{22} &= \frac{1}{12}\tau^2 \left( \frac{\partial \bar{v}_2}{\partial x_1} \right)^2 (c_1 + 6c_2 + c_3) \\ a_{33} &= -\frac{1}{6}\tau^2 \left( \frac{\partial \bar{v}_2}{\partial x_1} \right)^2 (c_1 + c_3) \\ a_{12} &= -\frac{1}{4}\tau^3 \left( \frac{\partial \bar{v}_2}{\partial x_1} \right)^3 (c_5 + c_6 + c_7) \end{aligned} \quad (14.6)$$

Inserting with values on the constants from [36] (see above) we obtain

$$\begin{aligned} a_{11} &= -\frac{0.5}{12}\tau^2 \left( \frac{\partial \bar{v}_2}{\partial x_1} \right)^2 \\ a_{22} &= \frac{0.82}{12}\tau^2 \left( \frac{\partial \bar{v}_2}{\partial x_1} \right)^2 \\ a_{33} &= -\frac{0.16}{12}\tau^2 \left( \frac{\partial \bar{v}_2}{\partial x_1} \right)^2, \quad a_{12} = 0 \end{aligned} \quad (14.7)$$

As can be seen the coefficient for  $a_{22}$  is larger than that in Eq. 14.5, and hence the model is slightly more sensitive to the secondary strain  $\partial \bar{v}_2 / \partial x_1$  than to the primary one  $\partial \bar{v}_1 / \partial x_2$ . Thus, the non-linear models are able to account for streamline curvature, but due to the choice of constants so that  $c_5 + c_6 + c_7 = 0$  this effect is weak.

## 15 The V2F Model

In the V2F model of [40, 41, 32] two additional equations, apart from the  $k$  and  $\varepsilon$ -equations, are solved: the wall-normal stress  $\overline{v_2'^2}$  and a function  $f$ . This is a model which is aimed at improving modelling of wall effects on the turbulence.

Walls affect the fluctuations in the wall-normal direction,  $\overline{v_2'^2}$ , in two ways. The wall damping of  $\overline{v_2'^2}$  is felt by the turbulence fairly far from the wall ( $x_2^+ \lesssim 200$ ) through the pressure field (i.e. the pressure-strain term) whereas the viscous damping takes place within the viscous and buffer layer ( $x_2^+ \lesssim 10$ ). In usual eddy-viscosity models both these effects are accounted for through damping functions. The damping of  $\overline{v_2'^2}$  is in the RSM accounted for through the modelled pressure-strain terms  $\Phi_{22,1w}$  and  $\Phi_{22,2w}$  (see Eqs. 11.91 and Eq. 11.92). They go to zero far away from the wall ( $x_2^+ \gtrsim 10$ ).

In the V2F model the problem of accounting for the wall damping of  $\overline{v_2'^2}$  is simply resolved by solving its transport equation. The  $\overline{v_2'^2}$  equation in boundary-layer form reads (see Eq. 9.16 at p. 77)

$$\frac{\partial \rho \bar{v}_1 \overline{v_2'^2}}{\partial x_1} + \frac{\partial \rho \bar{v}_2 \overline{v_2'^2}}{\partial x_2} = \frac{\partial}{\partial x_2} \left[ (\mu + \mu_t) \frac{\partial \overline{v_2'^2}}{\partial x_2} \right] - 2 \overline{v'_2} \frac{\partial p'}{\partial x_2} - \rho \varepsilon_{22} \quad (15.1)$$

in which the diffusion term has been modelled with an eddy-viscosity assumption, see Eq. 11.43 at p. 92. Note that the production term  $P_{22} = 0$  because in boundary-layer approximation  $\bar{v}_2 \ll \bar{v}_1$  and  $\partial/\partial x_1 \ll \partial/\partial x_2$ . The model for the dissipation  $\varepsilon_{22}$  is taken as in RSM (see Eq. 11.45)

$$\varepsilon_{22}^{model} = \frac{\overline{v_2'^2}}{k} \varepsilon$$

Add and subtract  $\varepsilon_{22}^{model}$  on the right side of Eq. 15.1 yields

$$\begin{aligned} \frac{\partial \rho \bar{v}_1 \overline{v_2'^2}}{\partial x_1} + \frac{\partial \rho \bar{v}_2 \overline{v_2'^2}}{\partial x_2} &= \\ \frac{\partial}{\partial x_2} \left[ (\mu + \mu_t) \frac{\partial \overline{v_2'^2}}{\partial x_2} \right] - 2 \overline{v'_2} \frac{\partial p'}{\partial x_2} - \rho \varepsilon_{22} + \rho \frac{\overline{v_2'^2}}{k} \varepsilon - \rho \frac{\overline{v_2'^2}}{k} \varepsilon \end{aligned} \quad (15.2)$$

In the V2F model  $\mathcal{P}$  is now defined as

$$\mathcal{P} = -\frac{2}{\rho} \overline{v'_2} \frac{\partial p'}{\partial x_2} - \varepsilon_{22} + \frac{\overline{v_2'^2}}{k} \varepsilon \quad (15.3)$$

so that Eq. 15.2 can be written as

$$\frac{\partial \rho \bar{v}_1 \overline{v_2'^2}}{\partial x_1} + \frac{\partial \rho \bar{v}_2 \overline{v_2'^2}}{\partial x_2} = \frac{\partial}{\partial x_2} \left[ (\mu + \mu_t) \frac{\partial \overline{v_2'^2}}{\partial x_2} \right] + \rho \mathcal{P} - \rho \frac{\overline{v_2'^2}}{k} \varepsilon \quad (15.4)$$

$\mathcal{P}$  is the source term in the  $\overline{v_2'^2}$ -equation above, and it includes the velocity-pressure gradient term and the difference between the exact and the modelled dissipation. Note that this term is commonly split into the pressure-strain term and a diffusion term as

$$\overline{v'_2} \frac{\partial p'}{\partial x_2} = \frac{\partial v'_2 p'}{\partial x_2} - p' \frac{\partial v'_2}{\partial x_2}$$

Physically, the main agent for generating wall-normal stress is indeed the pressure-strain term via re-distribution, see example in Section 11.12.

A new variable  $f = \mathcal{P}/k$  is defined and a relaxation equation is formulated for  $f$  as

$$\begin{aligned} L^2 \frac{\partial^2 f}{\partial x_2^2} - f &= -\frac{\Phi_{22}}{k} - \frac{1}{T} \left( \frac{\overline{v'_2}^2}{k} - \frac{2}{3} \right) \\ T &= \max \left\{ \frac{k}{\varepsilon}, C_T \left( \frac{\nu}{\varepsilon} \right)^{1/2} \right\} \\ \frac{\Phi_{22}}{k} &= \frac{C_1}{T} \left( \frac{2}{3} - \frac{\overline{v'_2}^2}{k} \right) + C_2 \frac{\nu_t}{k} \left( \frac{\partial \bar{v}_1}{\partial x_2} \right)^2 \\ L &= C_L \max \left\{ \frac{k^{3/2}}{\varepsilon}, C_\eta \left( \frac{\nu^3}{\varepsilon} \right)^{1/4} \right\} \end{aligned} \quad (15.5)$$

where  $\Phi_{22}$  is the IP model of the pressure-strain term, see Eqs. 11.53 and 11.86, the first term being the slow term, and the second the rapid term. The constants are given the following values:  $c_\mu = 0.23$ ,  $C_T = 6$ ,  $c_{e1} = 1.44$ ,  $c_{e2} = 1.9$ ,  $\sigma_k = 0.9$ ,  $\sigma_\varepsilon = 1.3$ ,  $C_1 = 1.3$ ,  $C_2 = 0.3$ ,  $C_L = 0.2$ ,  $C_\eta = 90$ .

The boundary condition for  $f$  is obtained from  $\overline{v'_2}^2$  equation. Near the wall, the  $\overline{v'_2}^2$  equation reads

$$0 = \nu \frac{\partial^2 \overline{v'_2}^2}{\partial x_2^2} + fk - \frac{\overline{v'_2}^2}{k} \varepsilon \quad (15.6)$$

The first and the last term behave as  $\mathcal{O}(x_2^2)$  as  $x_2 \rightarrow 0$  because Taylor analysis gives  $\overline{v'_2}^2 = \mathcal{O}(x_2^4)$ ,  $\varepsilon = \mathcal{O}(x_2^0)$  and  $k = \mathcal{O}(x_2^2)$ , see [5]. Furthermore,  $\varepsilon = 2\nu k / x_2^2$  [5] ; using this expression to replace  $k$  in Eq. 15.6 gives

$$0 = \frac{\partial^2 \overline{v'_2}^2}{\partial x_2^2} + \frac{f\varepsilon x_2^2}{2\nu^2} - \frac{2\overline{v'_2}^2}{x_2^2} \quad (15.7)$$

Assuming that  $f$  and  $\varepsilon$  are constant very close to the wall, this equation turns into an ordinary second-order differential equation with the solution

$$\overline{v'_2}^2 = Ax_2^2 + \frac{B}{x_2} - \varepsilon f \frac{x_2^4}{20\nu^2}$$

Since  $\overline{v'_2}^2 = \mathcal{O}(x_2^4)$  as  $x_2 \rightarrow 0$ , both constants must be zero, i.e.  $A = B = 0$ , so we get

$$f = -\frac{20\nu^2}{\varepsilon} \frac{\overline{v'_2}^2}{x_2^4} \quad (15.8)$$

For more details, see [42].

Above we have derived the  $\overline{v'_2}^2$  equation in boundary layer form assuming that  $x_2$  is the wall-normal coordinate. In general, three-dimensional flow it reads

$$\frac{\partial \rho \bar{v}_j v^2}{\partial x_j} = \frac{\partial}{\partial x_j} \left[ (\mu + \mu_t) \frac{\partial v^2}{\partial x_j} \right] + \rho fk - \rho \frac{v^2}{k} \varepsilon \quad (15.9)$$

In the V2F model a transport equation for the normal stress normal to walls is solved for. If the wall lies in the  $x_1 - x_3$  plane, then  $v^2 = \overline{v'_2}^2$ . However, if a wall lies in

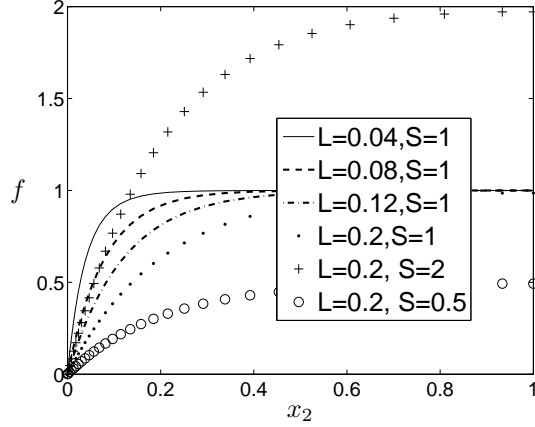


Figure 15.1: Illustration of Eq. 15.12

the  $x_2 - x_3$  plane, for example, this means that the transport equation for  $\overline{v'_2^2}$  is turned into an equation for  $\overline{v'_1^2}$ , i.e.  $v^2 = \overline{v'_1^2}$ . This is done automatically since in the general formulation in Eq. 15.9,  $\partial \bar{v}_1 / \partial x_2$  in the expression for  $\Phi_{22}$  is replaced by  $P^k$ . If the wall lies in the  $x_2 - x_3$  plane the largest velocity gradient will be  $\partial \bar{v}_2 / \partial x_1$  or  $\partial \bar{v}_3 / \partial x_1$ .

Why does the right side of Eq. 15.5 has the form it has? Far from the wall, the source term in the  $\overline{v'_2^2}$ -equation simplifies to  $\Phi_{22}$  plus isotropic dissipation (see Eq. 15.1). This is what happens, because far from the wall when  $\partial^2 f / \partial x_2^2 \simeq 0$ , and Eq. 15.5 yields ( $T = k/\varepsilon$ )

$$kf \equiv \mathcal{P} \rightarrow \Phi_{22} + \varepsilon(\overline{v'_2^2}/k - 2/3) \quad (15.10)$$

When this expression is inserted in Eq. 15.4 we get

$$\frac{\partial \rho \bar{v}_1 \overline{v'_2^2}}{\partial x_1} + \frac{\partial \rho \bar{v}_2 \overline{v'_2^2}}{\partial x_2} = \frac{\partial}{\partial x_2} \left[ (\mu + \mu_t) \frac{\partial \overline{v'_2^2}}{\partial x_2} \right] + \rho \Phi_{22} - \frac{2}{3} \rho \varepsilon \quad (15.11)$$

which is the usual form of the modelled  $\overline{v'_2^2}$ -equation with isotropic dissipation. Thus the  $f$  equation acts so as to let  $f$  go from the value of its source term to its (negative) wall value (see Eq. 15.8) over lengthscale  $L$ . This is how the reduction of the source term  $\mathcal{P}$  in Eq. 15.4 is achieved as the wall is approached. The behavior of the equation for  $f$  (Eq. 15.5) for different right sides is illustrated in the Fig. 15.1 where the equation

$$L^2 \frac{\partial^2 f}{\partial x_2^2} - f + S = 0 \quad (15.12)$$

has been solved with  $f = 0$  at the wall and with different  $L$  and  $S$ .

As can be seen,  $f$  is, as required, reduced as the wall is approached. Furthermore,  $f$  approaches the value of the source term as  $x_2 > L$ . The influence of the lengthscale  $L$  is nicely illustrated: the larger  $L$ , the further away from the wall does  $f$  go to its far-field value.

In the V2F model the turbulent viscosity is computed from

$$\nu_t = C_\mu \overline{v'_2^2} T \quad (15.13)$$

The  $k$  and  $\varepsilon$ -equations are also solved (without damping functions). For convenience, the boundary conditions are given again

$$\begin{aligned} k &= 0, \quad \overline{v_2'^2} = 0 \\ \varepsilon &= 2\nu k / x_2^2 \\ f &= -\frac{20\nu^2 \overline{v_2'^2}}{\varepsilon x_2^4} \end{aligned} \tag{15.14}$$

The boundary condition for  $f$  makes the equation system numerically unstable. One way to get around that problem is to solve both the  $k$ ,  $\varepsilon$  and  $\overline{v_2'^2}$ ,  $f$  equations coupled [42]. An alternative is to use the  $\zeta - f$  model [43] which is more stable. In this model they solve for the ratio  $\overline{v_2'^2}/k$  instead of for  $\overline{v_2'^2}$  which gives a simpler wall boundary condition for  $f$ , namely  $f = 0$ .

## 15.1 Modified V2F model

In [44] they proposed a modification of the V2F model allowing the simple explicit boundary condition  $f = 0$  at walls. They introduced a new variable

$$f^* = f - 5\varepsilon v^2/k^2$$

and they neglected the term

$$-5L^2 \frac{\partial^2}{\partial x_j \partial x_j} \left( \frac{\varepsilon v^2}{k^2} \right)$$

The resulting  $\overline{v_2'^2}$  and  $f^*$ -equation read [44]

$$\frac{\partial \bar{v}_j v^2}{\partial x_j} = \frac{\partial}{\partial x_j} \left[ (\nu + \nu_t) \frac{\partial v^2}{\partial x_j} \right] + kf^* - 6 \frac{v^2}{k} \varepsilon \tag{15.15}$$

$$\begin{aligned} -L^2 \frac{\partial^2 f^*}{\partial x_j \partial x_j} + f^* &= -\frac{1}{T} \left[ (C_1 - 6) \frac{v^2}{k} - \frac{2}{3} (C_1 - 1) \right] + C_2 \frac{P^k}{k} \\ P^k &= \nu_t \left( \frac{\partial \bar{v}_i}{\partial x_j} + \frac{\partial \bar{v}_j}{\partial x_i} \right) \frac{\partial \bar{v}_i}{\partial x_j} \\ T &= \max \left\{ \frac{k}{\varepsilon}, 6 \left( \frac{\nu}{\varepsilon} \right)^{1/2} \right\} \\ L &= C_L \max \left\{ \frac{k^{3/2}}{\varepsilon}, C_\eta \left( \frac{\nu^3}{\varepsilon} \right)^{1/4} \right\} \end{aligned} \tag{15.16}$$

Boundary conditions at the walls are

$$\begin{aligned} k &= 0, \quad v^2 = 0 \\ \varepsilon &= 2\nu k / x_2^2 \\ f^* &= 0 \end{aligned}$$

This modified model is numerically much more stable. Note that the modified model is identical to the original model far from the wall.

## 15.2 Realizable V2F model

The realizable condition for stagnation flow (see p. 115) is used also for the V2F model, and they read [44]

$$\begin{aligned} T &= \min \left[ \frac{k}{\varepsilon}, \frac{0.6k}{\sqrt{6}C_\mu v^2 (\bar{s}_{ij}\bar{s}_{ij})^{1/2}} \right] \\ L &= \min \left[ \frac{k^{3/2}}{\varepsilon}, \frac{k^{3/2}}{\sqrt{6}C_\mu v^2 (2\bar{s}_{ij}\bar{s}_{ij})^{1/2}} \right] \end{aligned} \quad (15.17)$$

These realizable conditions have been further investigated by Sveningsson [42, 45, 46, 47, 48], and it was found that the limitation on  $T$  is indeed important, whereas that for  $L$  is not. Furthermore, it was found that it is important to impose the limitation on  $T$  in a consistent manner. For instance, if the limit is used in the  $f$  equation, it must for consistency also be used for  $\varepsilon/k$  in Eq. 15.15.

## 15.3 To ensure that $v^2 \leq 2k/3$ [1]

In the V2F model,  $v^2$  denotes the generic wall-normal stress. Thus it should be the smallest one. This is not ensured in the V2F models presented above. Below the simple modification proposed by [1] is presented.

The source term  $kf$  in the  $v^2$ -equation (Eq. 15.15) includes the modelled velocity-pressure gradient term which is damped near walls as  $f$  goes to zero. Since  $v^2$  represents the wall-normal normal stress, it should be the smallest normal stress, i.e.  $\overline{v_2'^2} \leq \overline{v_1'^2}$  and  $\overline{v_2'^2} \leq \overline{v_3'^2}$ , and thus  $\overline{v_2'^2}$  should be smaller than or equal to  $\frac{2}{3}k$ . In the homogeneous region far away from the wall, the Laplace term is assumed to be negligible i.e.  $\partial^2 f / \partial x_j \partial x_j \rightarrow 0$ . Then Eq. 15.16 reduces to  $f = \text{right side}$ .

It turns out that in the region far away from the wall, the Laplace term is not negligible, and as a consequence  $v^2$  gets too large so that  $v^2 > \frac{2}{3}k$ . A simple modification is to use the right side of Eq. 15.16 as an upper bound on the source term  $kf$  in the  $v^2$ -equation, i.e.

$$v_{source}^2 = \min \left\{ kf, -\frac{\varepsilon}{k} \left[ (C_1 - 6)v^2 - \frac{2k}{3}(C_1 - 1) \right] + C_2 P^k \right\} \quad (15.18)$$

This modification ensures that  $v^2 \leq 2k/3$ . For more details, see [1].

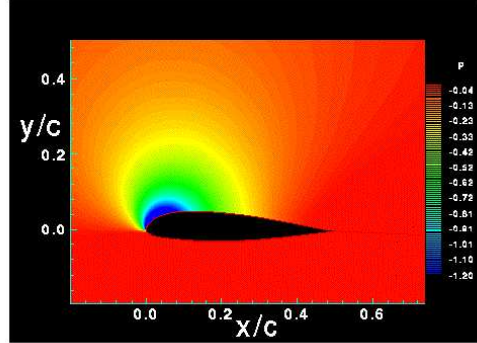


Figure 16.1: Flow around an airfoil. Pressure contours. Red: high pressure; blue: low pressure

## 16 The SST Model

The SST (Shear Stress Transport) model of [49] is an eddy-viscosity model which includes two main novelties:

1. It is combination of a  $k - \omega$  model (in the inner boundary layer) and  $k - \varepsilon$  model (in the outer region of the boundary layer as well as outside of it);
2. A limitation of the shear stress in adverse pressure gradient regions.

The  $k - \varepsilon$  model has two main weaknesses: it over-predicts the shear stress in adverse pressure gradient flows because of too large length scale (due to too low dissipation) and it requires near-wall modification (i.e. low-Re number damping functions/terms)

One example of adverse pressure gradient is the flow along the surface of an airfoil, see Fig. 16.1. Consider the upper surface (suction side). Starting from the leading edge, the pressure decreases because the velocity increases. At the crest (at  $x/c \simeq 0.15$ ) the pressure reaches its minimum and increases further downstream as the velocity decreases. This region is called the *adverse pressure gradient* (APG) region.

The  $k - \omega$  model is better than the  $k - \varepsilon$  model at predicting adverse pressure gradient flow and the standard model of [50] does not use any damping functions. However, the disadvantage of the standard  $k - \omega$  model is that it is dependent on the free-stream value of  $\omega$  [51].

In order to improve both the  $k - \varepsilon$  and the  $k - \omega$  model, it was suggested in [49] to combine the two models. Before doing this, it is convenient to transform the  $k - \varepsilon$  model into a  $k - \omega$  model using the relation  $\omega = \varepsilon / (\beta^* k)$ , where  $\beta^* = c_\mu$ . The left-hand side of the  $\omega$  equation will consist of the convection term,  $d\omega/dt$ , which denotes the material derivative assuming steady flow, see Eq. 2.23. Let us express the left-hand side of the  $\omega$  equation as a combination of the left-hand sides of the  $\varepsilon$  and the  $k$  equations by using the chain rule, i.e.

$$\begin{aligned} \frac{d\omega}{dt} &= \frac{d}{dt} \left( \frac{\varepsilon}{\beta^* k} \right) = \frac{1}{\beta^* k} \frac{d\varepsilon}{dt} + \frac{\varepsilon}{\beta^*} \frac{d(1/k)}{dt} \\ &= \frac{1}{\beta^* k} \frac{d\varepsilon}{dt} - \frac{\varepsilon}{\beta^* k^2} \frac{dk}{dt} = \frac{1}{\beta^* k} \frac{d\varepsilon}{dt} - \frac{\omega}{k} \frac{dk}{dt} \end{aligned} \quad (16.1)$$

Now we have transformed the left side of the  $\omega$  equation. The right side should be transformed in the same manner. For example, the production of the  $\omega$  equation will consist of two terms, one term from the  $\varepsilon$  equation

$$\frac{1}{\beta^* k} P_\varepsilon \quad (\text{the first term at the right side in Eq. 16.1}) \quad (16.2)$$

and one from the  $k$  equation

$$-\frac{\omega}{k} P^k \quad (\text{the second term at the right side in Eq. 16.1}) \quad (16.3)$$

In the same way we transform the entire right side inserting the modelled equations for  $k$  and  $\varepsilon$  so that

$$\begin{aligned} \frac{D\omega}{Dt} = & \underbrace{\left[ \frac{1}{\beta^* k} P_\varepsilon - \frac{\omega}{k} P^k \right]}_{\text{Production, } P_\omega} - \underbrace{\left[ \frac{1}{\beta^* k} \Psi_\varepsilon - \frac{\omega}{k} \Psi_k \right]}_{\text{Destruction, } \Psi_\omega} + \\ & \underbrace{\left[ \frac{1}{\beta^* k} D_\varepsilon^T - \frac{\omega}{k} D_k^T \right]}_{\text{Turbulent diffusion, } D_\omega^T} + \underbrace{\left[ \frac{\nu}{\beta^* k} \frac{\partial^2 \varepsilon}{\partial x_j^2} - \frac{\nu \omega}{k} \frac{\partial^2 k}{\partial x_j^2} \right]}_{\text{Viscous diffusion, } D_\omega^\nu} \end{aligned} \quad (16.4)$$

- Production term

$$\begin{aligned} P_\omega &= \frac{1}{\beta^* k} P_\varepsilon - \frac{\omega}{k} P^k = C_{\varepsilon 1} \frac{\varepsilon}{\beta^* k^2} P^k - \frac{\omega}{k} P^k \\ &= (C_{\varepsilon 1} - 1) \frac{\omega}{k} P^k \end{aligned} \quad (16.5)$$

- Destruction term

$$\begin{aligned} \Psi_\omega &= \frac{1}{\beta^* k} \Psi_\varepsilon - \frac{\omega}{k} \Psi_k = C_{\varepsilon 2} \frac{\varepsilon^2}{k} - \frac{\omega}{k} \varepsilon \\ &= (C_{\varepsilon 2} - 1) \beta^* \omega^2 \end{aligned} \quad (16.6)$$

- Viscous diffusion term

$$\begin{aligned} D_\omega^\nu &= \frac{\nu}{\beta^* k} \frac{\partial^2 \varepsilon}{\partial x_j^2} - \frac{\nu \omega}{k} \frac{\partial^2 k}{\partial x_j^2} = \frac{\nu}{k} \frac{\partial^2 \omega k}{\partial x_j^2} - \frac{\nu \omega}{k} \frac{\partial^2 k}{\partial x_j^2} \\ &= \frac{\nu}{k} \left[ \frac{\partial}{\partial x_j} \left( \omega \frac{\partial k}{\partial x_j} + k \frac{\partial \omega}{\partial x_j} \right) \right] - \nu \frac{\omega}{k} \frac{\partial^2 k}{\partial x_j^2} \\ &= \frac{\nu}{k} \left[ \frac{\partial \omega}{\partial x_j} \frac{\partial k}{\partial x_j} + \omega \frac{\partial^2 k}{\partial x_j^2} + \frac{\partial k}{\partial x_j} \frac{\partial \omega}{\partial x_j} + k \frac{\partial^2 \omega}{\partial x_j^2} \right] - \nu \frac{\omega}{k} \frac{\partial^2 k}{\partial x_j^2} \\ &= \frac{2\nu}{k} \frac{\partial \omega}{\partial x_j} \frac{\partial k}{\partial x_j} + \frac{\partial}{\partial x_j} \left( \nu \frac{\partial \omega}{\partial x_j} \right) \end{aligned} \quad (16.7)$$

The turbulent diffusion term is obtained as (the derivation is found in [52] which can be downloaded from [www.tfd.chalmers.se/~lada](http://www.tfd.chalmers.se/~lada))

$$\begin{aligned} D_\omega^T &= \frac{2\nu_t}{\sigma_\varepsilon k} \frac{\partial k}{\partial x_j} \frac{\partial \omega}{\partial x_j} + \frac{\omega}{k} \left( \frac{\nu_t}{\sigma_\varepsilon} - \frac{\nu_t}{\sigma_k} \right) \frac{\partial^2 k}{\partial x_j^2} + \\ &+ \frac{\omega}{k} \left( \frac{1}{\sigma_\varepsilon} - \frac{1}{\sigma_k} \right) \frac{\partial \nu_t}{\partial x_j} \frac{\partial k}{\partial x_j} + \frac{\partial}{\partial x_j} \left( \frac{\nu_t}{\sigma_\varepsilon} \frac{\partial \omega}{\partial x_j} \right) \end{aligned} \quad (16.8)$$

In the standard  $k - \varepsilon$  model we have  $\sigma_k = 1$  and  $\sigma_\varepsilon = 1.3$ . If we assume that  $\sigma_k = \sigma_\varepsilon$  in the second and third term of the right-hand side, we can considerably simplify the turbulence diffusion so that

$$D_\omega^T = \frac{2\nu_t}{\sigma_\varepsilon k} \frac{\partial k}{\partial x_j} \frac{\partial \omega}{\partial x_j} + \frac{\partial}{\partial x_j} \left( \frac{\nu_t}{\sigma_\varepsilon} \frac{\partial \omega}{\partial x_j} \right) \quad (16.9)$$

We can now finally write the  $\varepsilon$  equation formulated as an equation for  $\omega$

$$\begin{aligned} \frac{\partial}{\partial x_j} (\bar{v}_j \omega) &= \frac{\partial}{\partial x_j} \left[ \left( \nu + \frac{\nu_t}{\sigma_\varepsilon} \right) \frac{\partial \omega}{\partial x_j} \right] + \alpha \frac{\omega}{k} P^k - \beta \omega^2 \\ &\quad + \frac{2}{k} \left( \nu + \frac{\nu_t}{\sigma_\varepsilon} \right) \frac{\partial k}{\partial x_i} \frac{\partial \omega}{\partial x_i} \\ \alpha &= C_{\varepsilon 1} - 1 = 0.44, \beta = (C_{\varepsilon 2} - 1)\beta^* = 0.0828 \end{aligned} \quad (16.10)$$

Since the  $k - \varepsilon$  model will be used for the outer part of the boundary layer, the viscous part of the cross-diffusion term (second line) is usually neglected (the viscous term are negligible in the outer region).

In the SST model the coefficients are smoothly switched from  $k - \omega$  values in the inner region of the boundary layer to  $k - \varepsilon$  values in the outer region. Functions of the form

$$F_1 = \tanh(\xi^4), \quad \xi = \min \left[ \max \left\{ \frac{\sqrt{k}}{\beta^* \omega y}, \frac{500\nu}{y^2 \omega} \right\}, \frac{4\sigma_{\omega 2} k}{CD_\omega y^2} \right] \quad (16.11)$$

are used.  $F_1 = 1$  in the near-wall region and  $F_1 = 0$  in the outer region. The  $\beta$ -coefficient, for example, is computed as

$$\beta_{SST} = F_1 \beta_{k-\omega} + (1 - F_1) \beta_{k-\varepsilon} \quad (16.12)$$

where  $\beta_{k-\omega} = 0.075$  and  $\beta_{k-\varepsilon} = 0.0828$ . Since the standard  $k - \omega$  model does not include any cross-diffusion term, the last term in the  $\omega$  equation (second line in Eq. 16.10) should only be active in the  $k - \varepsilon$  region; hence it is multiplied by  $(1 - F_1)$ .

At p. 126 it was mentioned that the  $k - \omega$  model is better than the  $k - \varepsilon$  model in predicting adverse pressure-gradient flows because it predicts a smaller shear stress. Still, the predicted shear stress is too large. This brings us to the second modification (see p. 126). When introducing this second modification, the author in [49] noted that a model (the Johnson - King model [JK]) which is based on transport of the main shear stress  $\bar{v}'_1 \bar{v}'_2$ , predicts adverse pressure gradient flows much better than the  $k - \omega$  model. In the JK model, the  $\bar{v}'_1 \bar{v}'_2$  transport equation is built on Bradshaw's assumption [53]

$$-\overline{v'_1 v'_2} = a_1 k \quad (16.13)$$

where  $a_1 = c_\mu^{1/2} = \beta^{*1/2}$ . In boundary layer flow, the Boussinesq assumption can be written as

$$\begin{aligned} -\overline{v'_1 v'_2} &= \frac{k}{\omega} \frac{\partial \bar{v}_1}{\partial x_2} = \frac{c_\mu k^2}{\varepsilon} \frac{\partial \bar{v}_1}{\partial x_2} = c_\mu^{1/2} k \left[ \frac{c_\mu k^2}{\varepsilon^2} \left( \frac{\partial \bar{v}_1}{\partial x_2} \right)^2 \right]^{1/2} = c_\mu^{1/2} k \left( \frac{P^k}{\varepsilon} \right)^{1/2} \end{aligned} \quad (16.14)$$

It is found from experiments that in boundary layers of adverse pressure gradient flows the production is much larger than the dissipation ( $P^k \gg \varepsilon$ ) and  $-\overline{v'_1 v'_2} \simeq c_\mu^{1/2} k$ , which

explains why Eq. 16.14 over-predicts the shear stress and works poorly in this type of flow. To reduce  $|v'_1 v'_2|$  in Eq. 16.14 in adverse pressure gradient flow, [49] proposed to re-define the turbulent eddy viscosity including the expression in Eq. 16.13. We have two expressions for the turbulent viscosity

$$\nu_t = \frac{-\overline{v'_1 v'_2}}{\bar{\Omega}} = \frac{c_\mu^{1/2} k}{\bar{\Omega}} \quad (16.15a)$$

$$\nu_t = \frac{k}{\omega} = \frac{c_\mu^{1/2} k}{c_\mu^{1/2} \omega} \quad (16.15b)$$

where  $\bar{\Omega}$  is the absolute vorticity (in boundary layer flow  $\bar{\Omega} = \partial \bar{v}_1 / \partial x_2$ ); in (a) the Boussinesq assumption together with Eq. 16.13 were used and (b) is taken from the  $k - \omega$  model. We want (a) to apply only in the boundary layer and hence we multiply it with a function  $F_2$  (similar to  $F_1$ ) which is 1 near walls and zero elsewhere. Then we take the minimum of (a) and (b) so that

$$\nu_t = \frac{c_\mu^{1/2} k}{\max(c_\mu^{1/2} \omega, F_2 \bar{\Omega})} \quad (16.16)$$

When the production is large (i.e. when  $\bar{\Omega}$  is large), Eq. 16.16 reduces  $\nu_t$  according to the Johnson - King model, i.e. Eq. 16.15a. It is important to ensure that this limitation is not active in usual boundary layer flows where  $P^k \simeq \varepsilon$ . It can be seen that  $\nu_t$  is reduced only in regions where  $P^k > \varepsilon$ , because if  $P^k < \varepsilon$  then  $\bar{\Omega} < c_\mu^{1/2} \omega$  since

$$\bar{\Omega}^2 = \frac{1}{\nu_t} \nu_t \bar{\Omega}^2 = \frac{\omega}{k} P^k < \frac{\omega \varepsilon}{k} = c_\mu \omega^2 \quad (16.17)$$

Hence, in regions where  $P^k < \varepsilon$ , Eq. 16.16 returns to  $\nu_t = k/\omega$  as it should.

To summarize the SST modification:

- the second part,  $c_\mu^{1/2} k / \bar{\Omega}$  in Eq. 16.16 (which mimics the Johnson-King model), should be used in APG flow
- the first part,  $k/\omega$  in Eq. 16.16 (which corresponds to the usual Boussinesq model), should be in the remaining of the flow. Equation 16.17 shows that (it is likely that) the second part is only used in APG regions and not elsewhere.

Today, the SST model has been slightly further developed. Two modifications have been introduced [54]. The first modification is that the absolute vorticity  $\bar{\Omega}$  in Eq. 16.16 has been replaced by  $|\bar{s}| = (2\bar{s}_{ij}\bar{s}_{ij})^{1/2}$  which comes from the production term using the Boussinesq assumption (see Eq. 11.35), i.e.

$$\begin{aligned} |\bar{s}|^2 &= \left( \frac{\partial \bar{v}_i}{\partial x_j} + \frac{\partial \bar{v}_j}{\partial x_i} \right) \frac{\partial \bar{v}_i}{\partial x_j} = 2\bar{s}_{ij}(\bar{s}_{ij} + \bar{\Omega}_{ij}) = 2\bar{s}_{ij}\bar{s}_{ij} \\ \bar{\Omega}_{ij} &= \frac{1}{2} \left( \frac{\partial \bar{v}_i}{\partial x_j} - \frac{\partial \bar{v}_j}{\partial x_i} \right) \end{aligned} \quad (16.18)$$

where  $\bar{s}_{ij}\bar{\Omega}_{ij} = 0$  because  $\bar{s}_{ij}$  is symmetric and  $\bar{\Omega}_{ij}$  is anti-symmetric. Equation 16.16 with  $|\bar{s}|$  limits  $\nu_t$  in stagnation regions similar to Eq. 13.12. The second modification in the SST model is that the production term in the new SST model is limited by  $10\varepsilon$ , i.e.

$$P_{k,new} = \min(P^k, 10\varepsilon) \quad (16.19)$$

The final form of the SST model is given in Eq. 20.4 at p. 159.

## 17 Overview of RANS models

This section presents a short overview of the presented RANS models. First the models can be classified as models based on eddy viscosity (i.e. turbulent viscosity) or models in which equations are solved (algebraic or differential) to obtain the Reynolds stress tensor,  $\overline{v'_i v'_j}$ . Eddy-viscosity models, which are based on the Boussinesq assumption, see Eq. 11.30), are

- standard  $k - \varepsilon$  (see Section 11.8) and  $k - \omega$  models
- combination of  $k - \varepsilon$  and  $k - \omega$  models such as the SST model, see Section 16.

There are more elaborate eddy-viscosity models such as

- non-linear models, see Section 14

Models *not* based on the eddy-viscosity are the Reynolds stress models which include

- the Reynolds stress transport model (RSM or RSTM), in which *transport* equations are solved for  $\overline{v'_i v'_j}$ , see Eq. 11.97.
- the Algebraic Reynolds stress model, ASM, in which *algebraic* equations are solved for  $\overline{v'_i v'_j}$ , see Eq. 11.100.
- explicit Algebraic Reynolds stress models, in which *explicit* algebraic equations are solved for  $\overline{v'_i v'_j}$ , see Section 11.11.

Finally, there is a class of models which are somewhere in between two-equation eddy-viscosity models and Reynolds stress models, and that is

- V2F models, see Section 15

The V2F model is an addy-viscosity model and the model is based on four transport equations.

**Eddy-viscosity models**

**non-linear models**

**RSM**

**ASM**

**explicit ASM**

**V2F**

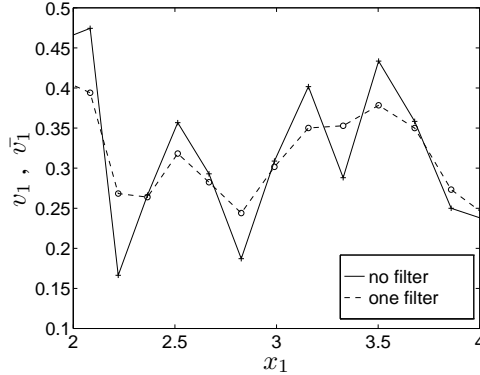


Figure 18.1: Filtering the velocity.

## 18 Large Eddy Simulations

### 18.1 Time averaging and filtering

In CFD we time average our equations to get the equations in steady form. This is called Reynolds time averaging:

$$\langle \Phi \rangle = \frac{1}{2T} \int_{-T}^T \Phi(t) dt, \quad \Phi = \langle \Phi \rangle + \Phi' \quad (18.1)$$

(note that we use the notation  $\langle \cdot \rangle$  for time averaging). In LES we filter (volume average) the equations. In 1D we get (see Fig. 18.1)

$$\bar{\Phi}(x, t) = \frac{1}{\Delta x} \int_{x-0.5\Delta x}^{x+0.5\Delta x} \Phi(\xi, t) d\xi$$

$$\Phi = \bar{\Phi} + \Phi''$$

Since in LES we do not average in time, the filtered variables are functions of space and time. The equations for the filtered variables have the same form as Navier-Stokes, i.e.

$$\begin{aligned} \frac{\partial \bar{v}_i}{\partial t} + \frac{\partial}{\partial x_j} (\bar{v}_i \bar{v}_j) &= -\frac{1}{\rho} \frac{\partial \bar{p}}{\partial x_i} + \nu \frac{\partial^2 \bar{v}_i}{\partial x_j \partial x_j} - \frac{\partial \tau_{ij}}{\partial x_j} \\ \frac{\partial \bar{v}_i}{\partial x_i} &= 0 \end{aligned} \quad (18.2)$$

where the subgrid stresses are given by

$$\tau_{ij} = \bar{v}_i \bar{v}_j - \bar{v}_i \bar{v}_j \quad (18.3)$$

Contrary to Reynolds time averaging where  $\langle v'_i \rangle = 0$ , we have here

$$\bar{v}'_i \neq 0$$

$$\bar{v}_i \neq \bar{v}_i$$

This is true for box filters. Note that for the spectral cut-off filter  $\bar{v}_i = \overline{\bar{v}_i}$ , see p. 134. However, in finite volume methods, box filters are always used. In this course we use box filters, if not otherwise stated.

Let's look at the filtering of Eq. 18.2 in more detail. The pressure gradient term, for example, reads

$$\overline{\frac{\partial p}{\partial x_i}} = \frac{1}{V} \int_V \frac{\partial p}{\partial x_i} dV$$

Now we want to move the derivative out of the integral. When is that allowed? The answer is “if the integration region is not a function of  $x_i$ ”, i.e. if  $V$  is constant. In finite volume methods, the filtering volume,  $V$ , is (almost always) identical to the control volume. In general, the size of the control volume varies in space. Fortunately, it can be shown that if  $V$  is a function of  $x_i$ , the error we do when moving the derivative out of the integral is proportional to  $V^2$  [55], i.e. it is an error of second order. Since this is the order of accuracy of our finite volume method anyway, we can accept this error. Now let's move the derivative out of the integral, i.e.

$$\overline{\frac{\partial p}{\partial x_i}} = \frac{\partial}{\partial x_i} \left( \frac{1}{V} \int_V p dV \right) + \mathcal{O}(V^2) = \frac{\partial \bar{p}}{\partial x_i} + \mathcal{O}(V^2)$$

All linear terms are treated in the same way.

Now we take a look at the non-linear term in Eq. 18.2, i.e. the convective term. First we filter the term and move the derivative out of the integral, i.e.

$$\overline{\frac{\partial v_i v_j}{\partial x_j}} = \frac{\partial}{\partial x_j} \left( \frac{1}{V} \int_V v_i v_j dV \right) + \mathcal{O}(V^2) = \frac{\partial}{\partial x_j} (\overline{v_i v_j}) + \mathcal{O}(V^2)$$

There is still a problem with the formulation of this term: it includes an integral of a product, i.e.  $\overline{v_i v_j}$ ; we want it to appear like a product of integrals, i.e.  $\overline{v_i} \overline{v_j}$ . To achieve this we simply add the term we want ( $\overline{v_i} \overline{v_j}$ ) and subtract the one we don't want ( $\overline{v_i v_j}$ ) on both the right and left side. This is how we end up with the convective term and the SGS term in Eq. 18.2.

## 18.2 Differences between time-averaging (RANS) and space filtering (LES)

In **RANS**, if a variable is time averaged twice ( $\langle\langle v \rangle\rangle$ ), it is the same as time averaging once ( $\langle v \rangle$ ). This is because  $\langle v \rangle$  is not dependent on time. From Eq. 18.1 we get

$$\langle\langle v \rangle\rangle = \frac{1}{2T} \int_{-T}^T \langle v \rangle dt = \frac{1}{2T} \langle v \rangle 2T = \langle v \rangle$$

This is obvious if the flow is steady, i.e.  $\partial \langle v \rangle / \partial t = 0$ . If the flow is unsteady, we must assume a separation in time scales so that the variation of  $\langle v \rangle$  during the time interval  $T$  is negligible, i.e.  $\partial / \partial t \ll 1/T$ . In practice this requirement is rarely satisfied.

In **LES**,  $\bar{v} \neq \overline{\bar{v}}$  (and since  $v = \bar{v} + v''$  we get  $\overline{v''} \neq 0$ ).

Let's filter  $\bar{v}_I$  once more (filter size  $\Delta x$ , see Fig. 18.2). For simplicity we do it in 1D. (Note that subscript  $I$  denotes node number.)

$$\begin{aligned} \bar{v}_I &= \frac{1}{\Delta x} \int_{-\Delta x/2}^{\Delta x/2} \bar{v}(\xi) d\xi = \frac{1}{\Delta x} \left( \int_{-\Delta x/2}^0 \bar{v}(\xi) d\xi + \int_0^{\Delta x/2} \bar{v}(\xi) d\xi \right) = \\ &= \frac{1}{\Delta x} \left( \frac{\Delta x}{2} \bar{v}_A + \frac{\Delta x}{2} \bar{v}_B \right). \end{aligned}$$

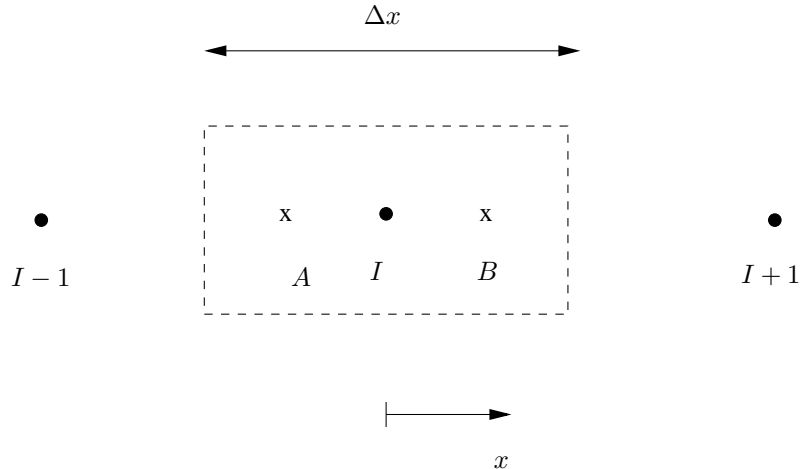


Figure 18.2: Box filter illustrated for a control volume.

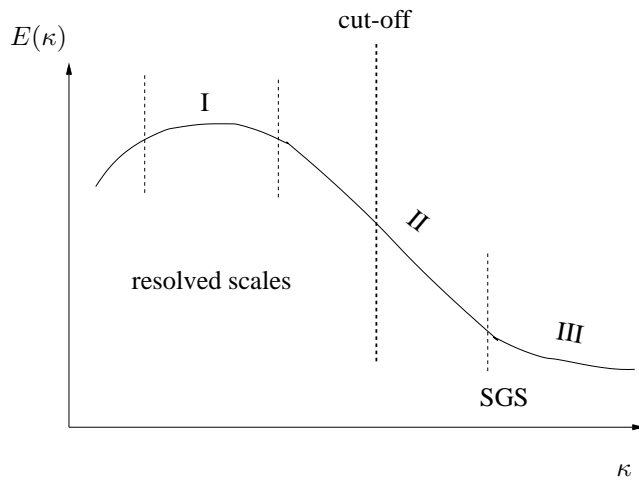


Figure 18.3: Spectrum of velocity.

The trapezoidal rule, which is second-order accurate, was used to estimate the integrals.  $\bar{v}$  at locations  $A$  and  $B$  (see Fig. 18.2) is estimated by linear interpolation, which gives

$$\begin{aligned}\bar{v}_I &= \frac{1}{2} \left[ \left( \frac{1}{4} \bar{v}_{I-1} + \frac{3}{4} \bar{v}_I \right) + \left( \frac{3}{4} \bar{v}_I + \frac{1}{4} \bar{v}_{I+1} \right) \right] \\ &= \frac{1}{8} (\bar{v}_{I-1} + 6\bar{v}_I + \bar{v}_{I+1}) \neq \bar{v}_I\end{aligned}\quad (18.4)$$

### 18.3 Resolved & SGS scales

The basic idea in LES is to resolve (large) grid scales (GS), and to model (small) subgrid-scales (SGS).

The limit (cut-off) between GS and SGS is supposed to take place in the inertial subrange (II), see Fig. 18.3.

- I: large, energy-containing scales
- II: inertial subrange (Kolmogorov  $-5/3$ -range)
- III: dissipation subrange

## 18.4 The box-filter and the cut-off filter

The filtering is formally defined as (1D)

$$\begin{aligned}\bar{v}(x) &= \int_{-\infty}^{\infty} G_B(r)v(x-r)dr \\ G_B(r) &= \begin{cases} 1/\Delta, & \text{if } r \leq \Delta/2 \\ 0, & \text{if } r > \Delta \end{cases} \\ \int_{-\infty}^{\infty} G_B(r)dr &= 1\end{aligned}\tag{18.5}$$

It is often convenient to study the filtering process in the spectral space. The filter in spectral space is particular simple: we simply set the contribution from wavenumbers larger than cut-off to zero. Hence the cut-off filter filters out all scales with wavenumber larger than the cut-off wavenumber  $\kappa_c = \pi/\Delta$ . It is defined as

$$\hat{G}_C(\kappa) = \begin{cases} 1/\Delta & \text{if } \kappa \leq \kappa_c \\ 0 & \text{otherwise} \end{cases}\tag{18.6}$$

The Fourier transform is defined as (see Section C)

$$\hat{v}(\kappa) = \frac{1}{2\pi} \int_0^{\infty} v(r) \exp(-\imath\kappa r) dr\tag{18.7}$$

and its inverse

$$v(r) = \int_0^{\infty} \hat{v}(\kappa) \exp(\imath\kappa r) d\kappa\tag{18.8}$$

where  $\kappa$  denotes the wavenumber and  $\imath = \sqrt{-1}$ . Note that it is physically meaningful to use Fourier transforms only in a homogeneous coordinate direction; in non-homogeneous directions the Fourier coefficients – which are not a function of space – have no meaning. Using the convolution theorem (saying that the integrated product of two functions is equal to the product of their Fourier transforms) the filtering in Eq. 18.5 is conveniently written

$$\begin{aligned}\bar{v}(\kappa) &= \hat{\bar{v}}(\kappa) = \int_0^{\infty} \bar{v}(\eta) \exp(-\imath\kappa\eta) d\eta \\ &= \int_0^{\infty} \int_0^{\infty} \exp(-\imath\kappa\eta) G_C(\rho) v(\eta - \rho) d\rho d\eta \\ &= \int_0^{\infty} \int_0^{\infty} \exp(-\imath\kappa\rho) \exp(-\imath\kappa(\eta - \rho)) G_C(\rho) v(\eta - \rho) d\rho d\eta \\ &= \int_0^{\infty} \int_0^{\infty} \exp(-\imath\kappa\rho) \exp(-\imath\kappa\xi) G_C(\rho) v(\xi) d\xi d\rho = \hat{G}_C(\kappa) \hat{v}(\kappa)\end{aligned}\tag{18.9}$$

If we filter twice with the cut-off filter we get (see Eq. 18.9)

$$\overline{\hat{v}} = \hat{G}_C \hat{G} \hat{v} = \hat{G}_C \hat{v} = \bar{v}\tag{18.10}$$

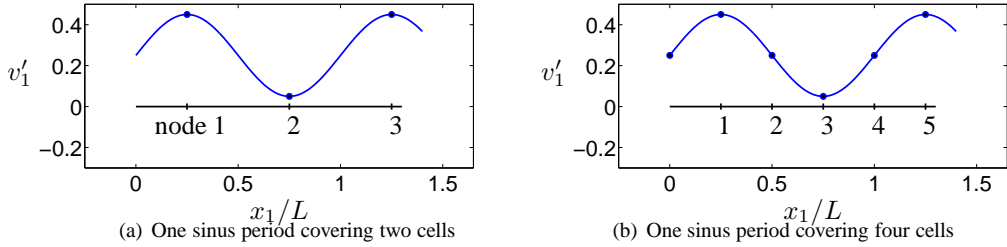


Figure 18.4: Physical and wavenumber space. Sinus curves with different wavenumbers illustrated in physical space.

using Eqs. 18.9 and 18.6. Thus, contrary to the box-filter (see Eq. 18.4), nothing happens when we filter twice in spectral space. The box filter is sharp in physical space but not in wavenumber space; for the cut-off filter it is vice versa.

In finite volume methods box filtering is always used. Furthermore *implicit* filtering is employed. This means that the filtering is the same as the discretization (=integration over the control volume which is equal to the filter volume, see Eq. 18.14).

## 18.5 Highest resolved wavenumbers

Any function can be expressed as a Fourier series such as Eq. 18.8 (see Section 5.3, Eq. C.28 and Section D) provided that the coordinate direction is homogeneous. Let's choose the fluctuating velocity in the  $x_1$  direction, i.e.  $v'_1$ , and let it be a function of  $x_1$ . We require it to be homogeneous, i.e. its RMS,  $v_{1,rms}$ , does not vary with  $x_1$ . Now we ask the question: on a given grid, what is the highest wavenumber that is resolved? Or, in other words, what is the cut-off wavenumber?

The wave shown in Fig. 18.4a reads

$$v'_1 = 0.25 [1 + 0.8 \sin(\kappa_1 x_1)], \quad \kappa_1 = 2\pi/L \quad (18.11)$$

and it covers two cells ( $\Delta x_1/L = 0.5$ ). If we define this as the cut-off wavenumber we get  $\kappa_{1,c}L = \kappa_{1,c}2\Delta x_1 = 2\pi$  so that

$$\kappa_{1,c} = 2\pi/(2\Delta x_1) = \pi/\Delta x_1 \quad (18.12)$$

It is of course questionable if  $v'_1$  in Fig. 18.4a really is resolved since the sinus wave covers only two cells. However this is the usual definition of the cut-off wavenumber.

If we require that the highest resolved wavenumber should be covered by four cells ( $\Delta x_1/L = 0.25$ ), as in Fig. 18.4b, then the cut-off wavenumber is given by  $\kappa_{1,c} = 2\pi/(4\Delta x_1) = \pi/(2\Delta x_1)$ .

## 18.6 Subgrid model

We need a subgrid model to model the turbulent scales which cannot be resolved by the grid and the discretization scheme.

The simplest model is the Smagorinsky model [56]:

$$\begin{aligned} \tau_{ij} - \frac{1}{3}\delta_{ij}\tau_{kk} &= -\nu_{sgs} \left( \frac{\partial \bar{v}_i}{\partial x_j} + \frac{\partial \bar{v}_j}{\partial x_i} \right) = -2\nu_{sgs} \bar{s}_{ij} \\ \nu_{sgs} &= (C_S \Delta)^2 \sqrt{2\bar{s}_{ij}\bar{s}_{ij}} \equiv (C_S \Delta)^2 |\bar{s}| \end{aligned} \quad (18.13)$$

and the filter-width is taken as the local grid size

$$\Delta = (\Delta V_{IJK})^{1/3} \quad (18.14)$$

The scalar  $|\bar{s}|$  is the norm (i.e. the “length”) of  $\partial \bar{v}_i / \partial x_j + \partial \bar{v}_j / \partial x_i$  in the Boussinesq assumption, see Eq. 16.18.

Near the wall, the SGS viscosity becomes quite large since the velocity gradient is very large at the wall. However, because the SGS turbulent fluctuations near a wall go to zero, so must the SGS viscosity. A damping function  $f_\mu$  is added to ensure this

$$f_\mu = 1 - \exp(-x_2^+/26) \quad (18.15)$$

A more convenient way to dampen the SGS viscosity near the wall is simply to use the RANS length scale as an upper limit, i.e.

$$\Delta = \min \left\{ (\Delta V_{IJK})^{1/3}, \kappa n \right\} \quad (18.16)$$

where  $n$  is the distance to the nearest wall.

Disadvantage of Smagorinsky model: the “constant”  $C_S$  is not constant, but it is flow-dependent. It is found to vary in the range from  $C_S = 0.065$  [57] to  $C_S = 0.25$  [58].

## 18.7 Smagorinsky model vs. mixing-length model

The eddy viscosity according to the mixing length theory reads in boundary-layer flow [59, 60]

$$\nu_t = \ell^2 \left| \frac{\partial \bar{v}_1}{\partial x_2} \right|.$$

Generalized to three dimensions, we have

$$\nu_t = \ell^2 \left[ \left( \frac{\partial \bar{v}_i}{\partial x_j} + \frac{\partial \bar{v}_j}{\partial x_i} \right) \frac{\partial \bar{v}_i}{\partial x_j} \right]^{1/2} = \ell^2 (2\bar{s}_{ij}\bar{s}_{ij})^{1/2} \equiv \ell^2 |\bar{s}|.$$

In the Smagorinsky model the SGS turbulent length scale corresponds to  $\ell = C_S \Delta$  so that

$$\nu_{sgs} = (C_S \Delta)^2 |\bar{s}|$$

which is the same as Eq. 18.13

## 18.8 Energy path

The path of kinetic energy is illustrated in Fig. 18.5. At cut-off, SGS kinetic energy is dissipated

$$\varepsilon_{sgs} = -\tau_{ij}\bar{s}_{ij} = 2\nu_{sgs}\bar{s}_{ij}\bar{s}_{ij} \quad (18.17)$$

from the resolved turbulence. This energy is transferred to the SGS scales and act as production term ( $P_{k_{sgs}}$ ) in the  $k_{sgs}$  equation. The SGS kinetic energy is then transferred to higher wave-numbers via the cascade effect and the kinetic energy is finally dissipated ( $\varepsilon$ =physical dissipation) in the dissipation range. It should be mentioned that this process is an idealized one. We assume that ALL dissipation takes place in the dissipation range. This is a good approximation, but in reality dissipation (i.e. transfer of energy from kinetic energy to internal energy, i.e. increase in temperature) takes place at all wave numbers, and the dissipation increases for increasing wave number.

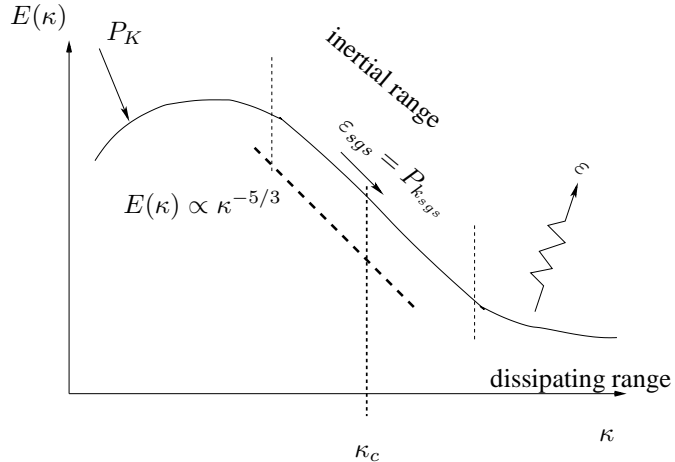


Figure 18.5: Energy spectrum.

## 18.9 SGS kinetic energy

The SGS kinetic energy  $k_{sgs}$  can be estimated from the Kolmogorov  $-5/3$  law. The total turbulent kinetic energy is obtained from the energy spectrum as

$$k = \int_0^\infty E(\kappa) d\kappa$$

Changing the lower integration limit to wavenumbers larger than cut-off (i.e.  $\kappa_c$ ) gives the SGS kinetic energy

$$k_{sgs} = \int_{\kappa_c}^\infty E(\kappa) d\kappa \quad (18.18)$$

The Kolmogorov  $-5/3$  law now gives

$$k_{sgs} = \int_{\kappa_c}^\infty C \kappa^{-5/3} \varepsilon^{2/3} d\kappa$$

(Note that for these high wavenumbers, the Kolmogorov spectrum ought to be replaced by the Kolmogorov-Pau spectrum in which an exponential decaying function is added for high wavenumbers [59, Chapter 3]). Carrying out the integration and replacing  $\kappa_c$  with  $\pi/\Delta$  we get

$$k_{sgs} = \frac{3}{2} C \left( \frac{\Delta \varepsilon}{\pi} \right)^{2/3} \quad (18.19)$$

In the same way as  $k_{sgs}$  can be computed from Eq. 18.18, the resolved turbulent kinetic energy,  $k_{res}$ , is obtained from

$$k_{res} = \int_0^{\kappa_c} E(\kappa) d\kappa$$

## 18.10 LES vs. RANS

LES can handle many flows which RANS (Reynolds Averaged Navier Stokes) cannot; the reason is that in LES large, turbulent scales are resolved. Examples are:

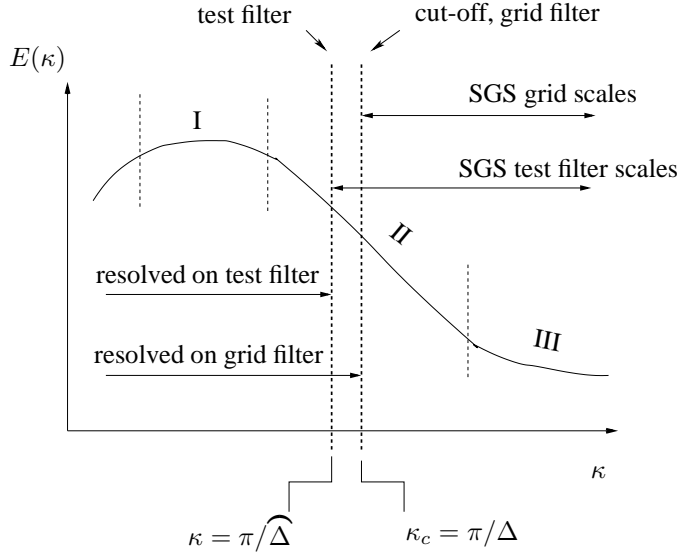


Figure 18.6: Energy spectrum with grid and test filter.

- o Flows with large separation
- o Bluff-body flows (e.g. flow around a car); the wake often includes large, unsteady, turbulent structures
- o Transition
  - In RANS all turbulent scales are modelled  $\Rightarrow$  inaccurate
  - In LES only small, isotropic turbulent scales are modelled  $\Rightarrow$  accurate
  - LES is *very* much more expensive than RANS.

## 18.11 The dynamic model

In this model of [61] the constant  $C$  is not arbitrarily chosen (or optimized), but it is computed.

If we apply two filters to Navier-Stokes [grid filter and a second, coarser filter (test filter, denoted by  $\widehat{\cdot}$ ) where  $\widehat{\Delta} = 2\Delta$ ] we get

$$\frac{\partial \widehat{v}_i}{\partial t} + \frac{\partial}{\partial x_j} \left( \widehat{v}_i \widehat{v}_j \right) = -\frac{1}{\rho} \frac{\partial \widehat{p}}{\partial x_i} + \nu \frac{\partial^2 \widehat{v}_i}{\partial x_j \partial x_j} - \frac{\partial T_{ij}}{\partial x_j} \quad (18.20)$$

where the subgrid stresses on the test level now are given by

$$T_{ij} = \widehat{v}_i \widehat{v}_j - \widehat{v}_i \widehat{v}_j \quad (18.21)$$

$$\begin{aligned} \frac{\partial \widehat{v}_i}{\partial t} + \frac{\partial}{\partial x_j} \left( \widehat{v}_i \widehat{v}_j \right) &= -\frac{1}{\rho} \frac{\partial \widehat{p}}{\partial x_i} + \nu \frac{\partial^2 \widehat{v}_i}{\partial x_j \partial x_j} - \frac{\partial \widehat{T}_{ij}}{\partial x_j} \\ &\quad - \frac{\partial}{\partial x_j} \left( \widehat{v}_i \widehat{v}_j - \widehat{v}_i \widehat{v}_j \right) \end{aligned} \quad (18.22)$$

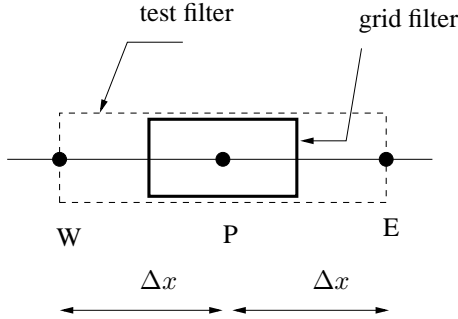


Figure 18.7: Control volume for grid and test filter.

Identification of Eqs. 18.20 and 18.22 gives

$$\widehat{\bar{v}_i \bar{v}_j} - \widehat{\bar{v}_i} \widehat{\bar{v}_j} + \widehat{\tau}_{ij} = T_{ij} \quad (18.23)$$

The *dynamic* Leonard stresses are now defined as

$$\mathcal{L}_{ij} \equiv \widehat{\bar{v}_i \bar{v}_j} - \widehat{\bar{v}_i} \widehat{\bar{v}_j} = T_{ij} - \widehat{\tau}_{ij} \quad (18.24)$$

The trace of this relation reads

$$\mathcal{L}_{ii} \equiv T_{ii} - \widehat{\tau}_{ii}$$

With this expression we can re-formulate Eq. 18.24 as

$$\mathcal{L}_{ij} - \frac{1}{3} \delta_{ij} \mathcal{L}_{kk} = T_{ij} - \frac{1}{3} \delta_{ij} T_{kk} - \left( \widehat{\tau}_{ij} - \frac{1}{3} \delta_{ij} \widehat{\tau}_{kk} \right) \quad (18.25)$$

In the energy spectrum, the test filter is located at lower wave number than the grid filter, see Fig. 18.6.

## 18.12 The test filter

The test filter is twice the size of the grid filter, i.e.  $\widehat{\Delta} = 2\Delta$ .

The test-filtered variables are computed by integration over the test filter. For example, the 1D example in Fig. 18.7  $\widehat{\bar{v}}$  is computed as ( $\widehat{\Delta}x = 2\Delta x$ )

$$\begin{aligned} \widehat{\bar{v}} &= \frac{1}{2\Delta x} \int_W^E \bar{v} dx = \frac{1}{2\Delta x} \left( \int_W^P \bar{v} dx + \int_P^E \bar{v} dx \right) \\ &= \frac{1}{2\Delta x} (\bar{v}_W \Delta x + \bar{v}_E \Delta x) = \frac{1}{2} \left( \frac{\bar{v}_W + \bar{v}_P}{2} + \frac{\bar{v}_P + \bar{v}_E}{2} \right) \\ &= \frac{1}{4} (\bar{v}_W + 2\bar{v}_P + \bar{v}_E) \end{aligned} \quad (18.26)$$

For 3D, filtering at the test level is carried out in the same way by integrating over

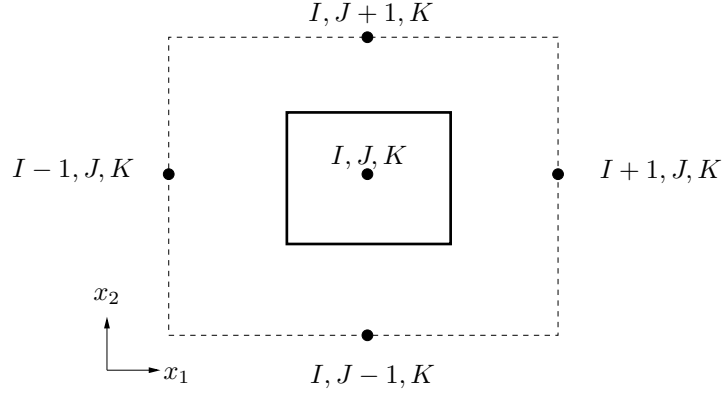


Figure 18.8: A 2D test filter control volume.

the test cell assuming linear variation of the variables [62], i.e. (see Fig. 18.8)

$$\begin{aligned} \widehat{\bar{v}}_{I,J,K} = & \frac{1}{8} (\bar{v}_{I-1/2,J-1/2,K-1/2} + \bar{v}_{I+1/2,J-1/2,K-1/2} \\ & + \bar{v}_{I-1/2,J+1/2,K-1/2} + \bar{v}_{I+1/2,J+1/2,K-1/2} \\ & + \bar{v}_{I-1/2,J-1/2,K+1/2} + \bar{v}_{I+1/2,J-1/2,K+1/2} \\ & + \bar{v}_{I-1/2,J+1/2,K+1/2} + \bar{v}_{I+1/2,J+1/2,K+1/2}) \end{aligned} \quad (18.27)$$

### 18.13 Stresses on grid, test and intermediate level

The stresses on the grid level, test level and intermediate level (dynamic Leonard stresses) have the form

$$\begin{aligned} \tau_{ij} &= \overline{v_i v_j} - \bar{v}_i \bar{v}_j \text{ stresses with } \ell < \Delta \\ T_{ij} &= \widehat{\bar{v}_i \bar{v}_j} - \widehat{\bar{v}_i} \widehat{\bar{v}_j} \text{ stresses with } \ell < \widehat{\Delta} \\ \mathcal{L}_{ij} &= T_{ij} - \widehat{\tau}_{ij} \text{ stresses with } \Delta < \ell < \widehat{\Delta} \end{aligned}$$

Thus the dynamic Leonard stresses represent the stresses with lengthscale,  $\ell$ , in the range between  $\Delta$  and  $\widehat{\Delta}$ .

Assume now that the same functional form for the subgrid stresses that is used at the grid level ( $\tau_{ij}$ ) also can be used at the test filter level ( $T_{ij}$ ). If we use the Smagorinsky model we get

$$\tau_{ij} - \frac{1}{3} \delta_{ij} \tau_{kk} = -2C\Delta^2 |\bar{s}| \bar{s}_{ij} \quad (18.28)$$

$$T_{ij} - \frac{1}{3} \delta_{ij} T_{kk} = -2C\widehat{\Delta}^2 |\widehat{s}| \widehat{s}_{ij} \quad (18.29)$$

where

$$\widehat{s}_{ij} = \frac{1}{2} \left( \frac{\partial \widehat{\bar{v}}_i}{\partial x_j} + \frac{\partial \widehat{\bar{v}}_j}{\partial x_i} \right), \quad |\widehat{s}| = \left( 2 \widehat{s}_{ij} \widehat{s}_{ij} \right)^{1/2}$$

Note that  $C$  in Eq. 18.28 is not squared (cf. the Smagorinsky model, Eq. 18.13 at p.135). Hence,  $C$  should be compared with  $C_S^2$ . Applying the test filter to Eq. 18.28 (assuming that  $C$  varies slowly), substituting this equation and Eq. 18.29 into Eq. 18.25 gives

$$\mathcal{L}_{ij} - \frac{1}{3}\delta_{ij}\mathcal{L}_{kk} = -2C \left( \widehat{\Delta}^2 |\widehat{s}| \widehat{s}_{ij} - \Delta^2 \widehat{|\bar{s}|} \widehat{s}_{ij} \right) \quad (18.30)$$

Note that the “constant”  $C$  really is a function of both space and time, i.e.  $C = C(x_i, t)$ .

Equation 18.30 is a tensor equation, and we have five ( $\bar{s}_{ij}$  is symmetric and traceless) equations for  $C$ . Lilly [63] suggested to satisfy Eq. 18.30 in a least-square sense. Let us define the error as the difference between the left-hand side and the right-hand side of Eq. 18.30 raised to the power of two, i.e.

$$Q = \left( \mathcal{L}_{ij} - \frac{1}{3}\delta_{ij}\mathcal{L}_{kk} + 2CM_{ij} \right)^2 \quad (18.31a)$$

$$M_{ij} = \left( \widehat{\Delta}^2 |\widehat{s}| \widehat{s}_{ij} - \Delta^2 \widehat{|\bar{s}|} \widehat{s}_{ij} \right) \quad (18.31b)$$

The error,  $Q$ , has a minimum (or maximum) when  $\partial Q/\partial C = 0$ . Carrying out the derivation of 18.31a gives

$$\frac{\partial Q}{\partial C} = 4M_{ij} \left( \mathcal{L}_{ij} - \frac{1}{3}\delta_{ij}\mathcal{L}_{kk} + 2CM_{ij} \right) = 0 \quad (18.32)$$

Since  $\partial^2 Q/\partial C^2 = 8M_{ij}M_{ij} > 0$  it is a minimum. Equation 18.31 is re-written so that

$$C = -\frac{\mathcal{L}_{ij}M_{ij}}{2M_{ij}M_{ij}} \quad (18.33)$$

It turns out that the dynamic coefficient  $C$  fluctuates wildly both in space and time. This causes numerical problems, and it has been found necessary to average  $C$  in homogeneous direction(s). Furthermore,  $C$  must be clipped to ensure that the total viscosity stays positive ( $\nu + \nu_{sgs} \geq 0$ ).

In real 3D flows, there is no homogeneous direction. Usually local averaging and clipping (i.e. requiring that  $C$  stays within pre-defined limits) of the dynamic coefficient is used.

Use of one-equation models solve these numerical problems (see p. 149).

## 18.14 Numerical dissipation

The main function of an SGS model is to dissipate (i.e. to dampen) resolved turbulent fluctuations. The SGS model is – hopefully – designed to give a proper amount of dissipation. This is the reason why in LES we should use a central differencing scheme, because this class of schemes does not give any *numerical* dissipation. All upwind schemes give numerical dissipation in addition to the modelled SGS dissipation. Indeed, there are LES-methods in which upwind schemes are used to create dissipation and where no SGS model is used at all (e.g. MILES [64]). However, here we focus on ensuring proper dissipation through an SGS model rather than via upwind differencing. It can be shown using Neumann stability analysis that all upwind schemes are dissipative (see *Further reading* at

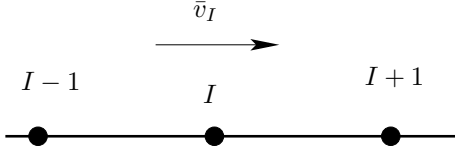


Figure 18.9: Numerical dissipation.

[http://www.tfd.chalmers.se/~lada/comp\\_turb\\_model/](http://www.tfd.chalmers.se/~lada/comp_turb_model/)). Below it is shown that first-order upwind schemes are dissipative.

The first-derivative in the convective term is estimated by first-order upwind differencing as (finite difference, see Fig. 18.9)

$$\bar{v}_I \left( \frac{\partial \bar{v}}{\partial x} \right) = \bar{v}_I \left( \frac{\bar{v}_I - \bar{v}_{I-1}}{\Delta x} + \mathcal{O}(\Delta x) \right) \quad (18.34)$$

where we have assumed  $\bar{v}_I > 0$ . Taylor expansion gives

$$\bar{v}_{I-1} = \bar{v}_I - \Delta x \left( \frac{\partial \bar{v}}{\partial x} \right)_I + \frac{1}{2} (\Delta x)^2 \left( \frac{\partial^2 \bar{v}}{\partial x^2} \right)_I + \mathcal{O}((\Delta x)^3)$$

so that

$$\frac{\bar{v}_I - \bar{v}_{I-1}}{\Delta x} = \left( \frac{\partial \bar{v}}{\partial x} \right)_I - \frac{1}{2} \Delta x \left( \frac{\partial^2 \bar{v}}{\partial x^2} \right)_I + \mathcal{O}((\Delta x)^2)$$

Insert this into Eq. 18.34

$$\bar{v} \left( \frac{\partial \bar{v}}{\partial x} \right) = \bar{v}_I \left( \left( \frac{\partial \bar{v}}{\partial x} \right)_I - \underbrace{\frac{1}{2} \Delta x \left( \frac{\partial^2 \bar{v}}{\partial x^2} \right)_I}_{\mathcal{O}(\Delta x)} + \mathcal{O}((\Delta x)^2) \right)$$

where the second term on the right side corresponds to the error term in Eq. 18.34. When this expression is inserted into the LES momentum equations, the second term on the right-hand side will act as an additional (numerical) diffusion term. The total diffusion term will have the form

$$\text{diffusion term} = \frac{\partial}{\partial x} \left\{ (\nu + \nu_{sgs} + \nu_{num}) \frac{\partial \bar{v}}{\partial x} \right\} \quad (18.35)$$

where the additional numerical viscosity,  $\nu_{num} \simeq 0.5 |\bar{v}_I| \Delta x$ . This means that the total dissipation due to SGS viscosity and numerical viscosity is (cf. Eq. 18.17)

$$\varepsilon_{sgs+num} = 2(\nu_{sgs} + \nu_{num}) \bar{s}_{ij} \bar{s}_{ij}$$

For more details on derivation of equations transport equations of turbulent kinetic energies, see [15].

## 18.15 Scale-similarity Models

In the models presented in the previous sections (the Smagorinsky and the dynamic models) the total SGS stress  $\tau_{ij} = \bar{v}_i \bar{v}_j - \bar{v}_i \bar{v}_j$  was modelled with an eddy-viscosity

hypothesis. In scale-similarity models the total stress is split up as

$$\begin{aligned}\tau_{ij} &= \overline{v_i v_j} - \bar{v}_i \bar{v}_j = \overline{(\bar{v}_i + v''_i)(\bar{v}_j + v''_j)} - \bar{v}_i \bar{v}_j \\ &= \overline{\bar{v}_i \bar{v}_j} + \overline{v_i v''_j} + \overline{v_j v''_i} + \overline{v''_i v''_j} - \bar{v}_i \bar{v}_j \\ &= (\overline{\bar{v}_i \bar{v}_j} - \bar{v}_i \bar{v}_j) + [\overline{\bar{v}_i v''_j} + \overline{v_j v''_i}] + \overline{v''_i v''_j}\end{aligned}$$

where the term in brackets is denoted the Leonard stresses, the term in square brackets is denoted cross terms, and the last term is denoted the Reynolds SGS stress. Thus

$$\begin{aligned}\tau_{ij} &= L_{ij} + C_{ij} + R_{ij} \\ L_{ij} &= \overline{\bar{v}_i \bar{v}_j} - \bar{v}_i \bar{v}_j \\ C_{ij} &= \overline{\bar{v}_i v''_j} + \overline{v_j v''_i} \\ R_{ij} &= \overline{v''_i v''_j}.\end{aligned}\tag{18.36}$$

Note that the Leonard stresses  $L_{ij}$  are *computable*, i.e. they are exact and don't need to be modelled.

In scale-similarity models the main idea is that the turbulent scales just above cut-off wavenumber,  $\kappa_c$ , (smaller than  $\Delta$ ) are similar to the ones just below  $\kappa_c$  (larger than  $\Delta$ ); hence the word "scale-similar". Looking at Eq. 18.36 it seems natural to assume that the cross term is responsible for the interaction between resolved scales ( $\bar{v}_i$ ) and modelled scales ( $v''_i$ ), since  $C_{ij}$  includes both scales.

## 18.16 The Bardina Model

In the Bardina model the Leonard stresses  $L_{ij}$  are computed explicitly, and the sum of the cross term  $C_{ij}$  and the Reynolds term is modelled as [65, 66]

$$C_{ij}^M = c_r(\bar{v}_i \bar{v}_j - \overline{\bar{v}_i \bar{v}_j})\tag{18.37}$$

and  $R_{ij}^M = 0$  (superscript  $M$  denotes Modelled). It was found that this model was not sufficiently dissipative, and thus a Smagorinsky model was added

$$\begin{aligned}C_{ij}^M &= c_r(\bar{v}_i \bar{v}_j - \overline{\bar{v}_i \bar{v}_j}) \\ R_{ij}^M &= -2C_S^2 \Delta^2 |\bar{s}| \bar{s}_{ij}\end{aligned}\tag{18.38}$$

## 18.17 Redefined terms in the Bardina Model

The stresses in the Bardina model can be redefined to make them Galilean invariant for any value  $c_r$  (see Appendix H). A modified Leonard stress tensor  $L_{ij}^m$  is defined as [67]

$$\begin{aligned}\tau_{ij}^m &= \tau_{ij} = C_{ij}^m + L_{ij}^m + R_{ij}^m \\ L_{ij}^m &= c_r(\overline{\bar{v}_i \bar{v}_j} - \overline{\bar{v}_i \bar{v}_j}) \\ C_{ij}^m &= 0 \\ R_{ij}^m &= R_{ij} = \overline{v''_i v''_j}\end{aligned}\tag{18.39}$$

Note that the modified Leonard stresses is the same as the "unmodified" one plus the modelled cross term  $C_{ij}$  in the Bardina model with  $c_r = 1$  (right-hand side of Eq. 18.37), i.e.

$$L_{ij}^m = L_{ij} + C_{ij}^M$$

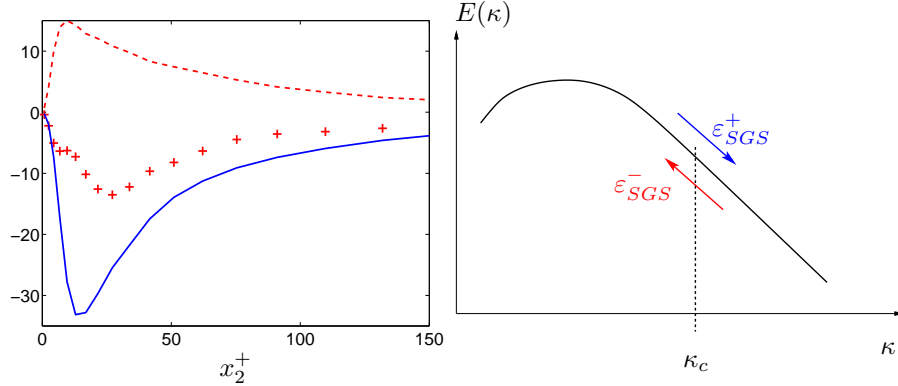


Figure 18.10: Dissipation terms and production term from DNS data.  $96^3$  mesh data filtered onto a  $48^3$  mesh.  $Re_\tau = 500$ . —:  $-\varepsilon_{SGS}^+$ ; - - -:  $-\varepsilon_{SGS}^-$ ; +:  $-\varepsilon_{SGS}$ .

In order to make the model sufficiently dissipative a Smagorinsky model is added, and the total SGS stress  $\tau_{ij}$  is modelled as

$$\tau_{ij} = \bar{v}_i \bar{v}_j - \bar{\bar{v}}_i \bar{\bar{v}}_j - 2(C_S \Delta)^2 |\bar{s}| \bar{s}_{ij} \quad (18.40)$$

Below we verify that the modified Leonard stress is Galilean invariant.

$$\begin{aligned} \frac{1}{c_r} L_{ij}^{m*} &= \overline{\bar{v}_i^* \bar{v}_j^*} - \overline{\bar{v}_i^*} \overline{\bar{v}_j^*} = \overline{(\bar{v}_i + V_i)(\bar{v}_j + V_j)} - \overline{(\bar{v}_i + V_i)} \overline{(\bar{v}_j + V_j)} \\ &= \overline{\bar{v}_i \bar{v}_j} + \overline{\bar{v}_i V_j} + \overline{\bar{v}_j V_i} - \overline{\bar{v}_i} \overline{\bar{v}_j} - \overline{V_i} \overline{V_j} \\ &= \overline{\bar{v}_i \bar{v}_j} - \overline{\bar{v}_i} \overline{\bar{v}_j} = \frac{1}{c_r} L_{ij}^m \end{aligned} \quad (18.41)$$

## 18.18 A dissipative scale-similarity model.

Above it was mentioned that when the first scale-similarity model was proposed it was found that it is not sufficiently dissipative [65]. An eddy-viscosity model has to be added to make the model sufficiently dissipative; these models are called *mixed* models. [68] (can be downloaded from [www.tfd.chalmers.se/~lada](http://www.tfd.chalmers.se/~lada)) presents and evaluates a dissipative scale-similarity model.

The filtered Navier-Stokes read

$$\frac{d\bar{v}_i}{dt} + \frac{1}{\rho} \frac{\partial \bar{p}}{\partial x_i} = \nu \frac{\partial^2 \bar{v}_i}{\partial x_k \partial x_k} - \frac{\partial \tau_{ik}}{\partial x_k} \quad (18.42)$$

where  $d/dt$  and  $\tau_{ik}$  denote the material derivative and the SGS stress tensor, respectively.

The SGS stress tensor is given by

$$\tau_{ik} = \bar{v}_i \bar{v}_k - \bar{\bar{v}}_i \bar{\bar{v}}_k. \quad (18.43)$$

When it is modelled with the standard scale-similarity model, it is not sufficiently dissipative. Let us take a closer look at the equation for the resolved, turbulent kinetic

energy,  $k = \langle v'_i v'_i \rangle / 2$ , which reads

$$\begin{aligned} \frac{dk}{dt} + \langle \bar{v}'_k \bar{v}'_i \rangle \frac{\partial \langle \bar{v}_i \rangle}{\partial x_k} + \frac{\partial \langle \bar{p}' \bar{v}'_i \rangle}{\partial x_i} + \frac{1}{2} \frac{\partial \langle \bar{v}'_k \bar{v}'_i \bar{v}'_i \rangle}{\partial x_k} &= \nu \left\langle \frac{\partial^2 \bar{v}'_i}{\partial x_k \partial x_k} \bar{v}'_i \right\rangle - \\ \left\langle \left( \frac{\partial \tau_{ik}}{\partial x_k} - \left\langle \frac{\partial \tau_{ik}}{\partial x_k} \right\rangle \right) \bar{v}'_i \right\rangle &= \nu \left\langle \frac{\partial^2 \bar{v}'_i}{\partial x_k \partial x_k} \bar{v}'_i \right\rangle - \left\langle \frac{\partial \tau_{ik}}{\partial x_k} \bar{v}'_i \right\rangle = \\ \nu \frac{\partial^2 k}{\partial x_k \partial x_k} - \underbrace{\nu \left\langle \frac{\partial \bar{v}'_i}{\partial x_k} \frac{\partial \bar{v}'_i}{\partial x_k} \right\rangle}_{\varepsilon} - \underbrace{\left\langle \frac{\partial \tau_{ik}}{\partial x_k} \bar{v}'_i \right\rangle}_{\varepsilon_{SGS}} & \end{aligned} \quad (18.44)$$

The first term on the last line is the viscous diffusion term and the second term,  $\varepsilon$ , is the viscous dissipation term which is always positive. The last term,  $\varepsilon_{SGS}$ , is a source term arising from the SGS stress tensor, which can be positive or negative. When it is positive, forward scattering takes place (i.e. it acts as a dissipation term); when it is negative, back scattering occurs.

Figure 18.10 presents SGS dissipation,  $\varepsilon_{SGS}$  in Eq. 18.44, computed from filtered DNS data. The forward scatter,  $\varepsilon_{SGS}^+$ , and back scatter,  $\varepsilon_{SGS}^-$ , SGS dissipation are defined as the sum of all instants when  $\varepsilon_{SGS}$  is positive and negative, respectively. As can be seen, the scale-similarity model is slightly dissipative (i.e.  $\varepsilon_{SGS} > 0$ ), but the forward and back scatter dissipation are both much larger than  $\varepsilon_{SGS}$ .

One way to make the SGS stress tensor strictly dissipative is to set the back scatter to zero, i.e.  $\max(\varepsilon_{SGS}, 0)$ . This could be achieved by setting  $\partial \tau_{ik} / \partial x_k = 0$  when its sign is different from that of  $\bar{v}'_i$  (see the last term in Eq. 18.44). This would work if we were solving for  $k$ . Usually we do not, and the equations that we do solve (the filtered Navier-Stokes equations) are not directly affected by the dissipation term,  $\varepsilon_{SGS}$ .

Instead we have to modify the SGS stress tensor as it appears in the filtered Navier-Stokes equations, Eq. 18.42. The second derivative on the right side is usually called a *diffusion* term because it acts like a diffusion transport term. When analyzing the stability properties of discretized equations to an imposed disturbance,  $\bar{v}'$ , using Neumann analysis (see, for example, Chapter 8 in [69]), this term is referred to as a *dissipation* term. In stability analysis the concern is to dampen numerical oscillations; in connection with SGS models, the aim is to dampen turbulent resolved fluctuations. It is shown in Neumann analysis that the diffusion term in the Navier-Stokes equations is dissipative, i.e. it dampens numerical oscillations. However, since it is the resolved *turbulent fluctuations*, i.e.  $k$  in Eq. 18.44, that we want to dissipate, we must consider the filtered Navier-Stokes equations for the fluctuating velocity,  $\bar{v}'_i$ . It is the diffusion term in this equation which appears in the first term on the right side (first line) in Eq. 18.44. To ensure that  $\varepsilon_{SGS} > 0$ , we set  $-\partial \tau_{ik} / \partial x_k$  to zero when its sign is different from that of the viscous diffusion term (cf. the two last terms on the second line in Eq. 18.44). This is achieved by defining a sign function; for details, see [68].

## 18.19 Forcing

An alternative way to modify the scale-similarity model is to omit the *forward* scatter, i.e. to include instants when the subgrid stresses act as *counter-gradient* diffusion. In hybrid LES-RANS, the stresses can then be used as forcing at the interface between URANS and LES. This new approach is the focus of [70].

## 18.20 Numerical method

A numerical method based on an implicit, finite volume method with collocated grid arrangement, central differencing in space, and Crank-Nicolson ( $\alpha = 0.5$ ) in time is briefly described below. The discretized momentum equations read

$$\begin{aligned}\bar{v}_i^{n+1/2} &= \bar{v}_i^n + \Delta t H \left( \bar{v}^n, \bar{v}_i^{n+1/2} \right) \\ &\quad - \alpha \Delta t \frac{\partial \bar{p}^{n+1/2}}{\partial x_i} - (1 - \alpha) \Delta t \frac{\partial \bar{p}^n}{\partial x_i}\end{aligned}\tag{18.45}$$

where  $H$  includes convective, viscous and SGS terms. In SIMPLE notation this equation reads

$$a_P \bar{v}_i^{n+1/2} = \sum_{nb} a_{nb} \bar{v}_i^{n+1/2} + S_U - \alpha \Delta t \frac{\partial \bar{p}^{n+1/2}}{\partial x_i} \Delta V$$

where  $S_U$  includes all source terms except the implicit pressure. The face velocities  $\bar{v}_{f,i}^{n+1/2} = 0.5(\bar{v}_{i,j}^{n+1/2} + \bar{v}_{i,j-1}^{n+1/2})$  (note that  $j$  denotes node number and  $i$  is a tensor index) do not satisfy continuity. Create an intermediate velocity field by subtracting the implicit pressure gradient from Eq. 18.45, i.e.

$$\bar{v}_i^* = \bar{v}_i^n + \Delta t H \left( \bar{v}^n, \bar{v}_i^{n+1/2} \right) - (1 - \alpha) \Delta t \frac{\partial \bar{p}^n}{\partial x_i}\tag{18.46a}$$

$$\Rightarrow \bar{v}_i^* = \bar{v}_i^{n+1/2} + \alpha \Delta t \frac{\partial \bar{p}^{n+1/2}}{\partial x_i}\tag{18.46b}$$

Take the divergence of Eq. 18.46b and require that  $\partial \bar{v}_{f,i}^{n+1/2} / \partial x_i = 0$  so that

$$\frac{\partial^2 \bar{p}^{n+1}}{\partial x_i \partial x_i} = \frac{1}{\Delta t \alpha} \frac{\partial \bar{v}_{f,i}^*}{\partial x_i}\tag{18.47}$$

The Poisson equation for  $\bar{p}^{n+1}$  is solved with an efficient multigrid method [71]. In the 3D MG we use a plane-by-plane 2D MG. The face velocities are corrected as

$$\bar{v}_{f,i}^{n+1} = \bar{v}_{f,i}^* - \alpha \Delta t \frac{\partial \bar{p}^{n+1}}{\partial x_i}\tag{18.48}$$

A few iterations (typically two) solving the momentum equations and the Poisson pressure equation are required each time step to obtain convergence. More details can be found [72]

1. Solve the discretized filtered Navier-Stokes equation, Eq. 18.46a, for  $\bar{v}_1$ ,  $\bar{v}_2$  and  $\bar{v}_3$ .
2. Create an intermediate velocity field  $\bar{v}_i^*$  from Eq. 18.46b.
3. The Poisson equation (Eq. 18.47) is solved with an efficient multigrid method [71].
4. Compute the face velocities (which satisfy continuity) from the pressure and the intermediate face velocity from Eq. 18.48
5. Step 1 to 4 is performed till convergence (normally two or three iterations) is reached.

	RANS	LES
<b>Domain</b>	2D or 3D	always 3D
<b>Time domain</b>	steady or unsteady	always unsteady
<b>Space discretization</b>	2nd order upwind	central differencing
<b>Time discretization</b>	1st order	2nd order (e.g. C-N)
<b>Turbulence model</b>	more than two-equations	zero- or one-equation

Table 18.1: Differences between a finite volume RANS and LES code.

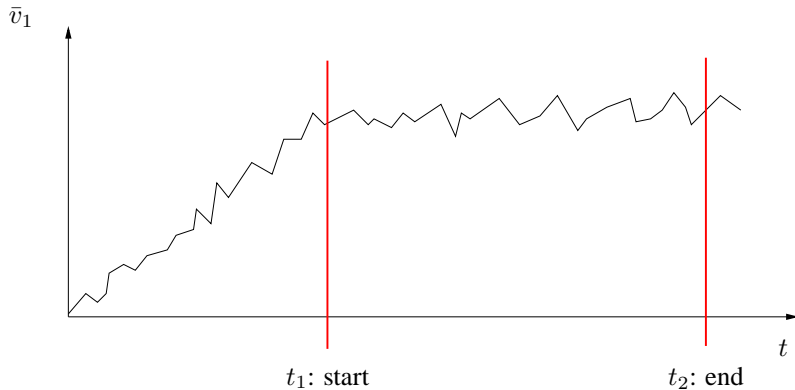


Figure 18.11: Time averaging in LES.

6. The turbulent viscosity is computed.

7. Next time step.

Since the Poisson solver in [71] is a nested MG solver, it is difficult to parallelize with MPI (Message Passing Interface) on large Linux clusters. Hence, when we do large simulations ( $> 20M$  cells) we use a traditional SIMPLE method.

### 18.20.1 RANS vs. LES

Above a numerical procedure suitable for LES was described. However, in general, any numerical procedure used for RANS can also be used for LES; for example pressure-correction methods such as SIMPLE [73, 74] are often used for LES. What are the specific requirements to carry out LES with a finite volume code? If you have a RANS finite volume code, it is very simple to transform that into an LES code. An LES code is actually simpler than a RANS code. Both the discretization scheme and the turbulence model are simpler in LES and RANS, see Table 18.1.

It is important to use a non-dissipative discretization scheme which does not introduce any additional numerical dissipation, see Section 18.14; hence a second-order (or higher) central differencing scheme should be employed.

The time discretization should also be non-dissipative. The Crank-Nicolson scheme is suitable.

As mentioned above, turbulence models in LES are simple. There are two reasons: first, only the small-scale turbulence is modelled and, second, no equation for the turbulent length scale is required since the turbulent length scale can be taken as the filter width,  $\Delta$ .

In LES we are doing unsteady simulations. The question then arises, when can we start to time average and for how long? This is exactly the same question we must ask our self whenever doing an experiment in, for example, a windtunnel. We start the windtunnel: when has the flow (and turbulence) reached fully developed conditions so that we can start the measure the flow. Next question: for how long should we carry out the measurements.

Both in LES and the windtunnel, the recorded time history of the  $\bar{v}_1$  velocity at a point may look like in Fig. 18.11. Time averaging can start at time  $t_1$  when the flow seems to have reached fully developed conditions. It is difficult to judge for how long one should carry out time averaging. Usually it is a good idea to form a non-dimensional time scale from a velocity,  $V$  (free-stream or bulk velocity), and a length scale,  $L$  (width of a wake, width or length of a recirculation region), and use this to estimate the required averaging time; 100 time units, i.e.  $100L/V$ , may be a suitable averaging time.

## 18.21 One-equation $k_{sgs}$ model

A one-equation model can be used to model the SGS turbulent kinetic energy. The equation can be written on the same form as the RANS  $k$ -equation, i.e.

$$\frac{\partial k_{sgs}}{\partial t} + \frac{\partial}{\partial x_j} (\bar{v}_j k_{sgs}) = \frac{\partial}{\partial x_j} \left[ (\nu + \nu_{sgs}) \frac{\partial k_{sgs}}{\partial x_j} \right] + P_{k_{sgs}} - \varepsilon \quad (18.49)$$

$$\nu_{sgs} = c_k \Delta k_{sgs}^{1/2}, \quad P_{k_{sgs}} = 2\nu_{sgs} \bar{s}_{ij} \bar{s}_{ij}, \quad \varepsilon = C_\varepsilon \frac{k_{sgs}^{3/2}}{\Delta}$$

Note that the production term,  $P_{k_{sgs}}$ , is equivalent to the SGS dissipation in the equation for the resolved turbulent kinetic energy (look at the flow of kinetic energy discussed at the end of [75]).

## 18.22 Smagorinsky model derived from the $k_{sgs}$ equation

We can use the one-equation model to derive the Smagorinsky model, Eq. 18.13. The length scale in the Smagorinsky model is the filter width,  $\Delta \propto \kappa_{II}$ , see Fig. 18.12. The cut-off takes place in the inertial subrange where diffusion and convection in the  $k_{sgs}$  equation are negligible (their time scales are too large so they have no time to adapt to rapid changes in the velocity gradients,  $\bar{s}_{ij}$ ). Hence, production and dissipation in Eq. 18.49 are in balance so that

$$P_{k_{sgs}} = 2\nu_{sgs} \bar{s}_{ij} \bar{s}_{ij} = \varepsilon \quad (18.50)$$

Let us replace  $\varepsilon$  by SGS viscosity and  $\Delta$ . We can write the SGS viscosity as

$$\nu_{sgs} = \varepsilon^a (C_S \Delta)^b \quad (18.51)$$

Dimensional analysis yields  $a = 1/3$ ,  $b = 4/3$  so that

$$\nu_{sgs} = (C_S \Delta)^{4/3} \varepsilon^{1/3}. \quad (18.52)$$

Eq. 18.50 substituted into Eq. 18.52 gives

$$\begin{aligned} \nu_{sgs}^3 &= (C_S \Delta)^4 \varepsilon = (C_S \Delta)^4 \nu_{sgs} (2\bar{s}_{ij} \bar{s}_{ij}) \\ \Rightarrow \nu_{sgs} &= (C_S \Delta)^2 |\bar{s}| \\ |\bar{s}| &= (2\bar{s}_{ij} \bar{s}_{ij})^{1/2} \end{aligned} \quad (18.53)$$

which is the Smagorinsky model.

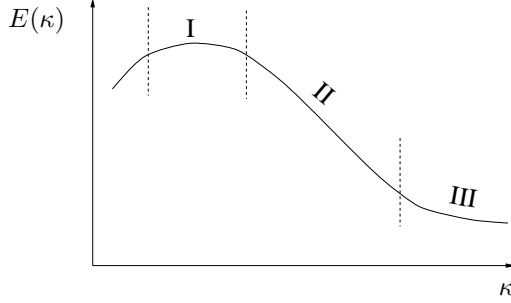


Figure 18.12: Spectrum for  $k$ . I: Range for the large, energy containing eddies; II: the inertial subrange for isotropic scales, independent of the large scales ( $\ell$ ) and the dissipative scales ( $\nu$ ); III: Range for small, isotropic, dissipative scales.

### 18.23 A dynamic one-equation model

One of the drawbacks of the dynamic model of [61] (see p. 138) is the numerical instability associated with the negative values and large variation of the  $C$  coefficient. Usually this problem is fixed by averaging the coefficient in some homogeneous flow direction. In real applications ad-hoc local smoothing and clipping is used. Below a dynamic one-equation model is presented. The main object when developing this model was that it should be applicable to real industrial flows. Furthermore, being a dynamic model, it has the great advantage that the coefficients are *computed* rather than being prescribed.

The equation for the subgrid kinetic energy reads [76, 77] (see also [78, 79])

$$\frac{\partial k_{sgs}}{\partial t} + \frac{\partial}{\partial x_j} (\bar{v}_j k_{sgs}) = P_{k_{sgs}} + \frac{\partial}{\partial x_j} \left( \nu_{eff} \frac{\partial k_{sgs}}{\partial x_j} \right) - C_* \frac{k_{sgs}^{3/2}}{\Delta} \quad (18.54)$$

$$P_{k_{sgs}} = -\tau_{ij}^a \bar{v}_{i,j}, \quad \tau_{ij}^a = -2C\Delta k_{sgs}^{\frac{1}{2}} \bar{s}_{ij}$$

with  $\nu_{eff} = \nu + 2C_{hom}\Delta k_{sgs}^{\frac{1}{2}}$ . The  $C$  in the production term  $P_{k_{sgs}}$  is computed dynamically (cf. Eq. 18.33). To ensure numerical stability, a *constant* value (in space) of  $C$  ( $C_{hom}$ ) is used in the diffusion term in Eq. 18.54 and in the momentum equations.  $C_{hom}$  is computed by requiring that  $C_{hom}$  should yield the same total production of  $k_{sgs}$  as  $C$ , i.e.

$$\langle 2C\Delta k_{sgs}^{\frac{1}{2}} \bar{s}_{ij} \bar{s}_{ij} \rangle_{xyz} = 2C_{hom} \langle \Delta k_{sgs}^{\frac{1}{2}} \bar{s}_{ij} \bar{s}_{ij} \rangle_{xyz}$$

The dissipation term  $\varepsilon_{k_{sgs}}$  is estimated as:

$$\varepsilon_{k_{sgs}} \equiv \nu T_f(v_{i,j}, v_{i,j}) = C_* \frac{k_{sgs}^{3/2}}{\Delta}. \quad (18.55)$$

Now we want to find a dynamic equation for  $C_*$ . The equations for  $k_{sgs}$  and  $K$  read in symbolic form

$$T(k_{sgs}) \equiv C_{k_{sgs}} - D_{k_{sgs}} = P_{k_{sgs}} - C_* \frac{k_{sgs}^{3/2}}{\Delta} \quad (18.56)$$

$$T(K) \equiv C_K - D_K = P^K - C_* \frac{K^{3/2}}{\Delta}$$

Since the turbulence on both the grid level and the test level should be in local equilibrium (in the inertial  $-5/3$  region), the left-hand side of the two equations in Eq. 18.56 should be close to zero. An even better approximation should be to assume  $T(k_{sgs}) = T(K)$ , i.e.

$$\widehat{P}_{k_{sgs}} - \frac{1}{\Delta} \overline{C_* k_{sgs}}^{3/2} = P^K - C_* \frac{K^{3/2}}{\Delta},$$

so that

$$C_*^{n+1} = \left( P^K - \widehat{P}_{k_{sgs}} + \frac{1}{\Delta} \overline{C_* k_{sgs}}^{3/2} \right) \frac{\Delta}{K^{3/2}}. \quad (18.57)$$

The idea is to put the local dynamic coefficients in the source terms, i.e. in the production and the dissipation terms of the  $k_{sgs}$  equation (Eq. 18.54). In this way the dynamic coefficients  $C$  and  $C_*$  don't need to be clipped or averaged in any way. This is a big advantage compared to the standard dynamic model of Germano (see discussion on p. 141).

## 18.24 A Mixed Model Based on a One-Eq. Model

Recently a new dynamic scale-similarity model was presented by [80]. In this model a dynamic one-equation SGS model is solved, and the scale-similarity part is estimated in a similar way as in Eq. 18.40.

## 18.25 Applied LES

At the Department we used LES for applied flows such as flow around a cube [81, 82], the flow and heat transfer in a square rotating duct [83, 84], the flow around a simplified bus [85, 82], a simplified car [86, 87, 88] and the flow around an airfoil [89, 90], detailed SUV [91], trains and buses subjected to sidewinds and wind gusts [92, 93, 94]. We have also done some work on buoyancy-affected flows [95, 96, 97, 98, 99, 100, 101].

## 18.26 Resolution requirements

The near-wall grid spacing should be about one wall unit in the wall-normal direction. This is similar to the requirement in RANS (Reynolds-Averaged Navier-Stokes) using low-Re number models. The resolution requirements in wall-parallel planes for a well-resolved LES in the near-wall region expressed in wall units are approximately 100 (streamwise) and 30 (spanwise). This enables resolution of the near-wall turbulent structures in the viscous sub-layer and the buffer layer consisting of high-speed in-rushes and low-speed ejections [102], often called the streak process. At low to medium Reynolds numbers the streak process is responsible for the major part of the turbulence production. These structures must be resolved in an LES in order to achieve accurate results. Then the spectra of the resolved turbulence will exhibit  $-5/3$  range, see figure on p. 46.

In applied LES, this kind of resolution can hardly ever be afforded. In outer scaling (i.e. comparing the resolution to the boundary layer thickness,  $\delta$ ), we can afford  $\delta/\Delta x_1$  and  $\delta/\Delta x_3$  in the region of 10 – 20 and 20 – 40, respectively. In this case, the spectra in the boundary layer will look something like that shown in Fig. 18.13 [103]. Energy spectra are actually not very reliable to judge if a LES simulation is well resolved or not.

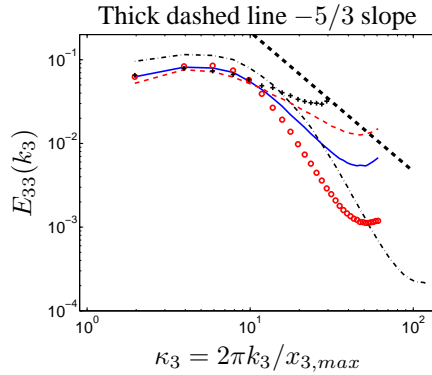


Figure 18.13: Energy spectra in fully developed channel flow [103].  $\delta$  denotes half channel width. Number of cells expressed as  $(\delta/\Delta x_1, \delta/\Delta x_3)$ . —: (10, 20); - - -: (20, 20); - - - -: (10, 40); ○: (5, 20); +: (10, 10).

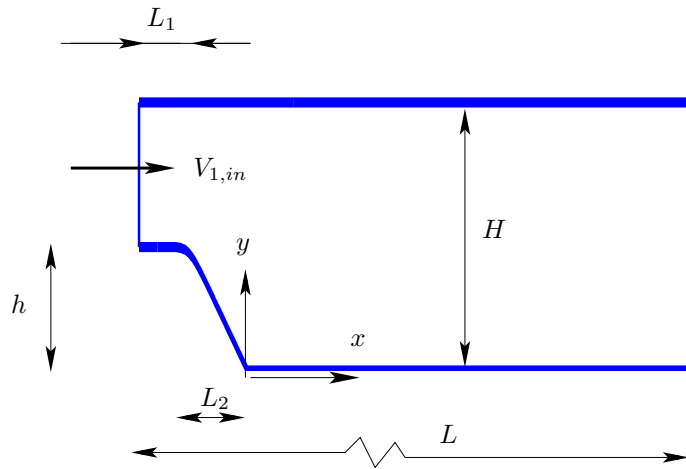


Figure 18.14: Onera bump. Computational domain (not to scale).

In [103, 104] different ways to estimate the resolution of an LES were investigated. The suggestion in these works was that two-point correlations is the best way to estimate if an LES is sufficiently resolved or not.

Even if the turbulence in boundary layer seldom can be resolved, the flow in recirculation regions and shear layer can. In [105] the flow ( $Re \simeq 10^6$ ) over a bump was computed. The geometry is shown in Fig. 18.14. The turbulence in the boundary layer on the bump was very poorly resolved:  $\Delta x_1/\delta_{in} = 0.33$ ,  $\Delta x_3/\delta_{in} = 0.44$ ,  $\Delta x_1^+ = 1300$  and  $\Delta x_3^+ = 1800$ . Nevertheless, the turbulence in the recirculation region and in the shear layer downstream the bump turned out to be well resolved, see Fig. 18.15.

Thus, for wall-bounded flows at high Reynolds numbers of engineering interest, the computational resource requirement of accurate LES is prohibitively large. Indeed, the requirement of near-wall grid resolution is the main reason why LES is too expensive for engineering flows, which was one of the lessons learned in the LESFOIL project [106, 107].

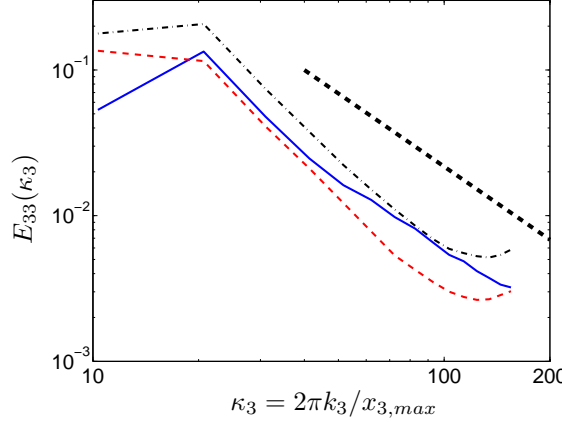


Figure 18.15: Energy spectra  $E_{33}(\kappa_3)$  in the recirculation region and the shear layer downstream the bump ( $x_1/H = 1.2$ ). Thick dashed line shows  $-5/3$  slope. —:  $x_2/H = 0.0035$  (near the wall); - - -:  $x_2/H = 0.13$ ; - · - :  $x_2/H = 0.34$  (in the shear layer).

## 19 Unsteady RANS

To perform an accurate LES, a very fine mesh must be used. This causes problems, for example, near walls. LES is very good for wake flow, where the flow is governed by large, turbulent structures, which can be captured by a fairly coarse mesh. However, if attached boundary layers are important, LES will probably give poor predictions in these regions, unless fine grids are used.

An alternative to LES for industrial flows can then be **unsteady RANS** (Reynolds-Averaged Navier-Stokes), often denoted **URANS** (Unsteady RANS) or **TRANS** (Transient RANS).

In URANS the usual Reynolds decomposition is employed, i.e.

$$\bar{v}(t) = \frac{1}{2T} \int_{t-T}^{t+T} v(t) dt, \quad v = \bar{v} + v'' \quad (19.1)$$

The URANS equations are the usual RANS equations, but with the transient (unsteady) term retained, i.e. (on incompressible form)

$$\begin{aligned} \frac{\partial \bar{v}_i}{\partial t} + \frac{\partial}{\partial x_j} (\bar{v}_i \bar{v}_j) &= -\frac{1}{\rho} \frac{\partial \bar{p}}{\partial x_i} + \nu \frac{\partial^2 \bar{v}_i}{\partial x_j \partial x_j} - \frac{\partial \bar{v}_i'' \bar{v}_j''}{\partial x_j} \\ \frac{\partial \bar{v}_i}{\partial x_i} &= 0 \end{aligned} \quad (19.2)$$

Note that the dependent variables are now not only function of the space coordinates, but also function of time, i.e.  $\bar{v}_i = \bar{v}_i(x_1, x_2, x_3, t)$ ,  $\bar{p} = \bar{p}(x_1, x_2, x_3, t)$  and  $\bar{v}_i'' \bar{v}_j'' = \bar{v}_i'' \bar{v}_j''(x_1, x_2, x_3, t)$ .

Even if the results from URANS are unsteady, one is often interested only in the time-averaged flow. We denote here the time-averaged velocity as  $\langle \bar{v} \rangle$ , which means that we can decompose the results from an URANS as a time-averaged part,  $\langle \bar{v} \rangle$ , a resolved fluctuation,  $\bar{v}'$ , and the modelled, turbulent fluctuation,  $v''$ , i.e.

$$v = \bar{v} + v'' = \langle \bar{v} \rangle + \bar{v}' + v'' \quad (19.3)$$

see Fig. 19.1. The modelled turbulent fluctuation,  $v''$ , is not shown in the figure; if this is added to  $\langle \bar{v} \rangle + \bar{v}'$  we obtain  $v$ .

What type of turbulence model should be used in URANS? That depends on type of flow. If the flow has strong vortex shedding, the standard high-Re number  $k - \varepsilon$  model can be used, i.e.

$$\frac{\partial \rho k}{\partial t} + \frac{\partial \rho \bar{v}_j k}{\partial x_j} = \frac{\partial}{\partial x_j} \left[ \left( \mu + \frac{\mu_t}{\sigma_k} \right) \frac{\partial k}{\partial x_j} \right] + P^k - \rho \varepsilon \quad (19.4)$$

$$\frac{\partial \rho \varepsilon}{\partial t} + \frac{\partial \rho \bar{v}_j \varepsilon}{\partial x_j} = \frac{\partial}{\partial x_j} \left[ \left( \mu + \frac{\mu_t}{\sigma_\varepsilon} \right) \frac{\partial \varepsilon}{\partial x_j} \right] + \frac{\varepsilon}{k} (c_{1\varepsilon} P^k - c_{\varepsilon 2} \rho \varepsilon) \quad (19.5)$$

$$\mu_t = c_\mu \rho \frac{k^2}{\varepsilon} \quad (19.6)$$

With an eddy-viscosity, the URANS equations read

$$\frac{\partial \rho \bar{v}_i}{\partial t} + \frac{\partial \rho \bar{v}_i \bar{v}_k}{\partial x_k} = -\frac{1}{\rho} \frac{\partial \bar{p}}{\partial x_i} + \frac{\partial}{\partial x_k} \left[ (\mu + \mu_t) \frac{\partial \bar{v}_i}{\partial x_k} \right] \quad (19.7)$$

So we are doing unsteady simulations, but still we time average the equations. How is this possible? The theoretical answer is that the time,  $T$ , in Eq. 19.1 should be much smaller than the resolved time scale, i.e. the modelled turbulent fluctuations,  $v''$ , should have a much smaller time scale than the resolved ones,  $\bar{v}'$ . This is called *scale separation*. In practice this requirement is often not satisfied [72]. On the other hand, how do the momentum equation, Eq. 19.7, know how they were time averaged? Or if they were volume filtered? The answer is that they don't. The URANS momentum equation and the LES momentum equation are exactly the same, except that we denote the turbulent viscosity in the former case by  $\nu_t$  and in the latter case by  $\nu_{sgs}$ . In URANS, much more of the turbulence is modelled than in LES, and, hence, the turbulent viscosity,  $\nu_t$ , is much larger than the SGS viscosity,  $\nu_{sgs}$ .

The common definition of URANS is that the turbulent length scale is not determined by the grid, whereas in LES it is. In URANS we do usually not care about scale

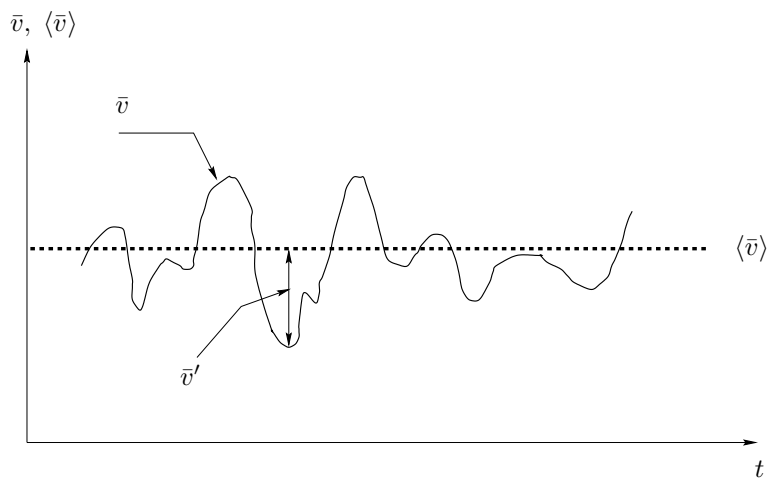


Figure 19.1: Decomposition of velocities in URANS.

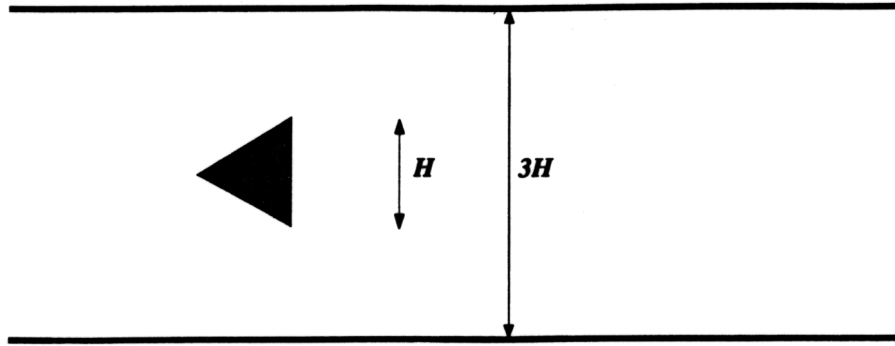


Figure 19.2: Configuration of the flow past a triangular flameholder. Flow from left to right

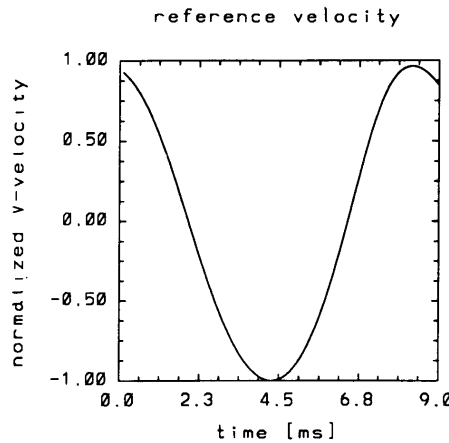


Figure 19.3: 2D URANS  $k - \varepsilon$  simulations [108]. One cycle of the  $\bar{v}_2$  velocity in a cell near the upper-right corner of the flameholder.

separation. What we care about is that the turbulence model and the discretization scheme should not be too dissipative, i.e. they should not kill the resolved fluctuations,  $\bar{v}'$ .

The standard  $k - \varepsilon$  model (Eq. 19.4 and 19.5) was used in [108] for URANS simulations computing the flow around a triangular flame-holder in a channel, see Fig. 19.2. This flow has a very regular vortex shedding, and the flow actually has a scale separation. In Fig. 19.3 the  $\bar{v}_2$  velocity in a point above the flame-holder is shown and it can be seen that the velocity varies with time in a sinusoidal manner.

When we're doing URANS, the question arises how the results should be time averaged, i.e. when should we start to average and for how long. This issue is the same when doing LES, and this was discussed in connection to Fig. 18.11.

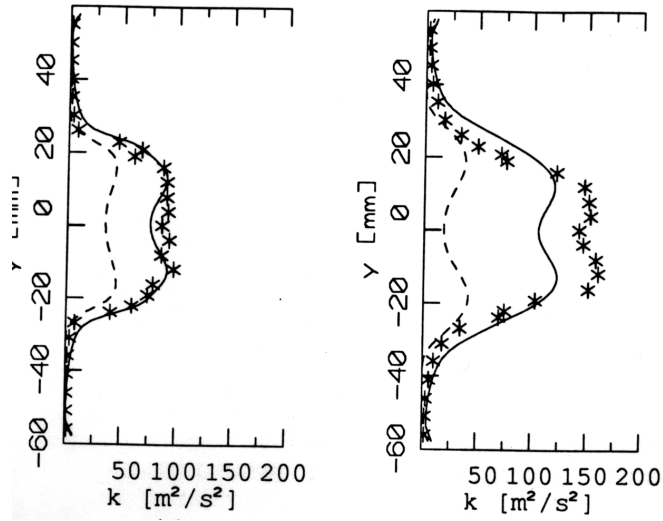


Figure 19.4: 2D URANS  $k - \varepsilon$  simulations compared with experiment [108]. Solid lines: total turbulent kinetic energy; dashed lines: resolved turbulent kinetic energy: \*: experimental data. Left figure:  $x = 0.43H$ ; right figure:  $x = 1.1H$  ( $x = 0$  at the downstream vertical plane of the flame-holder).

## 19.1 Turbulence Modelling

In URANS, part of the turbulence is modelled ( $v''$ ) and part of the turbulence is resolved ( $\bar{v}'$ ). If we want to compare computed turbulence with experimental turbulence, we must add these two parts together. Profiles downstream the flameholder are shown in Fig. 19.4. It can be seen that here the resolved and the modelled turbulence are of the same magnitude.

If the turbulence model in URANS generates "too much" eddy viscosity, the flow may not become unsteady at all, because the unsteadiness is damped out; the reason for this is that the turbulence model is too dissipative. It was found in [109, 110] when using URANS for the flow around a surface-mounted cube and around a car, that the standard  $k - \varepsilon$  model was too dissipative. Non-linear models like that of [111] was found to be less dissipative, and was successfully applied in URANS-simulations for these two flows.

## 19.2 Discretization

In LES it is well-known that non-dissipative discretization schemes should be used. The reason is that we don't want to dampen out resolved, turbulent fluctuations. The same is to some extent true also for URANS. In the predictions on the flame-holder presented above, the hybrid discretization scheme for the convective terms was used together with fully implicit first-order discretization in time; this gives first-order accuracy in both space and time. The turbulence model that was used was the standard  $k - \varepsilon$  model. Thus, both the discretization and the turbulence model have high dissipation. The reason why the unsteadiness in these computations was not damped out is that the vortex shedding in this flow is very strong.

In general a discretization scheme which has little numerical dissipation should be

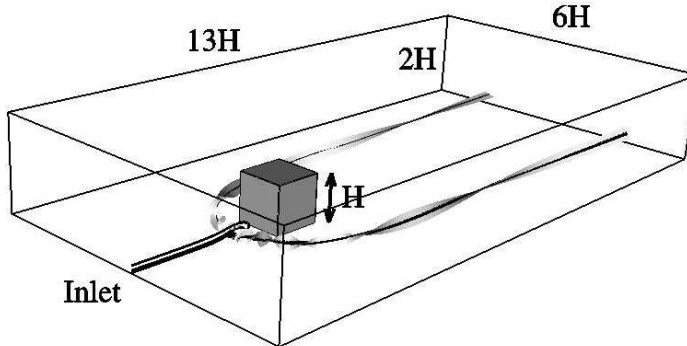


Figure 19.5: URANS simulations of the flow around a surface-mounted cube.

used. How dissipative a scheme needs to be in order to be stable is flow dependent; for some simple flows, it may work with no dissipation at all (i.e. central differencing), whereas for industrially complex flows maybe a bounded second-order scheme must be used. For time discretization, the second-order accurate Crank-Nicolson works in most cases.

In [109] LES and URANS simulations were carried out of the flow around a surface-mounted cube (Fig. 19.5) with a coarse mesh using wall-functions. Two different discretization schemes were used: the central scheme and the Mars scheme (a blend between central differencing and a bounded upwind scheme of second-order accuracy). In Fig. 19.6 the time-averaged velocity profile upstream of the cube ( $x_1 = -0.6H$ ) using URANS and LES with central differencing are shown together with URANS and Mars scheme. It is seen that with LES and central differencing unphysical oscillations are present (this was also found by [81]). However, LES with the Mars scheme (in which some numerical dissipation is present) and URANS with the central scheme (where the modelling dissipation is larger than in LES) no such unphysical oscillations are present. The main reason to the unphysical oscillations is that the predicted flow in this region does not have any resolved fluctuations. If turbulent unsteady inlet fluctuations are used, the unphysical oscillations do usually not appear, even if a central differencing scheme is used. In this case the turbulent, resolved fluctuations dominate over any numerical oscillations.

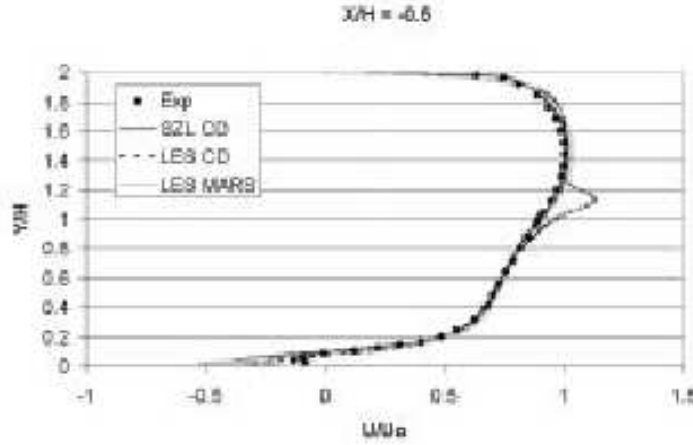


Figure 19.6: URANS simulations of the flow around a surface-mounted cube. Velocity profiles upstream the cube [109].

## 20 DES

DES (Detached Eddy Simulation) is a mix of LES and URANS. The aim is to treat the boundary layer with RANS and capture the outer detached eddies with LES. The model was originally developed for wings at very high angles of attack.

The RANS model that was originally used was the one-equation model by [112]. It can be written [112, 106, Sect. 4.6]

$$\frac{\partial \rho \tilde{\nu}_t}{\partial t} + \frac{\partial \rho \bar{v}_j \tilde{\nu}_t}{\partial x_j} = \frac{\partial}{\partial x_j} \left( \frac{\mu + \mu_t}{\sigma_{\tilde{\nu}_t}} \frac{\partial \tilde{\nu}_t}{\partial x_j} \right) + \frac{C_{b2}\rho}{\sigma_{\tilde{\nu}_t}} \frac{\partial \tilde{\nu}_t}{\partial x_j} \frac{\partial \tilde{\nu}_t}{\partial x_j} + P - \Psi \quad (20.1)$$

$$\nu_t = \tilde{\nu}_t f_1$$

The production term  $P$  and the destruction term  $\Psi$  have the form

$$P = C_{b1}\rho \left( \bar{s} + \frac{\tilde{\nu}_t}{\kappa^2 d^2} f_2 \right) \tilde{\nu}_t \quad (20.2)$$

$$\bar{s} = (2\bar{s}_{ij}\bar{s}_{ij})^{1/2}, \quad \Psi = C_{w1}\rho f_w \left( \frac{\tilde{\nu}_t}{d} \right)^2$$

$d$  in the RANS SA model is equal to the distance to the nearest wall.

In [113] the DES model was proposed in which  $d$  is taken as the minimum of the RANS turbulent length scale  $d$  and the cell length  $\Delta = \max(\Delta x_\xi, \Delta x_\eta, \Delta x_\zeta)$ , i.e.

$$\tilde{d} = \min(d, C_{des}\Delta) \quad (20.3)$$

$\Delta x_\xi, \Delta x_\eta$  and  $\Delta x_\zeta$  denote the cell length in the three grid directions  $\xi, \eta$  and  $\zeta$ . The constant  $C_{des}$  is usually set to 0.65.

In the boundary layer  $d < C_{des}\Delta$  and thus the model operates in RANS mode. Outside the turbulent boundary layer  $d > C_{des}\Delta$  so that the model operates in LES

mode. The modelled length scale is reduced and the consequence is that the destruction term  $\Psi$  increases, which gives a reduction in the turbulent viscosity  $\tilde{\nu}_t$ . A reduced  $\tilde{\nu}_t$  gives a smaller production term  $P$  so that the turbulent viscosity is further reduced.

At first sight it may seem that as the model switches from RANS mode to LES mode thus reducing  $d$ , this would give rise to an increased production term  $P$  through the second term (see Eq. 20.2). However, this second term is a viscous term and is active only close to the wall. This term is sometimes neglected [114]

## 20.1 DES based on two-equation models

The model described above is a one-equation model. In RANS mode it takes its length scale from the wall distance, which in many situations is not a relevant turbulent length scale. Recently, DES models based on two-equation models were proposed [115, 116, 117]. In these models the turbulent length scale is either obtained from the two turbulent quantities (e.g.  $k^{3/2}/\varepsilon$  or  $k^{1/2}/\omega$ ) or the filter width  $\Delta$ . A model based on the  $k - \varepsilon$  model can read

$$\begin{aligned} \frac{\partial k}{\partial t} + \frac{\partial}{\partial x_j} (\bar{v}_j k) &= \frac{\partial}{\partial x_j} \left[ \left( \nu + \frac{\nu_t}{\sigma_k} \right) \frac{\partial k}{\partial x_j} \right] + P^k - \varepsilon_T \\ \frac{\partial \varepsilon}{\partial t} + \frac{\partial}{\partial x_j} (\bar{v}_j \varepsilon) &= \frac{\partial}{\partial x_j} \left[ \left( \nu + \frac{\nu_t}{\sigma_\varepsilon} \right) \frac{\partial \varepsilon}{\partial x_j} \right] + \frac{\varepsilon}{k} (C_1 P^k - C_2 \varepsilon) \\ P^k &= 2\nu_t \bar{s}_{ij} \bar{s}_{ij}, \quad \nu_t = k^{1/2} \ell_t \end{aligned}$$

The turbulent length scale,  $\ell_t$ , and the turbulent dissipation,  $\varepsilon_T$ , are computed as [117, 118]

$$\begin{aligned} \ell_t &= \min \left( C_\mu \frac{k^{3/2}}{\varepsilon}, C_k \Delta \right) \\ \varepsilon_T &= \max \left( \varepsilon, C_\varepsilon \frac{k^{3/2}}{\Delta} \right) \end{aligned}$$

In other models [115, 54] only the dissipation term,  $\varepsilon_T$  is modified. When the grid is sufficiently fine, the length scale is taken as  $\Delta$ . The result is that the dissipation in the  $k$  equation increases so that  $k$  decreases which gives a reduced  $\nu_t$ . A third alternative is to modify only the turbulent length scale appearing in the turbulent viscosity [118]. In regions where the turbulent length scales are taken from  $\Delta$  (LES mode) the  $\varepsilon$ -equation is still solved, but  $\varepsilon$  is not used. However,  $\varepsilon$  is needed as soon as the model switches to RANS model again.

A rather new approach is to reduce the destruction term in the  $\varepsilon$  equation as in PANS [119, 120] (Partially Averaged Navier-Stokes) and PITM [121] (Partially Integrated Transport Modelling). In these models  $\varepsilon$  increases because of its reduced destruction term which decreases both  $k$  and  $\nu_t$ . A low-Reynolds number PANS was recently proposed [120] in which the near-wall modifications were taken from the AKN model [122].

In the RANS mode the major part of the turbulence is modelled. When the model switches to LES mode, the turbulence is supposed to be represented by resolved turbulence. This poses a major problem with this type of models. If the switch occurs at location  $x_1$ , say, it will take some distance  $L$  before the momentum equations start to resolve any turbulence. This is exactly what happens at an inlet in an LES simulation if no real turbulence is given as inlet boundary conditions. One way to get around this

is to impose turbulence fluctuations as forcing conditions [123, 124, 75, 125, 126, ] at the location where the model switches from RANS mode to LES mode. The forcing is added in the form of a source term (per unit volume) in the momentum equations.

## 20.2 DES based on the $k - \omega$ SST model

The standard  $k - \omega$  model SST reads [49, 54]

$$\begin{aligned} \frac{\partial k}{\partial t} + \frac{\partial}{\partial x_j} (\bar{v}_j k) &= \frac{\partial}{\partial x_j} \left[ \left( \nu + \frac{\nu_t}{\sigma_k} \right) \frac{\partial k}{\partial x_j} \right] + P_k - \beta^* k \omega \\ \frac{\partial \omega}{\partial t} + \frac{\partial}{\partial x_j} (\bar{v}_j \omega) &= \frac{\partial}{\partial x_j} \left[ \left( \nu + \frac{\nu_t}{\sigma_\omega} \right) \frac{\partial \omega}{\partial x_j} \right] + \alpha \frac{P_k}{\nu_t} - \beta \omega^2 \\ &\quad + 2(1 - F_1) \sigma_{\omega 2} \frac{1}{\omega} \frac{\partial k}{\partial x_i} \frac{\partial \omega}{\partial x_i} \\ F_1 &= \tanh(\xi^4), \quad \xi = \min \left[ \max \left\{ \frac{\sqrt{k}}{\beta^* \omega d}, \frac{500\nu}{d^2 \omega} \right\} \frac{4\sigma_{\omega 2} k}{CD_\omega d^2} \right] \quad (20.4) \\ \nu_t &= \frac{a_1 k}{\max(a_1 \omega, |\bar{s}| F_2)} \\ F_2 &= \tanh(\eta^2), \quad \eta = \max \left\{ \frac{2k^{1/2}}{\beta^* \omega d}, \frac{500\nu}{d^2 \omega} \right\} \end{aligned}$$

where  $d$  is the distance to the closest wall node. The SST model behaves as a  $k - \omega$  model near the wall where  $F_1 = 1$  and a  $k - \varepsilon$  model far from walls ( $F_1 = 0$ ). All coefficients are blended between the  $k - \omega$  and the  $k - \varepsilon$  model using the function  $F_1$ .

In DES the dissipation term in the  $k$  equation is modified as [54]

$$\begin{aligned} \beta^* k \omega &\rightarrow \beta^* k \omega F_{DES}, \quad F_{DES} = \max \left\{ \frac{L_t}{C_{DES} \Delta}, 1 \right\} \\ \Delta &= \max \{ \Delta x_1, \Delta x_2, \Delta x_3 \}, \quad L_t = \frac{k^{1/2}}{\beta^* \omega} \end{aligned}$$

Again, the DES modification is meant to switch the turbulent length scale from a RANS length scale ( $\propto k^{1/2}/\omega$ ) to a LES length scale ( $\propto \Delta$ ) when the grid is sufficiently fine. When  $F_{DES}$  is larger than one, the dissipation term in the  $k$  equation increases which in turn decreases  $k$  and thereby also the turbulent viscosity. With a smaller turbulent viscosity in the momentum equations, the modelled dissipation (i.e the damping) is reduced and the flow is induced to go unsteady. The result is, hopefully, that a large part of the turbulence is resolved rather than being modelled.

In some flows it may occur that the  $F_{DES}$  term switches to DES in the boundary layer because  $\Delta z$  is too small (smaller than the boundary layer thickness,  $\delta$ ). Different proposals have been made [127, 128] to protect the boundary layer from the LES mode

$$F_{DES} = \max \left\{ \frac{L_t}{C_{DES} \Delta} (1 - F_S), 1 \right\} \quad (20.5)$$

where  $F_S$  is taken as  $F_1$  or  $F_2$  (see Eq. 20.4) of the SST model.

## 21 Hybrid LES-RANS

When simulating bluff body flows, LES (Large Eddy Simulation) is the ideal method. Bluff body flows are dominated by large turbulent scales that can be resolved by LES without too fine a resolution and accurate results can thus be obtained at an affordable cost. On the other hand, it is a challenging task to make accurate predictions of wall-bounded flows with LES. The near-wall grid spacing should be about one wall unit in the wall-normal direction. This is similar to the requirement in RANS using low-Re number models. The resolution requirements in wall-parallel planes for a well-resolved LES in the near-wall region expressed in wall units are approximately 100 (streamwise) and 30 (spanwise). This enables resolution of the near-wall turbulent structures in the viscous sub-layer and the buffer layer consisting of high-speed in-rushes and low-speed ejections [102], often called the streak process.

An event of a high-speed in-rush is illustrated in Fig. 21.1. In the lower part of the figure the spanwise vortex line is shown. Initially it is a straight line, but due to a disturbance – e.g. a turbulent fluctuation – the mid-part of the vortex line is somewhat lifted up away from the wall. The mid-part of the vortex line experiences now a higher  $\bar{v}_1$  velocity (denoted by  $U$  in the figure) than the remaining part of the vortex line. As a result the mid-part is lifted up even more and a tip of a hairpin vortex is formed. The vorticity of the legs lift each other through self-induction which helps lifting the tip even more. In the  $x_1 - x_2$  plane (upper part of Fig. 21.1) the instantaneous and mean velocity profiles (denoted by  $U$  and  $\bar{U}$  in the figure, respectively) are shown as the hairpin vortex is created. It can be seen that an inflection point is created in the instantaneous velocity profile,  $U$ , and the momentum deficit in the inner layer increases for increasing  $x_1$ . Eventually the momentum deficit becomes too large and the high-speed fluid rushes in compensating for the momentum deficit. The in-rush event is also called a *sweep*. There are also events which occurs in the other direction, i.e. low-speed fluid is ejected away from the wall. These events are called *bursts* or *ejections*. The spanwise separation between sweeps and bursts is very small (approximately 100 viscous units, see Fig. 21.1). This is the main reason why the grid must be very fine in the spanwise direction. The streamwise distance between the events is related to the boundary layer thickness ( $4\delta$ , see Fig. 21.1). The process by which the events are formed is similar to the later stage in the transition process from laminar to turbulent flow. Figure 21.2 presents the instantaneous field of the streamwise velocity fluctuation,  $v'_1$  in the viscous wall region. As can be seen, the turbulent structures very elongated in the streamwise direction.

At low to medium Reynolds numbers the streak process is responsible for the major part of the turbulence production. These structures must be resolved in an LES in order to achieve accurate results. Thus, for wall-bounded flows at high Reynolds numbers of engineering interest, the computational resource requirement of accurate LES is prohibitively large. Indeed, the requirement of near-wall grid resolution is the main reason why LES is too expensive for engineering flows, which was one of the lessons learned in the LESFOIL project [106, 107].

The object of hybrid LES-RANS (and of DES) is to eliminate the requirement of high near-wall resolution in wall-parallel planes. In the near-wall region (the URANS region), a low-Re number RANS turbulence model (usually an eddy-viscosity model) is used. In the outer region (the LES region), the usual LES is used, see Fig. 21.3. The idea is that the effect of the near-wall turbulent structures should be modelled by the RANS turbulence model rather than being resolved. In the LES region, coarser grid spacing in wall-parallel planes can be used. The grid resolution in this region is

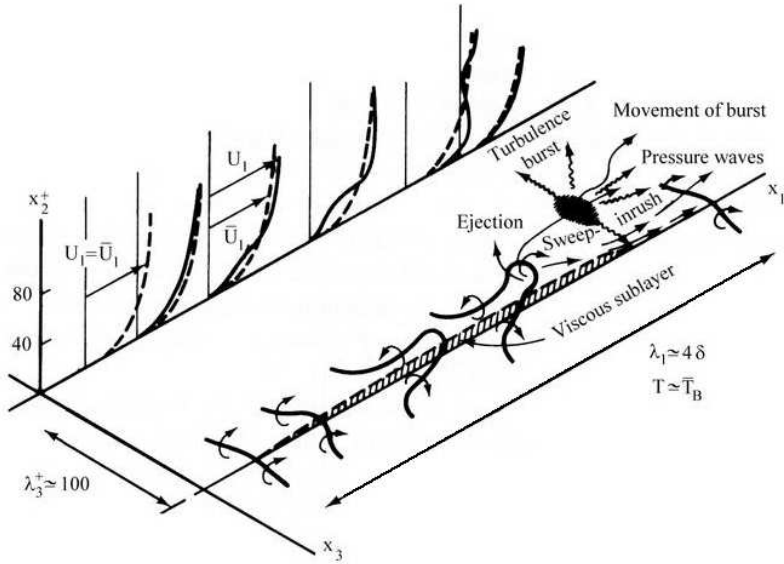


Figure 21.1: Illustration of near-wall turbulence (taken from [59]).

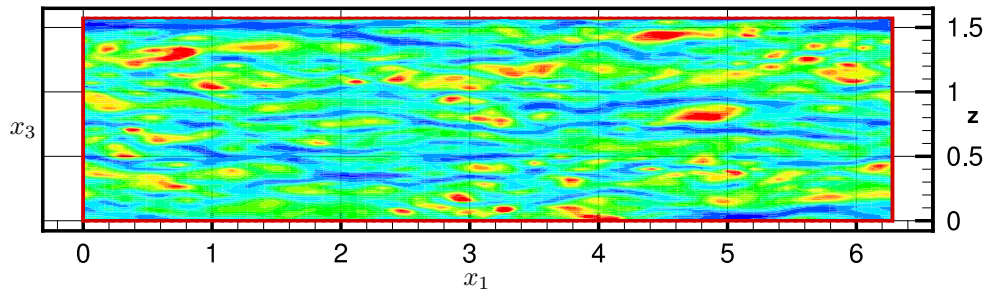
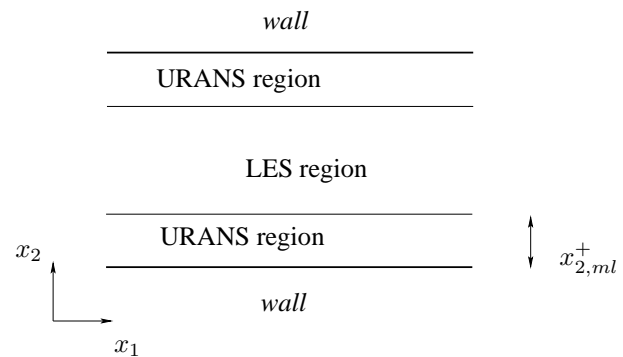
Figure 21.2: Fluctuating streamwise velocity in a wall-parallel plane at  $x_2^+ = 5$ . DNS of channel flow [75].

Figure 21.3: The LES and URANS region.

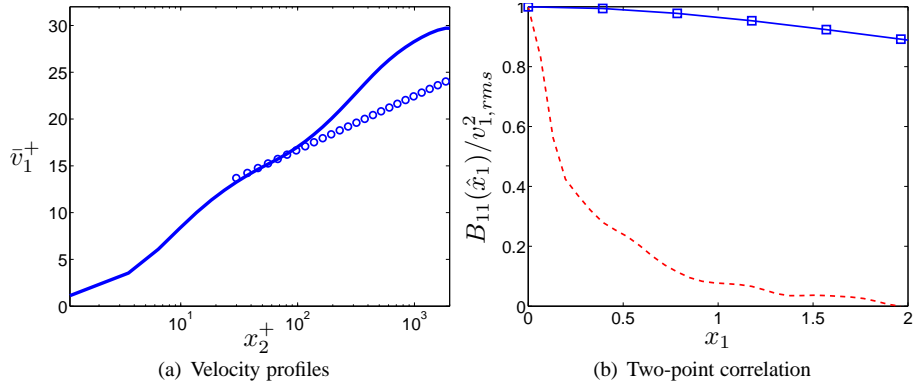


Figure 21.4: Comparison of standard hybrid LES-RANS in channel flow on a very coarse mesh ( $\Delta x_1^+ = 2\Delta x_3^+ = 785$ .  $\delta/\Delta x_1 \simeq 2.5$ ,  $\delta/\Delta x_3 \simeq 5$ .) [75]. — : hybrid LES-RANS;  $\circ$ :  $0.4 \ln(y^+) + 5.2$ . Markers in right figure indicate resolution.

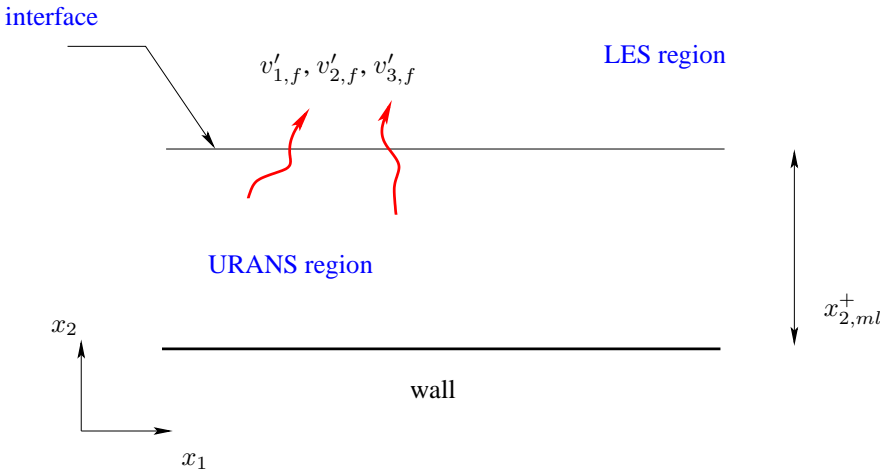


Figure 21.5: Using forcing at the interface between the LES and URANS region.

presumably dictated by the requirement of resolving the largest turbulent scales in the flow (which are related to the outer length scales, e.g. the boundary layer thickness) rather than the near-wall turbulent processes. The unsteady momentum equations are solved throughout the computational domain. The turbulent RANS viscosity is used in the URANS region, and the turbulent SGS viscosity is used in the LES region.

Much work on hybrid LES-RANS has been carried out. In [129, 72, 130] two-equation models were used in the URANS region and a one-equation SGS model was employed in the LES region. One-equation models were used in both regions in [131, 132]. The locations of the matching planes were determined in different ways. In some work [72, 130] it was chosen along a pre-selected grid plane. In [131] it was determined by comparing the URANS and the LES turbulent length scales or was computed from turbulence/physics requirements. In [129] they used a two-equation model in the URANS region and blended it into a one-equation model in the LES region. Different partial differential equations for automatically finding the matching plane were investigated in [132]. A one-equation model was used in both regions in [133], and the

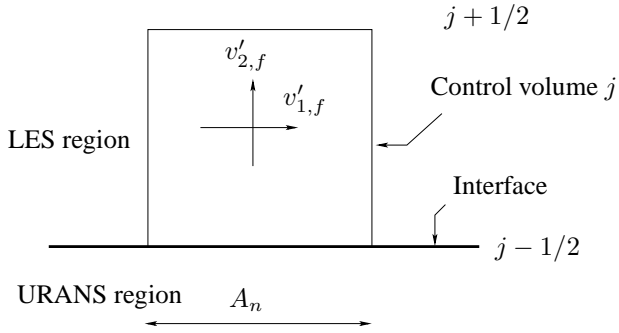


Figure 21.6: Added fluctuations,  $v'_{f,1}, v'_{f,2}, v'_{f,3}$ , in a control volume ( $j = j_{ml} + 1$ ) in the LES region adjacent to the interface. The fluctuations are either synthesized (subscript  $f = S$ ) or taken from channel DNS (subscript  $f = DNS$ ).

$c_\mu$  coefficient at the interface was computed dynamically to yield a smoother transition between the URANS and LES regions. In [134] they proposed a  $k - \varepsilon$  turbulence model, later also used by [135], in which the  $c_{\varepsilon 2}$  is made into a function of the ratio of the RANS and LES length scales. On a fine mesh the model switches smoothly to LES and in the limit  $c_{\varepsilon 1} = c_{\varepsilon 2}$  so that a pure DNS solution is obtained.

Hybrid LES-RANS is similar to DES (Detached Eddy Simulations) [113, 136, 128]. The main difference is that the original DES aims at covering the whole attached boundary layer with URANS, whereas hybrid LES-RANS aims at covering only the inner part of the boundary layer with URANS. In later work DES has been used as a wall model [137, 124], and, in this form, DES is similar hybrid LES-RANS.

Figure 21.4a presents comparison of LES and hybrid LES-RANS in channel flow at  $Re_\tau = 2000$  on a very coarse mesh. The momentum equations are solved in the entire domain and the turbulent viscosity is in both regions obtained from a one-equations  $k_{sgs}$  equation and an algebraic length scale (see Sections 21.1 and 21.2). The resolution in the wall-parallel plane is comparable to what can be afforded for boundary layer in real, industrial flows, at least in terms of viscous units ( $\Delta x_1^+$  and  $\Delta x_3^+$ ). The LES cannot resolve the flow at all. Hybrid LES-RANS gives much improved results, still not very good however. The normalized streamwise two-point correlation is shown in Fig. 21.4b. As can be seen, the streamwise lengthscale predicted with hybrid LES-RANS is extremely large. It should be mentioned that standard hybrid LES-RANS does – of course – give better results on finer grids [103], but these finer grids are rarely affordable in industrial flows.

Although the results obtained with hybrid LES-RANS are better than those obtained with LES, it has been found that the treatment of the interface between the URANS region and the LES region is crucial for the success of the method. The resolved turbulence supplied by the URANS region to the LES region has no reasonable turbulent characteristics and is not appropriate for triggering the LES equations to resolve turbulence. This results in too poorly resolved stresses in the interface region and thereby gives a ramp – also referred to as a shift – in the velocity profile approximately at the location of the matching plane [72, 137, 125, 130, 138, 131, 124]. The overly small resolved stresses in the LES region are translated into too small a wall shear stress. Several modifications have been proposed to remove this deficiency. In [138, 133], they suggested dampening the modelled stresses in the URANS region to

reduce the total (i.e. resolved plus modelled) shear stress in the URANS region and thereby reduce the jump in shear stress across the matching plane. Numerical smoothing was used at the interface in [131]. [130] proposed a modification of the discretized streamwise equation at the interface in order to avoid filtering out any resolved fluctuations at the interface. In [124] backscatter was introduced in the interface region with the object of generating resolved fluctuations.

One way to improve hybrid LES-RANS is to add fluctuations to the momentum equations at the interface [125, 75], see Figs. 21.5 and 21.6. The object is to trigger the equations to resolve turbulence. Adding fluctuations in order to trigger the equations to resolve turbulence is actually very similar to prescribing fluctuating turbulent inlet boundary conditions for DNS or LES (or hybrid LES-RANS). If no triggering inlet boundary conditions are prescribed in DNS or LES, the resolved turbulence near the inlet will be too small and a large streamwise distance is required before the equations trigger themselves into describing turbulent flow. This is also the case in hybrid LES-RANS: if no triggering (forcing) is applied at the interface between the LES region and the URANS region, the resolved turbulence in the LES region near the URANS region will be too small.

## 21.1 Momentum equations in hybrid LES-RANS

The incompressible Navier-Stokes equations with an added turbulent/SGS viscosity read

$$\frac{\partial \bar{v}_i}{\partial t} + \frac{\partial}{\partial x_j} (\bar{v}_i \bar{v}_j) = -\frac{1}{\rho} \frac{\partial \bar{p}}{\partial x_i} + \frac{\partial}{\partial x_j} \left[ (\nu + \nu_T) \frac{\partial \bar{v}_i}{\partial x_j} \right] \quad (21.1)$$

where  $\nu_T = \nu_t$  ( $\nu_t$  denotes the turbulent RANS viscosity) for  $x_2 \leq x_{2,ml}$  (see Fig. 21.3) and, for  $x_2 > x_{2,ml}$ ,  $\nu_T = \nu_{sgs}$ . The turbulent viscosity,  $\nu_T$ , is computed from an algebraic turbulent length scale (see Table 21.1) and  $k_T$ ; the latter is obtained by solving its transport equation, see Eq. 21.2.

## 21.2 The equation for turbulent kinetic energy in hybrid LES-RANS

A one-equation model is employed in both the URANS region and the LES region, which reads

$$\begin{aligned} \frac{\partial k_T}{\partial t} + \frac{\partial}{\partial x_j} (\bar{v}_j k_T) &= \frac{\partial}{\partial x_j} \left[ (\nu + \nu_T) \frac{\partial k_T}{\partial x_j} \right] + P_{k_T} - C_\varepsilon \frac{k_T^{3/2}}{\ell} \\ P_{k_T} &= -\tau_{ij} \bar{s}_{ij}, \quad \tau_{ij} = -2\nu_T \bar{s}_{ij} \end{aligned} \quad (21.2)$$

In the inner region ( $x_2 \leq x_{2,ml}$ )  $k_T$  corresponds to the RANS turbulent kinetic energy,  $k$ ; in the outer region ( $x_2 > x_{2,ml}$ ) it corresponds to the subgrid-scale kinetic turbulent energy ( $k_{sgs}$ ). No special treatment is used in the equations at the matching plane except that the form of the turbulent viscosity and the turbulent length scale are different in the two regions, see Table 21.1. At the walls,  $k_T = 0$ .

## 21.3 Results

Fully developed channel flow at  $Re_\tau = u_\tau \delta / \nu = 2000$  ( $\delta$  denotes the channel half width) is used as a test case to evaluate the effect of different forcing conditions. This flow may seem to be an easy test case, but it is not. In attempts to improve the performance of LES in wall-bounded flows, the Achilles' heel is the near-wall flow region.

	URANS region	LES region
$\ell$	$\kappa c_\mu^{-3/4} n [1 - \exp(-0.2 k^{1/2} n / \nu)]$	$\ell = \Delta$
$\nu_T$	$\kappa c_\mu^{1/4} k^{1/2} n [1 - \exp(-0.014 k^{1/2} n / \nu)]$	$0.07 k^{1/2} \ell$
$C_\varepsilon$	1.0	1.05

Table 21.1: Turbulent viscosity and turbulent length scales in the URANS and LES regions.  $n$  and  $\kappa$  denote the distance to the nearest wall and von Kármán constant ( $= 0.41$ ), respectively.  $\Delta = (\delta V)^{1/3}$

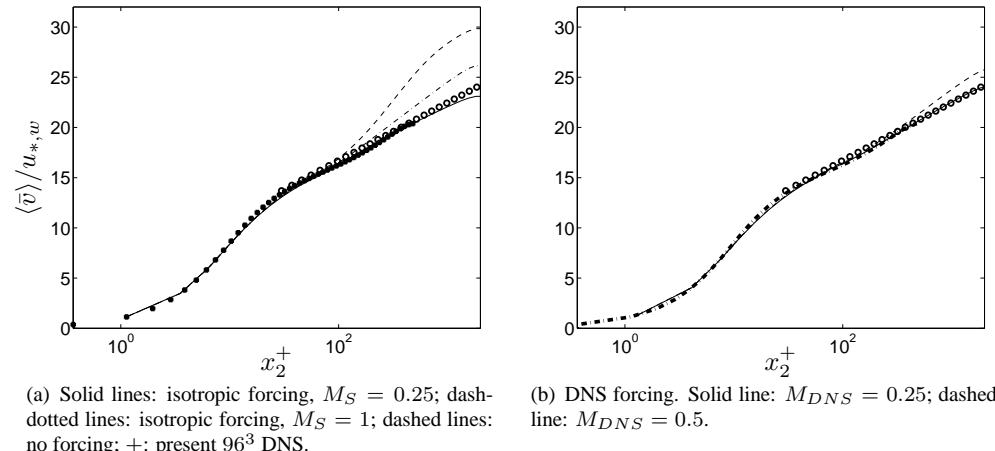


Figure 21.7: Streamwise velocities [75].  $\langle \bar{v} \rangle$  profiles.  $\circ: 2.5 \ln(x_2^+) + 5.2$ .

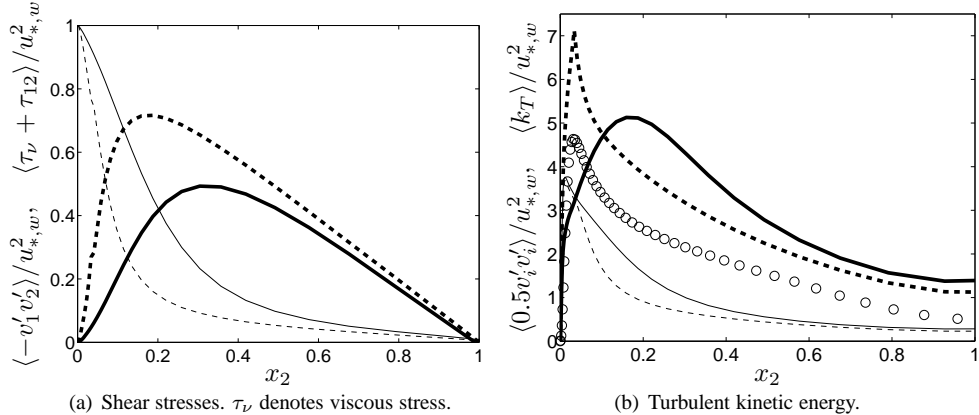


Figure 21.8: Shear stress and turbulent kinetic energy [75]. Solid lines: no forcing; dashed lines: forcing with isotropic fluctuations with  $M_S = 0.25$ ;  $\circ$ : present 96<sup>3</sup> DNS. Thick lines: resolved; thin lines: modelled.

The bulk velocity in fully developed channel flow with periodic boundary conditions (see Eq. 21.1) is entirely determined by the wall shear stress; consequently the flow is extremely sensitive to the turbulence in the near-wall region.

The streamwise velocity profiles obtained with and without forcing are compared in Fig. 21.7 with the present DNS and the log-law. It can be seen that the centerline velocity is strongly over-predicted when no forcing is used, whereas forcing with  $M_S = M_{DNS} = 0.25$  gives excellent agreement with the log-law ( $M_S$  and  $M_{DNS}$  denote forcing with synthetic and DNS fluctuations, respectively). The reason for the overly large velocities without forcing is that the resolved shear is too small. It can be seen in Fig. 21.8a that it is the resolved shear stress that increases when forcing is introduced, indicating that the resolved shear stress without forcing is too small. This was also observed by [124]: when forcing is introduced, the resolved shear stress increases, which reduces the bulk and centerline velocity.

Recently a novel way for generating fluctuations to be used as forcing at the interface was presented [103]. In this work backscatter obtained from a scale-similarity model was used.

## 22 The SAS model

### 22.1 Resolved motions in unsteady

When doing URANS or DES, the momentum equations are triggered through instabilities to go unsteady in regions where the grid is fine enough. In URANS or in DES operating in RANS mode, high turbulent viscosity often dampens out these instabilities. In many cases this is an undesired feature, because if the flow wants to go unsteady, it is usually a bad idea to force the equations to stay steady. One reason is that there may not be any steady solution. Hence, the equations will not converge. Another reason is that if the numerical solution wants to go unsteady, the large turbulent scales — i.e. part of the turbulent spectrum — will be resolved instead of being modelled. This leads to a more accurate prediction of the flow.

One way to improve a RANS model's ability to resolve large-scale motions is to use the SAS (Scale- Adaptive Simulation) model

### 22.2 The von Kármán length scale

The von Kármán length scale

$$L_{vK,1D} = \kappa \left| \frac{\partial \langle \bar{v} \rangle / \partial x_2}{\partial^2 \langle \bar{v} \rangle / \partial x_2^2} \right| \quad (22.1)$$

which includes the second velocity gradient is a suitable length scale for detecting unsteadiness. The von Kármán length scale is smaller for an instantaneous velocity profile than for a time averaged velocity, see Fig. 22.1. This is interesting because, as noted in [139], the von Kármán length scale decreases when the momentum equations resolve (part of) the turbulence spectrum.

The first and second derivatives in Eq. 22.1 are given in boundary layer form. We want to extend this expression to a general one, applicable in three dimensions. In the same way as in, for example, the Smagorinsky model, we take the first derivative as  $|\bar{s}| = (2\bar{s}_{ij}\bar{s}_{ij})^{1/2}$ . The second derivative can be generalized in a number of ways. In the SAS model it is taken as

$$U'' = \left( \frac{\partial^2 \bar{v}_i}{\partial x_j \partial x_j} \frac{\partial^2 \bar{v}_i}{\partial x_k \partial x_k} \right)^{0.5} \quad (22.2)$$

Hence, the general three-dimensional expression for the von Kármán length scale reads

$$L_{vK,3D} = \kappa \frac{|\bar{s}|}{|U''|} \quad (22.3)$$

In [140] they derived a one-equation  $\nu_t$  turbulence model where the von Kármán length scale was used. The model was called the SAS model. Later, based on the  $k - k^{1/2}L$  model of Rotta [141], Menter & Egorov [139] derived a new  $k - kL$  model using the von Kármán length scale. Finally, in [142] they modified the  $k - \omega$ -SST model to include the SAS features; they called this model the SST-SAS model. This model is described in more detail below.

### The SST-SAS model

The  $k - \omega$  SST model is given in Eq. 20.4 at p. 159 (see also the section starting at p. 126) Now, Menter & Egorov [142] introduced a SAS-term in the  $\omega$  equation. The

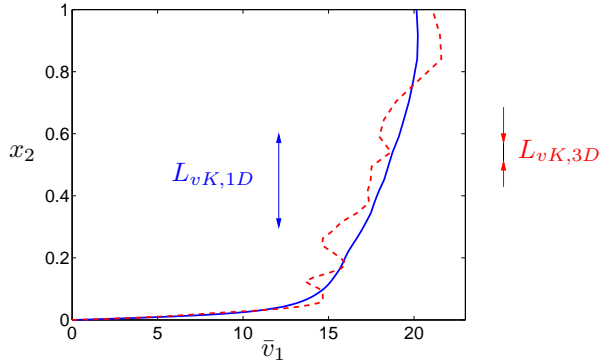


Figure 22.1: Velocity profiles from a DNS of channel flow. Solid line: time-averaged velocity with length scale  $L_{x,1D}$ , Eq. 22.1 ; dashed line: instantaneous velocity with length scale  $L_{vK,3D}$ , Eq. 22.3.

object of this term is to decrease the turbulent viscosity when unsteadiness is detected, i.e. when the von Kármán length scale becomes small. The production term in the  $\omega$  equation in the  $k-\omega$ -SST model reads  $P_\omega = \alpha P^k / \nu_t \propto |\bar{s}|^2$ . To decrease the turbulent viscosity we should increase  $\omega$ . Thus it seems reasonable to add a new production term proportional to  $P_\omega L_t / L_{vK,3D}$  where  $L_t$  denotes a RANS length scale. The additional term reads

$$\tilde{\zeta}_2 \kappa |\bar{s}|^2 \frac{L_t}{L_{vK,3D}}, \quad L_t = \frac{k^{1/2}}{\omega c_\mu^{1/4}} \quad (22.4)$$

When unsteadiness occurs — i.e. when the momentum equations attempt to resolve part of the turbulence spectrum — , this term reacts as follows:

- Local unsteadiness will create velocity gradients which decrease the turbulent length scale, see Fig. 22.1
- This results in a decrease in the von Kármán length scale,  $L_{vK,3D}$
- As a consequence the additional source, Eq. 22.4, in the  $\omega$  equation increases
- This gives an increase in  $\omega$  and hence a decrease in  $\nu_t$
- The decreased turbulent viscosity will allow the unsteadiness to stay alive and, perhaps, grow.

The last item in the list above is the main object of the SAS model. The reaction to local unsteadiness in an eddy-viscosity model without the SAS feature is as follows: the increased local velocity gradients will create additional production of turbulent kinetic energy and give an increased turbulent viscosity which will dampen/kill the local unsteadiness. As mentioned in the introduction to this chapter, this is an undesirable feature.

When incorporating the additional production term (Eq. 22.4) in the  $k - \omega$ -SST model, the last term in the  $\omega$  equation is replaced by (for further details, see [142])

$$\begin{aligned} P_{SAS} &= F_{SAS} \max(T_1 - T_2, 0) \\ T_1 &= \tilde{\zeta}_2 \kappa S^2 \frac{L}{L_{vK,3D}} \\ T_2 &= \frac{2k}{\sigma_\Phi} \max \left( \frac{1}{\omega^2} \frac{\partial \omega}{\partial x_j} \frac{\partial \omega}{\partial x_j}, \frac{1}{k^2} \frac{\partial k}{\partial x_j} \frac{\partial k}{\partial x_j} \right) \\ L &= \frac{k^{1/2}}{\omega c_\mu^{1/4}} \end{aligned} \quad (22.5)$$

Note that the term  $T_1$  is the “real” additional SAS term;  $T_2$  is included to make sure that the model in steady flow works as a  $k - \omega$  SST model.

## 22.3 The second derivative of the velocity

To compute  $U''$  in Eq. 22.2, we need to compute the second velocity gradients. In finite volume methods there are two main options for computing second derivatives.

Option I: compute the first derivatives at the faces

$$\left( \frac{\partial v}{\partial x_2} \right)_{j+1/2} = \frac{v_{j+1} - v_j}{\Delta x_2}, \quad \left( \frac{\partial v}{\partial x_2} \right)_{j-1/2} = \frac{v_j - v_{j-1}}{\Delta x_2}$$

and then

$$\Rightarrow \left( \frac{\partial^2 v}{\partial x_2^2} \right)_j = \frac{v_{j+1} - 2v_j + v_{j-1}}{(\Delta x_2)^2} + \frac{(\Delta x_2)^2}{12} \frac{\partial^4 v}{\partial x_2^4}$$

Option II: compute the first derivatives at the center

$$\left( \frac{\partial v}{\partial x_2} \right)_{j+1} = \frac{v_{j+2} - v_j}{2\Delta x_2}, \quad \left( \frac{\partial v}{\partial x_2} \right)_{j-1} = \frac{v_j - v_{j-2}}{2\Delta x_2}$$

and then

$$\Rightarrow \left( \frac{\partial^2 v}{\partial x_2^2} \right)_j = \frac{v_{j+2} - 2v_j + v_{j-2}}{4(\Delta x_2)^2} + \frac{(\Delta x_2)^2}{3} \frac{\partial^4 v}{\partial x_2^4}$$

In [143], Option I was used unless otherwise stated.

## 22.4 Evaluation of the von Kármán length scale in channel flow

In Fig. 22.2 the turbulent length scale,  $\langle L_{vK,3D} \rangle$ , is evaluated using DNS data of fully developed channel flow. When using DNS data only viscous dissipation of resolved turbulence affects the equations. This implies that the smallest scales that can be resolved are related to the grid scale. The von Kármán length scale based on instantaneous velocities,  $\langle L_{vK,3D} \rangle$ , is presented in Fig. 22.2. For  $x_2 > 0.2$ , its magnitude is close to  $\Delta x_2$  which confirms that the von Kármán length scale is related to the smallest resolvable scales. Closer to the wall,  $\langle L_{vK,3D} \rangle$  increases slightly whereas  $\Delta x_2$  continues to decrease.

The von Kármán length scale,  $L_{vK,1D}$ , based on the averaged velocity profile  $\langle \bar{v}_1 \rangle = \langle \bar{v}_1 \rangle(x_2)$  is also included in Fig. 22.2, and as can be seen it is much larger than  $\langle L_{vK,3D} \rangle$ . Near the wall  $L_{vK,1D}$  increases because the time-average second derivative,

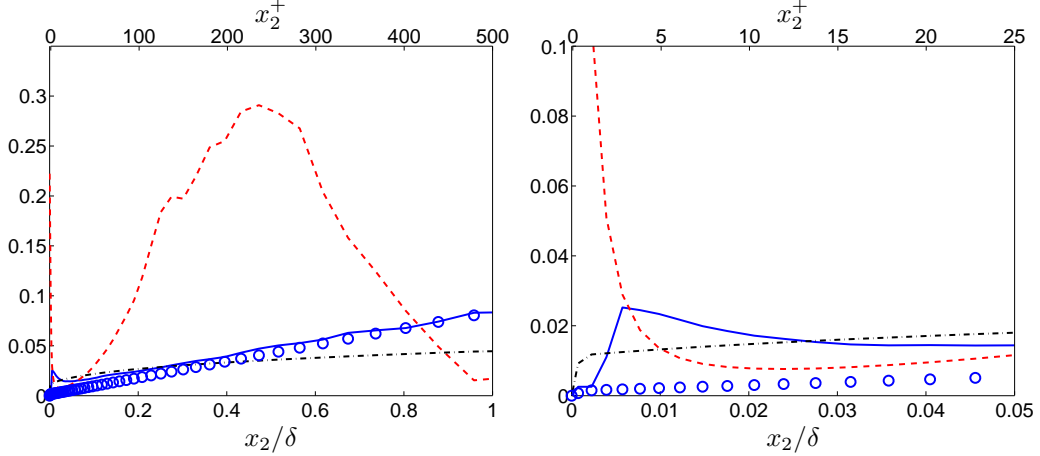


Figure 22.2: Turbulent length scales in fully developed channel flow. Left: global view; right: zoom. DNS.  $96^3$  mesh.  $Re_\tau = 500$ .  $\Delta x_1/\delta = 0.065$ ,  $\Delta x_3/\delta = 0.016$ ,  $x_2$ -stretching of 9%. —:  $\langle L_{vK,3D} \rangle$ ; - - -:  $L_{vK,1D}$ ; - - :  $(\Delta x_1 \Delta x_2 \Delta x_3)^{1/3}$ ; o:  $\Delta x_2$ .

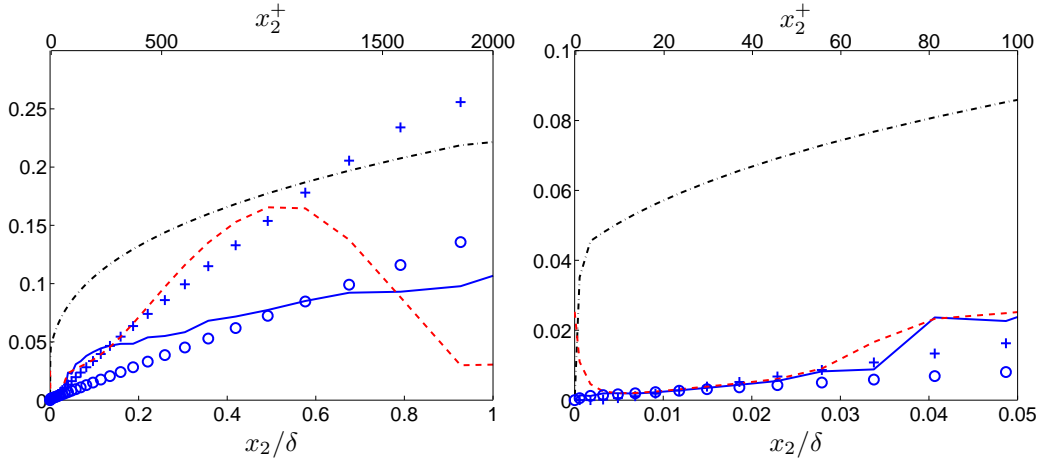


Figure 22.3: Turbulent length scales in fully developed channel flow. Hybrid LES-RANS. Left: global view; right: zoom.  $32 \times 64 \times 32$  mesh.  $Re_\tau = 2000$ .  $\Delta x_1/\delta = 0.39$ ,  $\Delta x_3/\delta = 0.19$ ,  $x_2$ -stretching of 17%. —:  $\langle L_{vK,3D} \rangle$ ; - - -:  $L_{vK,1D}$ ; - - :  $(\Delta x_1 \Delta x_2 \Delta x_3)^{1/3}$ ; o:  $\Delta x_2$ ; +:  $\ell_{k-\omega} = k^{0.5}/(c_\mu^{1/4} \omega)$ .

$\partial^2 \langle \bar{v}_1 \rangle / \partial x_2^2$ , goes to zero as the wall is approached. No such behavior is seen for the three-dimensional formulation,  $\langle L_{vK,3D} \rangle$ .

In Fig. 22.3, data from hybrid LES-RANS are used (taken from [75]). When using hybrid LES-RANS, part of the turbulence is resolved and part of the turbulence is modelled. The resolved turbulence is dissipated by a modelled dissipation,  $-2\langle \nu_T \bar{s}_{ij} \bar{s}_{ij} \rangle$  ( $\nu_T$  denotes SGS or RANS turbulent viscosity), and  $\nu_T \gg \nu$ . As a result, the length scale of the smallest resolved turbulence is larger in hybrid LES-RANS than in DNS. Close to the wall in the URANS region ( $x_2 < 0.031\delta$ ), the resolved turbulence is damped by the high turbulent viscosity, and as a result  $\langle L_{vK,3D} \rangle$  follows closely  $L_{vK,1D}$ .

The RANS turbulent length scale,  $\ell_{k-\omega}$ , from a 1D RANS simulation at  $Re_\tau =$

2000 with the  $k - \omega$  SST model is also included in Fig. 22.3. In the inner region ( $x_2 < 0.5\delta$ ), its behavior is close to that of the von Kármán length scale,  $L_{vK,1D}$ . In the center region the RANS turbulent length scale continues to increase which is physically correct. However, the von Kármán length scale,  $L_{vK,1D}$ , goes to zero because the velocity derivative goes to zero.

Two filter scales are included in Figs. 22.2 and 22.3. In the DNS-simulations,  $\Delta x_2 < (\Delta x_1 \Delta x_2 \Delta x_3)^{1/3}$  near the wall, whereas far from the wall  $\Delta x_2 > (\Delta x_1 \Delta x_2 \Delta x_3)^{1/3}$  because of the stretching in the  $x_2$  direction and because of small  $\Delta x_1$  and  $\Delta x_3$ . In the hybrid simulations, it can be noted that the three-dimensional filter width is more than twice as large as the three-dimensional formulation of the von Kármán length scale, i.e.  $(\Delta x_1 \Delta x_2 \Delta x_3)^{1/3} > 2\langle L_{vK,3D} \rangle$ .

In [143], the SST-SAS model has been evaluated in channel flow, flow in an asymmetric diffuser and flow over an axi-symmetric hill.

## 23 The PANS Model

The PANS method uses the so-called “partial averaging” concept, which corresponds to a filtering operation for a portion of the fluctuating scales [144].

For an instantaneous flow variable,  $F$ , we use  $\bar{f}$  to denote the partially-averaged part, namely  $\bar{f} = \mathcal{P}(F)$ , where  $\mathcal{P}$  denotes the partial-averaging operator. We consider incompressible flows. Applying the partial averaging to the governing equations gives

$$\frac{\partial \bar{v}_i}{\partial x_i} = 0 \quad (23.1)$$

$$\frac{\partial \bar{v}_i}{\partial t} + \frac{\partial(\bar{v}_i \bar{v}_j)}{\partial x_j} = -\frac{1}{\rho} \frac{\partial \bar{p}}{\partial x_i} + \frac{\partial}{\partial x_j} \left( \nu \frac{\partial \bar{v}_i}{\partial x_j} - \tau_{ij} \right) \quad (23.2)$$

where  $\tau_{ij}$  is the central second moment resulting from the partial averaging for the nonlinear terms, that is  $\tau_{ij} = (\mathcal{P}(v_i v_j) - \bar{v}_i \bar{v}_j)$ , where  $v_i$  indicates instantaneous velocity components. This term is similar to the Reynolds stress tensor resulting from the Reynolds averaging in RANS or to the subgrid-scale (SGS) stress tensor after the spatial filtering in LES. For simplicity, we also use the terminology of Reynolds stresses for the term  $\tau_{ij}$  in Eq. 23.2.

To close the system of the partially-averaged Navier-Stokes equations, as in RANS and LES, a model is needed for  $\tau_{ij}$ . In [144] they proposed using the conventional eddy viscosity concept so that  $\tau_{ij} = -2\nu_u \bar{s}_{ij}$ , where  $\bar{s}_{ij}$  is the strain-rate tensor of the computed flow and  $\nu_u$  is the PANS eddy viscosity.

In order to formulate the PANS eddy viscosity, they defined in [144] another two quantities, the partially-averaged turbulent kinetic energy,  $k_u$  and its dissipation rate  $\varepsilon_u$ , so that  $\nu_u = C_\mu k_u^2 / \varepsilon_u$ . In the derivation of the transport equations for  $k_u$  and  $\varepsilon_u$ , two parameters,  $f_k$  and  $f_\varepsilon$ , have been introduced, relating the unresolved to the resolved fluctuating scales. Parameter  $f_k$  defines the ratio of unresolved (partially-averaged) turbulent kinetic energy ( $k_u$ ) to the total kinetic energy ( $k$ ), and  $f_\varepsilon$  is the ratio between the unresolved ( $\varepsilon_u$ ) and the total ( $\varepsilon$ ) dissipation rates. These give

$$k = \frac{k_u}{f_k} \text{ and } \varepsilon = \frac{\varepsilon_u}{f_\varepsilon} \quad (23.3)$$

The extent of the resolved part is now determined by  $f_k$  and  $f_\varepsilon$ . In [145, 144] they employed the standard  $k - \varepsilon$  model as the base model.

The  $k_u$  equation is derived by multiplying the RANS  $k$  equation (Eq. 11.93) in the  $k - \varepsilon$  model by  $f_k$ , i.e. (for simplicity we omit the buoyancy term)

$$f_k \left\{ \frac{\partial k}{\partial t} + \bar{V}_j \frac{\partial k}{\partial x_j} \right\} = f_k \left\{ P^k - \varepsilon + \frac{\partial}{\partial x_j} \left[ \left( \nu + \frac{\nu_t}{\sigma_k} \right) \frac{\partial k}{\partial x_j} \right] \right\} \quad (23.4)$$

where  $V_i$  denotes the RANS velocity. The left side can be re-written

$$f_k \left\{ \frac{\partial k}{\partial t} + \bar{V}_j \frac{\partial k}{\partial x_j} \right\} = \frac{\partial k_u}{\partial t} + \bar{V}_j \frac{\partial k_u}{\partial x_j} = \frac{\partial k_u}{\partial t} + \bar{v}_j \frac{\partial k_u}{\partial x_j} + (\bar{V}_j - \bar{v}_j) \frac{\partial k_u}{\partial x_j} \quad (23.5)$$

The convective term must be expressed in  $\bar{v}_j$  (the PANS averaged velocity) rather than in  $\bar{V}_j$  (the RANS averaged velocity), because it is  $\bar{v}_j$  that transports  $k_u$  because  $\bar{v}_j$  represents the PANS resolved part of  $v_j$ . The last term on the right side in Eq. 23.5 is usually neglected.

The diffusion term is re-written using Eq. 23.3

$$\begin{aligned} f_k \left\{ \frac{\partial}{\partial x_j} \left[ \left( \nu + \frac{\nu_t}{\sigma_k} \right) \frac{\partial k}{\partial x_j} \right] \right\} &= \frac{\partial}{\partial x_j} \left[ \left( \nu + \frac{\nu_t}{\sigma_k} \right) \frac{\partial k_u}{\partial x_j} \right] \\ &= \frac{\partial}{\partial x_j} \left[ \left( \nu + \frac{\nu_u}{\sigma_{ku}} \right) \frac{\partial k_u}{\partial x_j} \right] \end{aligned} \quad (23.6)$$

where

$$\sigma_{ku} = \sigma_k \frac{f_k^2}{f_\varepsilon} \quad (23.7)$$

The sum of the source terms in Eq. 23.4 must be equal to the sum of the source terms of the  $k_u$  equation, i.e.

$$f_k (P^k - \varepsilon) = P_u - \varepsilon_u \quad (23.8)$$

This relation implies

$$P^k = \frac{1}{f_k} (P_u - \varepsilon_u) + \frac{\varepsilon_u}{f_\varepsilon} \quad (23.9)$$

Using Eqs. 23.5, 23.6 and 23.8 the final transport equation for  $k_u$  can now be written as

$$\frac{\partial k_u}{\partial t} + \frac{\partial(k_u \bar{v}_j)}{\partial x_j} = \frac{\partial}{\partial x_j} \left[ \left( \nu + \frac{\nu_u}{\sigma_{ku}} \right) \frac{\partial k_u}{\partial x_j} \right] + P_u - \varepsilon_u \quad (23.10)$$

where the production term,  $P_u$ , is expressed in terms of the PANS eddy viscosity,  $\nu_u$ , and the strain rate of PANS-resolved flow field, i.e.

$$P_u = \nu_u \left( \frac{\partial \bar{v}_i}{\partial x_j} + \frac{\partial \bar{v}_j}{\partial x_i} \right) \frac{\partial \bar{v}_i}{\partial x_j} \quad (23.11)$$

where

$$\nu_u = c_\mu \frac{k_u^2}{\varepsilon} \quad (23.12)$$

The  $\varepsilon_u$  equation is derived by multiplying the RANS  $\varepsilon$  equation by  $f_\varepsilon$ , i.e.

$$\begin{aligned} \frac{\partial \varepsilon_u}{\partial t} + \frac{\partial(\varepsilon_u \bar{v}_j)}{\partial x_j} &= f_\varepsilon \left[ \frac{\partial \varepsilon}{\partial t} + \frac{\partial(\varepsilon \bar{V}_j)}{\partial x_j} \right] \\ &= f_\varepsilon \left\{ \frac{\partial}{\partial x_j} \left[ \left( \nu + \frac{\nu_t}{\sigma_\varepsilon} \right) \frac{\partial \varepsilon}{\partial x_j} \right] + C_{\varepsilon 1} P_k \frac{\varepsilon}{k} - C_{\varepsilon 2} \frac{\varepsilon^2}{k} \right\} \end{aligned} \quad (23.13)$$

The diffusion term is re-written using Eq. 23.3

$$\begin{aligned} f_\varepsilon \left\{ \frac{\partial}{\partial x_j} \left[ \left( \nu + \frac{\nu_t}{\sigma_\varepsilon} \right) \frac{\partial \varepsilon}{\partial x_j} \right] \right\} &= \frac{\partial}{\partial x_j} \left[ \left( \nu + \frac{\nu_t}{\sigma_\varepsilon} \right) \frac{\partial \varepsilon_u}{\partial x_j} \right] \\ &= \frac{\partial}{\partial x_j} \left[ \left( \nu + \frac{\nu_u}{\sigma_{\varepsilon u}} \right) \frac{\partial \varepsilon_u}{\partial x_j} \right] \end{aligned} \quad (23.14)$$

where

$$\sigma_{\varepsilon ku} = \sigma_\varepsilon k \frac{f_k^2}{f_\varepsilon} \quad (23.15)$$

In the same way, the production and destruction terms are re-formulated as (using Eqs. 23.3 and 23.9)

$$\begin{aligned} f_\varepsilon \left\{ C_{\varepsilon 1} P_k \frac{\varepsilon}{k} - C_{\varepsilon 2} \frac{\varepsilon^2}{k} \right\} &= C_{\varepsilon 1} \frac{\varepsilon_u f_k}{k_u} \left( \frac{1}{f_k} (P_u - \varepsilon_u) + \frac{\varepsilon_u}{f_\varepsilon} \right) - C_{\varepsilon 2} \frac{\varepsilon_u^2 f_k}{f_\varepsilon k_u} \\ &= C_{\varepsilon 1} \frac{\varepsilon_u}{k_u} P_u - C_{\varepsilon 1} \frac{\varepsilon_u^2}{k_u} + C_{\varepsilon 1} \frac{\varepsilon_u^2 f_k}{k_u f_\varepsilon} - C_{\varepsilon 2} \frac{\varepsilon_u^2 f_k}{f_\varepsilon k_u} \\ &= C_{\varepsilon 1} \frac{\varepsilon_u}{k_u} P_u - C_{\varepsilon 2}^* \frac{\varepsilon_u^2}{k_u} \end{aligned} \quad (23.16)$$

where

$$C_{\varepsilon 2}^* = C_{\varepsilon 1} + \frac{f_k}{f_\varepsilon} (C_{\varepsilon 2} - C_{\varepsilon 1}) \quad (23.17)$$

The  $\varepsilon_u$  equation in the PANS model now takes the following form

$$\frac{\partial \varepsilon_u}{\partial t} + \frac{\partial (\varepsilon_u \bar{v}_j)}{\partial x_j} = \frac{\partial}{\partial x_j} \left[ \left( \nu + \frac{\nu_u}{\sigma_{\varepsilon u}} \right) \frac{\partial \varepsilon_u}{\partial x_j} \right] + C_{\varepsilon 1} P_u \frac{\varepsilon_u}{k_u} - C_{\varepsilon 2}^* \frac{\varepsilon_u^2}{k_u} \quad (23.18)$$

As in the  $k_u$  equation, the additional term  $(\bar{V}_j - \bar{v}_j) \partial \varepsilon_u / \partial x_j$  has been neglected.

The PANS equation for  $k_u$ , Eq. 23.10, was derived by multiplying the RANS equation for  $k$  by  $f_k$  which was assumed to be constant in space and in time. By referring to Eqs. 23.6, 23.12 and 23.7, the turbulent diffusion term was obtained as

$$f_k \frac{\partial}{\partial x_j} \left( \frac{\nu_t}{\sigma_k} \frac{\partial k}{\partial x_j} \right) = \frac{\partial}{\partial x_j} \left( \frac{\nu_t}{\sigma_k} \frac{\partial k_u}{\partial x_j} \right) \quad (23.19a)$$

$$= \frac{\partial}{\partial x_j} \left( \frac{\nu_u}{\sigma_{ku}} \frac{\partial k_u}{\partial x_j} \right) \quad (23.19b)$$

The expression on the right-hand side of Eq. 23.19(a) suggests that the turbulent transport for the PANS-modelled turbulent kinetic energy,  $k_u$ , is actually formulated in terms of the RANS turbulent viscosity from the base model. This is different from the turbulent diffusion in subgrid scale (SGS) modelling of LES with a one-equation  $k_{sgs}$  model, which reads

$$\frac{\partial}{\partial x_j} \left( \frac{\nu_{sgs}}{\sigma_k} \frac{\partial k_{sgs}}{\partial x_j} \right) \quad (23.20)$$

In Eq. 23.20 the SGS turbulent viscosity is invoked for the transport of  $k_{sgs}$ , whereas on the right-hand side of Eq. 23.19(a) the total (i.e. the RANS) turbulent viscosity has been used for  $k_u$ . Equation 23.19(a) suggests that, when used as an SGS model, the modelled turbulent diffusion in the PANS formulation is a factor of  $\sigma_k / \sigma_{ku} = f_\varepsilon / f_k^2$  larger than in Eq. 23.20, see Eqs. 23.10 and 23.19(b). With  $f_\varepsilon = 1$  and  $f_k = 0.4$ , for example, this factor is larger than six. The modification of the diffusion coefficient,  $\sigma_{ku}$ , is a unique property of the PANS model. In other models, such as DES [146], X-LES [117] and PITM [121], the sink term in the  $k$ ,  $\varepsilon$  or  $\omega$  equation is modified, but not the diffusion term. The only difference between PANS and PITM is that in the former model the diffusion coefficients in the  $k$  and  $\varepsilon$  are modified.

A Low Reynolds number PANS model was presented in [147]. A recently developed LRN PANS model is employed, for improved modelling of near-wall turbulence,

which reads [120]

$$\begin{aligned}
 \frac{\partial k_u}{\partial t} + \frac{\partial(k_u \bar{v}_j)}{\partial x_j} &= \frac{\partial}{\partial x_j} \left[ \left( \nu + \frac{\nu_u}{\sigma_{ku}} \right) \frac{\partial k_u}{\partial x_j} \right] + (P_u - \varepsilon_u) \\
 \frac{\partial \varepsilon_u}{\partial t} + \frac{\partial(\varepsilon_u \bar{v}_j)}{\partial x_j} &= \frac{\partial}{\partial x_j} \left[ \left( \nu + \frac{\nu_u}{\sigma_{\varepsilon u}} \right) \frac{\partial \varepsilon_u}{\partial x_j} \right] + C_{\varepsilon 1} P_u \frac{\varepsilon_u}{k_u} - C_{\varepsilon 2}^* \frac{\varepsilon_u^2}{k_u} \\
 \nu_u &= C_\mu f_\mu \frac{k_u^2}{\varepsilon_u}, C_{\varepsilon 2}^* = C_{\varepsilon 1} + \boxed{\frac{f_k}{f_\varepsilon}} (C_{\varepsilon 2} f_2 - C_{\varepsilon 1}) \\
 \sigma_{ku} &\equiv \sigma_k \boxed{\frac{f_k^2}{f_\varepsilon}}, \sigma_{\varepsilon u} \equiv \sigma_\varepsilon \boxed{\frac{f_k^2}{f_\varepsilon}}
 \end{aligned} \tag{23.21}$$

The modification introduced by the PANS modelling as compared to its parent RANS model is highlighted by boxes. The model constants take the same values as in the LRN model [122], i.e.

$$C_{\varepsilon 1} = 1.5, C_{\varepsilon 2} = 1.9, \sigma_k = 1.4, \sigma_\varepsilon = 1.4, C_\mu = 0.09 \tag{23.22}$$

## 24 Hybrid LES/RANS for Dummies

### 24.1 Introduction

Fluid flow problems are governed by the Navier-Stokes equations

$$\frac{\partial v_i}{\partial t} + \frac{\partial v_i v_j}{\partial x_j} = -\frac{1}{\rho} \frac{\partial p}{\partial x_i} + \nu \frac{\partial^2 v_i}{\partial x_j \partial x_j} \quad (24.1)$$

where  $v_i$  denotes the velocity vector,  $p$  is the pressure and  $\nu$  and  $\rho$  are the viscosity and density of the fluid, respectively. In turbulent flow, the velocity and pressure are unsteady and  $v_i$  and  $p$  include all turbulent motions, often called eddies. The spatial scale of these eddies vary widely in magnitude where the largest eddies are proportional to the size of the largest physical length (for example the boundary layer thickness,  $\delta$ , in case of a boundary layer). The smallest scales are related to the eddies where dissipation takes place, i.e. where the kinetic energy of the eddies is transformed into internal energy causing increased temperature. The ratio of the largest to the smallest eddies increases with Reynolds number,  $Re = |v_i| \delta / \nu$ . This has the unfortunate consequence – unless one is a fan of huge computer centers – that it is computationally extremely expensive to solve the Navier-Stokes equations for large Reynolds numbers.

#### 24.1.1 Reynolds-Averaging Navier-Stokes equations: RANS

In order to be able to solve the Navier-Stokes equations with a reasonable computational cost, the velocity vector and the pressure are split into a time-averaged part ( $V_i$  and  $P$ ) and a fluctuating part ( $v'_i$  and  $p'$ ), i.e.  $V_i = v_i + v'_i$ ,  $p = P + p'$ . The resulting equation is called the RANS (Reynolds-Averaging Navier-Stokes) equations

$$\frac{\partial V_i V_j}{\partial x_j} = -\frac{1}{\rho} \frac{\partial P}{\partial x_i} + \nu \frac{\partial^2 V_i}{\partial x_j \partial x_j} - \frac{\partial \bar{v}'_i \bar{v}'_j}{\partial x_j} = -\frac{1}{\rho} \frac{\partial P}{\partial x_i} + \frac{\partial}{\partial x_j} \left( (\nu + \nu_t) \frac{\partial V_i}{\partial x_j} \right) \quad (24.2)$$

The term in front of the second equal sign is called the Reynolds stress and it is unknown and must be modelled. All turbulent fluctuation are modelled with a turbulence model and the results when solving Eq. 24.2 are highly dependent on the accuracy of the turbulence model. On the right side of Eq. 24.2 the unknown Reynolds stresses are expressed by a turbulence model in which a new unknown variable is introduced which is called the turbulent viscosity,  $\nu_t$ . The ratio of  $\nu_t$  to  $\nu$  may be of the order of 1000 or larger. In industry today, CFD (Computationally Fluid Dynamics) based on finite volume methods is used extensively to solve the RANS equations, Eq. 24.2.

#### 24.1.2 Large Eddy Simulations: LES

A method more accurate than RANS is LES (Large Eddy Simulations) in which only the small eddies (fluctuations whose eddies are smaller than the computational cell) are modelled with a turbulence model. The LES equations read

$$\frac{\partial \bar{v}_i}{\partial t} + \frac{\partial \bar{v}_i \bar{v}_j}{\partial x_j} = -\frac{1}{\rho} \frac{\partial \bar{p}}{\partial x_i} + \nu \frac{\partial^2 \bar{v}_i}{\partial x_j \partial x_j} - \frac{\partial \tau_{ij}}{\partial x_j} = -\frac{1}{\rho} \frac{\partial \bar{p}}{\partial x_i} + \frac{\partial}{\partial x_j} \left( (\nu + \nu_{sgs}) \frac{\partial \bar{v}_i}{\partial x_j} \right) \quad (24.3)$$

Note that the time dependence term (the first term on the left side) has been retained, because the large, time dependent turbulent (i.e. the resolved) fluctuations are part of  $\bar{v}_i$  and  $\bar{p}$  and are not modelled with the turbulence model. The term in front of

the second equal sign includes the Reynolds stresses of the small eddies, which are called SGS (sub-grid stresses). This term must also – as in Eq. 24.2 – be modelled, and at the right side it has been modelled with a SGS turbulent viscosity,  $\nu_{sgs}$ . The difference of  $\nu_{sgs}$  compared to  $\nu_t$  in Eq. 24.2 is that it includes only the effect of the *small* eddies. The ratio of  $\nu_{sgs}$  to  $\nu$  is of the order of 1 to 100. However, the ratio of the resolved to the modelled turbulence,  $|\bar{v}'_i \bar{v}'_j| / |\tau_{ij}|$  (see Eqs. 24.2 and 24.3) is much smaller than one. Hence, LES is much more accurate than RANS because only a small part of the turbulence is modelled with the turbulence SGS model whereas in RANS all turbulence is modelled. The disadvantage of LES is that it is *much* more expensive than RANS because a finer mesh must be used and because the equations are solved in four dimensions (time and three spatial directions) whereas RANS can be solved in steady state (no time dependence).

When the flow near walls is of importance, it turns out that LES is prohibitively expensive because very fine cells must be used there. The reason is entirely due to physics: near the walls, the spatial scales of the “large” turbulent eddies which should be resolved by LES are in reality rather small. Furthermore, their spatial scales get smaller for increasing Reynolds number. Much research has the last ten years been carried out to circumvent this problem. All proposed methods combines RANS and LES where RANS is used near walls and LES is used some distance away from the walls, see Fig. 24.1. These methods are called Detached Eddy Simulation (DES), hybrid LES/RANS or zonal LES/RANS. The focus of this report is zonal LES/RANS.

#### 24.1.3 Zonal LES/RANS

Equations 24.2 and 24.3 can be written in a same form as

$$\frac{\partial \bar{v}_i}{\partial t} + \frac{\partial \bar{v}_i \bar{v}_j}{\partial x_j} = -\frac{1}{\rho} \frac{\partial \bar{p}}{\partial x_i} + \frac{\partial}{\partial x_j} \left( (\nu + \nu_T) \frac{\partial \bar{v}_i}{\partial x_j} \right) \quad (24.4)$$

Near the walls, a RANS turbulence model is used for the turbulent viscosity, i.e.  $\nu_T = \nu_t$  and away from the walls an LES turbulence model is employed, i.e.  $\nu_T = \nu_{sgs}$ . Note that the time dependence term is now retained also in the RANS region: near the wall we are using an *unsteady* RANS, i.e. URANS.

Above, we have describe how to use the zonal LES/RANS method for flows near walls. Another form of zonal LES/RANS is *embedded* LES, in which an LES mode is embedded in a RANS region. One example is prediction of aeroacoustic noise created by the turbulence around an external mirror on a vehicle [91]. The flow around the vehicle can be computed with RANS, but in order to predict the noise in the region of the external mirror we must predict the large turbulence fluctuations and hence LES must be used in this region. In Section 24.4 we will present simulations using embedded LES in a simplified configuration represented by the flow in a channel in which RANS is used upstream of the interface and LES is used downstream of it, see Fig. 24.4.

## 24.2 The PANS $k - \varepsilon$ turbulence model

In the present work, the PANS  $k - \varepsilon$  model is used to simulate wall-bounded flow at high Reynolds number as well as embedded LES. The turbulence model reads [119, 120], see Eq. 23.21 (here in a slightly simplified form to enhance readability)

$$\frac{\partial k}{\partial t} + \frac{\partial k \bar{v}_j}{\partial x_j} = \frac{\partial}{\partial x_j} \left[ \left( \nu + \frac{\nu_T}{\sigma_k} \right) \frac{\partial k}{\partial x_j} \right] + P_k - \varepsilon \quad (24.5)$$

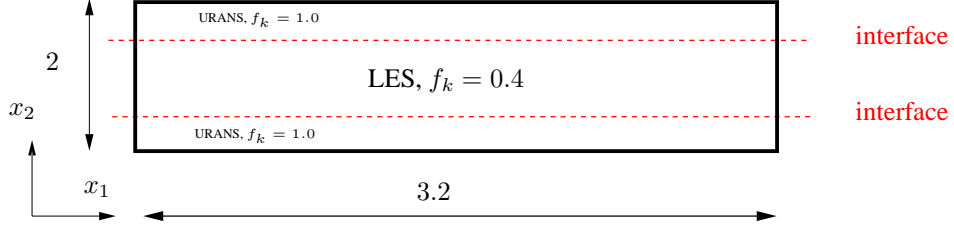


Figure 24.1: The LES and URANS regions. Fully developed channel flow. Periodic boundary conditions are applied at the left and right boundaries.

$$\frac{\partial \varepsilon}{\partial t} + \frac{\partial \varepsilon \bar{v}_j}{\partial x_j} = \frac{\partial}{\partial x_j} \left[ \left( \nu + \frac{\nu_T}{\sigma_\varepsilon} \right) \frac{\partial \varepsilon}{\partial x_j} \right] + C_{\varepsilon 1} P_k \frac{\varepsilon}{k} - \textcolor{red}{C}_{\varepsilon 2}^* \frac{\varepsilon^2}{k} \quad (24.6)$$

$$C_{\varepsilon 2}^* = C_{\varepsilon 1} + \textcolor{red}{f}_k (C_{\varepsilon 2} - C_{\varepsilon 1}), \quad C_{\varepsilon 1} = 1.5, \quad C_{\varepsilon 2} = 1.9 \quad (24.7)$$

$$\nu_T = C_\mu \frac{k^2}{\varepsilon}, \quad C_\mu = 0.09 \quad (24.8)$$

Note that  $k$  and  $\varepsilon$  are always positive. The key elements in the present use of the PANS  $k - \varepsilon$  model are highlighted in red. When  $f_k$  in Eq. 24.7 is equal to one, the model acts as a standard  $k - \varepsilon$  RANS model giving a large turbulent viscosity. When  $f_k$  is decreased (to 0.4 in the present study),  $C_{\varepsilon 2}^*$  in Eq. 24.7 decreases. As a result

- $\varepsilon$  increases because the destruction term (last term in Eq. 24.6 which is the main sink term) in the  $\varepsilon$  equation decreases,
- $k$  decreases because  $\varepsilon$  (last term in Eq. 24.5) is the main sink term in the  $k$  equation increases, and
- $\nu_T$  in Eq. 24.8 decreases because  $k$  decreases and  $\varepsilon$  increase.

Hence, the turbulence model in Eqs. 24.5–24.8 acts as a RANS turbulence model (large turbulent viscosity) when  $f_k = 1$  and it acts as an LES SGS turbulence model (small turbulent viscosity) when  $f_k = 0.4$ .

## 24.3 Zonal LES/RANS: wall modeling

### 24.3.1 The interface conditions

The interface plane (see Fig. 24.1) separates the URANS regions near the walls and the LES region in the core region. In the LES region  $f_k = 0.4$  and in the URANS region  $f_k = 1$ . In the former region, the turbulent viscosity  $\nu_T$  should be an SGS viscosity and in the latter region it should be an RANS viscosity. Hence  $\nu_T$  must decrease rapidly when going from the URANS region to the LES region. This is achieved by setting the usual convection and diffusion fluxes of  $k$  at the interface to zero. New fluxes are introduced using smaller SGS values [148].

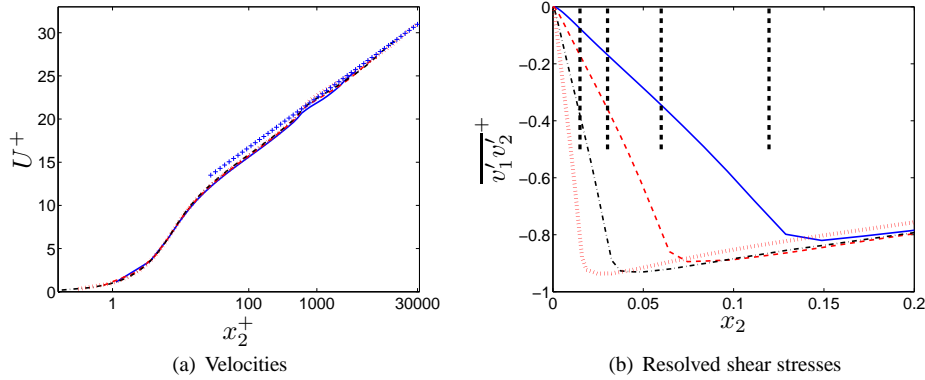


Figure 24.2: Velocities and resolved shear stresses.  $(N_x \times N_z) = (64 \times 64)$  — :  $Re_\tau = 4000$ ; - - :  $Re_\tau = 8000$ ; - · - :  $Re_\tau = 16000$ ; // :  $Re_\tau = 32000$ .

### 24.3.2 Results

Fully developed channel flow is computed for Reynolds numbers  $Re_\tau = u_\tau \delta / \nu = 4000, 8000, 16000$  and  $32000$ . The baseline mesh has  $64 \times 64$  cells in the streamwise ( $x_1$ ) and spanwise ( $x_3$ ) directions, respectively. The size of the domain is  $x_{1,max} = 3.2$ ,  $x_{2,max} = 2$  and  $x_{3,max} = 1.6$  ( $\delta = u_\tau = 1$ ). The grid in the  $x_2$  direction varies between 80 and 128 cells depending on Reynolds number. The interface is set to  $x_2^+ \simeq 500$  for all grids.

The velocity profiles and the resolved shear stresses are presented in Fig. 24.2. As can be seen, the predicted velocity profiles are in good agreement with the log-law which represents experiments. Figure 24.2b presents the resolved shear stresses. The interface is shown by thick dashed lines and it moves towards the wall for increasing Reynolds number since it is located at  $x_2^+ \simeq 500$  for all Reynolds numbers.

The turbulent viscosity profiles are shown in Fig. 24.3 for three different resolutions in the  $x_1 - x_3$  plane. It is interesting to note that the turbulent viscosity is not affected by the grid resolution. Hence, the model yields *grid independent* results contrary to other LES/RANS models.

The turbulent viscosity (Fig. 24.3) is sharply reduced when going across the interface from the URANS region to the LES region and the resolved fluctuations (the Reynolds shear stress in Fig. 24.2b) increase. This shows that the model is switching from RANS mode to LES mode as it should. More detailed results can be found in [148].

## 24.4 Zonal LES/RANS: embedded LES

### 24.4.1 The interface conditions

The interface plane is now vertical, see Fig. 24.4. The interface conditions for  $k$  and  $\varepsilon$  are treated in the same way as in Section 24.3.1. The difference is now that “inlet” turbulent fluctuations must be added to the LES  $\bar{v}_i$  equations (Eq. 24.3) to trigger the flow into turbulence-resolving mode. Anisotropic synthetic turbulent fluctuations are used [149, 150].

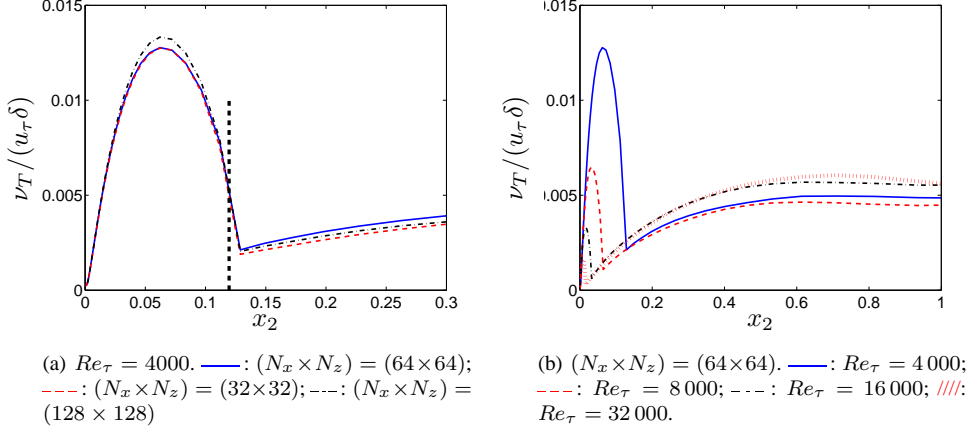


Figure 24.3: Turbulent viscosity.

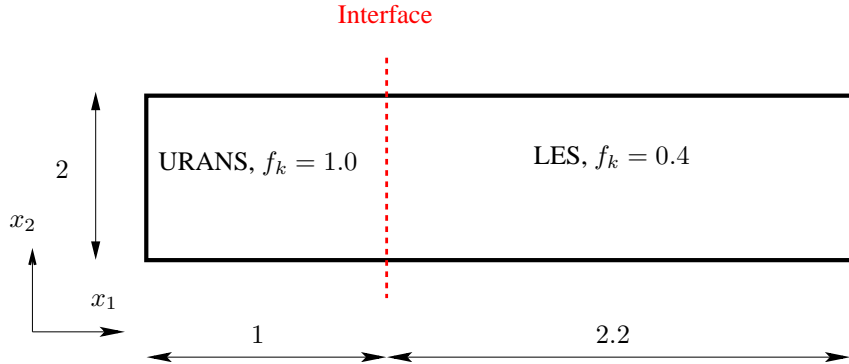
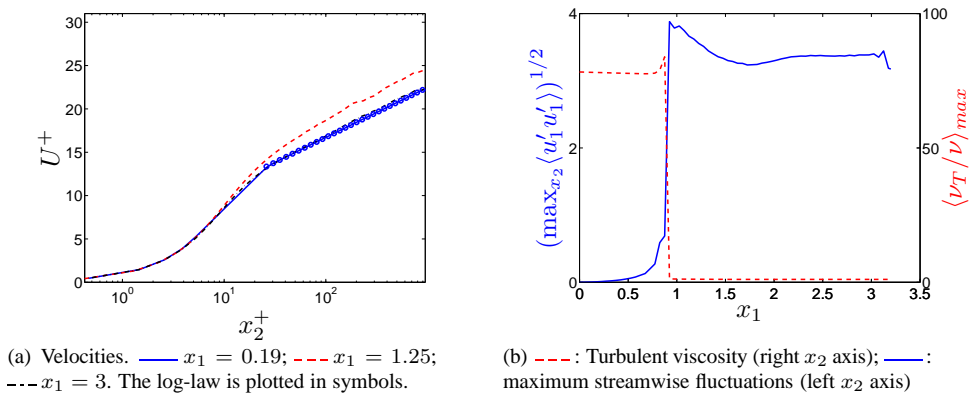


Figure 24.4: The LES and URANS regions. The left boundary is an inlet and the right boundary is an outlet.

Figure 24.5: Channel flow with inlet and outlet. (a) Velocities; (b) maximum resolved streamwise turbulent fluctuations and turbulent viscosity versus  $x_1$ .

#### 24.4.2 Results

The Reynolds number for the channel flow is  $Re_\tau = 950$ . With a  $3.2 \times 2 \times 1.6$  domain, a mesh with  $64 \times 80 \times 64$  cells is used in, respectively, the streamwise ( $x_1$ ), the wall-normal ( $x_2$ ) and the spanwise ( $x_3$ ) direction, see Fig. 24.4. Inlet conditions at  $x = 0$  are created by computing fully developed channel flow with the PANS  $k - \varepsilon$  model in RANS mode (i.e. with  $f_k = 1$ ).

Figure 24.5a presents the mean velocity and the resolved shear stresses at three streamwise locations,  $x_1 = 0.19, 1.25$  and  $3$  (recall that the interface is located at  $x_1 = 1$ ). At  $x_1 = 3$ , the predicted velocity agrees very well with the experimental log-law profile.

The resolved streamwise velocity fluctuations are zero in the RANS region, as they should (Fig. 24.5b), and the maximum resolved values increase sharply over the interface thanks to the imposed synthetic turbulent “inlet” fluctuations. The turbulent viscosity is reduced at the interface from its peak RANS value of approximately 80 to a small LES value of approximately one (these values are both fairly low because of the low Reynolds number). Hence, it is seen that the present model successfully switches from RANS to LES across the interface. The results will be presented in more detail in [148].

## 25 Inlet boundary conditions

In RANS it is sufficient to supply profiles of the mean quantities such as velocity and temperature plus the turbulent quantities (e.g.  $k$  and  $\varepsilon$ ). However, in unsteady simulations (LES, URANS, DES ...) the time history of the velocity and temperature need to be prescribed; the time history corresponds to turbulent, resolved fluctuations. In some flows it is critical to prescribe reasonable turbulent fluctuations, but in many flows it seems to be sufficient to prescribe constant (in time) profiles [105, 151].

There are different ways to create turbulent inlet boundary conditions. One way is to use a pre-cursor DNS or well resolved LES of channel flow. This method is limited to fairly low Reynolds numbers and it is difficult (or impossible) to re-scale the DNS fluctuations to higher Reynolds numbers.

Another method based partly on synthesized fluctuations is the vortex method [152]. It is based on a superposition of coherent eddies where each eddy is described by a shape function that is localized in space. The eddies are generated randomly in the inflow plane and then convected through it. The method is able to reproduce first and second-order statistics as well as two-point correlations.

A third method is to take resolved fluctuations at a plane downstream of the inlet plane, re-scale them and use them as inlet fluctuations.

Below we present a method of generating synthesized inlet fluctuations.

### 25.1 Synthesized turbulence

The method described below was developed in [153, 154, 75] for creating turbulence for generating noise. It was later further developed for inlet boundary conditions [155, 156, 149].

A turbulent fluctuating velocity fluctuating field (whose average is zero) can be expressed using a Fourier series, see Section 5.3 and Eq. C.17. Let us re-write this formula as

$$\begin{aligned} a_n \cos(nx) + b_n \sin(nx) = \\ c_n \cos(\alpha_n) \cos(nx) + c_n \sin(\alpha_n) \sin(nx) = c_n \cos(nx - \alpha_n) \end{aligned} \quad (25.1)$$

where  $a_n = c_n \cos(\alpha)$ ,  $b_n = c_n \sin(\alpha_n)$ . The new coefficient,  $c_n$ , and the phase angle,  $\alpha_n$ , are related to  $a_n$  and  $b_n$  as

$$c_n = (a_n^2 + b_n^2)^{1/2} \quad \alpha_n = \arctan\left(\frac{b_n}{a_n}\right) \quad (25.2)$$

A general form for a turbulent velocity field can thus be written as

$$\mathbf{v}'(\mathbf{x}) = 2 \sum_{n=1}^N \hat{u}^n \cos(\boldsymbol{\kappa}^n \cdot \mathbf{x} + \psi^n) \boldsymbol{\sigma}^n \quad (25.3)$$

where  $\hat{u}^n$ ,  $\psi^n$  and  $\boldsymbol{\sigma}_i^n$  are the amplitude, phase and direction of Fourier mode  $n$ . The synthesized turbulence at one time step is generated as follows.

### 25.2 Random angles

The angles  $\varphi^n$  and  $\theta^n$  determine the direction of the wavenumber vector  $\boldsymbol{\kappa}$ , see Eq. 25.3 and Eq. 25.1;  $\alpha^n$  denotes the direction of the velocity vector,  $\mathbf{v}'$ . For more details, see Appendix I.

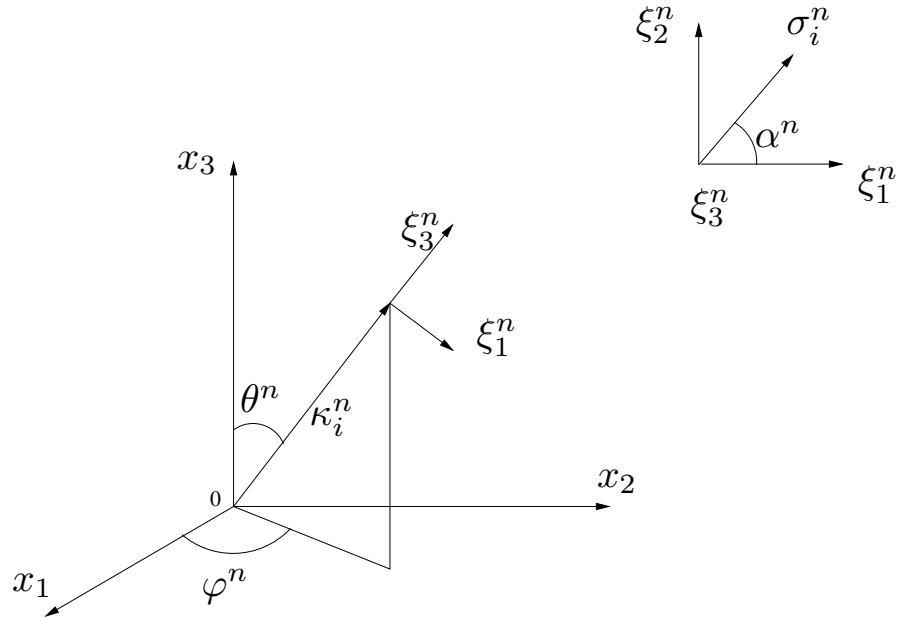


Figure 25.1: The wave-number vector,  $\kappa_i^n$ , and the velocity unit vector,  $\sigma_i^n$ , are orthogonal (in physical space) for each wave number  $n$ .

### 25.3 Highest wave number

Define the highest wave number based on mesh resolution  $\kappa_{max} = 2\pi/(2\Delta)$ , where  $\Delta$  is the grid spacing. The fluctuations are generated on a grid with equidistant spacing (or on a weakly stretched mesh),  $\Delta\eta = x_{2,max}/N_2$ ,  $\Delta x_3 = x_{3,max}/N_3$ , where  $\eta$  denotes the wall-normal direction and  $N_2$  and  $N_3$  denote the number of cells in the  $x_2$  and  $x_3$  direction, respectively. The fluctuations are set to zero at the wall and are then interpolated to the inlet plane of the CFD grid (the  $x_2 - x_3$  plane).

### 25.4 Smallest wave number

Define the smallest wave number from  $\kappa_1 = \kappa_e/p$ , where  $\kappa_e = \alpha 9\pi/(55L_t)$ ,  $\alpha = 1.453$ . The turbulent length scale,  $L_t$ , may be estimated in the same way as in RANS simulations, i.e.  $L_t \propto \delta$  where  $\delta$  denotes the inlet boundary layer thickness. In [155, 156, 149] it was found that  $L_t \simeq 0.1\delta_{in}$  is suitable.

Factor  $p$  should be larger than one to make the largest scales larger than those corresponding to  $\kappa_e$ . A value  $p = 2$  is suitable.

### 25.5 Divide the wave number range

Divide the wavenumber space,  $\kappa_{max} - \kappa_1$ , into  $N$  modes, equally large, of size  $\Delta\kappa$ .

## 25.6 von Kármán spectrum

A modified von Kármán spectrum is chosen, see Eq. 25.4 and Fig. 25.2. The amplitude  $\hat{u}^n$  of each mode in Eq. 25.3 is then obtained from

$$\begin{aligned}\hat{u}^n &= (E(\kappa)\Delta\kappa)^{1/2} \\ E(\kappa) &= c_E \frac{u_{rms}^2}{\kappa_e} \frac{(\kappa/\kappa_e)^4}{[1 + (\kappa/\kappa_e)^2]^{17/6}} e^{-2(\kappa/\kappa_\eta)^2} \\ \kappa &= (\kappa_i\kappa_i)^{1/2}, \quad \kappa_\eta = \varepsilon^{1/4}\nu^{-3/4}\end{aligned}\tag{25.4}$$

The coefficient  $c_E$  is obtained by integrating the energy spectrum over all wavenumbers to get the turbulent kinetic energy, i.e.

$$k = \int_0^\infty E(\kappa) d\kappa\tag{25.5}$$

which gives [59]

$$c_E = \frac{4}{\sqrt{\pi}} \frac{\Gamma(17/6)}{\Gamma(1/3)} \simeq 1.453\tag{25.6}$$

where

$$\Gamma(z) = \int_0^\infty e^{-z'} x^{z-1} dz'\tag{25.7}$$

## 25.7 Computing the fluctuations

Having  $\hat{u}^n$ ,  $\kappa_j^n$ ,  $\sigma_i^n$  and  $\psi^n$ , allows the expression in Eq. 25.3 to be computed, i.e.

$$\begin{aligned}v'_1 &= 2 \sum_{n=1}^N \hat{u}^n \cos(\beta^n) \sigma_1 \\ v'_2 &= 2 \sum_{n=1}^N \hat{u}^n \cos(\beta^n) \sigma_2 \\ v'_3 &= 2 \sum_{n=1}^N \hat{u}^n \cos(\beta^n) \sigma_3 \\ \beta^n &= k_1^n x_1 + k_2^n x_2 + k_3^n x_3 + \psi^n\end{aligned}\tag{25.8}$$

where  $\hat{u}^n$  is computed from Eq. 25.4.

In this way inlet fluctuating velocity fields  $(v'_1, v'_2, v'_3)$  are created at the inlet  $x_2 - x_3$  plane.

The code for generating the isotropic fluctuations can be downloaded [here](http://www.tfd.chalmers.se/~lada/projects/inlet-boundary-conditions/proright.html)

## 25.8 Introducing time correlation

A fluctuating velocity field is generated each time step as described above. They are independent of each other and their time correlation will thus be zero. This is unphysical.

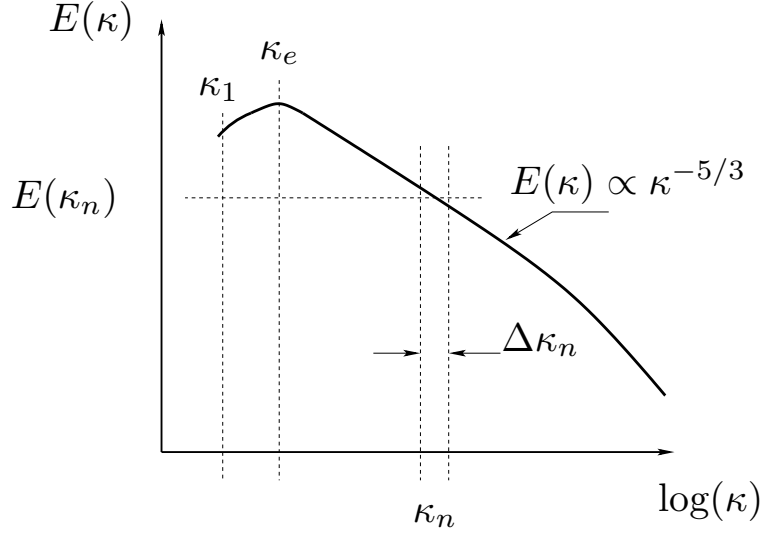


Figure 25.2: Modified von Kármán spectrum

To create correlation in time, new fluctuating velocity fields,  $\mathcal{V}'_1, \mathcal{V}'_2, \mathcal{V}'_3$ , are computed based on an asymmetric time filter

$$\begin{aligned} (\mathcal{V}'_1)^m &= a(\mathcal{V}'_1)^{m-1} + b(v'_1)^m \\ (\mathcal{V}'_2)^m &= a(\mathcal{V}'_2)^{m-1} + b(v'_2)^m \\ (\mathcal{V}'_3)^m &= a(\mathcal{V}'_3)^{m-1} + b(v'_3)^m \end{aligned} \quad (25.9)$$

where  $m$  denotes the time step number and  $a = \exp(-\Delta t/\mathcal{T})$ .

The second coefficient is taken as  $b = (1 - a^2)^{0.5}$  which ensures that  $\langle \mathcal{V}'_1^2 \rangle = \langle v_1'^2 \rangle$  ( $\langle \cdot \rangle$  denotes averaging). The time correlation will be equal to

$$\exp(-\tau/\mathcal{T}) \quad (25.10)$$

where  $\tau$  is the time separation and thus Eq. 25.9 is a convenient way to prescribe the turbulent time scale of the fluctuations. The inlet boundary conditions are prescribed as (we assume that the inlet is located at  $x_1 = 0$  and that the mean velocity is constant in the spanwise direction,  $x_3$ )

$$\begin{aligned} \bar{v}_1(0, x_2, x_3, t) &= V_{1,in}(x_2) + u'_{1,in}(x_2, x_3, t) \\ \bar{v}_2(0, x_2, x_3, t) &= V_{2,in}(x_2) + v'_{2,in}(x_2, x_3, t) \\ \bar{v}_3(0, x_2, x_3, t) &= V_{3,in}(x_2) + v'_{3,in}(x_2, x_3, t) \end{aligned} \quad (25.11)$$

where  $v'_{1,in} = (\mathcal{V}'_1)^m$ ,  $v'_{2,in} = (\mathcal{V}'_2)^m$  and  $v'_{3,in} = (\mathcal{V}'_3)^m$  (see Eq. 25.9). The mean inlet profiles,  $V_{1,in}$ ,  $V_{2,in}$ ,  $V_{3,in}$ , are either taken from experimental data, a RANS solution or from the law of the wall; for example, if  $V_{2,in} = V_{3,in} = 0$  we can estimate  $V_{1,in}$  as [157]

$$V_{1,in}^+ = \begin{cases} x_2^+ & x_2^+ \leq 5 \\ -3.05 + 5 \ln(x_2^+) & 5 < x_2^+ < 30 \\ \frac{1}{\kappa} \ln(x_2^+) + B & x_2^+ \geq 30 \end{cases} \quad (25.12)$$

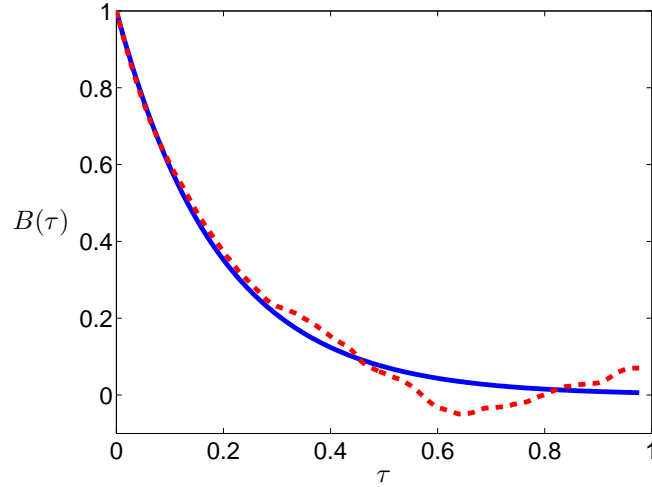


Figure 25.3: Auto correlation,  $B(\tau) = \langle v'_1(t)v'_1(t - \tau)_t \rangle$  (averaged over time,  $t$ ). — : Eq. 25.10; - - - : computed from synthetic data,  $(\mathcal{V}'_1)^m$ , see Eq. 25.9.

where  $\kappa = 0.4$  and  $B = 5.2$ .

The method to prescribed fluctuating inlet boundary conditions have been used for channel flow [149], for diffuser flow [151] as well as for the flow over a bump and an axisymmetric hill [158].

## 26 Overview of LES, hybrid LES-RANS and URANS models

DNS (Direct Numerical Simulation) is the most accurate method available. In DNS we solve the unsteady, 3D Navier-Stokes equations (see Eq. 2.7) numerically without any turbulence model. This gives the exact solution of the flow field in time and space. We can afford to do DNS only for low Reynolds number. The higher the Reynolds number gets, the finer the grid must be because the smallest turbulent length and time scales, which we must resolve in DNS, decrease with  $Re^{-3/4}$  and  $Re^{-1/2}$ , respectively, see Eq. 5.16. Hence the cell size in each coordinate of our CFD grid must decrease with  $Re^{-3/4}$  and the time step must decrease with  $Re^{-1/2}$ . Let's take an example. If the Reynolds number increases by a factor of two, the number of cells increases by

$$\frac{\Delta Re^{3/4}}{\text{x-direction}} \frac{\Delta Re^{3/4}}{\text{y-direction}} \frac{\Delta Re^{3/4}}{\text{z-direction}} \frac{\Delta Re^{1/2}}{\text{time}} = \Delta Re^{11/4} = 2^{11/4} = 6.7 \quad (26.1)$$

Above we assume that the lengthscales are reduced when the Reynolds numbers is increased. This implies that we assume that the Reynolds number is increased due to an increase in velocity or a decrease in viscosity. We can, of course, also consider the change of Reynolds number by changing the size of the object. For example, it is affordable to compute the flow around a small car such as those we played with as kids (for this car of, say, length of 5cm, the Reynolds number is very small). As we increase the size of the car we must increase the number of cells (the smallest cells cannot be enlarged, because the smallest turbulent scales will not increase). Also the time step cannot be increased, but we must compute longer time (i.e. increase the number of timesteps) in order to capture the largest time scales (assuming that the velocity of the small and the large car is the same).

Having realized that DNS is not feasible, we turn to LES, see Section 18. Here, the smallest scales are modelled, and only the eddies that are larger than the grid are resolved by the (filtered) Navier-Stokes. With LES, we can make the smallest grid cells somewhat larger (the cell side, say, 2 – 3 times larger).

However, it is found that LES needs very fine resolution near walls, see Section 21. To find an approximate solution to this problem we use RANS near the walls and LES away from the walls. The models which we have looked at are DES (Section 20), hybrid LES-RANS (Section 21), SAS (Section 22) and PANS (Section 23); see also Section 24 where PANS and Zonal PANS are discussed.

As stated above, the LES must at high Reynolds number be combined with a URANS treatment of the near-wall flow region. In the literature, there are different methods for bridging this problem such as Detached Eddy Simulation (DES) [113, 136, 146] hybrid LES/RANS [159] and Scale-Adapted Simulations (SAS) [160, 161] (for a review, see [162]). The two first classes of models take the SGS length scale from the cell size whereas the last (SAS) involves the von Kármán lengthscale.

The DES, hybrid LES/RANS and the SAS models have one thing in common: in the LES region, the turbulent viscosity is reduced. This is achieved in different ways. In some models, the turbulent viscosity is reduced indirectly by reducing the dissipation term in the  $k$  equation, see Eq. 20.5, as in two-equation DES [163]. In other models, such as the two-equation XLES model [117] and in the one-equation hybrid LES-RANS [75], it is accomplished by reducing the length scale in both the expression for the turbulent viscosity as well as for the dissipation term in the  $k$  equation, see Eq. 21.2 and Table 21.1.

In the partially averaged Navier-Stokes (PANS) model [119] and the Partially Integrated Transport Model (PITM) [121, 164], the turbulent viscosity is reduced by decreasing the destruction term in the dissipation ( $\varepsilon$ ) equation which increases  $\varepsilon$ , see Eq. 23.17. This decreases the turbulent viscosity in two ways: first, the turbulent viscosity is reduced because of the enhancement of  $\varepsilon$  ( $\nu_t = c_\mu k^2/\varepsilon$ , see Eq. 23.12), and, second, the turbulent kinetic energy ( $k$ ) decreases because of the increased dissipation term,  $\varepsilon$ . In the SAS model based on the  $k - \omega$  model, the turbulent viscosity is reduced by an additional source term,  $P_{SAS}$ , see Eq. 22.5, in the  $\omega$  equation. The source term is activated by resolved turbulence; in steady flow it is inactive. When the momentum equations are in turbulence-resolving mode,  $P_{SAS}$  increases which increases  $\omega$ . This decreases the turbulent viscosity in two ways: first, directly, because  $\omega$  appears in the denominator in the expression for the turbulent viscosity,  $\nu_t$ , and, second, because  $k$  is reduced due to the increased dissipation term  $\beta^* k \omega$ .

The PANS model and the PITM models are very similar to each other although their derivations are completely different. The only difference in the models is that in the PANS model the turbulent diffusion coefficients in the  $k$  and  $\varepsilon$  equations are modified. These two models do not use the filter width, and can hence be classified as URANS models. On the other hand, a large part of the turbulence spectrum is usually resolved which is in contrast to standard URANS models. PANS and PITM models have in [162] been classified as second-generation URANS models, or 2G-URANS models.

A short description of the models are given here.

**DES.** A RANS models is used near the walls and LES is used away from the walls.

The interface is usually defined automatic. In the original DES the entire boundary layer is covered by RANS. However, when the grid is refined in streamwise and spanwise directions, the interface moves closer to the wall. When a large part of the boundary layer is covered by LES, it is called WM-LES (Wall-Modelled LES). The LES lengthscale is the filterwidth.

**WM-LES**

**Hybrid LES-RANS.** The difference between DES and hybrid LES-RANS is that the original DES covers the entire boundary layer by RANS whereas hybrid LES-RANS treats most of the boundary layer in LES mode. Hybrid LES-RANS and WM-LES can be considered to be the same thing. The LES lengthscale is the filterwidth.

**PANS, PITM.** These models are able to operate both in LES and RANS mode. In LES mode the models do not use the filterwidth as a lengthscale. Hence they are usually defined as an URANS model (defined below). Since the models usually aim at resolving a substantial part of the turbulence spectrum, they can be defined as a second-generation URANS model (a 2G-URANS model [162]).

**SAS.** This is also a model that can operate both in LES and RANS mode. In unsteady mode the model does not use the filterwidth as a lengthscale. In unsteady mode this model usually resolved less turbulence than the other models mentioned above; hence it can be classified as an URANS model (first generation).

**URANS.** A RANS model is used in unsteady mode. In unsteady mode the model does not use the filterwidth as a lengthscale. Unless the flow is prone to go unsteady, the results will be steady (i.e. same as RANS). Usually a RANS model developed for steady flow is used. Only a small part of the turbulence is resolved.

The models listed above can be ranked in terms of accuracy and CPU cost:

1. **Hybrid LES-RANS, PANS, PITM, WM-LES.** Highest accuracy and CPU cost
2. **DES.**
3. **SAS.**
4. **URANS.** Lowest accuracy and CPU cost

## 27 Best practice guidelines (BPG)

In the early days of CFD, different CFD codes used to give different results. Even if the same grid and the same turbulence model were used, there could be substantial differences between the results. The reasons to these differences could be that the turbulence model was not implemented in exactly the same way in the two codes, or that the discretization scheme in one code was more diffusive than in the other. There could be small differences in the implementation of the boundary conditions in the two codes.

Today the situation is much improved. Two different CFD codes usually give the same results on the same grid. The main reason for this improved situation is because of workshops and EU projects where academics, engineers from industry and CFD software vendors regularly meet and discuss different aspects of CFD. Test cases with mandatory grids, boundary conditions, turbulence models etc are defined and the participants in the workshops and EU projects carry out CFD simulations for these test cases. Then they compare and discuss their results.

### 27.1 EU projects

Four EU projects in which the author has taken part can be mentioned

**LESFOIL:** Large Eddy Simulation of Flow Around Airfoils

<http://www.tfd.chalmers.se/~lada/projects/lesfoil/proright.html>

**FLOMANIA:** Flow Physics Modelling: An Integrated Approach

<http://cfd.mace.manchester.ac.uk/flomania/>

**DESIDER:** Detached Eddy Simulation for Industrial Aerodynamics

<http://cfd.mace.manchester.ac.uk/desider>

**ATAAC:** Advanced Turbulence Simulation for Aerodynamic Application Challenges

<http://cfd.mace.manchester.ac.uk/ATAAC/WebHome>

### 27.2 Ercoftac workshops

Workshops are organized by Ercoftac (European Research Community On Flow, Turbulence And Combustion). The Special Interest Group Sig15 is focused on evaluating turbulence models. The outcome from all workshop are presented

here

[http://www.ercoftac.org/fileadmin/user\\_upload/bigfiles/sig15/database/index.html](http://www.ercoftac.org/fileadmin/user_upload/bigfiles/sig15/database/index.html)

Ercoftac also organizes workshops and courses on Best Practice Guidelines. The publication *Industrial Computational Fluid Dynamics of Single-Phase Flows* can be ordered on

Ercoftac www page

[http://www.ercoftac.org/publications/ercoftac\\_best\\_practice\\_guidelines/single-phase\\_flows\\_spf/](http://www.ercoftac.org/publications/ercoftac_best_practice_guidelines/single-phase_flows_spf/)

### 27.3 Ercoftac Classical Database

A *Classical Database*, which includes some 100 experimental investigations, can be found at

[Ercoftac's www page](#)

[http://www.ercoftac.org/products\\_and\\_services/classic\\_collection\\_database](http://www.ercoftac.org/products_and_services/classic_collection_database)

### 27.4 ERCOFTAC QNET Knowledge Base Wiki

The QNET is also the responsibility of Ercoftac. Here you find descriptions of how CFD simulations of more than 60 different flows were carried out. The flows are divided into

**Application Areas.** These are sector disciplines such as Built Environment, Chemical and Process Engineering, External Aerodynamics, Turbomachinery, Combustion and Heat Transfer etc. Each Application Area is comprised of Application Challenges. These are realistic industrial test cases which can be used to judge the competency and limitations of CFD for a given Application Area.

**Underlying Flow Regimes.** These are generic, well-studied test cases capturing important elements of the key flow physics encountered across the Application Areas.

For more information, visit

[ERCOFTAC QNET Knowledge Base Wiki](#)

[http://www.ercoftac.org/products\\_and\\_services/wiki/](http://www.ercoftac.org/products_and_services/wiki/)

## A TME225: $\epsilon - \delta$ identity

The  $\epsilon - \delta$  identity reads

$$\epsilon_{inm}\epsilon_{mjk} = \epsilon_{min}\epsilon_{mjk} = \epsilon_{nmi}\epsilon_{mjk} = \delta_{ij}\delta_{nk} - \delta_{ik}\delta_{nj}$$

In Table A.1 the components of the  $\epsilon - \delta$  identity are given.

$i$	$n$	$j$	$k$	$\epsilon_{inm}\epsilon_{mjk}$	$\delta_{ij}\delta_{nk} - \delta_{ik}\delta_{nj}$
1	2	1	2	$\epsilon_{12m}\epsilon_{m12} = \epsilon_{123}\epsilon_{312} = 1 \cdot 1 = 1$	$1 - 0 = 1$
2	1	1	2	$\epsilon_{21m}\epsilon_{m12} = \epsilon_{213}\epsilon_{312} = -1 \cdot 1 = -1$	$0 - 1 = -1$
1	2	2	1	$\epsilon_{12m}\epsilon_{m21} = \epsilon_{123}\epsilon_{321} = 1 \cdot -1 = -1$	$0 - 1 = -1$
1	3	1	3	$\epsilon_{13m}\epsilon_{m13} = \epsilon_{132}\epsilon_{213} = -1 \cdot -1 = 1$	$1 - 0 = 1$
3	1	1	3	$\epsilon_{31m}\epsilon_{m13} = \epsilon_{312}\epsilon_{213} = 1 \cdot -1 = -1$	$0 - 1 = -1$
1	3	3	1	$\epsilon_{13m}\epsilon_{m31} = \epsilon_{132}\epsilon_{231} = -1 \cdot 1 = -1$	$0 - 1 = -1$
2	3	2	3	$\epsilon_{23m}\epsilon_{m23} = \epsilon_{231}\epsilon_{123} = 1 \cdot 1 = 1$	$1 - 0 = 1$
3	2	2	3	$\epsilon_{32m}\epsilon_{m23} = \epsilon_{321}\epsilon_{123} = -1 \cdot 1 = -1$	$0 - 1 = -1$
2	3	3	2	$\epsilon_{23m}\epsilon_{m32} = \epsilon_{231}\epsilon_{132} = 1 \cdot -1 = -1$	$0 - 1 = -1$

Table A.1: The components of the  $\epsilon - \delta$  identity which are non-zero.

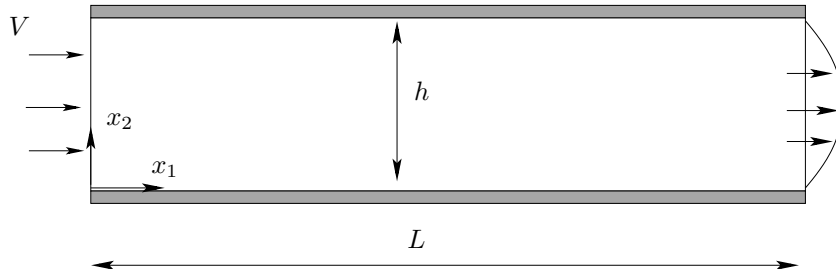


Figure B.1: Flow between two plates (not to scale).

## B TME225 Assignment 1: laminar flow

You will get results of a developing two-dimensional channel flow (i.e. flow between two parallel plates), see Fig. B.1. The flow is steady and incompressible. The simulations have been done with Calc-BFC [165]. The inlet boundary condition (left boundary) is  $v_1 = V_{in} = 0.7$ . The height of the channel is  $h = 0.011m$  and  $L = 0.6385m$ ; the fluid is air of  $20^\circ\text{C}$ . You will use Matlab to analyze the data. You can also use Octave on Linux/Ubuntu. Octave is a Matlab clone which can be downloaded for free.

- First, find out and write down the governing equations (N.B.: you cannot assume that the flow is fully developed).

From the course www page <http://www.tfd.chalmers.se/~lada/MoF/>, download the data file `channel_flow_data.dat` and the m-file `channel_flow.m` which reads the data and plot some results. Open Matlab and execute `channel_flow`.

Open `channel_flow.m` in an editor and make sure that you understand it. There are three field variables,  $v_1$ ,  $v_2$  and  $p$ ; the corresponding Matlab arrays are `v1_2d`, `v2_2d` and `p_2d`. The grid is  $199 \times 22$ , i.e.  $ni = 199$  grid points in the  $x_1$  direction and  $nj = 22$  grid points in the  $x_2$  direction. The field variables are stored at these grid points. We denote the first index as  $i$  and the second index as  $j$ , i.e. `v1_2d(i, j)`. Hence in

`v1_2d(:, 1)` are the  $v_1$  values at the lower wall;  
`v1_2d(:, nj)` are the  $v_1$  values at the upper wall;  
`v1_2d(1, :)` are the  $v_1$  values at the inlet;  
`v1_2d(ni, :)` are the  $v_1$  values at the outlet;

The work should be carried out in groups of two (you may also do it on your own, but we don't recommend it). At the end of this Assignment the group should write and submit a report (in English). Divide the report into sections corresponding to the sections B.1 – B.9. In some sections you need to make derivations; these should clearly be described and presented. Present the results in each section with a figure (or a numerical value). The results should also be discussed and – as far as you can – explained.

## B.1 Fully developed region

Fully developed conditions mean that the flow does not change in the streamwise direction, i.e.  $\partial v_1 / \partial x_1 = 0$ . If we define “fully developed” as the location where the velocity gradient in the center becomes smaller than 0.01, i.e.  $|\partial v_1 / \partial x_1| < 0.01$ , how long distance from the inlet does the flow become fully developed?

Another way to define fully developed conditions can be the  $x_1$  position where the centerline velocity has reached, for example, 99% of its final value. What  $x_1$  value do you get?

In Section 3.2.2, a distance taken from the literature is given. How well does this agree with your values?

In the fully developed region, compare the velocity profile with the analytical profile (see Section 3.2.2).

Look at the vertical velocity component,  $v_2$ . What value should it take in the fully developed region (see Section 3.2.2)? What value does it take (at  $x_2 = h/4$ , for example)?

## B.2 Wall shear stress

On the lower wall, the wall shear stress,  $\tau_{w,L}$  (index  $L$  denotes Lower), is computed as

$$\tau_{w,L} \equiv \tau_{21,w,L} = \mu \frac{\partial v_1}{\partial x_2} \Big|_L \quad (\text{B.1})$$

Recall that  $\tau_{12} = \mu(\partial v_1 / \partial x_2 + \partial v_2 / \partial x_1)$  (see Eqs. 2.4 and 1.5) but at the wall  $\partial v_2 / \partial x_1 = 0$ ;  $S_{kk} = 0$  because of the continuity equation, Eq. 2.3. Plot  $\tau_{w,L}$  versus  $x_1$ . Why does it behave as it does?

Now we will compute the wall shear stress at the upper wall,  $\tau_{w,U}$ . If you use Eq. B.1, you get the incorrect sign. Instead, use Cauchy’s formula (see [2], Chapt. 4.2)

$$t_i^{(\hat{n})} = \tau_{ji} n_j \quad (\text{B.2})$$

which is a general way to compute the stress vector on a surface whose (outward pointing) normal vector is  $\hat{n} = n_j$ . The expression for  $\tau_{ij}$  can be found in Eqs. 1.5 and 2.4; recall that the flow is incompressible. On the top wall, the normal vector points *out* from the surface (i.e.  $n_j = (0, -1, 0)$ ). Use Eq. B.2 to compute the wall shear stress at the upper wall. Plot the two wall shear stresses in the same figure. How do they compare? In the fully developed region, compare with the analytical value (see Eq. 3.30).

## B.3 Inlet region

In the inlet region the flow is developing from its inlet profile ( $v_1 = V = 0.7$ ) to the fully developed profile somewhere downstream. The  $v_1$  velocity is decelerated in the near-wall regions, and hence the  $v_1$  velocity in the center must increase due to continuity. Plot  $v_1$  in the center and near the wall as a function of  $x_1$ . Plot also  $\partial v_1 / \partial x_1$ . If you, for a fixed  $x_1$ , integrate  $v_1$ , i.e.

$$\xi(x_1) = \int_0^h v_1(x_1, x_2) dx_2$$

what do you get? How does  $\xi(x_1)$  vary in the  $x_1$  direction? How should it vary?

## B.4 Wall-normal velocity in the developing region

In Section B.3 we found that, in the developing region,  $v_1$  near the walls decreases for increasing  $x_1$ . What about  $v_2$ ? How do you explain the behaviour of  $v_2$ ?

## B.5 Vorticity

Do you expect the flow to be *irrotational* anywhere? Let's find out by computing the vorticity, see Section 1.3. Plot it in the fully developed region as  $\omega_3$  vs.  $x_2$ . Where is it largest? Plot the vorticity also in the inlet and developing regions; what happens with the vorticity in the inlet region? Now, is the flow rotational anywhere? Why? Why not?

## B.6 Deformation

In Section 1.5, we divided the velocity gradient into a strain-rate tensor,  $S_{ij}$ , and a vorticity tensor,  $\Omega_{ij}$ . Since the flow is two-dimensional, we have only two off-diagonal terms (which ones?). Plot and compare one of the off-diagonal term of  $S_{ij}$  and  $\Omega_{ij}$ . Where are they largest? Why? What is the physical meaning of  $S_{ij}$  and  $\Omega_{ij}$ , respectively? Compare  $\Omega_{ij}$  with the vorticity you plotted in Section B.5. Are they similar? Any comment?

## B.7 Dissipation

Compute and plot the dissipation,  $\Phi = \tau_{ji} \partial v_i / \partial x_j$ . What is the physical meaning of the dissipation? Where do you expect it to be largest? Where is it largest? Any difference in its behaviour in the inlet region compared to in the fully developed region?

The dissipation appears as a source term in the equation for internal energy, see Eq. 2.9. This means that dissipation increases the internal energy, i.e. the temperature. This is discussed in some detail at p. 24.

Use Eq. 2.14 to compute the temperature increase that is created by the flow (i.e. by dissipation). Start by integrating the dissipation over the entire computational domain. Next, re-write the left side on conservative form and then apply the Gauss divergence theorem. Assume that the upper and lower walls are adiabatic; furthermore we can neglect the heat flux by conduction,  $q_1$ , (see Eq. 2.11) at the inlet and outlet. Now you can compute the increase in bulk temperature,  $T_b$ , from inlet to outlet. The bulk temperature is defined at

$$T_b = \frac{\int_0^h v_1 T dx_2}{\int_0^h v_1 dx_2}$$

## B.8 Eigenvalues

Compute and plot the eigenvalues of the viscous stress tensor,  $\tau_{ij}$ . Use the Matlab command `eig`. If you have computed the four elements of the  $\tau_{ij}$  matrix you can use the following commands:

```
tau=[tau_11 tau_12; tau_21 tau_22];
[n,lambda]=eig(tau);
```

where `n` and `lambda` denote eigenvalues and eigenvectors, respectively. Note that `tau_11`, `tau_12`, `tau_21`, `tau_22` are scalars and hence the coding above must be inserted in `for` loops.

What is the physical meaning of the eigenvalues (see Chapter 1.7)? Pick an  $x_1$  location where the flow is fully developed. Plot one eigenvalue as a  $x - y$  graph (eigenvalue versus  $x_2$ ). Plot also the four stress components,  $\tau_{ij}$ , versus  $x_2$ . Is (Are) anyone(s) negligible? How does the largest component of  $\tau_{ij}$  compare with the largest eigenvalue? Any thoughts? And again: *what is the physical meaning of the eigenvalues?*

## B.9 Eigenvectors

Compute and plot the eigenvectors of  $\tau_{ij}$ . Recall that at each point you will get two eigenvectors, perpendicular to each other. It is enough to plot one of them. An eigenvector is, of course, a vector. Use the Matlab command `quiver` to plot the field of the eigenvectors. Recall that the sign of the eigenvector is not defined (for example, both  $\hat{\mathbf{v}}_1$  and  $-\hat{\mathbf{v}}_1$  in Fig. 1.10 at p. 19 are eigenvectors). Try to analyze why the eigenvectors behave as they do.

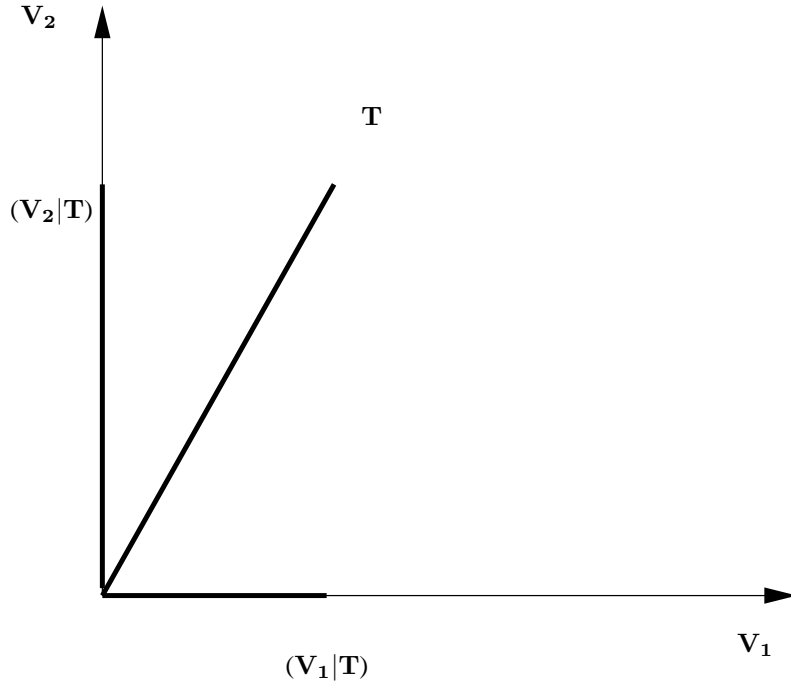


Figure C.1: Scalar product.

## C TME225: Fourier series

Here a brief introduction to Fourier series extracted from [166] is given.

### C.1 Orthogonal functions

Consider three vectors,  $\mathbf{V}_1$ ,  $\mathbf{V}_2$ ,  $\mathbf{V}_3$ , in physical space which form an orthogonal base in  $\mathbb{R}^3$  (i.e. their scalar products are zero). Let us call them *basis functions*. Any vector,  $\mathbf{T}$ , in  $\mathbb{R}^3$  can now be expressed in these three vectors, i.e.

$$\mathbf{T} = c_1 \mathbf{V}_1 + c_2 \mathbf{V}_2 + c_3 \mathbf{V}_3 \quad (\text{C.1})$$

see Fig. C.1. Now define the scalar product of two vectors,  $\mathbf{a}$  and  $\mathbf{b}$ , as  $\mathbf{a} \cdot \mathbf{b} = (\mathbf{a}|\mathbf{b})$ . The coordinates,  $c_i$ , can be determined by making a scalar product of Eq. C.1 and  $\mathbf{V}_i$  which gives

$$\begin{aligned} (\mathbf{T}|\mathbf{V}_i) &= (c_1 \mathbf{V}_1|\mathbf{V}_i) + (c_2 \mathbf{V}_2|\mathbf{V}_i) + (c_3 \mathbf{V}_3|\mathbf{V}_i) \\ &= (c_1 \mathbf{V}_1|\mathbf{V}_1) + (c_2 \mathbf{V}_2|\mathbf{V}_2) + (c_3 \mathbf{V}_3|\mathbf{V}_3) \\ &= c_1 |\mathbf{V}_1|^2 + c_2 |\mathbf{V}_2|^2 + c_3 |\mathbf{V}_3|^2 = c_i |\mathbf{V}_i|^2 \end{aligned} \quad (\text{C.2})$$

where  $|\mathbf{V}_i|$  denotes the length of  $\mathbf{V}_i$ ; the second line follows because of the orthogonality of  $\mathbf{V}_i$ . Hence the coordinates,  $c_i$ , are determined by

$$c_i = (\mathbf{T}|\mathbf{V}_i)/|\mathbf{V}_i|^2 \quad (\text{C.3})$$

Now let us define an infinite ( $\infty$ -dimensional) functional space,  $\mathbf{B}$ , with orthogonal basis functions  $\{g\}_1^\infty$ . The “scalar product” of two functions,  $f$  and  $g_n$ , is defined as

$$(f|g_n) = \int_a^b f(x)g_n(x)dx \quad (\text{C.4})$$

Then, in a similar way to Eq. C.1, any function can, over the interval  $[a, b]$ , be expressed as

$$f = \sum_{n=1}^{\infty} c_n g_n \quad (\text{C.5})$$

As above, we must now find the “coordinates” (cf. the coordinates,  $c_i$ , in Eq. C.1). Multiply, as in Eq. C.2,  $f$  with the basis functions,  $g_i$ , i.e.

$$(f|g_i) = \sum_{n=1}^{\infty} c_n (g_n|g_i) \quad (\text{C.6})$$

Since we know that all  $g_n$  are orthogonal, Eq. C.6 is non-zero only if  $i = n$ , i.e.

$$\begin{aligned} (f|g_i) &= (c_1 g_1|g_i) + (c_2 g_2|g_i) \dots c_i(g_i|g_i) \dots c_{i+1}(g_{i+1}|g_i) \dots = \\ &= c_i(g_i|g_i) = c_i \|g_i\|^2 \end{aligned} \quad (\text{C.7})$$

Similar to Eq. C.3, the “coordinates” can be found from (switch from index  $i$  to  $n$ )

$$c_n = (f|g_n)/\|g_n\|^2 \quad (\text{C.8})$$

The “coordinates”,  $c_n$ , are called the *Fourier coefficients* to  $f$  in system  $\{g\}_1^\infty$  and  $\|g_n\|$  is the “length” of  $g_n$  (cf.  $|\mathbf{V}_i|$  which is the length of  $\mathbf{V}_i$  in Eq. C.3), i.e.

$$\|g_n\| = (g_n|g_n)^{1/2} = \left( \int_a^b g_n(x)g_n(x)dx \right)^{1/2} \quad (\text{C.9})$$

Let us now summarize and compare the basis functions in physical space and the basis functions in functional space.

- |   |  |
|---|--|
| 1. Any vector in $\mathbf{R}^3$ can be expressed in the orthogonal basis vectors $\mathbf{V}_i$<br>2. The length of the basis vector, $\mathbf{V}_i$ , is $ \mathbf{V}_i $<br>3. The coordinates of $\mathbf{V}_i$ are computed as $c_i = (\mathbf{T} \mathbf{V}_i)/ \mathbf{V}_i ^2$ | 1. Any function in $[a, b]$ can be expressed in the orthogonal basis functions $g_n$<br>2. The length of the basis function, $g_n$ , is $\ g_n\ $<br>3. The coordinates of $g_n$ are computed as $c_n = (f g_n)/\ g_n\ ^2$ |
|---|--|

## C.2 Trigonometric functions

Here we choose  $g_n$  as trigonometric functions which are periodic in  $[-\pi, \pi]$ . The question is now how to choose the orthogonal function system  $\{g\}_1^\infty$  on the interval  $[-\pi, \pi]$ . In mathematics, we usually start by doing an intelligent “guess”, and then we prove that it is correct. So let us “guess” that the trigonometric series

$$[1, \sin x, \cos x, \sin(2x), \dots, \sin(nx), \cos(nx), \dots] \quad (\text{C.10})$$

is an orthogonal system. The function system in Eq. C.10 can be defined as

$$g_n(x) = \begin{cases} \phi_k(x), & \text{for } n = 2k = 2, 4, \dots \\ \psi_k(x), & \text{for } n = 2k + 1 = 1, 3, \dots \end{cases} \quad (\text{C.11})$$

where  $\phi_k(x) = \sin(kx)$  ( $k = 1, 2, \dots$ ) and  $\psi_k(x) = \cos(kx)$  ( $k = 0, 1, \dots$ ). Now we need to show that they are orthogonal, i.e. that the integral of the product of any two functions  $\phi_k$  and  $\psi_k$  is zero on  $\mathbf{B}[-\pi, \pi]$  and we need to compute their “length” (i.e. their norm).

#### Orthogonality of $\psi_n$ and $\psi_k$

$$\begin{aligned} (\psi_n | \psi_k) &= \int_{-\pi}^{\pi} \cos(nx) \cos(kx) dx = \frac{1}{2} \int_{-\pi}^{\pi} [\cos((n+k)x) + \cos((n-k)x)] dx \\ &= \frac{1}{2} \left[ \frac{1}{n+k} \sin((n+k)x) + \frac{1}{n-k} \sin((n-k)x) \right]_{-\pi}^{\pi} = 0 \text{ for } k \neq n \end{aligned} \quad (\text{C.12})$$

#### “Length” of $\psi_k$

$$\begin{aligned} (\psi_k | \psi_k) &= \|\psi_k\|^2 = \int_{-\pi}^{\pi} \cos^2(kx) dx = \left[ \frac{x}{2} + \frac{1}{4} \sin(2x) \right]_{-\pi}^{\pi} = \pi \text{ for } k > 0 \\ (\psi_0 | \psi_0) &= \|\psi_0\|^2 = \int_{-\pi}^{\pi} 1 \cdot dx = 2\pi \end{aligned} \quad (\text{C.13})$$

#### Orthogonality of $\phi_n$ and $\psi_k$

$$\begin{aligned} (\phi_n | \psi_k) &= \int_{-\pi}^{\pi} \sin(nx) \cos(kx) dx = \frac{1}{2} \int_{-\pi}^{\pi} [\sin((n+k)x) + \sin((n-k)x)] dx = \\ &- \frac{1}{2} \left[ \frac{1}{n+k} \cos((n+k)x) + \frac{1}{n-k} \cos((n-k)x) \right]_{-\pi}^{\pi} = 0 \end{aligned} \quad (\text{C.14})$$

#### Orthogonality of $\phi_n$ and $\phi_k$

$$\begin{aligned} (\phi_n | \phi_k) &= \int_{-\pi}^{\pi} \sin(nx) \sin(kx) dx = \frac{1}{2} \int_{-\pi}^{\pi} [\cos((n-k)x) - \cos((n+k)x)] dx \\ &= \frac{1}{2} \left[ \frac{1}{n-k} \sin((n-k)x) - \frac{1}{n+k} \sin((n+k)x) \right]_{-\pi}^{\pi} = 0 \text{ for } k \neq n \end{aligned} \quad (\text{C.15})$$

#### “Length” of $\phi_k$

$$(\phi_k | \phi_k) = \|\phi_k\|^2 = \int_{-\pi}^{\pi} \sin^2(kx) dx = \left[ \frac{x}{2} - \frac{1}{4} \sin(2x) \right]_{-\pi}^{\pi} = \pi \text{ for } k \geq 1 \quad (\text{C.16})$$

### C.3 Fourier series of a function

Now that we have proved that  $\{g\}_1^\infty$  in Eq. C.11 forms an orthogonal system of functions, we know that we can express any periodic function,  $f$  (with a period of  $2\pi$ ) in  $\{g\}_1^\infty$  as

$$f(x) = c + \sum_{n=1}^{\infty} (a_n \cos(nx) + b_n \sin(nx)) \quad (\text{C.17})$$

where  $x$  is a spatial coordinate. The Fourier coefficients are given by

$$b_n = (f|\phi_n)/||\phi_n||^2 = \frac{1}{\pi} \int_{-\pi}^{\pi} f(x) \sin(nx) dx \quad (\text{C.18a})$$

$$a_n = (f|\psi_n)/||\psi_n||^2 = \frac{1}{\pi} \int_{-\pi}^{\pi} f(x) \cos(nx) dx, n > 0 \quad (\text{C.18b})$$

$$c = (f|\psi_0)/||\psi_0||^2 = \frac{1}{2\pi} \int_{-\pi}^{\pi} f(x) dx \quad (\text{C.18c})$$

If we set  $c = a_0/2$ , then  $a_0$  is obtained from Eq. C.18b, i.e.

$$f(x) = \frac{a_0}{2} + \sum_{n=1}^{\infty} (a_n \cos(nx) + b_n \sin(nx)) \quad (\text{C.19a})$$

$$b_n = (f|\phi_n)/||\phi_n||^2 = \frac{1}{\pi} \int_{-\pi}^{\pi} f(x) \sin(nx) dx \quad (\text{C.19b})$$

$$a_n = (f|\psi_n)/||\psi_n||^2 = \frac{1}{\pi} \int_{-\pi}^{\pi} f(x) \cos(nx) dx \quad (\text{C.19c})$$

Note that  $a_0$  corresponds to the average of  $f$ . Taking the average of  $f$  (i.e. integrating  $f$  from  $-\pi$  to  $\pi$ ) gives (see Eq. C.19a)

$$\bar{f} = \int_{-\pi}^{\pi} f(x) dx = \pi a_0 \quad (\text{C.20})$$

Hence, if  $\bar{f} = 0$  then  $a_0 = 0$ .

### C.4 Derivation of Parseval's formula

Parseval's formula reads

$$\int_{-\pi}^{\pi} (f(x))^2 dx = \frac{\pi}{2} a_0^2 + \pi \sum_{n=1}^{\infty} (a_n^2 + b_n^2) \quad (\text{C.21})$$

We will try to prove this formula. Assume that we want to approximate the function  $f$  as well as possible with an orthogonal series

$$\sum_{n=1}^{\infty} a_n g_n \quad (\text{C.22})$$

Now we want to prove that the Fourier coefficients are the best choice to minimize the difference

$$||f - \sum_{n=1}^N a_n g_n|| \quad (\text{C.23})$$

Later we will let  $N \rightarrow \infty$ . Using the definition of the norm and the laws of scalar product we can write

$$\begin{aligned} \|f - \sum_{n=1}^N a_n g_n\|^2 &= \left( f - \sum_{n=1}^N a_n g_n \middle| f - \sum_{k=1}^N a_k g_k \right) \\ &= (f|f) - \sum_{n=1}^N a_n (f|g_n) - \sum_{k=1}^N a_k (f|g_k) + \sum_{n=1}^N \sum_{k=1}^N a_n a_k (g_n|g_k) = \quad (\text{C.24}) \\ &= (f|f) - 2 \sum_{n=1}^N a_n (f|g_n) + \sum_{n=1}^N a_n^2 (g_n|g_n) \end{aligned}$$

because of the orthogonality of the function system,  $\{g\}_1^N$ . Express  $f$  in the second term using the Fourier coefficients  $c_n$  (see Eqs. C.5 and C.8) gives

$$\begin{aligned} (f|f) - 2 \sum_{n=1}^N a_n c_n (g_n|g_n) + \sum_{n=1}^N a_n^2 (g_n|g_n) \\ = \|f\|^2 + \sum_{n=1}^N \|g_n\|^2 (a_n^2 - 2a_n c_n) \quad (\text{C.25}) \\ = \|f\|^2 + \sum_{n=1}^N \|g_n\|^2 (a_n - c_n)^2 - \sum_{n=1}^N \|g_n\|^2 c_n^2 \end{aligned}$$

The left side of Eq. C.24 is thus minimized if the coefficients  $a_n$  are chosen as the Fourier coefficients,  $c_n$  so that

$$\|f - \sum_{n=1}^N a_n g_n\|^2 = \|f\|^2 - \sum_{n=1}^N \|g_n\|^2 c_n^2 \quad (\text{C.26})$$

The left side must always be positive and hence

$$\sum_{n=1}^N \|g_n\|^2 c_n^2 \leq \|f\|^2 = \int_{-\pi}^{\pi} (f(x))^2 dx \quad \text{for all } N \quad (\text{C.27})$$

As  $N$  is made larger, the magnitude of the left side increases, and its magnitude gets closer and closer to that of the right side, but it will always stay smaller than  $\|f\|^2$ . This means that the series on the left side is *convergent*. Using the Fourier coefficients in Eq. C.19 and letting  $N \rightarrow \infty$  it can be shown that we get equality of the left and right side, which gives Parseval's formula,

$$\|f\|^2 \equiv \int_{-\pi}^{\pi} (f(x))^2 dx = \frac{\pi}{2} a_0^2 + \pi \sum_{n=1}^{\infty} (a_n^2 + b_n^2)$$

Note that  $\pi/2$  and  $\pi$  on the right side correspond to the “length” of  $\|g_n\|$ , i.e.  $\|\psi_0\|$ ,  $\|\psi_n\|$  and  $\|\phi_n\|$ , respectively.

Appendix M describes in detail how to create energy spectra from two-point correlations.

## C.5 Complex Fourier series

Equation C.19 gives the Fourier series of a real function. It is more convenient to express a Fourier series in complex variables even if the function  $f$  itself is real. On complex form it reads

$$f(x) = \sum_{n=-\infty}^{\infty} c_n \exp(\imath nx) \quad (\text{C.28a})$$

$$c_n = \frac{1}{2\pi} \int_{-\pi}^{\pi} f(x) \exp(-\imath nx) dx \quad (\text{C.28b})$$

where the Fourier coefficients,  $c_n$ , are complex. Below we verify that if  $f$  is real, then Eq. C.28 is equivalent to Eq. C.19. The Fourier coefficients,  $c_n$ , read – assuming that  $f$  is real – according to Eq. C.28

$$c_n = \frac{1}{2\pi} \int_{-\pi}^{\pi} f(x) (\cos(nx) - \imath \sin(nx)) dx = \frac{1}{2}(a_n - \imath b_n), \quad n > 0 \quad (\text{C.29})$$

where  $a_n$  and  $b_n$  are given by Eq. C.19. For negative  $n$  in Eq. C.28 we get

$$c_{-n} = c_n^* = \frac{1}{2\pi} \int_{-\pi}^{\pi} f(x) (\cos(nx) + \imath \sin(nx)) dx = \frac{1}{2}(a_n + \imath b_n), \quad n > 0 \quad (\text{C.30})$$

where  $c_n^*$  denotes the complex conjugate. For  $n = 0$ , Eq. C.28 reads

$$c_0 = \frac{1}{2\pi} \int_{-\pi}^{\pi} f(x) dx = \frac{1}{2}a_0 \quad (\text{C.31})$$

see Eq. C.19. Inserting Eqs. C.29, C.30 and C.31 into Eq. C.28 gives

$$\begin{aligned} f(x) &= \frac{1}{2}a_0 + \frac{1}{2} \sum_{n=1}^{\infty} (a_n - \imath b_n) \exp(\imath nx) + (a_n + \imath b_n) \exp(-\imath nx) \\ &= \frac{1}{2}a_0 + \frac{1}{2} \sum_{n=1}^{\infty} (a_n - \imath b_n)(\cos(nx) + \imath \sin(nx)) + (a_n + \imath b_n)(\cos(nx) - \imath \sin(nx)) \\ &= \frac{1}{2}a_0 + \sum_{n=1}^{\infty} a_n \cos(nx) - \imath^2 b_n \sin(nx) = \frac{1}{2}a_0 + \sum_{n=1}^{\infty} a_n \cos(nx) + b_n \sin(nx) \end{aligned} \quad (\text{C.32})$$

which verifies that the complex Fourier series for a real function  $f$  is indeed identical to the usual formulation in Eq. C.19 although the Fourier coefficients,  $c_n$ , are complex. One advantage of Eq. C.28 over the formulation in Eq. C.19 is that we don't need any special definition for the first Fourier coefficient,  $a_0$ . The trick in the formulation in Eq. C.28 is that the imaginary coefficients for negative and positive  $n$  cancel whereas the real coefficients add. This means that the real coefficients are multiplied by a factor two except the first coefficient,  $a_0$ , which makes up for the factor  $\frac{1}{2}$  in front of  $a_0$  in Eq. C.19.

## D TME225: Why has the energy spectrum, $E$ , such strange dimensions?

The energy spectrum,  $E$ , has the strange dimension  $v^2/\ell$ . The reason is that it is a spectral *density* so that the kinetic energy,  $k = \overline{v'_i v'_i}$ , is computed by integrating over all wavenumbers, see Eq. 5.10. The energy spectrum is a spectral density function in a similar way as  $f_v(v)$  in Eq. 7.2; the difference is that  $f_v(v)$  in Eq. 7.2 is the first *moment*. Equation 7.5 defines the second moment. The dimension of  $f_v(v)$  in Eq. 7.2 and  $f_{v'}(v')$  in Eq. 7.5 is one over velocity squared.

Since we have chosen to express the energy spectrum as a function of the wavenumber, dimension analysis gives  $E \propto \kappa^{-5/3}$ , see Eqs. 5.12 and 5.13. A similar dimension analysis for the kinetic energy of  $v'$  gives  $v'^2 \propto \kappa^{-2/3}$ . However, integrating  $v'^2$  over all wavenumbers does not give any useful integral quantity.

The integral of the energy spectrum in the inertial region can be estimated as (see Eqs. 5.10 and 5.13)

$$k = C_K \varepsilon^{2/3} \int_{\kappa_1}^{\kappa_2} \kappa^{-5/3} d\kappa \quad (\text{D.1})$$

We could also express  $E$  as a function of the turbulent length scale of the eddies,  $\ell_\kappa$  ( $\kappa = 2\pi/\ell_\kappa$ , see Eq. 5.7). The energy spectrum is then integrated as

$$\begin{aligned} k &= \int_{\kappa_1}^{\kappa_2} \underbrace{E(\kappa)}_{\kappa^{-5/3}} d\kappa = C_K \varepsilon^{2/3} \int_{\kappa_1}^{\kappa_2} \underbrace{\kappa^{-5/3}}_{\kappa^{-2/3}} d\kappa \\ &= C_K \varepsilon^{2/3} \int_{\kappa_1}^{\kappa_2} \kappa^{-5/3} \frac{d\kappa}{d\ell_\kappa} d\ell_\kappa = -C_K 2\pi \varepsilon^{2/3} \int_{\ell_1}^{\ell_2} \kappa^{-5/3} \ell_\kappa^{-2} d\ell_\kappa \quad (\text{D.2}) \\ &= C_K \left( \frac{\varepsilon}{2\pi} \right)^{2/3} \int_{\ell_2}^{\ell_1} \underbrace{\ell_\kappa^{-1/3}}_{\ell_\kappa^{2/3}} d\ell_\kappa = \int_{\ell_2}^{\ell_1} \underbrace{E^\ell(\ell_\kappa)}_{\kappa^{-1/3}} d\ell_\kappa \end{aligned}$$

As can be seen, the energy spectrum  $E^\ell(\ell_\kappa)$  obeys the  $-1/3$  law and  $E(\kappa)$  obeys the  $-5/3$  law. However, as mentioned above, the kinetic energy of  $v'_\kappa$  decays as  $\kappa^{-2/3}$ . The reason why  $E^\ell$  decays slower than  $v'^2$  is that as  $d\ell_\kappa$  in the last line of Eq. D.2 increases, the size of the eddies increases; large eddies have larger kinetic energy and hence  $E^\ell(\ell_\kappa)$  decreases slower. In the same way,  $E(\kappa)$  decays faster than  $v'^2$  because  $d\kappa$  in the first line of Eq. D.2 encompasses smaller and smaller eddies as  $\kappa$  increases.

### D.1 An example

Let's generate a fluctuating velocity,  $v'$ , using a Fourier series. For simplicity we make it symmetric so that only the cosine part needs to be used. We make it with four terms. It reads then (see Eq. C.19)

$$\begin{aligned} v' &= a_1^{0.5} \cos\left(\frac{2\pi}{L/1}x\right) + a_2^{0.5} \cos\left(\frac{2\pi}{L/2}x\right) \\ &\quad + a_3^{0.5} \cos\left(\frac{2\pi}{L/3}x\right) + a_4^{0.5} \cos\left(\frac{2\pi}{L/4}x\right) \quad (\text{D.3}) \end{aligned}$$

where the wavenumber  $n$  in Eq. C.19 corresponds to  $2\pi/(L/k)$  with  $k = (1, 2, 3, 4)$ . The first coefficient,  $a_0 = 0$ , in Eq. C.19 because the mean of the fluctuation  $v'$  is zero,

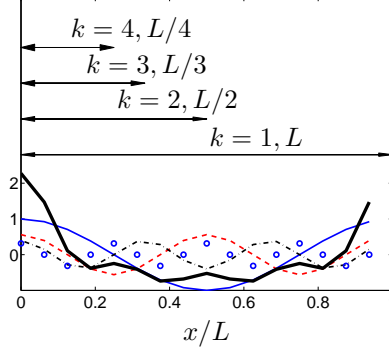


Figure D.1:  $v'$  in Eq. D.5 vs.  $x/L$ . —: term 1 ( $k = 1$ ); - - : term 2 ( $k = 2$ ); —: term 3 ( $k = 3$ ); ○: term 4 ( $k = 4$ ); thick line:  $v'$ . Matlab code is given in Section D.2.

i.e.

$$\int_0^L v' dx = 0 \quad (\text{D.4})$$

Equation Eq. D.3 is *continuous*, i.e. it is given for any  $x/L = [0, 1]$ . In unsteady CFD simulations we are always dealing with discrete points, i.e. a computational grid. Hence, let's express Eq. D.3 for  $N = 16$  discrete points with  $\Delta x = 1/(N - 1)$  as

$$v' = a_1^{0.5} \cos\left(\frac{2\pi(n-1)}{N/1}\right) + a_2^{0.5} \cos\left(\frac{2\pi(n-1)}{N/2}\right) \\ + a_3^{0.5} \cos\left(\frac{2\pi(n-1)}{N/3}\right) + a_4^{0.5} \cos\left(\frac{2\pi(n-1)}{N/4}\right) \quad (\text{D.5})$$

where  $(n-1)/N = x/L$  and  $n = [1, N]$ .

Now we want  $v'$  in Eq. D.5 to have an energy spectrum of  $-5/3$ . Parseval's formula, Eq. C.21, tells us that the kinetic energy of an eddy of wavenumber  $\kappa$  is simply the square of its Fourier coefficient. Hence we let the ratio of the  $a_k$  coefficients in Eq. D.5 decrease as  $k^{-5/3}$ , i.e.

$$a_1 = 1, \quad a_2 = 2^{-5/3}, \quad a_3 = 3^{-5/3}, \quad a_4 = 4^{-5/3} \quad (\text{D.6})$$

Figure D.1 shows how  $v'$  varies over  $x/L$ . The four terms in E. D.5 shown in Fig. D.1 can be regarded as the velocity fluctuations at one time instant of four eddies of length-scale  $L$ ,  $L/2$ ,  $L/3$  and  $L/4$ . The period of the four terms is  $L$ ,  $L/2$ ,  $L/3$ , and  $L/4$  corresponding to wavenumber  $2\pi/L$ ,  $2 \cdot 2\pi/L$ ,  $3 \cdot 3\pi/L$  and  $4 \cdot 2\pi/L$ .

Now let's make a DFT of the  $v'$  to get the energy spectrum (see Matlab code in Section D.2). In DFT, the integral in Eq. C.18

$$a_k = \frac{1}{\pi} \int_{-\pi}^{\pi} v'(x) \cos(\kappa x) dx = \frac{1}{\pi} \int_{-\pi}^{\pi} v'(x) \cos\left(\frac{2\pi k x}{L}\right) dx \quad (\text{D.7})$$

is replaced by a summation over discrete points, i.e.

$$A_k = \frac{1}{N} \sum_1^N v'(x) \cos\left(\frac{2\pi k(n-1)}{N}\right) \quad (\text{D.8})$$

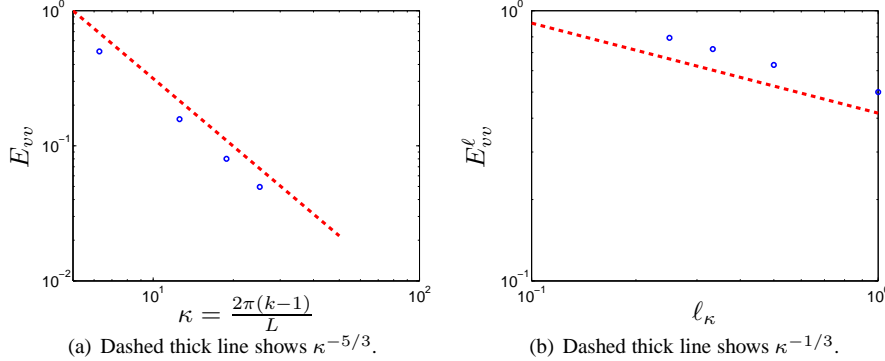


Figure D.2: Energy spectrum of  $v'$ .  $\circ$ :  $E_{vv} = A_k^2$ . Matlab code is given in Section D.2.

where  $(n - 1)/N = x/L$  (note that  $k = 0$  corresponds to the mean, which is zero, see Eq. D.4).

Now plot the energy spectrum,  $E_{vv} = A_k^2$  versus wavenumber, see Fig. D.2a. It can be seen that it decays as  $\kappa^{-5/3}$  as expected (recall that we chose the Fourier coefficients,  $a_k$ , to achieve this). The total energy is now computed as

$$\langle v'^2 \rangle_x = \sum_{k=1}^N A_k^2 = \sum_{k=1}^N E_{vv}(k) \quad (\text{D.9})$$

where  $\langle \cdot \rangle_x$  denotes averaging over  $x$ . Note that Eq. D.9 does not involve the wavenumber,  $\Delta\kappa$ , contrary to the continuous formulation in Eq. D.2. How come, then, that  $E_{vv}$  still decays as  $\kappa^{-5/3}$  and not as  $\kappa^{-2/3}$  as dimensional analysis of Eq. D.9 would give? The reason, as indicated at the end of Section D, is that  $E_{vv}$  is plotted versus the wavenumber which includes smaller and smaller eddies as it increases. This is best seen in Fig. D.1; as  $\kappa$  (indicated by  $k$  in Fig. D.1) increases, the turbulent length scale of the four eddies decreases as  $L, L/2, L/3, L/4$ . Hence,  $E_{vv}$  in Eq. D.9 decreases by one order of magnitude faster than expected ( $-5/3$  instead of  $-2/3$ ) because it is plotted versus a quantity ( $\kappa$ ) that includes smaller and smaller eddies as it increases.

Figure D.2b shows the computed energy spectrum,  $E^\ell(\ell_\kappa)$ , versus eddy size, see Matlab code in Section D.2. It decays as  $\ell_\kappa^{-1/3}$  as it should, see Eq. D.2.

## D.2 An example: Matlab code

```

close all
clear all

% number of cells
N=16;
L=1;

n=1:1:N;
x_over_L=(n-1)/N;

```

```
% E_vv=k^(-5/3)
a1=1;
a2=2^(-5/3);
a3=3^(-5/3);
a4=4^(-5/3);

for i=1:N
    arg2(i)=2*pi*(i-1)/N;
    arg2(i)=2*pi*x_over_L(i);
    v(i)=a1^0.5*cos(arg2(i))+a2^0.5*cos(2*arg2(i))+a3^0.5*cos(3*arg2(i))+a4^0.5*cos(4*arg2(i));
end

% take DFT
W_cos=zeros(1,N);
W_sin=zeros(1,N);
for k=1:N
    for i=1:N
        a=v(i);
        arg1=2*pi*(k-1)*(i-1)/N;
        W_cos(k)=W_cos(k)+a*cos(arg1)/N;
        W_sin(k)=W_sin(k)+a*sin(arg1)/N;
    end
end

% Note that all elements of W_sin are zero since v(i) is symmetric

%*****
figure(1)
f1=a1^0.5*cos(arg2);
f2=a2^0.5*cos(2*arg2);
f3=a3^0.5*cos(3*arg2);
f4=a4^0.5*cos(4*arg2);
plot(x_over_L,f1,'linew',2)
hold
plot(x_over_L,f2,'r--','linew',2)
plot(x_over_L,f3,'k-.','linew',2)
plot(x_over_L,f4,'o','linew',2)
plot(x_over_L,w,'k-','linew',4)

h=gca
set(h,'fontsiz',[20])
xlabel('x')
ylabel('y')
axis([0 1 -1 3])
print vprim_vs_L.ps -depsc2

%
```

```
%*****
%
figure(2)
%
% the power spectrum is equal to W*conj(W) = W_cos^2+W_sin^2
PW=W_cos.^2+W_sin.^2;

kx=2*pi*(n-1)/L;

% plot power spectrum; plot only one side of the symmetric spectrum and
% multiply by two so that all energy is accounted for
plot(kx(1:N/2),2*PW(1:N/2),'bo','linew',2)
hold
h=gca
set(h,'xscale','log')
set(h,'yscale','log')
axis([0 100 0.01 1])

% plot -5/3 line
xxx=[5 50];
yy0=1;
yyy(1)=yy0;
yyy(2)=yyy(1)*(xxx(2)/xxx(1))^-(-5/3);
plot(xxx,yyy,'r--','linew',4)

% compute the average of energy in physical space
int_phys=0;
for i=1:N
    int_phys=int_phys+v(i).^2/N;
end

% compute the average of energy in wavenumber space
int_wave=0;
for i=1:N
    int_wave=int_wave+PW(i);
end

set(h,'fontsi',[20])
xlabel('x')
ylabel('y')
print spectra_vs_kappa.ps -depsc2
%
%*****
%
figure(3)

% compute the length corresponding the wavenumber
lx=2*pi./kx;
```

```
% multiply PW by lx^(-2) to get the energy spectrum E(lx)
PW_L=PW.*lx.^(-2);

% plot power spectrum
plot(lx(1:N/2),2*PW_L(1:N/2),'bo','linew',2)
hold
h=gca
set(h,'xscale','log')
set(h,'yscale','log')

axis([0.1 3 .3 1])

% plot -1/3 line
xxx=[0.1 1]
ynnoll=0.9;
yyy(1)=ynnoll;
yyy(2)=yyy(1)*(xxx(2)/xxx(1))^{(-1/3)};
plot(xxx,yyy,'r--','linew',4);

set(h,'fontsi',[20])
xlabel('x')
ylabel('y')
print spectra_vs_L.ps -depsc2
```

## E TME225 Assignment 2: turbulent flow

In this exercise you will use data from a Direct Numerical Simulation (DNS) for fully developed channel flow. In DNS the unsteady, three-dimensional Navier-Stokes equations are solved numerically. The  $Re$  number based on the friction velocity and the half channel width is  $Re_\tau = u_\tau h/\nu = 500$  ( $h = \rho = u_\tau = 1$  so that  $\nu = 1/Re_\tau$ ).

A  $96 \times 96 \times 96$  mesh has been used. The streamwise, wall-normal and spanwise directions are denoted by  $x$  ( $x_1$ ),  $y$  ( $x_2$ ) and  $z$  ( $x_3$ ) respectively. The cell size in  $x$  and  $z$  directions are  $\Delta x = 0.0654$  and  $\Delta z = 0.0164$ . Periodic boundary conditions were applied in the  $x$  and  $z$  direction (homogeneous directions). All data have been made non-dimensional by  $u_\tau$  and  $\rho$ .

You can do the assignment on your own or in a group of two. You should write a report where you analyze the results following the heading E.1–E.11. It is recommended (but the not required) that you use L<sup>A</sup>T<sub>E</sub>X(an example of how to write in L<sup>A</sup>T<sub>E</sub>Xis available on the course www page). It is available on Linux. On Windows you can use, for example, MikTex ([www.miktex.org](http://www.miktex.org)) which is free to download.

### E.1 Time history

At [the course home page](http://www.tfd.chalmers.se/~lada/MoF/) <http://www.tfd.chalmers.se/~lada/MoF/> you find a file `u_v_time_4nodes.dat` with the time history of  $v_1$  and  $v_2$ . The file has eight columns of  $v_1$  and  $v_2$  at four nodes:  $x_2/\delta = 0.0039$ ,  $x_2/\delta = 0.0176$ ,  $x_2/\delta = 0.107$  and  $x_2/\delta = 0.47$ . With  $u_\tau = 1$  and  $\nu = 1/Re_\tau = 1/500$  this correspond to  $x_2^+ = 1.95$ ,  $x_2^+ = 8.8$ ,  $x_2^+ = 53.5$  and  $x_2^+ = 235$ . The sampling time step is  $\Delta t = 0.0033$  (every second time step). The four points are located in the viscous sublayer, the buffer layer and in the logarithmic layer, see Fig. 6.2 at p. 56.

Use the Matlab. You can also use Octave on Linux/Ubuntu. Octave is a Matlab clone which can be downloaded for free. Start the program `p1_time.m` which loads and plots the time history of  $v_1$ . Start Matlab and run the program `p1_time`. Recall that the velocities have been scaled with the friction velocity  $u_\tau$ , and thus what you see is really  $v_1/u_\tau$ . The time history of  $v_1$  at  $x_2/\delta = 0.0176$  and  $x_2/\delta = 0.107$  are shown. Study the time history of the blue line ( $x_2/\delta = 0.0176$ ) more in detail. Make a zoom between, for example,  $t = 10$  and  $t = 11$  and  $v_{1,min} = 3$  and  $v_{1,max} = 21$ . This is conveniently done with the command

```
axis([10 11 3 21])
```

In order to see the value at each sampling time step, change the plot command to

```
plot(t,u2,'b-',t,u2,'bo')
```

Use this technique to zoom, to look at the details of the time history. Alternatively, you can use the zoom buttons above the figure.

Plot  $v_1$  for all four nodes. How does the time variation of  $v_1$  vary for different positions? Plot also  $v_2$  at the four different positions. What is the differences between  $v_1$  and  $v_2$ ?

### E.2 Time averaging

Compute the average of the  $v_1$  velocity at node 2. Add the following code (before the plotting section)

```
umean=mean(u2)
```

Here the number of samples is  $n = 5000$  (the entire  $u2$  array). Find out how many samples must be used to get a correct mean value. Start by trying with 100 samples as

```
umean_100=mean(u2(1:100))
```

What is the maximum and minimum value of  $v_1$ ? Compare those to the mean.

Do the same exercise for the other three nodes.

Compute and plot also the instantaneous fluctuations;  $v'_1$  at node 1, for example, is computed as

```
u1_mean=mean(u1);
u1_fluct=u1-u1_mean;
```

### E.3 Mean flow

All data in the data files below have been stored every 10th time step.

Download the file `uvw_inst_small.mat`, `y.dat` and the Matlab file `p1_vel.m` which reads the data files. The data file includes  $v_1$ ,  $v_2$  and  $v_3$  from the same DNS as above, but now you are given the time history of all  $x_2$  nodes at one chosen  $x_1$  and  $x_3$  node. There are  $n_j = 98$  nodes in the  $x_2$  direction; node 1 and  $n_j$  are located at the lower and upper wall, respectively.

Your data are instantaneous. Compute the mean velocity. Plot it both as linear-linear plot and a log-linear plot (cf. Fig. 6.4).

In the log-linear plot, use  $x_2^+$  for the wall distance. Include the linear law,  $v_1^+ = x_2^+$ , and the log law,  $v_1^+ = \kappa^{-1} \ln x_2^+ + B$  ( $\kappa = 0.41$  is the von Kármán constant and  $B = 5.2$ ). How far out from the wall does the velocity profile follow the linear law? At what  $x_2^+$  does it start to follow the log-law?

Compute the bulk velocity

$$V_{1,b} = \frac{1}{2h} \int_0^{2h} \bar{v}_1 dx_2 \quad (\text{E.1})$$

(recall that  $h$  denote half the channel width) What is the Reynolds number based on  $V_{1,b}$  and centerline velocity,  $V_{1,c}$ , respectively?

### E.4 The time-averaged momentum equation

Let us time average the streamwise momentum equation. Since the flow is fully developed and two dimensional we get

$$0 = -\frac{1}{\rho} \frac{\partial \bar{p}}{\partial x_1} + \nu \frac{\partial^2 \bar{v}_1}{\partial x_2^2} - \frac{\partial \bar{v}'_1 \bar{v}'_2}{\partial x_2} \quad (\text{E.2})$$

This equation is very similar to fully developed laminar flow which you studied in Assignment 1, see Eq. 3.24; the difference is that we now have an additional term which is the derivative of the Reynolds shear stress. Recall that all terms in the equation above represent *forces* (per unit volume). Let us investigate how these forces (the pressure gradient, the viscous term and the Reynolds stress term) affect fluid particles located at different  $x_2$  locations. Compute and plot the three terms. (the file `uvw_inst_small.mat` does not include  $\bar{p}$ ; set  $\partial \bar{p} / \partial x = -1$ .)

If a term is positive it means that it pushes the fluid particle in the positive  $x_1$  direction. What about the viscous term? Is it always negative? Where is it largest? At that point? which term balances it? How large is the third term? The pressure term should be a *driving* force. Where is the Reynolds shear stress positive and where is it negative?

## E.5 Wall shear stress

Compute the wall shear stress at both walls. They should be equal. Are they?

## E.6 Resolved stresses

In Section E.3 you computed the mean velocities. From the instantaneous and the mean velocity, you can compute the fluctuations as

$$v'_i = v_i - \bar{v}_i \quad (\text{E.3})$$

Now you can easily compute all stresses  $\overline{v'_i v'_j}$ . Plot the normal stresses in one figure and the shear stresses in one figure (plot the stresses over the entire channel, i.e. from  $x_2 = 0$  to  $x_2 = 2h$ ). Which shear stresses are zero?

## E.7 Fluctuating wall shear stress

In the same way as the velocity, the wall shear stress can be decomposed into a mean value and a fluctuation. In general, any fluctuating variable,  $\phi$ , can be decomposed into a mean and fluctuation as  $\phi = \bar{\phi} + \phi'$ . The root-mean-square (RMS) is then defined as

$$\phi_{rms} = \left( \overline{\phi'^2} \right)^{1/2} \quad (\text{E.4})$$

Compute the RMS of the wall shear stress. This is a measure of the fluctuating tangential force on the wall due to turbulence. If heat transfer is involved, the fluctuating temperature at the wall inducing fluctuating heat transfer may be damaging to the material of the walls causing material fatigue. This is probably the most common form of fluid-solid interaction.

## E.8 Production terms

In order to understand why a stress is large, it is useful to look at its transport equation, see Eq. 9.12. Usually, a stress is large when its production term,  $P_{ij}$ , is large (there may be exceptions when other terms, such as the diffusion term, are largest). Plot the production terms for all non-zero stresses across the entire channel. Which ones are zero (or close to)? Does any production term change sign at the centerline? If so, what about the sign of the corresponding shear stress plotted in Section E.6?

## E.9 Pressure-strain terms

The pressure-strain term reads (see Eq. 9.14)

$$\Pi_{ij} = \overline{\frac{p'}{\rho} \left( \frac{\partial v'_i}{\partial x_j} + \frac{\partial v'_j}{\partial x_i} \right)} \quad (\text{E.5})$$

Our data are obtained from incompressible simulations, in which the pressure may vary unphysically in time ( $\partial p / \partial t$  does not appear in the equations). Hence, we prefer to compute the velocity-pressure gradient term

$$\Pi_{ij}^p = -\overline{\frac{v'_i}{\rho} \frac{\partial p'}{\partial x_j}} - \overline{\frac{v'_j}{\rho} \frac{\partial p'}{\partial x_i}}, \quad (\text{E.6})$$

see the second line in Eq. 9.3. The pressure diffusion term in the  $\overline{v'^2}$  equation – which is the difference between Eqs. E.5 and E.6 (the two first terms in Eq. 9.8) – is small except very close to the wall (see Figs. 9.2 and 9.3). Hence, the difference between  $\Pi_{ij}^p$  and  $\Pi_{ij}$  is small.

Download the data file `p_inst_small.mat` and the Matlab file `pl_press_strain.m` which reads the data file. The time histories of the pressure along five  $x_2$  lines  $[(x_1, x_2, x_3), (x_1 \pm \Delta x_1, x_2, x_3)$  and  $(x_1, x_2, x_3 \pm \Delta x_3)]$  are stored in this file. This allows you to compute all the three spatial derivatives of  $p'$ . Using the velocities stored in `uvw_inst_small.mat` (see Section E.3), you can compute all the terms in Eq. E.6.

Plot the pressure strain,  $\Pi_{ij}^p$ , for the three normal stresses and the shear stress across the channel. For which stresses is it negative and positive? Why?

Which term  $\Pi_{ij}^p$  is the largest source and sink term, respectively?

## E.10 Dissipation

The physical meaning of dissipation,  $\varepsilon$ , is transformation of turbulent kinetic energy into internal energy, i.e. increased temperature.

Download the files `y_half.dat`, `diss_inst.mat` and the Matlab file `pl_diss.m` which reads it. The data file includes the time history of the velocities along five  $x_2$  lines  $[(x_1, x_2, x_3), (x_1 \pm \Delta x_1, x_2, x_3)$  and  $(x_1, x_2, x_3 \pm \Delta x_3)]$  so that you can compute all spatial derivatives. The data cover only the lower half of the channel. Compute and plot

$$\varepsilon = \nu \overline{\frac{\partial v'_i}{\partial x_k} \frac{\partial v'_i}{\partial x_k}} \quad (\text{E.7})$$

see Eq. 8.14. Where is it largest? In which equation does this quantity appear?

Let us now consider the equations for the mean kinetic energy,  $K = \bar{v}_i \bar{v}_i / 2$  (Eq. 8.35) and turbulent kinetic energy,  $k = \overline{v'_i v'_i} / 2$  (Eq. 8.14). The dissipation in the  $K$  equation reads

$$\varepsilon_{mean} = \nu \overline{\frac{\partial \bar{v}_i}{\partial x_k} \frac{\partial \bar{v}_i}{\partial x_k}} \quad (\text{E.8})$$

The flow of kinetic energy between  $K$ ,  $k$  and  $\Delta T$  is illustrated in Fig. 8.5. The dissipations,  $\varepsilon$  and  $\varepsilon_{mean}$ , are defined in Eqs. E.7 and E.8, respectively. Compute and plot also  $\varepsilon_{mean}$  and  $P^k$ . Which is large and which is small? How is the major part of the kinetic energy transformed from  $K$  to  $\Delta T$ ? Is it transformed via  $k$  or directly from  $K$  to  $\Delta T$ ?

## E.11 Do something fun!

You have been provided with a lot of data which you have analyzed in many ways. Now think of some other way to analyze the data. There are many interesting things yet to be analyzed!

## F TME225 Learning outcomes 2012

### TME225 Learning outcomes 2012: week 1

1. Explain the difference between Lagrangian and Eulerian description
2. Watch the on-line lecture *Eulerian and Lagrangian Description, part 1 – 3* at  
[http://www.tfd.chalmers.se/~lada/flow\\_viz.html](http://www.tfd.chalmers.se/~lada/flow_viz.html)
  - i. Part 1 describes the difference between Lagrangian and Eulerian points and velocities.
  - ii. The formula  $\frac{\partial T}{\partial t} + v_i \frac{\partial T}{\partial x_i}$  is nicely explained in Part 2
3. Show which stress components,  $\sigma_{ij}$ , that act on the Cartesian surfaces of a quadrant (two dimensions). Show also the stress vector,  $t_i^{\hat{n}}$ . (see Fig. 1.2 and the Lecture notes of Toll & Ekh [3])
4. Show the relation between the stress tensor,  $\sigma_{ij}$ , and the stress vector,  $t_i^{\hat{n}}$ . (see the Lecture notes of Toll & Ekh [3])
5. Show that the product of a symmetric and an antisymmetric tensor is zero.
6. Explain the physical meaning of diagonal and off-diagonal components of  $S_{ij}$
7. Explain the physical meaning of  $\Omega_{ij}$
8. What is the definition of irrotational flow?
9. What is the physical meaning of irrotational flow?
10. Derive the relation between the vorticity vector and the vorticity tensor
11. Explain the physical meaning of the eigenvectors and the eigenvalues of the stress tensor (see Section 1.7 and the Lecture notes of Toll & Ekh [3])

## TME225 Learning outcomes 2012: week 2

1. Equation 1.3 states that mass times acceleration is equal to the sum of forces (per unit volume). Write out the momentum equation (without using the summation rule) for the  $x_1$  direction and show the surface forces and the volume force on a small, square fluid element (see lecture notes of Toll & Ekh [3]). Now repeat it for the  $x_2$  direction.
2. Derive the Navier-Stokes equation, Eq. 2.5 (use the formulas in the Formula sheet (it can be found on the course www page))
3. Simplify the Navier-Stokes equation for incompressible flow and constant viscosity (Eq. 2.7)
4. Derive the transport equation for the inner energy,  $u$ , Eq. 2.12 (again, use the Formula sheet). What is the physical meaning of the different terms?
5. Simplify the the transport equation for inner energy to the case when the flow is incompressible (Eq. 2.15).

## TME225 Learning outcomes 2012: week 3

1. Derive the transport equation for kinetic energy,  $v_i v_i / 2$ , Eq. 2.20. What is the physical meaning of the different terms?
2. Explain the energy transfer between kinetic energy and inner energy
3. Show how the left side of the transport equations can be written on conservative and non-conservative form
4. Starting from the Navier-Stokes equations (see Formula sheet), derive the flow equation governing the Rayleigh problem expressed in  $f$  and  $\eta$ ; what are the boundary conditions in time ( $t$ ) and space ( $x_2$ ); how are they expressed in the similarity variable  $\eta$ ?
5. Show how the boundary layer thickness can be estimated from the Rayleigh problem using  $f$  and  $\eta$  (Fig. 3.3)
6. Explain the flow physics at the entrance (smooth curved walls) to a plane channel
7. Explain the flow physics in a channel bend
8. Derive the flow equations for fully developed flow between two parallel plates, i.e. fully developed channel flow (Eqs. 3.18, 3.22 and 3.26)
9. Explain (using words and a figure) why vorticity can be created only by an imbalance (i.e. a gradient) of shear stresses. Explain why pressure cannot create vorticity.
10. The Navier-Stokes equation can be re-written on the form

$$\frac{\partial v_i}{\partial t} + \underbrace{\frac{\partial k}{\partial x_i}}_{\text{no rotation}} - \underbrace{\varepsilon_{ijk} v_j \omega_k}_{\text{rotation}} = -\frac{1}{\rho} \frac{\partial p}{\partial x_i} + \nu \frac{\partial^2 v_i}{\partial x_j \partial x_j} + f_i$$

Derive the transport equation (3D) for the vorticity vector, Eq. 4.20

11. Show that the divergence of the vorticity vector,  $\omega_i$ , is zero
12. Explain vortex stretching and vortex tilting
13. Show that the vortex stretching/tilting term is zero in two-dimensional flow
14. Derive the 2D equation transport equation for the vorticity vector from the 3D transport equation, Eq. 4.22
15. Show the similarities between the vorticity and temperature transport equations in fully developed flow between two parallel plates
16. Use the diffusion of vorticity to show that  $\frac{\delta}{\ell} \propto \sqrt{\frac{\nu}{U\ell}} = \sqrt{\frac{1}{Re}}$  (see also Eq. 3.14).
17. Watch the on-line lecture *Boundary layers parts 1* at  
[http://www.tfd.chalmers.se/~lada/flow\\_viz.html](http://www.tfd.chalmers.se/~lada/flow_viz.html)

- i. Consider the flow over the flat plate. How does the boundary layer thickness change when we move downstream?
- ii. What value does the fluid velocity take at the surface? What is this boundary conditions called: slip or no-slip? How do they define the boundary layer thickness?
- iii. How is the wall shear stress defined? How does it change when we move downstream? (how does this compare with the channel flow in TME075 Assignment 1?)
- iv. How is the circulation,  $\Gamma$ , defined? (cf. with Eq. 1.19) How is it related to vorticity? How do they compute  $\Gamma$  for a unit length ( $> \delta$ ) of the boundary layer? How large is it? How does it change when we move downstream on the plate?
- v. Where is the circulation (i.e. the vorticity) created? Where is the vorticity created in “your” channel flow (TME225 Assignment 1)? The vorticity is created at different locations in the flat-plate boundary layer and in the channel flow: can you explain why? (hint: in the former case

$$\frac{\partial p}{\partial x_1} = \mu \frac{\partial^2 v_1}{\partial x_2^2} \Big|_{wall} = 0,$$

but not in the latter; this has an implication for  $\gamma_{2,wall}$  [see Section 4.3])

- vi. How do they estimate the boundary layer thickness? (cf. Section 4.3.1)
18. Watch the on-line lecture *Boundary layers part 2* at  
[http://www.tfd.chalmers.se/~lada/flow\\_viz.html](http://www.tfd.chalmers.se/~lada/flow_viz.html)
  - i. How does the boundary layer thickness change at a given  $x$  when we increase the velocity? Explain why.
  - ii. Consider the flow in a contraction: what happens with the boundary layer thickness after the contraction?
  - iii. Why is the vorticity level higher after the contraction?
  - iv. Is the wall shear stress lower or higher after the contraction? Why?
  - v. Consider the flow in a divergent channel (a diffuser): what happens with the boundary layer thickness and the wall shear stress?
  - vi. What happens when the angle of the diffuser increases?
  - vii. What do we mean by a “separated boundary layer”? How large is the wall shear stress at the separation point?
  - viii. The second part of the movie deals with turbulent flow: we’ll talk about that in the next lecture (and the remaining ones).

## TME225 Learning outcomes 2012: week 4

1. Watch the on-line lecture *Boundary layers parts 2 (second half) & 3* at  
<http://www.tfd.chalmers.se/~lada/flowviz.html>
  - i. The flow is “tripped” into turbulence. How?
  - ii. When the flow along the lower wall of the diffuser is tripped into turbulent flow, the separation region is suppressed. Try to explain why.
  - iii. Two boundary layers – one on each side of the plate – are shown. The upper one is turbulent and the lower one is laminar. What is the difference in the two velocity profiles? (cf. my figures in the ‘summary of lectures’) Explain the differences.
  - iv. Why is the turbulent wall shear stress larger for the turbulent boundary layer? What about the amount of circulation (and vorticity) in the laminar and turbulent boundary layer? How are they distributed?
  - v. Consider the airfoil: when the boundary layer on the upper (suction) side is turbulent, stall occurs at a higher angle of incidence compared when the boundary layer is laminar. Why?
  - vi. Vortex generator are placed on the suction side in order to prevent or delay separation. Try to explain why separation is delayed.
2. What characterizes turbulence? Explain the characteristics. What is a turbulent eddy?
3. Explain the cascade process. How large are the largest scales? What is dissipation? What dimensions does it have? Which eddies extract energy from the mean flow? Why are these eddies “best” at extracting energy from the mean flow?
4. What are the Kolmogorov scales? Use dimensional analysis to derive the expression for the velocity scale,  $v_\eta$ , the length scale,  $\ell_\eta$  and the time scale,  $\tau_\eta$ .
5. Make a figure of the energy spectrum. The energy spectrum consists of three subregions: which? describe their characteristics. Show the flow of turbulent kinetic energy in the energy spectrum. Given the energy spectrum,  $E(\kappa)$ , how is the turbulent kinetic energy,  $k$ , computed? Use dimensional analysis to derive the  $-5/3$  Kolmogorov law.
6. What does isotropic turbulence mean?
7. How is the energy transfer from eddy-to-eddy,  $\varepsilon_\kappa$ , estimated? Show how the ratio of the large eddies to the dissipative eddies depend on the Reynolds number.
8. Describe the cascade process created by vorticity. Write the vortex stretching/tilting term in tensor notation. What is its physical meaning? Describe the physical process of vortex stretching which creates smaller and smaller eddies. Show and discuss the family tree of turbulence eddies and their vorticity. Show that in 2D flow the vortex stretching/tilting term vanishes.
9. Watch the on-line lecture *Turbulence part 1* at  
<http://www.tfd.chalmers.se/~lada/flowviz.html>

- i. Why does the irregular motion of wave on the sea not qualify as turbulence?
  - ii. How is the turbulence syndrome defined?
  - iii. The movie laminar shows flow in a pipe. The viscosity is decreased, and the pressure drop (i.e. the resistance, the drag, the loss) increases. Why? The viscosity is further decreased, and the pressure drop increases. Why? How does the characteristics of the water flow coming out of the pipe change due to the second decrease of viscosity?
  - iv. It is usually said that the flow in a pipe gets turbulent at a Reynolds number of 2300. In the movie they show that the flow *can* remain laminar up to 8 000. How do they achieve that?
  - v. Dye is introduced into the pipe. For laminar flow, the dye does not mix with the water; in turbulent flow it does. When the mixing occurs, what happens with the pressure drop?
10. Watch the on-line lecture *Turbulence part 2* at  
[http://www.tfd.chalmers.se/~lada/flow\\_viz.html](http://www.tfd.chalmers.se/~lada/flow_viz.html)
- i. Draw a laminar and turbulent velocity profile for pipe flow. What is the main difference? In which flow is the wall shear stress  $\tau_w = \mu \frac{\partial \bar{v}_1}{\partial x_2}$  largest, laminar or turbulent?
  - ii. In turbulent flow, the velocity near the wall is larger than in laminar flow. Why?
  - iii. Discuss the connection between mixing and the cross-stream (i.e.  $v'_2$ ) fluctuations.
  - iv. Try to explain the increased pressure drop in turbulent flow with the increased mixing.
  - v. The center part of the pipe is colored with blue dye and the wall region is colored with red dye: by looking at this flow, try to explain how turbulence creates a *Reynolds shear stress*.
  - vi. Two turbulent jet flows are shown, one at low Reynolds number and one at high Reynolds number. They look very similar in one way and very different in another way. Which scales are similar and which are different?
  - vii. The two turbulent jet flows have the same energy input and hence the same dissipation. Use this fact to explain why the smallest scales in the high Reynolds number jet must be smaller than those in the low Reynolds number jet.
  - viii. At the end of the presentation of the jet flow, they explain the *cascade process*.
  - ix. Explain the analogy of a water fall (cascade of water, the water passes down the cascade) and the turbulent cascade process.
11. Use the decomposition  $v_i = \bar{v}_i + v'_i$  to derive the time-averaged Navier-Stokes equation. A new terms appears: what is it called? Simplify the time-averaged Navier-Stokes equation for boundary layer. What is the total shear stress?

## TME225 Learning outcomes 2012: week 5

March 19, 2013

1. How is the friction velocity,  $u_\tau$ , defined? Define  $x_2^+$  and  $\bar{v}^+$ .
2. The wall region is divided into an inner and outer region. The inner region is furthermore divided into a viscous sublayer, buffer layer and log-layer. Make a figure and show where these regions are valid (Fig. 6.2)
3. What are the relevant velocity and length scales in the viscous-dominated region? Derive the linear velocity law in this region (Eq. 6.17). What are the suitable velocity and length scales in the inertial region? Derive the log-law.
4. In fully developed channel flow, the time-averaged Navier-Stokes consists only of three terms. Make a figure and show how the velocity and shear stress vary across the channel. After that, show how the three terms (i.e. their gradients plus the pressure gradient) vary across the channel. Which two terms balance each other in the outer region? Which terms drives (“pushes”) the flow in the  $x_1$  direction? Which two terms are large in the inner region? Which term drives the flow?
5. Consider fully developed channel flow. In which region (viscous sublayer, buffer layer or log-layer) does the viscous stress dominate? In which region is the turbulent shear stress large? Integrate the boundary layer equations and show that the total shear stress varies as  $1 - x_2/\delta$  (Eq. 6.15).
6. Derive the exact transport equation for turbulent kinetic energy,  $k$ . Discuss the physical meaning of the different terms in the  $k$  equation. Which terms do only transport  $k$ ? Which is the main source term? Main sink (i.e. negative source) term?
7. In the cascade process, we assume that the dissipation is largest at the smallest scales, i.e.  $\varepsilon(\kappa) \propto \kappa^{2/3}$ , see Eq. 8.18 at p. 68. Show this. For which eddies is the production largest? Why?
8. Watch the on-line lecture *Turbulence part 3* at  
[http://www.tfd.chalmers.se/~lada/flow\\_viz.html](http://www.tfd.chalmers.se/~lada/flow_viz.html)
  - i. The film says that there is a similarity of the small scales in a channel flow and in a jet flow. What do they mean?
  - ii. What happens with the small scales when the Reynolds number is increased? What happens with the large scales? Hence, how does the ratio of the large scales to the small scales change when the Reynolds number increases (see Eq. 5.16)
  - iii. In decaying turbulence, which scales dies first? The scenes of the clouds show this in a nice way.
  - iv. Even though the Reynolds number may be large, there are a couple of physical phenomena which may inhibit turbulence and keep the flow laminar: mention three.
  - v. Consider the flow in the channel where the fluid on the top (red) and the bottom (yellow) are separated by a horizontal partition. Study how the two fluids mix downstream of the partition. In the next example, the fluid on

the top is hot (yellow) **and light**, and the one at the bottom (dark blue) is cold (**heavy**); how do the fluids mix downstream of the partition, better or worse than in the previous example? This flow situation is called *stable stratification*. In the last example, the situation is reversed: cold, **heavy** fluid (dark blue) is moving on top of hot, **light** fluid (yellow). How is the mixing affected? This flow situation is called *unstable stratification*. Compare in meteorology where heating of the ground may cause unstable stratification or when *inversion* causes stable stratification. You can read about stable/unstable stratification in Section 12.1 at p. 109.

9. Given the exact  $k$  equation, give the equation for boundary-layer flow (Eq. 8.22). All spatial derivatives are kept in the dissipation term: why? In the turbulent region of the boundary layer, the  $k$  equation is dominated by two terms. Which ones? Which terms are non-zero at the wall?
10. Where is the production term,  $P^k = -\overline{v'_1 v'_2} \partial \bar{v}_1 / \partial x_2$ , largest? In order to explain this, show how  $-\overline{v'_1 v'_2}$  and  $\partial \bar{v}_1 / \partial x_2$  vary near the wall.

## TME225 Learning outcomes 2012: week 6

March 19, 2013

1. Discuss the difference of spatial transport of  $k$  and spectral transfer of  $k$ . Give an example of how they are combined in non-homogeneous turbulence. How is homogeneous turbulence defined?
2. Derive the exact transport equation for mean kinetic energy,  $K$ . Discuss the physical meaning of the different terms. One term appears in both the  $k$  and the  $K$  equations: which one? Consider the dissipation terms in the  $k$  and the  $K$  equations: which is largest? Why? Show where they appear in the energy spectrum.
3. Derive the exact transport equation for turbulent Reynolds stress,  $\overline{v'_i v'_j}$ . Take the trace of the  $\overline{v'_i v'_j}$  equation to obtain the  $k$  equation.
4. Show that the role of the convection and diffusion terms is purely to transport the quantity ( $k$  for example) and that they give no net effect except at the boundaries (use the Gauss divergence theorem)
5. Discuss the physical meaning of the different terms in the  $\overline{v'_i v'_j}$  equation.
6. Consider the pressure-strain term in the  $\overline{v'_i v'_j}$  equation. The *mean* normal stress can be defined as  $\overline{v'_{av}^2} = \overline{v'_i v'_i}/3$ ; what sign will the pressure-strain term have for normal stresses, respectively, larger and smaller than  $\overline{v'_{av}^2}$ ? What role does  $\Pi_{12}$  has? What sign? Why do we call the pressure-strain term the *Robin Hood* term?
7. Consider the dissipation term,  $\varepsilon_{12}$ , for the shear stress: how large is it?
8. Consider fully developed channel flow: how are the expressions for the production terms simplified? Which production terms are zero and non-zero, respectively? Consider the production term for  $\overline{v'_1 v'_2}$ : which sign does it have in the lower and upper part of the channel, respectively? Why is there no pressure-strain term in the  $k$  equation?
9. Consider the fully turbulent region in fully developed channel flow: which are the main source and sink terms in the  $\overline{v'_1^2}$ ,  $\overline{v'_2^2}$ ,  $\overline{v'_3^2}$  and  $\overline{v'_1 v'_2}$  equations? Which are the largest terms at the wall? Which terms are zero at the wall?
10. Consider channel flow and use physical reasoning to show that  $\overline{v'_1 v'_2}$  must be negative and positive in the lower and upper half of the channel, respectively. Is this consistent with the sign of  $P_{12}$ ?
11. Define the two-point correlation. How is it normalized? What is the physical meaning of the two-point correlation? How is it related to the largest eddies? How is the integral length scale defined?
12. Define the auto correlation. How is it normalized? What physical meaning does it have? The integral time scale is defined in analogy to the integral length scale: show how it is defined.

## TME225 Learning outcomes 2012: just for fun!

1. Watch the on-line lecture *Pressure field and acceleration part 1* at  
[http://www.tfd.chalmers.se/~lada/flow\\_viz.html](http://www.tfd.chalmers.se/~lada/flow_viz.html)
  - i. The water flow goes through the contraction. What happens with the velocity and pressure. Try to explain.
  - ii. Fluid particles become thinner and elongated in the contraction. Explain why.
  - iii. In the movie they show that the acceleration along  $s$ , i.e.  $V_s \frac{dV_s}{ds}$ , is related to the pressure gradient  $\frac{dp}{ds}$ . Compare this relation with the three-dimensional form of Navier-Stokes equations for incompressible flow, Eq. 2.7
2. Watch the on-line lecture *Pressure field and acceleration part 2* at  
[http://www.tfd.chalmers.se/~lada/flow\\_viz.html](http://www.tfd.chalmers.se/~lada/flow_viz.html)
  - i. Water flow in a manifold (a pipe with many outlets) is presented. The pressure decreases slowly downstream. Why?
  - ii. The bleeders (outlets) are opened. The pressure now increases in the downstream direction. Why?
  - iii. What is the stagnation pressure? How large is the velocity at a stagnation point?
  - iv. What is the static pressure? How can it be measured? What is the difference between the stagnation and the static pressures?
  - v. A venturi meter is a pipe that consists of a contraction and an expansion (i.e. a diffuser). The bulk velocities at the inlet and outlet are equal, but still the pressure at the outlet is lower than that at the inlet. There is a pressure drop. Why?
  - vi. What happens with the pressure drop when there is a separation in the diffuser?
  - vii. They increase the speed in the venturi meter. The pressure difference in the contraction region and the outlet increases. Since there is atmospheric pressure at the outlet, this means that the pressure in the contraction region must decrease as we increase the velocity of the water. Finally the water starts to boil, although the water temperature may be around  $10^\circ C$ . This is called cavitation (this causes large damages in water turbines).
  - viii. Explain how suction can be created by blowing in a pipe.
3. Watch the on-line lecture *Pressure field and acceleration part 3* at  
[http://www.tfd.chalmers.se/~lada/flow\\_viz.html](http://www.tfd.chalmers.se/~lada/flow_viz.html)
  - i. What is the Coanda effect?
  - ii. The water from the tap which impinges on the horizontal pipe attaches to the surface of the pipe because of the Coanda effect. How large is the pressure at the surface of the pipe relative to the surrounding pressure?
  - iii. Explain the relation between streamline curvature and pressure (cf. Section 3.2.1).

- iv. At the end of the contraction, there is an adverse pressure gradient ( $\partial p / \partial x > 0$ ). Explain why.

## G MTF270: Some properties of the pressure-strain term

In this Appendix we will investigate some properties of  $a_{ijkl}$  in Eq. 11.73 at p. 100.  
Introduce the two-point correlation function

$$B_{j\ell}(\mathbf{r}) = \overline{v'_j(\mathbf{x})v'_{\ell}(\mathbf{x} + \mathbf{r})}$$

Define the point  $\mathbf{x}' = \mathbf{x} + \mathbf{r}$  so that

$$B_{j\ell}(\mathbf{r}) = \overline{v'_j(\mathbf{x}' - \mathbf{r})v'_{\ell}(\mathbf{x}')} = \overline{v'_{\ell}(\mathbf{x}')v'_j(\mathbf{x}' - \mathbf{r})} = B_{\ell j}(-\mathbf{r})$$

We get

$$\frac{\partial B_{j\ell}(\mathbf{r})}{\partial r_i} = -\frac{\partial B_{\ell j}(-\mathbf{r})}{\partial r_i} \Rightarrow \frac{\partial^2 B_{j\ell}(\mathbf{r})}{\partial r_k \partial r_i} = \frac{\partial^2 B_{\ell j}(-\mathbf{r})}{\partial r_k \partial r_i} \quad (\text{G.1})$$

Since Eq. G.1 in the definition of  $a_{ijkl}$  in Eq. 11.73 is integrated over  $\mathbf{r}^3$  covering both  $\mathbf{r}$  and  $-\mathbf{r}$  (recall that  $v'_{\ell}$  and  $v'_j$  are separated by  $\mathbf{r}$ ),  $a_{ijkl}$  is symmetric with respect to index  $j$  and  $\ell$ , i.e.

$$a_{ijkl} = a_{iljk} \quad (\text{G.2})$$

Green's third formula (it is derived from Gauss divergence law) reads

$$\varphi(\mathbf{x}) = -\frac{1}{4\pi} \int_V \frac{\nabla^2 \varphi}{|\mathbf{y} - \mathbf{x}|} d\mathbf{y}^3 \quad (\text{G.3})$$

where the boundary integrals have been omitted. Setting  $\varphi = \overline{v'_{\ell}v'_j}$  in Eq. G.3 gives

$$\overline{v'_j v'_{\ell}} = -\frac{1}{4\pi} \int_V \frac{\partial^2 \overline{v'_{\ell}v'_j}}{\partial x_i \partial x_i} \frac{d\mathbf{y}^3}{|\mathbf{y} - \mathbf{x}|} = \frac{1}{2} a_{ijil} \quad (\text{G.4})$$

where the last equality is given by Equation 11.73.

## H MTF270: Galilean invariance

In [66] he found that the Leonard term  $L_{ij}$  and the cross term  $C_{ij}$  are not Galilean invariant by themselves, but only the sum  $L_{ij} + C_{ij}$  is. As a consequence, if the cross term is neglected, the Leonard stresses must not be computed explicitly, because then the modelled momentum equations do not satisfy Galilean invariance.

Below we repeat some of the details of the derivation given in [66]. Galilean invariance means that the equations do not change if the coordinate system is moving with a constant speed  $V_k$ . Let's denote the moving coordinate system by  $*$ , i.e.

$$x_k^* = x_k + V_k t, \quad t^* = t, \quad \bar{v}_k^* = \bar{v}_k + V_k \quad (\text{H.1})$$

By differentiating a variable  $\phi = \phi(t^*, x_i^*)$  we get

$$\begin{aligned} \frac{\partial \phi(x_i, t)}{\partial x_k} &= \frac{\partial x_j^*}{\partial x_k} \frac{\partial \phi}{\partial x_j^*} + \frac{\partial t^*}{\partial x_k} \frac{\partial \phi}{\partial t^*} = \frac{\partial \phi}{\partial x_k^*} \\ \frac{\partial \phi(x_i, t)}{\partial t} &= \frac{\partial x_k^*}{\partial t} \frac{\partial \phi}{\partial x_k^*} + \frac{\partial t^*}{\partial t} \frac{\partial \phi}{\partial t^*} = V_k \frac{\partial \phi}{\partial x_k^*} + \frac{\partial \phi}{\partial t^*}. \end{aligned} \quad (\text{H.2})$$

From Eq. H.2 it is easy to show that the Navier-Stokes (both with and without filter) is Galilean invariant [66, 167]. Transforming the material derivative from the  $(t, x_i)$ -coordinate system to the  $(t^*, x_i^*)$ -coordinate system gives

$$\begin{aligned} \frac{\partial \phi}{\partial t} + v_k \frac{\partial \phi}{\partial x_k} &= \frac{\partial \phi}{\partial t^*} + V_k \frac{\partial \phi}{\partial x_k^*} + (v_k^* - V_k) \frac{\partial \phi}{\partial x_k^*} \\ &= \frac{\partial \phi}{\partial t^*} + v_k^* \frac{\partial \phi}{\partial x_k^*}, \end{aligned}$$

It shows that the left hand side does not depend on whether the coordinate system moves or not, i.e. it is Galilean invariant.

Now, let's look at the Leonard term and the cross term. Since the filtering operation is Galilean invariant [66], we have  $\bar{v}_k^* = \bar{v}_k + V_k$  and consequently also  $v_k''^* = v_k''$ . For the Leonard and the cross term we get (note that since  $V_i$  is constant  $V_i = \bar{V}_i = \overline{V}_i$ )

$$\begin{aligned} L_{ij}^* &= \overline{\bar{v}_i^* \bar{v}_j^*} - \bar{v}_i^* \bar{v}_j^* = \overline{(\bar{v}_i + V_i)(\bar{v}_j + V_j)} - (\bar{v}_i + V_i)(\bar{v}_j + V_j) \\ &= \overline{\bar{v}_i \bar{v}_j} + \overline{\bar{v}_i} V_j + \overline{\bar{v}_j} V_i - \bar{v}_i \bar{v}_j - \bar{v}_i V_j - V_i \bar{v}_j \\ &= \overline{\bar{v}_i \bar{v}_j} - \bar{v}_i \bar{v}_j + V_j (\overline{\bar{v}_i} - \bar{v}_i) + V_i (\overline{\bar{v}_j} - \bar{v}_j) \\ &= L_{ij} - V_j \overline{v_i''} - V_i \overline{v_j''} \\ C_{ij}^* &= \overline{\bar{v}_i^* v_j''^*} + \overline{\bar{v}_j^* v_i''^*} = \overline{(\bar{v}_i + V_i)v_j''} + \overline{(\bar{v}_j + V_j)v_i''} = \\ &= \overline{\bar{v}_i v_j''} + \overline{v_j''} V_i + \overline{v_j v_i''} + \overline{v_i''} V_j = C_{ij} + \overline{v_j''} V_i + \overline{v_i''} V_j \end{aligned} \quad (\text{H.3})$$

From Eq. H.3 we find that the Leonard term and the cross term are different in the two coordinate systems, and thus the terms are not Galilean invariant. However, note that the sum is, i.e.

$$L_{ij}^* + C_{ij}^* = L_{ij} + C_{ij}. \quad (\text{H.4})$$

The requirement for the Bardina model to be Galilean invariant is that the constant must be one,  $c_r = 1$  (see Eq. 18.38). This is shown by transforming both the exact

$C_{ij}$  (Eq. 18.36) and the modelled one,  $C_{ij}^M$  (i.e. Eq. 18.37). The exact form of  $C_{ij}$  transforms as in Eq. H.3. The Bardina term transforms as

$$\begin{aligned} C_{ij}^{*M} &= c_r (\bar{v}_i^* \bar{v}_j^* - \bar{v}_i^* \bar{v}_j^*) \\ &= c_r [(\bar{v}_i + V_i)(\bar{v}_j + V_j) - \overline{(\bar{v}_i + V_i)} \overline{(\bar{v}_j + V_j)}] \\ &= c_r [\bar{v}_i \bar{v}_j - \overline{\bar{v}_i \bar{v}_j} - (\bar{v}_i - \bar{v}_i)V_j - (\bar{v}_j - \bar{v}_j)V_i] \\ &= C_{ij}^M + c_r [\overline{v''}_i V_j + \overline{v''}_j V_i]. \end{aligned} \quad (\text{H.5})$$

As is seen,  $C_{ij}^{*M} \neq C_{ij}^M$ , but here this does not matter, because provided  $c_r = 1$  the modelled stress,  $C_{ij}^M$ , transforms in the same way as the exact one,  $C_{ij}$ . Thus, as for the exact stress,  $C_{ij}$  (see Eq. H.4), we have  $C_{ij}^{*M} + L_{ij}^* = C_{ij}^M + L_{ij}$ . Note that in order to make the Bardina model Galilean invariant the Leonard stress *must* be computed explicitly.

## I MTF270: Computation of wavenumber vector and angles

For each mode  $n$ , create random angles  $\varphi^n$ ,  $\alpha^n$  and  $\theta^n$  (see Figs. I.1 and 25.1) and random phase  $\psi^n$ . The probability distributions are given in Table I.1. They are chosen so as to give a uniform distribution over a spherical shell of the direction of the wavenumber vector, see Fig. I.1.

### I.1 The wavenumber vector, $\kappa_j^n$

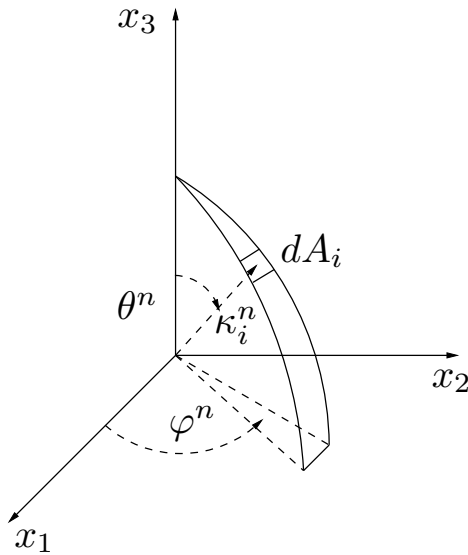


Figure I.1: The probability of a randomly selected direction of a wave in wave-space is the same for all  $dA_i$  on the shell of a sphere.

Compute the wavenumber vector,  $\kappa_j^n$ , using the angles in Section I according to Fig. I.1, i.e.

$$\begin{aligned}\kappa_1^n &= \sin(\theta^n) \cos(\varphi^n) \\ \kappa_2^n &= \sin(\theta^n) \sin(\varphi^n) \\ \kappa_3^n &= \cos(\theta^n)\end{aligned}\tag{I.1}$$

$p(\varphi^n) = 1/(2\pi)$	$0 \leq \varphi^n \leq 2\pi$
$p(\psi^n) = 1/(2\pi)$	$0 \leq \psi^n \leq 2\pi$
$p(\theta^n) = 1/2 \sin(\theta)$	$0 \leq \theta^n \leq \pi$
$p(\alpha^n) = 1/(2\pi)$	$0 \leq \alpha^n \leq 2\pi$

Table I.1: Probability distributions of the random variables.

$\kappa_i^n$	$\sigma_i^n$	$\alpha^n$
(1, 0, 0)	(0, 0, -1)	0
(1, 0, 0)	(0, 1, 0)	90
(0, 1, 0)	(0, 0, -1)	0
(0, 1, 0)	(-1, 0, 0)	90
(0, 0, 1)	(0, 1, 0)	0
(0, 0, 1)	(-1, 0, 0)	90

Table I.2: Examples of value of  $\kappa_i^n$ ,  $\sigma_i^n$  and  $\alpha^n$  from Eqs. I.1 and I.3.

## I.2 Unit vector $\sigma_i^n$

Continuity requires that the unit vector,  $\sigma_i^n$ , and  $\kappa_j^n$  are orthogonal. This can be seen by taking the divergence of Eq. 25.3 which gives

$$\nabla \cdot \mathbf{v}' = 2 \sum_{n=1}^N \hat{u}^n \cos(\kappa^n \cdot \mathbf{x} + \psi^n) \boldsymbol{\sigma}^n \cdot \boldsymbol{\kappa}^n \quad (\text{I.2})$$

i.e.  $\sigma_i^n \kappa_i^n = 0$  (superscript  $n$  denotes Fourier mode  $n$ ). Hence,  $\sigma_i^n$  will lie in a plane normal to the vector  $\kappa_i^n$ , see Fig. 25.1. This gives

$$\begin{aligned} \sigma_1^n &= \cos(\varphi^n) \cos(\theta^n) \cos(\alpha^n) - \sin(\varphi^n) \sin(\alpha^n) \\ \sigma_2^n &= \sin(\varphi^n) \cos(\theta^n) \cos(\alpha^n) + \cos(\varphi^n) \sin(\alpha^n) \\ \sigma_3^n &= -\sin(\theta^n) \cos(\alpha^n) \end{aligned} \quad (\text{I.3})$$

The direction of  $\sigma_i^n$  in this plane (the  $\xi_1^n - \xi_2^n$  plane) is randomly chosen through  $\alpha^n$ . Table I.2 gives the direction of the two vectors in the case that  $\kappa_i$  is along one coordinate direction and  $\alpha = 0$  and  $\alpha = 90^\circ$ .

## J MTF270: 1D and 3D energy spectra

The general two-point correlation  $B_{ij}$  of  $v'_i$  and  $v'_j$  (see Eq. 10.2) can be expressed by the energy spectrum tensor as [59, Chapter 3] (cf. Eq. 18.8)

$$B_{ij}(x_1, x_2, x_3) = \int_{-\infty}^{+\infty} \Psi_{ij}(\boldsymbol{\kappa}) \exp(i\kappa_m \hat{x}_m) d\kappa_1 d\kappa_2 d\kappa_3 \quad (\text{J.1})$$

where  $\hat{x}_m$  and  $\kappa_m$  are the separation vector the two points and the wavenumber vector, respectively. The complex Fourier transform  $\exp(i\kappa_m \hat{x}_m)$  is defined in Appendix C. The two-point correlation,  $B_{ij}$ , and the energy spectrum tensor,  $\Psi_{ij}$ , form a Fourier-transform pair

$$\Psi_{ij}(\boldsymbol{\kappa}) = \frac{1}{(2\pi)^3} \int_{-\infty}^{+\infty} B_{ij}(\hat{\mathbf{x}}) \exp(-i\kappa_m r_m) d\hat{x}_1 d\hat{x}_2 d\hat{x}_3 \quad (\text{J.2})$$

The separation between the two points is described by a general three-dimensional vector,  $\hat{x}_m$ . Both in experiments and in LES it is usually sufficient to study the two-point correlation and the energy spectra along a line. Hence, one-dimensional energy spectra,  $E_{ij}(\kappa)$ , which are a function of scalar wavenumber,  $\kappa$  ( $\kappa_1$ ,  $\kappa_2$  or  $\kappa_3$ ), are often used. They are formed by integrating over a wavenumber plane; the energy spectrum for the wavenumber  $\kappa_1$ , for example, reads

$$E_{ij}(\kappa_1) = \frac{1}{2} \int_{-\infty}^{+\infty} \Psi_{ij}(\boldsymbol{\kappa}) d\kappa_2 d\kappa_3 \quad (\text{J.3})$$

A factor of two is included because  $E \propto \Psi_{ii}/2$  is used to define a energy spectrum for the turbulent kinetic energy  $k = \overline{v'_i v'_i}/2$ , see Eqs. J.8 and J.10. Note that the maximum magnitude of the wavenumber vector contributing to  $E_{ij}(\kappa_1)$  is very large since it includes all  $\kappa_2$  and  $\kappa_3$ , i.e.  $-\infty < \kappa_2 < \infty$  and  $-\infty < \kappa_3 < +\infty$ . The one-dimensional two-point correlation,  $B_{ij}(\hat{x}_1)$ , for example, and the one-dimensional spectrum,  $E_{ij}(\kappa_1)$ , form a Fourier-transform pair, i.e.

$$B_{ij}(\hat{x}_1) = \frac{1}{2} \int_{-\infty}^{+\infty} E_{ij}(\kappa_1) \exp(i\kappa_1 \hat{x}_1) d\kappa_1 \quad (\text{J.4})$$

$$E_{ij}(\kappa_1) = \frac{2}{2\pi} \int_{-\infty}^{+\infty} B_{ij}(\hat{x}_1) \exp(-i\kappa_1 \hat{x}_1) d\hat{x}_1 \quad (\text{J.5})$$

where  $E_{ij}$  is *twice* the Fourier transform of  $B_{ij}$  because of the factor two in Eq. J.3. The diagonal components of the two-point correlation tensor are real and symmetric and hence the antisymmetric part of  $\exp(-i\kappa_1 \hat{x}_1)$  – i.e. the sinus part – is zero and Eqs. J.4 and J.5 are simplified as

$$\begin{aligned} B_{ij}(\hat{x}_1) &= \frac{1}{2} \int_{-\infty}^{+\infty} E_{ij}(\kappa_1) \cos(\kappa_1 \hat{x}_1) d\kappa_1 = \int_0^{\infty} E_{ij}(\kappa_1) \cos(\kappa_1 \hat{x}_1) d\kappa_1 \\ E_{ij}(\kappa_1) &= \frac{1}{\pi} \int_{-\infty}^{+\infty} B_{ij}(\hat{x}_1) \cos(\kappa_1 \hat{x}_1) d\hat{x}_1 = \frac{2}{\pi} \int_0^{+\infty} B_{ij}(\hat{x}_1) \cos(\kappa_1 \hat{x}_1) d\hat{x}_1 \end{aligned} \quad (\text{J.6})$$

The Reynolds stress  $\rho \overline{v'_1 v'_1}$ , for example, is equal to the two-point correlation tensor  $\rho B_{ij}$  with with zero separation distance. The  $\overline{v'_1 v'_1}$  can be computed both from the three-

dimensional spectrum (Eq. J.1) and one-dimensional spectrum (Eq. J.6)

$$\begin{aligned}\overline{v'_1^2} &= B_{11}(x_1, 0, 0) = \int_{-\infty}^{+\infty} \Psi_{ii}(\boldsymbol{\kappa}) d\kappa_1 d\kappa_2 d\kappa_3 \\ \overline{v'_1^2} &= B_{11}(0) = \int_0^\infty E_{11}(\kappa_1) d\kappa_1\end{aligned}\quad (\text{J.7})$$

Hence the turbulent kinetic energy,  $k = \overline{v'_i v'_i}/2$ , can be written as

$$k = \frac{1}{2} \int_{-\infty}^{+\infty} \Psi_{ii}(\boldsymbol{\kappa}) d\kappa_1 d\kappa_2 d\kappa_3 \quad (\text{J.8})$$

$$k = \frac{1}{2} \int_0^\infty E_{11}(\kappa_1) \kappa_1 + \frac{1}{2} \int_0^\infty E_{22}(\kappa_2) \kappa_2 + \frac{1}{2} \int_0^\infty E_{33}(\kappa_3) d\kappa_3 \quad (\text{J.9})$$

The integral in Eq. J.8 has no directional dependence: it results in a scalar,  $k$ . Instead of integrating over  $d\kappa_1 d\kappa_2 d\kappa_3$  we can integrate over a shell with radius  $\kappa$  and letting the radius go from zero to infinity, i.e.

$$k = \frac{1}{2} \int_0^\infty 4\pi\kappa^2 \Psi_{ii} d\kappa \quad (\text{J.10})$$

where  $4\pi\kappa^2$  is the surface area of the shell. We now define an energy spectrum,  $E(\kappa) = 4\pi\kappa^2 \Psi_{ii}$  so that

$$k = \int_0^\kappa E(\kappa) d\kappa \quad (\text{J.11})$$

where  $E(\kappa) = 2\pi\kappa^2 \Psi_{ii}(\kappa)$ .

The energy spectra  $E_{11}(\kappa_1)$  and  $E(\kappa)$ , for example, correspond to the square of the Fourier coefficient of the velocity fluctuation (see Parseval's formula, Eq. C.4), i.e.

$$\begin{aligned}E_{11}(\kappa_1) &= \hat{v}_1^2(\kappa_1) \\ E(\kappa) &= \frac{1}{2} (\hat{v}_1^2(\kappa) + \hat{v}_2^2(\kappa) + \hat{v}_3^2(\kappa))\end{aligned}\quad (\text{J.12})$$

Below the properties of the three energy spectra are summarized.

- The three-dimensional spectrum tensor,  $\Psi_{ij}(\boldsymbol{\kappa})$ , is a tensor which is a function of the wavenumber vector.
- The one-dimensional spectrum,  $E_{ij}(\kappa_1)$ , is a tensor which is a function of a scalar (one component of  $\kappa_m$ ).
- The energy spectrum,  $E(\kappa)$ , is a scalar which is a function of the length of the wavenumber vector,  $|\boldsymbol{\kappa}| \equiv \kappa$ .

## J.1 Energy spectra from two-point correlations

In connection to Eqs. J.4, J.5 and J.6 we stated that the one-dimensional energy spectra and the two-point correlations form Fourier-transform pairs. The proof is given in this section. The energy spectrum is given by the square of the Fourier coefficients, see Parseval's formula, Eq. C.4. Let  $\hat{u}$  be the Fourier coefficient of the velocity fluctuation  $u'$  in the  $x$  direction which is periodic with period  $L$ . Take the covariance of the Fourier

coefficients,  $\hat{u}(\kappa')$  and  $\hat{u}(\kappa)$  where  $\kappa$  and  $\kappa'$  denote two different wavenumbers and  $x$  and  $x'$  denote two points separated in the  $x$  directions so that

$$\begin{aligned}\langle \hat{u}(\kappa)\hat{u}(\kappa') \rangle &= \left\langle \frac{1}{L} \int_{-L}^L u(x) \exp(-i\kappa x) dx \frac{1}{L} \int_{-L}^L u(x') \exp(-i\kappa' x') dx' \right\rangle \\ &= \frac{1}{L^2} \int_{-L}^L \int_{-L}^L u(x) u(x') \exp(-i(\kappa x + \kappa' x')) dx dx' \end{aligned}\quad (\text{J.13})$$

where  $\langle \cdot \rangle$  denotes averaging over time; this equation corresponds to Eq. J.4 except the factor of two. Since we are performing a Fourier transform in  $x$  we must assume that this direction is homogeneous, i.e. all averaged turbulence quantities are independent of  $x$  and the two-point correlation is not dependent on  $x$  (or  $x'$ ) but only on the separation distance  $x - x'$ , see discussion in connection to Eq. 10.5. Hence we replace  $x'$  by  $y + x''$  so that

$$\begin{aligned}\langle \hat{u}(\kappa)\hat{u}(\kappa') \rangle &= \left\langle \frac{1}{L^2} \int_{-L}^L \left( \int_{-L-x}^{L-x} u(x) u(x + x'') \exp(-i(\kappa x + \kappa'(x + x''))) dx'' \right) dx \right\rangle \\ &= \left\langle \frac{1}{L} \int_{-L}^L \exp(-i(\kappa + \kappa')x) \left( \frac{1}{L} \int_{-L-x}^{L-x} B_{11}(x'') \exp(-i\kappa' x'') dx'' \right) dx \right\rangle\end{aligned}\quad (\text{J.14})$$

The second integral (in parenthesis) is the Fourier transform of the two-point correlation  $B_{11}$ , i.e.

$$\langle \hat{u}(\kappa)\hat{u}(\kappa') \rangle = \left\langle \hat{B}_{11}(x'') \frac{1}{L} \int_{-L}^L \exp(-i(\kappa + \kappa')x) dx \right\rangle\quad (\text{J.15})$$

where  $\hat{B}_{11}$  denotes the Fourier transform of  $B_{11}$  (cf. J.12) and since it does not depends on the spatial coordinate it has been moved out of the integral. Furthermore,  $\hat{B}_{11}$  is real and symmetric since  $B_{11}$  is real and symmetric. The remaining integral includes trigonometric function with wavelengths  $\kappa$  and  $\kappa'$ . They are orthogonal functions, see Appendix C, and the integral of these functions is zero unless  $\kappa = \kappa'$ . This integral in Eq. J.15 for  $\kappa = \kappa'$  is evaluated as (see ‘length of  $\psi_k$ ’ in Appendix C, Eq. C.13, and use  $\psi_1 = \cos(2\pi x/L)$ )

$$\begin{aligned}(\psi_1|\psi_1) &= \|\psi_1\|^2 = \int_{-L}^L \cos^2\left(\frac{2\pi x}{L}\right) dx \\ &= \left[ \frac{x}{2} + \frac{L}{8\pi} \sin\left(\frac{4\pi x}{L}\right) \right]_{-L}^L = L\end{aligned}\quad (\text{J.16})$$

Equation J.15 can now be written

$$\langle \hat{u}(\kappa)\hat{u}(\kappa) \rangle = \langle \hat{B}_{11}(x) \rangle\quad (\text{J.17})$$

Hence, it is seen that the Fourier transform of a two-point correlation (in this example  $\langle B_{11}(x_1) \rangle$ ) indeed gives the corresponding one-dimensional energy spectrum (in this example  $E_{11}(\kappa_1) = \langle (\hat{u}(\kappa))^2 \rangle$ ).

## K MTF270, Assignment 1: Reynolds averaged Navier-Stokes

### K.1 Two-dimensional flow

You can do the assignment on your own or in a group of two. It is recommended (but not required) that you use L<sup>A</sup>T<sub>E</sub>X(an example of how to write in L<sup>A</sup>T<sub>E</sub>Xis available on the course www page). It is available on Linux. On Windows you can use, for example, Lyx ([www.lyx.org](http://www.lyx.org)) or MikTex ([www.miktex.org](http://www.miktex.org)) which are both free to download.

You'll use data from a coarse DNS. Although some of the data are probably not fully accurate, in this exercise we consider the data to be exact. You will use Matlab. You can also use Octave on Linux/Ubuntu. Octave is a Matlab clone which can be downloaded for free. Use Matlab or Octave to read data files of the mean flow ( $\bar{v}_1$ ,  $\bar{v}_2$ ,  $\bar{p}$ ) and turbulent quantities. ( $v_1'^2$ ,  $v_2'^2$ ,  $v_3'^2$ ,  $v_1'v_2'$ , and  $\varepsilon$ ). You will analyze one of the following flows:

Case 1: Flow over a 2D hill.  $Re = 10\,595$  ( $\nu = 9.44 \cdot 10^{-5}$ ,  $\rho = 1$ ) based on the bulk velocity in the channel and the hill height.

Case 2: Flow over two small hills.  $Re = 10\,595$  ( $\nu = 9.44 \cdot 10^{-5}$ ,  $\rho = 1$ ) based on the bulk velocity bulk velocity in the channel and the height of the hill at the lower wall.

Case 3: Flow in a diverging/converging section  $Re = 18\,000$  ( $\nu = 5.56 \cdot 10^{-5}$ ,  $\rho = 1$ ) based on the bulk velocity in the channel and the width of the the channel.

Periodic boundary conditions are imposed in streamwise ( $x_1$ ) and spanwise ( $x_3$ ) directions in all flows.

The work should be carried out in groups of two (if you want to work on you own that is also possible). Contact the teacher to get a Case No. Download the data from [http://www.tfd.chalmers.se/~lada/comp\\_turb\\_model](http://www.tfd.chalmers.se/~lada/comp_turb_model). At the www-page you can download a M-file (`pl_vect.m`) which reads the data and plots the vector field and the pressure contours. You must also download the function `dphidx_dy.m` which computes the gradients. Make sure you put this function in the directory where you execute `pl_vect.m`.

The report, along with the Matlab files(s), should be submitted electronically at the Student Portal [www.student.portal.se](http://www.student.portal.se); the deadline can be found at the Student Portal.

### K.2 Analysis

Study the flow. In which regions do you expect the turbulence to be important?

Now let's find out. The two-dimensional time-averaged Navier-Stokes for the  $x_1$  momentum reads (the density is set to one, i.e.  $\rho = 1$ )

$$\frac{\partial \bar{v}_1 \bar{v}_1}{\partial x_1} + \frac{\partial \bar{v}_1 \bar{v}_2}{\partial x_2} = -\frac{\partial \bar{p}}{\partial x_1} + \nu \frac{\partial^2 \bar{v}_1}{\partial x_1^2} - \frac{\partial \bar{v}_1'^2}{\partial x_1} + \nu \frac{\partial^2 \bar{v}_1}{\partial x_2^2} - \frac{\partial \bar{v}_1' v_2'}{\partial x_2} \quad (\text{K.1})$$

Recall that all the terms on the right-hand side represent  $x$  components of forces per unit volume.

### K.2.1 The momentum equations

The file `p1_vect.m` loads the data file and plots the profiles of  $\bar{v}_1'^2$  at some  $x$  stations, the velocity vector field and a contour plot of velocity gradient  $\partial\bar{v}_1/\partial x_2$ . Compute all terms in Eq. K.1. You will need to compute the derivatives of e.g.  $\bar{v}_1$  and  $\bar{p}$ . In `p1_vect.m` the function `dphidx_dy.m` is used to compute  $\partial\bar{v}_1/\partial x_1$  and  $\partial\bar{v}_1/\partial x_2$ . Use this function to compute all derivatives that you need. Find two (or more)  $x_1$  locations (vertical grid lines) where the  $\bar{v}_1'^2$  stress is large and small, respectively. One way to find these locations is to use the Matlab `surf` command.

Assignment 1.1. Plot the stresses along vertical grid lines at these two locations using the Matlab command `plot(x,y)`. Please make sure that in your report the numbering on the axis and the text in the legend is large enough; you can use the command

```
h1=gca;
set(h1,'fontsize',[20]) %the number '20' gives the fontsize
```

The size of the labels and the title is similarly controlled by

```
xlabel('x/H','fontsize',[20])
ylabel('y/H','fontsize',[20])
title('velocity','fontsize',[20])
```

Assignment 1.2. Plot also all terms in Eq. K.1. To enhance readability you may omit the small terms or use two plots per vertical grid line. Make also a zoom near the walls. For example, for a  $x - y$  plot

```
plot(u,y,'linew',2) % linewidth=2
```

you may want to zoom in on  $y=[0 \ 0.01]$  and  $u=[-0.1 \ 0.4]$ ; this is achieved by

```
axis([-0.1 0.4 0 0.01])
```

The 'axis' command can be used together with any plot, e.g. with 'surf' and 'quiver'.

Which terms are negligible? Can you explain why they are negligible?

What about the viscous terms: where do they play an important role? Which terms are non-zero *at the wall*? (you can show that on paper).

So far we have looked at the  $\bar{v}_1$ -momentum equation. The database corresponds to a two-dimensional flow. Now let's think of the forces as vectors. The gradient of the normal stresses in the  $x_1 - x_2$  plane represent the force vector

$$\mathbf{F}_N = \left( -\frac{\partial \bar{v}_1'^2}{\partial x_1}, -\frac{\partial \bar{v}_2'^2}{\partial x_2} \right) \quad (\text{K.2})$$

and the corresponding force vector due to the shear stresses reads

$$\mathbf{F}_S = \left( -\frac{\partial \bar{v}_1' v_2'}{\partial x_2}, -\frac{\partial \bar{v}_1' v_2'}{\partial x_1} \right) \quad (\text{K.3})$$

Identify the first term in Eqs. K.2 and K.3 in the momentum equation for  $v_1$ , Eq. K.1. Write out the momentum equation also for  $\bar{v}_2$  and identify the other two terms in Eqs. K.2 and K.3. Note that  $\mathbf{F}_N$  and  $\mathbf{F}_S$  are forces per unit volume ( $[N/m^3]$ ).

Assignment 1.3. Plot the vector field  $\tau_N$  to find out some features. Zoom-in on interesting regions.

Assignment 1.4. Plot also vector fields of the shear stress,  $\tau_S$  (see Eq. K.3), the pressure gradient and the viscous terms. Zoom up in interesting regions. Anything interesting? When  $\overline{v_2'^2}$  reaches a maximum or a minimum along a grid line normal to the wall, what happens with the vector field? Zoom-in on interesting regions.

### K.2.2 The turbulent kinetic energy equation

The exact transport equation for the turbulent kinetic energy,  $k$ , reads

$$\begin{aligned} \frac{\partial}{\partial x_j} (\bar{v}_j k) &= \nu \frac{\partial^2 k}{\partial x_j \partial x_j} + P_k + D_k - \varepsilon \\ P_k &= -\overline{v_i' v_j'} \frac{\partial \bar{v}_i}{\partial x_j} \end{aligned} \quad (\text{K.4})$$

Assignment 1.5. Plot the production term along the two grid lines. Explain why it is large at some locations and small at others. The production term consists of the sum of four terms, two of which involve the shear stress while the other include the normal stresses. Compare the contributions due to the shear stress and the normal stresses.

Assignment 1.6. Plot the dissipation and compare it with the production. Do you have local equilibrium (i.e.  $P^k \simeq \varepsilon$ ) anywhere?

### K.2.3 The Reynolds stress equations

The modelled transport equation for the Reynolds stresses can be written as

$$\begin{aligned} \frac{\partial}{\partial x_k} \left( \bar{v}_k \overline{v_i' v_j'} \right) &= \nu \frac{\partial^2 \overline{v_i' v_j'}}{\partial x_k \partial x_k} + P_{ij} + \Phi_{ij} + D_{ij} - \varepsilon_{ij} \\ P_{ij} &= -\overline{v_i' v_k'} \frac{\partial \bar{v}_j}{\partial x_k} - \overline{v_j' v_k'} \frac{\partial \bar{v}_i}{\partial x_k} \end{aligned} \quad (\text{K.5})$$

The pressure-strain term,  $\Phi_{ij}$ , and the diffusion term,  $D_{ij}$ , need to be modelled. Here we use the models in Eqs. 11.87, 11.53, 11.86, 11.91 and 11.92.

1. In the damping function,  $f$  (see Eq. 11.88),  $|x_i - x_{i,n}|$  denotes the distance to the nearest wall. If, for example, the lower wall is the closest wall to node  $(I, J)$ , then

$$|x_i - x_{i,n}| = \{(x(I, J) - x(I, 1))^2 + (y(I, J) - y(I, 1))^2\}^{1/2} \quad (\text{K.6})$$

2. If we assume, again, that the lower wall is the closest wall to cell  $(I, J)$  and that the lower wall is horizontal, then  $n_{i,w} = (0, 1)$ . To compute  $n_{i,w}$  for the general case (see Eqs. 11.91 and 11.92), compute first the vector which is parallel to the wall,  $s_{i,w}$ , and compute then  $n_{i,w}$  from  $s_{i,w}$  (see Eq. K.11)

3. The diffusion terms  $D_{ij}$  and  $D^\varepsilon$  can be modelled using the Generalized Gradient Diffusion Hypothesis GGDH of [168]

$$D_{ij} = \frac{\partial}{\partial x_m} \left( c \bar{u}_k \bar{u}_m \frac{k}{\varepsilon} \frac{\partial \bar{v}'_i \bar{v}'_j}{\partial x_k} \right) \quad (\text{K.7})$$

This diffusion model can cause numerical problems, and the GGDH is then replaced by a simple eddy viscosity model

$$D_{ij} = \frac{\partial}{\partial x_m} \left( \frac{\nu_t}{\sigma_k} \frac{\partial \bar{v}'_i \bar{v}'_j}{\partial x_m} \right), \nu_t = C_\mu k^2 / \varepsilon \quad (\text{K.8})$$

The following constants should be used:

$$(c_\mu, c_1, c_2, c_{1w}, c_{2w}, \sigma_k) = (0.09, 1.5, 0.6, 0.5, 0.3, 1)$$

Assignment 1.7. Choose two stresses. Plot the different terms in the equations for one vertical grid line fairly close to the inlet (not too close!). Use the simple eddy viscosity model for the turbulent diffusion term. If the figure becomes too crowded, use two plots per vertical grid line or simply omit terms that are negligible. Try to explain why some terms are large and vice versa. Usually, a stress is large in locations where its production (or pressure-strain) term is large. Is that the case for you?

Assignment 1.8. Compute the stresses using the Boussinesq assumption, i.e.  $\bar{v}'_i \bar{v}'_j = -2\nu_t \bar{s}_{ij} + (2k/3)\delta_{ij}$  where  $\nu_t = c_\mu k^2 / \varepsilon$ . Compare the eddy-viscosity stresses with two of the Reynolds stresses from the database. Make also a zoom-in near walls.

When using the Boussinesq assumption the production of turbulent kinetic energy

$$P^k = 2\nu_t \bar{s}_{ij} \bar{s}_{ij} \quad (\text{K.9})$$

is always positive. The exact production of turbulent kinetic energy (see Eq. K.4) is usually positive. It can however become negative.

Assignment 1.9. Compute the exact production in Eq. K.4 in the entire domain to investigate if the production is negative anywhere. If so, explain why.

The reason why the eddy-viscosity production in Eq. K.9 must be positive is of course that neither  $\nu_t$  nor  $\bar{s}_{ij} \bar{s}_{ij}$  can go negative. Another way to explain this fact is that the modelled Reynolds stress,  $\bar{v}'_i \bar{v}'_j$ , and the strain rate tensor,  $\partial \bar{v}_i / \partial x_j$  are parallel. To find out to what degree the exact Reynolds stress and the strain rate are parallel, one can compute the eigenvectors.

Assignment 1.10. Compute the eigenvalues and eigenvectors of the strain tensor,  $\bar{s}_{ij}$ . The eigenvalues correspond to the normal strain in the direction of the eigenvectors (see Section 13). If the shear strains (i.e. the off-diagonal components) dominate, you will get eigenvectors in the direction  $\pm\pi/4 \pm \pi/2$  and if the normal strains (i.e. the diagonal components) dominate the direction of the eigenvectors will be along the  $x_1$  and  $x_2$  axes (explain why!). Plot the eigenvectors as a vector field. Our flow is 2D; thus we get two eigenvectors and two eigenvalues. Since the two eigenvectors are perpendicular to each other it is sufficient to plot one of them (for example, the eigenvectors  $(\pi/4, \pi/4)$ ,  $(-\pi/4, \pi/4)$ ,  $(-\pi/4, -\pi/4)$  and  $(\pi/4, -\pi/4)$ , all represent the same principal coordinate system). Zoom in on interesting regions.

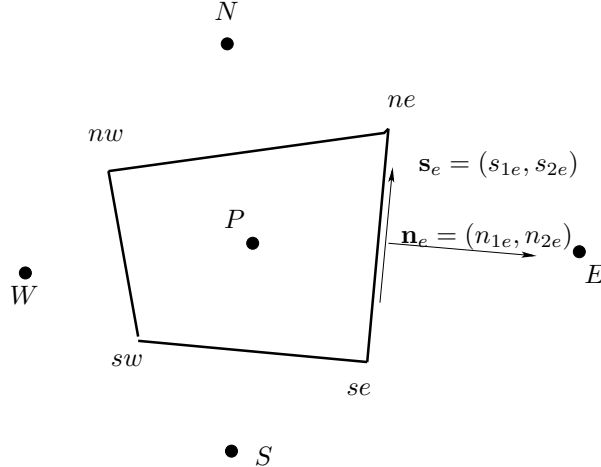


Figure K.1: *Control volume. The velocity  $v_1$  is stored at the corners (ne, nw, ...). Coordinates  $x_1, x_2$  are given at the corners (ne, nw, ...).*

Assignment 1.11. Compute the eigenvalues and eigenvectors of the Reynolds stresses,  $\overline{v'_i v'_j}$ . The eigenvalues correspond to the normal stresses in the direction of the eigenvectors. Zoom in on interesting regions. In which regions are the eigenvectors of the Reynolds stress tensor and those of the strain tensor not parallel? This should indicate regions in which an eddy-viscosity model would perform poorly. Zoom in on interesting regions.

### K.3 Compute derivatives on a curvi-linear mesh

In this appendix we describe how the derivatives on a curvi-linear grid are computed in the provided Matlab function `dphidx_dy.m`. On a Cartesian grid it is more convenient to use the built-in Matlab function `gradient`, but the approach used below works for all meshes, including Cartesian ones.

The data you have been given,  $x_1$  and  $x_2$  and all variables are stored at the grid points, i.e. at  $(x_{1,sw}, x_{2,sw})$ ,  $(x_{1,se}, x_{2,se})$ ,  $(x_{1,nw}, x_{2,nw})$  and  $(x_{1,ne}, x_{2,ne})$ . When you need a variable, say  $v_1$ , at the center of the cell, compute it as

$$v_{1,P} = \frac{1}{4}(v_{1,sw} + v_{1,se} + v_{1,nw} + v_{1,ne}) \quad (\text{K.10})$$

Let's compute  $\partial v_1 / \partial x_1$ . In order to do that we use Gauss' law over a control volume centered at face  $e$  (dashed control volume in Fig. K.1). The divergence theorem for a scalar,  $\phi$ , reads

$$\int_V \frac{\partial \phi}{\partial x_i} dV = \int_A \phi n_i dA$$

To compute  $\partial v_1 / \partial x_1$  we set  $\phi = v_1$  and  $i = 1$  which gives

$$\int_V \frac{\partial v_1}{\partial x_1} dV = \int_A v_1 n_1 dA$$

Assuming that  $\partial v_1 / \partial x_1$  is constant in the volume  $V$  we obtain

$$\frac{\partial v_1}{\partial x_1} = \frac{1}{V} \int_A v_1 n_1 dA$$

In discrete form we can write (see Fig. K.1)

$$\left( \frac{\partial v_1}{\partial x_1} \right) = \frac{1}{V} \sum_{i=e,n,w,w} (v_1 n_1 A)_i =$$

$$\frac{1}{V} \{ (v_1 A n_1)_e + (v_1 A n_1)_n + (v_1 A n_1)_w + (v_1 A n_1)_s \}$$

### K.3.1 Geometrical quantities

It is useful to first compute the unit vectors  $\mathbf{s}$  along the control volume. For the east face, for example, we get

$$s_{1e} = \frac{x_{1,ne} - x_{1,se}}{d_e}$$

$$s_{2e} = \frac{x_{2,ne} - x_{2,se}}{d_e}$$

$$d_e = \sqrt{(x_{1,ne} - x_{1,se})^2 + (x_{2,ne} - x_{2,se})^2}$$

(note that the area of the east face  $A_e$  is equal to  $d_e$  since  $\Delta z = 1$ ). The relation between the normal vector  $\mathbf{n}$ ,  $\mathbf{s}$  and the unit vector in the  $z$ -direction

$$\begin{aligned} \mathbf{s} \cdot \mathbf{n} &= 0 \\ \mathbf{s} \times \hat{z} &= \mathbf{n}, \end{aligned}$$

gives us the normal vector for the east face as

$$\begin{aligned} n_{1e} &= s_{2e} \\ n_{2e} &= -s_{1e}. \end{aligned} \tag{K.11}$$

## L MTF270, Assignment 2: LES

You can do the assignment on your own or in a group of two. You will receive data from a DNS of fully developed flow in a channel. It is recommended (but not required) that you use L<sup>A</sup>T<sub>E</sub>X(an example of how to write in L<sup>A</sup>T<sub>E</sub>Xis available on the course www page). It is available on Linux. On Windows you can use, for example, Lyx ([www.lyx.org](http://www.lyx.org)) or MikTex ([www.miktex.org](http://www.miktex.org)) which are both free to download.

The equations that have been solved are

$$\begin{aligned} \frac{\partial v_i}{\partial x_i} &= 0 \\ \frac{\partial v_i}{\partial t} + \frac{\partial}{\partial x_j} (v_i v_j) &= \delta_{i1} - \frac{\partial p}{\partial x_i} + \frac{1}{Re_\tau} \frac{\partial^2 v_i}{\partial x_j \partial x_j} \end{aligned} \quad (\text{L.1})$$

The *Re* number based on the friction velocity and the half channel width is  $Re_\tau = u_\tau h / \nu = 500$  ( $h = \rho = u_\tau = 1$  so that  $\nu = 1/Re_\tau$ ).

A  $96 \times 96 \times 96$  mesh has been used. The streamwise, wall-normal and spanwise directions are denoted by  $x$  ( $x_1$ ),  $y$  ( $x_2$ ) and  $z$  ( $x_3$ ) respectively. The cell size in  $x$  and  $z$  directions are  $\Delta x = 0.0654$  and  $\Delta z = 0.0164$ . Periodic boundary conditions were applied in the  $x$  and  $z$  direction (homogeneous directions). The size od the domain is  $(L, h, Z_{max})$  in  $(x, y, z)$ , see Fig.L.1.

At the www-page ([http://www.tfd.chalmers.se/~lada/comp\\_turb\\_model](http://www.tfd.chalmers.se/~lada/comp_turb_model)) you find data files with three instantaneous flow fields (statistically independent). The data files include the instantaneous variables  $u$  ( $v_1$ ),  $v$  ( $v_2$ ),  $w$  ( $v_3$ )and  $p$  (made non-dimensional by  $u_\tau$  and  $\rho$ ). Use Matlab to analyze the data. You can also use Octave on Linux/Ubuntu. Octave is a Matlab clone which can be downloaded for free. You find a Matlab/Octave program at the www-page which reads the data and computes the mean velocity. The data files are Matlab binary files. Since the data files are rather large, it is recommended that you do all tasks using only data files '1'. When everything works, then use also data files '2' and '3' averaging by use of the three files.

### L.1 Task 2.1

We decompose the instantaneous variables in time-averaged and fluctuating quantities as

$$v_i = \langle v_i \rangle + v'_i, \quad p = \langle p \rangle + p'$$

The symbol  $\langle \cdot \rangle$  denotes averaging in the homogeneous directions  $x$  and  $z$ . Note that in reality  $\langle \cdot \rangle$  always denote time averaging. It is only in this special academic test case where we have *three* homogeneous directions  $(x, z, t)$  where we can – in addition to time averaging – also can use  $x$  and  $z$  averaging. Compute the six stresses of the stress tensor,  $\langle v'_i v'_j \rangle$ . Use the definition to compute the stresses, for example

$$\begin{aligned} \langle v'_1 v'_2 \rangle &= \langle (v_1 - \langle v_1 \rangle) (v_2 - \langle v_2 \rangle) \rangle \\ &= \langle v_1 v_2 \rangle - \langle v_1 \langle v_2 \rangle \rangle - \langle v_2 \langle v_1 \rangle \rangle + \langle \langle v_1 \rangle \langle v_2 \rangle \rangle \\ &= \langle v_1 v_2 \rangle - 2\langle v_1 \rangle \langle v_2 \rangle + \langle v_1 \rangle \langle v_2 \rangle = \langle v_1 v_2 \rangle - \langle v_1 \rangle \langle v_2 \rangle. \end{aligned} \quad (\text{L.2})$$

Wait with analysis of the results till you have done next part.

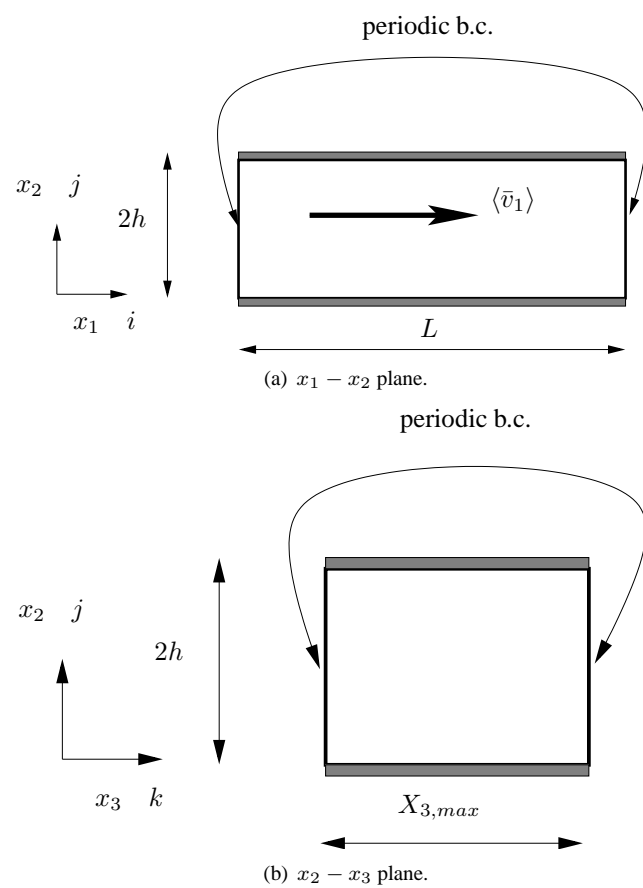


Figure L.1: Channel domain.

## L.2 Task 2.2

Compute the production term and the pressure-strain terms

$$\begin{aligned} P_k &= -\langle v'_1 v'_2 \rangle \frac{\partial \langle v_1 \rangle}{\partial y} \\ P_{11} &= -2 \langle v'_1 v'_2 \rangle \frac{\partial \langle v_1 \rangle}{\partial y} \\ P_{12} &= -\langle v'_2 v'_2 \rangle \frac{\partial \langle v_1 \rangle}{\partial y} \\ \Phi_{11} &= 2 \left\langle p' \frac{\partial v'_1}{\partial x} \right\rangle \\ \Phi_{12} &= \left\langle p' \frac{\partial v'_1}{\partial y} \right\rangle + \left\langle p' \frac{\partial v'_2}{\partial x} \right\rangle \\ \Phi_{22} &= 2 \left\langle p' \frac{\partial v'_2}{\partial y} \right\rangle \end{aligned}$$

Do the production terms and the pressure-strain term appear as you had expected? (see the previous course MTF256)

Now analyze the fluctuations in the previous subsection. Which stresses do you think are symmetric with respect to the centerline? or anti-symmetric? What's the reason?

When averaging, we use only three time steps (three files). If we would use many more time steps – or, in general, if we let  $T \rightarrow \infty$  when time averaging, e.g.

$$\langle \phi \rangle = \lim_{T \rightarrow \infty} \frac{1}{2T} \int_{-T}^{+T} \phi dt$$

then some of the stresses would be zero: which ones? Why?

## L.3 Task 2.3

Plot  $v_1$  and  $v_2$  along  $x_1$  at two different  $x_2$  values at  $x_3 = x_{3,max}/2$ .

1. Filter  $v_1$  and  $v_2$  to get  $\bar{v}_1$  and  $\bar{v}_2$  using a 1D box-filter (in the  $x_1$  direction) with filter width  $\Delta = 2\Delta x_1$  (this corresponds to a test filter, see Eq. 18.26. Compare  $\bar{v}_1$  and  $\bar{v}_2$  with  $v_1$  and  $v_2$ ).
2. Do the same thing again but with a filter width of  $\Delta = 4\Delta x_1$  (now you must derive the expression on your own!). Discuss the differences between no filter,  $\Delta = 2\Delta x_1$  and  $\Delta = 4\Delta x_1$ .

In LES we almost always assume that the filter width is equal to the control volume (i.e. we use an *implicit* filter). Above, in Item 1 and 2 you have just carried out *explicit* filtering.

Repeat Item 1, but now for a 2D filter ( $x_1$  and  $x_3$  direction); the formula for a 3D filter is given in Eq. 18.27. Compare the results along the same lines as in Item 1 and 2.

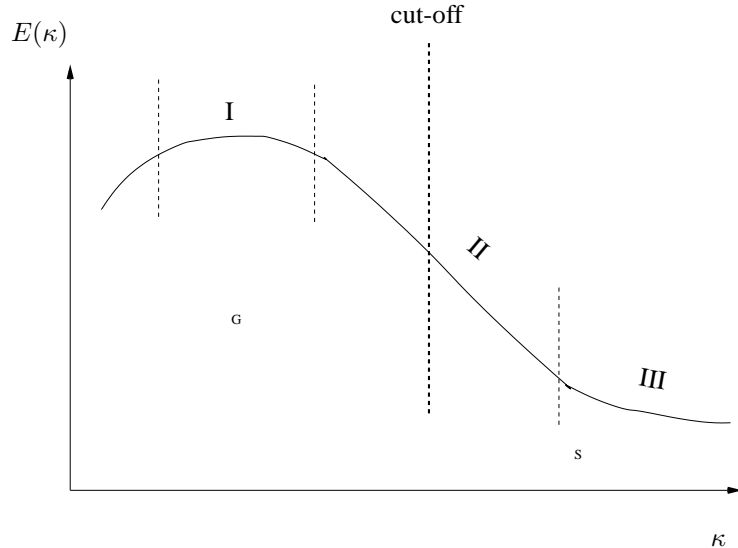


Figure L.2: Spectrum with cut-off.

## L.4 Task 2.4

Compute the SGS stress  $\tau_{12}$  from the Smagorinsky model, which reads

$$\begin{aligned}\tau_{ij} &= -2\nu_{sgs}\bar{s}_{ij}, \quad \nu_{sgs} = (C_s f_\mu \Delta)^2 \sqrt{2\bar{s}_{ij}\bar{s}_{ij}} \\ \bar{s}_{ij} &= \frac{1}{2} \left( \frac{\partial \bar{v}_i}{\partial x_j} + \frac{\partial \bar{v}_j}{\partial x_i} \right) \\ f_\mu &= 1 - \exp(-x_2^+/26)\end{aligned}\tag{L.3}$$

The filtered velocities,  $\bar{v}_i$ , are taken from Task 2.3 using the 2D filter (in  $x_1$  and  $x_3$ ); we should really have used a 3D filter, but in order to keep it simple, we use the 2D filter. Before doing the 2D filter, look in the Lecture Notes how a 3D filter is done. The constant  $C_s = 0.1$ .

Compare the SGS stress  $\langle \tau_{12} \rangle$  with the resolved stress  $\langle u'v' \rangle$  and compare the SGS viscosity with the physical one. Plot them across the channel. Any thoughts?

As an alternative to the damping function,  $f_\mu$ , compute the filter length as

$$\Delta = \min\{\kappa n, \Delta\}\tag{L.4}$$

where  $n$  is the distance to the nearest wall and  $\kappa = 0.4$  (von Kàrmàn constant). In this case you should set  $f_\mu = 1$ .

## L.5 Task 2.5

Repeat the Task 2.4, but now for the WALE model by [169], which reads

$$\begin{aligned} g_{ij} &= \frac{\partial \bar{v}_i}{\partial x_j}, \quad g_{ij}^2 = g_{ik}g_{kj} \\ \bar{s}_{ij}^d &= \frac{1}{2}(g_{ij}^2 + g_{ji}^2) - \frac{1}{3}\delta_{ij}g_{kk}^2 \\ \nu_{sgs} &= (C_m \Delta)^2 \frac{(\bar{s}_{ij}^d \bar{s}_{ij}^d)^{3/2}}{(\bar{s}_{ij} \bar{s}_{ij})^{5/2} + (\bar{s}_{ij}^d \bar{s}_{ij}^d)^{5/4}} \end{aligned} \quad (\text{L.5})$$

with  $C_m = 0.325$  which corresponds to  $C_s = 0.1$ .

## L.6 Task 2.6

Compute the dissipation

$$\varepsilon = \nu \left\langle \frac{\partial v'_i}{\partial x_j} \frac{\partial v'_j}{\partial x_i} \right\rangle$$

and plot  $\varepsilon$  across the channel.

In LES we introduce a filter which is assumed to cut off the spectrum at  $\kappa_c$  in the inertial region, see Fig. L.2. At cut-off, kinetic energy is extracted from the resolved flow by the SGS dissipation  $\varepsilon_{sgs}$ . Since the cut-off is assumed to be located in the inertial sub-range (II), the SGS dissipation is at high  $Re$  numbers equal to the dissipation.

Introduce a 2D filter ( $2\Delta x_1$  and  $2\Delta x_3$ ) as in Tasks 2.3 & 2.4 and filter all velocities to obtain  $\bar{v}_1$ ,  $\bar{v}_2$  and  $\bar{v}_3$ . Compute the SGS stresses from the definition

$$\tau_{ij} = \bar{v}_i \bar{v}_j - \bar{v}_i \bar{v}_j \quad (\text{L.6})$$

and compute the SGS dissipation

$$\varepsilon_{sgs} = -\langle \tau_{ij} \frac{\partial \bar{v}_i}{\partial x_j} \rangle \quad (\text{L.7})$$

Now, what is the relation between  $\varepsilon_{sgs}$  and  $\varepsilon$ ? Considering the cascade process, what did you expect?

Recall that when we do traditional Reynolds decomposition, the production term in the equation for turbulent kinetic energy appears as a sink term in the equation for the mean kinetic energy, see Eq. 8.35. This is the case also in LES, but now we have a decomposition into time-averaged filtered velocity,  $\langle \bar{v}_i \rangle$ , resolved fluctuation,  $\bar{v}'_i$ , and SGS fluctuation,  $v''_i$ , i.e.

$$v_i = \bar{v}_i + v''_i = \langle \bar{v}_i \rangle + \bar{v}'_i + v''_i \quad (\text{L.8})$$

Now we have three equations for kinetic energy:  $\bar{K} = \frac{1}{2}\langle \bar{v}_i \rangle \langle \bar{v}_i \rangle$ ,  $\bar{k} = \frac{1}{2}\langle \bar{v}'_i \bar{v}'_i \rangle$  and  $k_{sgs} = \frac{1}{2}\langle v''_i v''_i \rangle$ . The flow of kinetic energy can be illustrated as in Fig. L.3 (cf. Fig. 20 in [75])

The transport equation for  $\langle \frac{1}{2}\bar{v}'_i \bar{v}'_i \rangle$  is derived in [15]. (can be downloaded from [www.tfd.chalmers.se/~lada](http://www.tfd.chalmers.se/~lada)).

When deriving the  $k_{sgs}$  equation, no decomposition into time-averaged,  $\langle \bar{v}_i \rangle$ , and resolved fluctuations,  $\bar{v}'_i$ , is made. Hence the SGS dissipation in Eq. L.7 appears as an instantaneous production term in the equation for  $k_{sgs}$  [76, 77, ] (can be downloaded from [www.tfd.chalmers.se/~lada](http://www.tfd.chalmers.se/~lada)).

Plot (along  $x_2$ ), compare and discuss the four dissipations (see Fig. L.3)

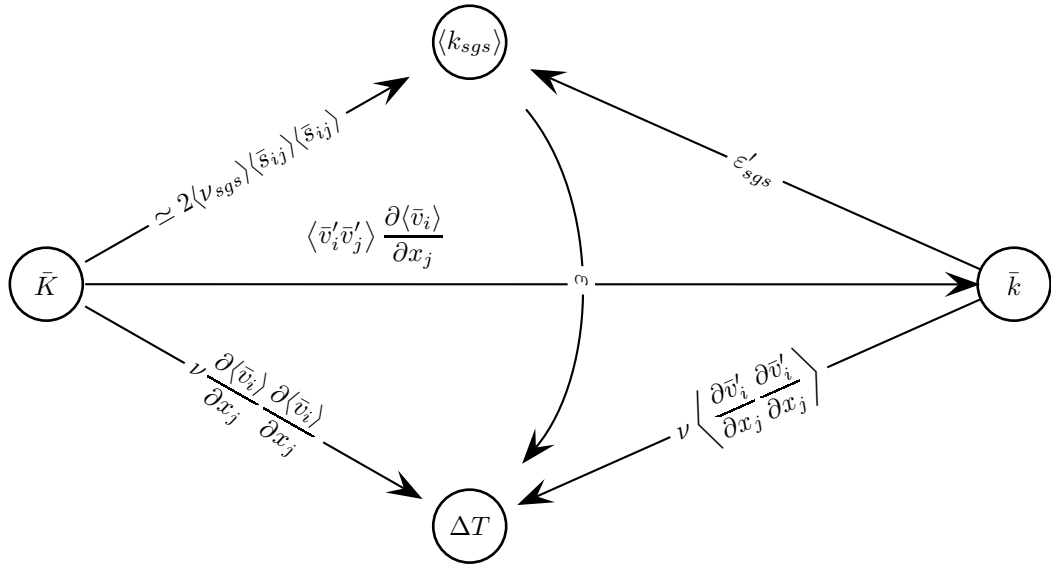


Figure L.3: Transfer of kinetic turbulent energy.  $\bar{K} = \frac{1}{2} \langle \bar{v}_i \rangle \langle \bar{v}_i \rangle$  and  $\bar{k} = \frac{1}{2} \langle \bar{v}'_i \bar{v}'_i \rangle$  denote time-averaged kinetic and resolved turbulent kinetic energy, respectively.  $\Delta T$  denotes increase in internal energy, i.e. dissipation.

$\langle \bar{v}'_1 \bar{v}'_2 \rangle \frac{\partial \langle \bar{v}_1 \rangle}{\partial x_2}$ : dissipation (which is equal to production with minus sign) by resolved turbulence in the  $\bar{K}$  equation

$\varepsilon'_{sgs} = \left\langle \left( \nu_{sgs} \frac{\partial \bar{v}_i}{\partial x_j} \frac{\partial \bar{v}_j}{\partial x_i} \right)' \right\rangle \simeq \langle \nu_{sgs} \frac{\partial \bar{v}'_i}{\partial x_j} \frac{\partial \bar{v}'_j}{\partial x_i} \rangle$ : SGS dissipation term in the  $\bar{k}$  equation. This is the *modelled* SGS dissipation. The exact SGS dissipation is computed as (since  $\varepsilon'_{sgs}$  is a product of two fluctuating quantities, we compute it with the same formula as in Eq. L.2)

$$\varepsilon'_{sgs} = \left\langle -\tau'_{ij} \frac{\partial \bar{v}'_i}{\partial x_j} \right\rangle = - \left\langle \tau_{ij} \frac{\partial \bar{v}_i}{\partial x_j} \right\rangle + \langle \tau_{ij} \rangle \frac{\partial \langle \bar{v}_i \rangle}{\partial x_j} \quad (\text{L.9})$$

Note that  $\varepsilon'_{sgs}$  is defined using the *fluctuating* velocity gradient (see [15]<sup>4</sup>), contrary to  $\varepsilon_{sgs} = P_{k_{sgs}}$  in Eq. L.7.

$\nu \left\langle \frac{\partial \bar{v}'_i}{\partial x_j} \frac{\partial \bar{v}'_i}{\partial x_j} \right\rangle$ : viscous dissipation term in the  $\bar{k}$  equation

$\left\langle \nu_{sgs} \frac{\partial \bar{v}_1}{\partial x_2} \right\rangle \frac{\partial \langle \bar{v}_1 \rangle}{\partial x_2} \simeq \langle \nu_{sgs} \rangle \left( \frac{\partial \langle \bar{v}_1 \rangle}{\partial x_2} \right)^2$ : SGS dissipation term in the  $\bar{K}$  equation.

## L.7 Task 2.7

Above the filtered velocities were computed using the filter width  $\Delta = 2\Delta x_1$ . In dynamic models, we often define the test filter as twice the usual filter, i.e.  $\widehat{\Delta} = 2\Delta$ .

<sup>4</sup>can be downloaded from course home page

Use this definition (1D filter, i.e.  $\widehat{\Delta} = 4\Delta x_1$ ) to compute the dynamic Leonard stress  $\langle \mathcal{L}_{12} \rangle$  from the definition

$$\mathcal{L}_{ij} = \widehat{\bar{v}_i \bar{v}_j} - \widehat{\bar{v}_i} \widehat{\bar{v}_j} \quad (\text{L.10})$$

and compare it (across the channel) with the resolved stress  $\langle v'_1 v'_2 \rangle$  and the SGS stress  $\langle \tau_{12} \rangle$  defined in Eq. L.6. Do you expect the magnitude of stresses to be similar?

## L.8 Task 2.8

What is the near-wall behavior of  $\langle v_1 \rangle$ ,  $\langle v_1'^2 \rangle$  and  $\langle v_2'^2 \rangle$  (i.e., for  $v_1$ , what is  $m$  in  $\langle v_1 \rangle = \mathcal{O}(x_2^m)$ ). In order to estimate  $m$ , plot the quantities in log-log coordinates. Do the quantities exhibit the near-wall behaviour that you expected?

## L.9 Task 2.9

The two-point correlation for  $u'$

$$B_{11}(x_2, \zeta_m) = \frac{1}{96 \times 96} \sum_{I=1}^{96} \sum_{K=1}^{96} v'_1(x_1^I, x_2, x_3^K) v'_1(x_1^I, x_2, x_3^K - \zeta_m) \quad (\text{L.11})$$

where  $x_3^K$  and  $\zeta_m$  are the spanwise locations of the two points. Take advantage of the fact that the flow is periodic, but be careful when integrating the correlation above in the  $x_3$  direction. We have 96 cells in the  $x_3$  direction. If, for example,  $\zeta_m = 2\Delta x_3$ , and one of the points ( $x_3^1$ ) is at  $K = 1$  then the other ( $x_3^1 - 2\Delta$ ) is at  $K = 95$ .

Plot the two-point correlation at a couple of  $x_2$  positions. When plotting two-point correlations, it is no point showing both symmetric parts; show only half of it (cf. the two-point correlations in Section 10.1 and Fig. M.1).

Compute and plot the integral length scale,  $\mathcal{L}_1$ , which is defined by

$$\mathcal{L}_1(x_2) = \frac{1}{v_{1,rms}^2} \int_0^\infty B_{11}(x_2, \zeta) d\zeta \quad (\text{L.12})$$

Compute also  $\mathcal{L}_3$ . What's the difference between  $\mathcal{L}_1$  and  $\mathcal{L}_3$ ?

## L.10 Task 2.10

The energy spectrum of any second moment can be obtained by taking the FFT of the corresponding two-point correlation. The energy spectrum of any second moment can be obtained by taking the FFT of the corresponding two-point correlation. You can find some details on how to use Matlab's FFT in Appendix M.

If you have computed the Fourier coefficients properly, the sum of all coefficients should give the energy. The reason is that the Fourier coefficients correspond to the energy spectrum, and if we integrate the energy spectrum over all wave numbers we get the total energy. When we take the FFT of Eq. L.11, for example, we get

$$\hat{B}_{11}(\kappa_z) = FFT(B_{11})$$

and summation gives

$$v_{1,rms}^2 = \sum_1^N \hat{B}_{11}/N \quad (\text{L.13})$$

see Appendix M

Plot the energy spectra at a couple of  $x_2$  locations. Confirm that Eq. L.13 is satisfied. When plotting two energy spectrum, it is no point showing both symmetric parts; show only half of it (cf. the energy spectrum in Fig. M.5 b).

### L.11 Task 2.11

Think of an interesting turbulent quantity and plot it and analyze it!

## M MTF270: Compute energy spectra from LES/DNS data using Matlab

### M.1 Introduction

When analyzing DNS or LES data, we are interested to look at the energy spectra. From these we can find out in which turbulence scales (i.e. at which wave numbers) the fluctuating kinetic turbulent energy reside. By taking the Fourier transform of the time signal (a fluctuating turbulent velocity) and then taking the square of the Fourier coefficients we obtain the energy spectrum versus frequency.

If we want to have the energy spectrum versus wavenumber, we Fourier transform  $N$  instantaneous signals in space and then time average the  $N$  Fourier transforms. An alternative way is to Fourier transform of a (time-averaged) two-point correlation,  $B_{33}(\hat{x}_3)$ , which is defined as (see Eq. 10.2)

$$B(x_3, \hat{x}_3) = \langle v'_3(x_3 - \hat{x}_3) v'_3(x_3) \rangle \quad (\text{M.1})$$

where  $\hat{x}_3$  is the separation between the two points. Here we assume that  $x_3$  is an homogeneous direction so that  $B_{33}$  is independent of  $x_3$ , i.e.  $B_{33} = B_{33}(\hat{x}_3)$ . The two-point correlation for an infinite channel flow is shown in Fig. M.1. On discrete form the expression for  $B_{33}$  reads

$$B_{33}(k\Delta z) = \frac{1}{M} \sum_{m=1}^M v'_3(x_3 - k\Delta z) v'_3(x_3) \quad (\text{M.2})$$

where  $m$  denotes summation in homogeneous directions (i.e. time plus spatial homogeneous directions).

In the following section we give a simple example how to use Matlab to Fourier transform a signal where we know the answer. Then we show how to derive the energy spectrum from a spatial two-point correlation. Finally, some comments are given on how to create an energy spectrum versus frequency from an autocorrelation (i.e. from a two-point correlation in time).

### M.2 An example of using FFT

Here we will present a simple example. Consider the function

$$u = 1 + \cos(2\pi x/L) = 1 + \cos(2\pi(n-1)/N) \quad (\text{M.3})$$

where  $L$  is the length of the domain and  $N = 16$  is the number of discrete points, see Fig. M.2. Let's use this function as input vector for the discrete Fourier transform (DFT) using Matlab. The function  $u$  is symmetric, so we expect the Fourier coefficients to be real. In Matlab the DFT of  $u$  is defined as (type `help fft` at the Matlab prompt)

$$U(k) = \sum_{n=1}^N u_n \exp \left\{ \frac{-i2\pi(k-1)(n-1)}{N} \right\} \quad (\text{M.4})$$

$$1 \leq k \leq N$$

where  $k$  is the non-dimensional wavenumber and  $i = \sqrt{-1}$ . The ratio  $(n-1)/N$  corresponds to the physical coordinate,  $x$ , in the the continuous FFT

$$U^c(\kappa) = \frac{1}{L} \int_{-L}^L u(x) \exp(-i\kappa x) dx, \quad \kappa = 2\pi/L \quad (\text{M.5})$$

Note that the discrete Fourier  $U(k)$  coefficients in Eq. M.4 must be divided by  $N$ , i.e.  $U(k)/N$ , in order to correspond to the Fourier coefficients  $U^c$  ( $N$  corresponds to  $L$  in Eq. M.5). Furthermore, it can be noted that in Eq. M.4 the period  $[0, 2\pi]$  is used whereas the formulation in Eq. M.5 is based on the interval  $[-\pi, \pi]$ .

In Matlab, we generate the function  $u$  in Eq. M.3 using the commands

```
N=16;
n=1:1:N;
u=1+cos(2*pi*(n-1)/N);
```

The  $u$  function is shown in Fig. M.2. 16 nodes are used; node 1 is located at  $x = 0$  and node 16 is located at  $15L/16$ .

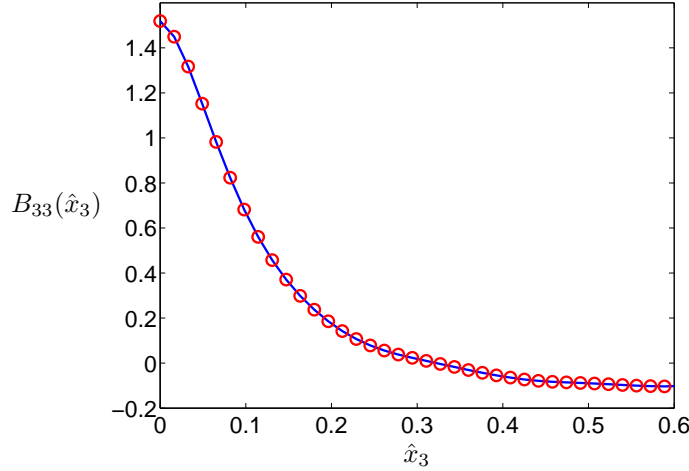


Figure M.1: Two-point correlation,  $B(\hat{x}_3) = \langle v'_3(x_3 - \hat{x}_3)v'_3(x_3) \rangle$ , of DNS data in channel flow taken from [75].

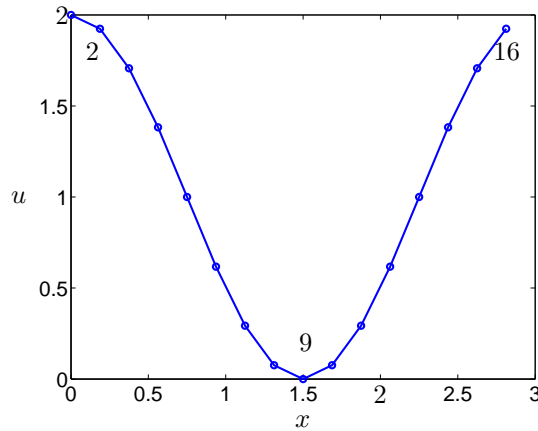


Figure M.2: The  $u$  function.

Now we take the discrete Fourier transform of  $u$ . Type

```
U=fft(u);
```

Instead of using the built-in `fft` command in Matlab we can program Eq. M.4 directly in Matlab as

```
U=zeros(1,N);
for k=1:N
    for n=1:N
        arg1=2*pi*(k-1)*(n-1)/N;
        U(k)=U(k)+u(n)*cos(-arg1);
    end
end
```

Note that since  $u$  is symmetric, we have only used  $\cos(-x) = \cos(x)$  (the symmetric part of  $\exp(-ix)$ ).

The resulting Fourier coefficients are shown in Fig. M.3. Since the function  $u$  includes only one cosine function and a mean (which is equal to one) only three Fourier coefficient are non-zero. Two of them,  $U(2)/N = 0.5$ ,  $U(16)/N = 0.5$ , correspond to the cosine functions (there must be two since  $U$  is symmetric)

$$\begin{aligned} \cos(2\pi(n-1)/N) \\ \cos((N-1)2\pi(n-1)/N) = \cos(-2\pi(n-1)/N) = \cos(2\pi(n-1)/N) \end{aligned} \quad (\text{M.6})$$

which corresponds to  $\cos(2\pi x/L)$  in Eq. M.3. It can be noted that the interval  $[k = N/2 + 1, N = 9, 16]$  corresponds to the negative, symmetric part of the wavenumbers in the physical formulation (cf. Eqs. M.4 and M.5). The first Fourier coefficient corresponds – as always – to the mean of  $u$ , i.e.  $U(1)/N = \langle u \rangle$ . This is easily verified from Eq. M.4 by inserting  $k = 1$ . The remaining coefficients are zero.

In Fig. M.3,  $U/N$  is plotted versus non-dimensional wavenumber,  $k$ , and versus wavenumber  $\kappa = 2\pi(n-1)/L$ .

The energy,  $\langle u^2 \rangle$ , of the signal in Fig. M.2 can be computed as

$$\langle u^2 \rangle = \frac{1}{L} \int_0^L u^2(x) dx = \sum_{n=1}^N u_n^2 / N = 1.5 \quad (\text{M.7})$$

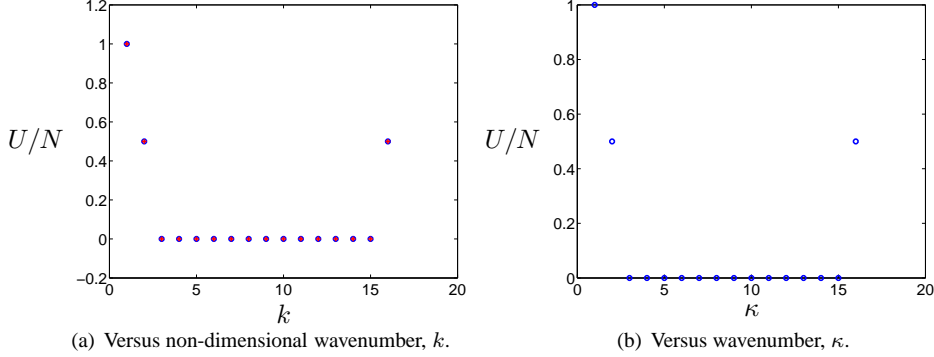
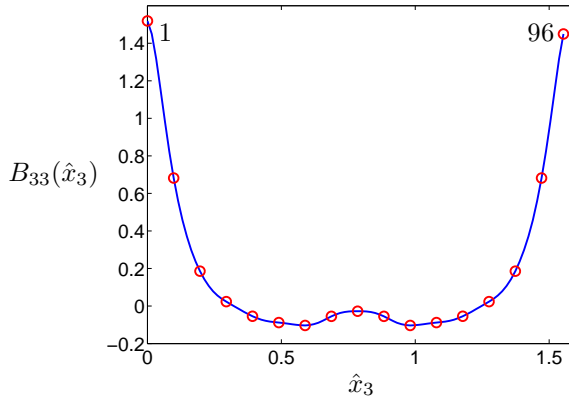
In wavenumber space the energy is – according to Parseval’s formula, see Eq. C.4 – equal to the integral of the square of the Fourier coefficients, i.e.

$$\langle u^2 \rangle = \frac{1}{L} \int_0^\infty U^2(\kappa) d\kappa = \frac{1}{N} \sum_{n=1}^N U_n^2 / N = 1.5 \quad (\text{M.8})$$

### M.3 Energy spectrum from the two-point correlation

Now that we have learnt how to use the FFT command in Matlab, let’s use it on our two-point correlation in Eq. M.1 and Fig. M.1. Equation M.4 reads

$$\hat{B}_{33}(k) = \sum_{n=1}^N B_{33}(n) \exp \left\{ \frac{-i2\pi(k-1)(n-1)}{N} \right\} \quad (\text{M.9})$$

Figure M.3: The  $U/N$  Fourier coefficients.Figure M.4: Periodic two-point correlation,  $B_{33}(\hat{x}_3) = \langle v'_3(x_3)v'_3(x_3 + \hat{x}_3) \rangle$ , of DNS data in channel flow taken from [75].

The simulations have been carried out with periodic boundary conditions in  $x_3$  direction (and  $x_1$ ), and hence  $B_{33}(\hat{x}_3)$  is symmetric, see Fig. M.4. Thus, it is sufficient to use the cosine part of Eq. M.9, i.e.

$$\hat{B}_{33}(k) = \sum_{n=1}^N B_{33}(n) \cos \left\{ \frac{2\pi(k-1)(n-1)}{N} \right\} \quad (\text{M.10})$$

In Fig. M.5a the Fourier coefficients  $\hat{B}_{33}\kappa_3$  are presented versus wavenumber  $\kappa_3 = 2\pi(n-1)/x_{3,max}$ , where  $x_{3,max} \simeq 1.55$ , see Fig. M.4. Figure M.5b shows the same energy spectra in log-log scale (only half of the spectrum is included), which is the common way to present energy spectra. The dashed line shows the  $-5/3$  slope which indicates that the energy spectra from the DNS follows the Kolmogorov  $-5/3$  decay.

As usual, the Fourier coefficient for the first non-dimensional wavenumber, i.e.  $\hat{B}_{33}(1)/N$  is equal to the mean of  $B_{33}$ , i.e.

$$\langle B_{33} \rangle = \frac{1}{N} \sum_{n=1}^N B_{33}(n) \equiv \frac{1}{N} \hat{B}_{33}(1) \quad (\text{M.11})$$

compare with Eq. M.10. Note that this is almost the same expression as that for the

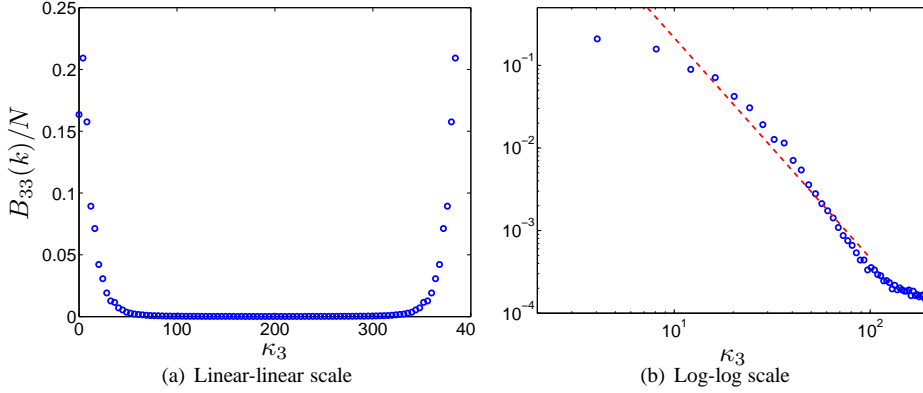


Figure M.5: The energy spectrum of  $\overline{v'_3}^2$  versus wavenumber,  $\kappa_3$ . Dashed line in b) show  $-5/3$  slope.

integral length scale which reads (see Eq. 10.5)

$$L_{int}(x_3) = \frac{1}{\overline{v'_3}^2} \int_0^\infty B_{33}(x_3, \hat{x}_3) d\hat{x}_3 = \frac{\langle B_{33} \rangle}{\overline{v'_3}^2} \quad (\text{M.12})$$

Hence the integral length scale is related to the first Fourier mode as

$$L_{int} = \frac{\hat{B}_{33}(1)}{N \overline{v'_3}^2} \quad (\text{M.13})$$

The two-point correlation for zero separation is equal to  $\overline{v'_3}^2$ , i.e.  $B_{33}(0) = \overline{v'_3}^2 = 1.51$ . Another way to obtain  $\overline{v'_3}^2$  is to integrate the energy spectrum in Fig. M.5, i.e.

$$\overline{v'_3}^2 = \int_0^\infty \hat{B}_{33}(\kappa_3) d\kappa_3 = \frac{1}{N} \sum_{n=1}^N \hat{B}_{33}(n) = 1.51 \quad (\text{M.14})$$

#### M.4 Energy spectra from the autocorrelation

When computing the energy spectra of the  $v'_3$  velocity, say, versus frequency, the time series of  $v'_3(t)$  is commonly Fourier transformed and the energy spectrum is obtained by plotting the square of the Fourier coefficients versus frequency,  $f$ . We can also split the time signal into a number subsets, Fourier transform each subset and then average. In Matlab, the command `pwelch` is a convenient command which does all this.

In the previous section we computed the energy spectrum versus wavenumber by Fourier transforming the two-point correlation. We can use the same approach in time. First we create the autocorrelation  $B_{33}(\tau) = \langle v'_3(t)v'_3(t + \tau) \rangle$  (this can be seen as a two-point correlation in time). Then  $B_{33}(\tau)$  is Fourier transformed to get  $\hat{B}_{33}(f)$  in the same way as in Section M.3. The only difference is that  $\hat{B}_{33}(\tau)$  is a function of frequency whereas  $\hat{B}_{33}(\kappa_3)$  is a function of wavenumber.

## N MTF270, Assignment 4: Hybrid LES-RANS

In this exercise you will use data from a Hybrid LES-RANS for fully developed channel flow. The turbulence model is the same as in [75] (no forcing), but the domain and Reynolds number is taken from [148]. The  $Re$  number based on the friction velocity and the half channel width is  $Re_\tau = u_\tau h/\nu = 8000$ . 28 cells (29 nodes including the boundary) are located in the URANS region at each wall. The matching line is located at  $x_2^+ \simeq 500$ ,  $x_2/\delta = 0.06$ .

A  $64 \times 96 \times 64$  mesh has been used. The cell size in  $x_1$  and  $x_3$  directions are  $\Delta x_1 = 0.05$  and  $\Delta x_3 = 0.025$ . Periodic boundary conditions were applied in the  $x_1$  and  $x_3$  direction (homogeneous directions). All data have been made non-dimensional by  $u_\tau$  and  $\rho$ .

At the course www page you find data files with instantaneous flow fields (statistically independent) of The data files include the instantaneous variables  $u$ ,  $v$ ,  $w$  and  $k_T$  (made non-dimensional by  $u_\tau$  and  $\rho$ ). Use Matlab or Octave on Linux/Ubuntu. Octave is a Matlab clone which can be downloaded for free. Use one of these programs to analyze the data. You find a Matlab/Octave program at the www page which reads the data and computes the mean velocity. The data files are Matlab binary files. Since the data files are rather large, it is recommended that you do all tasks using only data files '1'. When everything works, then use also data files '2', '3' and '4', averaging by use of the four files.

You will also find a file with time history of  $u$ .

### N.1 Time history

At the www page you find a file `u_v_time_4nodes_hybrid.dat` with the time history of  $\bar{v}_1$  and  $\bar{v}_2$ . The file has nine columns of  $\bar{v}_1$  and  $\bar{v}_2$  at four nodes (and time):  $x_2/\delta = 0.0028$ ,  $x_2/\delta = 0.015$ ,  $x_2/\delta = 0.099$  and  $x_2/\delta = 0.35$ . Hence, two nodes are located in the URANS region and two nodes in the LES region. With  $u_\tau = 1$  and  $\nu = 1/Re_\tau = 1/8000$ , this correspond to  $x_2^+ = 22$ ,  $x_2^+ = 120$ ,  $x_2^+ = 792$  and  $x_2^+ = 2800$ , respectively. The sampling time step is  $6.250E-4$  (every time step). Use the Matlab program `pl_time_hybrid` to load and plot the time history of  $\bar{v}_1$ .

Recall that the velocities have been scaled with the friction velocity  $u_\tau$ , and thus what you see is really  $\bar{v}_1/u_\tau$ . The time history of  $\bar{v}_1$  at  $x_2/\delta = 0.015$  and  $x_2/\delta = 0.35$  are shown. To study the profiles in closer detail, use the `axis-command` in the same way as when you studied the DNS data.

Plot  $\bar{v}_1$  for all four nodes. How does the time variation of  $\bar{v}_1$  differ for different positions? Recall that the two points closest the wall are located in the URANS region and the other two are located in the LES region. In the URANS region the turbulent viscosity is much larger than in the LES region. How do you expect that the difference in  $\nu_t$  affects the time history of  $\bar{v}_1$ . Does the time history of  $\bar{v}_1$  behave as you expect? What about  $\bar{v}_2$ ?

Compute the autocorrelation of the four points

```
imax=500;
two_uu_1_mat=autocorr(u1,imax);
```

Above we See the maximum separation in time to 500 samples. Then compute the integral timescale

```

dt=t(1);
int_T_1=trapz(two_uu_1_mat)*dt;

Plot the autocorrelation.

plot(t(1:imax),two_uu_1_mat(1:imax),'linew',2)
xlabel('t')
ylabel('B_{uu}')
handle=gca
set(handle,'fontsiz',[20])

```

How does it compare to the integral timescale. Compute the autocorrelation and integral timescale also for the other three points. Do you see any difference between the points in the URANS region and the LES region?

## N.2 Mean velocity profile

After having performed a hybrid LES-RANS, we want to look at the time-averaged results. Use the file `pl_uvw_hybrid.m` to look at the mean velocity profiles. `pl_uvw_hybrid.m` reads the instantaneous  $\bar{v}_1$  field and performs an averaging in the homogeneous directions  $x_1$  and  $x_3$ . The time averaged velocity profile is compared with the log profile (markers). There are four files with instantaneous values of  $\bar{v}_1$ . Use more than one file to perform a better averaging.

## N.3 Resolved stresses

We want to find out how much of the turbulence that has been resolved and how much that has been modelled. Compute first `vmean` (this quantity should be very small, but if you use only one file this may not be the case due to too few samples). Now compute  $\langle v'_1 v'_2 \rangle$ . Here's an example how to do:

```

uv=zeros(nj,1);
for k=1:nk
for j=1:nj
for i=1:ni
    ufluct=u3d(i,j,k)-umean(j);
    vfluct=v3d(i,j,k)-vmean(j);
    uv(j)=uv(j)+ufluct*vfluct;
end
end
end
uv=uv/ni/nk;

```

Plot it in a new figure (a figure is created by the command `figure(2)`).  
Compute also the resolved turbulent kinetic energy

$$k_{res} = 0.5 (\langle v'_1^2 \rangle + \langle v'_2^2 \rangle + \langle v'_3^2 \rangle)$$

and plot it in a new figure.

	URANS region	LES region
$\ell$	$2.5n[1 - \exp(-0.2k_T^{1/2}n/\nu)]$	$\ell = \Delta = (\delta V)^{1/3}$
$\nu_T$	$0.09 \cdot 2.5k_T^{1/2}n[1 - \exp(-0.014k_T^{1/2}n/\nu)]$	$0.07k_T^{1/2}\ell$

Table N.1: Expressions for  $\ell$  and  $\nu_T$  in the LES and URANS regions.  $n$  denotes the distance from the wall.

## N.4 Turbulent kinetic energy

Now plot and compare the resolved and modelled turbulent kinetic energies. Note that the modelled turbulent kinetic energy,  $k_T$  (`te1_hybrid.mat`, `te2_hybrid.mat`, ...), can be downloaded from the www page and loaded at the beginning of `p1_uvw_hybrid.m`. Which is largest? Which is largest in the URANS region and in the LES region, respectively? What about the sum? The magnitude of resolved and modelled turbulent kinetic energies is discussed in the last subsection in [75].

## N.5 The modelled turbulent shear stress

We have computed the resolved shear stress. Let's find the modelled shear stress.

The modelled turbulent kinetic energy,  $k_T$  (file `te1_hybrid.mat`, ...), will be used. Recall that  $\nu = 1/8000$ . Compute the turbulent viscosity according to Table N.1 and do the usual averaging. When computing  $\Delta$ , you need the volume,  $\delta V$ , of the cells. It is computed as  $\delta V = (\Delta x_1 \Delta x_2 \Delta x_3)$ ;  $\Delta x_1$  and  $\Delta x_3$  are constant and  $\Delta x_2$  is stored in the array `dy(j)`, look at the beginning of the m-file. Plot  $\langle \nu_T \rangle / \nu$ . Where is it large and where is it small? (Recall that the URANS region is located in the first 28 cells). Is it smooth? Do you need more samples? If so, use more files.

Compute the modelled shear stress from the Boussinesq assumption

$$\tau_{12} = -2\nu_T \bar{s}_{12} = -\nu_T \left( \frac{\partial \bar{v}_1}{\partial x_2} + \frac{\partial \bar{v}_2}{\partial x_1} \right)$$

Plot it and compare with the resolved shear stress (see Section N.3). Are they smooth across the interface? (recall that forcing is used) Is the resolved shear stress large in the URANS region? Should it be large? Why/why not?

## N.6 Turbulent length scales

Compute and plot the turbulent length scales given in Table N.1. Plot the  $\ell_{SGS}$  and  $\ell_{URANS}$  length scales in both regions. Which is largest? Any surprises? Compare them with  $\Delta x_2$  and  $(\Delta x_1 \Delta x_2 \Delta x_3)^{1/3}$ . One would expect that  $(\Delta x_1 \Delta x_2 \Delta x_3)^{1/3} < \ell_{URANS}$  everywhere. Is this the case?

## N.7 SAS turbulent length scales

Compute the 1D von Kármán length scale defined as

$$L_{vK,1D} = \kappa \left| \frac{\partial \langle \bar{v}_1 \rangle / \partial x_2}{\partial^2 \langle \bar{v}_1 \rangle / \partial x_2^2} \right| \quad (N.1)$$

Note that you should take the derivatives of the *averaged*  $\bar{v}_1$  velocity, i.e. of  $\langle \bar{v}_1 \rangle$ . Zoom up near the wall. How does it behave (i.e. what is  $n$  in  $\mathcal{O}(x_2^n)$ )? What should  $n$  be?

Compare that with the von Kármán length scale defined from instantaneous  $\bar{v}_1$ , i.e.

$$L_{vK,1D,inst} = \kappa \left| \left\langle \frac{\partial \bar{v}_1 / \partial x_2}{\partial^2 \bar{v}_1 / \partial x_2^2} \right\rangle \right| \quad (\text{N.2})$$

How does it compare with  $L_{vK,1D}$ ?

When we're doing real 3D simulations, the first and second derivative must be defined in 3D. One way of defining the von Kármán length scale in 3D is [142, 143]

$$\begin{aligned} L_{vK,3D,inst} &= \kappa \left| \frac{S}{U''} \right| \\ S &= (2\nu_t \bar{s}_{ij} \bar{s}_{ij})^{0.5} \\ U'' &= \left( \frac{\partial^2 \bar{v}_i}{\partial x_j \partial x_j} \frac{\partial^2 \bar{v}_i}{\partial x_j \partial x_j} \right)^{0.5} \end{aligned} \quad (\text{N.3})$$

The second derivative is then computed as

$$\begin{aligned} U''^2 &= \left( \frac{\partial^2 \bar{v}_1}{\partial x_1^2} + \frac{\partial^2 \bar{v}_1}{\partial x_2^2} + \frac{\partial^2 \bar{v}_1}{\partial x_3^2} \right)^2 \\ &\quad + \left( \frac{\partial^2 \bar{v}_2}{\partial x_1^2} + \frac{\partial^2 \bar{v}_2}{\partial x_2^2} + \frac{\partial^2 \bar{v}_2}{\partial x_3^2} \right)^2 \\ &\quad + \left( \frac{\partial^2 \bar{w}_3}{\partial x_1^2} + \frac{\partial^2 \bar{w}_3}{\partial x_2^2} + \frac{\partial^2 \bar{w}_3}{\partial x_3^2} \right)^2 \end{aligned} \quad (\text{N.4})$$

Plot the von Kármán length scale using Eqs. N.3 and N.4. Compare them with Eq. N.1. What's the difference? What effect do the different length scales give for  $P_{SAS}$  (i.e.  $T_1$  in Eq. 22.5) and what effect does it give to  $\omega$ ?

Another way to compute the second derivative is

$$\begin{aligned} U''^2 &= \left( \frac{\partial^2 \bar{v}}{\partial x^2} \right)^2 + \left( \frac{\partial^2 \bar{v}}{\partial y^2} \right)^2 + \left( \frac{\partial^2 \bar{v}}{\partial z^2} \right)^2 \\ &\quad + \left( \frac{\partial^2 \bar{v}}{\partial x^2} \right)^2 + \left( \frac{\partial^2 \bar{v}}{\partial y^2} \right)^2 + \left( \frac{\partial^2 \bar{v}}{\partial z^2} \right)^2 \\ &\quad + \left( \frac{\partial^2 \bar{w}}{\partial x^2} \right)^2 + \left( \frac{\partial^2 \bar{w}}{\partial y^2} \right)^2 + \left( \frac{\partial^2 \bar{w}}{\partial z^2} \right)^2 \end{aligned} \quad (\text{N.5})$$

Plot and compare the von Kármán length scales using the second derivatives defined in Eqs. N.4 and N.5.

## O MTF270, Assignment 5: Embedded LES with PANS

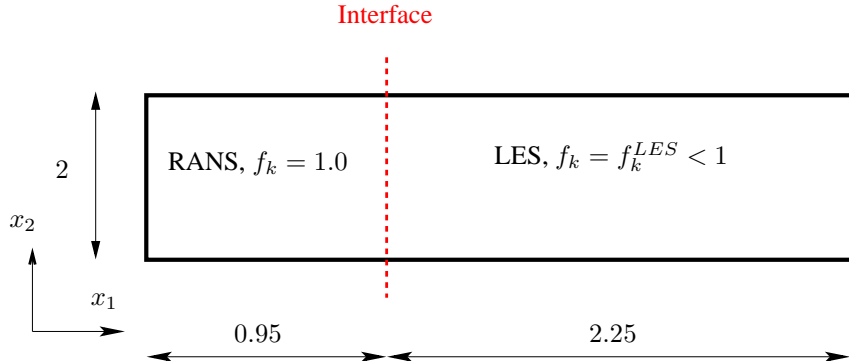


Figure O.1: Channel flow configuration. The interface separates the RANS and the LES regions.

In this exercise you will use data from an embedded PANS of channel flow. The data are taken from [150]. The  $k_u$  (Eq. 23.10) and the  $\varepsilon_u$  (Eq. 23.18) equations are solved. The turbulent viscosity is computed from Eq. 23.12. The PANS model is a modified  $k - \varepsilon$  model which can operate both in RANS mode and LES mode.

The Reynolds number for the channel flow is  $Re_\tau = 950$  based on the friction velocity,  $u_\tau$ , and half the channel width,  $\delta$ . In the present simulations, we have set  $\rho = 1$ ,  $\delta = 1$  and  $u_\tau \simeq 1$ , see Fig. O.1. With a  $3.2 \times 2 \times 1.6$  domain, a mesh with  $64 \times 80 \times 64$  cells is used in, respectively, the streamwise ( $x$ ), the wall-normal ( $y$ ) and the spanwise ( $z$ ) direction, see Fig. O.1. The resolution is approximately (the wall shear stress varies slightly along the wall)  $48 \times (0.6 - 103) \times 24$  in viscous units. Inlet conditions at  $x = 0$  are created by computing fully developed channel flow with the LRN PANS model in RANS mode (i.e. with  $f_k = 1$ ). The RANS part extends up to  $x_1 = 0.95$ ; downstream the equations operate in LES mode ((i.e.  $f_k = 0.4$ ).

Anisotropic synthetic fluctuations are added at the interface. The interface condition for  $\varepsilon_u$  is computed with the baseline value  $C_s = 0.07$ , where  $k_{RANS}$  is taken at  $x = 0.5$ , see Fig. O.1. The modelled dissipation,  $\varepsilon_{inter}$ , is set from  $k_{inter}$  and an SGS length scale,  $\ell_{sgs}$ , which is estimated from the Smagorinsky model as

$$\ell_{sgs} = C_s \Delta \quad (\text{O.1})$$

and the interface condition for  $k_u$  is computed as

$$k_{inter} = f_k^{LES} k_{RANS} \quad (\text{O.2})$$

with  $f_k^{LES} = 0.4$ . The interface conditions on  $k_u$  and  $\varepsilon_u$  will make the turbulent viscosity steeply decrease from its large values in the RANS region to much smaller values appropriate for the LES region.

### O.1 Time history

At the www-page you find a file `u_time_interior.dat` with the time history of  $\bar{v}_2$ . The file has eight columns of  $\bar{v}_2$  along two lines:  $x_2 = 0.0139$  ( $x_2^+ \simeq 13$ ) and

$x_2 = 0.24$  ( $x_2^+ \simeq 230$ ); they are located at  $x_1 = 0.775, 1.175, 1.675, 2.175$ . The sampling time step is 0.000625 (every time step). Use Matlab. You can also use Octave on Linux/Ubuntu. Octave is a Matlab clone which can be downloaded for free. Use the Matlab/Octave program `pl_time_pans` to load and plot the time history of  $\bar{v}_2$ .

The time history of  $\bar{v}_2$  at  $x_2 = 0.0139$  at  $x_1 = 0.775$  and  $x_1 = 1.675$  are shown. To study the profiles in closer detail, use the `axis`-command in the same way as when you studied the DNS data. Why is there such a big difference in the fluctuations?

If you're not interested in integral time scales, skip the rest of this section and proceed to Section O.2.

In Matlab figure 2, the autocorrelation is plotted. The autocorrelation is defined as

$$B(\tau) = \int_0^\infty v(t)v(t-\tau)dt \quad (O.3)$$

Study the coding and try to understand it. When prescribing the time correlation of the synthetic fluctuations, the integral timescale  $\mathcal{T}$  is used, see Eq. 11 in [150]. The integral time scale is defined as

$$\mathcal{T} = \int_0^\infty B^{norm}(\tau)d\tau \quad (O.4)$$

where  $B^{norm} = B(\tau)/B(0)$  so that  $B^{norm}(0) = 1$ . The constant  $a$  is in [150] set to 0.954 and from Eq. 11 in [150] we can then compute the prescribed integral timescale. In the Matlab file the integral timescale is computed from the autocorrelation. Try to understand the coding.

Plot  $\bar{v}_2$  for the other nodes and study the differences. Compute the autocorrelations and the integral timescales.

## O.2 Resolved stresses

Now we will look at the time-averaged results. Use the file `pl_uuvvww_2d.m` to look at the mean quantities such as velocity, resolved and modelled stresses, turbulent viscosities etc. `pl_uuvvww_2d.m` reads the fields and transforms them into 2D arrays such as `u_2d`, `uu_2d`.

Run `pl_uuvvww_2d..` The resolved stresses  $\langle \bar{v}_1'^2 \rangle$  are plotted vs  $x_2$  (figure 1) and vs.  $x_1$  (figure 2).

Two  $x_1$  stations are shown in figure 1,  $x_1 = 1.175$  and  $x_1 = 2.925$ . Plot the resolved stress also in the RANS region, i.e. for  $x_1 < 0.95$ . The  $\langle \bar{v}_1'^2 \rangle$  profiles are very different in the RANS region ( $x_1 < 0.95$ ) and in the LES ( $x_1 > 0.95$ ), aren't they? Why? This can also be seen in figure 2 where  $\langle \bar{v}_1'^2 \rangle$  is plotted vs.  $x_1$

Now plot the resolved shear stresses,  $\langle \bar{v}_1' \bar{v}_2' \rangle$ , both in the RANS region and in the LES region. You find the same difference between RANS and LES region as for  $\langle \bar{v}_1'^2 \rangle$ , don't you?

## O.3 Turbulent viscosity

Plot the turbulent viscosity vs.  $x_2$  in both regions. Normalize it with  $\langle \nu \rangle$ , i.e. plot  $\langle \nu_u \rangle / \nu$ . Where is it large and where is it small? Why? Now plot it also vs.  $x_1$ . Something drastically happens at  $x_1 = 0.95$ , right?

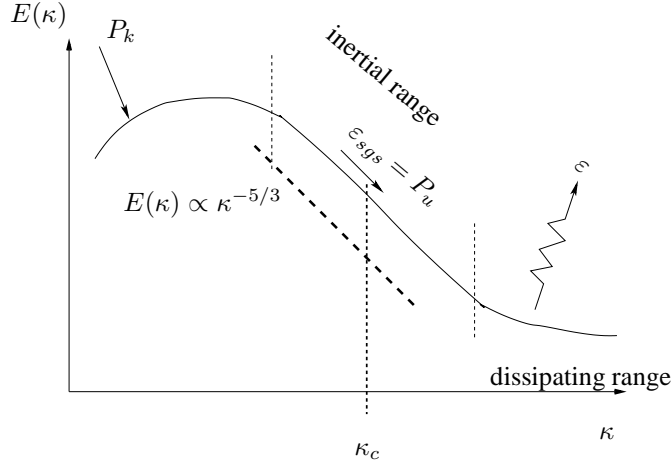


Figure O.2: Energy spectrum.

## O.4 Modelled stresses

In Section O.2 you looked at the resolved Reynolds stresses. Now let's look at the *modelled* stresses. Computer the modelled Reynolds stresses from the Boussinesq assumption

$$\langle \bar{v}_i' \bar{v}_j' \rangle_{mod} = -\langle \nu_u \rangle \left( \frac{\partial \langle \bar{v}_i \rangle}{\partial x_j} + \frac{\partial \langle \bar{v}_j \rangle}{\partial x_i} \right) + \frac{2}{3} \delta_{ij} \langle k_u \rangle \quad (\text{O.5})$$

Compare the resolved and the modelled shear stress and streamwise normal stresses in the RANS region and in the LES region.

## O.5 Turbulent SGS dissipation

In an LES the resolved turbulent fluctuations can be represented by a energy spectrum as in Fig. O.2. The resolved turbulence extracts kinetic energy via the production term,  $P^k$ , which represents a source term in the  $k$  equation (Eq. 8.14) and a sink term in the  $\bar{k}$  equation (Eq. 8.35). The energy flow is visualized in Fig. L.3 where the energy in  $\bar{k}$  mostly goes to resolved turbulence,  $\bar{k}$ , then to modelled turbulence,  $k_{sgs}$  (or  $k_u$ ) and finally to internal energy via dissipation,  $\varepsilon_u$ .

In RANS mode, however, there is no resolved turbulence. Hence the kinetic energy goes directly from  $\bar{k}$  to the modelled turbulence,  $k_u$ .

In the LES region, the production term in the  $k_u$  equation includes both mean and fluctuating strain rates since

$$P_u = \varepsilon_{sgs} = \left\langle \nu_u \left( \frac{\partial \bar{v}_i}{\partial x_j} + \frac{\partial \bar{v}_j}{\partial x_i} \right) \frac{\partial \bar{v}_i}{\partial x_j} \right\rangle$$

which in the Matlab file is stored as `pksgs_2d`.

Now investigate the LES region the relation between  $P_u = \varepsilon_{sgs}$  and the production,  $P^k$ , due to the resolved turbulence

$$P^k = -\langle \bar{v}_i' \bar{v}_j' \rangle \frac{\partial \langle \bar{v}_i \rangle}{\partial x_j}$$

Compare also  $P^k$  in the LES region and in the RANS region.

In both the RANS and the LES region the process of viscous dissipation takes place via  $\varepsilon_u$ . Hence, plot also this quantity. Is the turbulence in local equilibrium, i.e. does the relation  $P_u = \varepsilon_u$  hold?

## P MTF270: Transformation of a tensor

The rotation of a vector from the  $x_{i*}$  coordinate system to  $x_i$  reads (see, e.g., Chapter 1 in [20])

$$u_i = b_{ij} u_{j*} \quad (\text{P.1})$$

where  $b_{ij}$  denotes the cosine between the axis

$$b_{ij} = \cos(x_i, x_{j*}) \quad (\text{P.2})$$

In Fig. P.1, the  $b_{ij}$  is given by

$$\begin{aligned} b_{11} &= \cos \alpha, & b_{12} &= \cos \beta = -\sin \alpha \\ b_{21} &= \cos(\pi/2 - \alpha) = \sin \alpha, & b_{22} &= \cos \alpha \end{aligned} \quad (\text{P.3})$$

The relations  $b_{ik}b_{jk} = b_{ki}b_{kj} = \delta_{ij}$  are fulfilled as they should.

For a second-order tensor, the transformation reads

$$u_{ij} = b_{ik}b_{jm}u_{k*m*} \quad (\text{P.4})$$

As an example, set  $\alpha = \pi/4$ . Equation P.3 gives

$$b_{11} = 1/\sqrt{2}, \quad b_{12} = -1/\sqrt{2}, \quad b_{21} = 1/\sqrt{2}, \quad b_{22} = 1/\sqrt{2} \quad (\text{P.5})$$

Inserting Eq. P.5 into Eq. P.4 gives

$$u_{11} = b_{11}b_{11}u_{1*1*} + b_{12}b_{11}u_{2*1*} + b_{11}b_{12}u_{1*2*} + b_{12}b_{12}u_{2*2*} \quad (\text{P.6a})$$

$$= \frac{1}{2}(u_{1*1*} - u_{2*1*} - u_{1*2*} + u_{2*2*})$$

$$u_{12} = b_{11}b_{21}u_{1*1*} + b_{12}b_{21}u_{2*1*} + b_{11}b_{22}u_{1*2*} + b_{12}b_{22}u_{2*2*} \quad (\text{P.6b})$$

$$= \frac{1}{2}(u_{1*1*} - u_{2*1*} + u_{1*2*} - u_{2*2*})$$

$$u_{21} = b_{21}b_{11}u_{1*1*} + b_{22}b_{11}u_{2*1*} + b_{21}b_{12}u_{1*2*} + b_{22}b_{12}u_{2*2*} \quad (\text{P.6c})$$

$$= \frac{1}{2}(u_{1*1*} + u_{2*1*} - u_{1*2*} - u_{2*2*})$$

$$u_{22} = b_{21}b_{21}u_{1*1*} + b_{22}b_{21}u_{2*1*} + b_{21}b_{22}u_{1*2*} + b_{22}b_{22}u_{2*2*} \quad (\text{P.6d})$$

$$= \frac{1}{2}(u_{1*1*} + u_{2*1*} + u_{1*2*} + u_{2*2*})$$

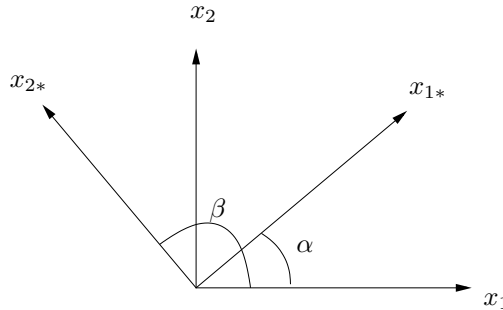


Figure P.1: Transformation between the coordinate systems  $(x_{1*}, x_{2*})$  and  $(x_1, x_2)$ .

## P.1 Rotation to principal directions

Consider fully developed flow in a channel, see Appendix B. The strain-rate tensor,  $s_{ij}$ , reads

$$s_{11} = 0, \quad s_{12} = \frac{1}{2} \frac{\partial v_1}{\partial x_2}, \quad s_{21} = s_{12}, \quad s_{22} = 0 \quad (\text{P.7})$$

Assume that the  $x_1$  and  $x_2$  coordinates in Fig. P.1 correspond to the streamwise and wall-normal directions, respectively. Let the  $x_{1*} - x_{2*}$  coordinate system denote the eigenvectors. The transformation from  $x_1 - x_2$  to  $x_{1*} - x_{2*}$  reads

$$s_{i*j*} = c_{ik}s_{km}, \quad c_{ij} = \cos(x_{i*}, x_j) \quad (\text{P.8})$$

where

$$\begin{aligned} c_{11} &= \cos \alpha, & c_{12} &= \cos(\pi/2 - \alpha) = \sin \alpha \\ c_{21} &= \cos \beta = -\cos \alpha, & c_{22} &= \cos \alpha \end{aligned} \quad (\text{P.9})$$

see Fig. P.1. It can be seen that the relation  $c_{ji} = b_{ij}$  is satisfied as it should. The eigenvectors for Eq. P.7 are any two orthogonal vectors with angles  $\pm\pi/4, \pm3\pi/4$ . Let us choose  $\pi/4$  and  $3\pi/4$  for which the transformation in Eq. P.8 reads ( $\alpha = \pi/4$ )

$$s_{1*1*} = c_{11}c_{11}s_{11} + c_{12}c_{11}s_{21} + c_{11}c_{12}s_{12} + c_{12}c_{12}s_{22} \quad (\text{P.10a})$$

$$= \frac{1}{2}(s_{11} + s_{21} + s_{12} + s_{22})$$

$$s_{1*2*} = c_{11}c_{21}s_{11} + c_{12}c_{21}s_{21} + c_{11}c_{22}s_{12} + c_{12}c_{22}s_{22} \quad (\text{P.10b})$$

$$= \frac{1}{2}(-s_{11} - s_{21} + s_{12} + s_{22})$$

$$s_{2*1*} = c_{21}c_{11}s_{11} + c_{22}c_{11}s_{21} + c_{21}c_{12}s_{12} + c_{22}c_{12}s_{22} \quad (\text{P.10c})$$

$$= \frac{1}{2}(-s_{11} + s_{21} - s_{12} + s_{22})$$

$$s_{2*2*} = c_{21}c_{21}s_{11} + c_{22}c_{21}s_{21} + c_{21}c_{22}s_{12} + c_{22}c_{22}s_{22} \quad (\text{P.10d})$$

$$= \frac{1}{2}(-s_{11} - s_{21} - s_{12} + s_{22})$$

The fully developed channel flow is obtained by inserting Eq. P.7

$$s_{1*1*} = s_{12}, \quad s_{1*2*} = 0, \quad s_{2*1*} = 0, \quad s_{2*2*} = -s_{21} \quad (\text{P.11})$$

Since the diagonal elements are zero it confirms that the coordinate system  $x_{1*} - x_{2*}$  with  $\alpha = \pi/4$  is indeed a principal coordinate system. The eigenvalues,  $\lambda^{(k)}$ , of  $s_{ij}$  correspond to the diagonal elements in Eq. P.11, i.e.

$$\lambda^{(1)} \equiv s_{1*1*} = s_{12} = \frac{1}{2} \frac{\partial v_1}{\partial x_2}, \quad \lambda^{(2)} \equiv s_{2*2*} = -s_{21} = -\frac{1}{2} \frac{\partial v_1}{\partial x_2} \quad (\text{P.12})$$

## P.2 Transformation of a velocity gradient

Consider the velocity gradient  $A_{ij} = \partial v_i / \partial x_j$ . Apply the transformation from the  $x_1 - x_2$  system to the  $x_{1*} - x_{2*}$  in Eqs. P.10a-P.10d with  $\alpha = \pi/4$

$$\begin{aligned} A_{1*1*} &= \frac{1}{2}(A_{11} + A_{21} + A_{12} + A_{22}) \\ A_{1*2*} &= \frac{1}{2}(-A_{11} - A_{21} + A_{12} + A_{22}) \\ A_{2*1*} &= \frac{1}{2}(-A_{11} + A_{21} - A_{12} + A_{22}) \\ A_{2*2*} &= \frac{1}{2}(-A_{11} - A_{21} - A_{12} + A_{22}) \end{aligned} \quad (\text{P.13})$$

Insert Eq. P.9 with  $\alpha = \pi/4$  and replace  $A_{ij}$  by the velocity gradient

$$\frac{\partial v_{1*}}{\partial x_{1*}} = \frac{\partial v_{1*}}{\partial x_{2*}} = \frac{1}{2} \frac{\partial v_1}{\partial x_2}, \quad \frac{\partial v_{2*}}{\partial x_{1*}} = \frac{\partial v_{2*}}{\partial x_{2*}} = -\frac{1}{2} \frac{\partial v_1}{\partial x_2}, \quad (\text{P.14})$$

It can be seen that  $\partial v_{1*} / \partial x_{1*} = s_{1*1*}$  and  $\partial v_{1*} / \partial x_{2*} + \partial v_{2*} / \partial x_{1*} = 2s_{1*2*} = 0$  (see Eqs. P.12 and P.14) as it should.

## Q MTF270: Green's formulas

In this appendix we will derive Green's three formulas from Gauss divergence law. In the last section we will derive the analytical solution to the Poisson equation. The derivations below are partly taken from [170].

### Q.1 Green's first formula

Gauss divergence law reads

$$\int_V \frac{\partial F_i}{\partial x_i} dV = \int_S F_i n_i dS \quad (\text{Q.1})$$

where  $S$  is the bounding surface of the volume,  $V$ , and  $n_i$  is the normal vector of  $S$  pointing out of  $V$ . Replacing  $F_i$  by  $\varphi \frac{\partial \psi}{\partial x_i}$  gives

$$\int_V \frac{\partial}{\partial x_i} \left( \varphi \frac{\partial \psi}{\partial x_i} \right) dV = \int_S \varphi \frac{\partial \psi}{\partial x_i} n_i dS \quad (\text{Q.2})$$

The left side is re-written as

$$\frac{\partial}{\partial x_i} \left( \varphi \frac{\partial \psi}{\partial x_i} \right) = \varphi \frac{\partial^2 \psi}{\partial x_i \partial x_i} + \frac{\partial \psi}{\partial x_i} \frac{\partial \varphi}{\partial x_i} \quad (\text{Q.3})$$

which inserted in Eq. Q.2 gives

$$\int_V \varphi \frac{\partial^2 \psi}{\partial x_i \partial x_i} dV + \int_V \frac{\partial \psi}{\partial x_i} \frac{\partial \varphi}{\partial x_i} dV = \int_S \varphi \frac{\partial \psi}{\partial x_i} n_i dS \quad (\text{Q.4})$$

This is Green's first formula.

### Q.2 Green's second formula

Switching  $\varphi$  and  $\psi$  in Eq. Q.4 gives

$$\int_V \psi \frac{\partial^2 \varphi}{\partial x_i \partial x_i} dV + \int_V \frac{\partial \varphi}{\partial x_i} \frac{\partial \psi}{\partial x_i} dV = \int_S \psi \frac{\partial \varphi}{\partial x_i} n_i dS \quad (\text{Q.5})$$

Subtract Eq. Q.5 from Q.4 gives

$$\int_V \left( \varphi \frac{\partial^2 \psi}{\partial x_i \partial x_i} - \psi \frac{\partial^2 \varphi}{\partial x_i \partial x_i} \right) dV = \int_S \left( \varphi \frac{\partial \psi}{\partial x_i} - \psi \frac{\partial \varphi}{\partial x_i} \right) n_i dS \quad (\text{Q.6})$$

This is Green's second formula.

### Q.3 Green's third formula

In Green's second formula, Eq. Q.6, set

$$\psi(\mathbf{r}) = \frac{1}{|\mathbf{r} - \mathbf{r}_P|} \quad (\text{Q.7})$$

As usual we are considering a volume  $V$  with bounding surface  $S$  and normal vector  $n_i$ . Since function  $\psi(\mathbf{r})$  is singular for  $\mathbf{r} = \mathbf{r}_P$ , consider a small sphere in  $V$ , see Fig. Q.1.

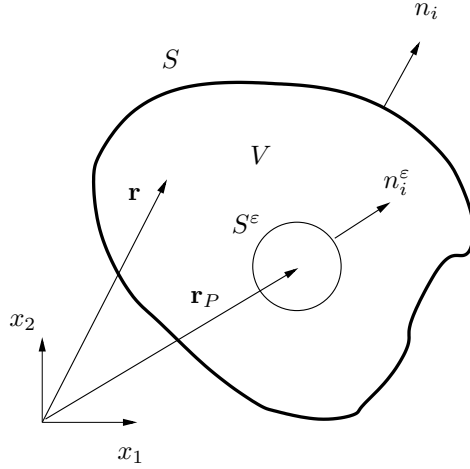


Figure Q.1: Green's third formula. A volume  $V$  with bounding surface  $S$  with normal vector  $n_i$ . In  $V$  there is a small sphere  $S^\varepsilon$  located at  $\mathbf{r}_P$  with radius  $\varepsilon$  and normal vector  $n_i^\varepsilon$ .

In Eq. Q.6 we need the first and the second derivative of  $\psi$ . The first derivative of  $1/r_i$  is computed as

$$\frac{\partial}{\partial x_i} \left( \frac{1}{r} \right) = -\frac{\partial r / \partial x_i}{r^2} = -\frac{r_i}{r^3} \quad (\text{Q.8})$$

since the derivative of a distance  $X$  is a vector along the increment of the distance, i.e.  $\partial X / \partial x_i = X_i / X$  where  $X = |X_i|$ . The second derivative is obtained as

$$\begin{aligned} \frac{\partial^2}{\partial x_i \partial x_i} \left( \frac{1}{r} \right) &= -\frac{\partial}{\partial x_i} \left( \frac{r_i}{r^3} \right) = -\frac{\partial r_i}{\partial x_i} \left( \frac{1}{r^3} \right) + \frac{\partial r}{\partial x_i} \left( \frac{3r_i}{r^4} \right) \\ &= -3 \left( \frac{1}{r^3} \right) + \frac{r_i}{r} \left( \frac{3r_i}{r^4} \right) = -\frac{3}{r^3} + \frac{r^2}{r} \left( \frac{3}{r^4} \right) = 0 \end{aligned} \quad (\text{Q.9})$$

To get the right side on the second line we used the fact that  $r_i r_i = r^2$ . Now we replace  $r_i = \mathbf{r}$  by  $\mathbf{r} - \mathbf{r}_P = r_i - r_{P,i}$  in Eqs. Q.8 and Q.9 which gives

$$\begin{aligned} \frac{\partial}{\partial x_i} \left( \frac{1}{|\mathbf{r} - \mathbf{r}_P|} \right) &= -\frac{r_i - r_{P,i}}{|\mathbf{r} - \mathbf{r}_P|^3} \\ \frac{\partial^2}{\partial x_i \partial x_i} \left( \frac{1}{|\mathbf{r} - \mathbf{r}_P|} \right) &= 0 \end{aligned} \quad (\text{Q.10})$$

for  $r_i \neq r_i^P$ , i.e. for  $V$  excluding the sphere  $S^\varepsilon$ , see Fig. Q.1. Apply Green's second formula for this volume which has the bounding surfaces  $S$  and  $S^\varepsilon$  with normal vectors  $n_i$  (outwards) and  $n_i^\varepsilon$  (inwards), respectively. We get

$$\begin{aligned} - \int_{V - S^\varepsilon} \frac{1}{|\mathbf{r} - \mathbf{r}_P|} \frac{\partial^2 \varphi}{\partial x_i \partial x_i} dV &= \int_S \left( -\varphi \frac{r_i - r_i^P}{|\mathbf{r} - \mathbf{r}_P|^3} - \frac{1}{|\mathbf{r} - \mathbf{r}_P|} \frac{\partial \varphi}{\partial x_i} \right) n_i dS \\ &\quad + \int_{S^\varepsilon} \left( -\varphi \frac{r_i - r_i^P}{|\mathbf{r} - \mathbf{r}_P|^3} - \frac{1}{|\mathbf{r} - \mathbf{r}_P|} \frac{\partial \varphi}{\partial x_i} \right) (-n_i^\varepsilon) dS \end{aligned} \quad (\text{Q.11})$$

where the volume integral is taken over the volume  $V$  but excluding the sphere  $S^\varepsilon$ , i.e.  $V - S^\varepsilon$ . Note the minus sign in front of the normal vector in the  $S^\varepsilon$  integral; this is

because the normal vector must point *out* of the volume  $V - S^\varepsilon$ , i.e. into the sphere,  $S^\varepsilon$ . In the sphere the normal vector,  $n_i^\varepsilon$ , is the direction from point  $\mathbf{r}_P$ , i.e.

$$-n_i^\varepsilon = \frac{\mathbf{r} - \mathbf{r}_P}{|\mathbf{r} - \mathbf{r}_P|} = \frac{r_i - r_{P,i}}{|r_i - r_{P,i}|} \quad (\text{Q.12})$$

where we have normalized the vector  $r_i - r_{P,i}$  in order to make its length equal to one. The length of the vector  $r_i - r_{P,i}$  is the radius of sphere  $S^\varepsilon$ , i.e.

$$|\mathbf{r} - \mathbf{r}_P| = \varepsilon \quad (\text{Q.13})$$

The surface area,  $dS$ , for sphere  $S^\varepsilon$  can be expressed in spherical coordinates as

$$dS = \varepsilon^2 \Omega = \varepsilon^2 \sin \theta d\theta d\alpha \quad (\text{Q.14})$$

where  $\Omega$  is the solid angle. Inserting Eqs. Q.12, Q.13 and Q.14 in the last integral in Eq. Q.11 gives

$$I_{S^\varepsilon} = \int_{S^\varepsilon} \left( \frac{\varphi}{\varepsilon^2} + \frac{r_i - r_{P,i}}{\varepsilon^2} \frac{\partial \varphi}{\partial x_i} \right) \varepsilon^2 d\Omega = \int_{S^\varepsilon} \left( \varphi + (r_i - r_{P,i}) \frac{\partial \varphi}{\partial x_i} \right) d\Omega \quad (\text{Q.15})$$

To re-write this integral we will use the *mean value theorem* for integrals. In one dimension this theorem simply states that for the integral of a function,  $g(x)$ , over the interval  $[a, b]$ , there exists (at least) one point for which the relation

$$\int_a^b g(x) dx = (b - a)g(x_Q) \quad (\text{Q.16})$$

holds, where  $x_Q$  denotes a point on  $[a, b]$ . Applying this theorem to the integral in Eq. Q.15 gives

$$I_{S^\varepsilon} = \varphi(\mathbf{r}_Q) \int_{S^\varepsilon} d\Omega + \left[ r_{Q,i} - r_{P,i} \frac{\partial \varphi}{\partial x_i}(\mathbf{r}_Q) \right] \int_{S^\varepsilon} d\Omega \quad (\text{Q.17})$$

where  $\mathbf{r}_Q \equiv r_{Q,i}$  denotes a point on  $S^\varepsilon$ . As we let  $Q \rightarrow P$ , the radius,  $\varepsilon$ , of sphere  $S^\varepsilon$  goes to zero so that the integral in Eq. Q.17 reads

$$\lim_{\varepsilon \rightarrow 0} I_{S^\varepsilon} = 4\pi \varphi(\mathbf{r}_Q) \quad (\text{Q.18})$$

since  $\int_{S^\varepsilon} d\Omega = 4\pi$ . Inserted in Eq. Q.18 gives

$$\begin{aligned} \varphi(\mathbf{r}_P) &= -\frac{1}{4\pi} \int_V \frac{1}{|\mathbf{r} - \mathbf{r}_P|} \frac{\partial^2 \varphi}{\partial x_i \partial x_i} dV \\ &+ \frac{1}{4\pi} \int_S \varphi \frac{r_i - r_i^P}{|\mathbf{r} - \mathbf{r}_P|^3} n_i dS + \frac{1}{4\pi} \int_S \frac{1}{|\mathbf{r} - \mathbf{r}_P|} \frac{\partial \varphi}{\partial x_i} n_i dS \end{aligned} \quad (\text{Q.19})$$

This is Green's third formula.

The singularity  $1/|\mathbf{r} - \mathbf{r}_P|$  in the volume integral in Eq. Q.19 is not a problem. Consider a small sphere with radius  $r_1 = |\mathbf{r} - \mathbf{r}_P|$  centered at point  $P$ . In spherical coordinates the volume element can then be expressed as

$$dV = r_1^2 \sin \theta dr_1 d\theta d\alpha = r_1^2 dr_1 d\Omega \quad (\text{Q.20})$$

Hence it is seen that the volume element  $dV$  goes to zero faster than the singularity  $1/|\mathbf{r} - \mathbf{r}_P|$ .

## Q.4 Analytical solution to Poisson's equation

Poisson's equation reads

$$\frac{\partial^2 \varphi}{\partial x_j \partial x_j} = f \quad (\text{Q.21})$$

where we assume that  $\varphi$  goes to zero at infinity and that the right side is limited. Green's third formula, Eq. Q.19, gives

$$\begin{aligned} \varphi(\mathbf{r}_P) &= -\frac{1}{4\pi} \int_V \frac{f(\mathbf{r})}{|\mathbf{r} - \mathbf{r}_P|} dV \\ &\quad + \frac{1}{4\pi} \int_S \varphi \frac{r_i - r_i^P}{|\mathbf{r} - \mathbf{r}_P|^3} n_i dS + \frac{1}{4\pi} \int_S \frac{1}{|\mathbf{r} - \mathbf{r}_P|} \frac{\partial \varphi}{\partial x_i} n_i dS \end{aligned} \quad (\text{Q.22})$$

We choose the volume as a large sphere with radius  $R$ . Using Eqs. Q.12, Q.13 and Q.14, the first surface integral can be written as

$$\frac{1}{4\pi} \int_S \varphi \frac{r_i - r_i^P}{|\mathbf{r} - \mathbf{r}_P|^3} n_i dS = \frac{1}{4\pi R^2} \int_S \varphi n_i n_i dS = \frac{1}{4\pi} \int_S \varphi d\Omega \quad (\text{Q.23})$$

using  $n_i n_i = 1$ . This integral goes to zero since  $\varphi \rightarrow 0$  as  $R \rightarrow \infty$ .

The second integral in Eq. Q.22 can be re-written using Eq. Q.13, Gauss divergence law and Eq. Q.21 as

$$\begin{aligned} \frac{1}{4\pi} \int_S \frac{1}{|\mathbf{r} - \mathbf{r}_P|} \frac{\partial \varphi}{\partial x_i} n_i dS &= \frac{1}{4\pi R} \int_S \frac{\partial \varphi}{\partial x_i} n_i dS \\ &= \frac{1}{4\pi R} \int_S \frac{\partial^2 \varphi}{\partial x_i \partial x_i} dV = \frac{1}{4\pi R} \int_V f dV \end{aligned} \quad (\text{Q.24})$$

This integral also goes to zero for large  $R$  since we have assumed that  $f$  is limited. Hence the final form of Eq. Q.22 reads

$$\varphi(\mathbf{r}_P) = -\frac{1}{4\pi} \int_V \frac{f(\mathbf{r})}{|\mathbf{r} - \mathbf{r}_P|} dV \quad (\text{Q.25})$$

This is the analytical solution to Poisson's equation, Eq. Q.21.

## R MTF270: Learning outcomes for 2012

### Week 1

1. How is the buoyancy term,  $\rho g_i$ , re-written in incompressible flow?
2. Given the transport equation for the temperature,  $\theta$ , and the transport equation for  $\bar{\theta}$ , Derive the transport equation for  $v'_i \theta'$  (Eq. 11.19). Discuss the physical meaning of the different terms. Which terms need to be modelled?
3. What is the expression for the total heat flux that appear in the  $\bar{\theta}$  equation?
4. Which terms in the  $\overline{v'_i v'_j}$  equation need to be modelled? Explain the physical meaning of the different terms in the  $\overline{v'_i v'_j}$  equation.
5. Derive the Boussinesq assumption.
6. Show how the turbulent diffusion (i.e. the term including the triple correlation) in the  $k$  equation is modelled.
7. How is the production term modelled in the  $k - \varepsilon$  model (Boussinesq)? Show how it can be expressed in  $\bar{s}_{ij}$
8. Given the modelled  $k$  equation, derive the modelled  $\varepsilon$  equation.
9. Discuss and show how the dissipation term,  $\varepsilon_{ij}$ , is modelled.

## Week 2

1. How are the Reynolds stress,  $\overline{v'_i v'_j}$ , and the turbulent heat flux,  $\overline{v'_i \theta'}$ , modelled in the Boussinesq approach?
2. Use physical reasoning to derive a model for the diagonal components of the pressure-strain term (slow part).
3. Derive the exact Poisson equation for the pressure fluctuation, Eq. 11.61.
4. For a Poisson equation

$$\frac{\partial^2 \varphi}{\partial x_j \partial x_j} = f$$

there exists an exact analytical solution

$$\varphi(\mathbf{x}) = -\frac{1}{4\pi} \int_V \frac{f(\mathbf{y}) dy_1 dy_2 dy_3}{|\mathbf{y} - \mathbf{x}|} \quad (\text{R.1})$$

Use Eqs. 11.61 and R.1 to derive the exact analytical solution for the pressure-strain term. What are the “slow” and “rapid” terms?

5. Derive the algebraic stress model (ASM). What main assumption is made?
6. Describe the physical effect of the pressure-strain term in the near-wall region. What sign must hence  $\Phi_{22,1w}$  have?
7. The modelled slow and rapid pressure strain term read  $\Phi_{ij,1} = -c_1 \rho \frac{\varepsilon}{k} \left( \overline{v'_i v'_j} - \frac{2}{3} \delta_{ij} k \right)$  and  $\Phi_{ij,2} = -c_2 \left( P_{ij} - \frac{2}{3} \delta_{ij} P^k \right)$ , respectively. Give the expression for the production terms, modelled pressure-strain terms and modelled dissipation terms for a simple shear flow (e.g. boundary layer, channel flow, jet flow ...). In some stress equations there is no production terms nor any dissipation term. How come? Which is the main source term (or sink term) in these equations?
8. Describe the physical effect of stable stratification and unstable stratification on turbulence.
9. Consider buoyancy-dominated flow with  $x_3$  vertically upwards. The production term for the  $\overline{v'_i v'_j}$  and the  $\overline{v'_i \theta'}$  equations read

$$G_{ij} = -g_i \beta \overline{v'_j \theta'} - g_j \beta \overline{v'_i \theta'}, \quad P_{i\theta} = -\overline{v'_i v'_k} \frac{\partial \bar{\theta}}{\partial x_k}$$

respectively. Show that the Reynolds stress model dampens and increases the vertical fluctuation in stable and unstable stratification, respectively, as it should. Show also that  $k$  in the  $k - \varepsilon$  model is affected in the same way.

10. Consider streamline curvature for a streamline formed as a circular arc (convex curvature). Show that the turbulence is damped if  $\partial v_\theta / \partial r > 0$  and that it is enhanced if the sign of  $\partial v_\theta / \partial r$  is negative.
11. Streamline curvature: now consider a boundary layer where the streamlines are curved away from the wall (concave curvature). Show that the Reynolds stress model gives an enhanced turbulence production (as it should) because of positive feedback between the production terms. Show that the effect of streamline curvature in the  $k - \varepsilon$  model is much smaller.

12. Consider stagnation flow. Show that in the Reynolds stress model, there is only a small production of turbulence whereas eddy-viscosity models (such as the  $k - \varepsilon$  model) give a large production of turbulence.
13. What is a realizability constraint? There are two main realizability constraints on the normal and the shear stresses: which ones?
14. Show that the Boussinesq assumption may give negative normal stresses. In which coordinate system is the risk largest for negative normal stresses? Derive an expression (2D) how to avoid negative normal stresses by reducing the turbulent viscosity (Eq. 13.12).
15. What is the two-component limit? What requirement does it put on the pressure-strain models? Show that the standard IP model and the Rotta model do not satisfy this requirement.
16. What is a non-linear eddy-viscosity model? When formulating a non-linear model, the anisotropy tensor  $a_{ij} = -2\nu_t \bar{s}_{ij}/k$  is often used. Show the three first terms ( $S^2, \Omega^2, S\Omega$ ) in the non-linear model in the lecture notes. Show that each term has the same properties as  $a_{ij}$ , i.e. non-dimensional, traceless and symmetric.

## Week 3

1. Which equations are solved in the V2F model?
2. The transport equation for  $\overline{v_2'^2}$  reads (the turbulent diffusion terms are modelled)

$$\frac{\partial \rho \bar{v}_1 \overline{v_2'^2}}{\partial x_1} + \frac{\partial \rho \bar{v} \overline{v_2'^2}}{\partial x_2} = \frac{\partial}{\partial x_2} \left[ (\mu + \mu_t) \frac{\partial \overline{v_2'^2}}{\partial x_2} \right] - \underbrace{2 \overline{v'_2} \frac{\partial p' / \partial x_2}{\partial x_2}}_{\Phi_{22}} - \rho \varepsilon_{22}$$

Show how this equation is re-written in the V2F model.

3. The  $f$  equation in the V2F model reads

$$L^2 \frac{\partial^2 f}{\partial x_2^2} - f = -\frac{\Phi_{22}}{k} - \frac{1}{T} \left( \frac{\overline{v_2'^2}}{k} - \frac{2}{3} \right), \quad T \propto \frac{k}{\varepsilon}, \quad L \propto \frac{k^{3/2}}{\varepsilon}$$

Show how the magnitude of the right side and  $L$  affect  $f$ . How does  $f$  enter into the  $\overline{v_2'^2}$  equation? What is the physical meaning of  $f$ ? Show that far from the walls, the V2F model (i.e. the  $f$  and the  $\overline{v_2'^2}$  equation) returns to the  $\overline{v_2'^2}$  equation in the Reynolds stress model.

4. What does the acronym SST mean? The SST model is a combination of the  $k - \varepsilon$  and the  $k - \omega$  model. In which region is each model being used and why? How is  $\omega$  expressed in  $k$  and  $\varepsilon$ ?

## Week 4

1. Derive a transport equation for  $\omega$  from the  $k$  and  $\varepsilon$  transport equations.
2. Describe the  $k - \omega$  SST model.
3. In the SST model, a blending function  $F_1$  is used; what does this function do? In which region is each model being used and why?
4. What is the purpose of the shear stress limiter in the SST model? Show that the eddy-viscosity assumption gives too high shear stress in APG since  $P^k/\varepsilon \gg 1$  (Eq. 16.14).
5. Show the difference between volume averaging (filtering) in LES and time-averaging in RANS.
6. Consider the spatial derivative of the pressure in the filtered Navier-Stokes: show that the derivative can be moved outside the filtering integral (it gives an additional second-order term).
7. The filtered non-linear term has the form

$$\overline{\frac{\partial v_i v_j}{\partial x_j}}$$

Show that it can be re-written as

$$\overline{\frac{\partial \bar{v}_i \bar{v}_j}{\partial x_j}}$$

giving an additional term

$$-\frac{\partial}{\partial x_j}(\bar{v}_i \bar{v}_j) + \frac{\partial}{\partial x_j}(\bar{v}_i \bar{v}_j) = -\frac{\partial \tau_{ij}}{\partial x_j}$$

on the right side.

8. Consider a 1D finite volume grid. Carry out a second filtering of  $\bar{v}$  at node  $I$  and show that  $\bar{v}_I \neq \bar{v}_I$ .
9. Consider the energy spectrum. Show the three different regions (the large energy-containing scales, the  $-5/3$  range and the dissipating scales). Where should the cut-off be located? What does cut-off mean? Show where the SGS scales, grid (i.e resolved) scales and the cut-off,  $\kappa_c$  are located in the spectrum.
10. Show how a sinus wave  $\sin(\kappa_c x)$  corresponding to cut-off is represented on a grid with two and four nodes, respectively. How is  $\kappa_c$  related to the grid size  $\Delta x$  for these cases? Using the sin wave, derive the relation between  $\kappa_c$  and  $\Delta$ .
11. Derive the one-equation  $k_{sgs}$  equation
12. Consider the energy spectrum and discuss the physical meaning of  $P_{k_{sgs}}$  and  $\varepsilon_{sgs}$ .
13. Derive the Smagorinsky model in two different ways (Sections 18.6 and 18.22)

## Week 5

1. Discuss the energy path in connection to the source and sink terms in the  $\bar{k}$ ,  $\bar{K}$  and the  $k_{sgs}$  equations, see Fig. L.3. How are  $\bar{k}$  and  $k_{sgs}$  computed from the energy spectrum?
2. What is a test filter? Grid and test filter Naiver-Stokes equation and derive the relation

$$\widehat{\bar{v}_i \bar{v}_j} - \widehat{\bar{v}_i} \widehat{\bar{v}_j} + \widehat{\tau}_{ij} = T_{ij} \quad (\text{R.2})$$

Draw an energy spectrum and show which wavenumber range  $\bar{k}$ ,  $k_{sgs}$ ,  $k_{sgs,test}$  cover.

3. Formulate the Smagorinsky model for the grid filter SGS stress,  $\tau_{ij}$ , and the test filter SGS stress,  $T_{ij}$ . Use Eq. R.2 and derive the relation

$$\mathcal{L}_{ij} - \frac{1}{3} \delta_{ij} \mathcal{L}_{kk} = -2C \left( \widehat{\Delta}^2 |\widehat{s}| \widehat{s}_{ij} - \Delta^2 |\bar{s}| \widehat{\bar{s}}_{ij} \right)$$

This equation is a tensor equation for  $C$ . Use this relation and derive the final expression for the dynamic coefficient,  $C$ , Eq. 18.33.

4. Show that when a first-order upwind schemes is used for the convection term, an additional diffusion term and dissipation terms appear because of a numerical SGS viscosity.
5. We usually define the SGS stress tensor as  $\tau_{ij} = \overline{v'_i v'_j} - \bar{v}_i \bar{v}_j$ . In scale-similarity models  $\tau_{ij}$  is written as three different terms. Derive these three terms. What are they called? What does the work “scale-similar” mean?
6. What are the five main differences between a RANS finite volume CFD code and a LES finite volume CFD code? What do you need to consider in LES when you want to compute time-averaged quantities? (see Fig. 18.11)
7. When doing LES, how fine does the mesh need to be in the wall region be? Why does it need to be that fine?
8. What is DES? The length scale in the RANS S-A model reads  $\left(\frac{\tilde{\nu}_t}{d}\right)^2$ ; how is it computed in the corresponding DES model?
9. How is the length scale computed in a  $k - \varepsilon$  two-equation DES model? Where in a boundary layer does the DES model switch from RANS to LES (see “Summary of lectures”)
10. The modified (reduced) length scale in two-equation DES models can be introduced in different equations. Which equations and which term? What is the effect on the modelled, turbulent quantities?
11. Describe hybrid LES-RANS based on a one-equation model.
12. Describe URANS. How is the instantaneous velocity decomposed? What turbulence models are used? What is scale separation?
13. Discuss the choice of discretization scheme and turbulence model in URANS (see Sections 19.1 and 19.2)

## Week 6

1. Describe the SAS model. How is the von Kármán length scale defined? An additional source term is introduced in the  $\omega$  equation: what is the form of this term? What is the object of this term? When is it large and small, respectively?
2. Describe the PANS model. What is the main modification compared to the standard  $k - \varepsilon$  model? What is the physical meaning of  $f_k$ ? Describe what happens to the equation system when  $f_k$  is reduced.
3. Give a short description of the method to generate synthetic turbulent inlet fluctuations. What form on the spectrum is assumed? How are the maximum and minimum wavelengths,  $\kappa_{max}$ ,  $\kappa_{min}$ , determined. With this method, the generated shear stress is zero: why? How is the correlation in time achieved?

## S References

- [1] L. Davidson, P.V. Nielsen, and A. Sveningsson. Modifications of the  $v^2 - f$  model for computing the flow in a 3D wall jet. In K. Hanjalić, Y. Nagano, and M.J. Tummers, editors, *Turbulence Heat and Mass Transfer 4*, pages 577–584, New York, Wallingford (UK), 2003. begell house, inc.
- [2] J.N. Reddy. *An Introduction to Continuum Mechanics*. Cambridge University Press, New York, 2008.
- [3] S. Toll and M. Ekh. Mechanics of solids & fluids. Part I: Fundamentals. Report, Div. of Material and Computational Mechanics, Dept. of Applied Mechanics, Chalmers University of Technology, Göteborg, Sweden, 2011.
- [4] H. Abedi. Aerodynamic loads on rotor blades. MSc Thesis 2011:18, Division of Fluid Dynamics, Department of Applied Mechanics, Chalmers University of Technology, Göteborg, Sweden, 2011.
- [5] L. Davidson. An introduction to turbulence models. Technical Report 97/2, Dept. of Thermo and Fluid Dynamics, Chalmers University of Technology, Gothenburg, 1997.
- [6] J. Wojtkowiak and C.O. Popiel. Inherently linear annular-duct-type laminar flowmeter. *Journal of Fluids Engineering*, 128(1):196–198, 2006.
- [7] S.B. Pope. *Turbulent Flow*. Cambridge University Press, Cambridge, UK, 2001.
- [8] H. Tennekes and J.L. Lumley. *A First Course in Turbulence*. The MIT Press, Cambridge, Massachusetts, 1972.
- [9] P. Bradshaw. *Turbulence*. Springer-Verlag, Berlin, 1976.
- [10] S. Hoyas and J. Jiménez. Scaling of the velocity fluctuations in turbulent channels up to  $Re_\tau = 2003$ . *Physics of Fluids A*, 18(011702), 2006.
- [11] S. Hoyas and J. Jiménez. <http://torroja.dmt.upm.es/ftp/channels/data/statistics/>. 2006.
- [12] Th. von Kármán. Mechanische Ähnlichkeit und Turbulenz. *Nachrichten von der Gesellschaft der Wissenschaften zu Göttingen, Fachgruppe I (Mathematik)*, 5:58–76, 1930.
- [13] P.R. Spalart. Direct simulation of a turbulent boundary layer up to  $R_\theta = 1410$ . *Journal of Fluid Mechanics*, 187:61–98, 1988.
- [14] A.A. Townsend. Equilibrium layers and wall turbulence. *Journal of Fluid Mechanics*, 11:97–120, 1961.
- [15] L. Davidson. Transport equations in incompressible URANS and LES. Report 2006/01, Div. of Fluid Dynamics, Dept. of Applied Mechanics, Chalmers University of Technology, Göteborg, Sweden, 2006.
- [16] K. Hanjalić. Advanced turbulence closure models: A view of current status and future prospects. *Int. J. Heat and Fluid Flow*, 15:178–203, 1994.

- [17] D.C. Wilcox. *Turbulence Modeling for CFD*. DCW Industries, Inc., 5354 Palm Drive, La Cañada, California 91011, 2 edition, 1998.
- [18] K. Hanjalić and B.E. Launder. A Reynolds stress model of turbulence and its application to thin shear flows. *Journal of Fluid Mechanics*, 52:609–638, 1972.
- [19] J.C. Rotta. Statistische theorie nichthomogener turbulenz. *Zeitschrift für Physik*, 129:547–572, 1951.
- [20] G.E. Mase. *Continuum Mechanics*. Schaum's Outline Series. McGraw-Hill, 1970.
- [21] S. Fu, B.E. Launder, and D.P. Tselepidakes. Accomodating the effects of high strain rates in modelling the pressure-starin correlation. Technical Report TFD/87/5, UMIST, Mechanical Engineering Dept., 1987.
- [22] B.E. Launder, G.J. Reece, and W. Rodi. Progress in the development of a Reynolds-stress turbulence closure. *Journal of Fluid Mechanics*, 68(3):537–566, 1975.
- [23] D. Naot, A. Shavit, and M. Wolfshtein. Interactions between components of the turbulent velocity correlation tensor. *Israel J. Techn.*, 8:259, 1970.
- [24] B. E. Launder. An introduction to single-point closure methodology. In T.B. Gatski, M.Y. Hussaini, and J.L. Lumley, editors, *Simulation and Modeling of Turbulent Flows*, New York, 1996. Oxford University Press.
- [25] M.M. Gibson and B.E. Launder. Ground effects on pressure fluctuations in the atmospheric boundary layer. *Journal of Fluid Mechanics*, 86:491–511, 1978.
- [26] S.B. Pope. A more general effective-viscosity hypothesis. *Journal of Fluid Mechanics*, 472:331–340, 1975.
- [27] P. Bradshaw. Effects of streamline curvature on turbulent flow. Agardograph progress no. 169, AGARD, 1973.
- [28] W. Rodi and G. Scheuerer. Calculation of curved shear layers with two-equation turbulence models. *Physics of Fluids*, 26:1422–1435, 1983.
- [29] B.E. Thompson and J.H. Whitelaw. Characteristics of a trailing-edge flow with turbulent boundary-layer separation. *Journal of Fluid Mechanics*, 157:305–326, 1985.
- [30] S. Wallin and A.V. Johansson. Modelling streamline curvature effects in explicit algebraic reynolds stress turbulence models. *International Journal of Heat and Fluid Flow*, 23(5):721–730, 2002.
- [31] L. Davidson. Prediction of the flow around an airfoil using a Reynolds stress transport model. *Journal of Fluids Engineering*, 117:50–57, 1995.
- [32] P.A. Durbin. On the  $k - 3$  stagnation point anomaly. *International Journal of Heat and Fluid Flow*, 17:89–90, 1996.
- [33] J. Hult. *Cartesiska tensorer: Ett praktiskt fikonspråk*. Almqvist & Wiksell, 1972.

- [34] J.L. Lumley. Computational modeling of turbulent flows. *Advances in Applied Mechanics*, 18:123–176, 1978.
- [35] T.J. Craft and B.E. Launder. A Reynolds stress closure designated for complex geometries. *International Journal of Heat and Fluid Flow*, 17(3):245–254, 1996.
- [36] T.J. Craft, B.E. Launder, and K. Suga. Prediction of turbulent transitional phenomena with a nonlinear eddy-viscosity model. *International Journal of Heat and Fluid Flow*, 18:15–28, 1997.
- [37] T.B. Gatski and C.G. Speziale. On explicit algebraic stress models for complex turbulent flows. *Journal of Fluid Mechanics*, 154:59–78, 1993.
- [38] T.-H. Shih, J. Zhu, and J.L. Lumley. A new Reynolds stress algebraic equation model. *Comput. Methods Appl. Engng.*, 125:287–302, 1995.
- [39] S. Wallin and A.V. Johansson. A new explicit algebraic Reynolds stress model for incompressible and compressible turbulent flows. *Journal of Fluid Mechanics*, 403:89–132, 2000.
- [40] P.A. Durbin. Near-wall turbulence closure modeling without damping functions. *Theoretical and Computational Fluid Dynamics*, 3:1–13, 1991.
- [41] P.A. Durbin. Application of a near-wall turbulence model to boundary layers and heat transfer. *International Journal of Heat and Fluid Flow*, 14(4):316–323, 1993.
- [42] A. Sveningsson. Analysis of the performance of different  $\overline{v^2} - f$  turbulence models in a stator vane passage flow. Thesis for licentiate of engineering, Dept. of Thermo and Fluid Dynamics, Chalmers University of Technology, Göteborg, Sweden, 2003.
- [43] K. Hanjalic, M. Popovacx, and M. Habziabdic. A robust near-wall elliptic relaxation eddy-viscosity turbulence model for CFD. *International Journal of Heat and Fluid Flow*, 2004.
- [44] F-S Lien and G. Kalitzin. Computations of transonic flow with the v2f turbulence model. *International Journal of Heat and Fluid Flow*, 22(1):53–61, 2001.
- [45] A. Sveningsson and L. Davidson. Assessment of realizability constraints in  $\overline{v^2} - f$  turbulence models. *International Journal of Heat and Fluid Flow*, 25(5):785–794, 2004.
- [46] A. Sveningsson and L. Davidson. Computations of flow field and heat transfer in a stator vane passage using the  $\overline{v^2} - f$  turbulence model. Paper GT2004-53586, ASME TURBO EXPO 2004, Vienna, 2004.
- [47] A. Sveningsson and L. Davidson. Computations of flow field and heat transfer in a stator vane passage using the  $\overline{v^2} - f$  turbulence model. *Journal of Turbomachinery*, 127(3):627–634, 2005.
- [48] A. Sveningsson. *Turbulence Transport Modelling in Gas Turbine Related Applications*. PhD thesis, Div. of Fluid Dynamics, Dept. of Applied Mechanics, Chalmers University of Technology, Göteborg, Sweden, 2006.

- [49] F.R. Menter. Two-equation eddy-viscosity turbulence models for engineering applications. *AIAA Journal*, 32:1598–1605, 1994.
- [50] D.C. Wilcox. Reassessment of the scale-determining equation. *AIAA Journal*, 26(11):1299–1310, 1988.
- [51] F.R. Menter. Influence of freestream values on  $k - \omega$  turbulence model predictions. *AIAA Journal*, 30(6):1657–1659, 1992.
- [52] J. Bredberg. On two-equation eddy-viscosity models. Report 01/8, can be downloaded from [www.tfd.chalmers.se/~lada/allpaper.html](http://www.tfd.chalmers.se/~lada/allpaper.html), Dept. of Thermo and Fluid Dynamics, Chalmers University of Technology, 2001.
- [53] P. Bradshaw, D.H. Ferriss, and N.P. Atwell. Calculation of boundary-layer development using the turbulent energy equation. *Journal of Fluid Mechanics*, 28:593–616, 1967.
- [54] F.R. Menter, M. Kuntz, and R. Langtry. Ten years of industrial experience of the SST turbulence model. In K. Hanjalić, Y. Nagano, and M.J. Tummers, editors, *Turbulence Heat and Mass Transfer 4*, pages 624–632, New York, Wallingford (UK), 2003. begell house, inc.
- [55] S. Ghosal and P. Moin. The basic equations for the large eddy simulation of turbulent flows in complex geometry. *J. Comp. Phys.*, 118:24–37, 1995.
- [56] J. Smagorinsky. General circulation experiments with the primitive equations. *Monthly Weather Review*, 91:99–165, 1963.
- [57] P. Moin and J. Kim. Numerical investigation of turbulent channel flow. *Journal of Fluid Mechanics*, 118:341–377, 1982.
- [58] W.P. Jones and M. Wille. Large eddy simulation of a jet in a cross-flow. In *10th Symp. on Turbulent Shear Flows*, pages 4:1 – 4:6, The Pennsylvania State University, 1995.
- [59] J.O. Hinze. *Turbulence*. McGraw-Hill, New York, 2nd edition, 1975.
- [60] H. Schlichting. *Boundary-Layer Theory*. McGraw-Hill, New York, 7 edition, 1979.
- [61] M. Germano, U. Piomelli, P. Moin, and W.H. Cabot. A dynamic subgrid-scale eddy viscosity model. *Physics of Fluids A*, 3:1760–1765, 1991.
- [62] Y. Zang, R.L. Street, and J.R. Koseff. A dynamic mixed subgrid-scale model and its application to turbulent recirculating flows. *Physics of Fluids A*, 5:3186–3196, 1993.
- [63] D.K. Lilly. A proposed modification of the Germano subgrid-scale closure method. *Physics of Fluids A*, 4:633–635, 1992.
- [64] J.P. Boris, F.F. Grinstein, E.S. Oran, and R.L. Kolbe. New insights into large eddy simulation. *Fluid Dynamic Research*, 10:199–228, 1992.
- [65] J. Bardina, J.H. Ferziger, and W.C. Reynolds. Improved subgrid scale models for large eddy simulation. AIAA 80-1357, Snomass, Colorado, 1980.

- [66] C.G. Speziale. Galilean invariance of subgrid-scale stress models in the large-eddy simulation of turbulence. *Journal of Fluid Mechanics*, 156:55–62, 1985.
- [67] M. Germano. A proposal for a redefinition of the turbulent stresses in the filtered Navier-Stokes equations. *Phys. Fluids A*, 7:2323–2324, 1986.
- [68] L. Davidson. A dissipative scale-similarity model. In V. Armenio, B. Geurts, and J. Fröhlich, editors, *DLES7: Direct and Large-Eddy Simulations 7*, volume 13 of *ERCOFTAC series*, pages 261–266, 2010.
- [69] C. Hirsch. *Numerical Computation of Internal and External Flows: Fundamentals of Numerical Discretization*, volume 1. John Wiley & Sons, Chichester, UK, 1988.
- [70] L. Davidson. Hybrid LES-RANS: back scatter from a scale-similarity model used as forcing. *Phil. Trans. of the Royal Society A*, 367(1899):2905–2915, 2009.
- [71] P. Emvin. *The Full Multigrid Method Applied to Turbulent Flow in Ventilated Enclosures Using Structured and Unstructured Grids*. PhD thesis, Dept. of Thermo and Fluid Dynamics, Chalmers University of Technology, Göteborg, 1997.
- [72] L. Davidson and S.-H. Peng. Hybrid LES-RANS: A one-equation SGS model combined with a  $k - \omega$  model for predicting recirculating flows. *International Journal for Numerical Methods in Fluids*, 43:1003–1018, 2003.
- [73] S.V. Patankar. *Numerical Heat Transfer and Fluid Flow*. McGraw-Hill, New York, 1980.
- [74] H.K. Versteegh and W. Malalasekera. *An Introduction to Computational Fluid Dynamics - The Finite Volume Method*. Longman Scientific & Technical, Harlow, England, 1995.
- [75] L. Davidson and M. Billson. Hybrid LES/RANS using synthesized turbulence for forcing at the interface. *International Journal of Heat and Fluid Flow*, 27(6):1028–1042, 2006.
- [76] L. Davidson. Large eddy simulation: A dynamic one-equation subgrid model for three-dimensional recirculating flow. In *11th Int. Symp. on Turbulent Shear Flow*, volume 3, pages 26.1–26.6, Grenoble, 1997.
- [77] L. Davidson. Large eddy simulations: A note on derivation of the equations for the subgrid turbulent kinetic energies. Technical Report 97/11, Dept. of Thermo and Fluid Dynamics, Chalmers University of Technology, Gothenburg, 1997.
- [78] A. Sohankar, L. Davidson, and C. Norberg. Large eddy simulation of flow past a square cylinder: Comparison of different subgrid scale models. *Journal of Fluids Engineering*, 122(1):39–47, 2000.
- [79] A. Sohankar, L. Davidson, and C. Norberg. Erratum. *Journal of Fluids Engineering*, 122(3):643, 2000.

- [80] S. Krajnović and L. Davidson. A mixed one-equation subgrid model for large-eddy simulation. *International Journal of Heat and Fluid Flow*, 23(4):413–425, 2002.
- [81] S. Krajnović and L. Davidson. Large eddy simulation of the flow around a bluff body. *AIAA Journal*, 40(5):927–936, 2002.
- [82] S. Krajnović. *Large Eddy Simulations for Computing the Flow Around Vehicles*. PhD thesis, Dept. of Thermo and Fluid Dynamics, Chalmers University of Technology, Göteborg, Sweden, 2002.
- [83] J. Pallares and L. Davidson. Large-eddy simulations of turbulent flow in a rotating square duct. *Physics of Fluids*, 12(11):2878–2894, 2000.
- [84] J. Pallares and L. Davidson. Large-eddy simulations of turbulent heat transfer in stationary and rotating square duct. *Physics of Fluids*, 14(8):2804–2816, 2002.
- [85] S. Krajnović and L. Davidson. Numerical study of the flow around the bus-shaped body. *Journal of Fluids Engineering*, 125:500–509, 2003.
- [86] S. Krajnović and L. Davidson. Flow around a simplified car. part I: Large eddy simulations. *Journal of Fluids Engineering*, 127(5):907–918, 2005.
- [87] S. Krajnović and L. Davidson. Flow around a simplified car. part II: Understanding the flow. *Journal of Fluids Engineering*, 127(5):919–928, 2005.
- [88] S. Krajnović and L. Davidson. Influence of floor motions in wind tunnels on the aerodynamics of road vehicles. *Journal of Wind Engineering and Industrial Aerodynamics*, 92(5):677–696, 2005.
- [89] S. Dahlström and L. Davidson. Large eddy simulation applied to a high-Reynolds flow around an airfoil close to stall. AIAA paper 2003-0776, 2003.
- [90] S. Dahlström. *Large Eddy Simulation of the Flow Around a High-Lift Airfoil*. PhD thesis, Dept. of Thermo and Fluid Dynamics, Chalmers University of Technology, Göteborg, Sweden, 2003.
- [91] J. Ask and L. Davidson. Flow and dipole source evaluation of a generic SUV. *Journal of Fluids Engineering*, 132(051111), 2010.
- [92] H. Hemida and S. Krajnović. LES study of the impact of the wake structures on the aerodynamics of a simplified ICE2 train subjected to a side wind. In *Fourth International Conference on Computational Fluid Dynamics (ICCFD4)*, 10-14 July, Ghent, Belgium, 2006.
- [93] H. Hemida and S. Krajnović. Numerical study of the unsteady flow structures around train-shaped body subjected to side winds. In *ECCOMAS CFD 2006*, 5-8 September, Egmond aan Zee, The Netherlands, 2006.
- [94] S. Krajnović. Numerical simulation of the flow around an ICE2 train under the influence of a wind gust. In *International Conference on Railway Engineering 2008 (IET ICRE2008)*, 25-28 March, Hong Kong, China, 2008.
- [95] S.-H. Peng and L. Davidson. On a subgrid-scale heat flux model for large eddy simulation of turbulent thermal flow. *International Journal of Heat and Mass Transfer*, 45:1393–1405, 2002.

- [96] S.-H. Peng and L. Davidson. Large eddy simulation for turbulent buoyant flow in a confined cavity. *International Journal of Heat and Fluid Flow*, 22:323–331, 2001.
- [97] S.-H. Peng. *Modeling of Turbulent flow and Heat Transfer for Building Ventilation*. PhD thesis, Dept. of Thermo and Fluid Dynamics, Chalmers University of Technology, Göteborg, 1998.
- [98] D.G. Barhaghi and L. Davidson. Natural convection boundary layer in a 5:1 cavity. *Physics of Fluids*, 19(125106), 2007.
- [99] D. Barhaghi. *A Study of Turbulent Natural Convection Boundary Layers Using Large-Eddy Simulation*. PhD thesis, Div. of Fluid Dynamics, Dept. of Applied Mechanics, Chalmers University of Technology, Göteborg, Sweden, 2007.
- [100] D.G. Barhaghi, L. Davidson, and R. Karlsson. Large-eddy simulation of natural convection boundary layer on a vertical cylinder. *International Journal of Heat and Fluid Flow*, 27(5):811–820, 2006.
- [101] D.G. Barhaghi and L. Davidson. Les of mixed convection boundary layer between radiating parallel plates. In *5th International Symposium on Turbulence, Heat and Mass Transfer*, September 25-29, 2006, Dubrovnik, Croatia, 2006.
- [102] S.R. Robinson. Coherent motions in the turbulent boundary layer. *Annual Review of Fluid Mechanics*, 23:601–639, 1991.
- [103] L. Davidson. Large eddy simulations: how to evaluate resolution. *International Journal of Heat and Fluid Flow*, 30(5):1016–1025, 2009.
- [104] L. Davidson. How to estimate the resolution of an LES of recirculating flow. In M. V. Salvetti, B. Geurts, J. Meyers, and P. Sagaut, editors, *ERCOFTAC*, volume 16 of *Quality and Reliability of Large-Eddy Simulations II*, pages 269–286. Springer, 2010.
- [105] L. Davidson. Inlet boundary conditions for embedded LES. In *First CEAS European Air and Space Conference*, 10-13 September, Berlin, 2007.
- [106] L. Davidson, D. Cokljat, J. Fröhlich, M.A. Leschziner, C. Mellen, and W. Rodi, editors. *LESFOIL: Large Eddy Simulation of Flow Around a High Lift Airfoil*, volume 83 of *Notes on Numerical Fluid Mechanics*. Springer Verlag, 2003.
- [107] C.P. Mellen, J. Fröhlich, and W. Rodi. Lessons from LESFOIL project on large eddy simulation of flow around an airfoil. *AIAA Journal*, 41(4):573–581, 2003.
- [108] S. Johansson, L. Davidson, and E. Olsson. Numerical simulation of vortex shedding past triangular cylinders at high reynolds numbers using a  $k - \varepsilon$  turbulence model. *International Journal for Numerical Methods in Fluids*, 16:859–878, 1993.
- [109] S. Perzon and L. Davidson. On CFD and transient flow in vehicle aerodynamics. In *SAE Technical Paper 2000-01-0873, Detroit*, 2000.
- [110] S. Perzon and L. Davidson. On transient modeling of the flow around vehicles using the Reynolds equation. In J.-H. Wu, Z.-J. Zhu, F.-P. Jia, X.-B. Wen, and W. Hu, editors, *ACFD 2000*, Bejing, 2000.

- [111] T.H. Shih, J. Zhu, and J. L. Lumley. A realizable Reynolds stress algebraic equation model. Technical memo 105993, NASA, 1993.
- [112] P. Spalart and S. Allmaras. A one equation turbulence model for aerodynamic flows. AIAA paper 92-0439, Reno, NV, 1992.
- [113] P.R. Spalart, W.-H. Jou, M. Strelets, and S.R. Allmaras. Comments on the feasibility of LES for wings and on a hybrid RANS/LES approach. In C. Liu and Z. Liu, editors, *Advances in LES/DNS, First Int. conf. on DNS/LES*, Louisiana Tech University, 1997. Greyden Press.
- [114] F.R. Menter, M. Kuntz, and R. Bender. A scale-adaptive simulation model for turbulent flow prediction. AIAA paper 2003-0767, Reno, NV, 2003.
- [115] A.K. Travin, M. Shur, , M. Strelets, and P.R. Spalart. Physical and numerical upgrades in the detached-eddy simulations of complex turbulent flows. In R.Friederich and W.Rodi, editors, *Fluid Mechanics and its Applications. Advances in LES of Complex Flows*, volume 65 of *Euromech Colloquium 412. Fluid Mechanics and its Applications. Advances in LES of Complex Flows*, pages 239–254. Academic Publishers, Dordrecht, 2002.
- [116] C. De Langhe, B. Merci, K. Lodefier, and E. Dick. Hybrid RANS-LES modelling with the renormalization group. In K. Hanjalić, Y. Nagano, and M.J. Tummers, editors, *Turbulence Heat and Mass Transfer 4*, pages 697–704, New York, Wallingford (UK), 2003. begell house, inc.
- [117] J.C. Kok, H.S. Dol, B. Oskam, and H. van der Ven. Extra-large eddy simulation of massively separated flows. AIAA paper 2004-264, Reno, NV, 2004.
- [118] J. Yan, C. Mocket, and F. Thiele. Investigation of alternative length scale substitutions in detached-eddy simulation. *Flow, Turbulence and Combustion*, 74:85–102, 2005.
- [119] S.S. Girimaji. Partially-Averaged Navier-Stokes model for turbulence: A Reynolds-averaged Navier-Stokes to direct numerical simulation bridging method. *Journal of Fluids Engineering*, 73(2):413–421, 2006.
- [120] J. Ma, S.-H. Peng, L. Davidson, and F. Wang. A low Reynolds number variant of Partially-Averaged Navier-Stokes model for turbulence. *International Journal of Heat and Fluid Flow*, 32(3):652–669, 2011.
- [121] R. Schiestel and A. Dejoan. Towards a new partially integrated transport model for coarse grid and unsteady turbulent flow simulations. *Theoretical and Computational Fluid Dynamics*, 18(6):443–468, 2005.
- [122] K. Abe, T. Kondoh, and Y. Nagano. A new turbulence model for predicting fluid flow and heat transfer in separating and reattaching flows - 1. Flow field calculations. *Int. J. Heat Mass Transfer*, 37(1):139–151, 1994.
- [123] P. Batten, U. Goldberg, and S. Chakravarthy. Interfacing statistical turbulence closures with large-eddy simulation. *AIAA Journal*, 42(3):485–492, 2004.
- [124] U. Piomelli, E. Balaras, H. Pasinato, K.D. Squire, and P.R. Spalart. The inner-outer layer interface in large-eddy simulations with wall-layer models. *International Journal of Heat and Fluid Flow*, 24:538–550, 2003.

- [125] L. Davidson and S. Dahlström. Hybrid LES-RANS: An approach to make LES applicable at high Reynolds number. *International Journal of Computational Fluid Dynamics*, 19(6):415–427, 2005.
- [126] J. Larsson, F.S. Lien, and E. Yee. The artificial buffer layer and the effects of forcing in hybrid LES/RANS. *International Journal of Heat and Fluid Flow*, 28(6):1443–1459, 2007.
- [127] F.R. Menter and M. Kuntz. Adaption of eddy-viscosity turbulence models to unsteady separated flows behind vehicles. In Rose McCallen, Fred Browand, and James Ross, editors, *The Aerodynamics of Heavy Vehicles: Trucks, Buses, and Trains*, volume 19 of *Lecture Notes in Applied and Computational Mechanics*. Springer Verlag, 2004.
- [128] M. Strelets. Detached eddy simulation of massively separated flows. AIAA paper 2001–0879, Reno, NV, 2001.
- [129] X. Xiao, J.R. Edwards, and H.A. Hassan. Inflow boundary conditions for LES/RANS simulations with applications to shock wave boundary layer interactions. AIAA paper 2003–0079, Reno, NV, 2003.
- [130] F. Hamba. An approach to hybrid RANS/LES calculation of channel flow. In W. Rodi and N. Fueyo, editors, *Engineering Turbulence Modelling and Experiments 5*, pages 297–305. Elsevier, 2003.
- [131] P. Tucker and L. Davidson. Zonal k-l based large eddy simulation. *Computers & Fluids*, 33(2):267–287, 2004.
- [132] P. Tucker. Differential equation based length scales to improve DES and RANS simulations. AIAA paper 2003-3968, 16th AIAA CFD Conference, 2003.
- [133] L. Temmerman, M. Hadžiadicbic, M.A. Leschziner, and K. Hanjalić. A hybrid two-layer URANS-LES approach for large eddy simulation at high Reynolds numbers. *International Journal of Heat and Fluid Flow*, 26:173–190, 2005.
- [134] A. Dejoan and R. Schiestel. Large-eddy simulation of non-equilibrium pulsed turbulent flow using transport equations subgrid model. In E. Lindborg, A. Johansson, J. Eaton, J. Humphrey, N. Kasagi, M. Leschziner, and M. Sommerfeld, editors, *The Second International Symp. on Turbulence and Shear Flow Phenomena*, volume 2, pages 341–346, Stockholm, 2001.
- [135] S. Kenjereš and K. Hanjalić. LES, T-RANS and hybrid simulations of thermal convection at high RA numbers. In W. Rodi and M. Mulas, editors, *Engineering Turbulence Modelling and Measurements 6*, pages 369–378. Elsevier, 2005.
- [136] P.R. Spalart. Strategies for turbulence modelling and simulations. *International Journal of Heat and Fluid Flow*, 21:252–263, 2000.
- [137] N.V. Nikitin, F. Nicoud, B. Wasistho, K.D. Squires, and P. Spalart. An approach to wall modeling in large-eddy simulations. *Physics of Fluids*, 12(7):1629–1632, 2000.

- [138] L. Temmerman, M.A. Leschziner, and K. Hanjalić. A-priori studies of near-wall RANS model within a hybrid LES/RANS scheme. In W. Rodi and N. Fueyo, editors, *Engineering Turbulence Modelling and Experiments 5*, pages 317–326. Elsevier, 2002.
- [139] F.R. Menter and Y. Egorov. Revisiting the turbulent length scale equation. In *IUTAM Symposium: One Hundred Years of Boundary Layer Research*, Göttingen, 2004.
- [140] F.R. Menter, M. Kuntz, and R. Bender. A scale-adaptive simulation model for turbulent flow predictions. AIAA-2003-0767, Reno, 2003.
- [141] J.C. Rotta. *Turbulente Strömungen*. Teubner Verlag, Stuttgart, 1972.
- [142] F.R. Menter and Y. Egorov. A scale-adaptive simulation model using two-equation models. AIAA paper 2005-1095, Reno, NV, 2005.
- [143] L. Davidson. Evaluation of the SST-SAS model: Channel flow, asymmetric diffuser and axi-symmetric hill. In *ECCOMAS CFD 2006*, September 5-8, 2006, Egmond aan Zee, The Netherlands, 2006.
- [144] S.S. Girimaji. Partially-averaged Navier-Stokes model for turbulence: A Reynolds-averaged Navier-Stokes to direct numerical simulation bridging method. *ASME Journal of Applied Mechanics*, 73(2):413–421, 2006.
- [145] S.S. Girimaji and K. S. Abdol-Hamid. Partially-Averaged Navier-Stokes model for turbulence: Implementation and Validation. AIAA paper 2005-0502, Reno, N.V., 2005.
- [146] M. L. Shur, P.R. Spalart, M. Kh. Strelets, and A.K. Travin. A hybrid RANS-LES approach with delayed-DES and wall-modelled LES capabilities. *International Journal of Heat and Fluid Flow*, 29:1638–1649, 2008.
- [147] J. Ma, S.-H. Peng, L. Davidson, and F. Wang. A low Reynolds number partially-averaged Navier-Stokes model for turbulence. In *8th International ERCOFTAC Symposium on Engineering Turbulence, Modelling and Measurements*, Marseille, France, 9-11 June, 2010.
- [148] L. Davidson. A new approach of zonal hybrid RANS-LES based on a two-equation  $k - \varepsilon$  model. In *ETMM9: 9th International ERCOFTAC Symposium on Turbulence Modelling and Measurements*, Thessaloniki, Greece, 2012.
- [149] L. Davidson. Using isotropic synthetic fluctuations as inlet boundary conditions for unsteady simulations. *Advances and Applications in Fluid Mechanics*, 1(1):1–35, 2007.
- [150] L. Davidson and S.-H. Peng. Emddedded LES with PANS. In *6th AIAA Theoretical Fluid Mechanics Conference*, AIAA paper 2011-3108, 27-30 June, Honolulu, Hawaii, 2011.
- [151] L. Davidson. Hybrid LES-RANS: Inlet boundary conditions for flows including recirculation. In *5th International Symposium on Turbulence and Shear Flow Phenomena*, volume 2, pages 689–694, 27-29 August, Munich, Germany, 2007.

- [152] N. Jarrin, S. Benhamadouche, D. Laurence, and R. Prosser. A synthetic-eddy-method for generating inflow conditions for large-eddy simulations. *International Journal of Heat and Fluid Flow*, 27(4):585–593, 2006.
- [153] M. Billson. *Computational Techniques for Turbulence Generated Noise*. PhD thesis, Dept. of Thermo and Fluid Dynamics, Chalmers University of Technology, Göteborg, Sweden, 2004.
- [154] M. Billson, L.-E. Eriksson, and L. Davidson. Jet noise prediction using stochastic turbulence modeling. AIAA paper 2003-3282, 9th AIAA/CEAS Aeroacoustics Conference, 2003.
- [155] L. Davidson. Hybrid LES-RANS: Inlet boundary conditions. In B. Skallerud and H.I. Andersson, editors, *3rd National Conference on Computational Mechanics – MekIT'05 (invited paper)*, pages 7–22, Trondheim, Norway, 2005.
- [156] L. Davidson. Hybrid LES-RANS: Inlet boundary conditions for flows with recirculation. In *Second Symposium on Hybrid RANS-LES Methods*, Corfu island, Greece, 2007.
- [157] J.R. Welty, C.E. Wicks, and R.E. Wilson. *Fundamentals of Momentum, Heat, and Mass Transfer*. John Wiley & Sons, New York, 3 edition, 1984.
- [158] L. Davidson. HYBRID LES-RANS: Inlet boundary conditions for flows with recirculation. In *Advances in Hybrid RANS-LES Modelling*, volume 97 of *Notes on Numerical Fluid Mechanics and Multidisciplinary Design*, pages 55–66. Springer Verlag, 2008.
- [159] Lars Davidson and Shia-Hui Peng. Hybrid LES-RANS: A one-equation SGS model combined with a  $k - \omega$  for predicting recirculating flows. *International Journal for Numerical Methods in Fluids*, 43(9):1003–1018, 2003.
- [160] F.R. Menter and Y. Egorov. The scale adaptive simulation method for unsteady turbulent flow predictions. Part 1: Theory and description. *Flow, Turbulence and Combustion*, 85:113–138, 2010.
- [161] Y. Egorov, F.R. Menter, R. Lechner, and D. Cokljat. The scale adaptive simulation method for unsteady flow predictions. Part 2: Application to complex flows. *Flow, Turbulence and Combustion*, 85:139–165, 2010.
- [162] J. Fröhlich and D. von Terzi. Hybrid LES/RANS methods for the simulation of turbulent flows. *Progress in Aerospace*, 44(5):349–377, 2008.
- [163] A. Travin, M. Shur, M. Strelets, and P. Spalart. Detached-eddy simulations past a circular cylinder. *Flow Turbulence and Combustion*, 63(1/4):293–313, 2000.
- [164] B. Chaouat and R. Schiestel. A new partially integrated transport model for subgrid-scale stresses and dissipation rate for turbulent developing flows. *Physics of Fluids*, 17(065106), 2005.
- [165] L. Davidson and B. Farhanieh. CALC-BFC: A finite-volume code employing collocated variable arrangement and cartesian velocity components for computation of fluid flow and heat transfer in complex three-dimensional geometries. Rept. 95/11, Dept. of Thermo and Fluid Dynamics, Chalmers University of Technology, Gothenburg, 1995.

- [166] F. Eriksson. *Flerdimensionell analys (in Swedish)*. Studentlitteratur, Lund, Sweden, 4 edition, 1977.
- [167] R.L. Panton. *Incompressible Flow*. John Wiley & Sons, New York, 1984.
- [168] B.J. Daly and F.H. Harlow. Transport equation in turbulence. *Physics of Fluids*, 13:2634–2649, 1970.
- [169] F. Nicoud and F. Ducros. Subgrid-scale stress modelling based on the square of the velocity gradient tensor. *Flow, Turbulence and Combustion*, 62(3):183–200, 1999.
- [170] O. Brander. *Vektoranalys (in Swedish)*. Studentlitteratur, Lund, Sweden, 2007.